π-Conjugated Si=Si Systems with (Oligo-)Aromatic Linking Units and their Regiodivergent Reactivity towards Acetylenes.

Dissertation

zur Erlangung des Grades

des Doktors der Naturwissenschaften

der Naturwissenschaftlich-Technischen Fakultät

der Universität des Saarlandes

Von

M. Sc. Naim Obeid

Saarbrücken

10/2017

Tag des Kolloquiums: 21.December 2017

Dekan: Prof. Dr. Guido Kickelbick

Berichterstatter: Prof. Dr. David Scheschkewitz

Prof. Dr. Gregor Jung

Vorsitz: Prof. Dr. Claus Jacob

Akad. Mitarbeiter: Prof. Dr. Volker Huch

The work described in this thesis was carried out from Februray 2014 until October 2017 at Saarland University, Naturwissenschaftlich-Technische Fakultät, Fachrichtung Chemie, Krupp-Chair of General and Inorganic Chemistry under supervision of Prof. Dr. David Scheschkewitz.

Abstract

Nucleophilic disilenides allow for the incorporation of Si=Si units into conjugated organic systems, a crucial step to exploit their unique physical and chemical properties. An optimized reaction protocol for the Si=Si transfer suppresses undesired redox reactions, allowing for high yields even for sterically demanding substrates. Various aryl disilenes $Tip_2Si{=}Si(Tip)Ar$ and *para*-arylene bridged tetrasiladienes, $Tip_2Si{=}Si(Tip)$-LU-$Si(Tip){=}SiTip_2$ were obtained by reaction of aryl halides and dihalides with the disilenide $Tip_2Si{=}SiTipLi$ (Tip = 2,4,6-$iPr_3C_6H_2$, Ar = aryl substituent, LU = *para*-arylene linking unit). The products with oligoaromatic bridging units exhibit weak fluorescence at room temperature, a rare phenomenon in species with Si=Si bonds.

Additionally, the reactivity of disilenes and tetrasiladienes towards alkynes such as phenyl acetylene has been examined. In the majority of cases, [2+2] cycloaddition between the Si=Si moieities and C≡C bonds takes place and air stable compounds featuring σ-π conjugation along the molecule backbone were obtained. The regiospecific [2+2] cycloaddition of C≡C bonds to Si=Si bonds also allowed the preparation of ethynyl-terminated extended monomers from 1,4-bis(ethynyl)benzene and the corresponding *para*-arylene bridged tetrasiladienes with different linking units (LU = biphenylene, acetylene and anthracene).

Zusammenfassung

Nukleophile Disilenide ermöglichen den Einbau von Si=Si-Einheiten in konjugierte organische Systeme. Dieser Schritt ermöglicht die Erforschung ihrer einzigartigen physikalischen und chemischen Eigenschaften. Eine optimierte Reaktionsvorschrift für den Si=Si Transfer ermöglicht die Unterdrückung unerwünschter RedOx Reaktionen und liefert hohe Ausbeuten selbst bei der Umsetzung mit sterisch anspruchsvollen Substraten. Verschiedene Aryl-Disilene $Tip_2Si=Si(Tip)Ar$ und para-arylene verbrückte Tetrasiladiene $Tip_2Si=Si(Tip)$-LU-$Si(Tip)=SiTip_2$ wurden durch Reaktion von Arylhaliden und Dihaliden mit dem Disilenid $Tip_2Si=SiTipLi$ erhalten. (Tip = 2,4,6-$iPr_3C_6H_2$, Ar = aryl Substituent, LU = *para*-Arylene linking unit). Die Produkte mit oligoaromatischen Brückeneinheiten zeigen schwache Fluoreszenz bei Raumtemperatur, was bei Spezies mit einer Si=Si Einheit ein seltenes Phänomen ist.

Darüberhinaus wurde die Reaktivität vin Diselenen und Tetrasiladienen gegenüber Alkinen wie Phenylacetylen untersucht. In den meisten Fällen treten [2+2] Cycloadditionen zwischen den Si=Si Einheiten und C≡C bindungen auf und luftstabile Verbindungen mit einer σ-π Konjugation über das Grundgerüst des Moleküls.

Die Regiospezifische [2+2] Cycloaddition von C≡C bindungen mit Si=Si bindungen ermöglichte außerdem die Synthese von Ethynyl-terminierten Erweiterten Monomeren von 1-4-bis(ethynyl)benzol und den korrespondierenden para-arylene Verbrückten Tetrasiladienen mit verschiedenen Linking Units (LU = biphenylene, acetylen und Anthracene).

Annotation

This thesis has been published in parts in:

- N. M. Obeid, L. Klemmer, D. Maus, M. Zimmer, I. Bejan, V. Huch, A. J. P. White, G. Jung, D. Scheschkewitz, **(Oligo)aromatic species with one or two conjugated Si=Si bonds: near-IR emission of anthracenyl-bridged tetrasiladiene**, *Dalton Trans.* **2017**

“Whoever Allah wants good for him, he puts them to test. He puts them through difficulties; like a diamond or gold that has to be burnt after which anything bad from it is removed so that what you have is the pure diamond or the pure gold.”

Prophet Muhammad
peace be upon him

Acknowledgements

Firstly, I would like to express my sincere gratitude to my advisor **Prof. Dr. David Scheschkewitz** for the continuous support of my PhD study and related research, for his patience, motivation, and immense knowledge. The door to **Prof. Dr. David Scheschkewitz** office was always open whenever I ran into a trouble spot or had a question about my research or writing. His guidance helped me in all the time of research and writing of this thesis. I could not have imagined having a better advisor and mentor for my PhD study.

I am grateful to **Prof. Dr.** Gregor Jung for agreeing to take the duty of examination.

Specials Thanks to **Lukas Klemmer** for performing DFT-calculations.

Many thanks to **Susanne Harling** for measuring the elementary analyzes.

I am particularly grateful to **Daniel Maus** and **Prof. Dr. Gregor Jung** for recording the fluorescence spectra.

I would like aslo to thank **Dr. Volker Huch** for performing the X-ray diffraction experiments of my compounds.

Many thanks to **Dr. Michael Zimmer** for carrying out the VT NMR experiments and the help of NMR spectroscopic problems.

Many Thanks to all other former and current members group: **Dr. Prasenjit Bag, Dr. Cem B. Yildiz, Hui Zhao, Isabell Omlor, Nadine Poitiers, Marcel Lambert, Dr. Kinga Leszczyńska, Dr. Carsten Präsang, Dr. Philipp Willmes, Dr. David Nieder, Yvonne Kaiser, Yannic Heider, Thomas Büttner, Dr. Andreas Rammo, Ramona Cullmann, Evelyne Altmeyer, Andreas Adolf, Bettina Piro and Günther Berlin.**

To the best secretary in the world, **Bianca Iannuzzi**, I thank you for your support in all sorts of bureaucratic matters and friendly cooperation.

A very special thanks to **my Parents** for their invaluable and loving support throughout the time of my PhD work.

Table of Contents

List of Abbreviations

DFT	**D**ensity **F**unctional **T**heory
B3LYP	**B**ecke hybrid-**3**-parameter functional and the correlation functional of **L**ee, **Y**ang and **P**ar
CGMT	**C**arter-**G**oddard-**M**alrieu-**T**rinquier
dec.	**d**ecomposition
mp.	**m**elting **p**oint
C	**C**elsius
Dip	2,6-**Di**i**s**opropy**p**henyl
Dis	Bis(trimetylsilyl)methyl
Mes	2,4,6-Trimethylphenyl
^{t}Bu	***t**ert*.-**Bu**tyl, -C4H9
Ph	**P**henyl
DME	1,2-**dim**ethoxy**e**thylene
Me	**M**ethyl, -CH$_3$
Tip	1,3,5-**T**ri**i**sopropyl**p**henyl
iPr	**i**so-**Pr**opyl, -C3H7
TMS	Trimethylsilyl
EMind	1,1,3,3,7,7-Hexaethyl-5,5-dimethyl-s-hydrindacen-4-yl
M	**M**olar
eq	**eq**uivalents
h	**h**our(s)

HOMO	**H**ighest **O**ccupied **M**olecular **O**rbital
LUMO	**L**owest **U**noccupied **M**olecular **O**rbital
MO	**M**olecular **O**rbital
NMR	**N**uclear **M**agnetic **R**esonance
ppm	**P**arts **p**er **m**illion
rt	**R**oom **T**emperature
VT	**V**ariable **T**emperature
thf	**t**etra**h**ydro**f**uran
Et_2O	Diethylether
UV	**U**ltra-**V**iolet
vis	**v**isible
IR	Infrared
λ_{max}^{exc}	Maximum Excitation Wavelength
λ_{max}^{em}	Maximum Emission Wavelength
ε	Molar Extinction Coefficient
Δ_{EST}	Singlet-triplet energy splitting
Ar	**Ar**omatic substituent
LU	**L**inking **U**nits
Å	**A**ngstrom
CP-MAS	**C**ross **P**olarization-**M**agic **A**ngle **S**pinning

List of Figures

List of Schemes

List of Tables

Foreword

There is little doubt that silicon as the prototypical semiconductor is one of the most important elements for human society at the start of the 21st century. Silicon-based technologies such as microprocessors or photovoltaics lead to vigorous progress in virtually all aspects of our daily life.[1]

We are living on the silicon planet, the planet of the element most abundant (27.7% by weight) in the earth crust after oxygen (46.6% by weight).[2] A virtually endless number of minerals contain silicon,[2] although almost exclusively in combination with oxygen as silicates or related materials.[3]

Discovery of elemental silicon was complicated process taking several decades to conclude. In 1787 French scientist Lavoisier (1743–1794) predicted that silica is not an elemental matter and but rather a compound of an element, probably of a metal, with oxygen.[4] In 1808 English scientist Sir Humphry Davy (1778–1829) developed the technique of melt flow electrolysis that allows for the isolation of (semi-)metallic elements from compounds, which otherwise resist most chemical reduction protocols. The technique was successful for producing elemental sodium, potassium, calcium, and several other elements for the first time, but he failed with elemental silicon.[5] Berzelius finally succeeded in getting the new element in pure form via the reduction of silicon tetrafluoride (SiF_4) by potassium metal in 1824.[6] The English name silicon was suggested by Thomas Thomson (1773–1852) in 1831 based on the Latin word for "flint" (silex) and the ending –on, presumably to reflect the similarity with the nonmetals carbon and boron.[7] In 1858, Wöhler first showed that thermal decomposition of silane affords elemental silicon as red-brown mirror.[8]

Since the middle of last century, synthetic organosilicon polymers, the polysiloxanes (silicones), are increasingly being applied in virtually all branches of industry, agriculture, medicine and end consumer products.[9] The basic molecular precursor for such polymers is dimethyldichlorosilane (Me_2SiCl_2), which is obtained by the so-called "Direct Process" from methyl chloride and metallurgical silicon in the presence of copper (Müller-Rochow method).[10] In an idealized reaction sequence, the hydrolysis of

Me_2SiCl_2 results in the polycondensation of intermediate silanedioles to linear silicones (Scheme 1).[11]

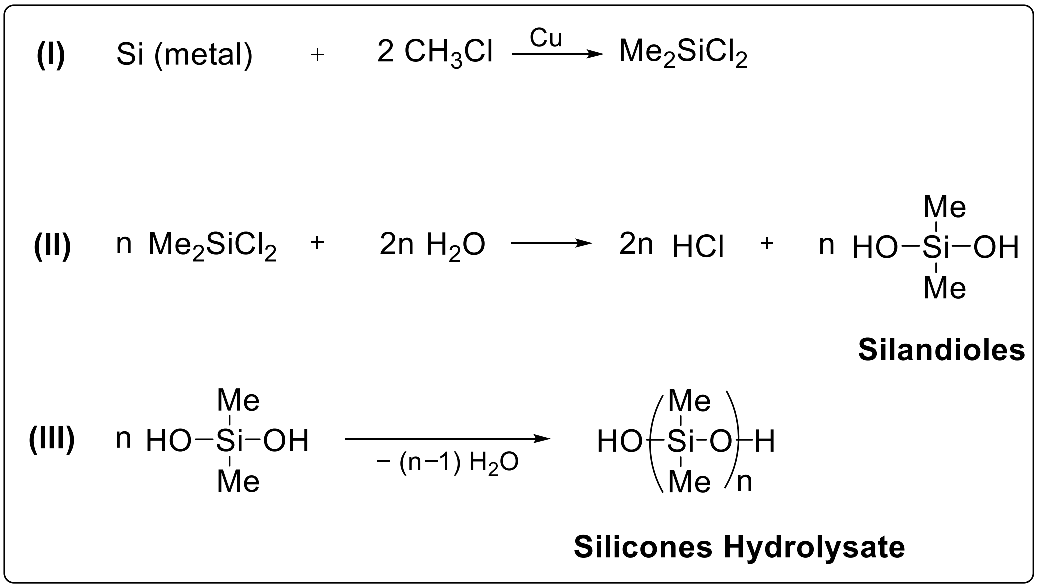

Scheme 1. Reaction between methyl chloride and metallurgical silicon in the presence of copper (Direct Process) and idealized reaction of dimethyldichlorosilane (Me_2SiCl_2) with water followed by polycondensation.[11] **(I):** Direct Process; **(II):** Hydrolysis and **(III):** Polycondensation.

While polysiloxanes show desirable properties that add convenience to applications that can also been achieved with other materials, the availability of elemental silicon with its semi-conducting properties changed the world beyond anything that could have been imagined: the first diode based silicon was patented for the first time in 1905[12] while the first silicon solar cell was reported in 1941.[13] The floating zone process (developed in 1945) is the key for the generation of high purity silicon, which opens the door for the use of silicon in semiconductor industry.[14] At present, about 99% of all semiconductor devices are made from monocrystalline silicon.[14] Silicon technology is the basis for radioelectronics, microelectronics, computer chips and optoelectronics. Concerning the special characteristic of silicon over 6000 articles denoted to its synthesis and application appeared in the early 21st century alone. Silicon science can thus not be ignored in any technological development yet to come. [15]

Preface

As one of the tools that promoted an increased understanding of our world, the science of chemistry (study of matter and the changes it undergoes) developed slowly until near the end of the eighteenth century. By that time, two branches of chemistry were starting to be distinguished. One branch was concerned with matter obtained from natural or living sources and was called organic chemistry. The other branch dealt with substances derived from nonliving matter minerals and the like. It was called inorganic chemistry.

A major contributor to the development of organic chemistry (and of course also the wide range of organic substrates in nature) is the ability of carbon to form single, double and triple bonds with itself and with other atoms. π- and σ-components of these bonds are of comparable strength leading to relative kinetic inertness. This led to the question whether a similar variability in bonding could be realized for the heavier main group elements of Group 14 (Si, Ge, Sn and Pb), which could serve as building blocks for the synthesis of complex "inorganic" molecules.

However, attempts by Frederic Stanley Kipping at Nottingham to isolate "silicones" ($R_2Si=O$; silaketones in modern nomenclature)[16] and "silicoethylene" ($R_2Si=SiR_2$; disilenes)[17] in the early 20th century century failed. The anticipated access to "silicones" via the dehydration of silandioles afforded polysiloxanes instead – which to this day are referred to as silicones in colloquial terms.[16] Other efforts to form multiple bonds between elements of the third row of the periodic table were also unsuccessful[18] and the components mainly consisted of five- or six-membered oligomers.[19] These findings resulted in the so called “double bond rule”, which states that compounds with multiple bonds to main group elements heavier than the second row were unstable and thus non-existent. According to Pitzer [20] and Muliken,[21] this is due to repulsive interactions of their inner electronic shells.

In 1975, Jutzi predicted that a π-bond between heavier elements should be accessible by the incorporation of sterically demanding substituents, which would stabilize the compounds kinetically against oligomerization.[22] One year later, this principle was indeed successfully applied for the isolation of the first heavier analogues of alkenes (distannene **1** and digermene **2**) by Lappert and co-workers.[23]

This milestone achievement opened the door for the isolation of the first silene **3** (Si=C) by Brook,[24] disilene **4** (Si=Si) by West[25] and diphosphene **5** (P=P) by Yoshifuji,[26] all three isolated only a few years later and kinetically stabilized by bulky substituents (Scheme 2).

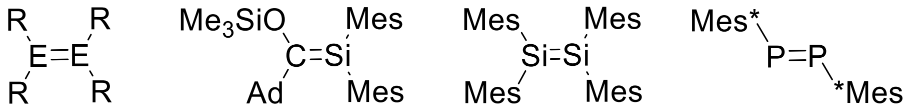

1,2 **3** **4** **5**

(**1**: E=Sn, **2**: E=Ge)

Scheme 2. First examples of unsaturated heavy main group elements: Lappert's distannene and digermene **1** and **2**; Brook´s silene **3**; West's disilene **4** and Yoshifuji's diphosphene **5** (R = $CH(SiMe_3)_2$, Mes = 2,4,6-trimethylphenyl, Ad = 1-adamantyl, Tip = 2,4,6-triisopropylphenyl, Mes* = 2,4,6-tri-tert-butylphenyl).[23,24,25,26]

Since then, the specific field of low-valent heavier main group elements has been remarkably developed by the efforts of many research groups. This growth reflects the impressive advances made in the chemistry of low valent silicon, which is flourishing nowadays with many spectacular achievements. The following chapter provides a brief introduction into structural aspects of heavy double bonds, which is followed by selected published examples based on silicon.

1. Introduction

1.1. The landmark Work of West

A first allusion to the long-desired multiply bonded silicon species was provided in 1973 by Peddle and Roark.[27] They reported the formation of elusive tetramethyl disilene via a retro-Diels-Alder process at 380 °C and subsequently trapped the product in a Diels-Alder reaction with anthracene. The intermediacy of the proposed product was verified by the disilene's distinct mass-spectrometric fragment signal at $m/z = 116$.[27]

The preparative breakthrough came in 1981 with the isolation of the first stable compound containing a Si=Si bond by West, Michl and Fink.[25] Initially, UV irradiation of the acyclic trisilane **6** in a hydrocarbon matrix leads to the elimination of $Me_3SiSiMe_3$ and hence to the blue silylene **7** (Scheme 3), which was characterized by UV/vis at cryogenic temperatures ($\lambda_{max} = 580$ nm).[28] Upon annealing of the matrix, silylene **7** dimerizes to yellow orange disilene **4** ($\lambda_{max} = 420$ nm).[25]

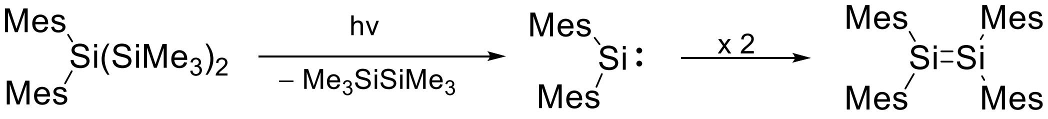

6 **7** **4**

Scheme 3. Synthesis of the first stable disiline **4** reported by West (Mes = mesityl, 2,4,6-trimethylphenyl).[25]

Protected by four mesityl groups as bulky substituents (Mes = 2,4,6-trimethylphenyl), the Si=Si bond in disilene **4** is stable at room temperature in the absence of air or moisture. Due to this pioneering work, the direct observation of physical and optical properties of a disilene was finally possible.

1.2. Bonding in Carbon's Heavier Congeners

The dissimilarities between the 2nd and the 3rd row of the periodic table are most pronounced in Group 14. Compared to carbon species, compounds of Si, Ge, Sn and Pb exhibit completely differing physical properties, chemical behavior and structural features.[29] The theoretical framework of organic chemistry cannot be applied to the chemistry of heavier Group 14 elements without changes and amendments: a typical example is the markedly different electronic structure of olefines ($R_2C=CR_2$) and heavier alkene analogues ($R_2E=ER_2$). The C-C double bond of ethylene in a rigid, perfectly planar geometrical arrangement can readily be explained by valence bond theory and its hybridization model.[30] In contrast, the first structurally characterized heavier analogues of ethylene exhibited marked structural distortions from the planar structure.[22] Thus, apart from the dihedral angle (φ) which is also observed in conjugated organic alkenes, ie deviations of the $R_2E=ER_2$ framework from planarity are described by two fundamental structural deformations namely, *trans*-bending (*trans*-bent angle θ) and twisting (twist angle τ). The *trans*-bending geometry results from the pyramidalization at silicon centers due to the inherent reluctance to hybridize, whereas the dihedral distortion of the idealized bonding planes with respect to one another is typically a result of severe steric interactions and thus not electronic in nature (Figure 1).

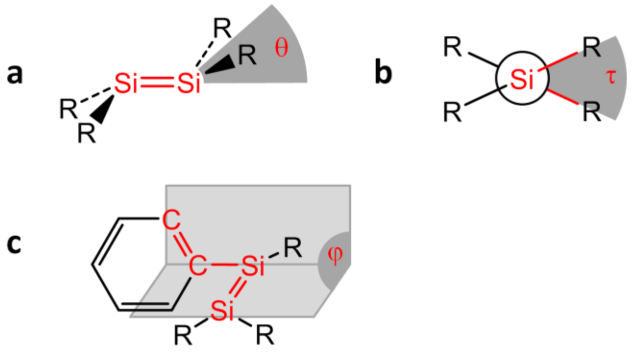

Figure 1. Illustration of non-classical double bond deformations: (a) *trans*-bent angle θ_{Si} = 90° - (angle between the Si-Si vector and the normal to the plane defined by Si and the pendant substituents), (b) twist angle τ = angle between the normals to the two planes defined by the silicon atoms and the pendant substituents, (c) dihedral distortion from co-planarity given by dihedral angle φ.

The model of Carter, Goddard, Malrieu and Trinquier CGMT Model provides a clear explanation for this non-classical, *trans*-bent double bond (Figure 2).[31] They proposed the *Gedankenexperiment* of the homolytic cleavage of a double bond into two distinct fragments that correspond to carbenes or their heavier analogues, the tetrylenes. According to Hund's rule, the two non-bonding electrons are only paired in one orbital, *i.e.* the lone pair of electrons, if an appreciable HOMO-LUMO gap is present: the tetrylene is in the singlet state. Conversely, two unpaired non-bonding electrons occur in case of two (nearly) degenerate MOs, which is referred to as the triplet state. In practice, the two unpaired electrons are typically arranged in one σ-type and one π-type orbital (Figure 2).[32a]

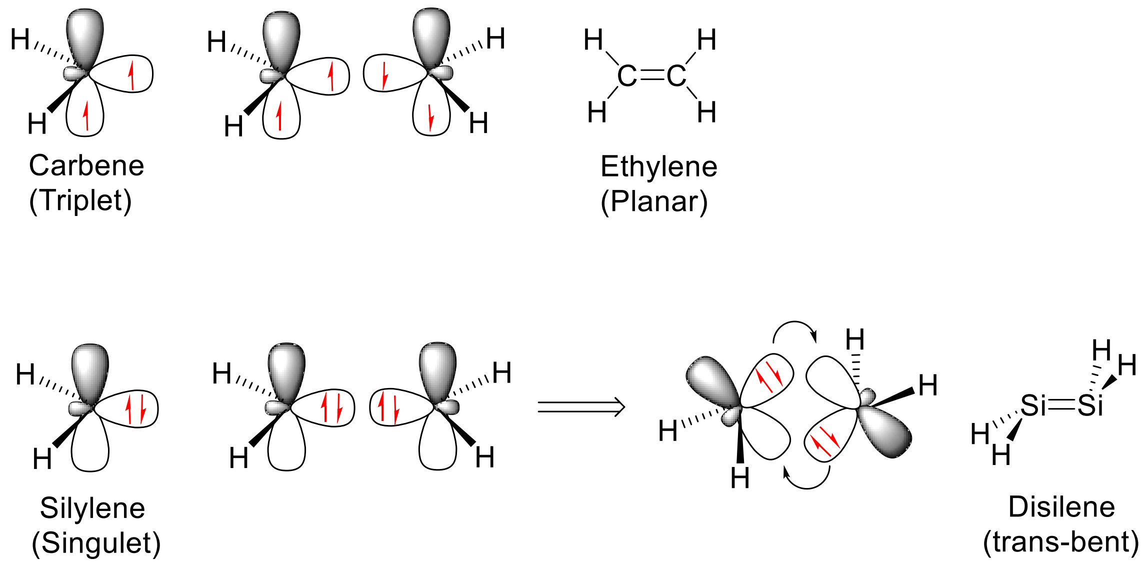

Figure 2. Classical and non-classical double bond characteristics according to CGMT-model from carbene-like singlet fragments.

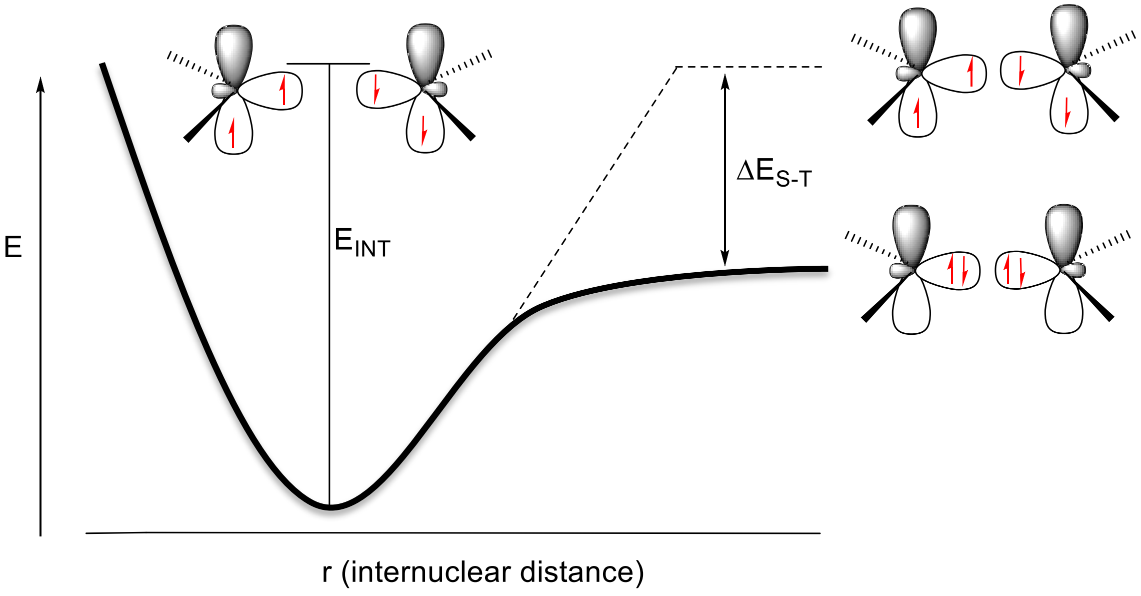

Figure 3. Homolytic cleavage of a double bond between Group 14 elements carbene-like fragments. E_{INT} = Total bond energy and $\Delta E_{S\text{-}T}$ = Difference between the fragment´s singlet and triplet state.[32b]

Essentially, this model describes the double bond topology as being a function of the energy gap between the two electronic states ($\Delta E_{S\text{-}T}$) of the carbene-like fragments formally constituting the double bond (Figure 3).[32b]

The relation between the double bond energy $E_{\sigma+\pi}$ and the singlet-triplet gap of the constituting carbene-like fragments ($\Delta E_{S\text{-}T}$) is given by the equation $E_{\sigma+\pi} = E_{INT} - 2\Delta E_{S\text{-}T}$, in which E_{INT} refers to energy required for the homolytic cleavage of the double bond into two triplet fragments.[31] With this formula, rough predictions of the geometry of the double bond of an unknown alkene analogue are possible. If the ground state is a triplet, the S-T gap is small or even vanishing compared to the $E_{\sigma+\pi}$ ($E_{\sigma+\pi} > 2\Delta E_{S\text{-}T}$). The combination of the two triplet fragments results in the classical double bond (planar geometry) as in the case of C-C double bonds (Figure 2). Conversely, if the singlet state is more favorable, the double bond's energy is smaller than the sum of singlet-triplet gaps: $E_{\sigma+\pi} < 2\Delta E_{S\text{-}T}$. The preparation energy required for the formation of a triplet carbene fragment cannot be over-compensated by the energy released by double bond formation. The fragments have to remain in the singlet state, which induces considerable Pauli repulsion between the lone electron pairs upon mutual approach. This repulsion can be reduced by inclining the bonding planes of the atoms that constitute the double bonds in opposite directions.[31] Consequently, the doubly occupied, formally sp^2 hybridized orbital of each of the two fragments forms a donor-acceptor bond to the empty p_z orbital of the other (Figure 2), which leads to the so-called *trans*-bent structure of the double bond. Lastly, if the energy difference between the lone pair of electrons and the accepting vacant orbital of the other tetrylene fragment is too high ($E_{\sigma+\pi} < \Delta E_{S\text{-}T}$) no double bond formation at all occurs and the monomers are stable.[31]

1.3. Disilenes Conformation

According to theoretical calculations, the parent disilene Si_2H_4 displays a *trans*-bent arrangement (θ calculated = 12.9°) due to the singlet ground state of the parent silylene.[33] The experimentally known disilenes, however, exhibit a whole variety of structures ranging from *trans*-bent to planar arrangements. This conformational flexibility is highly dependent on the substituent effects. In 1990, Karni and Apeloig reported the first systematic *ab initio* study concerning the impact of the substituents on the structure of disilenes.[33] While electropositive substituents (Li, BH_2, BeH and SiH_3) favor the triplet state of constituting tetrylene fragments and thus a planar arrangement of the Si=Si bond, π-donating as well as electronegative substituents (OH, F and NH_2) stabilize the singlet state and force the Si=Si unit into a *trans*-bent conformation.[33]

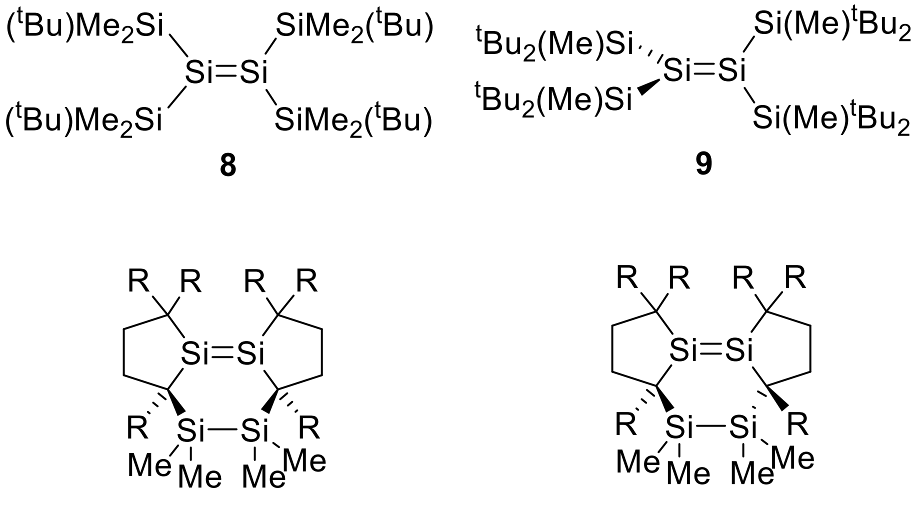

8 **9**

***cis*-10** ***trans*-10**

Scheme 4. Stable disilenes illustrating the conformational flexibility of the Si=Si Bond. (Mes = 2,4,6-trimethylphenyl; Tip = 2,4,6-triisopropylphenyl; R = $SiMe_3$).

Indeed, although necessary for kinetic stabilization, sterically demanding groups have a large impact on the structure of disilenes. The potential energy surface for the conformation of disilenes is generally very flat. As shown in Scheme 4 the Si=Si can adopt a broad variety of conformations ranging from planar **8**[34] and twisted **9**,[35] to different degrees of *trans*-bending as in the *cis*- and *trans*- isomers of **10**.[36] For instance, increased steric bulk in disilene **9** causes a considerable twisting of the planar coordination environments of each silicon atom between the two Si planes (τ = 54.5°),[35] while the sterically less encumbered disilene **8** is almost perfectly planar.[34] Similarly, the more pronounced ring strain in *trans*-**10** causes much larger *trans*-bending and twisting in comparison with *cis*-**10**.[36] Even co-crystallized solvent can have a noticable influence on the conformation of disilenes. In case of disilene **4**, three different conformations were detected depending on the solvate (solvent free: τ = 3°, θ = 14°;[37] toluene: τ = 12°, θ = 18°;[38] thf: τ = 13°, θ = 0°).[39]

Therefore, the substituent's electronic and steric properties as well as co-crystallized solvent types have considerable influence on the geometry about the Si=Si double bond.

UV/vis Spectroscopy

Disilenes are characterized by a significantly smaller HOMO-LUMO gap compared to their carbon analogues, which explains the absorption of disilenes in the visible region of the electromagnetic spectrum and thus the intense color of these compounds – in sharp contrast to the often colorless olefins. The HOMO-LUMO energies of the parent systems (disilene and ethylene) were theoretically examined by Kira and Iwamoto. They found that disilene showed about half the energy gap of ethylene due to a raised HOMO and a lowered LUMO (Figure 4).[40]

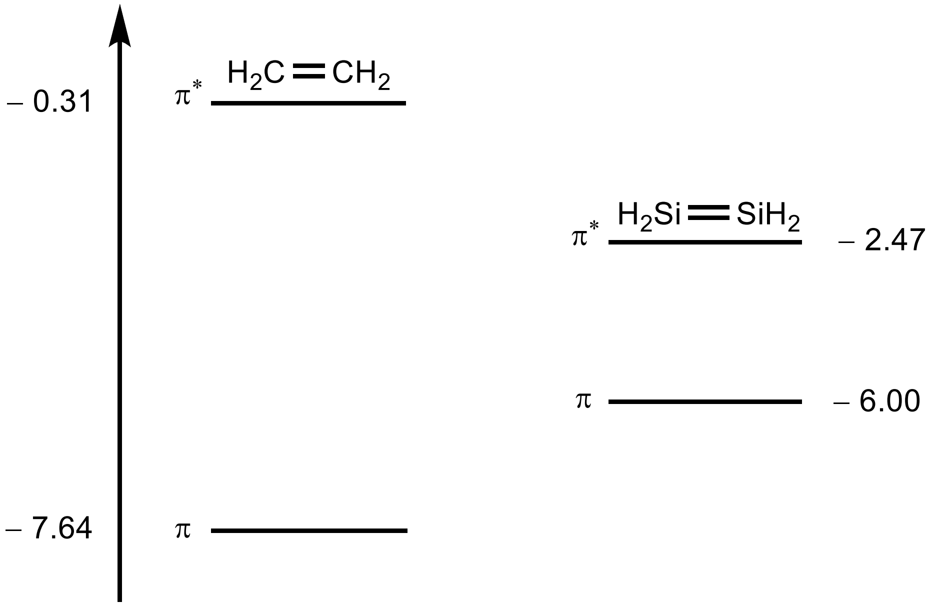

Figure 4. Energy levels of HOMO and LUMO in parent systems.[40]

The conformational flexibility of disilenes is another important factor determining the size of HOMO-LUMO gap. As illustrated in Figure 5,[41] an increasing deviation from planarity (larger θ and τ) results in a narrowing of the π-π^* gap and thus a red-shift of the longest wavelength absorption.

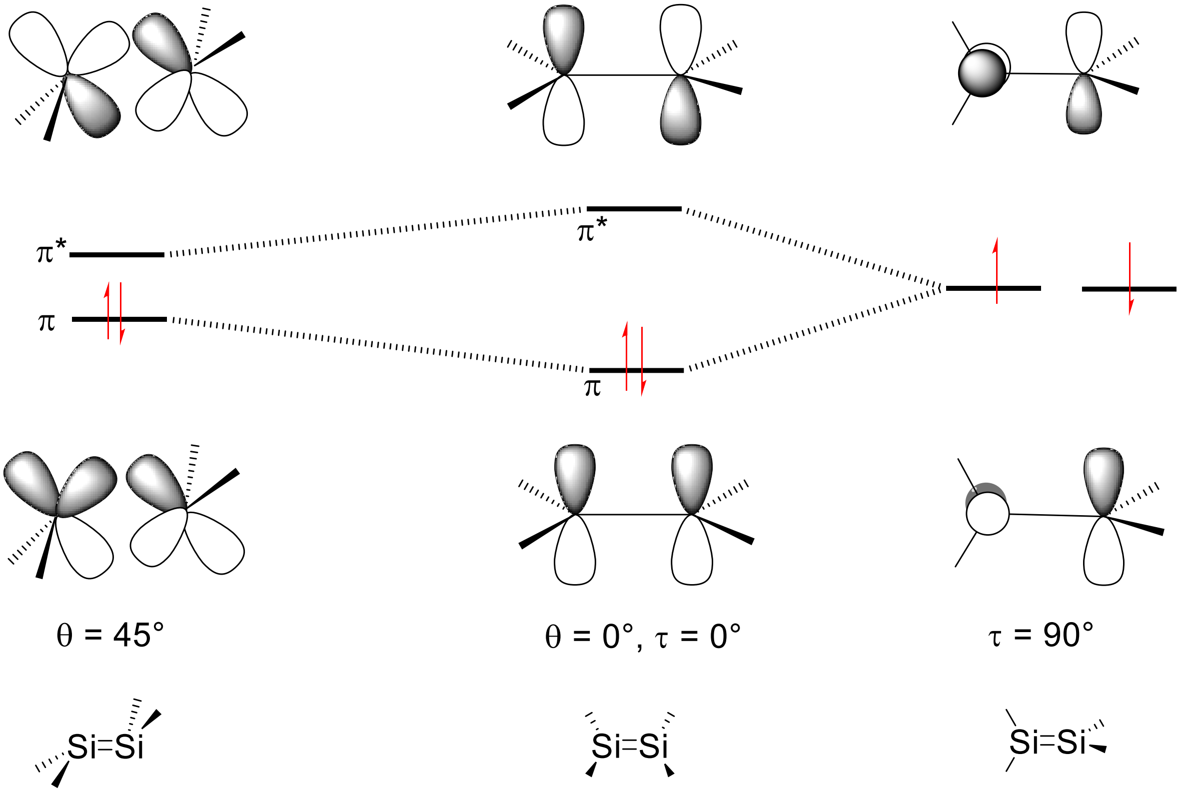

Figure 5. Effect of bending and twisting of disilenes on the HOMO-LUMO gap.[41]

The relationship between structural distortion of the disilenes and their HOMO-LUMO gap was confirmed numerous times. For instance, a strong red-shift was found for the longest wavelength absorption in the UV/vis of twisted disilene **9** (blue, λ_{max} = 612 nm)[35] compared to the planar disilene **8** (yellow, λ_{max} = 412 nm).[34] As mentioned before, the more pronounced ring strain in red *trans*-**10** causes much larger *trans*-bending and twisting in comparison with the yellow isomer *cis*-**10**, which explains the larger red-shift of the longest wavelength UV/vis absorption of *trans*-**10** (Scheme 4).[36]

In addition to the reduction of the HOMO-LUMO gap in disilenes by substituent effects, conjugation of multiple Si=Si units effectively lowers the frontier orbital energy difference, as in case of the corresponding conjugated C=C systems. The first example of well-characterized two conjugated Si=Si bonds in one and the same molecule was obtained by Weidenbruch *et al.*[42] in 1997. A considerable red-shift of the longest wavelength UV-vis absorption by about 100 nm (λ_{max} = 518 nm) was found for tetrasilabutadiene **11** (Scheme 5) compared to disilene **4**, which suggests a significant π-conjugation between the two Si=Si double bonds.

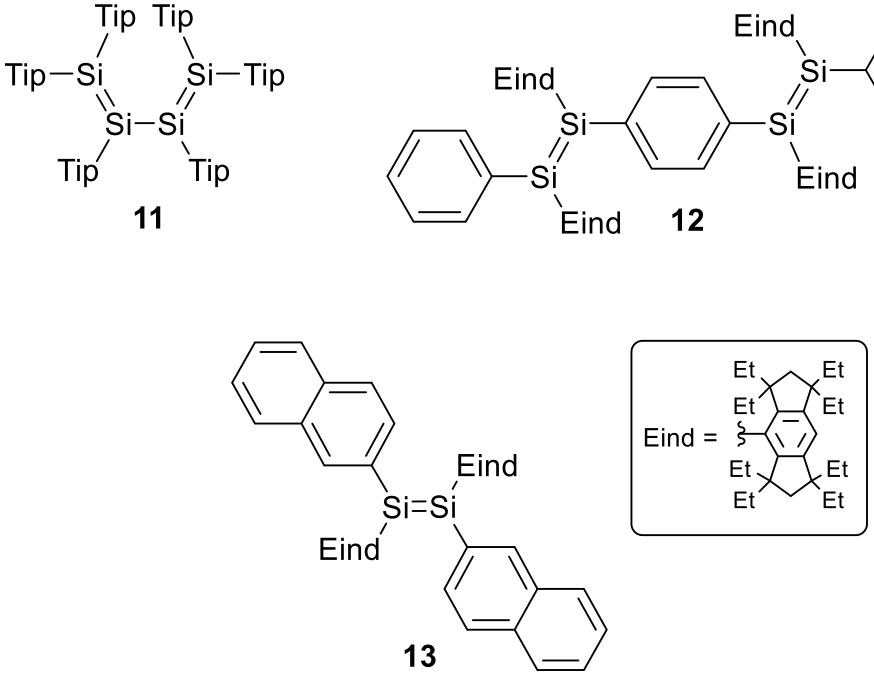

Scheme 5. First conjugated tetrasiladienes **11** and an air-stable emissive tetrasiladiene **12** and disilene **13**.

It should also be noted that the conformational flexibility of disilenes allows for the adaption to steric and electronic influences by the choice of substituents. On the other hand, large substituents may effectively quench photoluminescence by the large number of degrees of freedom typically available. Nevertheless, in 1984 West reported a weak luminescence for disilene **4** at low temperature (−196 °C).[37] Room temperature fluorescence of a tetrasiladiene **12** was observed for the first time in 2007 by Tamao *et al.*[43] and recently they have provided the first observation of electroluminescence (EL) from the disilene **13** as the organic photoactive layer in a prototypical organic light-emitting diode (OLED).[44] In these particular cases the rigidity of the tricyclic substituents appears to diminish the otherwise commonly observed quenching of fluorescence. Clearly, the optoelectronic properties of disilenes require further investigations for a comprehensive understanding of their rather versatile behavior.

1.4. Preparation of Disilenes

A significant advance in the field of disilene chemistry emerged since the discovery of the first stable disilene **4** by West *et al.* in 1981.[25] In 1996, just 27 disilenes had been isolated and completely characterized,[45] while by know hundreds of examples have been reported.

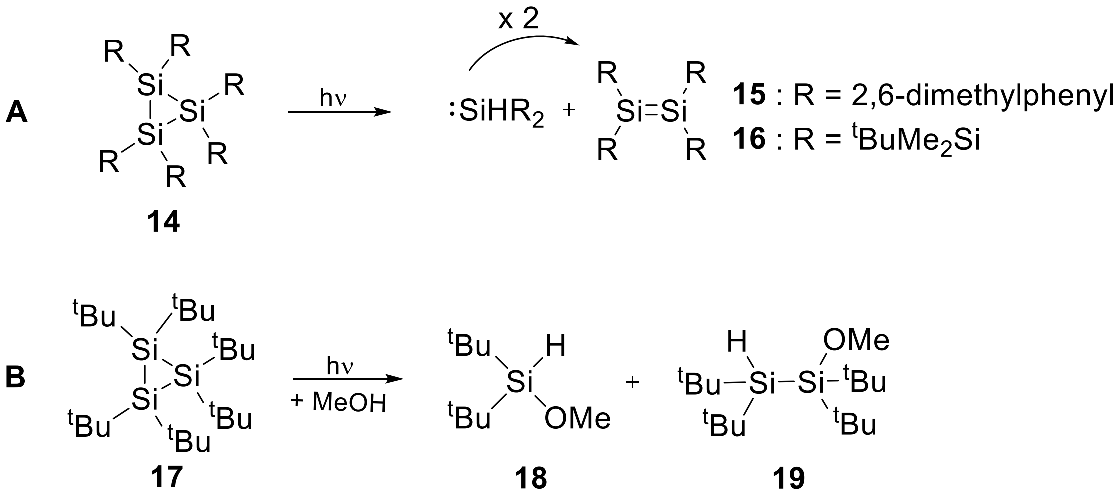

Scheme 6. Photolytic cleavage of cyclotrisilanes, **A** = synthesis of disilenes **15** and **16** reported by Masamune[46] and Kira[47], respectively; **B** = trapping reaction of the reaction intermediates with methanol.[48]

The successful photolytic generation of disilene **4** had been the starting point of these developments and was therefore adapted numerous times. For instance, Masamune successfully applied this concept to cyclotrisilane **14** as precursor in 1982. The mechanism in that case involves an initial formation of disilene **15** and a silylene that subsequently dimerizes to **15.**[46] By using a similar route, Kira *et al.* were able to synthesize tetrasilyl substituted disilene **16** in 1994 (Scheme 6A).[47] The reaction mechanism was investigated in detail by Weidenbruch and co-workers. Photolysis of cyclotrisilane **17** in the presence of equimolar amounts of MeOH as trapping agent yields the corresponding quenching products **18** and **19**, a proof for simultaneous silylene and disilene formation (Scheme 6 B).[48] Another main pathway that can be employed to form Si=Si double bond is the reductive coupling of bulky 1,1-dihalosilanes. In 1987, Watanabe *et al.*[49] reported the reaction of Tip_2SiCl_2 with two equivalents of lithium naphthalenide as a reducing agent affording disilene **20** in moderate yields. In the same year Masamune[50] followed this strategy to generate disilene **21** by using the $(Me_3Si)_2CH$ group as bulky substituent (Scheme 7).

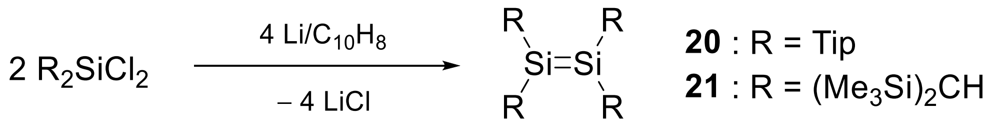

Scheme 7. Disilenes **20** and **21** generated via reductive coupling of 1,1-dihalosilanes.

In order to prepare unsymmetrically substituted disilenes, Kira and coworkers developed a more sophisticated reductive technique of prebuilt disilane scaffolds. Reduction of 1,2-dibromo-disilanes **22a,b** yielded the corresponding disilenes **23a,b** and hence allowed for the characterization of disilenes of the $A_2Si=SiB_2$ type by an X-ray structure study for the first time (Scheme 8).[51]

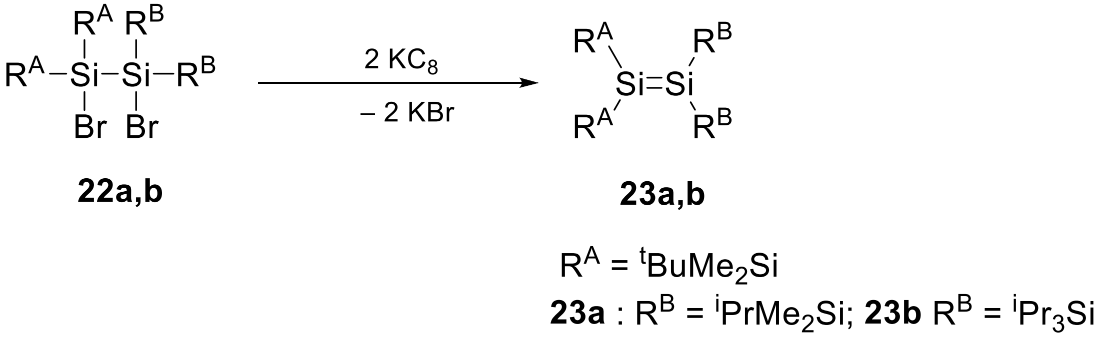

Scheme 8. Disilenes **23a,b** generated via reductive dehalogenation of 1,2-dibromosilanes **22a,b**.

In 2001, Sekiguchi reported a more straightforward preparative approach to disilenes of the $A_2Si=SiB_2$ type. Reduction of silacyclopropenes **24a,b** with lithium metal yields 1,1-

dilithiosilanes **25a,b**[52] that can be reacted as dinucleophiles with dihalosilanes to afford the final disilenes **26a,d** in excellent yields (Scheme 9).[53]

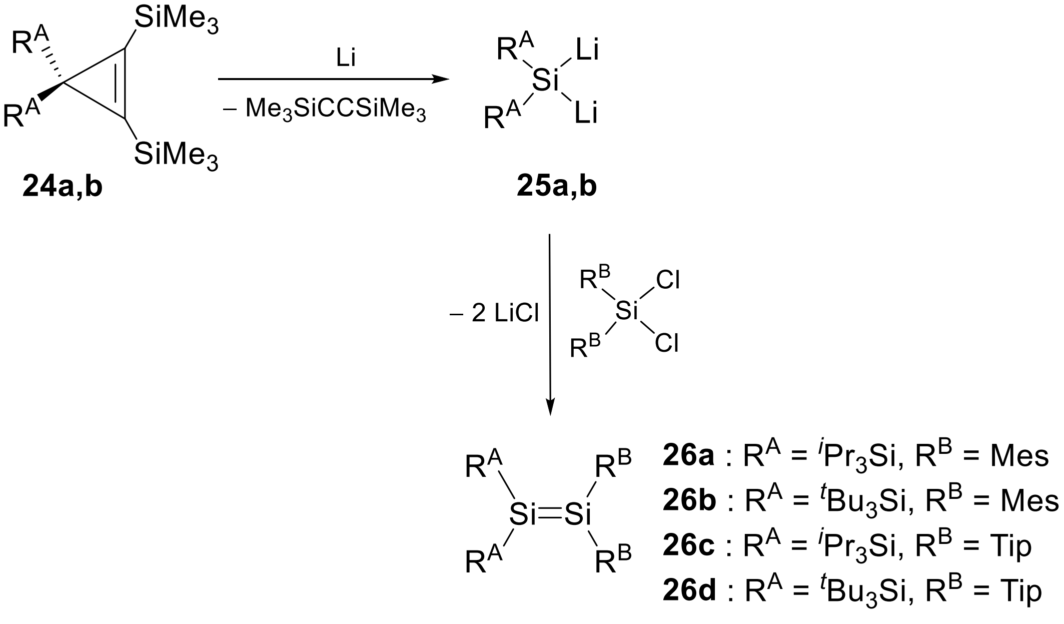

24a,b

25a,b

26a : $R^A = {}^iPr_3Si$, R^B = Mes
26b : $R^A = {}^tBu_3Si$, R^B = Mes
26c : $R^A = {}^iPr_3Si$, R^B = Tip
26d : $R^A = {}^tBu_3Si$, R^B = Tip

26a,d

Scheme 9. Generation of 1,1-dilithiosilanes **25a,b** and subsequent conversion to the unsymmetrical disilenes **26a-d**.

1.5. Synthesis of Disila Analogues of Vinyl Anions (Disilenides)

In order to be able to transfer prebuilt Si=Si units, either a nucleophilic or an electrophilic functionality is required in the periphery of the unsaturated heavy atoms.[54]

In the seminal work by Weidenbruch *et al.* on the synthesis of the first tetrasilabutadiene **11**[42] the authors assumed that lithium disilenide **27** was first generated as a plausible intermediate and then reacted with half an equivalent of mesityl bromide to form the required tetrasilabutadiene **11** (Scheme 10).[42] In line with this postulate and in analogy to what had been reported by Masamune *et al.* for $Tip_2Ge{=}GeTip_2$,[55] Weidenbruch *et al.* treated Watanabe´s disilene **20**[49] with two equivalents of metallic lithium in 1,2-dimethoxyethane (dme) to yield disilenide **27** by reductive cleavage of one of the four Tip substituents.[56] Even though the isolation of the final product **11** lent the proposed intermediacy of **27** significant support, Weidenbruch *et al.* did not isolate **27**. These observations inspired Scheschkewitz to attempt the direct reduction of Tip_2SiCl_2 with an appropriate excess of lithium powder in dme. Indeed, the isolation of disilenide **27** in an acceptable yield of 51% was achieved and hence led to the first structural characterization of a disilenide in 2004 (Scheme 10).[57]

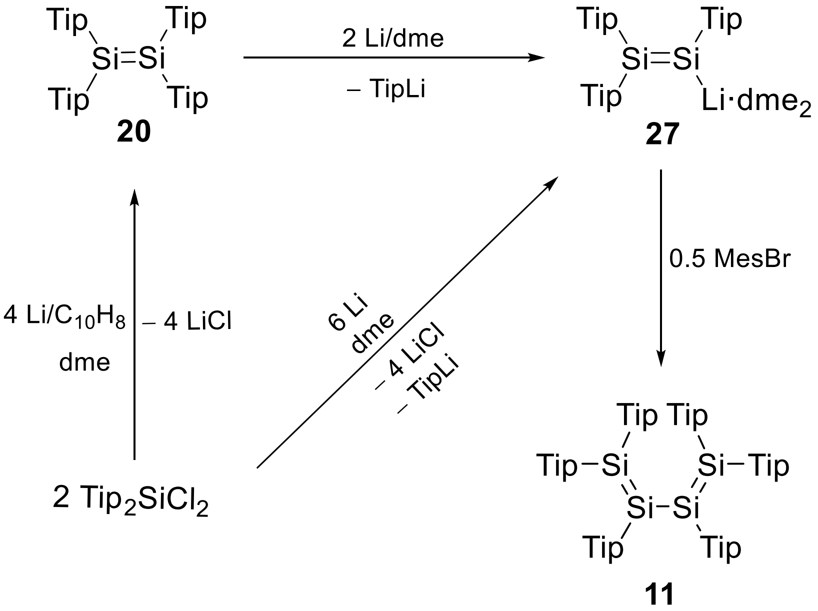

Scheme 10. Proposed intermediacy of disilenide **27** in the synthesis of tetrasilabutadiene **11** (Tip: 2,4,6-$iPr_3C_6H_2$; Mes: 2,4,6-$Me_3C_6H_2$),[42] original synthesis of Watanabe's disilene **20**,[49] as well as the "direct" synthesis of disilenide **27** according to Scheschkewitz.[57]

After the disclosure of Scheschkewitz´s disilenide, several more examples were isolated and characterized.

Sekiguchi investigated a broad range of starting materials and reagents for disilenide formation. For instance, the reaction of tetrasilabutadiene **28** with ^tBuLi resulted in the formal cleavage of the central Si-Si bond to yield disilenide **29** (Scheme 11).[58] Furthermore, Sekiguchi *et al.* were able to isolate potassium disilenide **30** from the reduction of **28** with potassium graphite in thf.[59] In 2005, the same group found that reduction of disilene **9** with different metal/naphthalene leads to disilenides **31a-c** (Scheme 11).[60]

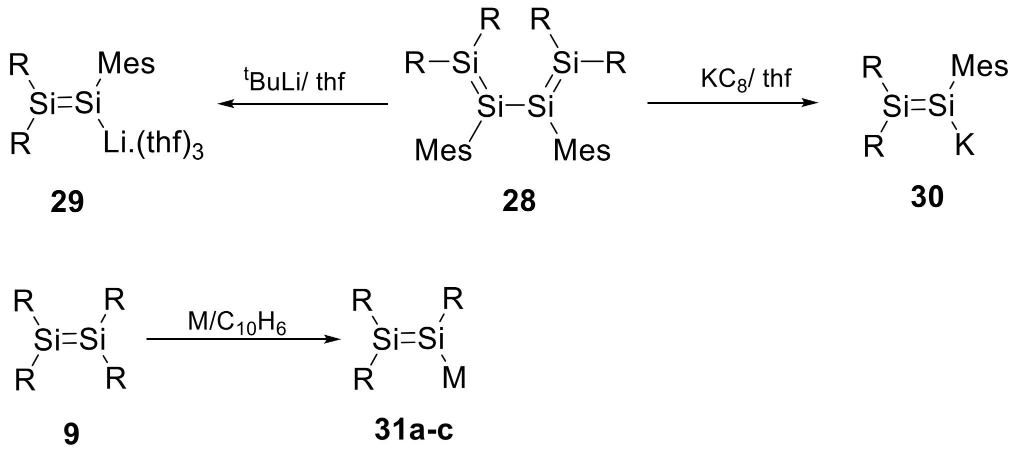

Scheme 11. Synthesis of disilenides **29**, **30**, and **31a-c** (**a**: M = Li, **b**: M = Na, **c**: M = K) reported by Sekiguchi (R = ^{t}Bu$_2$MeSi, Mes = 2,4,6-trimethylphenyl).

In addition, Sekiguchi reported the preparation of disilenide **33**[61] and **34**[62] from disilyne **32** by employing the addition of MeLi and LiH (from ^{t}BuLi), respectively. Notably, **34** is the first stable disilenide with a hydrogen directly attached to the Si=Si bond (Scheme 12). In 2009, Kira reported the sole example of a trialkyl substituted disilenide **36** via the reductive dehalogenation of trichlorosilane **35** with potassium graphite in thf (Scheme 12).[63]

The Scheschkewitz group succeeded in the transmetallation of lithium disilenide **27** with magnesium bromide and the reduction of dichlorosilyl substituted disilene **38** with activated magnesium to afford magnesium disilenide **37** and magnesium trisilen-1,3-diide **39**, respectively, as the sole two examples for alkaline earth metal disilenides so far (Scheme 12).[64,65]

Scheme 12 also shows a cyclic disilenide derivative, which was reported by Sekiguchi in 2009. The separation of the lithium cation from the trisilapentadienyl anion **40** effected by 12-crown-4 leads to a 1,2-migration of the substituent R and thus the formation of **41**.[66]

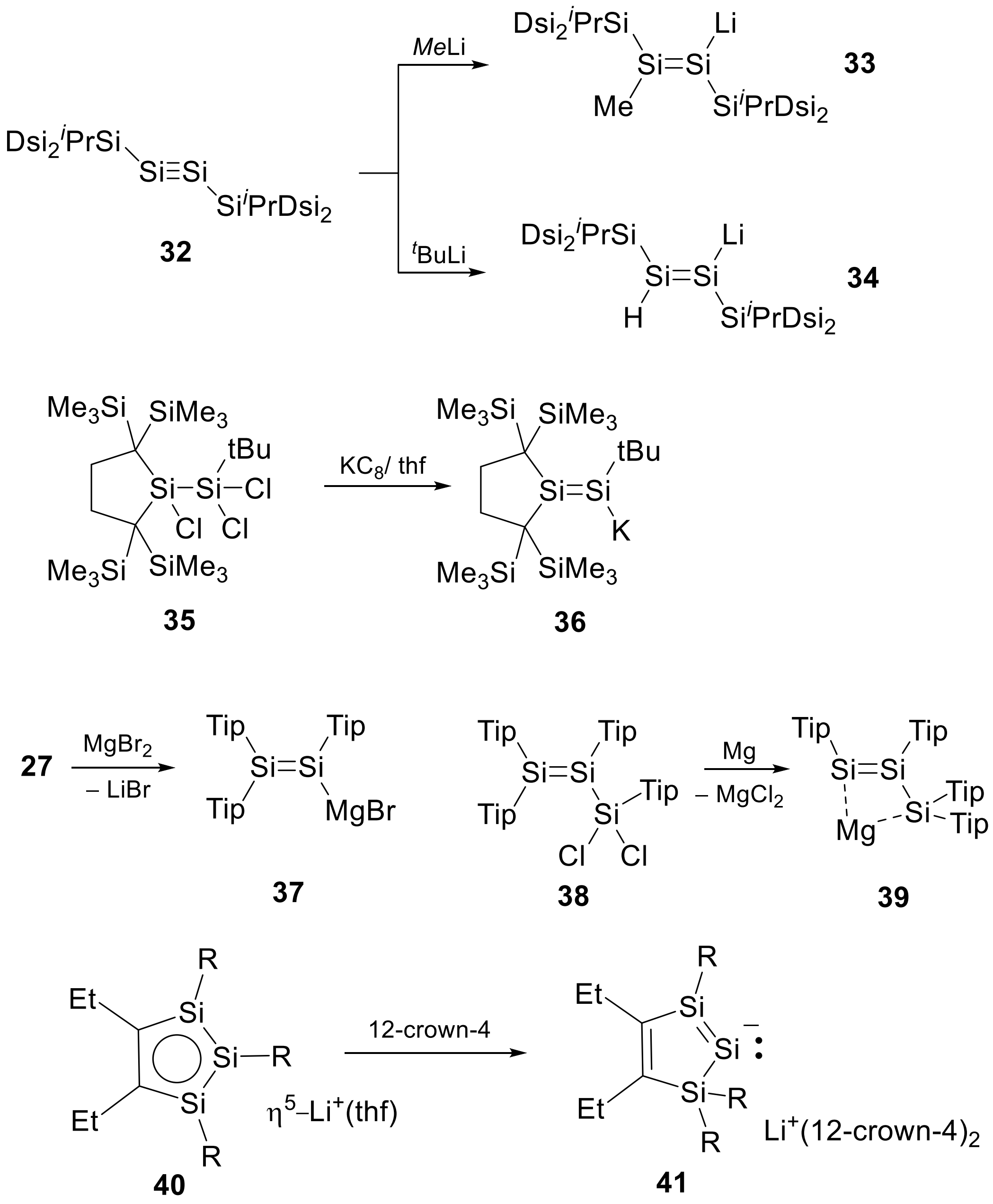

Scheme 12. Synthesis of disilenides **33**, **34** (Dsi = $CH(SiMe_3)_2$), **36**, **37**, **39** and **41** (R = $^tBu_2MeSi$).

1.6. Reactivity of Disilenides towards Main group and Transition-Metal Electrophiles.

The transfer of the Si=Si unit to various organic and inorganic substrates became possible through the recent synthesis of disilenides as anionic reagents with silicon-silicon double bonds and the functionalization of the Si=Si double bonds with main group functionalities therefore a viable option. Sekiguchi *et al.* were able to synthesize straightforwardly the first boryl substituted disilenes **42a,b** by reacting disilenide **29** with the appropriate boronic acid chlorides (Scheme 13).[67] In addition, disilenide **27** turned out to be a viable starting point for the rational synthesis of unsymmetrically substituted disilenes of the $A_2Si{=}SiAB$ type, which are otherwise difficult to prepare. For instance, Scheschkewitz and coworkers successfully isolated phosphino substituted disilenes **43a-d** from the reaction of disilenide **27** with dialkyl or diaryl chlorophosphines (Scheme 13).[68]

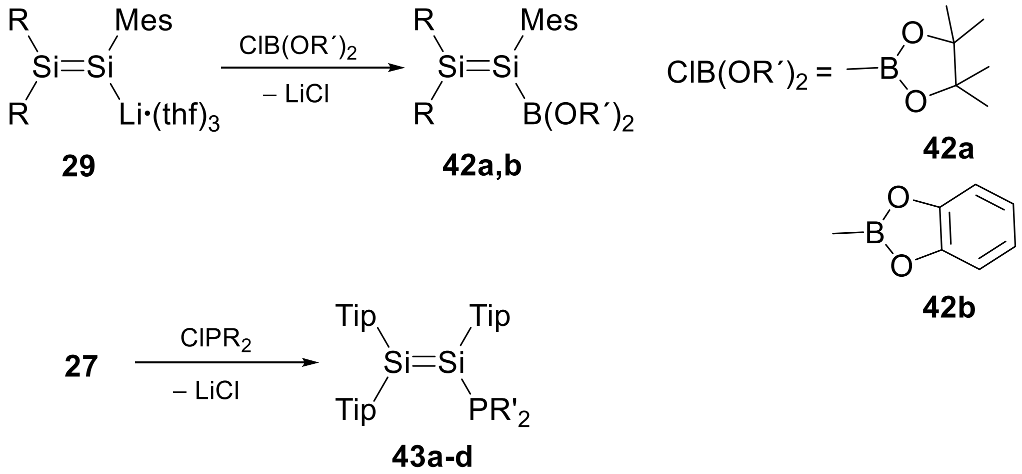

Scheme 13. Synthesis of boryl substituted disilenes **42a,b** (R = $^tBu_2MeSi$) reported by Sekiguchi and phosphino substituted disilenes **43a-d** (**a:** R = Ph; **b:** R = ^{i}pr; **c:** R = Cy; **d:** R = ^{t}Bu) reported by Scheschkewitz group (Cy = cyclohexyl).

Furthermore, the Scheschkewitz group found that the treatment of disilenide **27** with monochlorinated silanes or stannanes, main group 14 halides, yields silyl-substituted disilene **44** and the corresponding stannyl substituted derivatives **45a-d**, respectively (Scheme 14). [69,70]

Conversely, the reaction of **27** with dichlorosilanes or dichlorodimethyl stannane leads to a cyclization reaction under consumption of the double bonds and thus the formation of chloro functionalized cyclotrisilanes **46a,b** and disilastannirane **47**, respectively (Scheme 14).[69,70] Similarly, reaction of excess silicon tetrachloride with disilenide **27** affords the unsymmetrically substituted 1,1,2-trichlorocyclotrisilane **46c** (Scheme 14).[71]

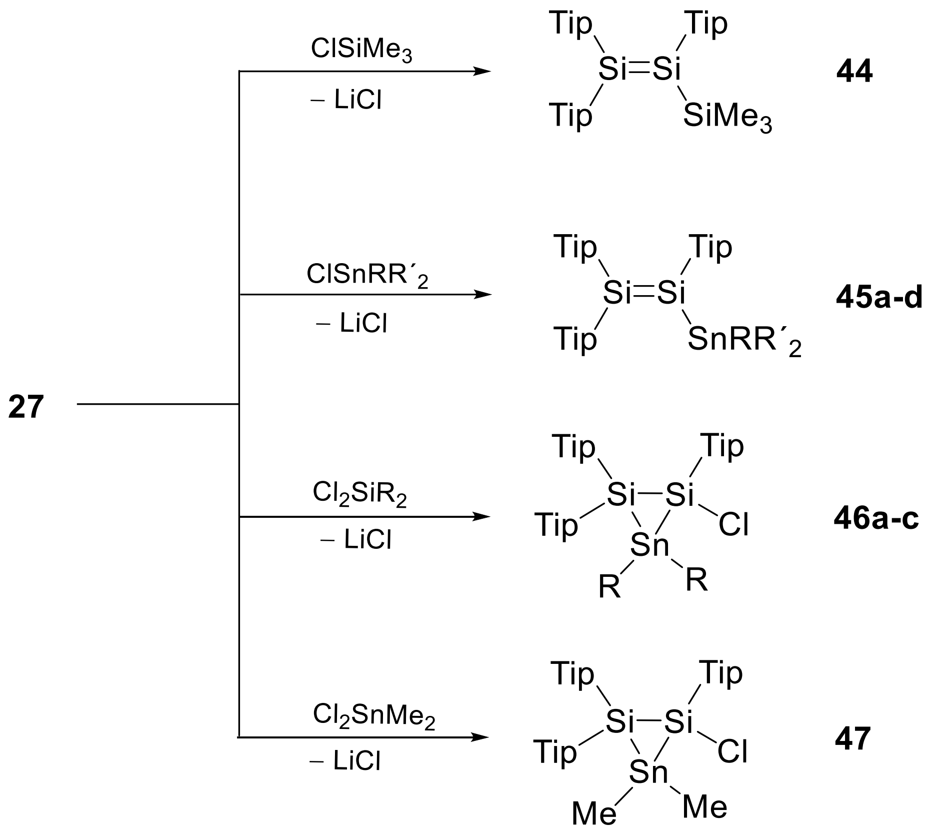

Scheme 14. Synthesis of trimethylsilyl substituted disilene **44**, stanyl substituted disienes **45a-d** (**a:** R = R´= Me; **b:** R = R´ = Ph; **c:** R = R´ = ^{n}Bu; **d:** R = Cl, R´ = ^{t}Bu), chlorocyclotrisilanes **46a-c** (**a:** R = Me; **b:** R = Ph; **c:** R = Cl) and chlorodisilastanirane **47** reported by Scheschkewitz group (Cy = cyclohexyl).

The possibility of coordinating disilenide **27** as a ligand to a transition metal was also probed by the Scheschkewitz group (Scheme 15).

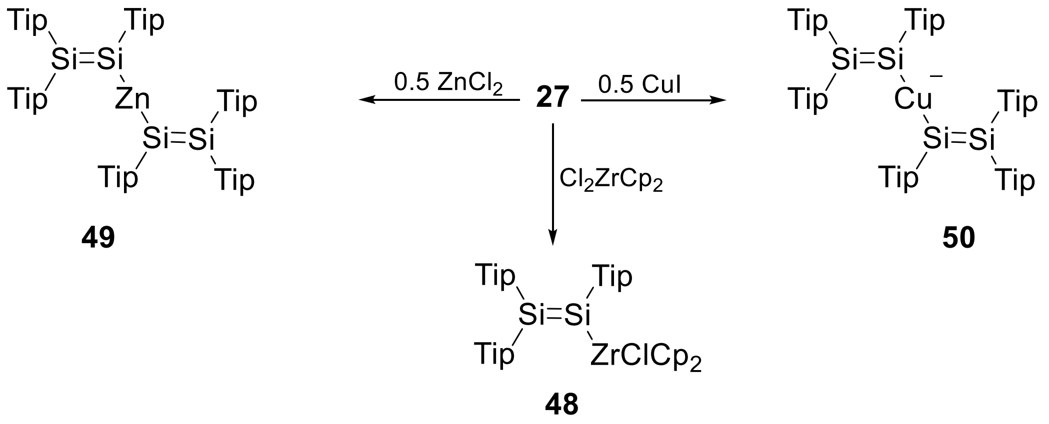

Scheme 15. Synthesis of transition metals (zirconocene, zinc and copper) substituted disilenes complexes **48**, **49**, and **50** (Cp = cyclopentadienyl).

The isolation of the first η^1-disilenyl transition metal complex **48**, from the reaction of lithium disilenide **27** with Cp_2ZrCl_2 can be taken as proof of this concept. The intensely green compound **48** shows an unusually red-shifted absorption band in the near infra-red region λ_{max} = 715 nm. This finding could be explained by ligand-to-metal charge transfer (Scheme 15).[72]

In a similar reaction, transmetallation of **27** with the corresponding transition metal chlorides yields the corresponding bis(disilenyl)zinc complex **49** and the cuprate **50**, respectively (Scheme 15).[64] Interestingly, both compounds **49** and **50** exhibit a significant red-shift of the longest wavelength absorption in the UV/vis spectra revealing an interaction between the two disilenyl moieties through the transition metal center (Scheme 15).[64]

1.7. Synthesis of Halodisilenes

Halodisilenes can be considered as the heavier analogues of vinyl halides in low valent silicon chemistry. Due to the electron-withdrawing halogen substituent, halodisilenes are relatively electron-poor and can be seen as the electrophilic counterpart to disilenides. In 2002, Wiberg *et al.* realized the first synthetic approaches to halodisilenes when they combined a mixture of halotrisilanes **51** and **52** with tri(tert-butyl) silylsodium in boiling benzene to afford dichlorodisilene **53** in 12% yield (Scheme 16).[73]

Recently, Tokitoh *et al.* were able to isolate dibromo disilenes **55** stabilized by bulky Bbt substituents (Bbt = 2,6-($(Me_3Si)_2CH)_2$-4-($(Me_3Si)_3C$)-C_6H_2) via the reduction of tribromo Bbt-silane **54** with two equivalents of lithium/naphthalene (Scheme 16) in thf at low temperature (−78°C).[74] A similar approach was applied by Tamao *et al.* to synthesize dibromo disilene **57** stabilized by EMind-groups (EMind = 1,1,3,3,7,7-hexaethyl-5,5-dimethyl-s-hyndrindacen-4-yl) in a more recent work (Scheme 16).[75]

The Scheschkewitz group reported the use of disilenide **27** to prepare the corresponding iododisilene **58** via the oxidation (and thus umpolung) of disilenide **27** with elemental iodine (Scheme 16).[68]

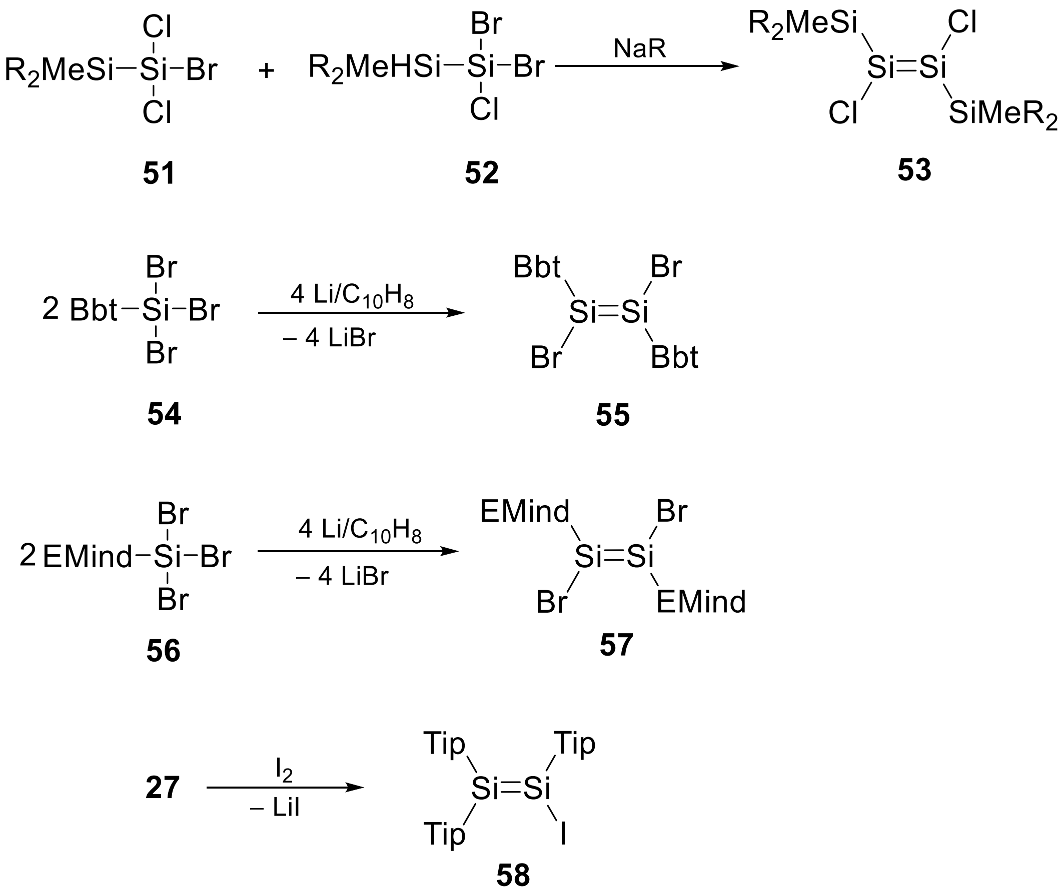

Scheme 16. Synthesis of dichlorodisilenes **53** (R = Si(^{t}Bu)$_3$); dibromodisilene **55** (Bbt = 2,6-((Me$_3$Si)$_2$CH)$_2$-4-(Me$_3$Si)$_3$C)-C$_6$H$_2$); dibromodisilene **57** (EMind = 1,1,3,3,7,7-hexaethyl-5,5-dimethyl-s-hyndrindacen-4-yl) and iododisilene **58**.

1.8. Reactivity of Halodisilenes

The positively polarized silicon atom of halodisilenes provides an electrophilic center that should be an equally useful building block. For instance, the removal of the existing halogens via reduction in 1,2-dihalodisilenes allows to generate a Si-Si triple bond as heavier group 14 analogues of alkynes. The reductive dehalogenation of 1,2-dichlorodisilene **53** with alkaline metal/naphthalene or the 1,2-dibromodisilene **55** with tert-butyllithium affords the disilynes **59**[76] and **60**,[77] respectively (Scheme 17).

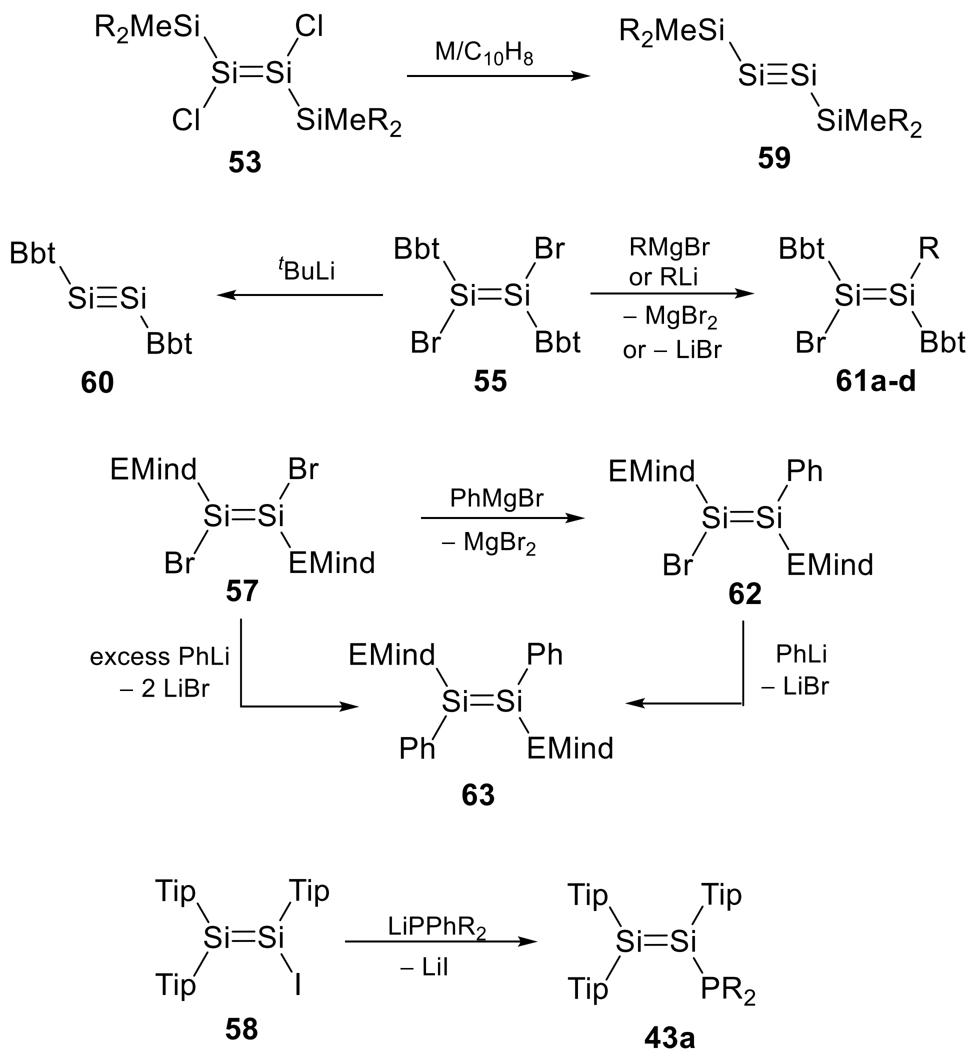

Scheme 17. Synthesis of disilyne **59**, **60** (M = Li, Na, K; R = $Si(^tBu)_3$); monosubstitution disilenes produts **61a-d** (**a**: R = Me, **b**: R = Et, **c**: R = ^nBu, **d**: R = Ph); mono- and disubstitution products **62** and **63**; and phosphinodisilene **43a**. (Bbt = 2,6-($((Me_3Si)_2CH)_2$-4-$(Me_3Si)_3C$)-C_6H_2); EMind = 1,1,3,3,7,7-hexaethyl-5,5-dimethyl-s-hyndrindacen-4-yl).

The electrophilic halogen-substituted Si=Si center in principle also allows for the derivatization of the disilenes with variable substituents. In this regard, the 1,2-dichlorodisilene **53** turns out to be sterically too crowded to be attacked by nucleophiles at the unsaturated silicon centers. In contrast, 1,2-dibromodisilene **55** can be reacted with one equivalent of various organolithium and magnesium reagents to yield **61a-d** (Scheme 17).[78] According to the authors, however, attempts to substitute both bromo functionalities failed, due to a slightly higher LUMO energy of **61a-d** than that of **55**. Whereas, in the case of **57**, mono- or disubstituted derivatives **62** and **63** are attainable from the reaction with one or two equivalents phenyl lithium/phenyl magnesium bromide, respectively (Scheme 17).[79]

The reaction of compound **58** as the counterpart of disilenide **27** with $LiPPh_2$ leads to the formation of phosphino disilene **43a** (Scheme 17), which is an alternative synthetic route to that shown in Scheme 13.[68]

1.9. Recent Advances in π-Organic Systems Comprising Disilenes Moieties

Double bonds to silicon, such as C=Si and Si=Si, have attracted widespread attention because of their unique fundamental properties and chemistry, as well as their potential role in polysilane chemistry and material sciences. So far, this field of chemistry is still in its infancy, and much remains to be done. For instance, little is known on the synthesis and properties of bridged tetrasilabutadienes which have two conjugated double bonds. As mentioned before, a landmark experimental breakthrough in the field was the synthesis and characterization of the first stable tetrasilabutadiene **11**,[42] a compound containing two directly connected conjugated Si=Si double bonds, in 1997 by Weidenbruch *et al.* (Scheme 5 and 10).[42] Weidenbruch showed that **11** exhibits a considerable red-shift of the longest wavelength absorption at λ_{max} = 518 nm compared to related non-conjugated compounds.[42] A second tetrasilabutadiene derivative **28** was prepared by Sekiguchi[62] with an absorption maximum at λ_{max} = 531 nm, hence with a similar red-shift as Weidenbruch´s example. The synthesis proceeded via the reaction of two equivalents of $(^tBu_2MeSi)_2SiLi_2$ with $(MesSiCl_2)_2$ leading to **28** in 11% yield (scheme 18). Recently, Kira *et al.* found that the reduction of **64** in toluene yields the third example of a tetrasilabutadiene **65** in 13% yield (Scheme 18).[78] The absorption maximum of 510 nm is well in line with the absorptions of **11** and **28**. These three examples display a significant conjugation between the two directly connected Si=Si double bonds.

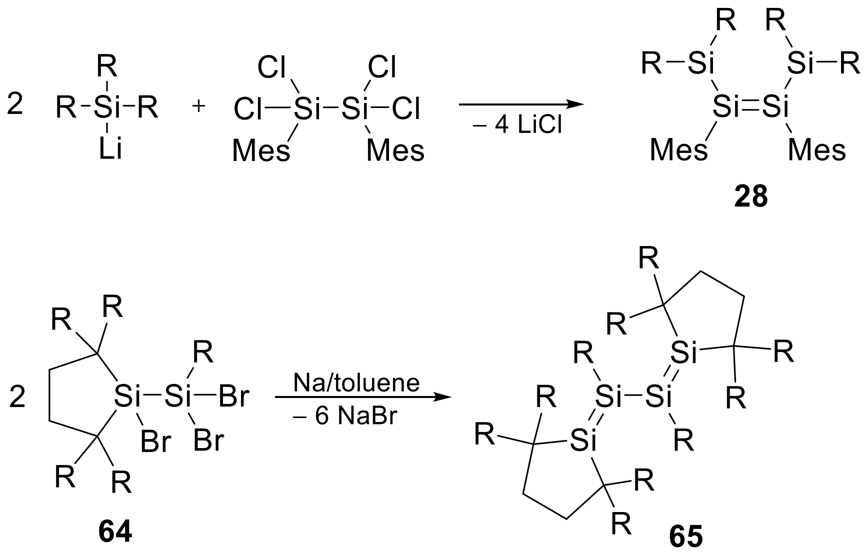

Scheme 18. Synthesis of tetrasilabutadienes **28** (R = ${}^{t}Bu_2MeSi$, Mes = 2,4,6-trimethylphenyl) and **65** (R = $SiMe_3$).

As the carbon-based conjugated π-systems find more and more commercial electronic applications in devices such as light emitting diodes or thin-film transistors, it is not surprising that the incorporation of heavier main group elements into such systems is of great contemporary interest.[79]

Notably, the conformation flexibility and the inherently smaller HOMO-LUMO gap of disilenes (see section1.3 and 1.4) prompted attempts to integrate Si=Si bond(s) with organic π-conjugated systems.

After the groundbreaking work of the Scheschkewitz group in 2007,[80a] the study of organic π-conjugated systems incorporating Si=Si bonds has been remarkably developed. They showed that the reaction of **27** with phenyl iodide affords the corresponding phenyl substituted disilene **66** in 58% yield, an unsymmetrically substituted disilene of the $A_2Si{=}SiAB$ type. Additionally, when **27** is treated with half an equivalent 1,4-diiodobenzene, the *para*-phenylene-bridged tetrasiladiene **67** is obtained in 72% yield (Scheme 19). The tetrasiladiene **67** constitutes the first model system for the up to then unknown silicon analogues to oligo(*para*-phenylenevinylene)s (Si-OPVs).

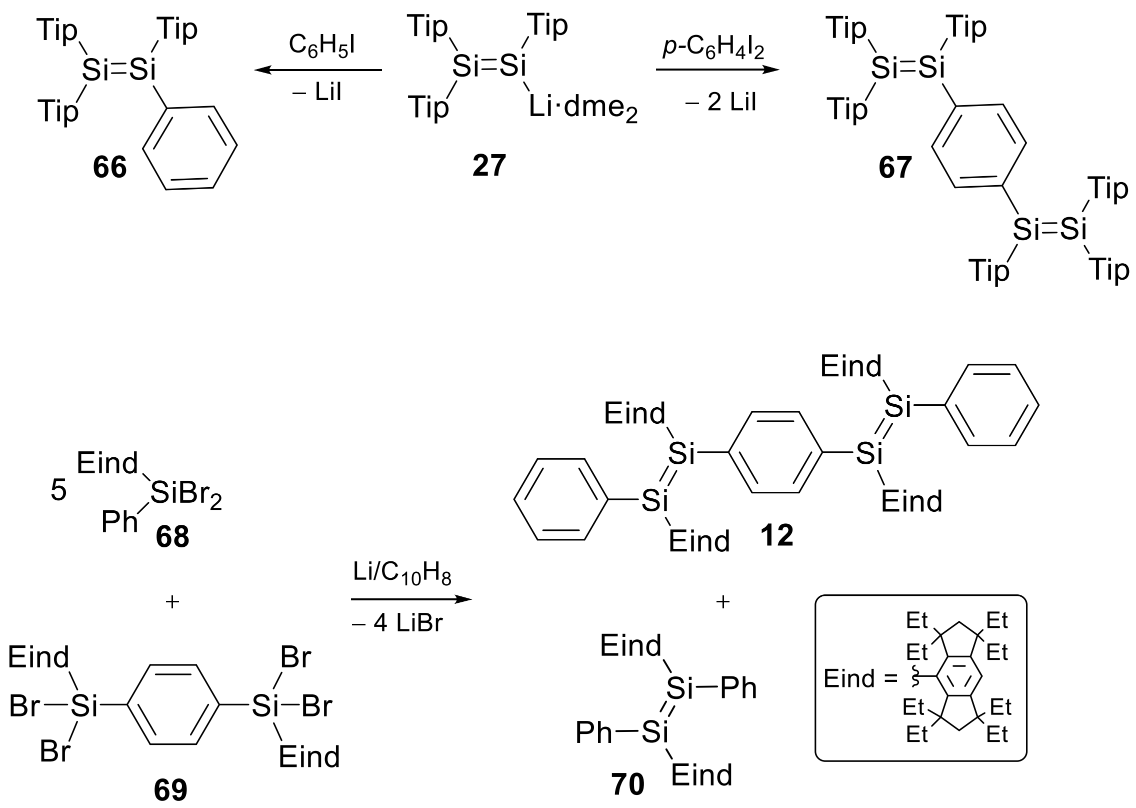

Scheme 19. Synthesis of disilenes and tetrasiladienes containing a phenylene spacer.

The substantial red-shift of the longest wavelength UV/Vis absorption of **67** is indicative of appreciable conjugation between the two Si=Si bonds (**66**: λ_{max} = 493 nm, **67**: λ_{max} = 508 nm).[80a] In comparison with the tetrasilabutadienes **11**, **28** and **65**, a strong conjugation of the two Si=Si bonds over the phenylene ring can be taken for granted.

Just a few months later, Tamao *et al.* reported on disilene **70** and *para*-phenylene bridged tetrasiladiene **12** featuring the very rigid and bulky hindracenyl substituents (Eind).[43] The homocoupling reaction of the dibromosilane **68** with lithium/naphthalene affords **70** in 76% yield. Similarly, the tetrasiladiene **12** was obtained by the reductive coupling of the two dibromosilanes **68** and **69** in a 5:1 ratio with lithium/naphthalene in thf (Scheme 19).[43] It should be noted, however, that the synthesis of **12** is intrinsically low yielding (15%) due to the Wurtz-type coupling methodology employed and involves the separation of **12** from the major product diphenyldisilene **70** (Scheme 19). In contrast to tetrasiladiene **67**, the very rigid environment of **12** not only results in more efficient π-conjugation (as evident in the even more red-shifted longest wavelength absorption at $\lambda_{max} = 543$ nm), but also in the first observation of fluorescence of a disilene at room temperature with an emission at $\lambda_{max} = 612$ nm and a moderate quantum yield of $\varphi = 0.10$. The two Si=Si bonds and the phenyl-/phenylene rings/spacers in **12** are in coplanar arrangement, thus facilitating electronic interaction between the Si=Si moieties. Remarkably, **12** is a rare example for an air-stable unsaturated silicon species in the solid state, although it decomposes in solution within two days after exposure to air.

A series of trialkyldisilenes **71a-c** with single polycyclic aromatic substituents (naphthyl, phenanthryl and anthryl) was reported by Iwamoto *et al*. in 2009. Reaction of potassium disilenide **36** with the appropriate aryl bromide affords **71a-b** (yellow) and **71c** (blue purple) in moderate yields (Scheme 20). [81]

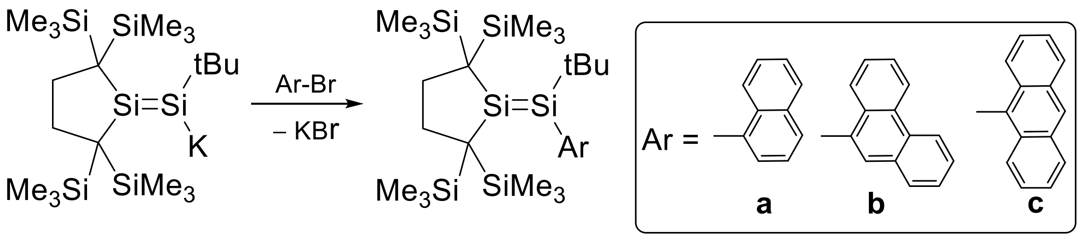

36 **71a-c**

Scheme 20. Synthesis of polycyclic aromatic substituted disilenes **71a-c** by Kira *et al.*

Unlike in the cases of disilenes **66** and **70** the conjugation with the aromatic substituent is suppressed, because the sterically very demanding 1-naphthyl, 9-phenanthryl, and 9-anthryl groups adopt a perpendicular conformation with respect to the Si=Si double bond. This leads to distinct absorption bands in the UV/vis spectrum that were identified by the authors as intramolecular charge transfer from the Si=Si π bond to the π^* orbital of the polyaromatic ligand.

In complementary results to that regarding **12** (which contains *two* Si=Si units on *one* central benzene ring), the disilenes **13** and **72** with *two* π-extended polycyclic aromatic groups on *one* disilene unit exhibit red fluorescence in the solid state and thf even at room temperature.[82] Notably, while the fluorescence of these disilenes in thf at room temperature is weak (**13**: $\lambda_{max} = 586$ nm, $\varphi < 0.01$; **72**: $\lambda_{max} = 575$ nm, $\varphi = 0.01$), they show much stronger emissions in the solid state with λ_{max} = 619 nm (φ = 0.23) for **13** and 600 nm (φ = 0.2) for **72**.

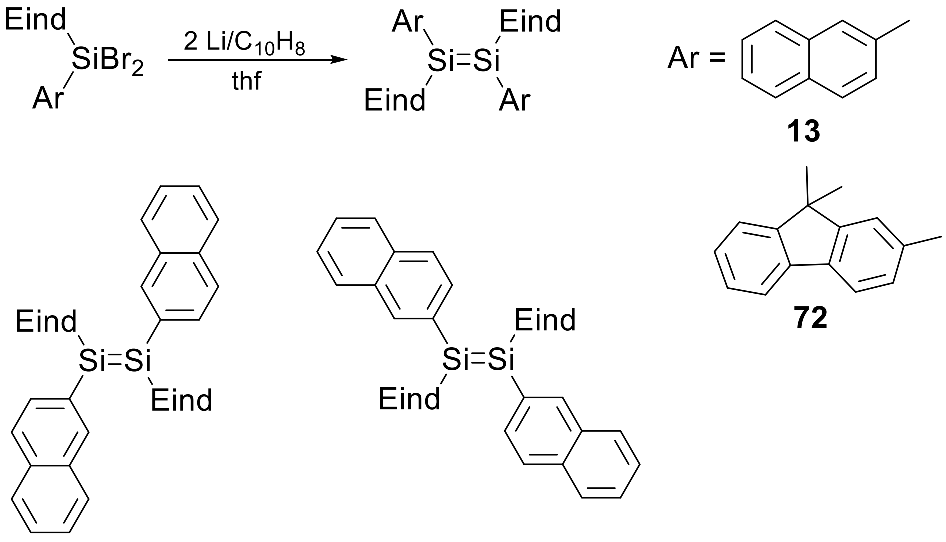

13

72

13(*s-cis, s-cis*) **13**(*s-trans, s-trans*)

Scheme 21. Synthesis of polycyclic aromatic substituted disilenes.

The Eind-stabilized di(2-naphthyl)disilene **13** and di(2-fluorenyl)disilene **72** were prepared straightforwardly by the reduction of the corresponding dibromosilane, as shown in Scheme 21. Disilene **13** exists as a mixture of two conformers in the solid state, **13**(s-*trans*, s-*trans*) and **13**(s-*cis*, s-*cis*), in the ratio of 6 : 4. The X-ray structural analysis of **13** revealed that the Si=Si moiety is entirely co-planar with the two naphthalene groups in both isomers. Indeed, the presence of efficient π-delocalization over the dinaphthyl substituted disilene **13** skeleton is supported by the UV/vis spectrum exhibiting a bathochromic shift of the longest wavelength absorption by about 43 nm compared to diphenyl substituted disilene **70** (**13**: λ_{max} = 504 nm, **70**: λ_{max} = 461 nm). The absorption maximum of **72** was observed at 510 nm. It was also found that disilenes **13** and **72** are stable in air for months, at least in the solid state.[86]

In analogy to the procedure for the preparation of Si-OPV dimer **12**, Tamao *et al.*[83] developed in 2015 the synthesis of a higher oligomers of Si-OPVs up to the tetramer starting from a new bulky ligand (HexO)MEind with a pending hexoxy group to improve solubility. The reductive coupling of the two dibromosilanes **73** and **74** with lithium naphthalenide in thf followed by column chromatography affords the four oligomers **75** to **78** in very low yield (Scheme 22).[83].

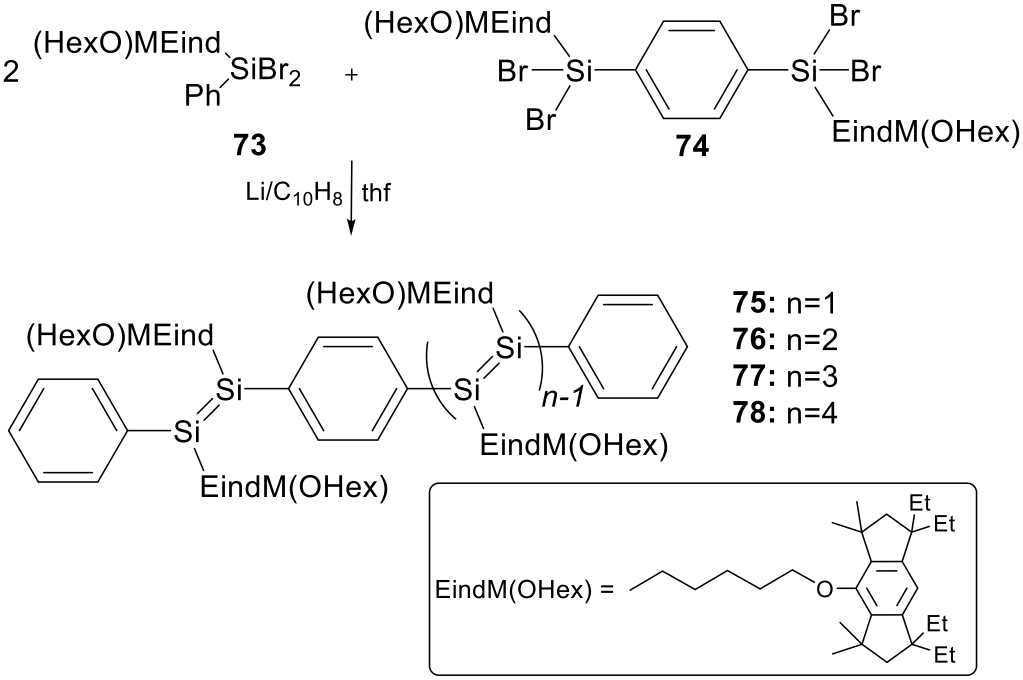

Scheme 22. Synthesis of Si-OPVs **75−78** by using a new conn ligand (HexO)MEind.

The experimental and theoretical studies of the Si-OPVs **75-78** demonstrate the fully extended π-conjugation of the Si-OPV main chains. Single crystal X-ray analyses of the monomer **75** and the dimer **76** revealed the highly coplanar Si-OPV backbones facilitating the effective extension of the π-conjugation, which had further been validated by the significant increases in the absorption maxima from 465 nm for the monomer **75** to 610 nm for the tetramer **78**. Additionally, the Si-OPVs **76−78** show an intense fluorescence from 613 to 668 nm at room temperature with the quantum yields up to 0.48.

Very recently, Tamao *et al.*[84] disclosed the synthesis of 1,2-diaryl disilenes with two pyrenyl substituents as emissive aryldisilenes with low quantum yields in both solution and solid state at room temperature.

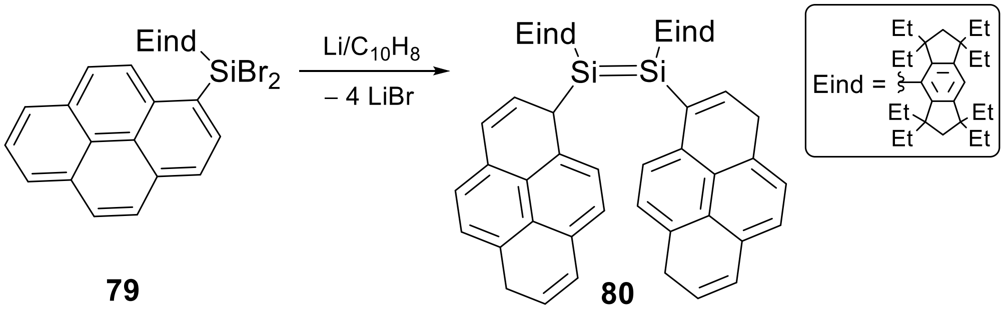

79

80

Scheme 23. Synthesis of (Z)-1,2-di(1-pyrenyl)disilene **80**.

The reductive coupling reaction of the corresponding dibromosilane **79** with lithium/naphthalene yields (Z)-1,2-di(1-pyrenyl)disilene **80** (Scheme 23) in which the two pyrenyl groups interact intramolecularly through π stacking with a distance of 3.635 Å between the centers of the two pyrene rings. This disilene exhibits a π(Si−Si) → π*(pyrene) intramolecular charge-transfer (ICT) fluorescence at room temperature at wavelengths that depend on the solvent polarity.

1.10. Reactivity of Disilenes toward Alkynes

As mentioned above (Figure 4), disilenes have an energetically higher lying HOMO and lower lying LUMO compared to ethylene. This small band gap is directly responsible for the high reactivity of Si=Si double towards a broad range of substrates. For instance, numerous functionalized silanes have been isolated by taking advantage of the general tendency of disilenes to react with all kind of polar reagents (such as water, hydrogen halides,[85] alcohols,[85,86] ammonia,[87] or haloalkanes[88]) under consumption of the Si=Si double bonds.

The reactivity of disilenes toward alkynes was examined for the first time in 1985 by Sakurai and co-workers.[89] They have found that the Si=Si of *trans*- or *cis*-disilene **81** undergo facile formal [2+2] cycloadditions with the C≡C of diphenylacetylene to form a mixture of diastereomeric 1,2-disilacyclobutenes **83**. The formation of a biradical intermediate **82** in the stepwise mechanism for this reaction was suggested by the authors (Scheme 24).[89] The concerted thermal [2+2] cyclo addition would be symmetry forbidden according to the Woodward-Hoffmann rules and was therefore ruled out.

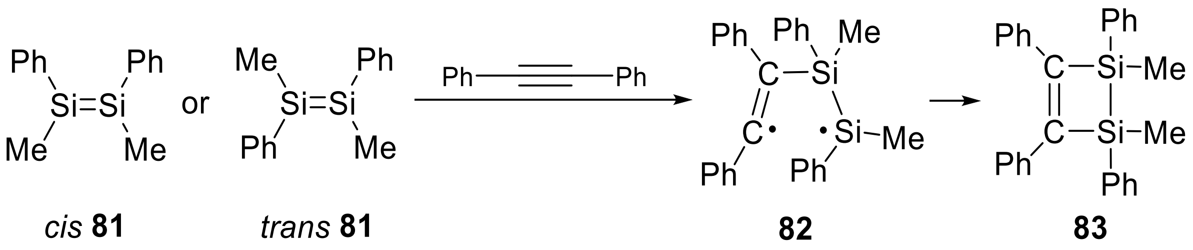

Scheme 24. Synthesis of 1,2-disilacyclobutenes **83** via the addition of diphenylacetylene to *cis-/trans*-disilene **81**.

One year later, West *et al.* found that the reaction of disilenes **4** and **84** with a variety of alkynes yields the corresponding air-stable disilacyclobutenes **85a-d** and **86a-b** (Scheme 25).[90]

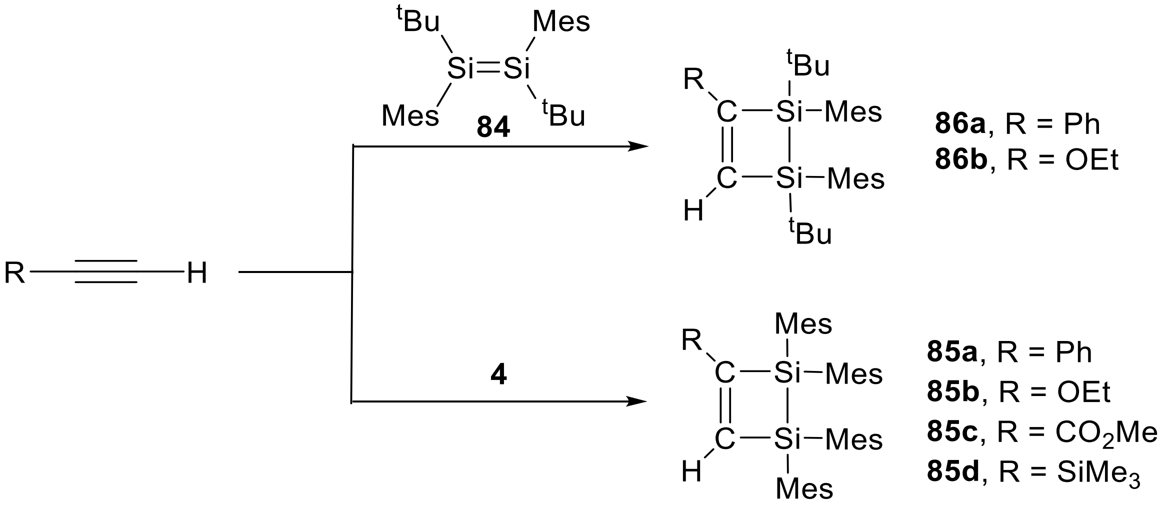

Scheme 25. Synthesis of disilacyclobutenes **85a-d** and **86a-b** reported by West.

It should be noted that no reaction was observed between disilene **4** and alkynes such as acetylene, diphenylacetylene, dimethyl acetylenedicarboxylate and phenyl(trimethylsilyl)acetylene. West *et al.* proposed an ionic mechanism for the reaction of disilene **4** with the terminal alkynes that may behave as a nucleophile.[90] However, the nature of intermediate formed in both Sakurai and West's examples remains unclear so far.

Recently, the unsymmetrical disilene **87** has been employed by our group in a similar protocol, in which a disilacyclobutene **88** was generated almost quantitatively upon the addition of phenylacetylene to **87** at room temperature (Scheme 26).[91]

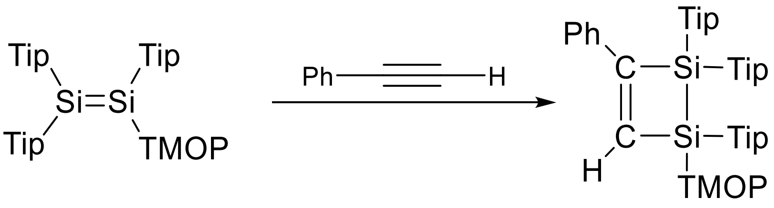

87 **88**

Scheme 26. Formation of disilacyclobutenes **88** reported by our group (TMOP = 2,4,6-$(MeO)_3C_6H_2$).

Our group has also reported the air-stable 1,2-disilacyclobutenes **89a,b** derived from the regiospecific addition of phenyl acetylene or tert-butyl acetylene to the unsymmetrically substituted phenyl disilene **66,** respectively (Scheme 27).[92]

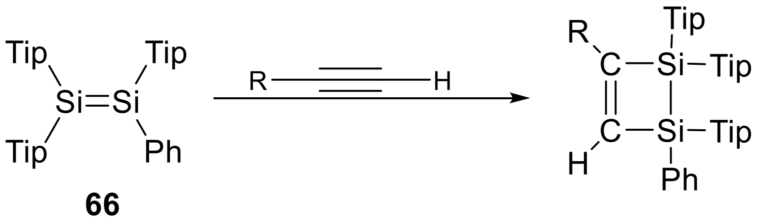

66

89a, R = Ph
89b, R = ^{t}Bu

Scheme 27. Formation of disilacyclobutenes **89a,b**.

In an attempt to extend this reactivity towards bifunctional reagents, the reaction of *para*-phenylene bridged tetrasiladiene **67** with phenyl acetylene resulted in the formation of the [2+2] cycloadduct **90**.

When **67** is added dropwise to a large excess of 1,4-diethynyl benzene in benzene at room temperature, a mixture of two diastereomers of air-stable ethynyl-terminated extended monomers **M1** and **M2** in a 4 : 1 ratio was obtained (Scheme 28). Further addition of tetrasiladiene **67** with slight excess of 1,4-diethynyl benzene to the bifunctional co-monomers allowed for the preparation of σ–π conjugated organosilicon polymers.[92]

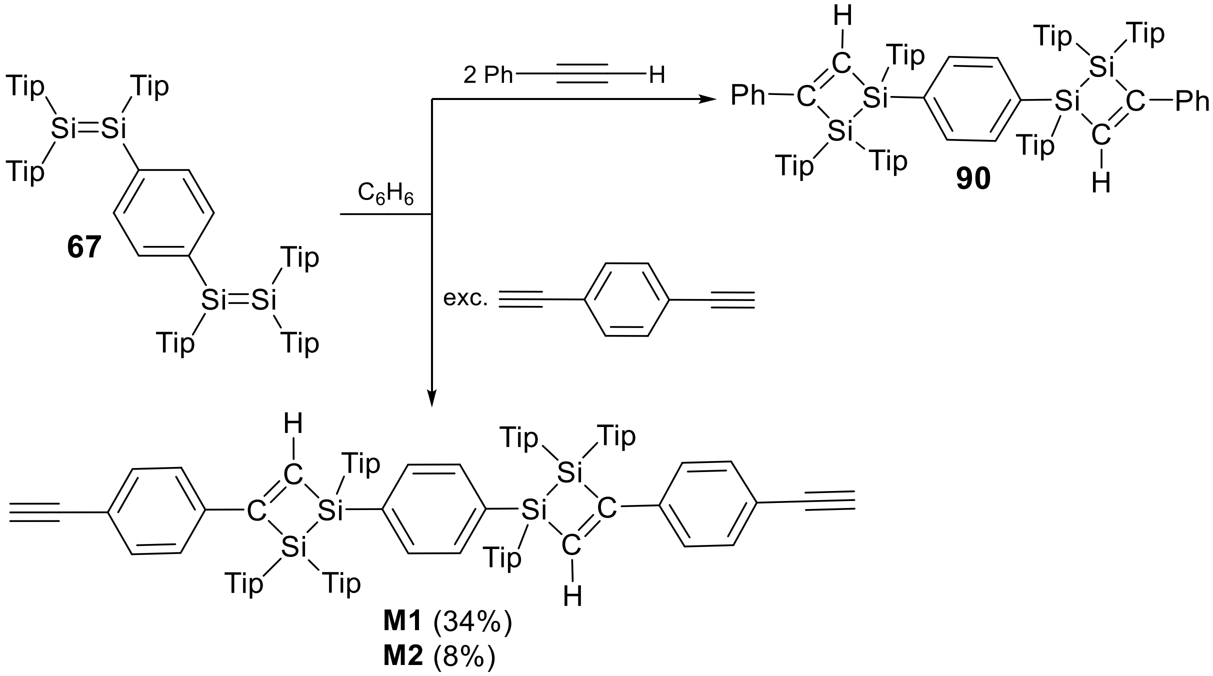

Scheme 28. [2+2] cycloaddition of tetrasiladiene **67** with phenyl acetylene and **67** with a large excess of 1,4-diethynyl benzene.

2. Aims and Scope

The development of new carbon-based π-systems incorporating heavier main group elements is of considerable interest owing to their potential applications in organic electronics.[79] Due to the inherent high reactivity as well as synthetic challenges, heavier *multiple* bonds have been employed relatively rarely in this context,[93] although after the ground-breaking work of the Protasiewicz and Gates groups[94] multiple bonds to phosphorus or even heavier Group 15 elements enjoy renewed attention recently.[95] Notably, only few reports exist on conjugated systems involving silicon in the conjugation path, although the increased admixture of σ- and σ*-orbitals to the π-π* set of orbitals of disilene typically results in a further reduced HOMO-LUMO separation.[96a] It was the objective of this work to prepare further examples of Si=Si bonds incorporated into carbon-based π-systems, and to study the properties of the obtained species. In order for the low-valent silicon atoms to be a part of the π-aromatic substituents/spacers, the disilenide **27** was the natural choice. Indeed, the nucleophilic center in the periphery of unsaturated silicon atoms of disilenide **27** had been successfully utilized as building block for conjugated materials.[93a,d]

The second major task of the project was to study the principle of regioselective [2+2] cycloaddition of polar multiple bonds to Si=Si moieties by the addition of phenyl acetylene to the various disilenes and bridged tetrasiladienes obtained. The elucidation of optimal reaction conditions as well as mechanistic details was anticipated to allow for the preferably selective syntheses of further bifunctional monomers with terminal alkynyl groups with a variety of linking units. The use of novel linking units between Si=Si bonds was expected to allow for the more selective synthesis of organosilicon polymers with alternating saturated Si_2 motifs and π-conjugated fragments (LU) and thus extend the σ-π conjugation along the polymer backbone.

3. Results and Discussion

3.1. Synthesis of Aryl Disilenes and *para*-Arylene Bridged Tetrasiladienes

In previous work, the Si=Si transfer reaction effectuated by lithium disilenide **27** was employed by our group to not only obtain *meta*- and *para*-phenylene bridged tetrasiladienes **67**, but also phenyl-substituted disilenes of type **66** with, in part, residual functionality X (Scheme 29).[80b]

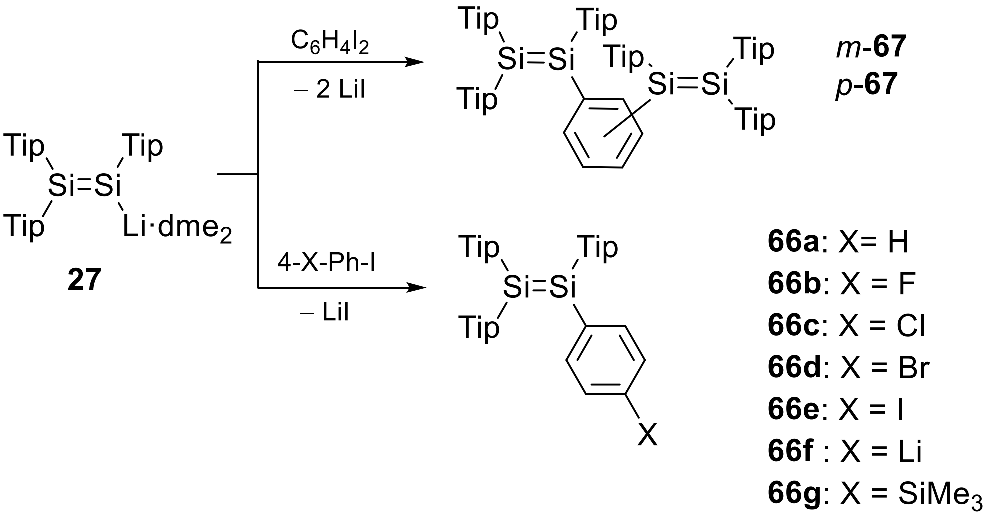

Scheme 29. Synthesis of and phenylene bridged tetrasiladiene *m*-**67** and *p*-**67** as well as *para*-functionalized phenyl-substituted disilenes of type **66** (Tip = 2,4,6-^{i}Pr$_3$C$_6$H$_2$).[80b]

It was therefore decided to investigate the single or double grafting of disilenyl functionalities, Tip$_2$Si=SiTip-, to (poly)aromatic systems as organic π-linking units and thus extend the scope of the Si=Si transfer protocol to include sterically rather demanding substrates.

As will be shown, the disilenyl group can indeed be transferred to the different (poly)aromatic systems by reacting the corresponding aryl (di)halides with the nucleophilic disilenide **27** if the reaction parameters, namely the choice of solvent and temperature, are carefully optimized. Besides, the molecular structures and

NMR spectroscopic properties of the products are elucidated, as well as the influence of the organic linking unit (LU) on the photophysical properties. An exploration of the scope of the thus developed synthetic protocol for the formation of different aryl substituted disilenes and *para*-arylene bridged tetrasiladienes is also presented.

3.1.1. Synthetic Strategy

For the planning a synthetic strategy for the formation of aryl disilenes and *para*-arylene bridged tetrasiladienes, it is important to consider the homocoupling of disilenide **27** to a tetrasilabutadiene **11** as potential undesired side reaction. There are two main mechanistic scenarios for the formation of tetrasilabutadiene **11** (Scheme 30):

(a) As proposed by Weidenbruch, a metal halogen-exchange between disilenide **27** would lead to a transiently occurring halodisilene **27a**, which could plausibly react with residual disilenide **27** in a salt elimination reaction to give **11**.

(b) The one electron oxidation of **27** would generate a very reactive disilenyl radical **27b** that simply needed to dimerize to produce **11**.

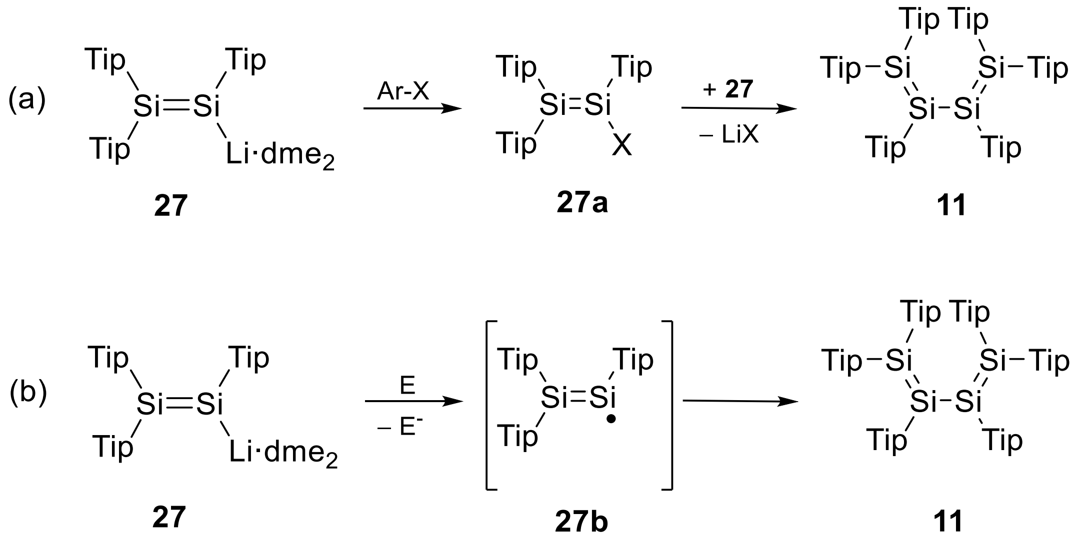

Scheme 30. (a) Metal halogen-exchange followed by salt elimination between the thus-formed halodisilene **27a** and residual disilenide **27**. (b) Dimerisation of disilenyl radicals **27b** generated from the oxidation of **27** by the intended electrophile.

While it is difficult to discern the two alternative mechanisms, it can be speculated that (b) should be favored by entropic considerations as the halogen exchange according to (a) would require a highly ordered transition state. Of course, the desired formal nucleophilic substitution at the halo arene although typical transition states for substitution provide more degrees of freedom than that of a metal-halogen exchange reaction.

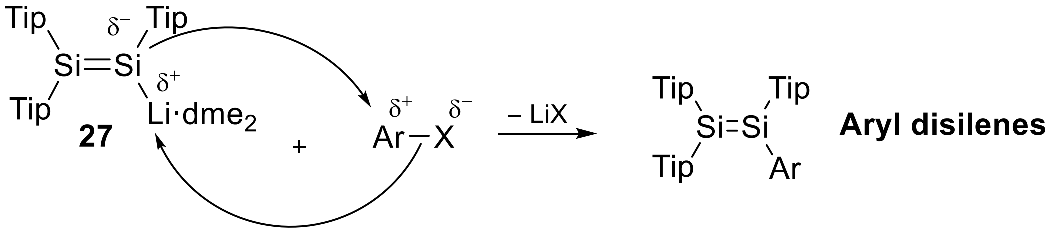

Scheme 31. Suggested aromatic S_N2-type mechanism for the formation of aryl disilenes from the reaction of aryl haildes and disilenide **27** under elimination of lithium halides.

The reactivity of disilenide **27** with the aryl halides of the type C_6H_5X (X = F, Cl, Br, I) had been investigated previously.[80b] The reaction of **27** with iodo or bromobenzene had yielded the phenyl-substituted disilenes **66a** in a smooth reaction with the cleavage of LiX (X = I, Br). In contrast to the cases of bromo- and iodobenzene, no reaction at all had been observed after one week at room temperature using either chloro- or fluorobenzene. If the nucleophilic aromatic substitution reactions S_NAr mechanism were active, the reaction with aryl fluorides should be the most rapid because the reactivity of the aryl halides Ar-X decreases in the order X = F> Cl> Br> I.[80b] Therefore, The S_NAr reaction mechanism for the reaction of disilenide **27** with aryl halides had been ruled out. On this basis, plausible mechanisms for the reactions of **27** with the different halo arenes in this project involve S_N2-like aromatic substitution (Scheme 31).

The ^{29}Si NMR signals spectra (Figure 6) of most reactions without optimization of the reaction conditions predominantly reveal resonances at $\delta = 88.46$ and 44.04 ppm, suggesting almost exclusive formation of **11**.

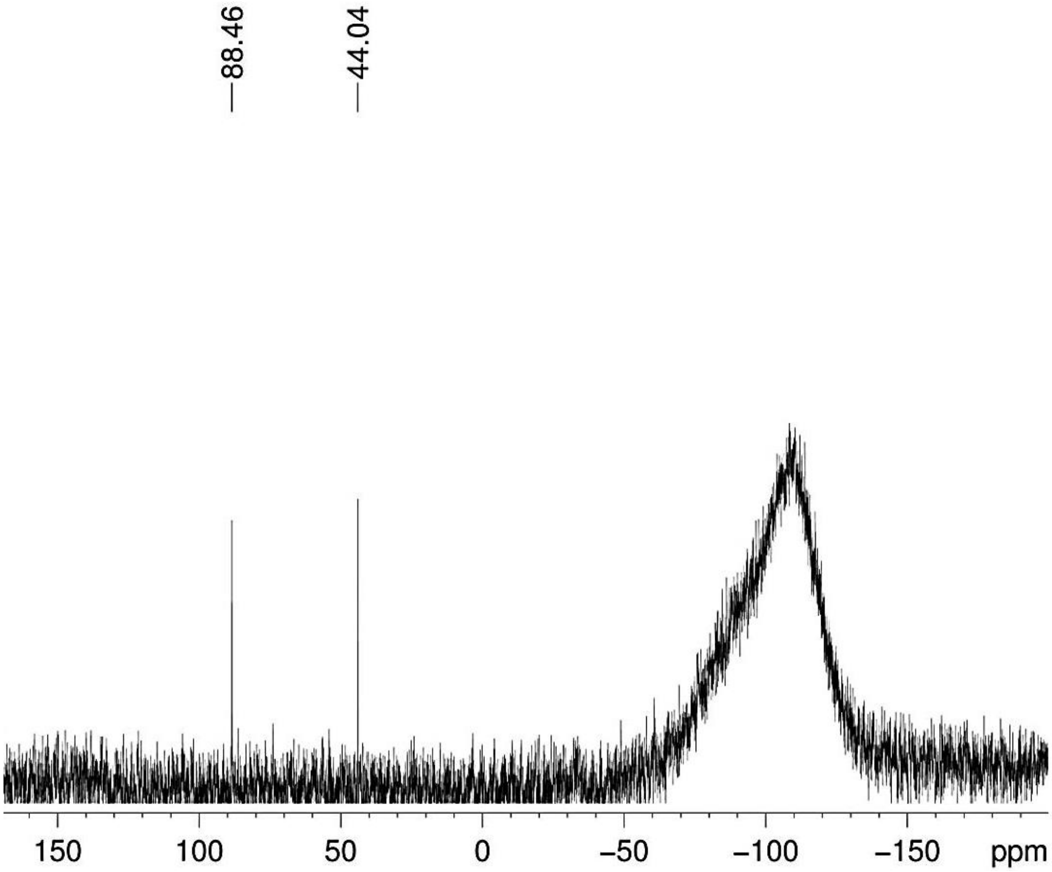

Figure 6. Example of ^{29}Si NMR spectrum of the reaction mixture of 1-iododurene **93** with disilenide **27** in C_6D_6 at 300 K.

Indeed, Weidenbruch *et al.* reported the isolation of tetrasilabutadiene **11** from the reaction disilenide **27** with MesBr in 1,2-dimethoxyethane as a solvent.[42]

Although, an n-donor solvent could in principle enhance the nucleophilicity of disilenide **27**, the formal nucleophilic substitution at the halo arene probably requires **27** in the form of the contact ion pair to sufficiently decrease its reduction potential and thus suppress electron loss to the disilenyl radical **27b**.

On the basis of above considerations, it was further expected that a lowering of the temperature might favor substitution over the competing redox chemistry. Benzene as a solvent was preferred over toluene in order to reduce erratic radical type reactivity.

In order to prevent the formation of **11**, all reactions were carried out by the slow addition of a pre-cooled benzene solution of one equivalent of disilenide **27** to a solution of the different aryl halides (Ar-X) in benzene at about 7 °C. The use of a dropping funnel pre-cooled with ice water in the cooling mantle is obligatory for good results. The reaction mixture is brought to room temperature and stirred for additional 22 hours. Following an analogous protocol, the appropriate aryl dihalides (X-LU-X) were treated with two equivalents of disilenide **27**. As will be shown, the synthetic technique used in this project is selective and suitable to obtain new compounds in high yields (Figure 7).

Figure 7. Photographic image of precooled funnel used for the addition of a solution of disilenide **27** in benzene to halo arene substrates.

3.1.2. Reactivity of Disilenide 27 towards Aryl Halides (Ar-X)

3.1.2.1. Reactivity of Disilenide 27 towards MesBr 91

Applying the above synthetic strategy, a pre-cooled solution of one equivalent disilenide **27** in benzene was added to mesityl bromide **91** in benzene at 7 °C (Scheme 32).

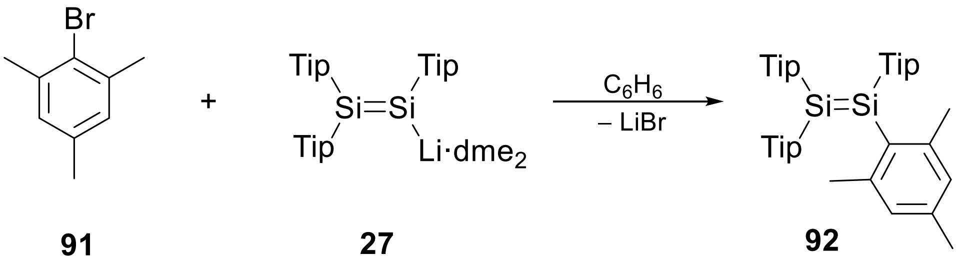

Scheme 32. Synthesis of mesityl substituted disilene **92**.

This leads to a change of color from intense orange to yellow orange, indicating that a reaction takes place and that only little – if any – of the intensely purple-colored tetrasilabutadiene **11** had been formed. The precipitation of a white solid, presumably lithium bromide, also hinted towards the intended substitution reaction.

The quantitative formation of a new Si=Si-containing species was confirmed by the NMR spectra obtained from the reaction mixture. The ^{29}Si NMR shows two signals of equal intensity at δ = 55.95 and 55.58 ppm in the expected region for aryl substituted disilenes alongside very minor impurities at higher field (Figure 8).[97]

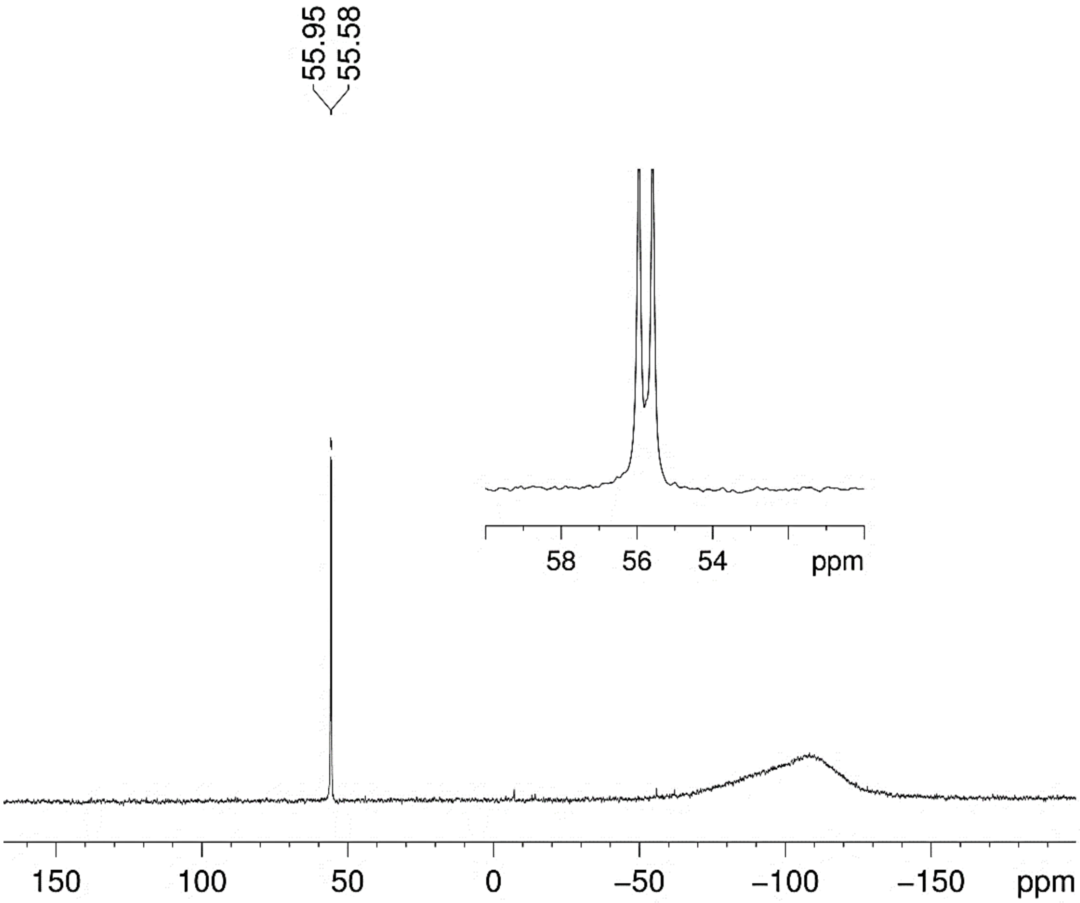

Figure 8. ^{29}Si NMR of the reaction mixture of disilenide **27** with MesBr **91** after work-up.

The ^{1}H NMR spectrum confirms the selective formation of a single product. The three singlet upfield resonances at δ = 2.66, 2.53 and 2.02 ppm can be attributed to the three methyl groups of the mesityl moiety. The low field region shows the expected three singlet resonances at δ = 7.02 ,7.00 and 6.98 ppm for the three inequivalent Tip groups next to the two singlet signals at δ = 6.67 and 6.65 ppm, which are typical for the two aromatic protons of the mesityl group.

A yellow-orange solid product was obtained in 93% yield (mp. 160°C) after filtration and removal of the solvent and single crystals of **92** were grown from a concentrated hexane solution. X-ray diffraction confirmed the constitution of mesityl substituted disilene **92** (Figure 9).

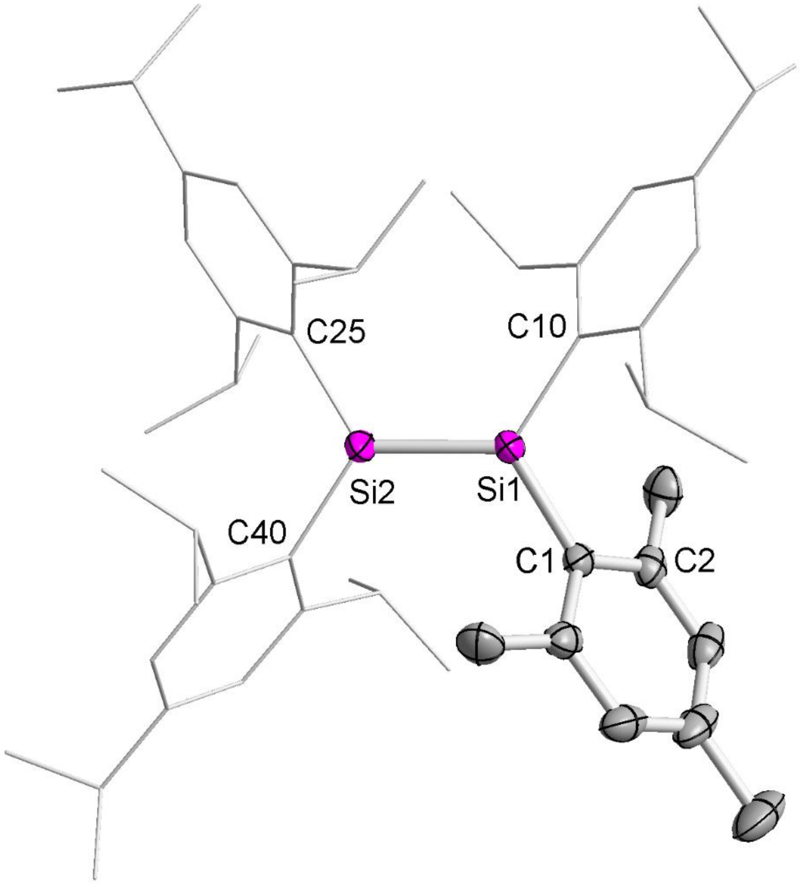

Figure 9. Solid state molecular structure of **92** (50% probability ellipsoids, H atoms and disordered ^{i}Pr groups are omitted for clarity). Selected bond lengths [Å]: Si1-Si2 2.1452(6), Si1-C1 1.8739(17), Si1-C10 1.8820(16), Si2-C40 1.8872(17), Si2-C25 1.8865(17), C(1)-Si(1)-C(10) 114.69(7), C(1)-Si(1)-Si(2) 122.46(5), C(10)-Si(1)-Si(2) 122.34(5), C(40)-Si(2)-C(25) 114.79(7), C(40)-Si(2)-Si(1) 122.43(6), C(25)-Si(2)-Si(1) 122.19(5).

Disilene **92** shows a nearly planar coordination environment at the silicon atoms, the sum of the bond angles around the Si1 and Si2 atoms are 359.48° and 359.41°, respectively (Figure 9). The Si=Si bond is determined to 2.1452(6) Å, which is at the short end of the range of values found for aryl substituted disilenes (2.140 to 2.229 Å)[98] and thus significantly shorter than the corresponding bond of the previously reported phenyl disilene **66a**[80a] [2.1754(11) Å for **66a**]. This observation is in line with the considerably more pronounced *trans*-bending of the Si=Si bond in **66a**[80a] compared to the moderately *trans*-bent **92** (**92**: θ_{SiTip} = 6.7°; θ_{SiTip2} = 7.2°; **66a**: θ_{SiTip} = 23.6°, θ_{SiTip2} = 22.3°). The CGMT model predicts a weakening of the Si=Si bond as the extent of *trans*-bending increases.[31] The mesitylene ring is twisted out of the plane with a torsion angle of 50.6° for Si2−Si1−C1−C2.

UV/vis spectroscopy shows a maximum absorption wavelength of **92** at λ_{max} = 430 nm (ε = 21200 $M^{-1}cm^{-1}$), which is comparable to the values reported for nearly planar disilenes (385-430 nm).

3.1.2.2. Reactivity of Disilenide 27 towards Mono-Iododurene 93

Mono-iododurene **93** as a substrate with slightly higher steric demand due to the so-called buttressing effect[95b] was reacted with one equivalent of disilenide **27** in benzene (Scheme 33).

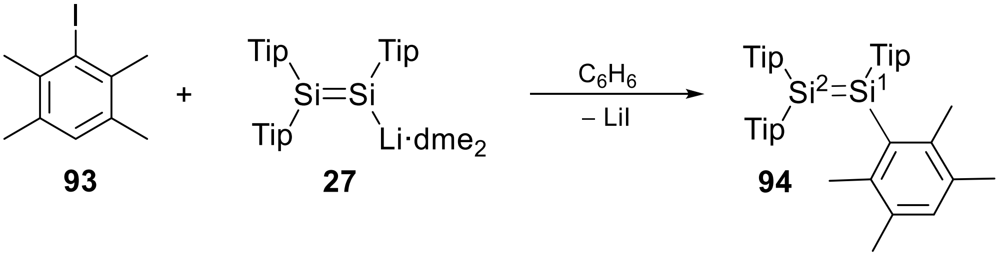

Scheme 33. Synthesis of duryl substituted disilene **94**.

A color change from the orange-red color of disilenide **27** to a yellow orange tint was observed. The ^{29}Si NMR spectrum (Figure 10) after work-up revealed uniform conversion to a new product with two resonances at δ = 57.88 and 52.95 ppm in the typical range for disilenes[97] suggesting the formation of disilene **94**.

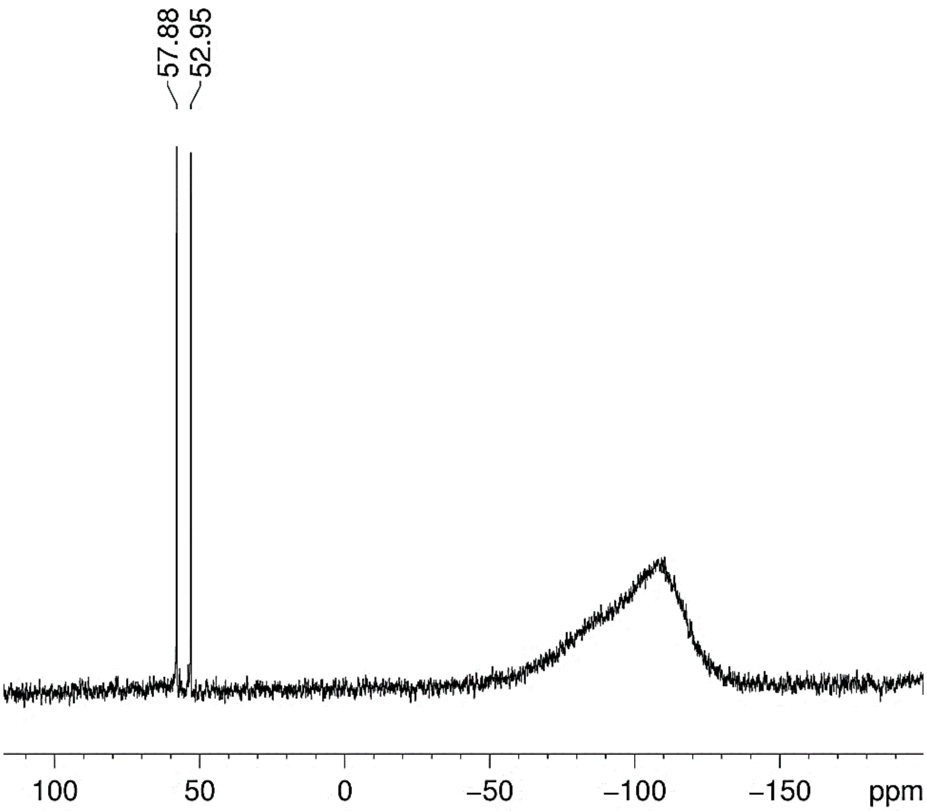

Figure 10. ^{29}Si NMR spectrum of the reaction mixture of 1-iododurene **93** with disilenide **27**.

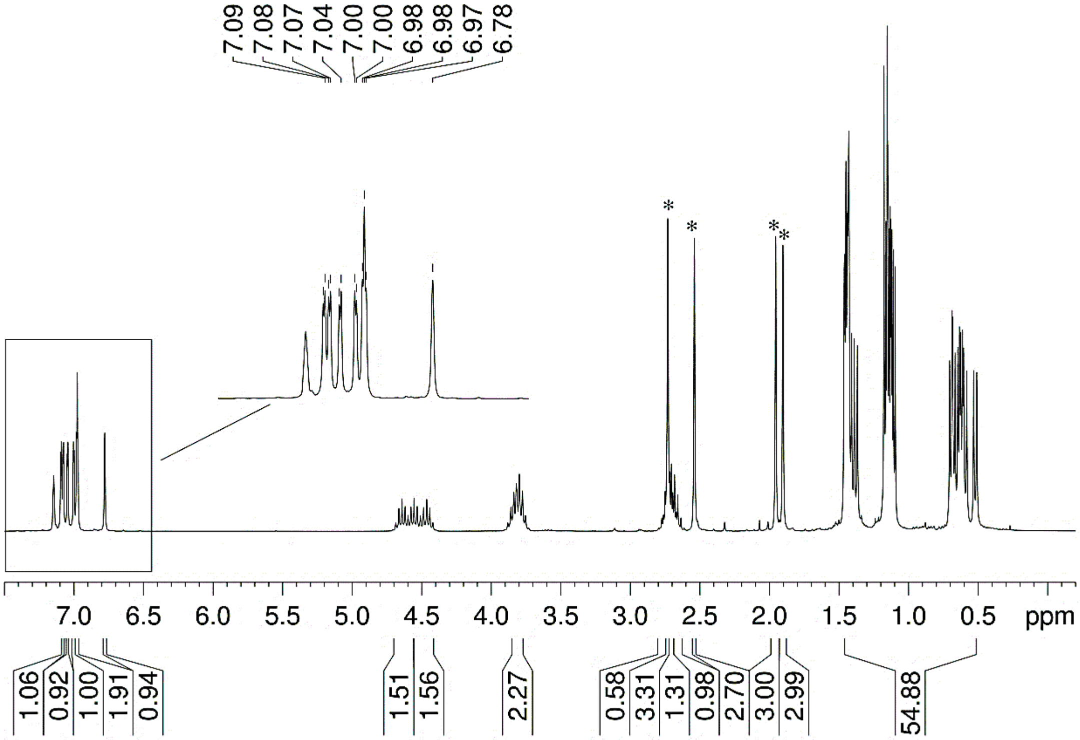

Figure 11. ^{1}H NMR spectrum of the reaction mixture of 1-iododurene **93** with disilenide **27**, $*$ = Selected signals assigned to CH_3 groups of the duryl moiety.

The ^{1}H NMR spectrum (Figure 11) shows four singlet upfield resonances for the methyl protons of the duryl moiety at δ = 2.73, 2.54, 1.95 and 1.90 ppm suggesting that the rotation of the duryl group about the Si-C bond is slow on the NMR time-scale. Similarly, the Tip groups on Si2 show individual resonances as a doublet signal for each aromatic proton at δ = 7.09, 7.07, 7.04 and 6.99 ($^4J_{H\text{-}H}$ = 1.65 Hz) ppm. In contrast, the aryl-hydrogen atoms of the Tip group at Si1 shows just a single ^{1}H singlet resonance at δ = 6.97 ppm, which confirms chemical equivalence and thus fast rotation of that group on the NMR time scale. The *para*-hydrogen of the duryl group is observed at δ = 6.78 ppm as a singlet.

Indeed, the 2D ^{29}Si-^{1}H correlation NMR spectrum shows a cross-peak of this particular resonance to the more low-field silicon atom signal, and thus the ^{29}Si NMR signals resonances at δ = 57.88 and 52.95 ppm should arise from Si1Tip and Si2Tip$_2$ units, respectively (Figure 12).

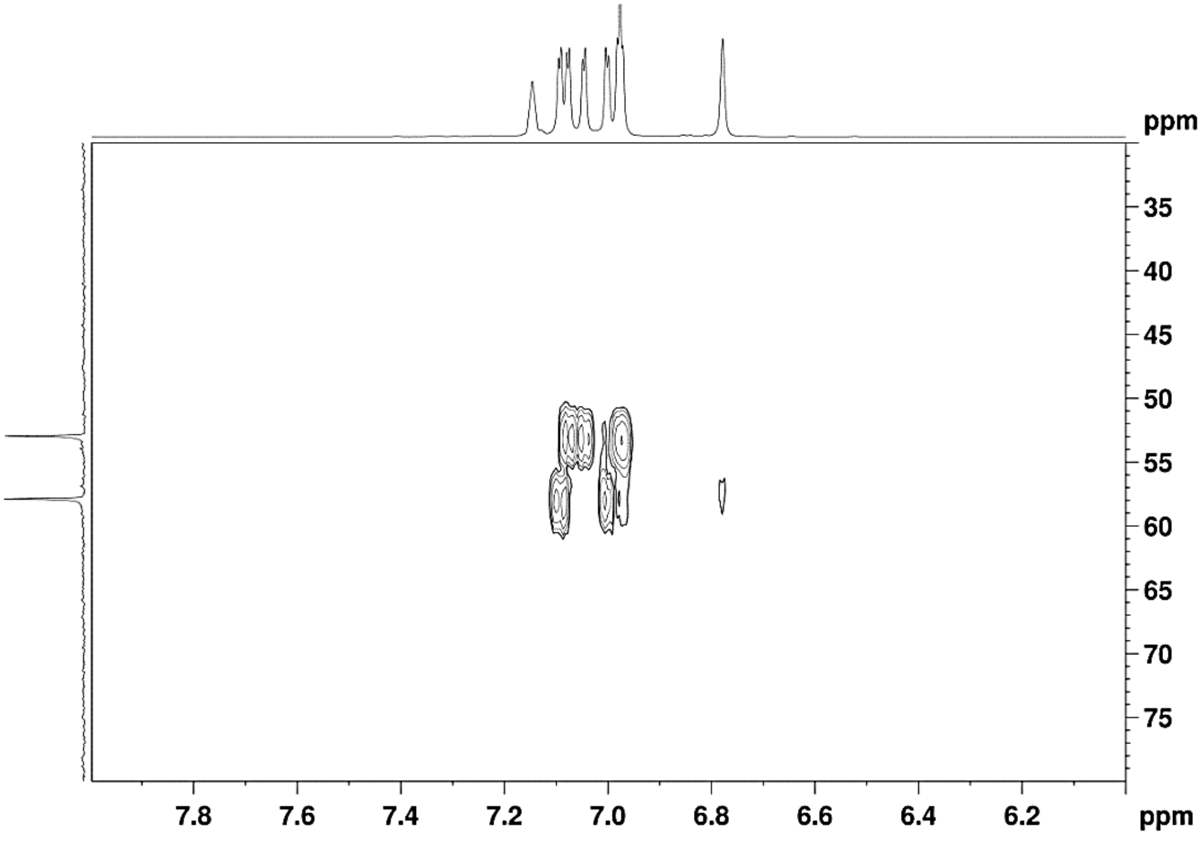

Figure 12. 2D ^{29}Si-^{1}H NMR correlation spectrum of disilene **94**.

Disilene **94** can be isolated as large yellow single crystals in 88% yield (mp. 145°C) after crystallization from hexane solution. The constitution of **94** was verified by X-ray diffraction (Figure 13).

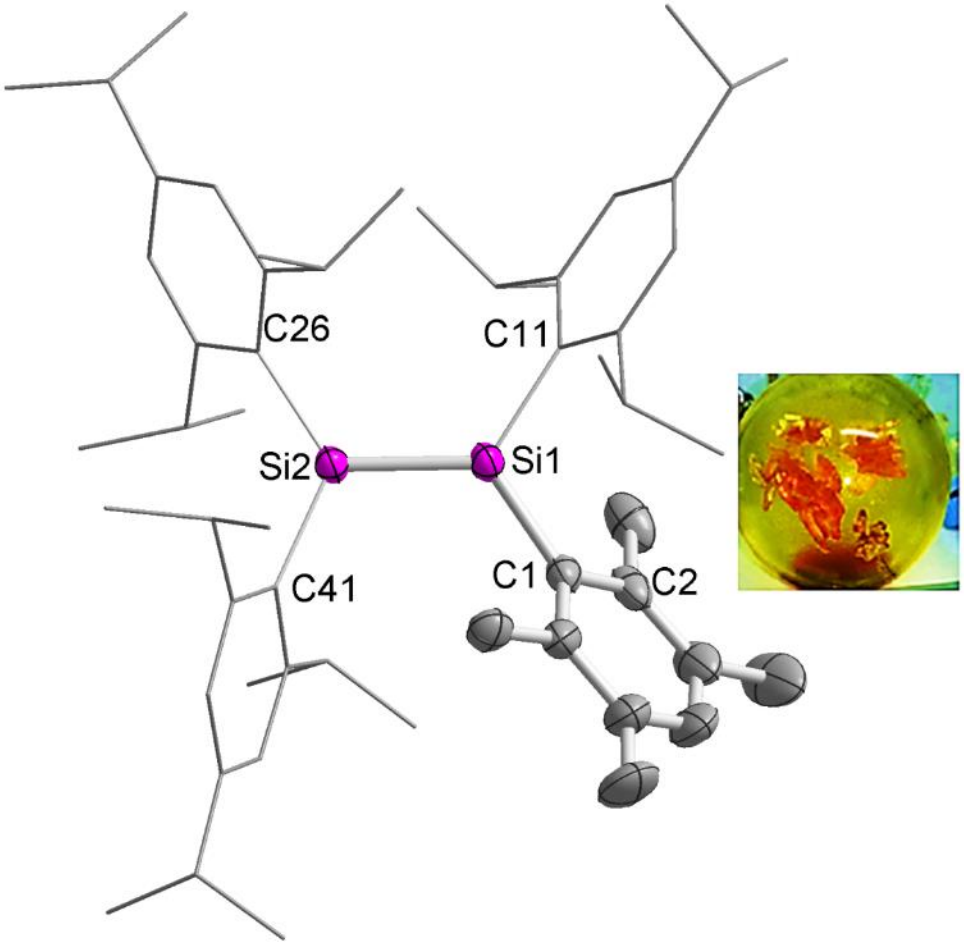

Figure 13. Molecular structure of **94** in the solid state (thermal ellipsoids at 50%, H atoms and disordered ^{i}Pr groups are omitted for clarity). Insert shows photographic image of crystals of **94**. Selected bond lengths [Å] and bond angles [°]: Si1-Si2 2.1516(7), Si1-C1 1.8825(19), Si1-C11 1.8853(17), Si2-C41 1.8860(17), Si2-C26 1.8907(18), C(1)-Si(1)-C(11) 112.85(8), C(1)-Si(1)-Si(2) 121.26(6), C(11)-Si(1)-Si(2) 121.25(6), C(41)-Si(2)-C(26) 122.76(8), C(41)-Si(2)-Si(1) 116.00(6), C(26)-Si(2)-Si(1) 121.22(6).

The Si=Si bond length in **94** is determined to 2.1516(7) Å, which is only slightly elongated compared to the corresponding Si=Si bond of 2.1453(6) Å in the related **92**. The bond distance between the silicon atom and the *ipso*-C atom of the duryl group in **94** (Si1-C1 1.8825(19) Å), which is in good agreement with other aryl substituted disilenes (lit. 1.851 Å to 1.890 Å).[98] The disilenyl unit experiences a significant twist (τ =

10.6°) and moderate *trans*-bent arrangement with θ_{SiTip} = 7.5°; θ_{SiTip2} = 1.7°. Similar to **92**, despite the near-perfect planarity of the molecule **94** around the two Si=Si bonds (ΣSi1 = 359.3° and ΣSi2 = 359.9°), the durene ring is also twisted out of the plane with a torsion angle of 56.30° for Si2−Si1−C1−C2.

UV/vis spectroscopy of disilene **94** shows a similar longest wavelength absorption maximum as the disilene **92** at λ_{max} = 430 nm, albeit slightly blue-shifted by $\Delta\lambda$ = 9 nm compared to the more *trans*-bent **66** (λ_{max} = 439 nm).[80]

3.1.2.3. Reactivity of Disilenide 27 towards 1-Bromo-4-(phenylethynyl) Benzene 95

In order to increase absorbance in the visible region and possibly induce fluorescence in the product, 1-bromo-4-(phenylethynyl)benzene **95** with a C≡C bond between the two phenylene units seemed to be a promising substrate for the reaction with disilenide **27**. Disilenide **27** was treated with an equimolar amount of **95** in benzene. It was anticipated that the corresponding product **96** would be formed (Scheme 34).

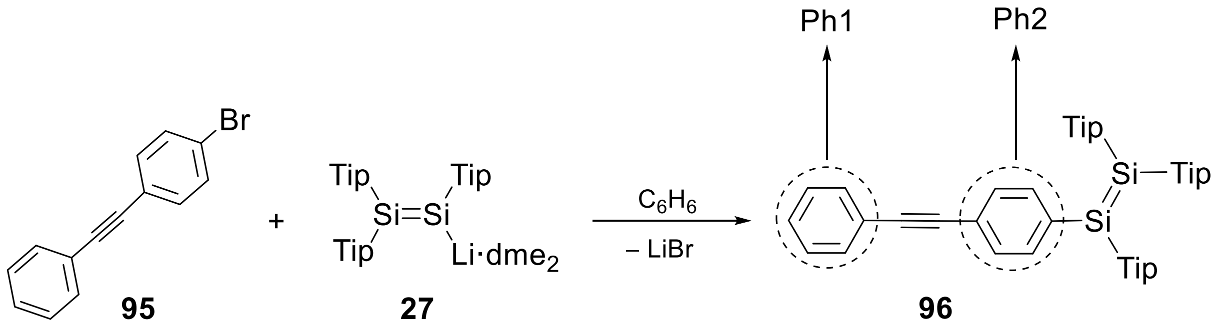

Scheme 34. Anticipated reaction of one equivalent disilenide **27** with **95**.

Since crystallization attempts remained unsuccessful, the crude product was obtained as red solid in excellent yield 94% (mp. 155°C) after filtration and evaporation of hexane under vacuum and was characterized by multinuclear NMR analysis and UV/vis spectroscopy.

The three different singlet resonances at δ = 7.12, 7.09 and 7.03 ppm in the ^{1}H NMR spectrum are assigned to the three sets of two aromatic hydrogen atoms of the chemically inequivalent Tip substituents. Chemical shift for protons of Ph1 appear at δ = 7.32-7.30 and 7.28 ppm as one multiplet and one singlet resonances, while the one singlet and one multiplet resonances at δ = 7.17 and 6.93-6.90 are assigned to the chemical shift for protons of Ph2 (Figure 14).

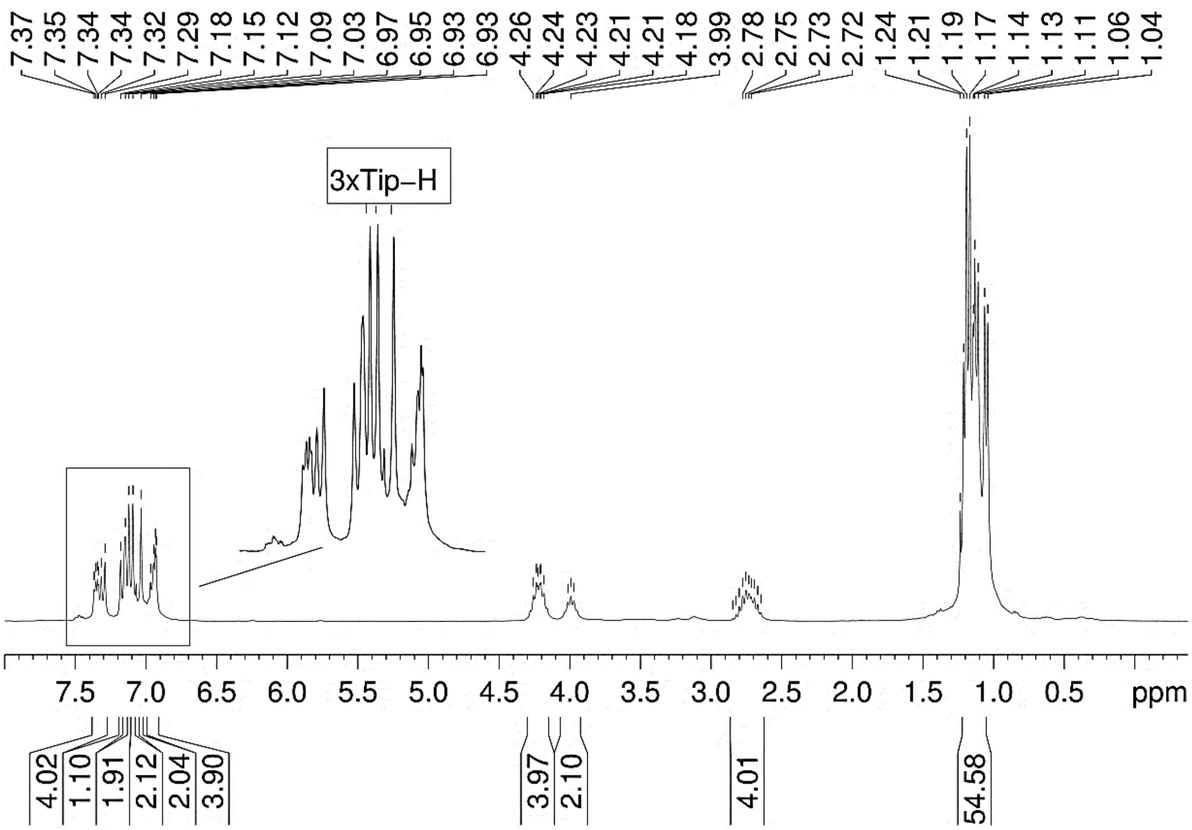

Figure 14. ^{1}H NMR of the reaction mixture of one equivalent disilenide **27** with **95** in C_6D_6 at 300 K.

Two signals are found in the ^{29}Si NMR at δ = 69.71 and 57.77 ppm, which are attributed to the Si=Si bond (Figure 15).

In addition to the typical signals for the three inequivalent Tip groups, the ^{13}C NMR spectrum exhibits two resonances at δ = 90.79 and 90.52 ppm characteristic of the C≡C bond (Figure 16), which clearly indicates the presence of an uncompromised carbon-carbon triple bond in **96**.

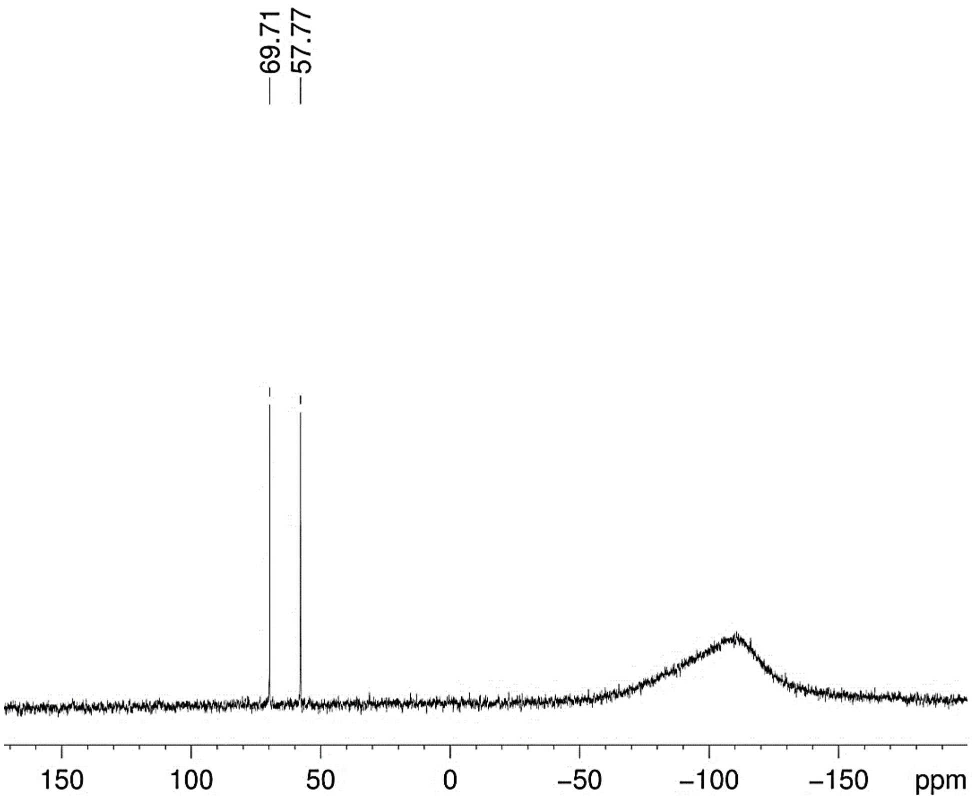

Figure 15. ^{29}Si NMR spectrum of anticipated disilene **96** in C_6D_6 at 300 K.

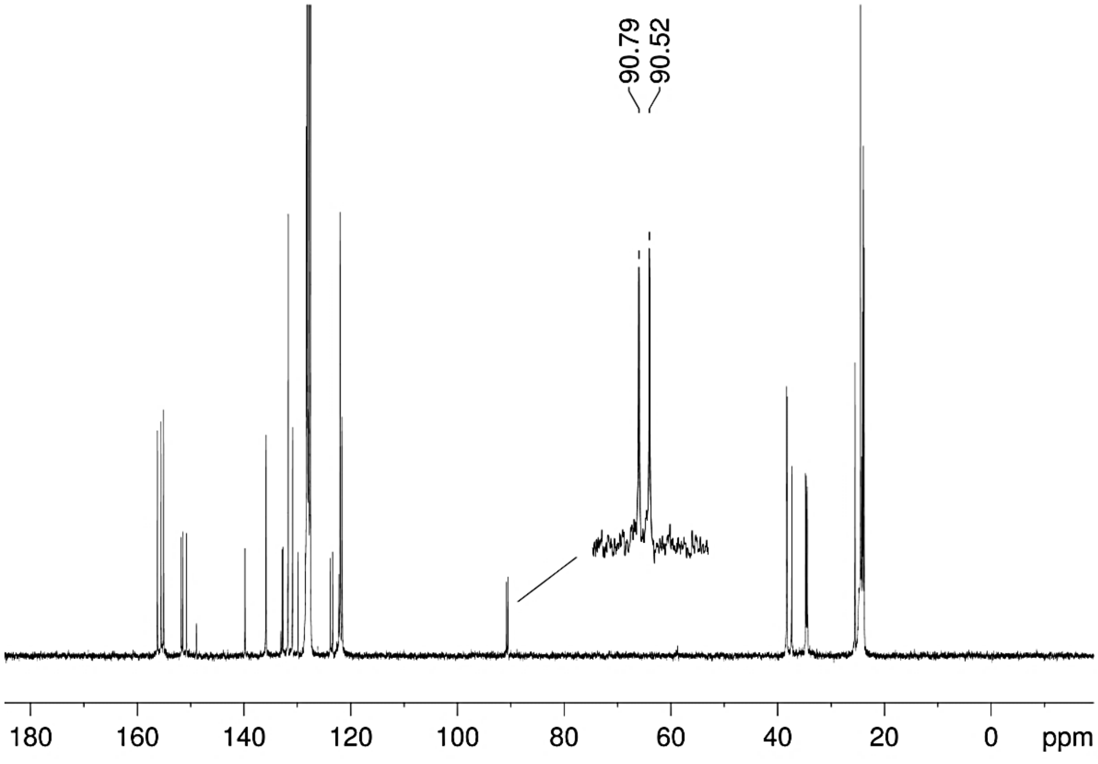

Figure 16. ^{13}C NMR spectrum of anticipated disilene **96** in C_6D_6 at 300 K.

On the basis of a two-dimensional ^{29}Si-^{1}H correlation analysis (Figure 17), the high-field resonance shows two equally intense cross-peaks to the aryl hydrogen atoms of two Tip moieties and is therefore assigned to $SiTip_2$ moiety. In contrast, for the low-field resonance cross-peaks to one Tip group and the Ph2 moiety are observed; the ^{29}Si NMR signal at 69.71 ppm must therefore be due to the SiTip-unit. No cross-peaks of the two ^{29}Si NMR resonances are observed to the hydrogen atoms of Ph1, which appears to be too far away for significant coupling of the nuclei.

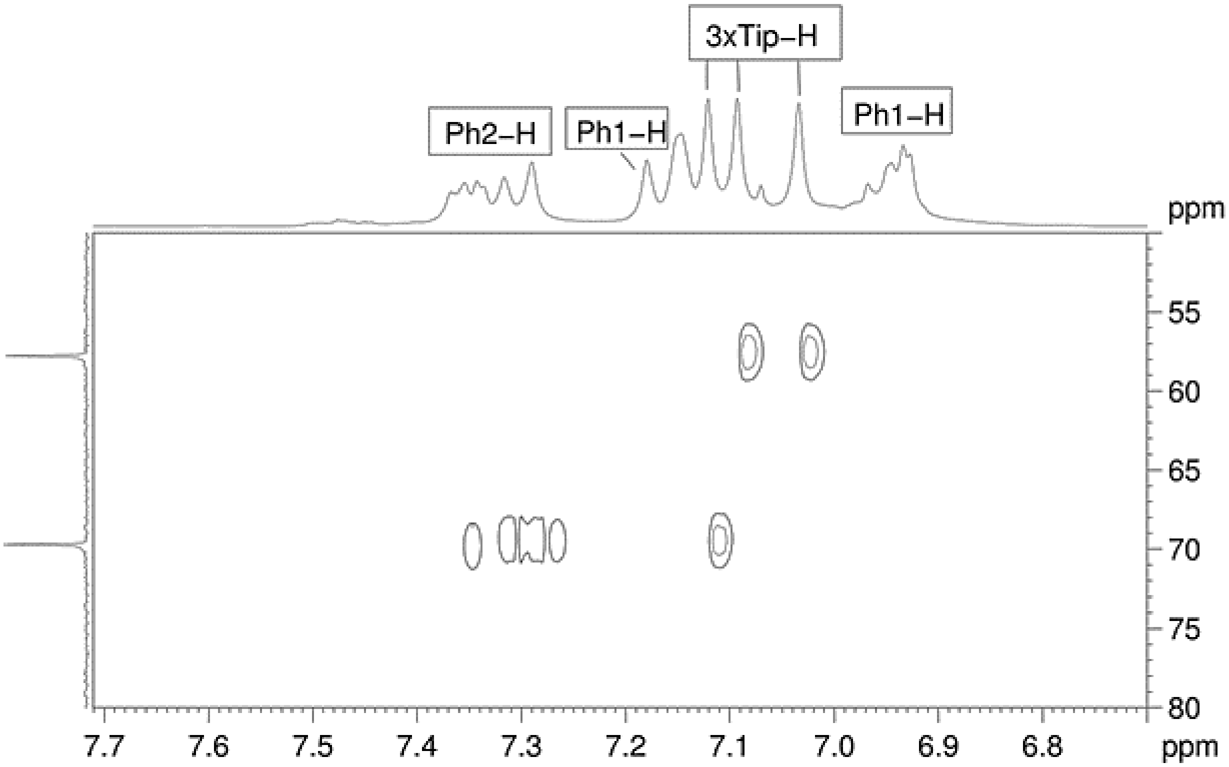

Figure 17. 2D ^{29}Si-^{1}H NMR correlation spectrum of anticipated disilene **96**.

UV/vis spectroscopy shows a maximum absorption wavelength at λ_{max} = 472 nm (ε = 4880 $M^{-1}cm^{-1}$), which is much more red-shifted compared to than in (phenyl, mesityl, duryl and naphthyl) disilenes. This red-shift is either due to the extended conjugated system over the Si=Si and phenyl ring through C≡C bond unit or to a more pronounced *trans*-bending induced by the sterically less demanding diphenylethynyl linker, which cannot be decided in the absence of a solid state structure. The NMR and UV/vis spectroscopic data, however, still provide unambiguous prove for the suggested constitution as disilene **96**.

3.1.2.4. Reactivity of Disilenide 27 towards Bromo Naphthalene 97

As outlined in the introduction, the UV/vis spectra of Iwamoto's polycyclic aromatic substituted disilenes **71a-c** showed characteristic intramolecular charge transfer (ICT) absorption bands in addition to the usual absorption bands of the π-π* transitions (around 370–380 nm). X-ray analyses of single crystals of **71a-c** revealed that the disilene π(πSi) and aromatic π(πC) systems are almost perpendicular to each other indicating very little conjugative interaction between π(πSi) and aromatic π(πC). Theoretical calculations confirmed that the Si–Si π orbital bond and the oligoaromatic ligand's π* orbital of **71a-c** function as donor and acceptor of that ICT, respectively.[81] In order to compare whether the reactivity of disilenide **27** towards oligo-aromatic halides substituents has similar properties with respect to the charge transfer transition, such compounds were subsequently prepared and tested.

One equivalent disilenide **27** was anticipated to react with 2-bromo naphthalene **97** to afford the naphthyl substituted disilene **98** (Scheme 35).

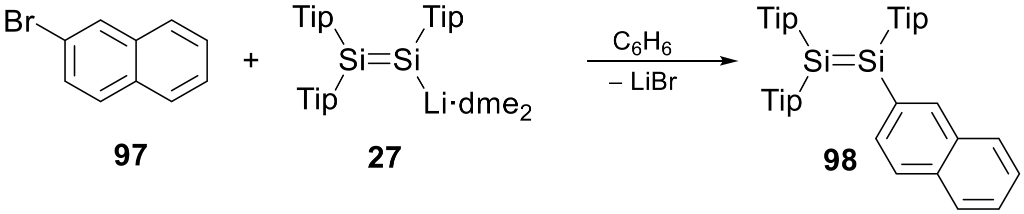

Scheme 35. Synthesis of naphthyl substituted disilene **98**.

The reaction was carried out by addition of a benzene solution of disilenide **27** to a benzene solution of 2-bromo naphthalene **97**. Even though no visible color change of the orange-red reaction mixture occurred, multinuclear NMR spectroscopy confirmed the quantitative conversion to the corresponding disilene **98.**

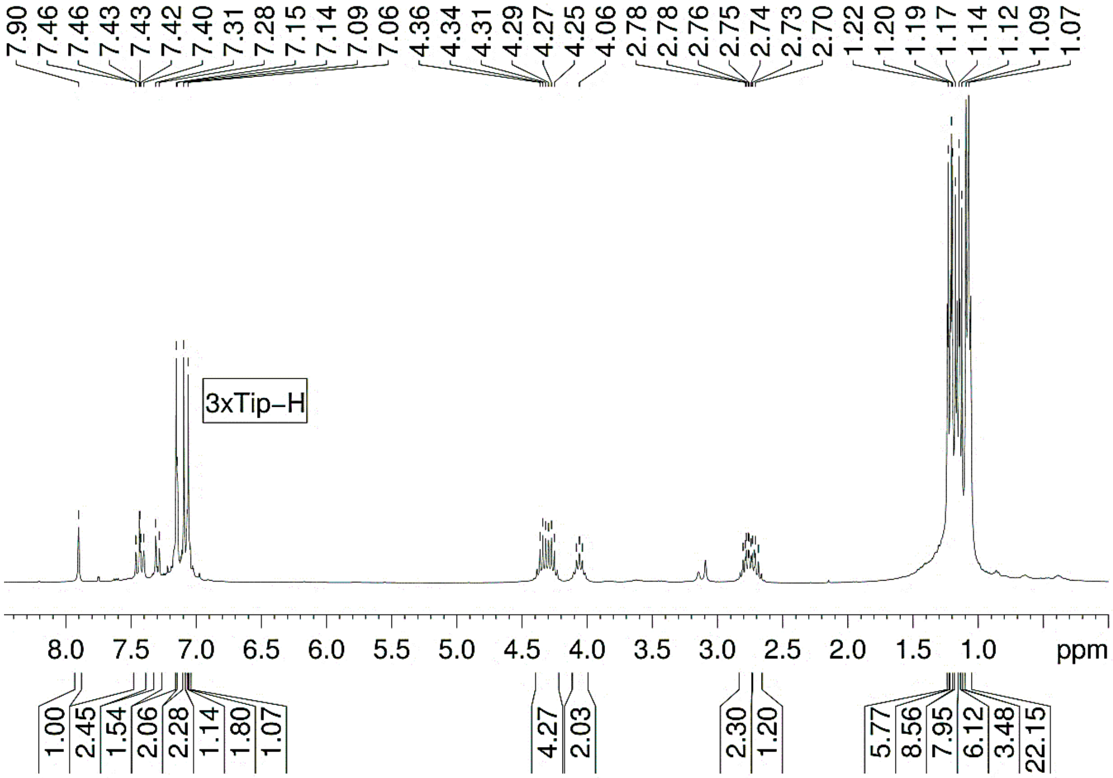

Figure 18. ^{1}H NMR spectrum of disilene **98** in C_6D_6 at room temperature, showing clearly the three-different low-field singlet resonances for the aromatic Tip protons.

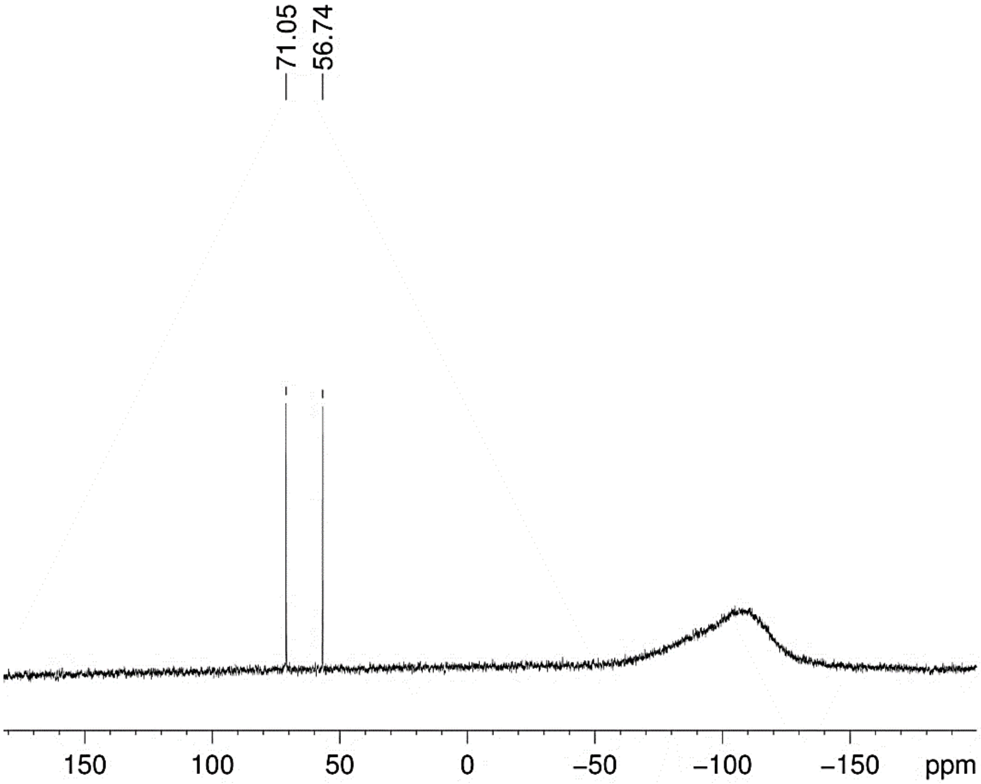

Figure 19. ^{29}Si NMR spectrum of disilene **98** in C_6D_6 at 300 K.

The ^{1}H NMR spectrum shows different low-field signals for the different naphthalene protons in **98** at δ = 7.90, 7.43, 7.31 and 7.06 ppm. Additionally, three diagnostic singlet signals at δ = 7.15, 7.09, 7.06 ppm represent the aromatic protons of the three chemically inequivalent Tip groups about the Si=Si moiety (Figure 18).

The ^{29}Si NMR signals spectrum (Figure 19) shows resonances at δ = 71.05 and 56.74 ppm. The low-field signal is assigned to the naphthyl-substituted silicon atom on the basis of a 2D ^{29}Si-^{1}H correlation analysis.

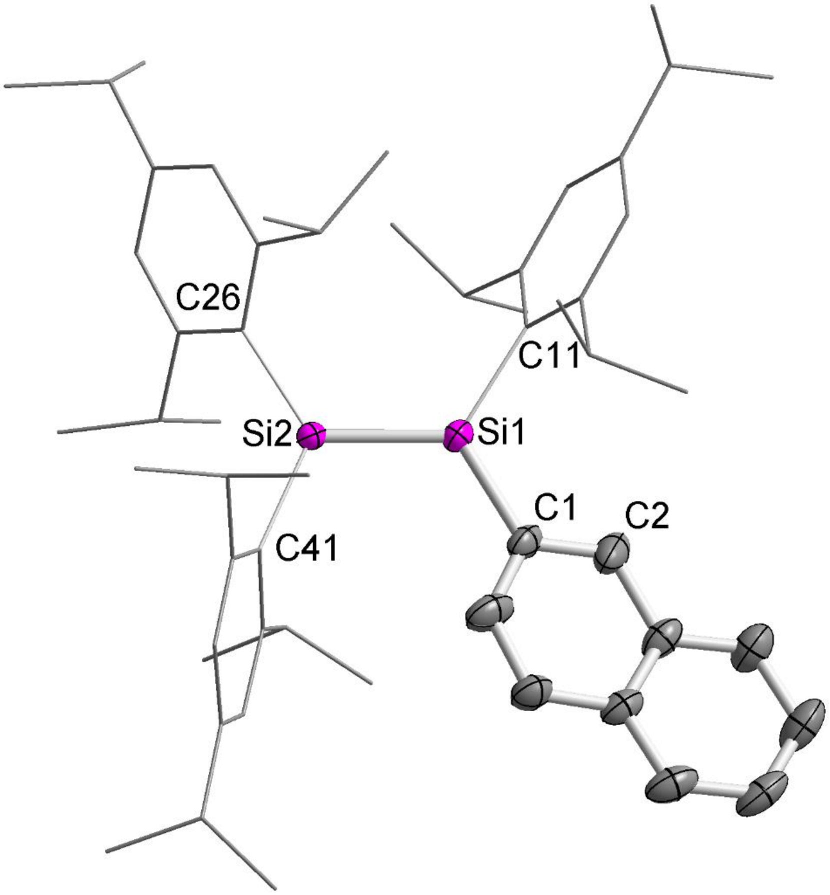

Figure 20. Molecular structure of **98** in the solid state (thermal ellipsoids at 50%, H atoms and disordered ^{i}Pr groups are omitted for clarity). Selected bond lengths [Å] and bond angles [°]: Si1-Si2 2.1525(6), Si1-C1 1.8700(18), Si1-C11 1.8846(17), Si2-C41 1.8875(16), Si2-C26 1.8874(16), C(1)-Si(1)-C(11) 115.91(8), C(1)-Si(1)-Si(2) 120.06(6), C(11)-Si(1)-Si(2) 122.54(5), C(26)-Si(2)-C(41) 124.14(7), C(41)-Si(2)-Si(1) 115.25(5), C(26)-Si(2)-Si(1) 120.50(5).

Single crystals of **98** (mp. 120°C) were obtained as red orange blocks from a concentrated hexane solution in 85% yield and an X-ray diffraction study expectedly revealed the structure of **98** (Figure 20). Both unsaturated silicon centers show only slight deviation from planarity (Σ of angles Si1: 358.51 and Si2 359.89 Å). The Si=Si bond length 2.1525(6) Å is very similar to the duryl substituted disilene **94** and significantly shorter than the corresponding bonds of the previously reported phenyl disilene **66a** (2.1754(11) Å).[80a] Furthermore, twisting of the Si-Si bond (τ = 10.4°) is observed for **98**, which is almost identical to the value for duryl disilene **94** and slightly larger than that of the phenyl disilene **66a** (τ = 5°).[80a] Si-C bond distances to the aryl-substituents range from 1.8700(18) Å to 1.8875(16) Å, which is also in good agreement with literature values of aryl substituted disilenes (lit: 1.851 Å to 1.890 Å).[98] The naphthalene ring is only mildly distorted from planarity with a torsion angle of just 21.29° for Si2−Si1−C1−C2, which is significantly smaller than the corresponding angle in duryl substituted disilene **94** (φ = 56.30°). Despite the less pronounced *trans*-bending in **98** (θ_{SiTip} = 11.6°; θ_{SiTip2} = 3.2°) compared to phenyl substituted disilene **66a**, a red-shift is found for the longest wavelength absorption at λ_{max} = 463 nm (ε = 6800 $\text{M}^{-1}\text{cm}^{-1}$).

3.1.2.5. Reactivity of Disilenide 27 towards Bromo Anthracene 99

Another substitution reaction of the related disilenide **27** with bromo anthracene **99** was investigated. The treatment of one equivalent disilenide **27** with 9-bromoanthracene **99** in benzene (Scheme 36) results in the formation of a deep-purple solution. The NMR measurements of the reaction mixture indicated the full conversion into disilene **100.**

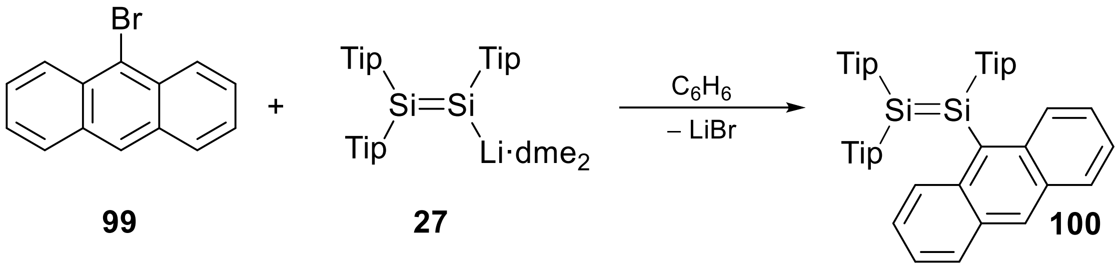

Scheme 36. Synthesis of anthracyl substituted disilene **100**.

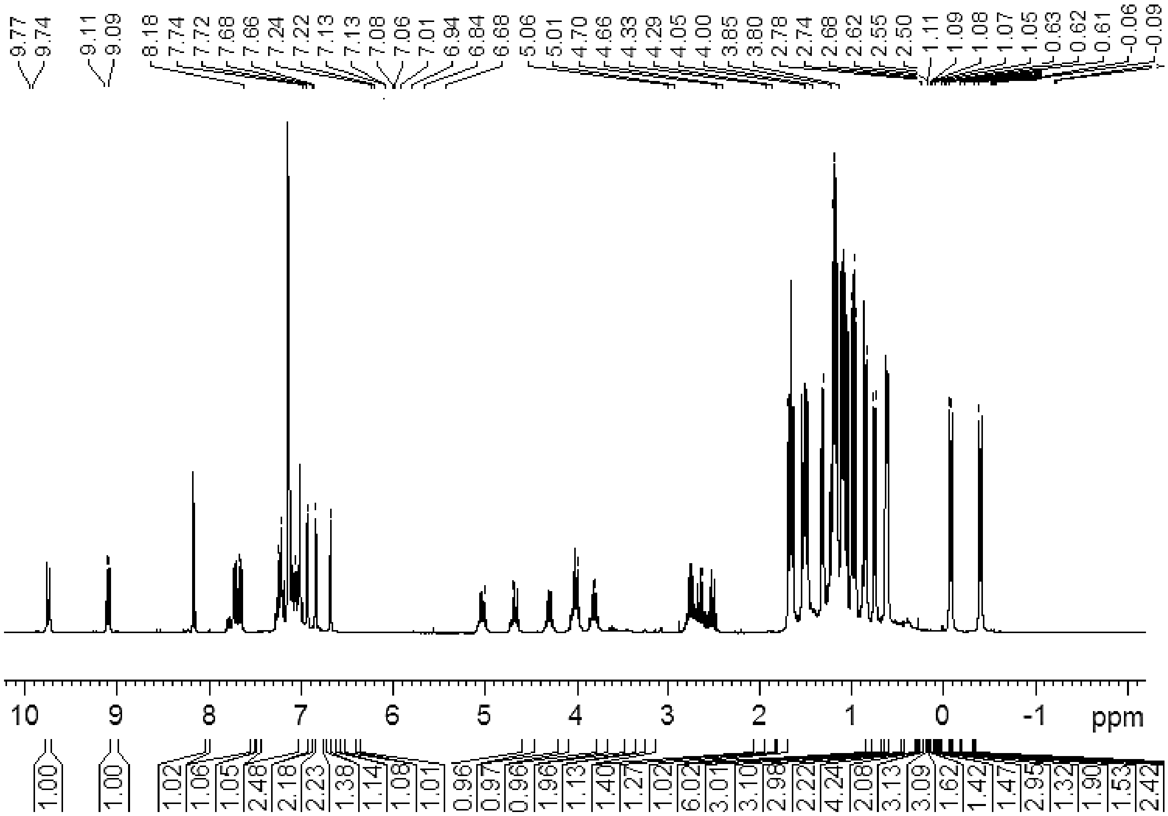

Figure 21. ^{1}H NMR spectrum of the reaction mixture of disilenide **27** with **99** after work-up.

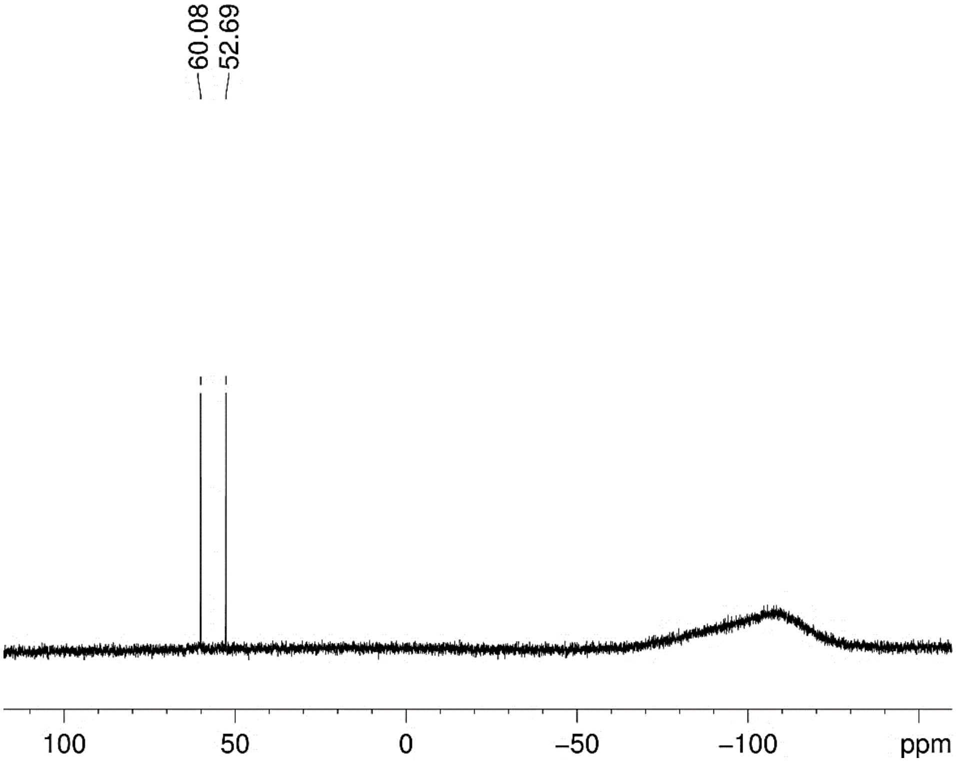

Figure 22. ^{29}Si NMR spectrum of the reaction mixture of disilenide **27** with **99** after work-up.

The ^{1}H NMR spectrum (Figure 21) shows diagnostically sharp low-field signals for the different anthracene protons at δ = 9.75, 9.09, 8.18, 7.69, 7.01, 6.93, 6.84, and 6.68 ppm. The multiplets in the range 7.02 to 7.27 ppm, overlapping with the protons of the aromatic systems, can be attributed to the aromatic protons of the Tip units. Furthermore, the distinct heptets in the isopropyl region and the well-resolved doublets of equal intensity in the alkyl region indicate that the reaction proceeds in a selective manner.

The ^{29}Si NMR spectrum exhibits only two resonances at δ = 60.08 and 52.69 ppm characteristic of the disilene silicon atoms (Figure 22).

Crystallization at −26 °C from pentane yields 1.10 g (87%) as purple crystals (mp. 168 °C).

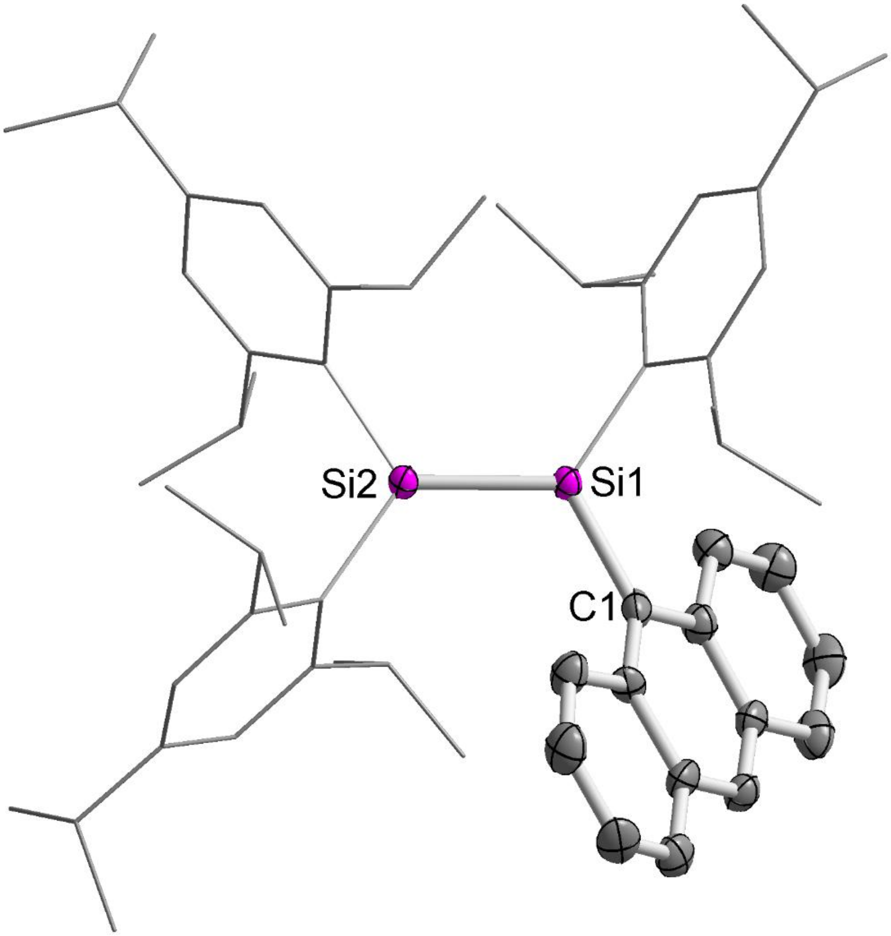

Figure 23. Molecular structure of **100** in the solid state (thermal ellipsoids at 50%, H atoms and disordered ^{i}Pr groups are omitted for clarity). Quality of data insufficient for discussion of bonding parameters.

X-ray analysis confirmed the NMR spectroscopic findings and revealed the structure of disilene **100** (Figure 23). Due to unsatisfactory crystal quality of **100**, only the connectivities could be confirmed, but no bond lengths or angles can be reliably discussed.

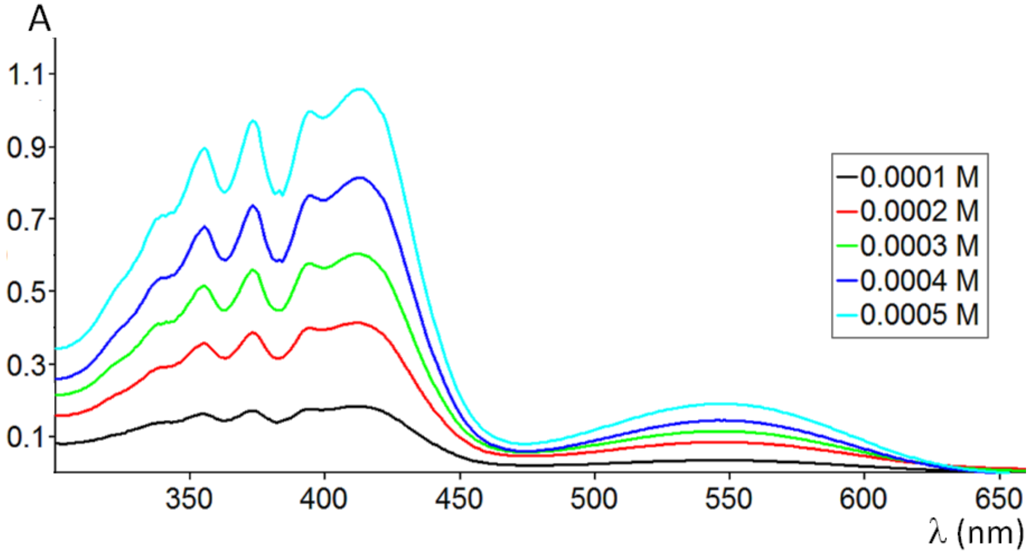

Figure 24. UV/vis spectra of **100** in hexane at different concentrations.

The UV/vis spectrum of disilene **100** in hexane shows a broad absorption band with maximum absorption wavelength at λ_{max} = 412 nm (ε = 21500 $M^{-1}cm^{-1}$) accompanied by a weaker more red-shifted band at λ_{max} = 550 nm (ε = 3800 $M^{-1}cm^{-1}$). In addition, disilene **100** exhibits several broad overlapping bands between 300 and 400 nm with an extinction coefficient of approximately $\varepsilon \cong$ 19500 $M^{-1}cm^{-1}$ that can be assigned to the anthracene ring itself (Figure 24).

3.1.2.6. Reactivity of Disilenide 27 towards Bromo di(naphtyl) Anthracene 101

In order to investigate how an increased π-conjugation of the organic linker would influence the incorporation of disilenide **27**, 2-bromo-9,10-di(2-naphthyl) anthracene **101** was reacted with with one equivalent disilenide **27** in benzene solution (Scheme 37).

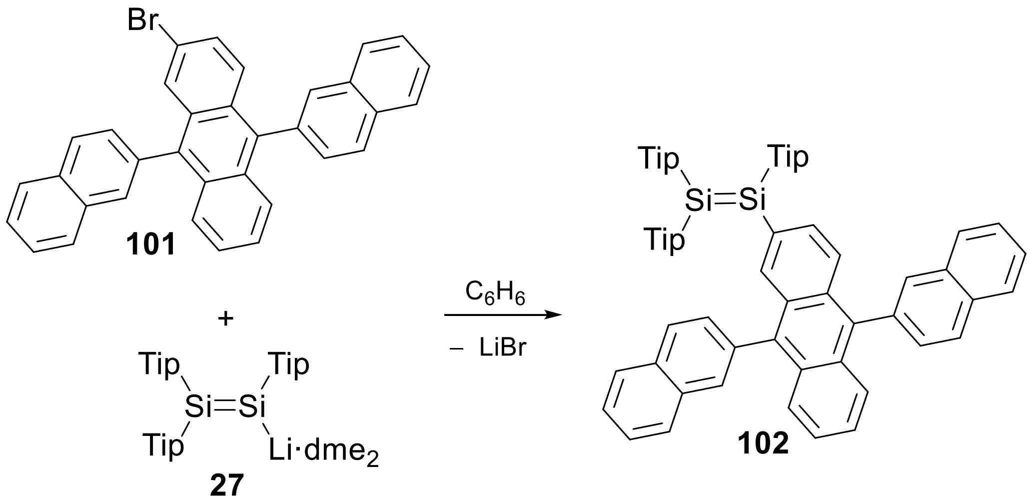

Scheme 37. Reaction of **101** with one equivalent disilenide **27** and the postulated product **102**.

A color change from the orange-red color of disilenide **27** to a burgundy red was observed. Full conversion into disilene **102** was checked by ^{1}H NMR and ^{29}Si NMR spectroscopy.

While most of the diagnostic aromatic signals in the ^{1}H NMR spectrum are a complex multiplet due to the overlapping peaks and are not suitable for analysis, two singlet resonances at δ = 7.00 and 7.03 ppm that can be assigned to the aromatic protons of two of the three inequivalent Tip groups are observed (Figure 25).

The ^{29}Si NMR spectrum of the reaction mixture revealed the quantitative formation of a new Si=Si-containing species with only two resonances at δ = 70.79 and 57.56 ppm in the typical range for disilenes[97] suggesting the formation of disilene **102** (Figure 26).

The reaction proceeded cleanly to afford the anticipated disilene **102** as a burgundy red precipitate from hexane.

Recrystallization of the precipitate from hexane, or pentane, led to microcrystals product in 86% yield (mp. 180°C), which were of insufficient quality for analysis by X-ray diffraction. Despite repeated crystallization from several solvents (pentane, hexane, benzene and toluene), no measurable single crystals could be obtained.

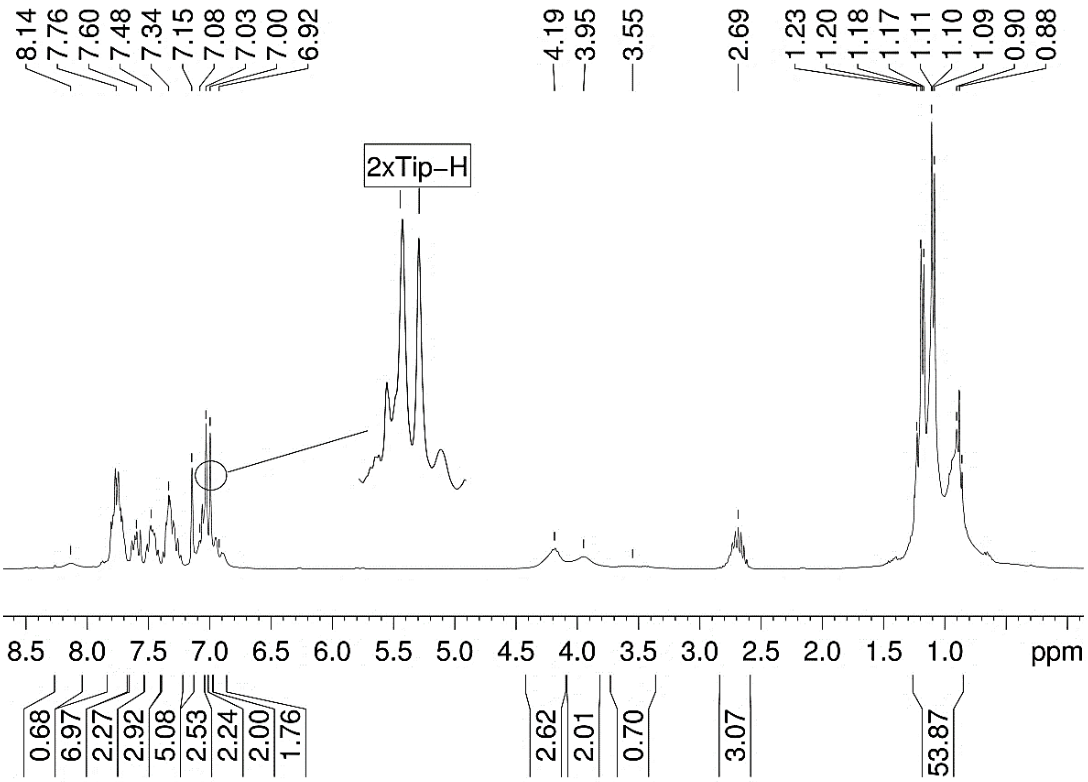

Figure 25. ^{1}H NMR of the reaction mixture of one equivalent disilenide **27** with **101** in C_6D_6 at 300 K.

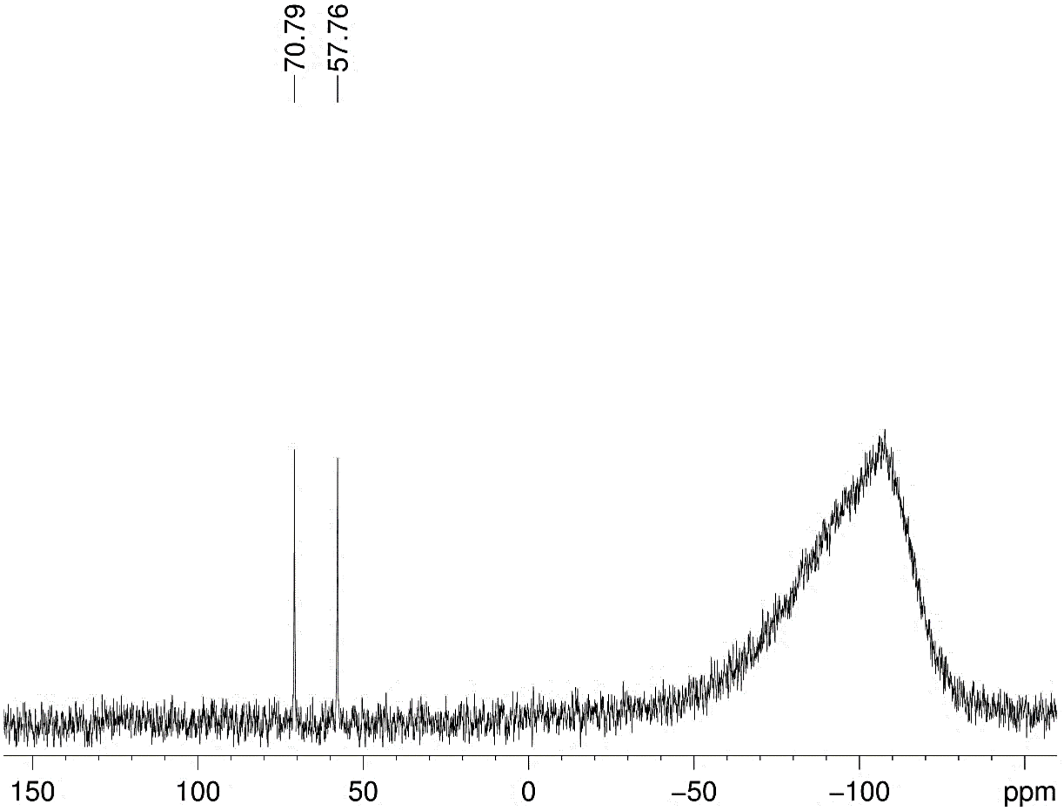

Figure 26. ^{29}Si NMR of the reaction mixture of one equivalent disilenide **27** with **101** in C_6D_6 at 300 K.

Similar to anthryl substituted disilene **100**, the UV/vis spectrum of disilene **102** in hexane shows a broad absorption band with maximum absorption wavelength at λ_{max} = 406 nm (ε = 38800 $M^{-1}cm^{-1}$) accompanied by another band at λ_{max} = 530 nm with a lower molar extinction coefficient (ε = 23000 $M^{-1}cm^{-1}$). Disilene **102** exhibits several broad absorption bands between 350 and 400 nm, probably due to the organic substituent itself (Figure 27).

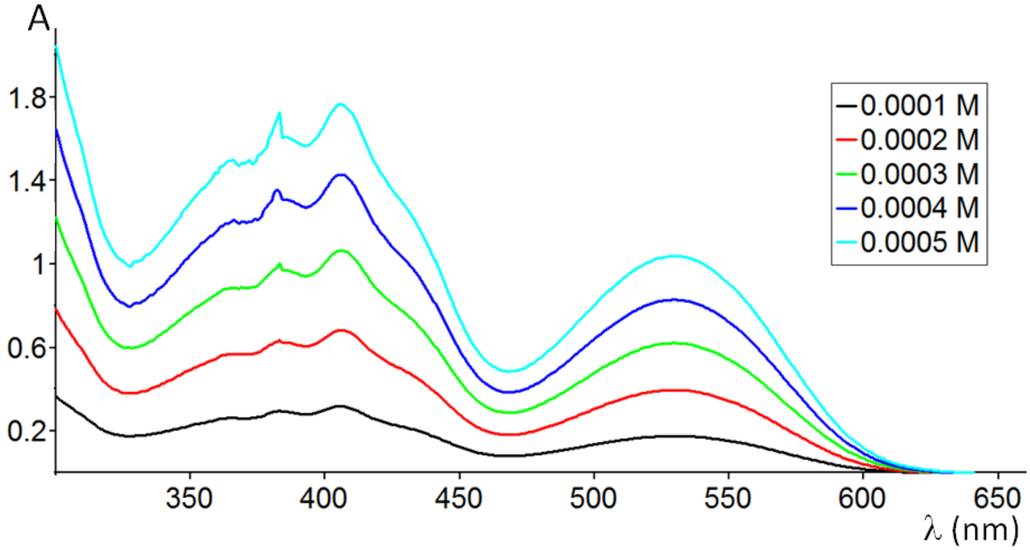

Figure 27. UV/vis spectra of pure **102** in hexane at different concentrations.

Figure 28. Pure disilene **102** at ambient temperature in solid state. (left) under room light, (right) under irradiation at 360 nm.

More importantly, the incorporation of Si=Si moieties into π-conjugated systems in case of pure disilene **102** results in fluorescence at room temperature in solid state (Figure 28) and hexane solution.

Thus, disilene **102** was subjected to fluorescence spectroscopic measurements in order to characterize its excitation and emission properties. The excitation spectra were determined by measuring the emission intensity at a fixed wavelength, while varying the excitation wavelength. Similarly, the emission spectra were obtained by recording at a fixed excitation wavelength.

In hexane solution at room temperature, **102** shows the maximum wavelength excitation at λ_{max}^{exc} = 404 nm for λ_{em} = 460 nm, and the maximum wavelength emission at λ_{max}^{em} = 431 nm for λ_{ex} = 350 nm (Figure 29).

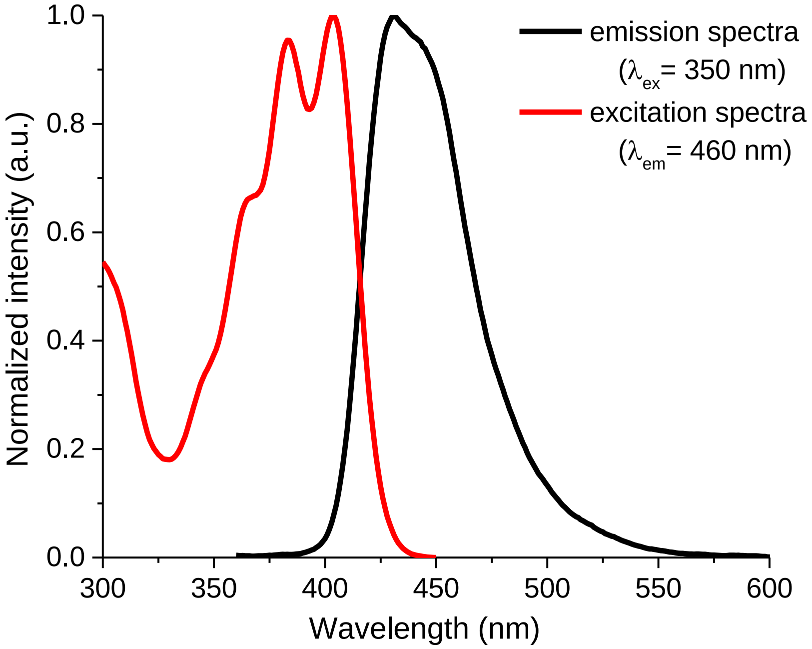

Figure 29. Excitation and emission spectra of **102** in hexane solution at room temperature.

In similar fashion, but in solid state at room temperature, compound **102** has a maximum wavelength excitation at λ_{max}^{exc} = 596 nm for a detectable emission intensity (λ_{em} = 710 nm), while a maximum emission wavelength (λ_{max}^{em} = 587 nm) occurs at a unique excitation wavelength of 560 nm (Figure 30).

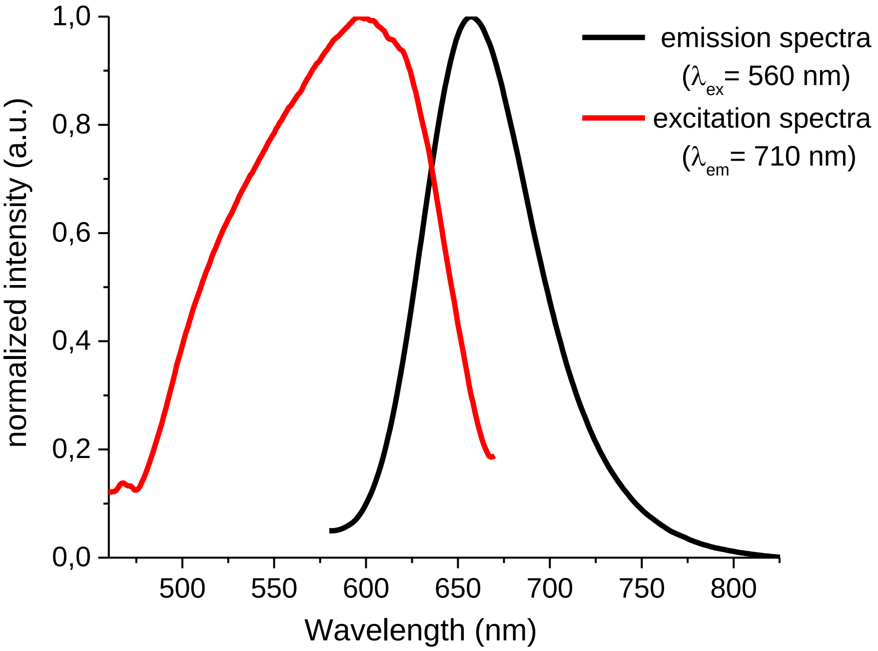

Figure 30. Excitation and emission spectra of **102** in solid state at room temperature.

Unfortunately, the quality of the emission data was insufficient for the extraction of reliable lifetime data for this system. It should be noted, however, that disilene **102** shows an enhanced photoemission in solid state compared to solution with a slightly increased albeit still low quantum yield (Φ = 0.11% in the solid state; $\Phi = 0.06\%$ in solution).

3.1.2.7. Reactivity of Disilenide 27 towards Bromo (naphtyl) Carbazole 103

Inspired by previous results, the reactivity of **27** towards oligoaromatic containing tertiary amine functionality was also examined by metathesis of disilenide **27** with compound **103** (Scheme 38).

No color change of the orange-red reaction mixture was detected after addition of the one equivalent of **27** to **103** in benzene solution. However, the formation of a white precipitate (presumably LiBr) indicated that a reaction had taken place.

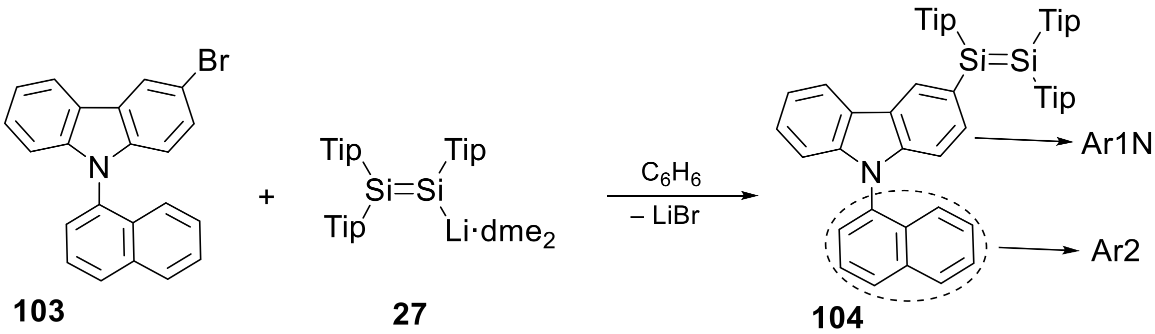

Scheme 38. Anticipated reaction of one equivalent disilenide **27** with **103**.

NMR spectroscopic analysis of the reaction mixture showed the quantitative conversion to disilene **104**. The ^{29}Si NMR in C_6D_6 (Figure 31) features only two signals at δ = 74.40 and 52.28 ppm in the expected range for Si-Si double bonds.

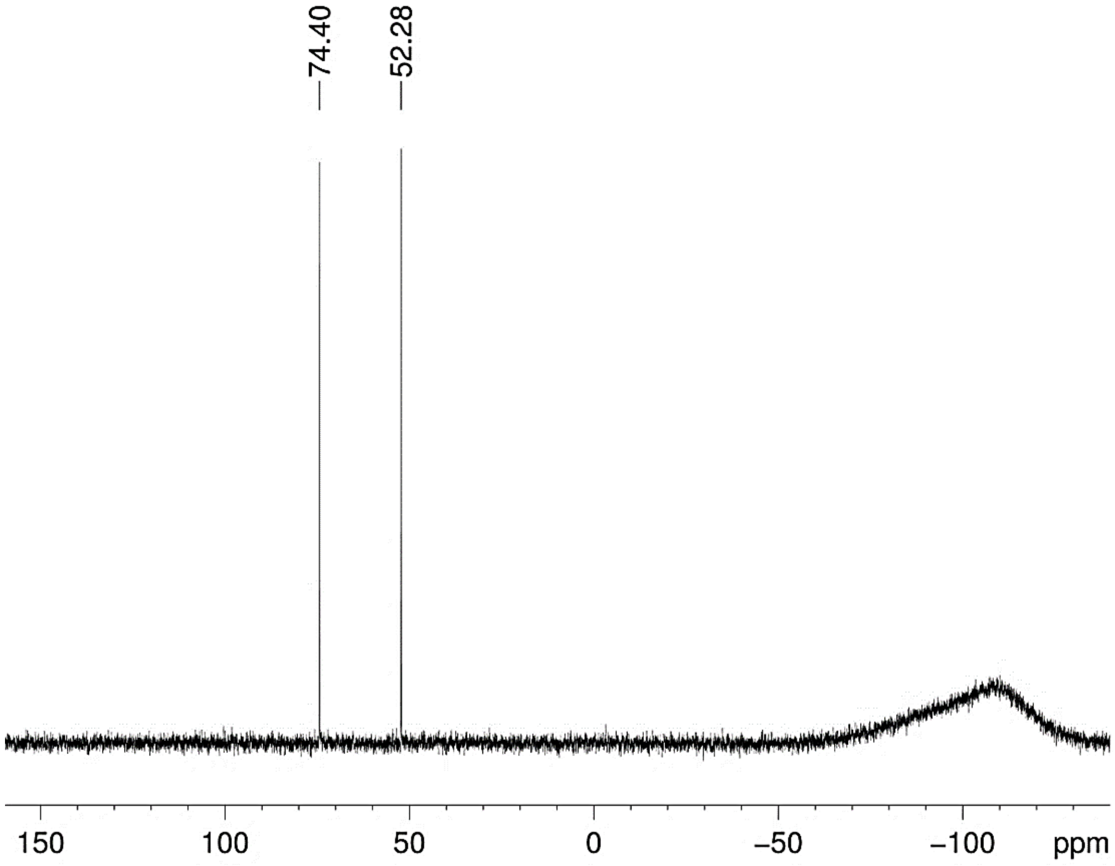

Figure 31. ^{29}Si NMR spectrum of anticipated disilene **104** in C_6D_6 at 300 K.

Furthermore, in the ^{1}H NMR spectrum the three characteristically sharp singlets at chemical shifts at δ = 7.10, 7.14 and 7.21 ppm can be assigned to the aromatic protons of the Tip units (Figure 32).

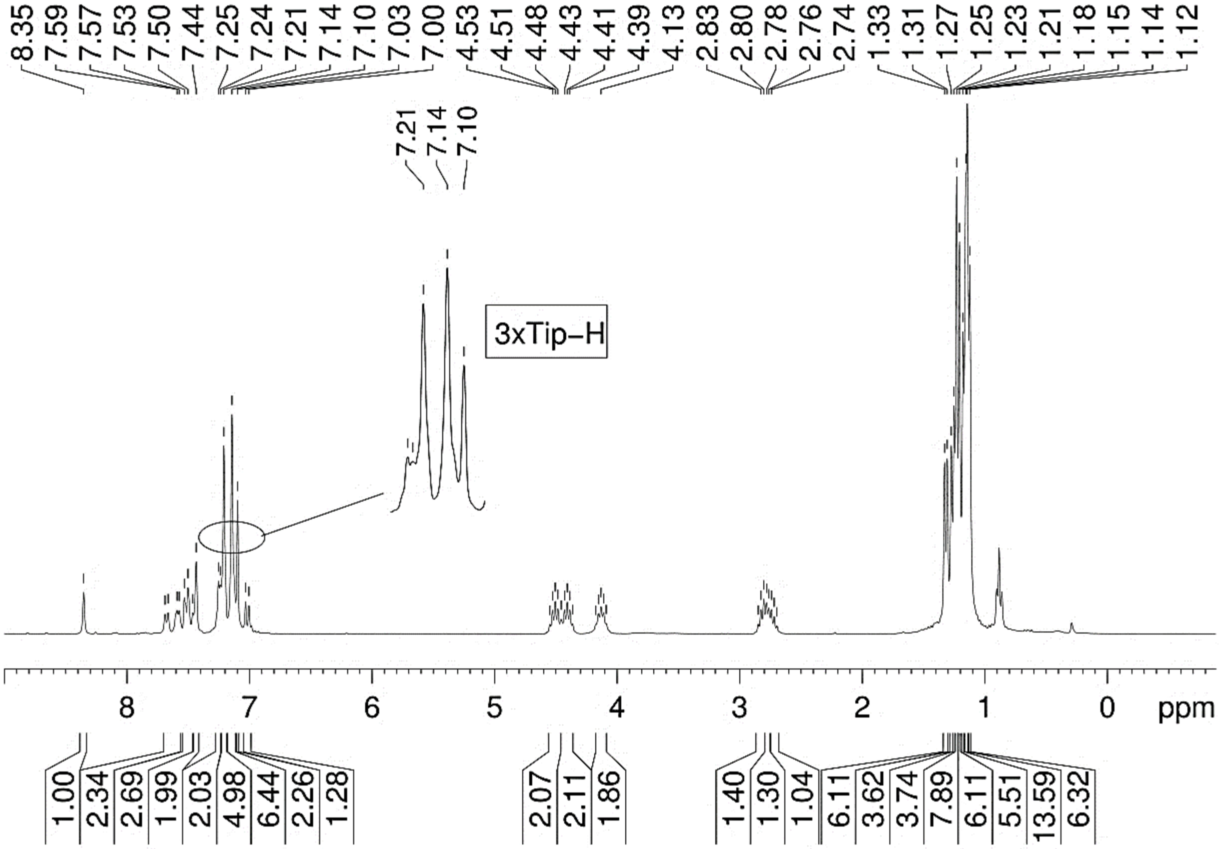

Figure 32. ^{1}H NMR of the reaction mixture of one equivalent disilenide **27** with **103** in C_6D_6 at 300 K.

The two-dimensional ^{29}Si-^{1}H correlation (Figure 33) is a very useful tool to distinguish between aromatic protons of Ar1N, Ar2 and the Tip units. No cross-peaks are detected between the two ^{29}Si NMR resonances and the protons of the remote Ar2 unit. The more shielded resonance shows two equally intense cross-peaks to the aryl hydrogen atoms of two Tip moieties, while for the low-field resonance only one equally intense cross-peak to one Tip group as well as a somewhat weaker cross-peak to the Ar1N moiety are observed. It should be noted that the employed HMQC experiment is optimized for coupling constants of the size typically observed between ^{29}Si and the aryl hydrogen atoms of directly bonded Tip groups.

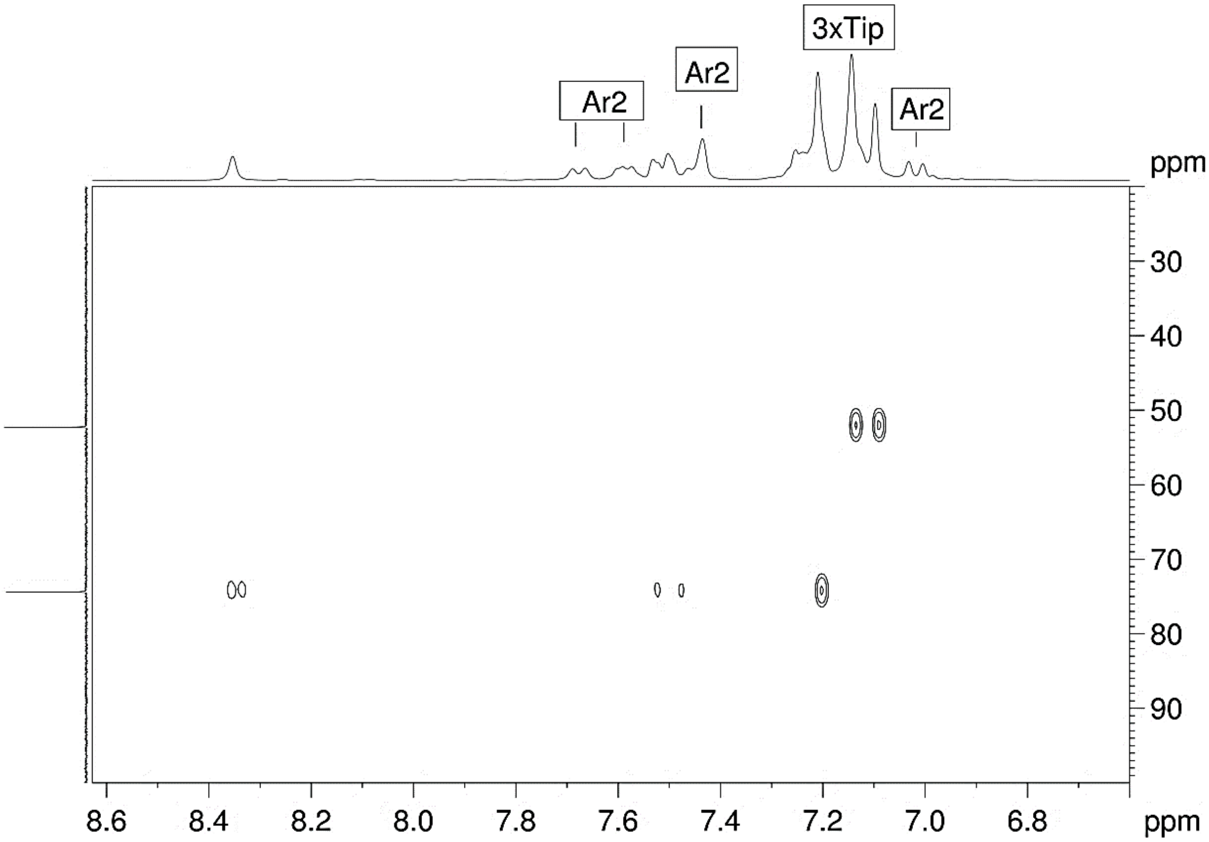

Figure 33. 2D ^{29}Si-^{1}H NMR correlation spectrums of anticipated disilene **104**.

Crystallization attempts from a variety of solvents (pentane, hexane, benzene and toluene) remained unsuccessful. However, an orange solid (mp. 163 °C) was obtained in 90% yield as a precipitate from hexane.

UV/vis spectroscopy shows a maximum absorption wavelength at λ_{max} = 447 nm (ε = 17300 $M^{-1}cm^{-1}$), which is a reasonable value for a Si=Si moiety. The absorption maxima of the naphthyl carbazole derivative are slightly red-shifted compared to other aryl-substituted disilenes. The naphthyl carbazole based backbone may force the Si=Si into a more pronounced *trans*-bending or twisting due to the increased rigidity, a reasoning that cannot be confirmed in the absence of a solid state structure.

Multinuclear NMR analysis and UV/vis spectroscopy, however, strongly support the anticipated formation of the desired carbazole substituted disilene **104**.

3.1.3. Reactivity of Disilenide 27 towards Aryl Dihalides (X-LU-X)

Encouraged by the successful substitution reactions with oligo(aromatic) halides as substrates, the next step was to establish selective reactions with oligo(aromatic) dihalides.

3.1.3.1. Reactivity of Disilenide 27 towards Diiododuryl 105

Diiododurene **105** was reacted with two equivalents of disilenide **27** in benzene two give a red orange reaction mixture (Scheme 39).

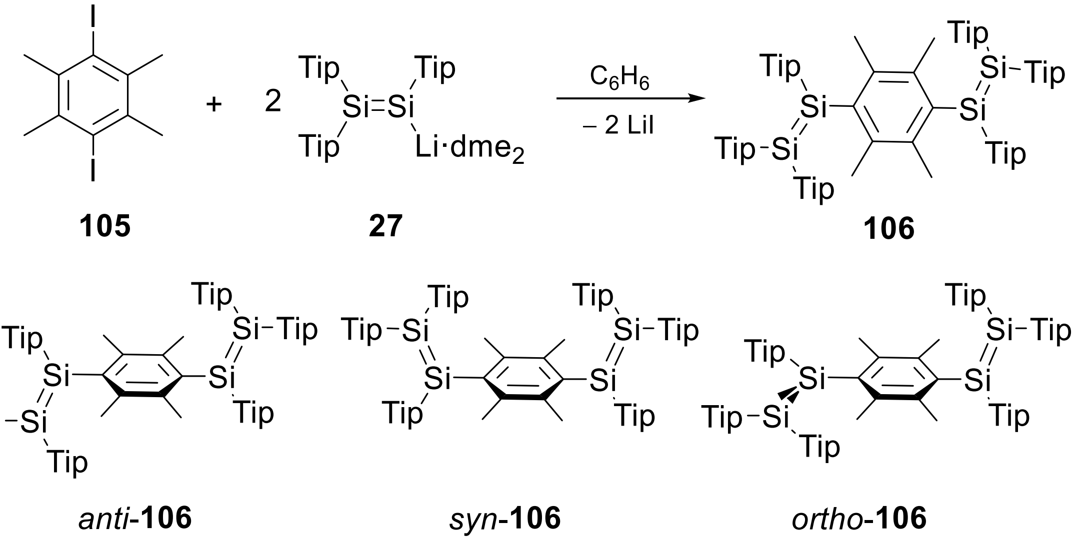

Scheme 39. Reaction of **105** with 2 equivalents disilenide **27** and postulated *syn-*, *anti-*, and *ortho-*conformations of resulting bridged tetrasiladienes.

Most of the signals in the ^{1}H NMR of the reaction mixture are overlapping and do not lend themselves to straightforward analysis.

The DEPT135 NMR spectrum (Figure 34), however, shows two high-field signals at δ = 34.60 and 34.39 ppm in a similar region as in the spectrum of duryl disilene **94**, which suggests that a presumably symmetric compound with two disilenyl groups attached to the durene moiety could have been formed.

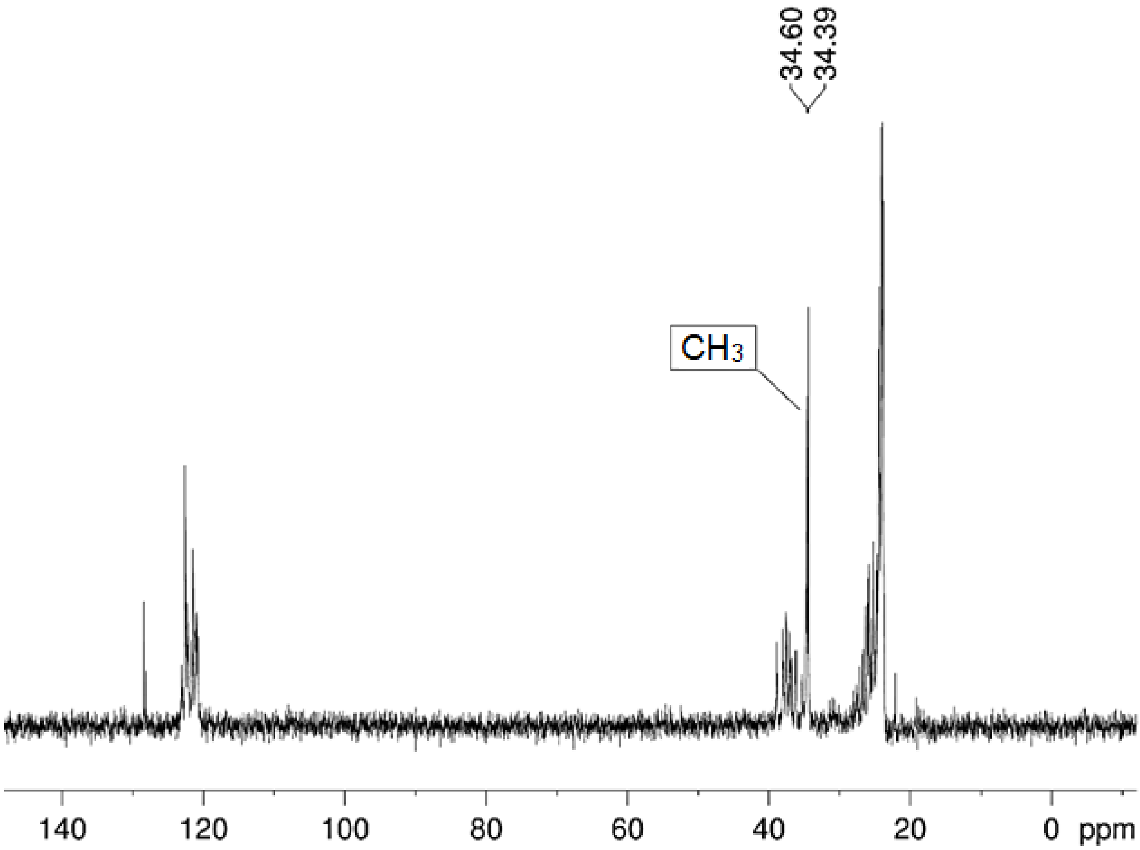

Figure 34. Dept135 NMR spectrum of reaction mixture between diiododurene **105** and disilenide **27**.

The ^{29}Si NMR (Figure 35) shows a surprisingly large number of signals in the typical range for disilenes from δ = 52.12 and 58.75 ppm, which at first could be interpreted as an indication for a product mixture, *e.g.* of mono- and disubstitution product. As this hypothesis would only account for two sets of signals, the question was raised whether the three sets of two ^{29}Si signals each could instead be attributed to the presence of different rotational conformers that interconvert only slowly on the NMR timescale.

Crystallization at room temperature overnight from hexane yields 0.67 g (65%) of **106** as well-shaped orange crystals (mp. 184°C). The NMR data of the crystalline material did not show any changes in comparison to the crude reaction mixture, which lends support to the assumption that slowly interconverting rotamers are responsible for the large number of signals.

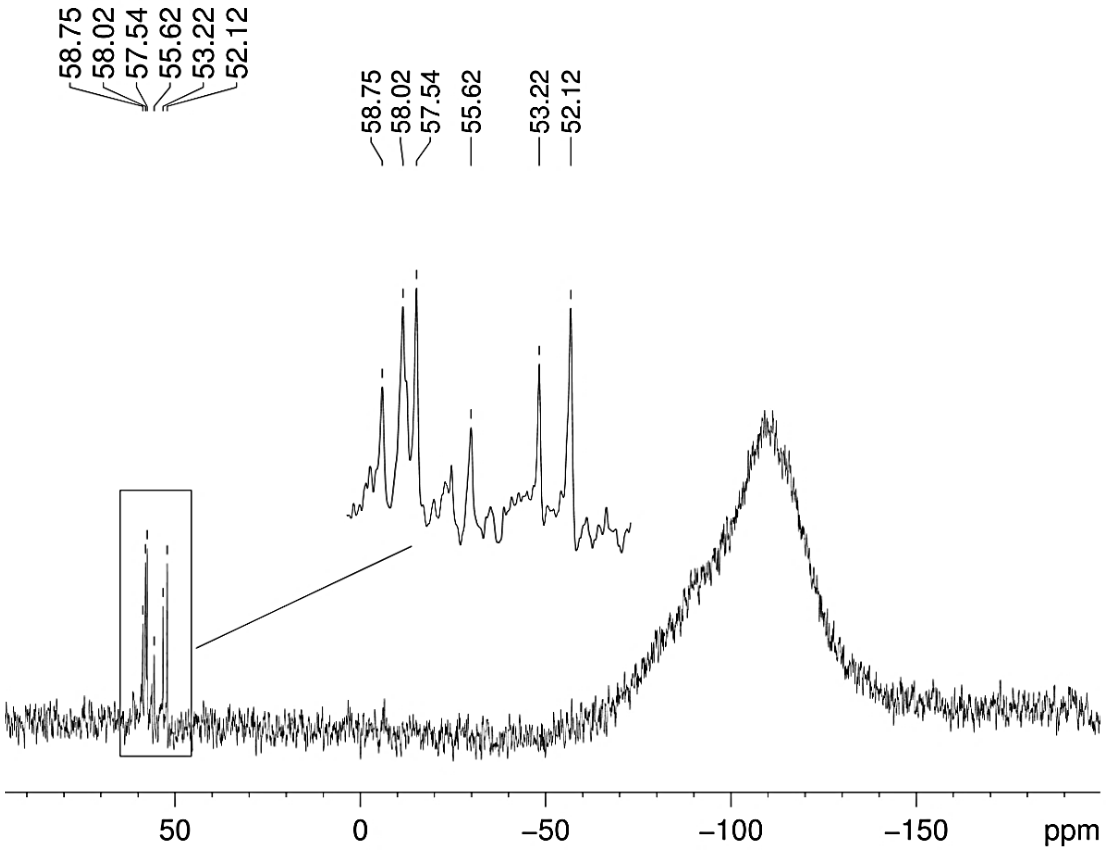

Figure 35. ^{29}Si NMR spectrum of reaction mixture resulting from diiododurene **105** and disilenide **27**.

In order to prove the hypothesis, the compound was investigated by ^{29}Si NMR at variable temperature (Figure 36). Cooling to 253 K resulted in a significant sharpening of the signals. The four more intense signals can be tentatively assigned to the rotamers of higher symmetry with chemical equivalence of the disilenyl groups. The set of slightly higher intensity at δ = 52.11 and 57.44 ppm is plausibly due to the sterically slightly more favorable *anti* arrangement of the disilenyl moieties (*anti*-**106**, C_i symmetry), while the lower intensity pair at δ = 53.23 and 58.03 ppm is attributed to *syn*-**106** (C_s symmetry). The additional four ^{29}Si NMR signals at δ = 55.61, 56.30, 57.92 and 58.76 ppm of equal intensity apparently stem from a less symmetric rotamer, probably *ortho*-**106** in which only one of the disilenyl groups assumes the sterically favorable orthogonal position to the durylene linker, while the other remains in the electronically preferred coplanar conformation. At 253 K, the three rotamers *anti*, *syn* and *ortho*-**106** are observed in the approximate ratio of 7: 3: 2), respectively. Increasing the temperature should accelerate the interconversion of the rotamers and indeed only two sharp peaks (57.84 and 52.92 ppm) are observed in the ^{29}Si NMR at 353 K. Evidently, at higher temperature the exchange is fast on the NMR time scale and ^{29}Si VT-NMR analysis thus unambiguously proves the presence of a single and uniform compound, the durylene-bridged tetrasiladiene **106**.

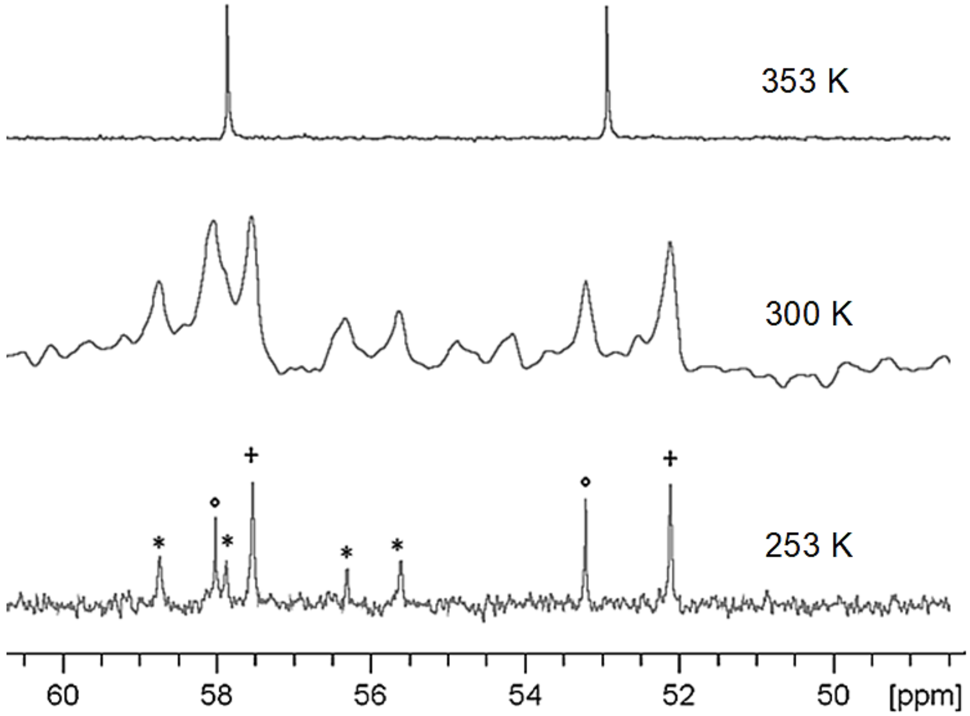

Figure 36. ^{29}Si VT-NMR of durene-bridged tetrasiladiene **106** at different temperatures in d_8-toluene (253 K- 353 K), and the resonances for the expected 3 rotamers, (+): signals can be assigned to *anti*-**106**, (°): signals can be assigned to *syn*-**106** and (∗): signals can be assigned to *ortho*-**106**.

Furthermore, the well-resolved CP-MAS ^{29}Si NMR of **106** (Figure 37) shows only one signal in at δ = 55.42 ppm thus lending the hypothesis of conformational equilibria of **106** in solution further support. Apparently, the two expected signals in the range of aryl disilenes overlap in one signal (55.42 ppm), which is, however, irrelevant for the prove of purity of the bulk of **106.**

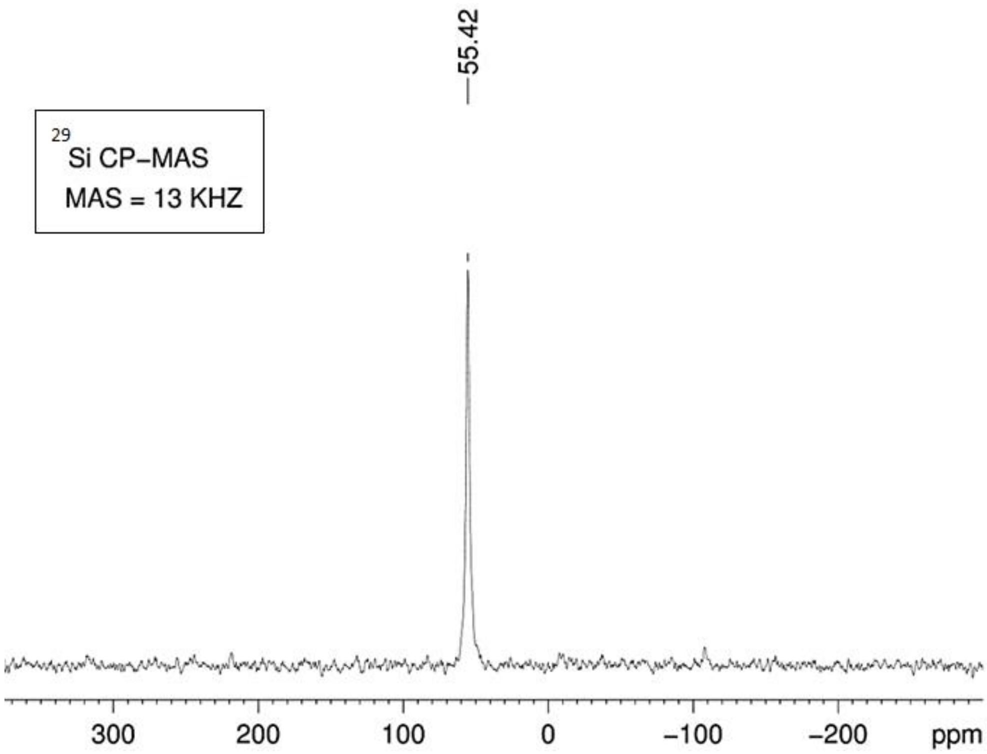

Figure 37. CP-MAS ^{29}Si NMR of **106** in solid state at 300 K.

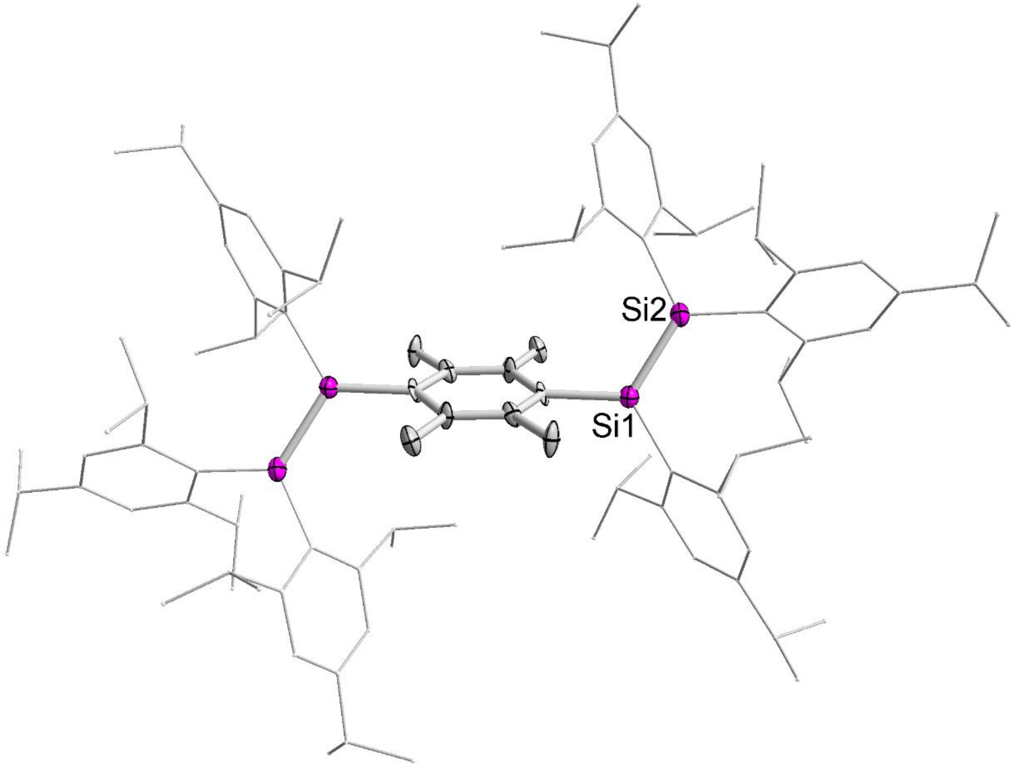

Figure 38. Molecular structure of *anti*-**106** in the solid state (thermal ellipsoids at 50%, H atoms and disordered ^{i}Pr groups are omitted for clarity). Quality of data insufficient for discussion of bonding parameters.

The structure of **106** was finally confirmed by X-ray diffraction on single crystals showing only the *anti*-conformer (Figure 38), although the considerable disorder in the crystals is prohibitive with regards to a discussion of structural parameters.

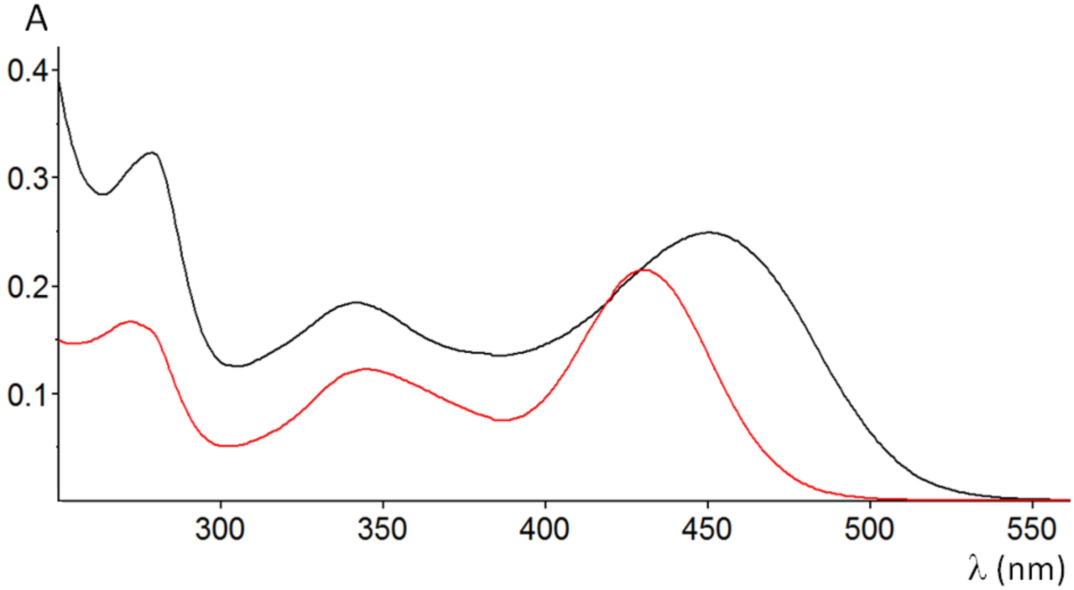

Figure 39. Normalized UV/vis spectrum of disilene **94** (red) and tetrasiladiene **106** (black) together in hexane at room temperature using same c = 0.0005 M.

UV/vis spectroscopy (Figure 39) shows a moderate red-shift of $\Delta\lambda$ = 20 nm of the longest wavelength absorption of **106** (λ_{max} = 450 nm) compared to that of disilene **94** (λ_{max} = 430 nm). The intensity (ε = 19700 $M^{-1}cm^{-1}$) is comparable to that of **94** (ε = 17300 $M^{-1}cm^{-1}$). This can again be explained by the presence of different conformers in solution. Unlike in the case of the para-phenylene bridged tetrasiladiene **67** (λ_{max} = 508 nm), the pronounced orthogonality of the disilenyl groups and the durylene linker in **106**, leads to an effective disruption of the conjugation path. Only the proposed ortho-conformer would be conjugated, albeit just with the participation of one coplanar Si=Si unit. This limited conjugation would be in accordance with the slightly narrower HOMO-LUOMO gap necessary for such a red-shift.

3.1.3.2. Reactivity of Disilenide 27 towards Diiodobiphenyl 107

Stirring a mixture of 4,4´-diiodobiphenyl **107** with two equivalents of disilenide **27** in benzene (Scheme 40) led to full conversion into tetrasiladiene **108** according to the appearance of two new signals at δ = 71.04 and 56.01 ppm in the ^{29}Si NMR spectrum (Figure 40).

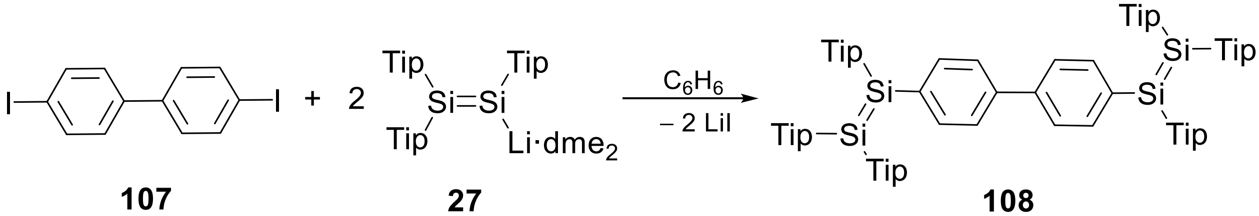

107 **27** **108**

Scheme 40. Synthesis of biphenylene bridged tetrasiladiene **108**.

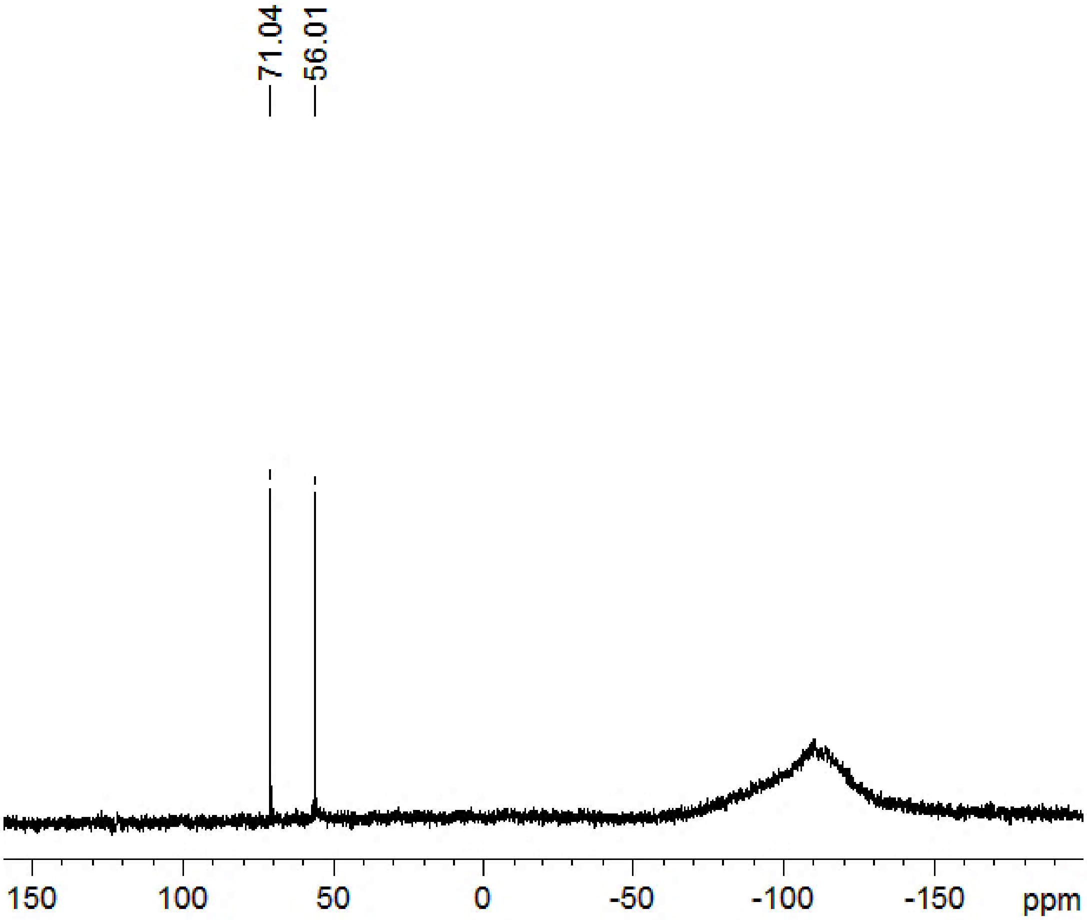

Figure 40. ^{29}Si NMR of the reaction mixture of two equivalents disilenide **27** with **107**.

The ^1H NMR spectrum shows two doublet signals at δ = 6.99 (slightly overlapping with its neighbor singlet signal) and 7.35 ppm that are diagnostic for the biphenylene linker alongside three singlet signals of equal intensity at δ = 7.13, 7.11 and 7.04 ppm for the three individual Tip substituents of each disilenyl functionality in **108** (Figure 41).

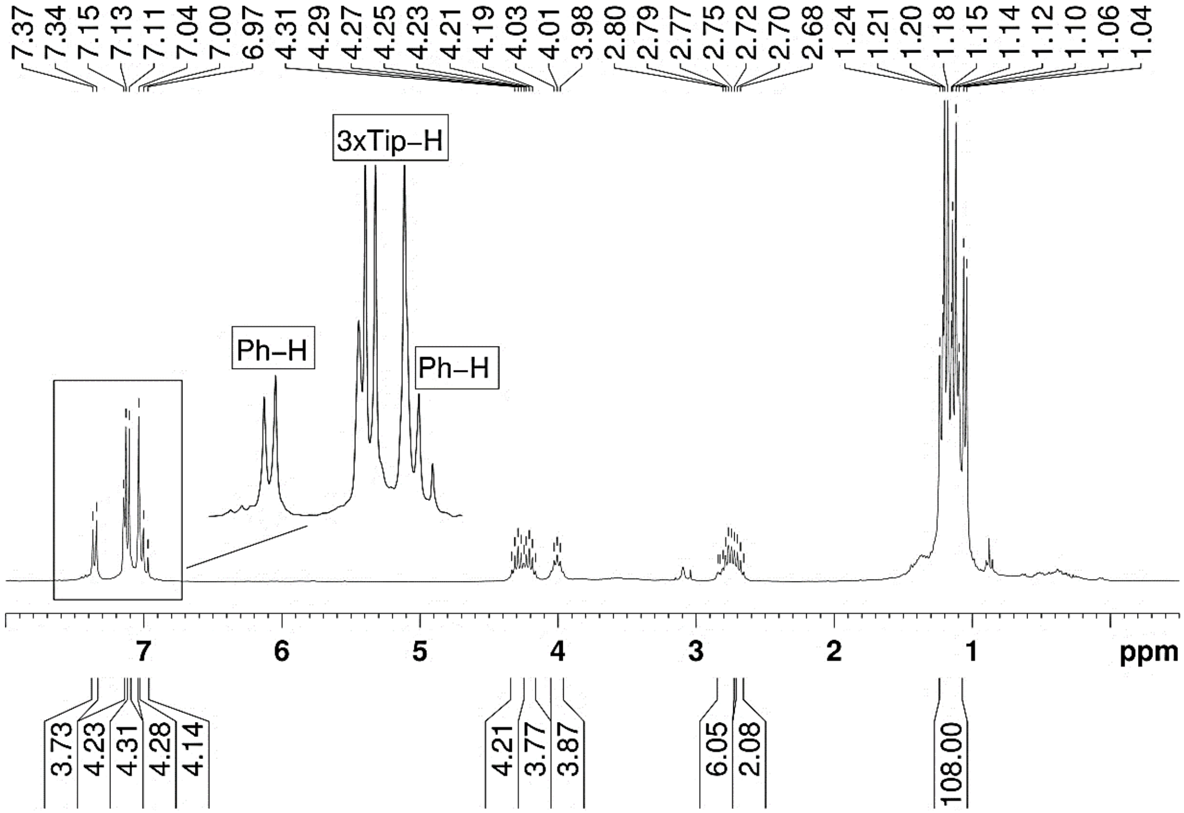

Figure 41. ^1H NMR spectra of biphenylene bridged tetrasiladiene **108**.

On the basis of a ^{29}Si-^1H correlation 2D spectrum, the low-field resonance is as expected assigned to SiTip unit, while the signal at δ = 56.00 ppm is attributed to $SiTip_2$ moieties (Figure 42).

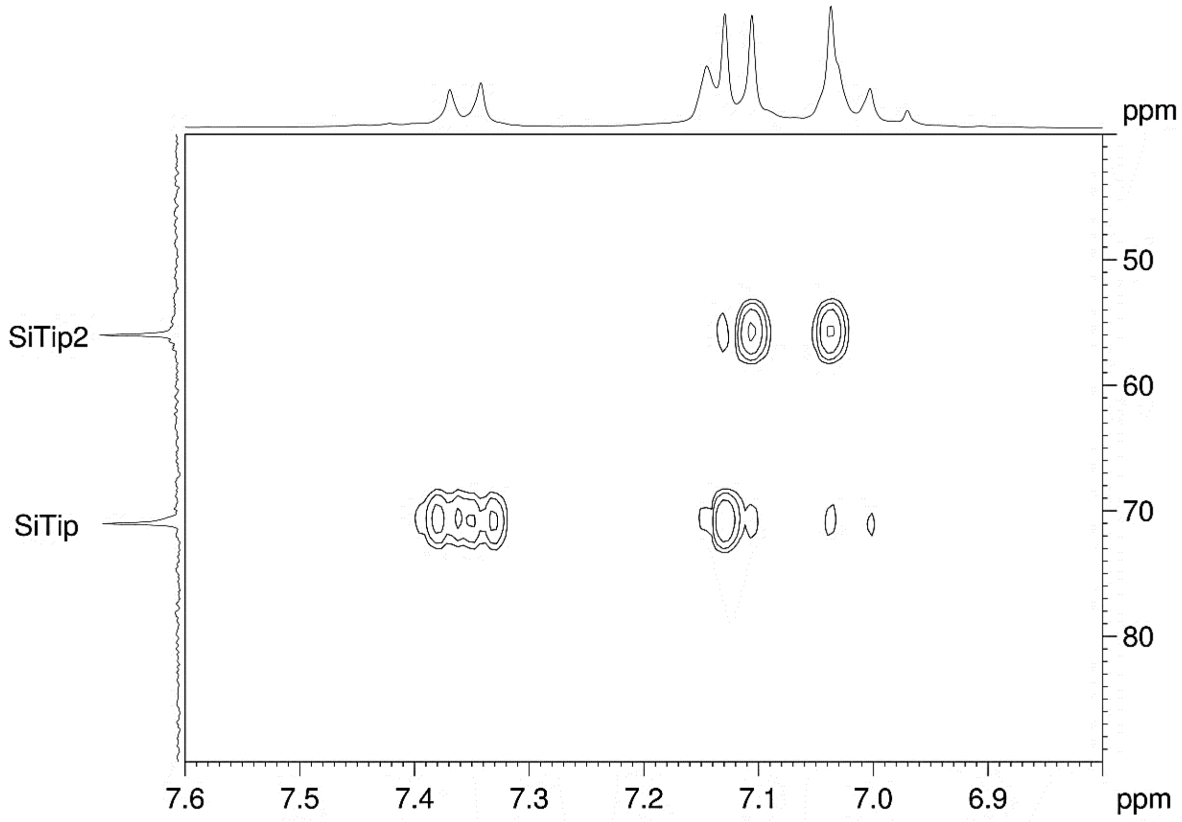

Figure 42. 2D ^{29}Si-^{1}H NMR correlation spectrums of tetrasiladiene **108**.

The product crystallizes from hexane at room temperature as red crystals in 88% yield (mp. 178°C). An X-ray diffraction study confirmed the constitution of **108** as biphenylene-bridged tetrasiladiene (Figure 43).

The coordination environments of the two Si-Si double bonds are almost planar (Σ of angles around Si1 359.52°, Si2 359.8°), but the biphenylene bridge is twisted out of the plane with a torsion angle of 24.85° for Si2−Si1−C1−C2. The two Si=Si bonds crystallographically equivalent and show a bond distance of 2.1460(8) Å, which is in the expected region for aryl substituted disilenes, and at the short end of typical values of planar disilenes.[98] Notably, the Si=Si distance is significantly shorter than the corresponding bonds of the previously reported tetrasiladiene *p*-**67**[80a] [2.1460(8) for **108** vs. 2.1674(8) Å for *p*-**67**]. This somewhat counterintuitive observation can be rationalized by considering the more pronounced *trans*-bending of phenylene-bridged tetrasiladiene *p*-**67** compared to the moderately *trans*-bent **108** (**3a**: θ_{SiTip} = 6.7°; θ_{SiTip2} =

4.2°; *p*-**67**: θ_{SiTip} = 16.5°; θ_{SiTip2} = 19.3°). Also, a twist angle of τ = 11.4° in **108** was observed.

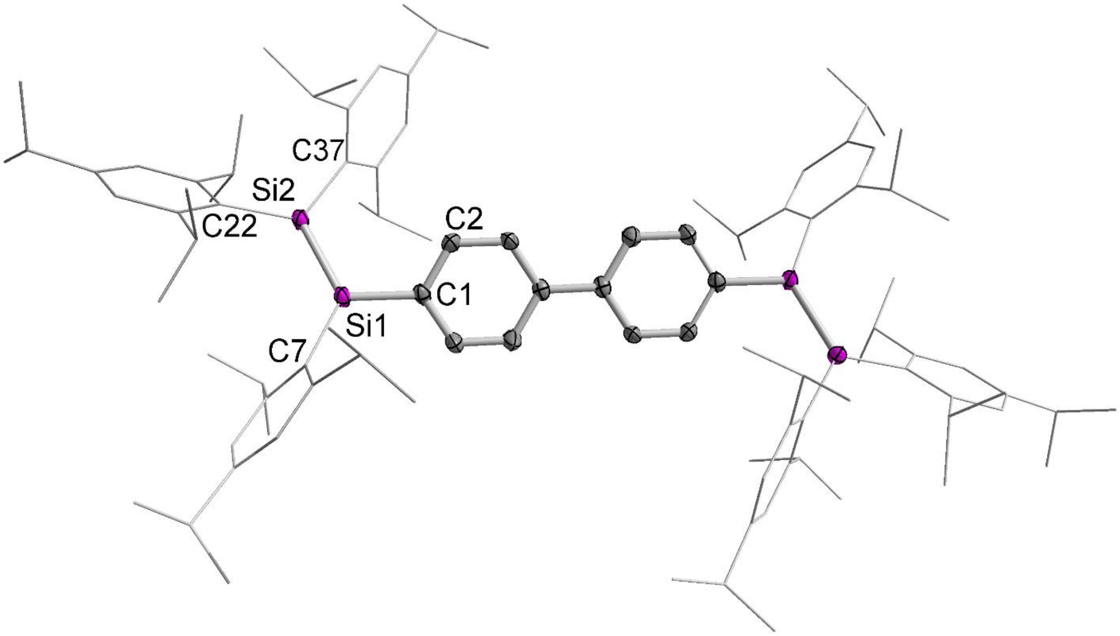

Figure 43. Molecular structure of **108** in the solid state (thermal ellipsoids at 50%, H atoms and disordered ^{i}Pr groups are omitted for clarity). Selected bond lengths [Å] and bond angles [°]: Si1-Si2 2.1460(8), Si1-C1 1.855(2), Si1-C7 1.876(2), Si2-C22 1.884(2), Si2-C37 1.895(2), C(1)-Si(1)-C(7) 117.03(9), C(1)-Si(1)-Si(2) 116.52(7), C(7)-Si(1)-Si(2) 125.97(7), C(22)-Si(2)-C(37) 116.12(9), C(22)-Si(2)-Si(1) 126.15(7), C(37)-Si(2)-Si(1) 117.53 (7).

Compound **108** shows a similar maximum absorption wavelength in the UV/vis spectrum as naphthyl disilene **98** (463 nm), which is strongly blue-shifted by about 45 nm compared to tetrasiladiene *p*-**67**.[80] Despite the more extended conjugated π-electron system in **108** compared to *p*-**67**, the twist along the biphenylene axis (φ = 65. 67°) in **108** possibly disturbs the π-electron and hence lowers the observed λ_{max} value. The intensity of the longest wavelength absorption of **108** (ε = 21000 $M^{-1}cm^{-1}$) is smaller compared to *p*-**67** (ε = 27000 $M^{-1}cm^{-1}$).[80a] A second absorption band in the UV/vis spectrum of **108** is located at λ = 277 nm (35000 $M^{-1}cm^{-1}$) and can be attributed to an internal transition associated to the biphenylene linking group.

3.1.3.3. Reactivity of Disilenide 27 towards Dibromo *para*-terphenyl 109

In analogy to the synthesis of **106** but with one more phenylene moiety in the organic linker**,** two equivalents disilenide **27** were expected to react with 4,4′-dibromo-p-terphenyl **109** to the *para*-terphenylene-bridged tetrasiladiene **110** (Scheme 41).

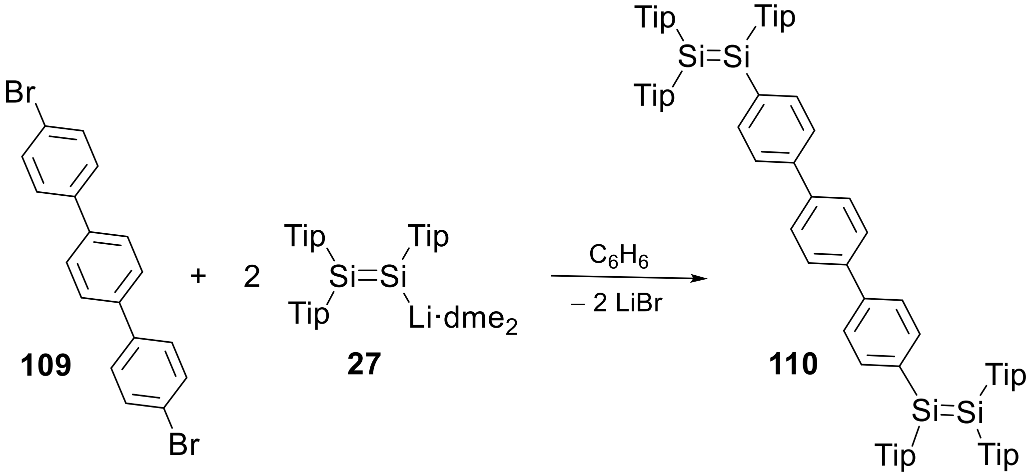

Scheme 41. Reaction of compound **109** with two equivalents disilenide **27** and the postulated product **110**.

No color change of the orange-red reaction mixture was observed after addition of the disilenide **27** to the diborminated *para*-terphenyl substrate. After work-up, however, the ^{29}Si NMR spectrum shows only two signals at δ = 70.90 and 56.11 ppm (Figure 44). These low-field signals are a strong indication for the presence of Si-Si double bond moieties and thus the formation of the targeted terphenylene-bridged tetrasiladiene **110**. The ^{1}H NMR spectrum reveals signals of aromatic protons system in the range of 7.06 to 7.48 ppm. The low-field doublet of the signal at δ = 7.46 ppm can be attributed to the terphenylene protons. Additionally, three singlet signals with same intensity at δ = 7.30, 7.16 and 7.06 ppm can be assigned to the three different aromatic protons of the Tip groups. Furthermore, the signal at δ = 7.14 ppm is of high intensity compared to the other signals. The overlap of terphenylene protons with C_6D_6 merges the expected signals into one signal at δ = 7.14 ppm (Figure 45).

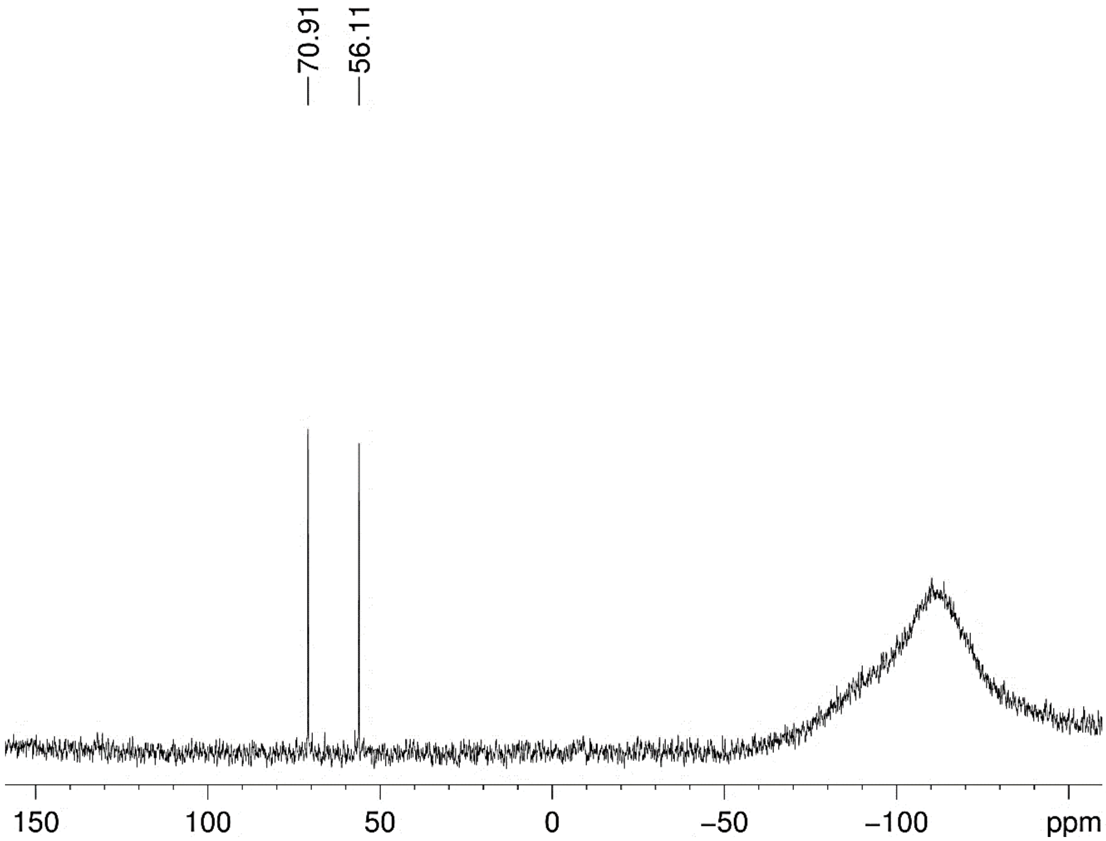

Figure 44. ^{29}Si NMR spectrum of anticipated tetrasiladene **110** in C_6D_6 at 300 K.

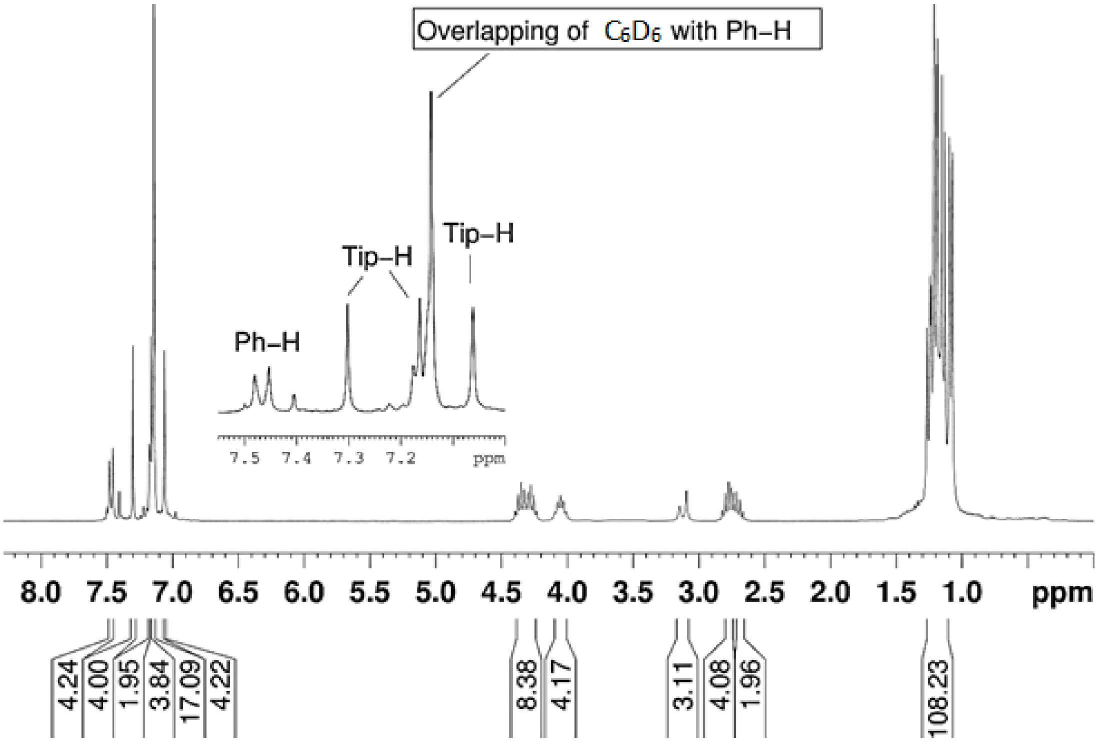

Figure 45. ^{1}H NMR of the reaction mixture of two equivalents disilenide **27** with **109** in C_6D_6 at 300 K.

Crystallization from hexane at room temperature from hexane overnight yields 0.95 g (75 %) as red orange microcrystals (mp. 177°C). Attempts to grow single crystals from benzene, pentane, thf and toluene at room temperature as well as at lower temperature (0 to −20 °C) failed.

The longest wavelength absorption observed in the UV/vis spectrum of **110** (Figure 46) is identical to that observed for biphenylene-bridged tetrasiladiene **108** at λ_{max} = 463 nm. This observation is an agreement with that for the twisted **108**, the abruption of which is also highly blue-shifted in relation to *p*-**67**. Therefore, it is concluded that even the more extended terphenylene linker of tetrasiladiene **110** disrupts the conjugation path by twisting and hence leads to a lower than anticipated λ_{max} value.

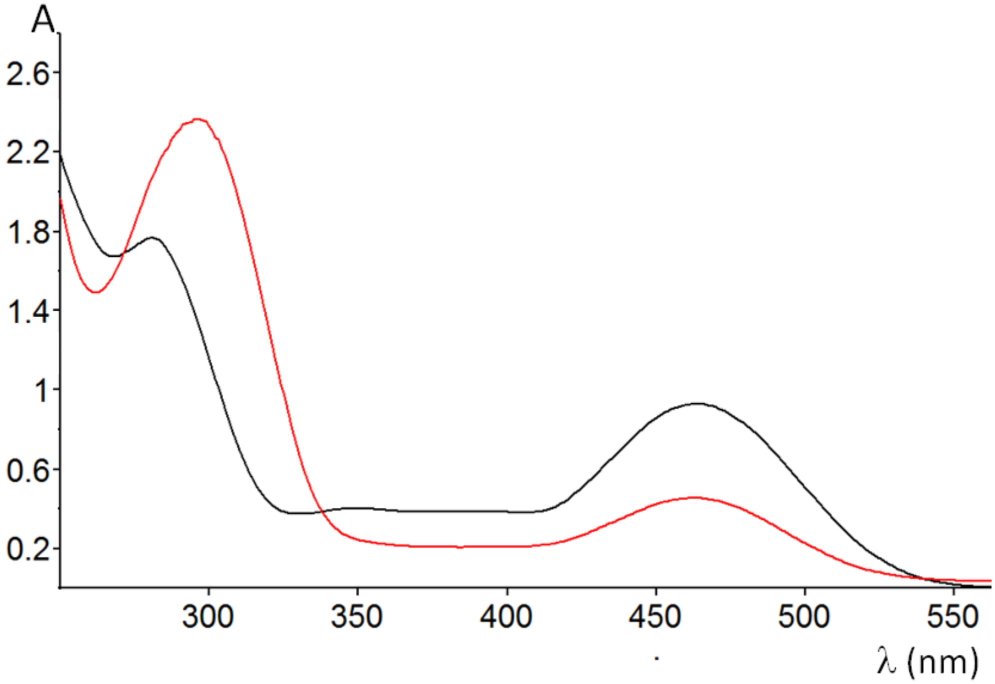

Figure 46. UV/vis spectra of biphenylene- linked tetrasiladiene **108** (black) and terphenylene-linked **110** (red) in hexane at room temperature at identical concentrations (c = 0.0005 M).

The intensity of the longest wavelength absorption of **110** (ε = 8300 $M^{-1}cm^{-1}$) is significantly smaller than that of the corresponding absorption of **108** (ε = 21000 $M^{-1}cm^{-1}$). Apparently, the intensity of the longest wavelength absorption decreases with the number of phenylene bridges, which suggests a decreasing efficiency of the π-conjugation due to the additional conformational freedom associated to longer oligophenylene bridges. An additional absorption band at λ = 296 nm can be assigned to the linking unit itself. Indeed this ligand-centered absorption is red-shifted compared to **108** (λ = 277 nm), which is in accord with the extended π-system going from biphenyl to terphenyl. Moreover, the intensity of the absorption attributed to the linker in **110** is larger (ε = 44600 $M^{-1}cm^{-1}$) compared to **108** (ε = 35000 $M^{-1}cm^{-1}$).

3.1.3.4. Reactivity of Disilenide 27 towards Bis(4-bromophenyl)Acetylene 111

With the goal to further extend the conjugated π-electron system without the possibility of dihedral distortions detrimental to the conjugation efficiency, the reaction of bis(4-bromophenyl)acetylene **111** with two equivalents disilenide **27** was considered (Scheme 42).

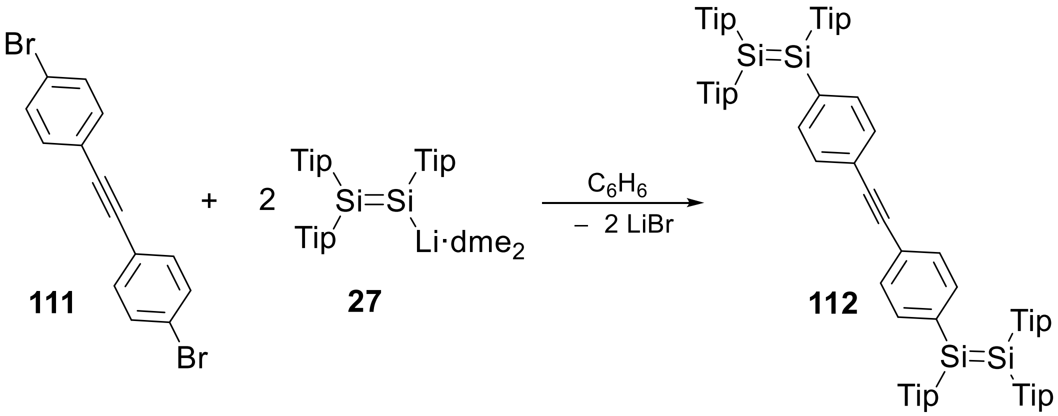

Scheme 42. Synthesis of tetrasiladiene **112**.

After addition of disilenide to the substrate **111**, the reaction mixture turns red and its ^{29}Si NMR spectra reveals two resonances at δ = 69.91 and 57.52 ppm, which are attributed to the two Si=Si bonds (Figure 47).

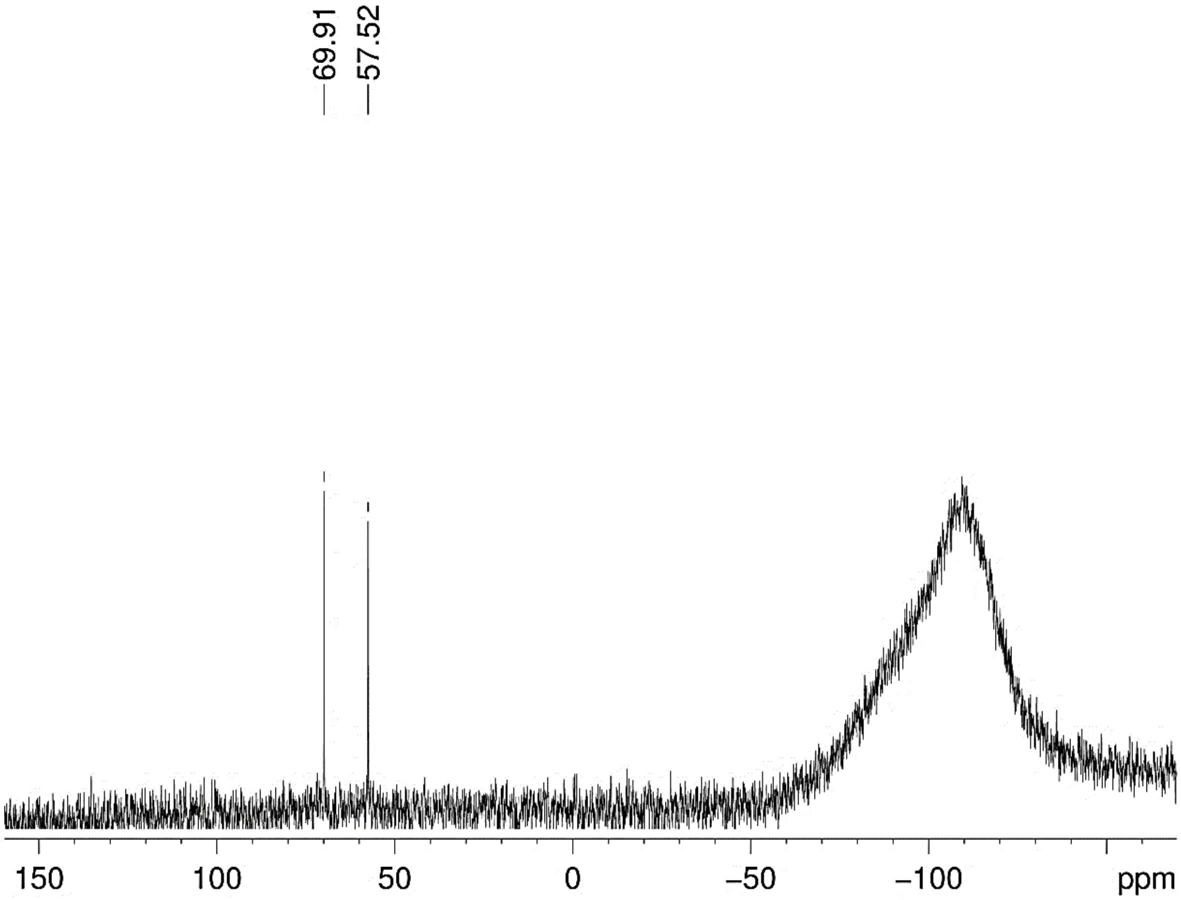

Figure 47. ^{29}Si NMR of the reaction mixture of two equivalents disilenide **27** with **111**.

The low-field region of the ^{1}H NMR spectrum (Figure 48) shows the expected two doublet signals at δ = 7.25 and 7.02 (overlapping with the adjacent singlet signals) ppm for the protons of the two phenylene linker as well as three singlet resonances at δ = 7.11, 7.08 and 7.03 ppm for the three inequivalent Tip groups of each disilenyl functionality. The coupling constants for the two doublets of the phenylene bridge are the same $^{3}J_{H\text{-}H}$ = 8.14 Hz.

The ^{13}C NMR spectrum exhibits a characteristic resonance at δ = 91.43 ppm attributable to the alkyne moiety (Figure 49), which clearly proves the presence of an uncompromised C-C triple bond in the product **112**.

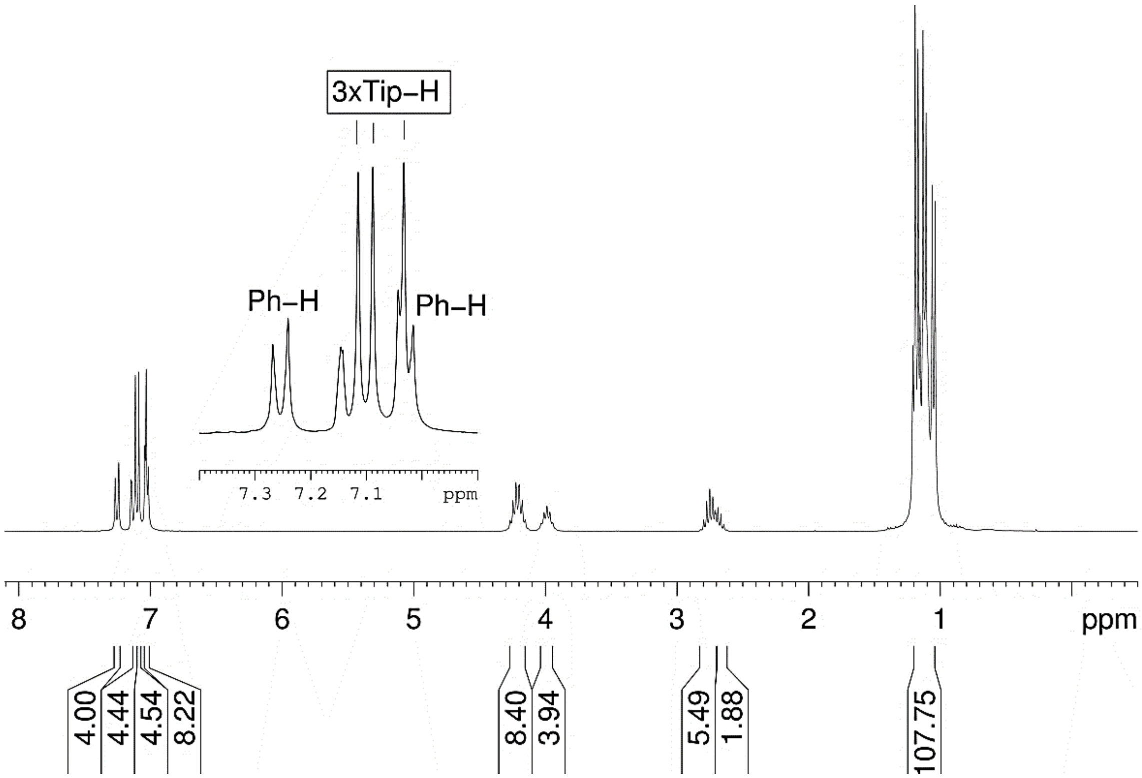

Figure 48. ^{29}H NMR of the reaction mixture of two equivalents disilenide **27** with **111.**

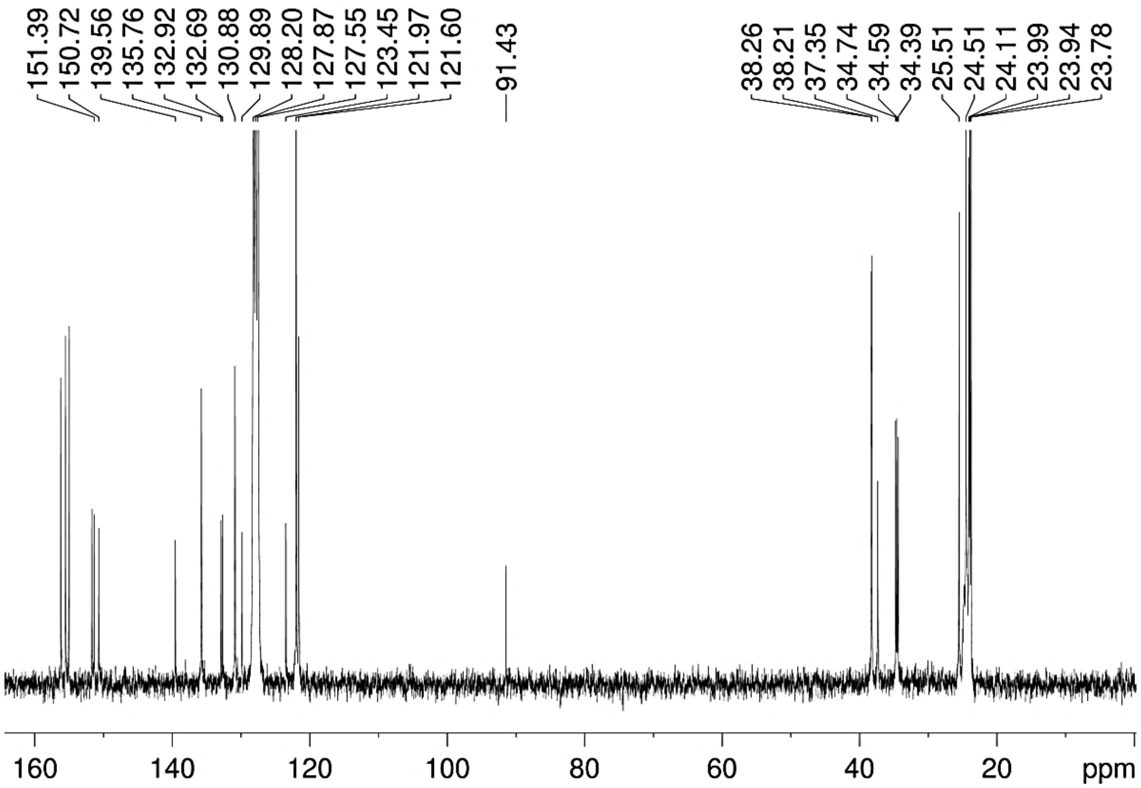

Figure 49. ^{13}C NMR of the reaction mixture of two equivalents disilenide **27** with **111**.

On the basis of a two-dimensional ^{29}Si-^{1}H correlation analysis (Figure 50), the more shielded resonance in the ^{29}Si NMR shows two equally intense cross-peaks to the aryl hydrogen atoms of the Tip substituents. For the low-field resonance cross-peaks to one Tip and phenylene moieties are observed. Therefore, the low-field resonance at δ = 69.91 ppm is assigned to a SiTip-units while the signal at δ = 57.52 ppm is attributed to SiTip$_2$ moities.

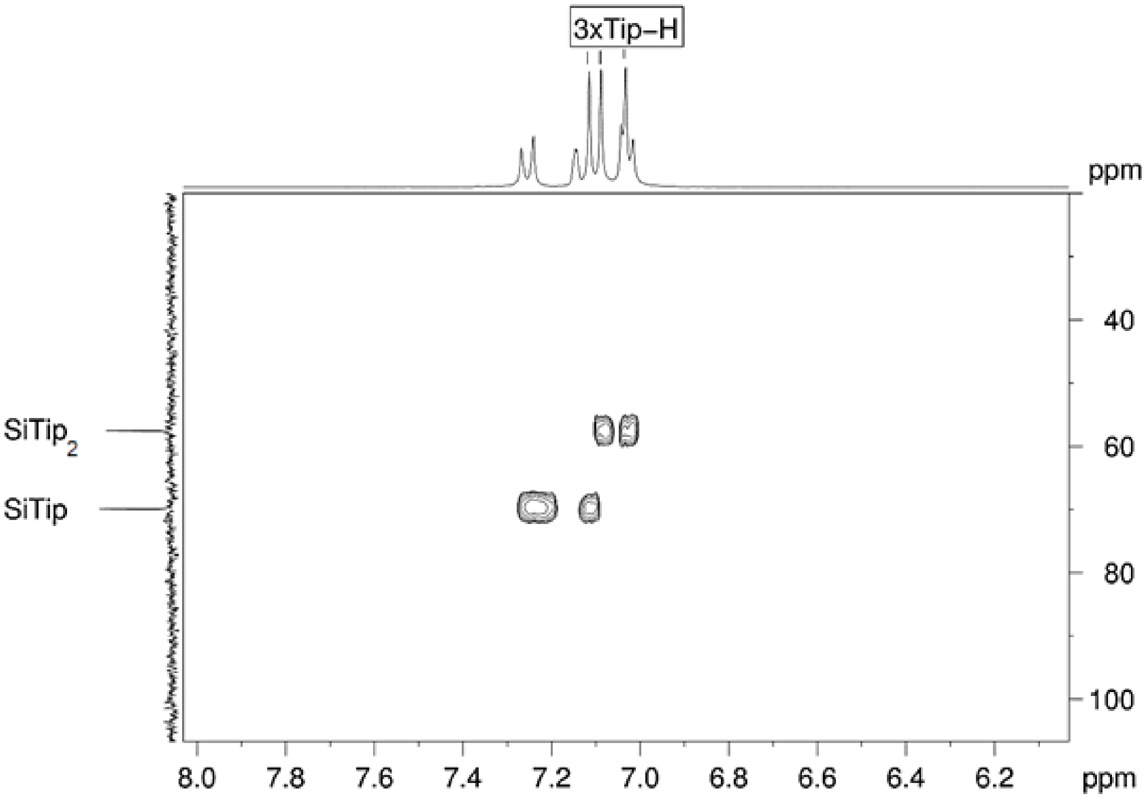

Figure 50. 2D ^{29}Si-^{1}H NMR correlation spectrum of tetrasiladiene **112**.

Red crystals of **112** (mp. 184°C) suitable for X-ray diffraction analysis were obtained in excellent yield 94% by crystallization from hexane. The structure of **112** in the solid state (Figure 51) confirms the constitution as bis(phenyl)acetylene-bridged tetrasiladiene.

Tetrasiladiene **112** crystallizes (Figure 51) in triclinic space group (P-1). The silicon centers show only slight deviation from planarity (Σ of angles Si1: 357.43 and Si2 358.86 Å). The two Si=Si bonds distances (2.1530(8) Å) are in accordance with literature values (2.140 to 2.229 Å) for aryl substituted disilenes[98] and shorter than that of phenylene-bridged tetrasiladiene *p*-**67** (2.1674(8) Å).[80a] This observation is, however, in line with the strong *trans*-bending of the Si=Si bond in *p*-**67** compared to the moderately *trans*-bent **112** (θ_{SiTip} = 15.3°; θ_{SiTip2} = 9.7°). A twist angle of τ = 6.4° is found for **112**. All silicon carbon bond distances are in good agreement with other aryl substituted disilene values (Si1-C1 1.8587(18), Si1-C8 1.8765(18), Si2-C23 1.885(2), Si2-C38 1.885(2) Å).[98] The organic linker is twisted out of the plane defined by the Si=Si moieties with a torsion angle of 45.9° for Si2−Si1−C1−C2.

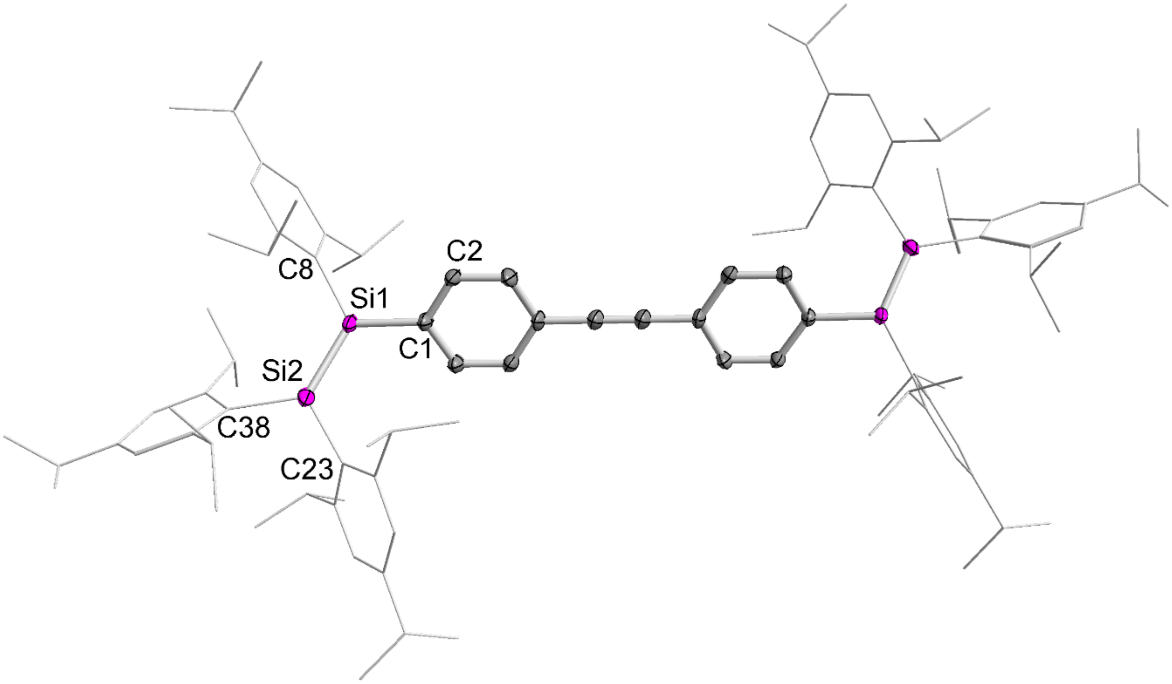

Figure 51. Molecular structure of **112** in the solid state (thermal ellipsoids at 50%, H atoms and disordered ^{i}Pr groups are omitted for clarity). Selected bond lengths [Å] and bond angles [°]: Si1-Si2 2.1530(8), Si1-C1 1.8587(18), Si1-C8 1.8765(18), Si2-C23 1.885(2), Si2-C38 1.885(2), C4-C7 1.432(3), C7-C7' 1.196(4), C(1)-Si(1)-C(8) 115.69(8), C(1)-Si(1)-Si(2) 117.96(6), C(8)-Si(1)-Si(2) 121.78(6), C(23)-Si(2)-C(38) 110.78(9), C(23)-Si(2)-Si(1) 122.84(6), C(38)-Si(2)-Si(1) 125.24 (8).

UV/vis spectroscopy shows a maximum absorption wavelength at λ_{max} = 488 nm associated with the highest molar extinction coefficient (ε = 46000 $M^{-1}cm^{-1}$) in this series of Si=Si unit containing derivatives. The longest wavelength absorption is red-shifted by about 16 nm compared to that of disilene **96** (λ_{max} = 472 nm), which indicates more extended conjugation upon the introduction of a second Si=Si unit to the system. The hypsochromic shift (blue) of $\Delta\lambda = 20$ nm compared to that of phenylene bridged tetrasiladiene *p*-**67** (λ_{max} = 508 nm)[80a] can be attributed to a less pronounced *trans*-bending in **112**. An additional absorption band at λ = 309 nm with ε = 47690 $M^{-1}cm^{-1}$ that can be assigned to the linker unit is observed.

Notably, tetrasiladiene **112** exhibits visible fluorescence in hexane solution and in the solid state at room temperature (Figure 52 and 53).

In hexane solution, compound **112** has a maximum wavelength excitation λ_{max}^{exc} = 514 nm for λ_{em} = 610 nm and a maximum wavelength emission λ_{max}^{em} = 570 nm for λ_{ex} = 480 nm (Figure 52).

Whereas, the maximum excitation and emission wavelength for compound **112** in solid state are λ_{max}^{exc} = 574 nm, λ_{max}^{em} = 619 nm for a specific wavelength λ_{em} = 700 nm, λ_{ex} = 510 nm, respectively (Figure 53).

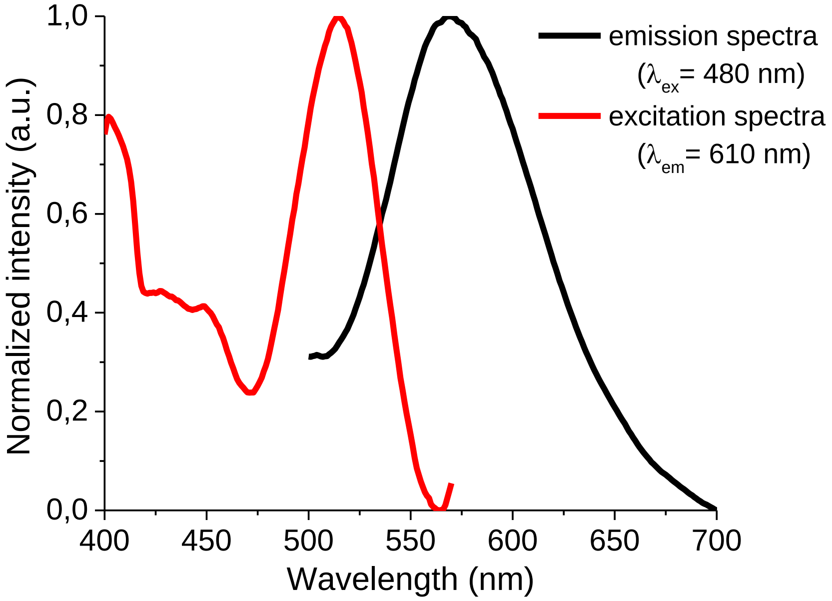

Figure 52. Excitation and emission spectra of **112** in hexane at room temperature.

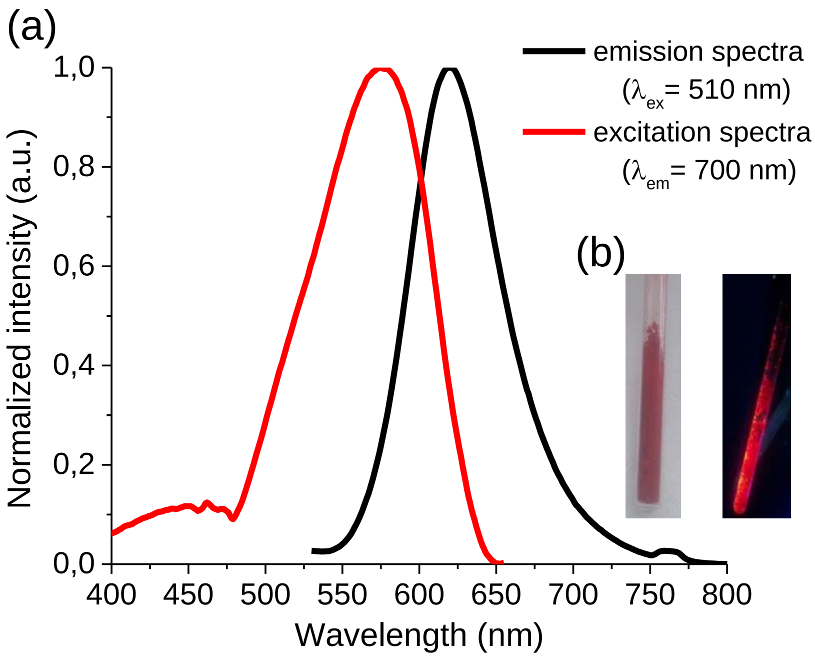

Figure 53. (a) Excitation and emission spectra of **112** in solid state at room temperature, (b) Solid-state color under room light and 360 nm UV light of **112** at room temperature.

As shown in Figure 53b, **112** is red fluorescent in solid state albeit with a low quantum yield both in solution ($\Phi < 0.01\%$) and in the solid state ($\Phi = 0.015\%$).

3.1.3.5. Reactivity of Disilenide 27 towards Dibromo Naphthalene 113

In order to add more rigidity to the linking unit and thus decrease the degrees of freedom available for radiation-less relaxation, the introduction of oligoaromatic substituents and linking units was considered as a viable measure. In order to allow an estimate on this effect, the comparatively small naphthalene moiety was chosen as initial subject of the investigation, while the steric demand of the oligoaromatic substrate was subsequently to be increased in a stepwise manner.

Dibromonaphthalene **113** and two equivalents disilenide **27** were thus combined in benzene using the same methodology as described before (Scheme 43).

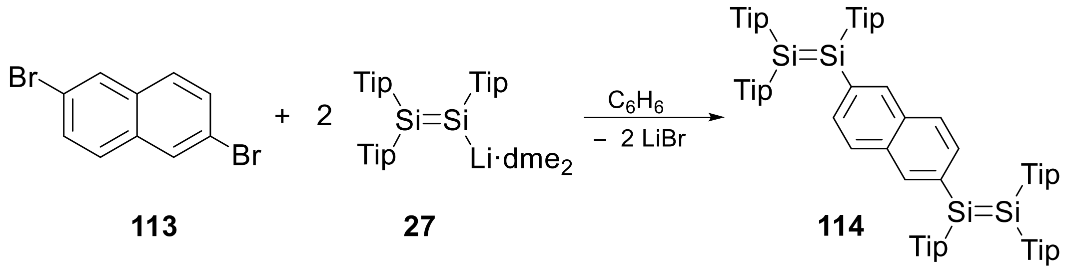

Scheme 43. Synthesis of naphthalene bridged tetrasiladiene **114**.

The deep orange solution changed its color to red and the ^{29}Si NMR spectrum of the reaction mixture revealed uniform conversion to a new product with only two resonances (δ = 71.46 and 56.67) ppm in the typical range for Si=Si, suggesting the formation of tetrasiladiene **114** (Figure 54).

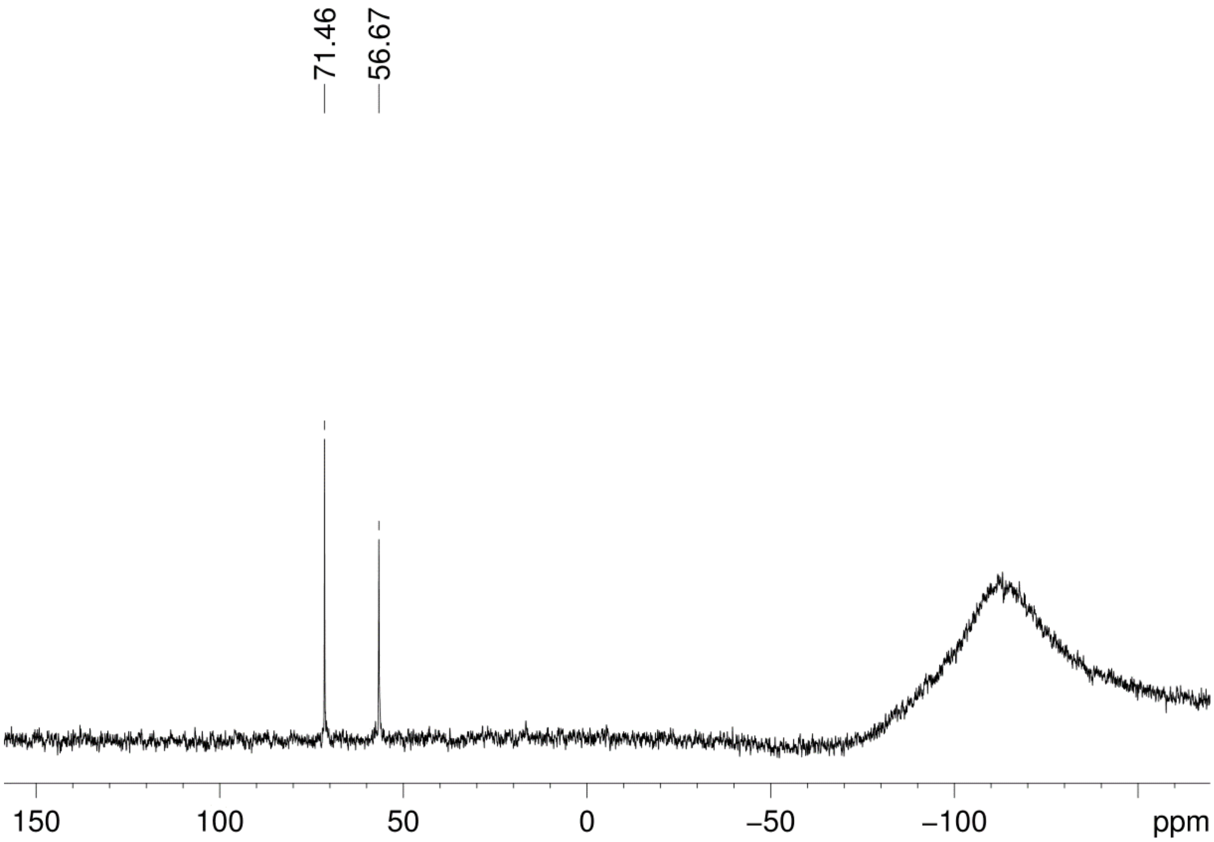

Figure 54. ^{29}Si NMR of the reaction mixture of two equivalents disilenide **27** with **113.**

The ^{1}H NMR spectrum shows one low-field singlet and two doublet signals at δ = 7.67, 7.27 and 6.75 ppm, which can be attributed to the three pairs of chemically equivalent naphthalene protons of the linking unit. The coupling constant for the two doublets of naphthalene protons are the same $^3J_{H\text{-}H}$ = 8.26 Hz. Additionally, three diagnostic singlet signals for the aromatic Tip protons are visible at δ = 7.12, 7.06 and 7.04 ppm (Figure 55).

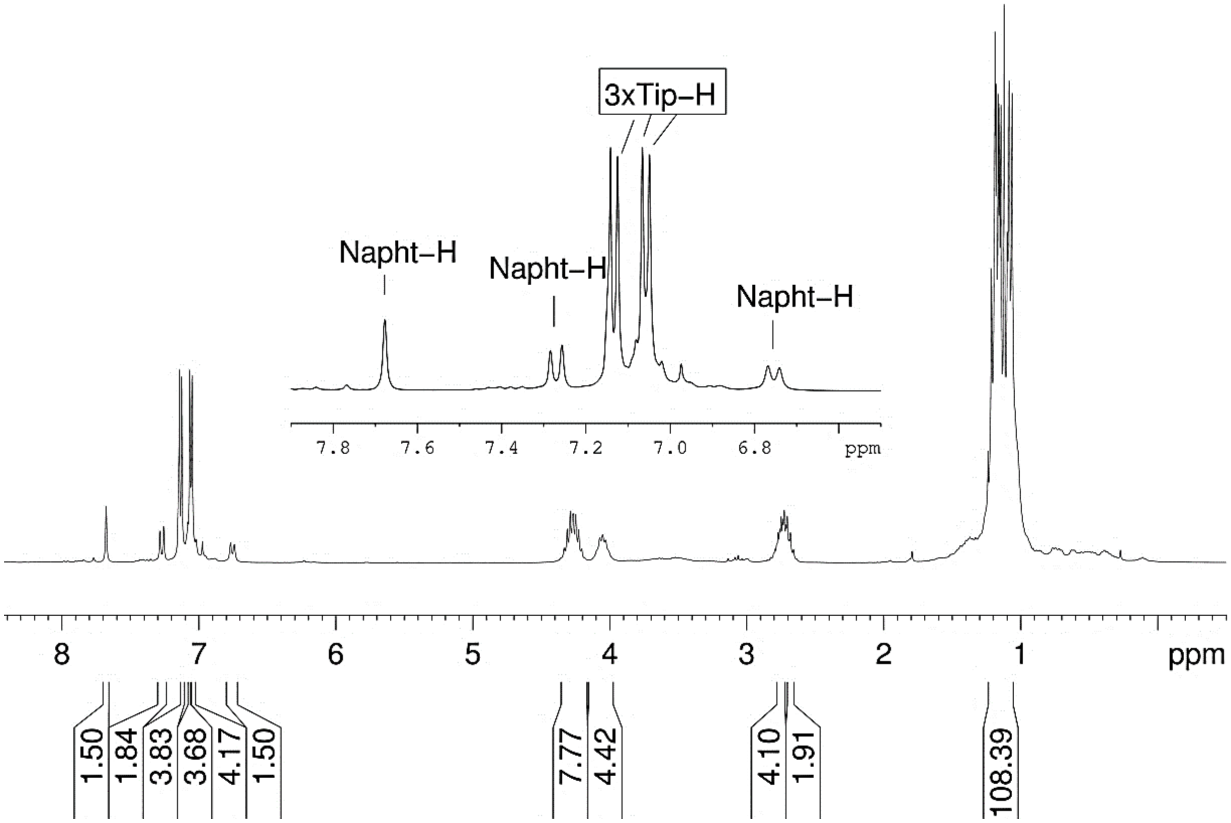

Figure 55. ^{1}H NMR of the reaction mixture of two equivalents disilenide **27** with **113**.

The ^{29}Si NMR resonance at low field belongs to the silicon atom bonded to the naphthalene unit and one Tip group on the basis of Si-H correlation 2D spectra. The more shielded resonance is assigned to the silicon atom with two Tip moieties due to the appearance of two cross-peaks (Figure 56).

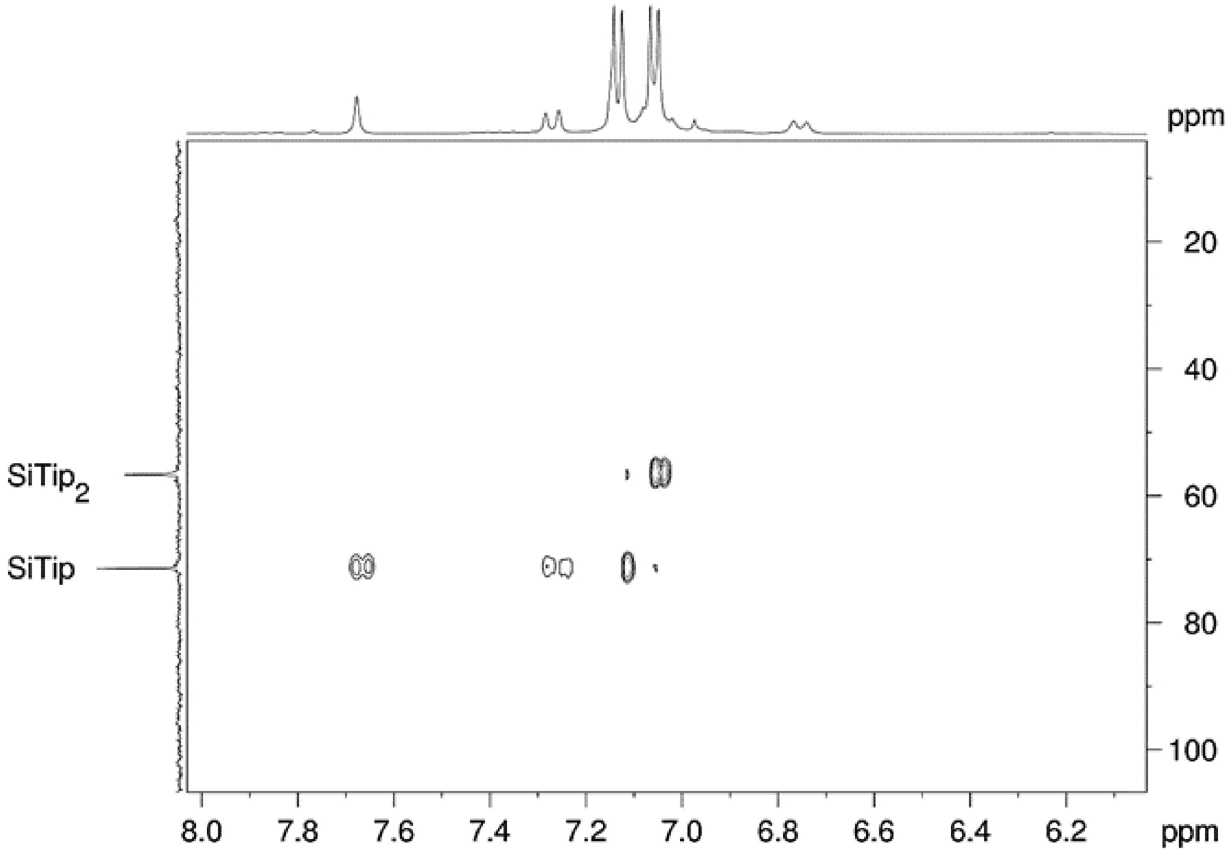

Figure 56. 2D ^{29}Si-^{1}H NMR correlation spectrums of tetrasiladiene **114**.

Orange-red crystals were obtained from benzene in 74% yield (mp. 150°C). The structure of **114** in the solid state was verified by X-ray diffraction on a single crystal (Figures 57).

Tetrasiladiene **114** adopts an almost planar geometry about the Si atoms; the sum of bond angles about the Si atoms are Si1 359.64° and Si2 360°. Even though both ends of the Si-Si double bond of **114** show a rather low degree of *trans*-bending (θ_{SiTip} = 5.5°; θ_{SiTip2} = 1.5°), the length of the Si-Si double bond in **114** [2.1622(6) Å] is comparable to the strongly *trans*-bent phenylene-bridged tetrasiladiene *p*-**67** (2.1674(8) Å). The naphthalene ring is not coplanar with the Si=Si bond, but substantially twisted with a torsion angle of 38.7° for Si2−Si1−C1−C2. The Si-C bonds to the Tip and naphthalene carbons range from 1.8547(19) to 1.8836(16) Å, which is an agreement with literature values for aryl disilenes.[95]

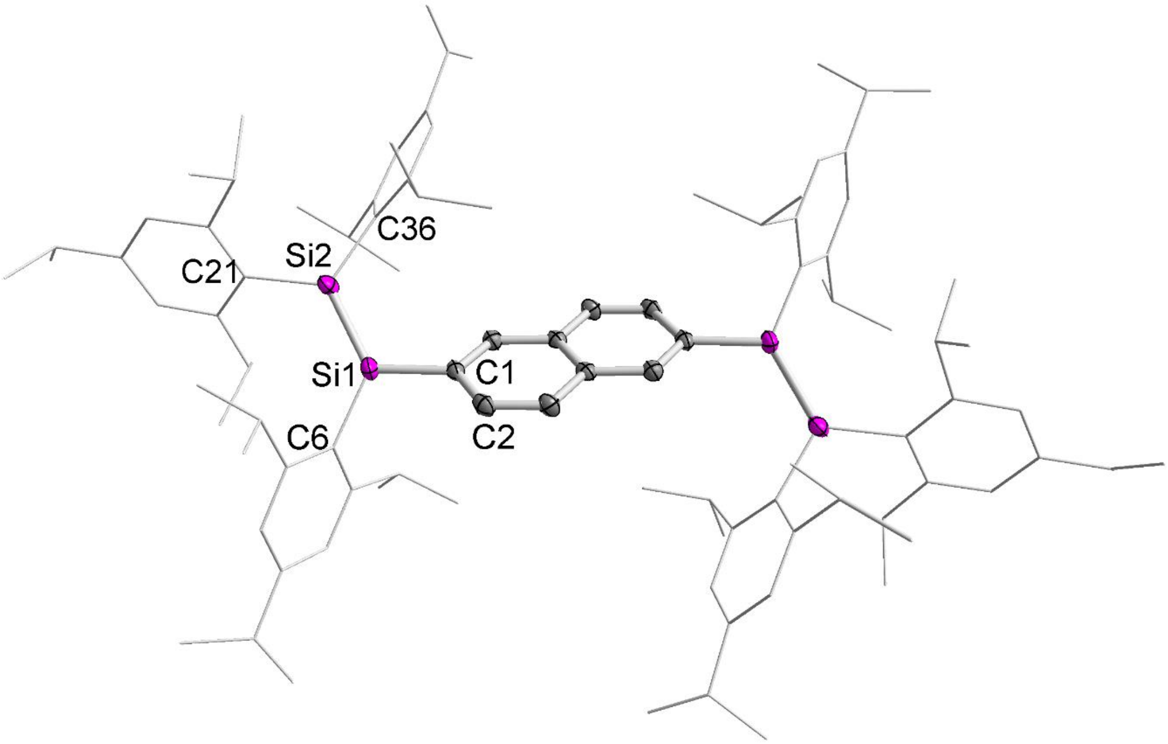

Figure 57. Molecular structure of **114** in the solid state (thermal ellipsoids at 50%, H atoms and disordered ^{i}Pr groups are omitted for clarity). Selected bond lengths [Å] and bond angles [°]: Si1-Si2 2.1622(6), Si1-C1 1.8547(19), Si1-C6 1.8678(16), Si2-C21 1.8803(15), Si2-C36 1.8836(16), C(1)-Si(1)-C(6) 111.68(8), C(1)-Si(1)-Si(2) 119.01(7), C(6)-Si(1)-Si(2) 128.95(5), C(21)-Si(2)-C(36) 114.04(7), C(21)-Si(2)-Si(1) 124.27(5), C(36)-Si(2)-Si(1) 121.66 (6).

UV/vis spectroscopy reveals a red-shift of $\Delta\lambda = 21$ nm of the longest wavelength absorption of **114** (λ_{max} = 484 nm) compared to that of naphthalene disilene **98** (λ_{max} = 463 nm). The intensity of the longest wavelength absorption of **114** (ε = 12200 $M^{-1}cm^{-1}$) is nearly twice as large as compared to **98** (ε = 6800 $M^{-1}cm^{-1}$). The bathochromic shift is likely due to the extension of the conjugated system upon introduction of another Si=Si to the organic linker.

Tetrasiladiene **114** shows an orange fluorescence (Scheme 59b) with a very low quantum yield both in solution (Φ < 0.01%) and in the solid state (Φ = 0.04%).

In hexane solution at room temperature, **114** shows a maximum wavelength excitation λ_{max}^{exc} = 525 nm for λ_{em} = 610 nm, and a maximum wavelength emission λ_{max}^{em} = 574 nm for λ_{ex} = 450 nm (Figure 58). In the solid state at room temperature, **114** has a maximum wavelength excitation at λ_{max}^{exc} = 552 nm for a detectable emission intensity

(λ_{em} = 670 nm), while a maximum emission wavelength (λ_{max}^{em} = 587 nm) occurs at a unique excitation wavelength of 450 nm (Figure 59).

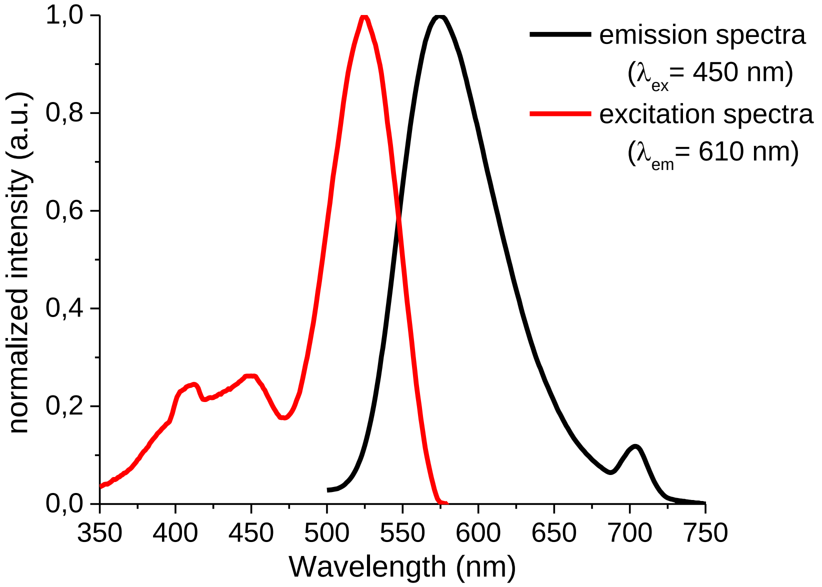

Figure 58. Excitation and emission spectra of **114** in hexane solution at room temperature.

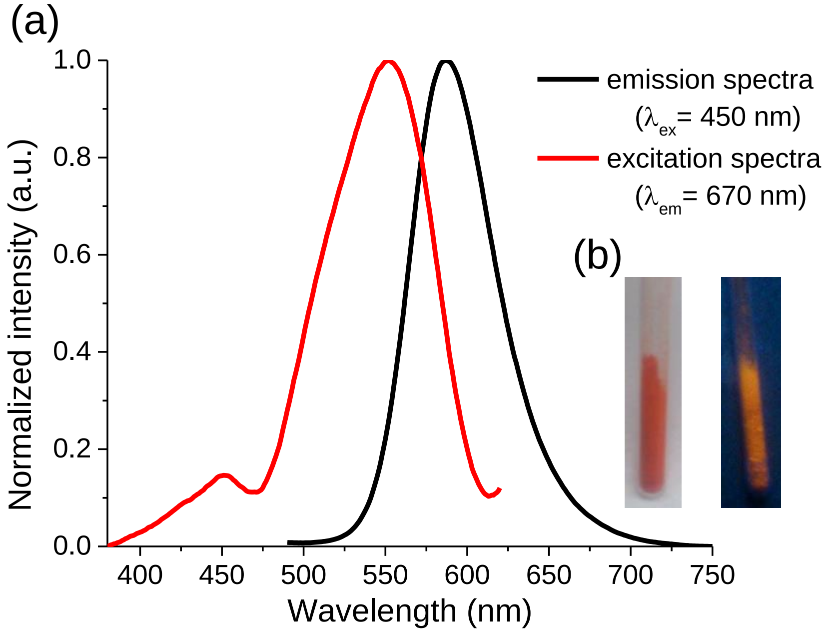

Figure 59. (a) Excitation and emission spectra of **114** in solid state at room temperature, (b) solid-state color under room light and 360 nm UV light of **114** at room temperature.

3.1.3.6. Reactivity of Disilenide 27 towards Dibromo Anthracene 115

The reaction of 9,10-dibromoanthracene **115** with two equivalents disilenide **27** in benzene (Scheme 44) results in the formation of dark green solution and a white precipitate (probably lithium bromide) clearly indicating that a reaction has taken place. Furthermore, the dark-green color of the solution was taken as a first hint that despite the steric demand of the substrate, the formation of the undesired unbridged tetrasilabutadiene side product **11** was minimal at most.

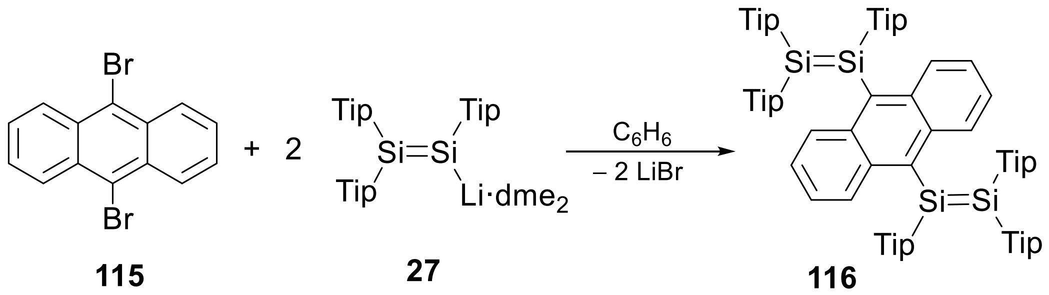

Scheme 44. Anticipated reaction of two equivalents disilenide **27** with **115**.

After workup, the desired anthracene-bridged tetrasiladiene **116** can be isolated as dark blue-green microcrystalline material in 88% yield (mp. 189°C) from a concentrated thfsolution, which was left standing for two days at −10°C.

Despite the poor solubility of **116** and the resulting mediocre signal to noise ratio, the ^{29}Si NMR spectrum (Figure 60) reveals several weak signals in the range of 52.24 to 62.72 ppm, along with two slightly more prominent resonances at δ = 53.94 and 59.71 ppm. Although the absence of signals in the typical area for oxidation or hydrolysis products cannot be confirmed with certainty due to the very bad signal/noise ration of ^{29}Si spectrum in solution, the large number of resonances in the unsaturated region is likely due to the presence of different rotational conformers of **116**.In contrast to durene bridged tetrasiladiene **106**, it proved impossible to substantiate this assertion by coalescence of the signals at elevated temperature due to the insufficient thermal stability of **116**. As a consequence, the ^{1}H and ^{13}C NMR spectra of **116** feature a large number of signals in various intensity ratios, which do not lend themselves to meaningful interpretation.

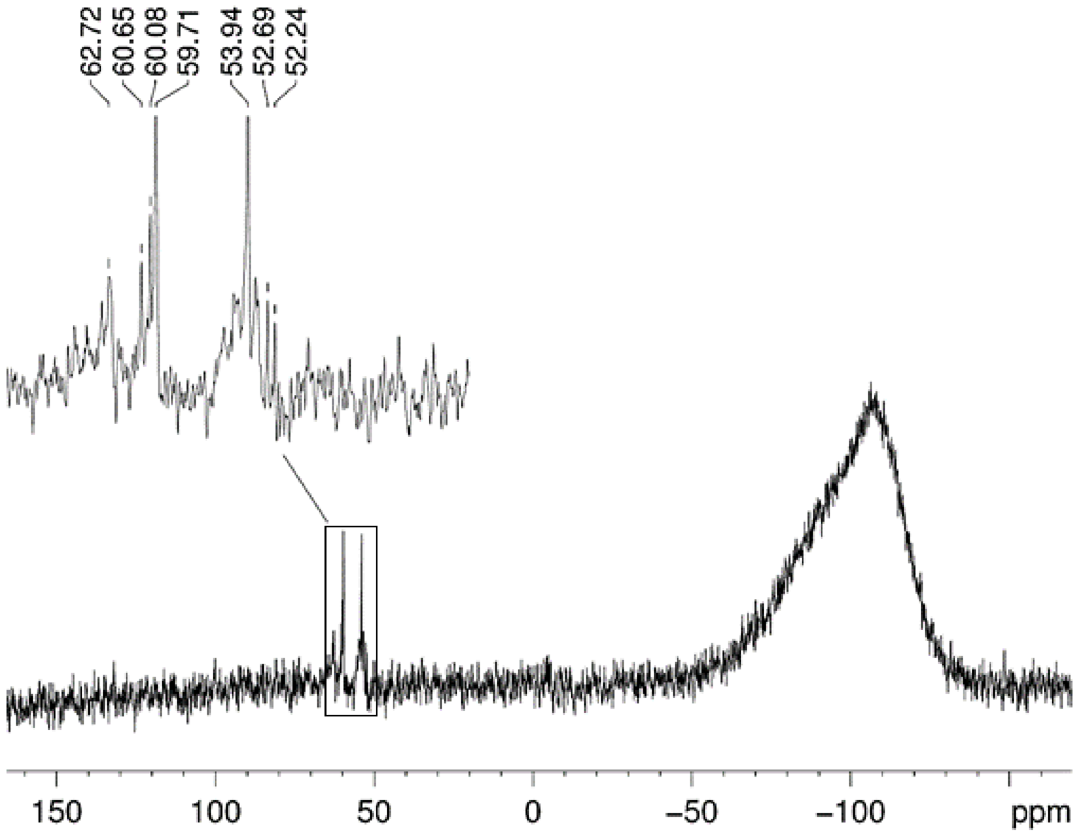

Figure 60. ^{29}Si NMR spectrum of tetrasiladiene **116** in C_6D_6 at 300 K.

Due to its poor solubility in organic solvents and the comparatively low thermal stability of **116**, solid state NMR was performed in order to obtain some support for the assumed presence of different rotamers in solution. Qualitatively, the chemical shift regions in the ^{13}C NMR are in accordance with a CP-MAS ^{13}C NMR spectrum in the solid state.

The well-resolved CP-MAS ^{29}Si NMR (Figure 61) provides unambiguous prove for the purity of the bulk crystalline material **116** though. It shows only two signals in at δ = 65.14 and 54.01 ppm (alongside rotational side bands and very minor signals of unknown impurities at δ = −2.25 and −6.30 ppm), which is consistent with the description as anthracene-bridged tetrasiladiene **116**.

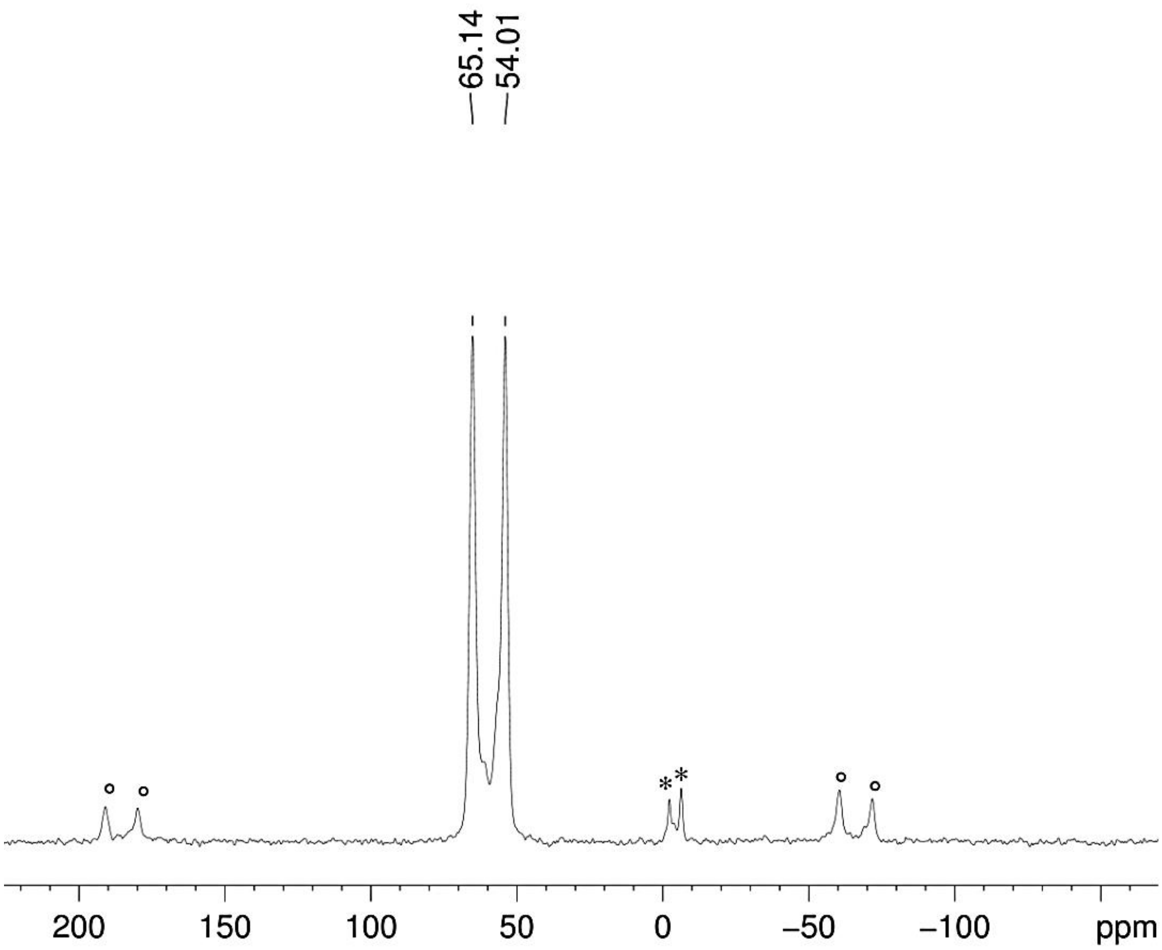

Figure 61. CP-MAS ^{29}Si NMR of **116** in solid state at 300 K, ∗ = minor signals for unknown impurities,° = Rotational side band with MAS rotation rate = 5000 Hz.

The ^{29}Si NMR spectra in solution for both species with durylene and anthracene bridges (**116** and **106**) showed several unsaturated signals in the typical region of aryl substituted disilenes, while the number of these signals for each compound was reduced to one or two signal(s) in the CP-MAS ^{29}Si NMR (solid state). This unambiguously proves that the multitude of signals for both compounds (**116** and **106**) are due to a solution process, which is unlikely to be anything else than an equilibrium between different conformers.

In an attempt to improve crystal quality, microcrystalline **116** was redissolved in benzene. Single crystals were grown from benzene and investigated by X-ray diffraction (Figure 62).

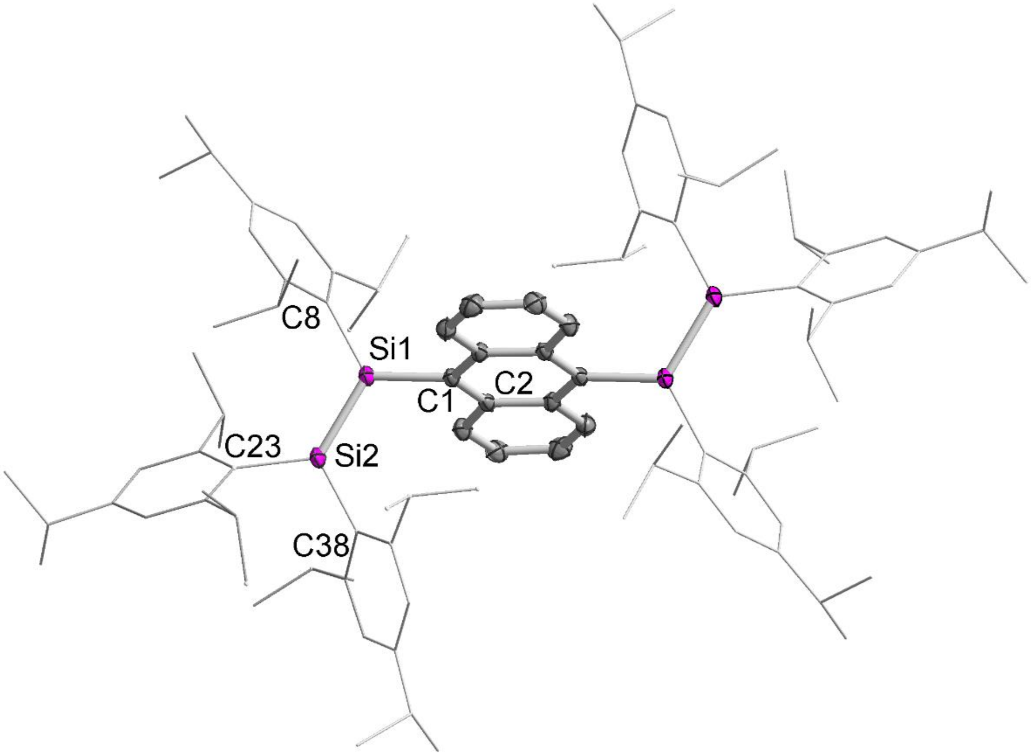

Figure 62. Molecular structure of **116** in the solid state (thermal ellipsoids at 50%, H atoms and disordered ^{i}Pr groups are omitted for clarity). Selected bond lengths [Å] and bond angles [°]: Si1-Si2 2.1483 (8), Si1-C1 1.899(2), Si1-C8 1.883(2), Si2-C23 1.893(2), Si2-C38 1.887(2), C(1)-Si(1)-C(8) 119.83(9), C(1)-Si(1)-Si(2) 118.74(7), C(8)-Si(1)-Si(2) 121.20(7), C(23)-Si(2)-C(38) 111.47(10), C(23)-Si(2)-Si(1) 126.68(7), C(38)-Si(2)-Si(1) 121.70 (7).

The length of the Si-Si double bond in **116** is with 2.1483(8) Å at the short end of typical values of disilenes.[98] As a consequence both unsaturated silicon centers show a nearly planar geometry (Σ of angles around Si1 359.8°, Si2 359.9°). The Si-Si bonds adopt an almost planar geometry, since the anthracene and Tip groups fit together in a gear-like arrangement around the disilene core with rather small *trans*-bent and twist angles (θ_{SiTip} = 4.7°; θ_{SiTip2} = 3.5°; and τ = 1.8°). Moreover, the anthracene ring is not coplanar with the Si=Si bond, but substantially twisted with a torsion angle of 74.63° for Si2−Si1−C1−C2. The Si-C bonds to the Tip and anthracene carbons range from 1.883(2) to 1.8899(2) Å, which is an agreement with literature values for aryl substituted disilenes.[98]

The UV/vis spectrum of **116** (Figure 63) in hexane shows a broad absorption band with maximum absorption wavelength at λ_{max} = 422 nm (ε = 36600 $M^{-1}cm^{-1}$) accompanied by another weaker broad band absorption at λ_{max} = 597 nm (ε = 7500 $M^{-1}cm^{-1}$).

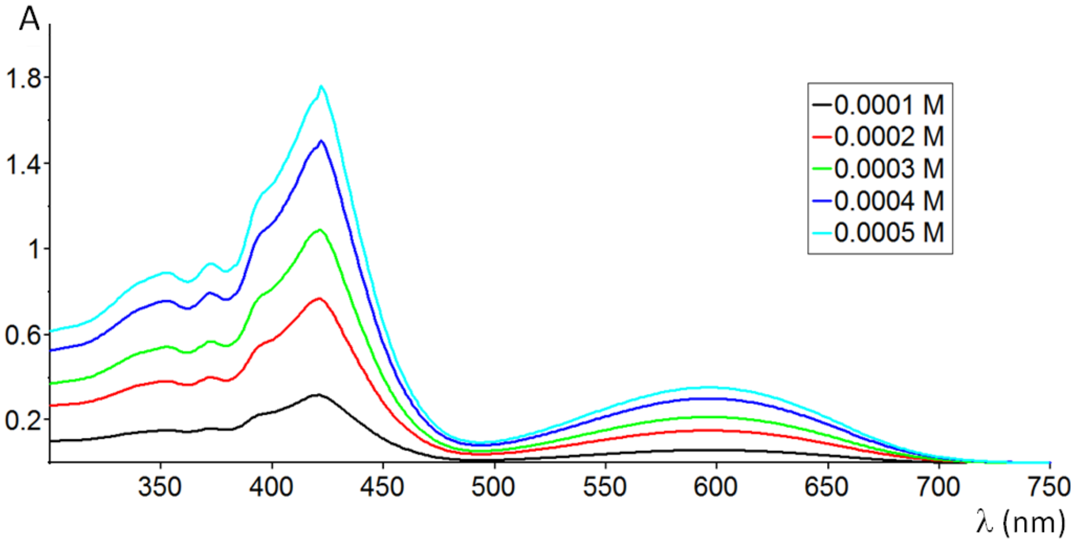

Figure 63. UV/vis spectra of **116** in hexane at different concentrations.

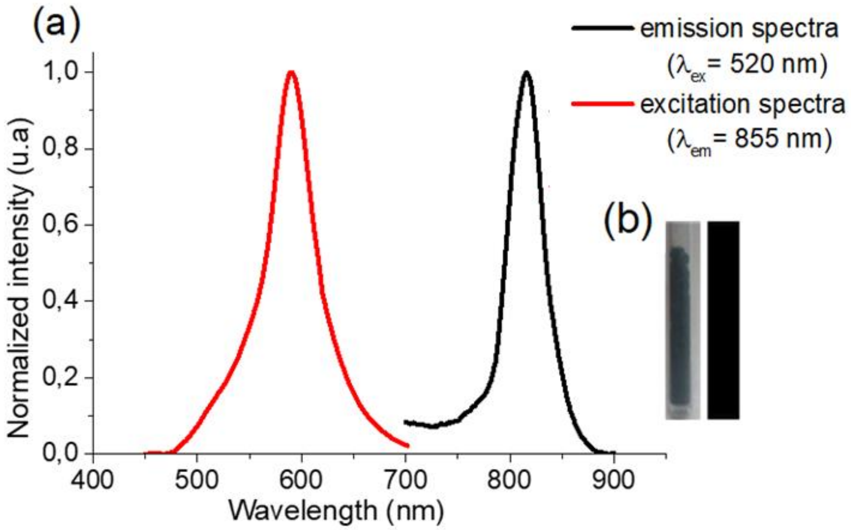

Figure 64. (a) Excitation and emission spectra of **116** in solid state at room temperature, (b) Solid-state color under room light and under 360 nm UV light of **116** at room temperature.

In contrast to solution, tetrasiladiene **116** exhibits weak fluorescence in the solid state at room temperature. The maximum excitation and emission wavelengths for compound **116** are λ_{max}^{exc} = 590 nm and λ_{max}^{em} = 816 nm for a specific wavelength λ_{em} = 855 nm and λ_{ex} = 520 nm, respectively (Figure 64). Tetrasiladiene **116** thus exhibits weak near-infrared (nIR) fluorescence with a low quantum yield (0.05%).

The reaction of disilenide **27** with the same precursor dibromoanthracene **115** in benzene but in a 1:1 ratio leads to an immediate change color from intense orange to dark green indicating that a reaction takes place (Scheme 45).

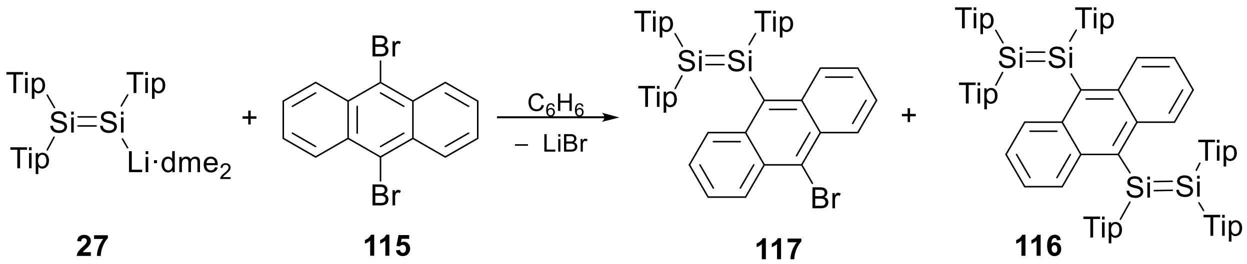

27 **115** **117** **116**

Scheme 45. Reaction of one equivalent disilenide **27** to a one equivalent **115.**

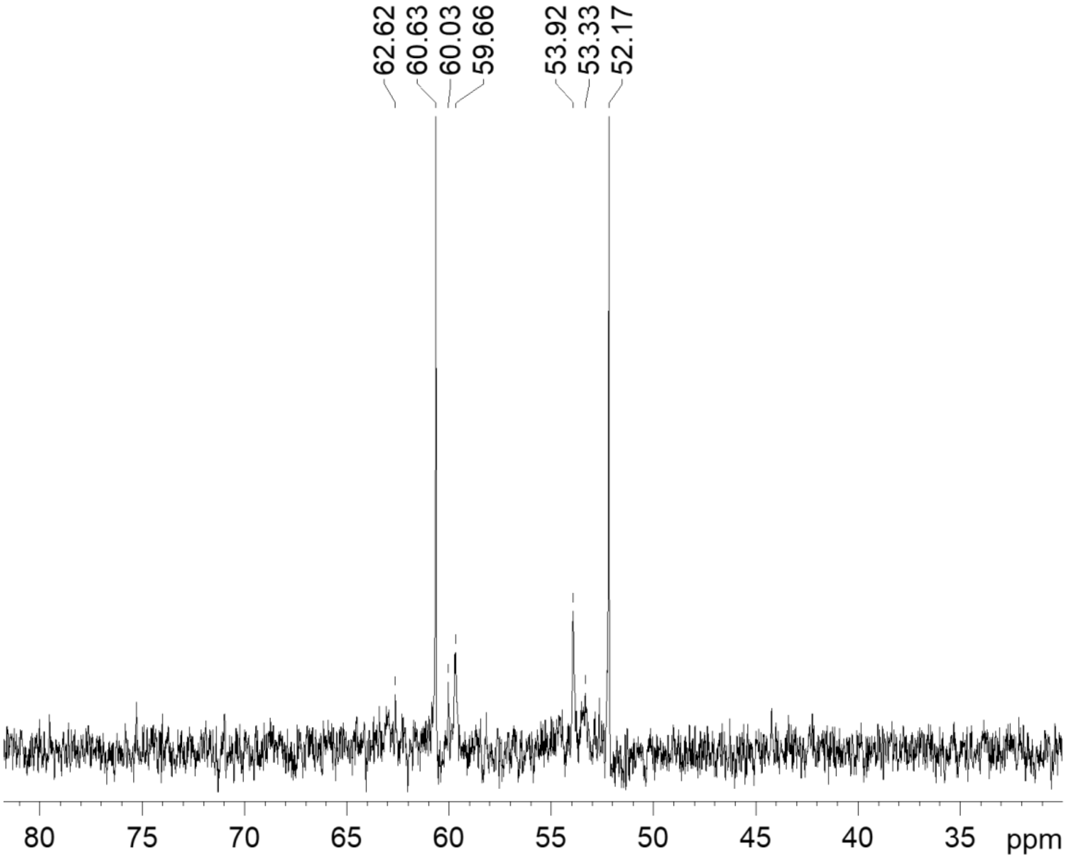

Figure 65. Low-field section of the ^{29}Si NMR after reaction of disilenide **27** with dibromoanthracene **115** in a ratio (1:1).

The ^{29}Si NMR of the reaction mixtures after drying and filtration reveals several weak signals in the range of 53.33 to 62.62 ppm that are assigned to the anthracene-bridged tetrasiladiene **116**, along with two resonances of much higher intensity at δ = 52.17 and 60.63 ppm strongly suggesting the predominant formation of the monosubstitution product, bromoanthracenyl-substituted disilene **117** (Figure 65).

Despite the precise 1:1 stoichiometry, the expected bromoanthracene disilene **117** was obtained in a mixture with about 9% of the disubstitution product **116** and unreacted dibromoanthracene **115**.

In order to increase the selectivity of the reaction, disilenide **27** was added to an excess of the diarylhalide **115** (1 : 1.5). A ^{29}Si NMR taken after work-up does shows the exclusive formation of a single species, presumably the monosubstitution product **117** (Figure 66).

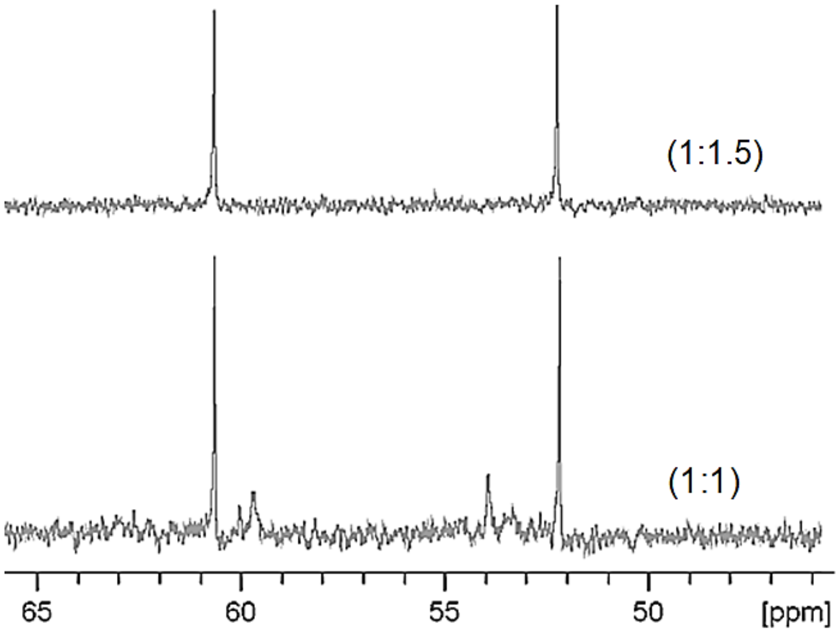

Figure 66. Low-field ^{29}Si NMR after reaction of disilenide **27** with dibromoanthracene **115** (blue = mixture (1:1)) and (red = mixture (1:1.5)) in benzene.

The ^{1}H NMR of the reaction mixture (Figure 67) showed several new signals of a seemingly pure product. Additional sharp low-field signals for anthracene protons in the range of 6.65 to 9.87 ppm are observed that are in line with a bromoanthryl substituent.

Although the multiplets in the range 7.04 to 7.25 ppm, overlapping with the protons of the aromatic systems, can be attributed to the aromatic protons of the Tip units. Furthermore, the well-separated distinct heptets in the isopropyl region and the well-resolved doublets of comparable intensity in the alkyl region indicate that the reaction proceeds in a selective way.

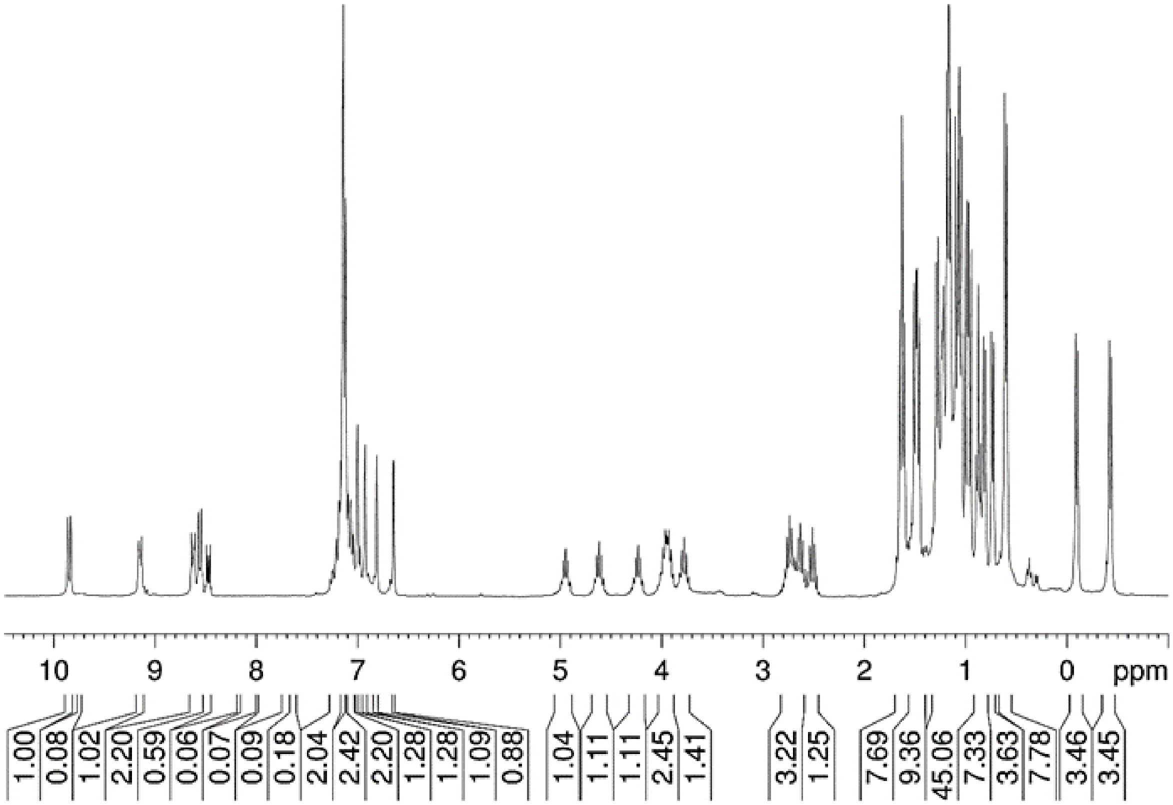

Figure 67. ^{1}H NMR of the reaction mixture of one equivalent **27** with one and half equivalents of **115**.

Indeed, the bromine functionality in bromoanthryl disilene **117** could offer an alternative point of entry for further manipulations in the periphery of the Si=Si bond and several attempts were therefore made to obtain **117** in analytically pure form. However, despite the clean NMR data, no single crystals suitable for an X-ray structure analyses have been obtained yet.

3.1.3.7. Reactivity of Disilenide 27 towards Dibromo Pyrene 118

As the increased steric strain of the anthracene linker apparently gives rise to selectivity issues, pyrene was chosen as linking unit with somewhat smaller steric congestion. in particular, 2,7-dibromopyrene **118** seemed to be a promising substrate due to the existence of tetrabenzenoid aromatics rings fused to each other via a common C=C bond (Scheme 43).

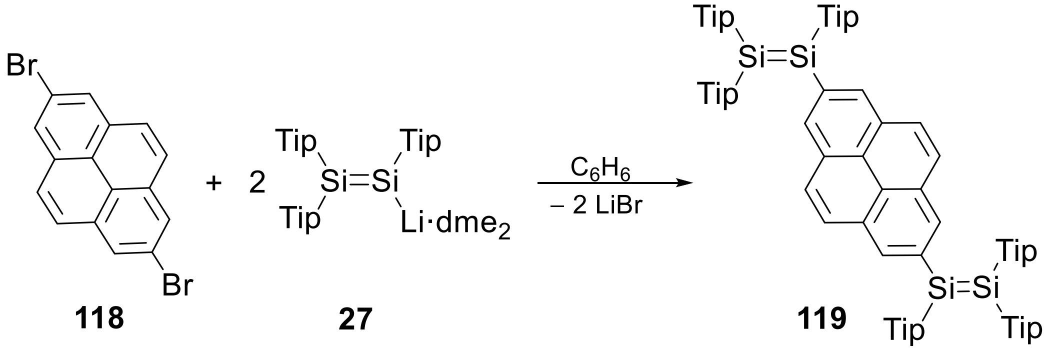

Scheme 46. Reaction of **118** with two equivalents disilenide **27** and the postulated product **119**.

The reaction of 2,7-dibromopyrene **118** with two equivalents disilenide **27** in benzene at room temperature leads to a dark red solution. The ^{29}Si NMR of the reaction mixture (Figure 68) shows two signals in the typical chemical shift range of saturated silicon species at δ = −14.27 and −61.90 ppm, along with one major unsaturated silicon species at δ = 71.15 and 57.01 ppm that is consistent with the targeted tetrasiladiene **119**. The highfield shifts are attributed to the protonation of disilenide **27** by water traces in the dibrompyrene substrate followed by dimerization of the resulting transient hydrido disilene Tip$_2$Si=Si(Tip)H to a cyclotetrasilane derivative.

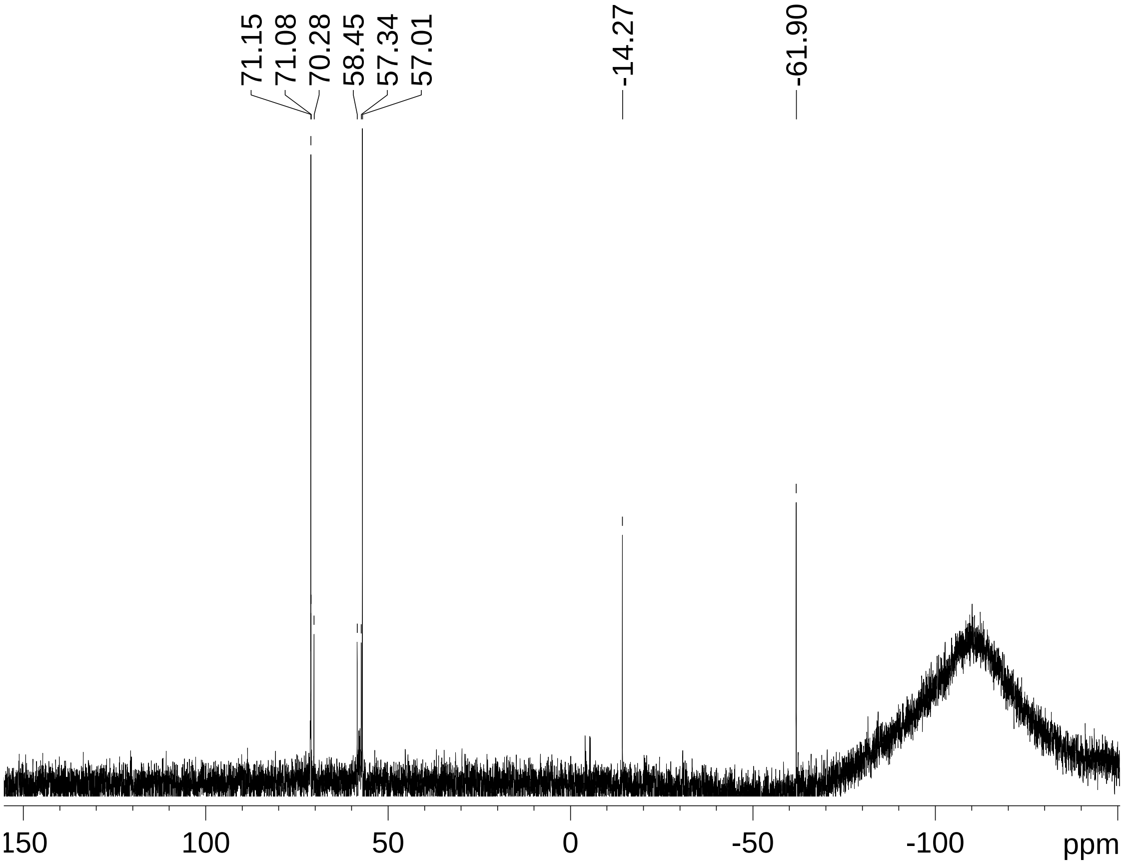

Figure 68. ^{29}Si NMR spectrum of the reaction mixture between **27** and dibromopyrene **118**.

To overcome this problem, the commercial 2,7-dibromo pyrene starting material **118** was recrystallized from a minimum amount of hot dry toluene under argon followed by rapid filtration in order to remove any trace of insoluble impurities. Subsequent cooling to room temperature yielded pure and water-free 2,7-dibromopyrene **118** as colorless crystals. After drying the colorless crystals obtained under vacuum over two hours at 80°C, the reaction of **118** with two equivalents disilenide **27** was repeated. After the completion of disilenide addition, the reaction mixture turned to an orange red instead of the dark red color observed in the previous attempt, indicating that the reaction takes place in a different manner.

Indeed, the ^{29}Si NMR of the reaction mixture shows only two resonances at δ = 71.13 and 56.93 ppm (Figure 69). These values indicate a complete and uniform conversion to a new product and thus the formation of the pyrene-bridged tetrasiladiene **119**.

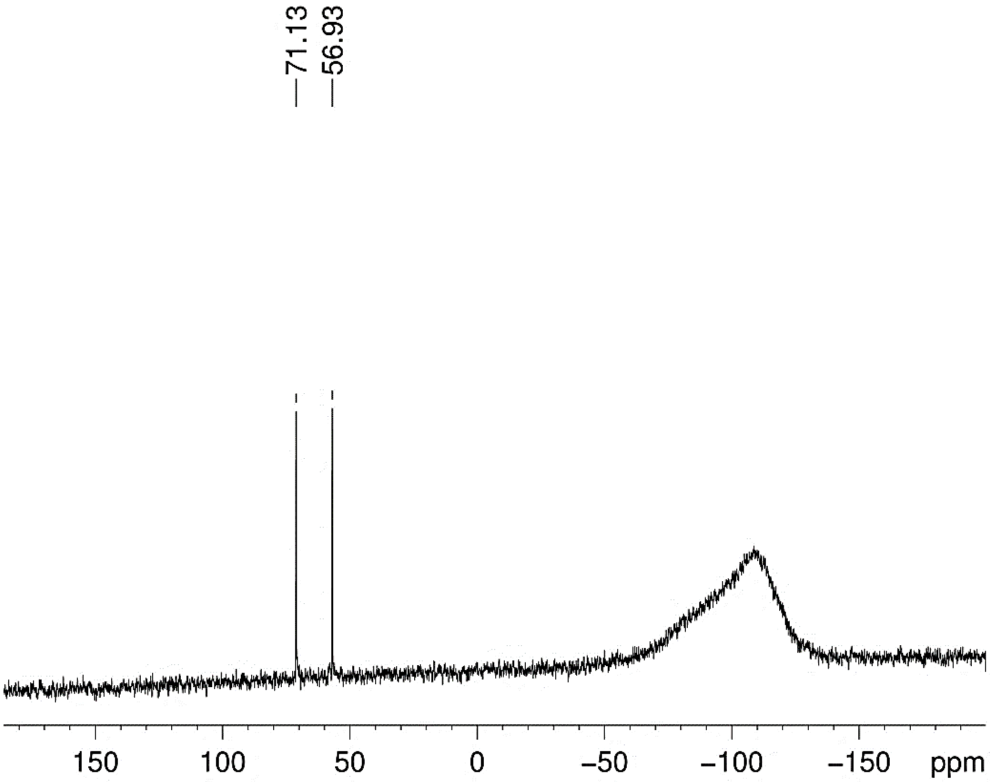

Figure 69. ^{29}Si NMR spectrum of the reaction mixture between **27** and dibromopyrene **118** after purification of **118**.

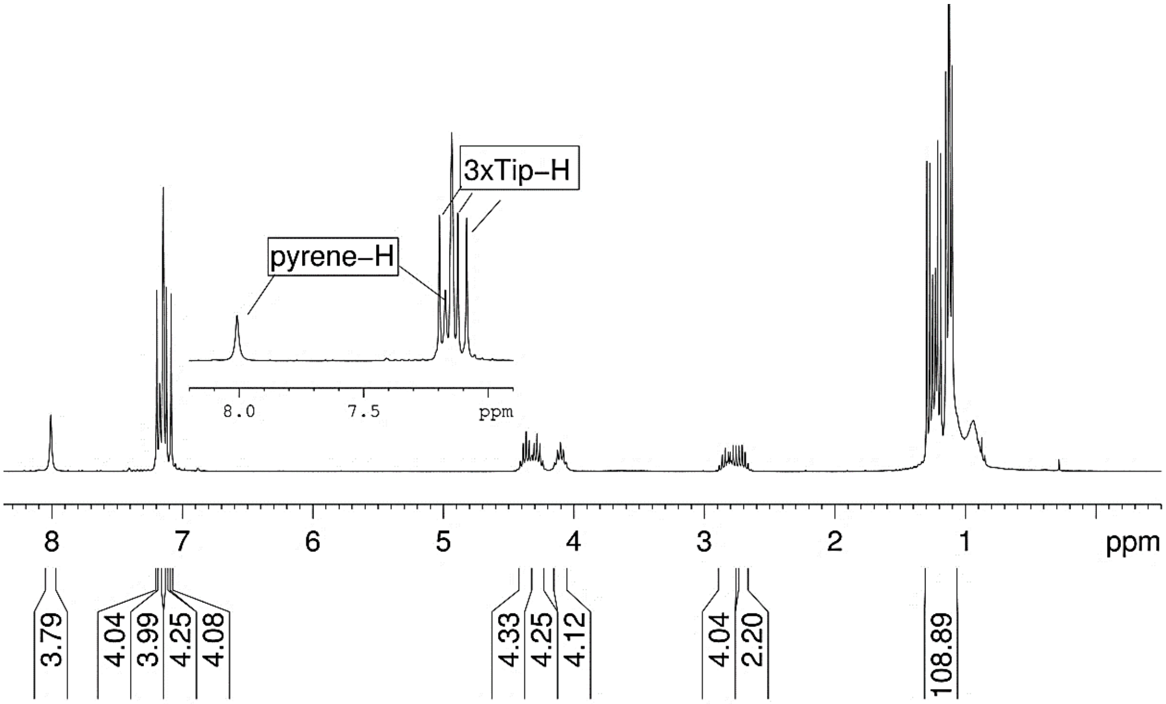

Figure 70. ^{29}H NMR spectrum of the reaction mixture between **27** and dibromopyrene **118**.

Additionally, the low-field region of the ^{1}H NMR spectrum (Figure 70) shows the two diagnostic singlet resonances at δ = 8.00 and 7.17 ppm for the aromatic protons of the pyrene moiety as well as the three singlet signals of equal intensity at δ = 7.19, 7.12 and 7.08 ppm for the three inequivalent Tip groups.

The 2D ^{29}Si-^{1}H correlation NMR (Figure 71) shows that the lowfield ^{29}Si NMR resonance is assignable to the SiTip units while the signals at δ = 56.93 ppm can be attributed to the SiTip$_2$ moieties.

Crystallization at room temperature from hexane overnight led to red-orange microcrystals (mp. 189°C) in excellent yield (95%). All this experimental data hints strongly towards the reaction as proposed in Scheme 43, but a final proof by X-ray diffraction was not possible due to the insufficient size of crystals of **119**.

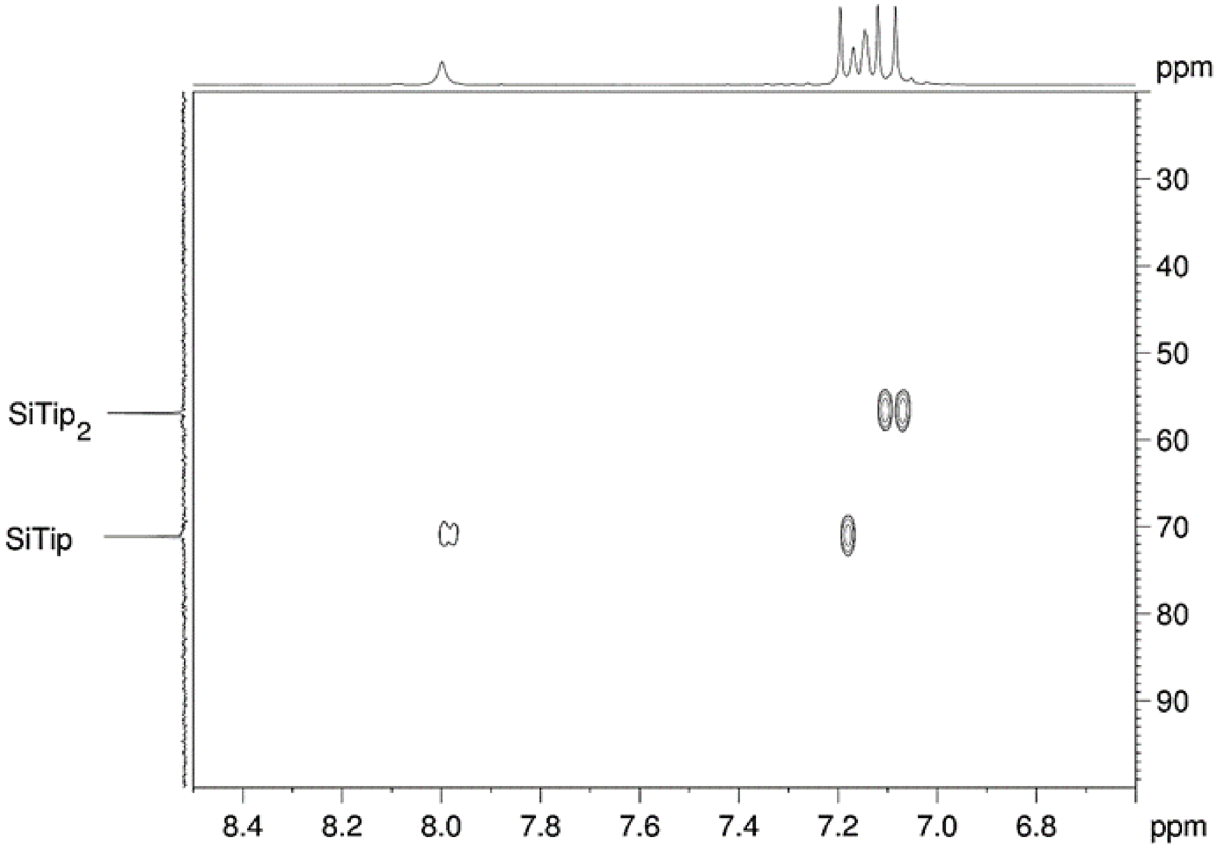

Figure 71. 2D ^{29}Si-^{1}H NMR correlation spectrums of pyrene-bridged tetrasiladiene **119**.

The absence of any other signals in the typical region of unsaturated silicon atoms of disilenes allowed basic UV/vis analysis of the crude product. The maximum absorption was found at λ_{max} = 470 nm (ε = 9700 M^{-1}cm^{-1}) which is significantly blue-shifted compared to phenyl tetrasiladiene *p*-**67** (λ_{max} = 508 nm). This hypsochromic shift by about 38 nm can be attributed to a less pronounced *trans*-bending in **119** and cannot be rationalized any further without X-ray structure analysis. In addition, **119** exhibits several more blue-shifted absorption bands between 300 and 350 nm values, presumably due to internal excitations of the pyrene linker itself (Figure 72).

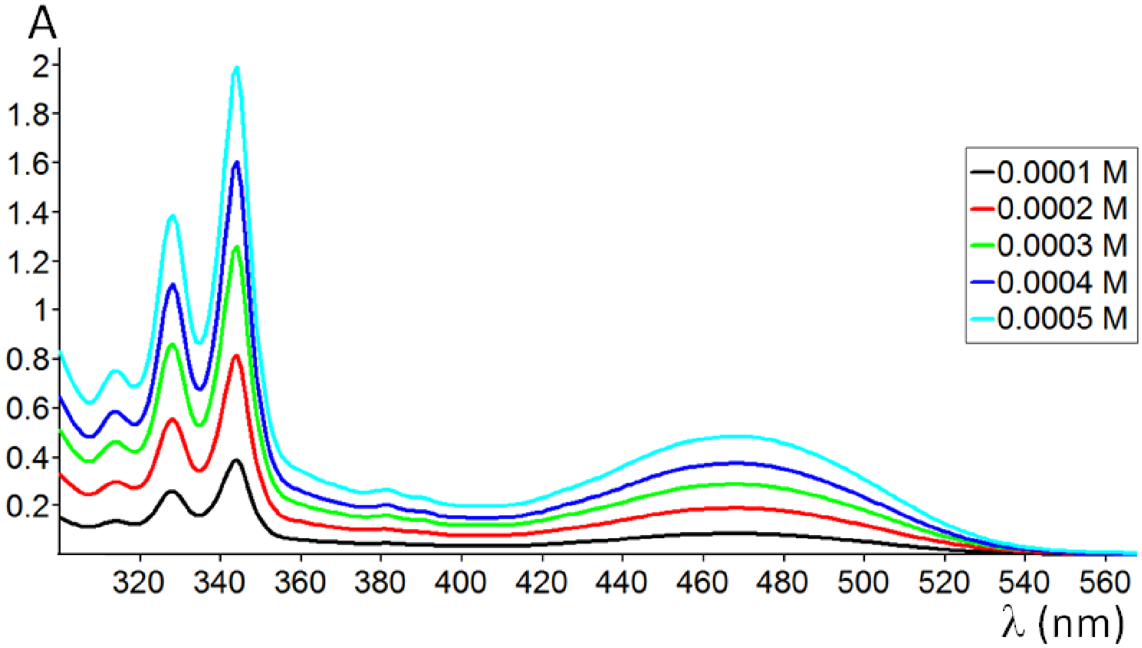

Figure 72. UV/vis spectra of **119** in hexane at different concentrations.

3.1.4. Comparison of the Electronic Properties of all isolated Disilenes and Bridged Tetrasiladienes

This chapter has been published in part as article in Dalton Transactions.[99]

The electronic properties of all successfully isolated compounds (Figure 73) on the basis of obtained NMR spectroscopy, X-ray structures, photophysical properties as well as theoretical studies were summarized and grouped together in this section for comparison and further discussions.

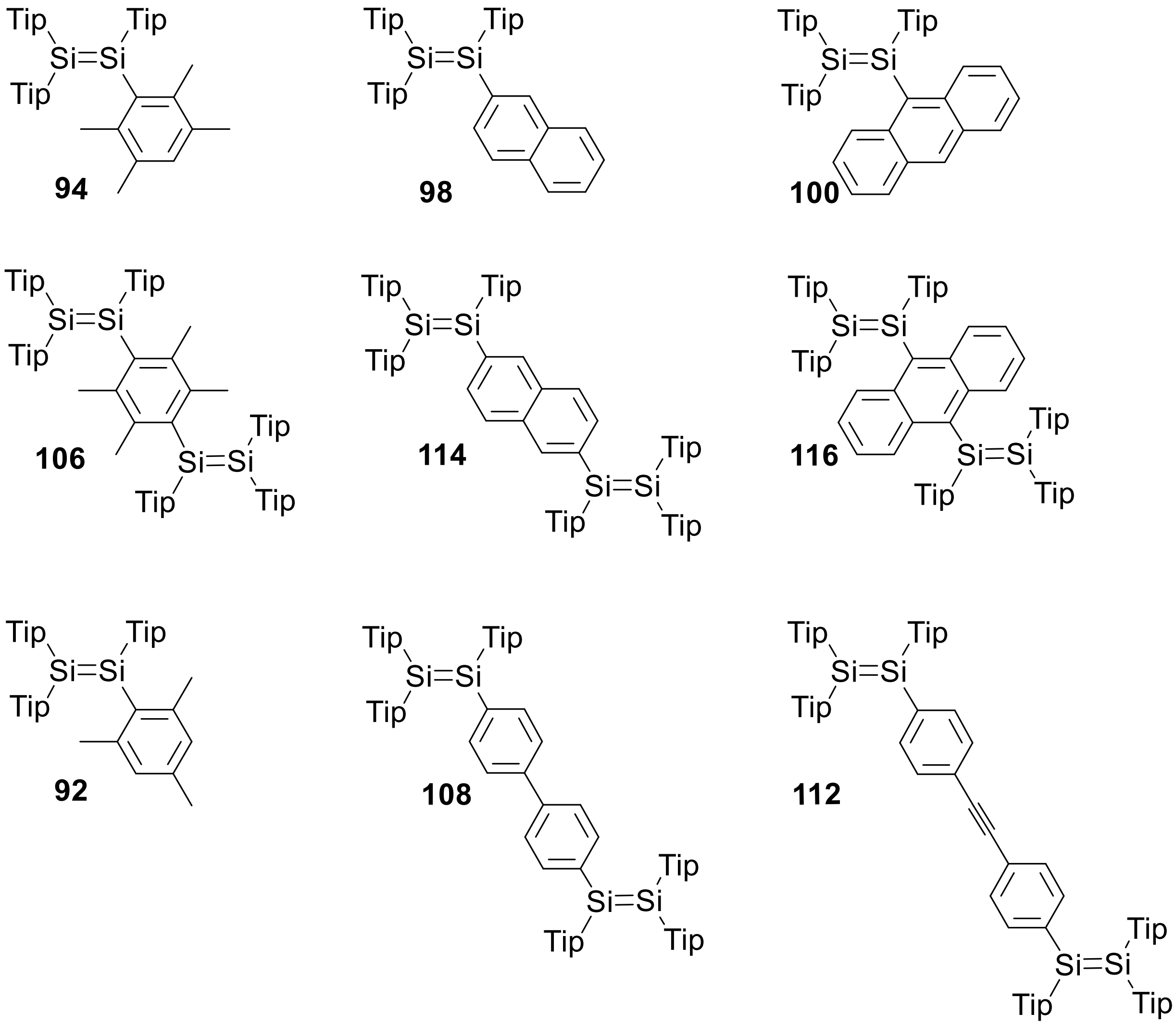

Figure 73. Series of different isolated aryl disilenes **92-100** and para-arylene bridged tetrasiladienes **106-116**.

3.1.4.1. Nuclear Magnetic Resonance and X-ray Structures

In all cases except for **106** and **116**, the quantitative formation of a new Si=Si-containing species was confirmed by the ^{29}Si NMR spectra obtained from the product mixtures. As shown in Table 1, each show two signals between 52.68 and 71.46 ppm in the typical range for aryl-substituted disilenes.[97] While In contrast, in case of **106** and **116**, the large number of signals in the ^{29}Si NMR solution spectra was rationalized by the presence of different rotational conformers in solution. Nonetheless, the well-resolved solid state CP-MAS ^{29}Si NMR spectra of **106** and **116** as well as the coalescence of three sets of signals of **106** into a single pair at elevated temperature (see Figure 36-37 in section 3.1.3.1 and Figure 61 in section 3.1.3.6) provide unambiguous evidence for this explanation and therefore the purity of **106** and **116**.

Table 1. ^{29}SiNMR data and structural parameters of isolated disilenes **92-100** and tetrasiladienes **108-116**.

Disilenes	**92**	**94**	**98**	**100**
δ^{29}Si1 (ppm)	55.76	57.88	71.05	60.08
δ^{29}Si2 (ppm)	55.42	52.95	56.74	52.68
ΣSi1 (°)	359.48	359.3	358.51	-
ΣSi2 (°)	359.41	359.9	359.89	-
Si1-Si2 (Å)	2.1453(6)	2.1516(7)	2.1525(6)	-
θ_{Si1} (°)	6.7	7.5	11.6	-
θ_{Si2} (°)	7.2	1.7	3.2	-
τ (°)	0.5	10.6	10.4	-
φ (°)	50.6	56.3	21.3	-
Tetrasiladienes	**108**	**112**	**114**	**116**
δ^{29}Si1 (ppm)	71.04	69.91	71.46	65.14
δ^{29}Si1 (ppm)	65.00	57.52	56.67	54.01
ΣSi1 (°)	359.52	357.43	359.64	359.8
ΣSi2 (°)	359.8	358.86	359.98	359.9
Si1-Si2 (Å)	2.1460(8)	2.1530(8)	2.1622(6)	2.1483(8)
θSi1 (°)	6.7	15.3	5.5	4.7
θSi2 (°)	4.2	9.7	1.3	3.5
τ (°)	11.4	6.4	7.7	1.8
φ (°)	24.8	45.9	38.7	74.6

All compounds appear to have a close to planar geometry about the silicon atoms as the sum of the bond angles at Si1 and Si2 ranges from 357.43 to 359.98°. Variable twisting angles τ are observed for the Si=Si bonds of isolated compounds, which may simply be taken as a measure of the differing steric congestion (Table 1; τ = 0.5 to 11.4°). The Si=Si bond distances (2.1453(6) to 2.1622(6) Å) are nevertheless at the short end of the range of literature values for aryl substituted disilenes (2.140 to 2.229 Å).[98] In fact, the Si=Si bonds of all new species are slightly shorter than the corresponding bonds of the less congested phenyl disilene **66** and phenyl tetrasiladiene *p*-**67**[80a] (2.1754(11) Å for **66** vs. 2.1674(8) Å for *p*-**67**). This somewhat counterintuitive observation can be rationalized by considering the more pronounced *trans*-bending of **66** and *p*-**67** compared to that in the new compounds (Table 1; **66**: θ_{SiTip} = 23.6°, θ_{SiTip2} = 22.3°; *p*-**67:** θ_{SiTip} = 16.5(2)°, θ_{SiTip2} = 19.3(2)°).[80a] As had been pointed out previously, a correlation exists between the sum of *trans*-bent angles and the Si=Si bond length for disilenes with electronically comparable substitution patterns.[80b]

Notably, **114** appears to contradict this correlation, which is based on the bonding model developed by Carter, Goddard, Malrieu, and Trinquier (the CGMT model).[31] Naphthalene-bridged tetrasiladiene **114** shows a unusually long Si=Si bond of 2.1622(6) Å despite the absence of significant *trans*-bending. This can probably be taken as an indication of more efficient delocalization of Si=Si π–bonding electron density towards the linking unit. Indeed, the bond distance between silicon and the naphthalene *ipso*-carbon atoms is short compared to that of **98** (Si-C(ipso) = 1.8700(18) for **98** vs. 1.8547(19) Å for **114**). The out-of-plane distortion of the linking unit in **114** appears to be sufficiently moderate to allow for effective conjugation (φ = 38.7°).

Remarkably, with φ = 74.6° the anthracene-bridged **116** exhibits the highest torsion angle, approaching orthogonality, which is expected to interrupt the conjugation between Si=Si and the triaromatic linker in **116** and hence could give rise to an intramolecular charge transfer transition (ICT) from the Si π system to the C π^* system as had been observed by Iwamoto *et al.* in related species.[81]

3.1.4.2. Photophysical Properties and Theoretical Studies

All isolated disilenes and tetrasiladienes were investigated by UV/vis spectroscopy, fluorescence spectroscopy and TD-DFT calculations in order to determine the influence of the organic linking unit (LU) on the photophysical properties of the compounds (Table 2). DFT-calculations were performed by Lukas Klemmer from our group whereas the fluorescence spectra were recorded by Daniel Maus from the group of Prof. Dr. Gregor Jung (Saarland University, Germany) using a Jasco Spectrofluorometer FP-6500.

Table 2. Photophysical data of isolated products and calculated wavelength maxima with HOMO LUMO gap energy of their optimized structure.

	State	λ_{max} (nm)	ε (M^{-1} cm^{-1})	λ_{max}^{exc} (nm)	λ_{max}^{em} (nm)	Φ[%]	$\lambda_{cal.max}$ (nm)	$E_{H\rightarrow L}$ (eV)
92	Hex	430	21200	-	-	-	-	-
94	Hex	430	17300	-	-	-	427	2.90
98	Hex	463	6800	-	-	-	468	2.64
100	Hex	550	3800	-	-	-	604	2.05
106	Hex	450	19700	-	-	-	-	-
108	Hex	463	21000	-	-	-	505	2.45
112	Hex	488	46000	514	570	<0.01	545	2.27
	Solid	-	-	574	619	0.015		
114	Hex	484	12000	525	574	<0.01	513	2.33
	Solid	-	-	552	587	0.04		
116	Hex	597	7500	-	-	-	657	1.88
	Solid	-	-	590	816	0.05		

The disilenes with the monoaromatic substituents **92** and **94** (**92**: Ar = Mes, **94**: Ar = Dur) show unremarkable longest wavelength absorptions in hexane solution at λ_{max} = 430 nm, which are just slightly blue-shifted by $\Delta\lambda$ = 9 nm compared to the more *trans*-bent **66a** (λ_{max} = 439 nm).[80a] In contrast, the oligoaromatic substituents of **98** and **100** (**89**: Ar = 2-naphthyl, **100**: Ar = 9-anthryl) result in a considerable red-shift of the longest wavelength absorptions at the expense of progressively reduced extinction coefficients (Table 2). Iwamoto *et al.* had identified the longest wavelength transition of their 9-anthryl substituted disilene **71c** at λ_{max} = 525 nm as an intramolecular charge transfer (ICT) band with an even smaller extinction coefficient of ε = 480 $M^{-1}cm^{-1}$.[81] This is undoubtedly a consequence of less efficient conjugation compared to **100**, an aspect that will be subject to closer inspection by DFT calculations (*vide infra*).

The lowest energy transitions of the bridged tetrasiladienes are as expected more or less red-shifted compared to disilenes with just one Si=Si unit. For **108**, however, the longest wavelength absorption at λ_{max} = 463 nm is blue-shifted by $\Delta\lambda$ = 45 nm compared to *p*-**67** with a single *para*-phenylene bridge.[80a] The in principle more extended conjugated π-electron system in **108** is apparently disrupted in solution by the twisting of the two biphenylene aryl rings, which is clearly confirmed by the solid state structure of **108** as determined by X-ray diffraction on a single crystal. Indeed, the introduction of an acetylene spacer between the two phenylene moieties as in **112** results in a red-shift of $\Delta\lambda$ = 25 nm compared to **108** as well as the by far highest molar extinction coefficient in this series of Si=Si unit containing derivatives (ε = 46000 $M^{-1}cm^{-1}$). As anticipated, the acetylene spacer of **112** conveys an efficient conjugative interaction between the two Si=Si units due to the relative unimportance of dihedral distortion of this linking unit due to the two orthogonal sets of π-orbitals in that case.

The moderate red-shift by about $\Delta\lambda$ = 20 nm of the longest wavelength absorption of durylene and naphthalene-bridged (**106** and **114**) compared to that of duryl and naphthyl-substituted (**94** and **98**) indicates a slightly less efficient π-conjugation in comparison to that observed between **66** and *p*-**67**[80a]. Furthermore, the intensities of the longest wavelength absorptions of **106** and **94** are nearly identical. While the extinction coefficient in naphthalene system is only approximately doubled along with the number of Si=Si units and hence of no diagnostic value (Figure 74).

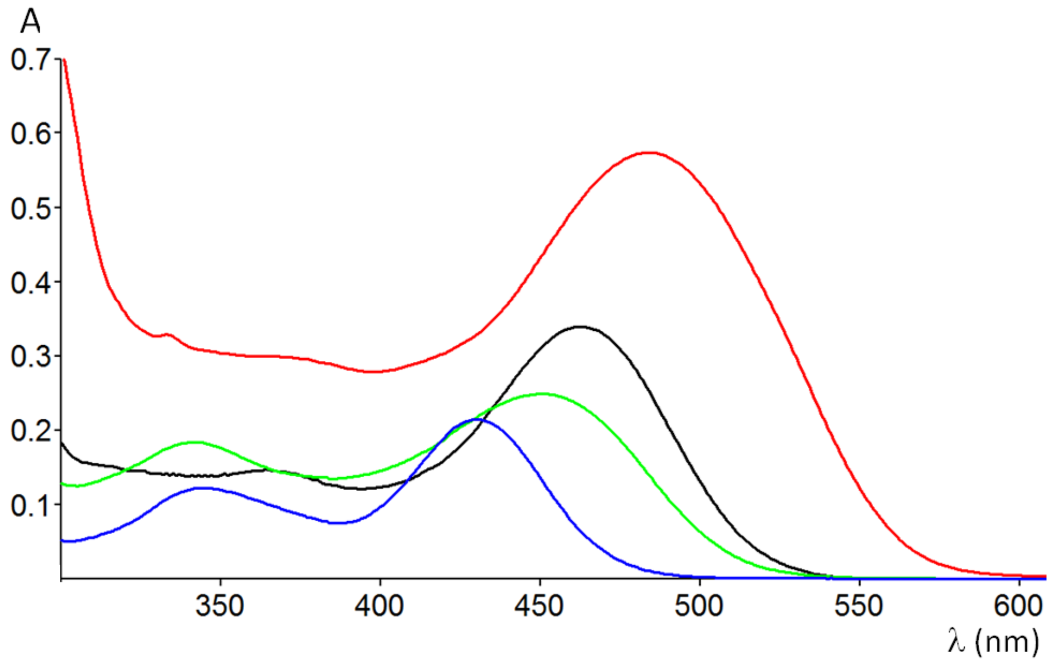

Figure 74. Normalized UV/vis spectra of **94** (blue), **98** (black), **106** (green) and **114** (red) in hexane (0.0005 M) at room temperature.

The dominant UV/vis absorption of a hexane solution of **116** (Figure 75) at λ_{max} = 422 nm (ε = 36600 $M^{-1}cm^{-1}$) is accompanied by another significantly weaker band at λ_{max} = 597 nm (ε = 7500 $M^{-1}cm^{-1}$), which is red-shifted by $\Delta\lambda$ = 47 nm compared to the corresponding absorption of **100** at λ_{max} = 550 nm (ε = 3800 $M^{-1}cm^{-1}$). This considerable red-shift together with the extinction coefficients being one order of magnitude larger than that reported for **71c** suggests that the electronic transition in case of **100** and **116** may in fact be best represented by a combination of π-π* and ICT transition despite the inversion symmetry of **116**.[100] Support for the ICT notion is gathered from the solvent dependency of the absorption bands. In the more polar thf solvent, the longest wavelength bands of **100** and **116** are shifted to λ = 568 nm (ε = 4000 $M^{-1}cm^{-1}$) and λ = 621 nm (ε = 8000 $M^{-1}cm^{-1}$), respectively (Figure 74). Solvatochromic effects are a typical feature of charge transfer transitions,[101] and had also been observed in case of the mono(disilenyl) substituted **71c**.[81] Interestingly, large changes of the static dipole moment upon excitation were previously observed for other non-planar antracene-derivatives.[102] An exhaustive experimental and theoretical treatment of the torsional potential and the symmetry-breaking influence of the solvent, however, is beyond the scope of this study.[103] Both, **100** and **116** also exhibit several additional overlapping bands between 300 and 400 nm that can be readily assigned to excitations of the anthracene system itself (*e.g.* λ_{max} of 9-(pentamethyldisilanyl) anthracene appears at 373 nm[104]).

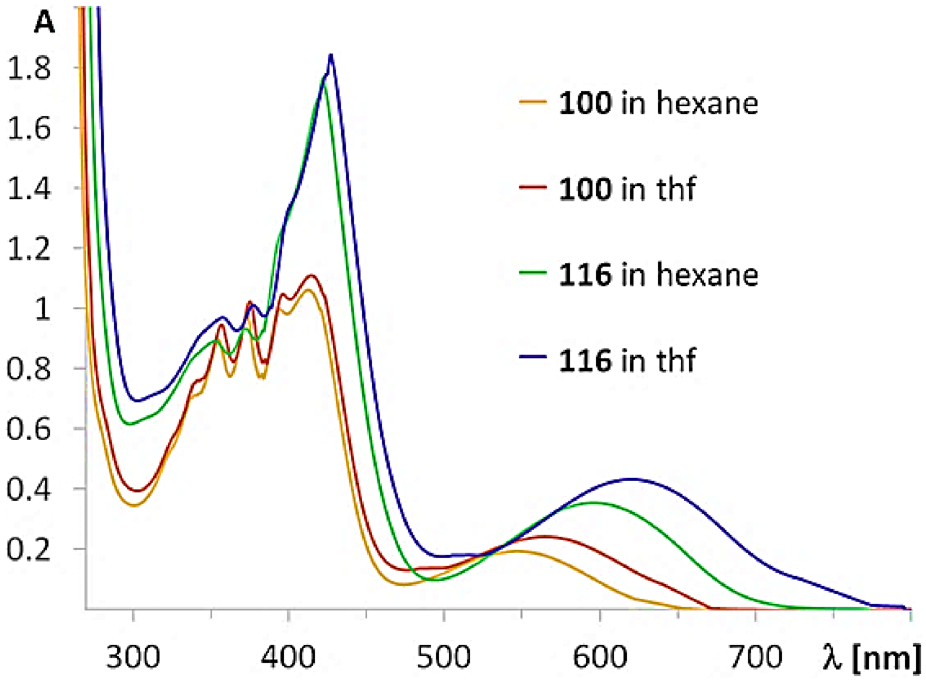

Figure 75. UV/vis spectra of **100** and **116** in hexane (0.0005 M) and thf (0.0005 M) solution at room temperature.

Given the dihedral distortion of the anthryl group and the Si=Si bonds of **100** and **116** a significant mixing of Si=Si and ligand- or bridge-centered orbitals would be unexpected. On the other hand, as had been pointed out before the conformational flexibility of the Si=Si unit in concert with the admixture of σ-electrons could allow for conjugative interactions even in cases when π-orbital overlap is small.[96] Alternatively, the absorption red-shift going from **100** to **116** may be an indication of excitonic interaction of the nearby, but not conjugated Si=Si units.

In order to shed light on these questions, and in particular, to obtain a better understanding of the extended π-conjugation features, possible intramolecular charge transfer and interplay between the two, density functional theory (DFT) calculations were performed at the B3LYP/6-31G(d,p)[105] level of theory using the Gaussian09 program package[106] where the Tip groups were simplified to the computationally less demanding Dip groups (Dip = 2,6-iPr$_2$C$_6$H$_3$).

The molecular structure of disilenes **94-100** and tetrasiladienes **108-116** determined by X-ray crystallography are reproduced well in the fully optimized structures of **(94-100)Dip** and **(108-116)Dip** (see Appendix). The calculated Si=Si bond distances of **(94-100)Dip** and **(108-116)Dip** are with 2.1675(5) to 2.182(6) Å reasonably close to the experimental values. The anthracene ring is substantially twisted from the Si=Si vector in both **100Dip** and **116Dip** with dihedral angles of φ = 64° and 65°, respectively. In the experimental case in the solid state, **116** shows a similar geometry with even slightly more twisting φ = 74.6°). For **100**, the experimental bond lengths or angles in the solid state cannot be reliably discussed due to issues with the quality of the data set. It should be noted, however, that Iwamoto's anthryl disilene **71c** showed a dihedral distortion of φ = 88° and thus very close to perfect orthogonality of ligand and Si=Si moiety.[81]

The frontier orbitals for **(94-100)Dip** and **(108-116)Dip** are shown in Figure 76 (for **98Dip** and **(108,114)Dip** see Appendix). The HOMOs predominantly consist of the π(Si-Si) orbital in all cases, with relatively minor participation from the p_z atomic orbitals (AOs) of the organic substituents or bridge. In stark contrast, the LUMO structure differs significantly depending on the nature of the organic moiety. For the duryl and naphthyl disilenes **94Dip** and **98Dip**, the LUMOs delocalize almost over the entire molecules. In tetrasiladienes **(108-114)Dip**, the LUMOs equally involve substantial π^*(Si−Si)−π^*(organic linker) mixing.

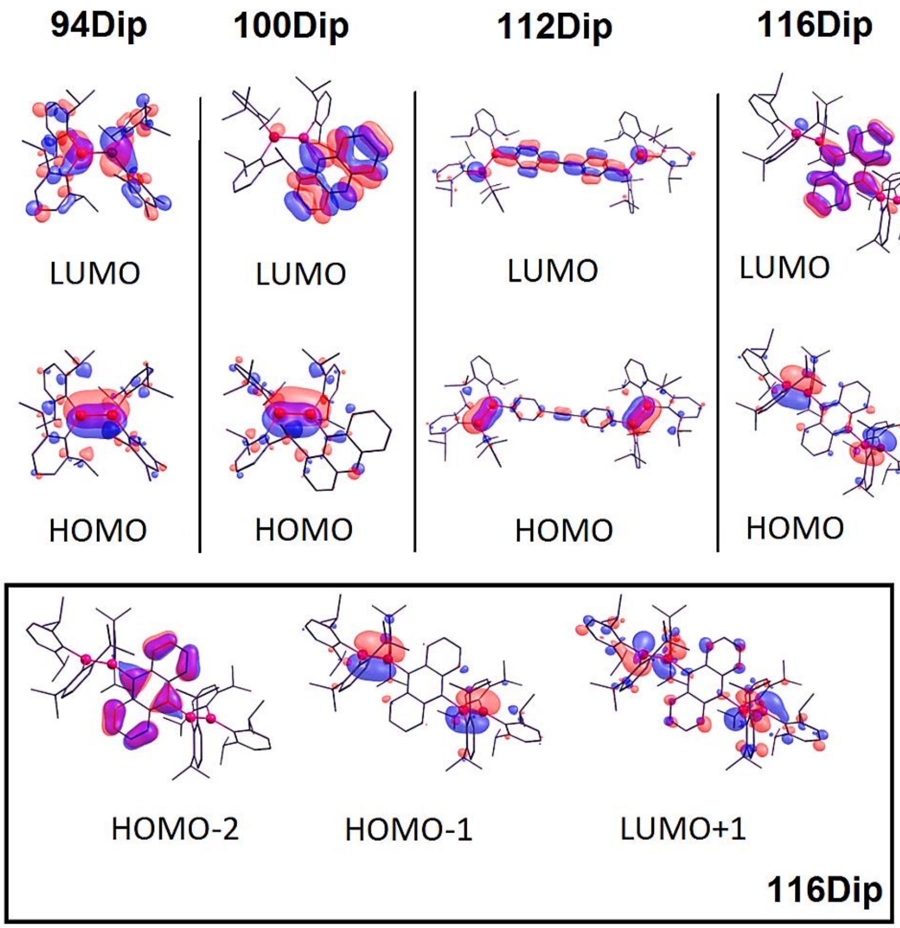

Figure 76. Selected frontiel orbitals of disilenes (**94,100)Dip** and tetrasiladienes (**112,116)Dip** (isovalue for all orbital plots = 0.03 a.u).

In contrast, the LUMOs of **100Dip** and **116Dip** are primarily represented by the π^*(anthracene) orbital with much less, but nonetheless significant contribution of the π^*(Si−Si) orbitals. In fact, an approximate reciprocal relationship between the dihedral twisting of the substituent/linking unit from the plane of the Si=Si units on the one hand and the amount of admixture of Si=Si centered π^* orbitals is apparent from visual inspection of the frontier orbitals (Figure 76). This is also in line with Iwamoto's anthryl disilene **71c** in which the anthryl group was shown to be close to being orthogonal to the Si=Si moiety and consequently no admixture of the Si-Si π^* orbitals to the ligand-centered LUMO can be discerned.[81] Indeed, the two bonding π orbitals HOMO and HOMO−1 of the anthryl-bridged tetrasiladienes **116** are not degenerate (as to be expected for isolated Si=Si bond), but separated by 0.1 eV instead. As shown in Table 2, the HOMO-LUMO gap decreases without exception when increasing the number of repeat Si=Si units from disilenes **(98,100)Dip** to tetrasiladiene **(114,116)Dip**. For instance, in case of naphthalene bridged disilene and tetrasiladiene the resulting overall decrease in the energy gap from 2.64 eV (**98Dip**) to 2.33 eV (**114Dip**) further supports the fact that the π-electron system extends over the two Si=Si units which are in conjugation through the naphthalene linker. TD-DFT calculations on (**94-100)Dip** and **(108-116)Dip** reproduce the absorption spectra of **94-100** and **108-116** (see Appendix) in a reasonably accurate manner (Table 2). The longest wavelength absorptions thus mainly originate from the HOMO→LUMO transitions.

In contrast to Iwamoto's anthryl disilene,[81] **112**-**116** exhibit fluorescence in solid state and in hexane solution at room temperature although the observed quantum yields are very poor, in fact close to the detection limit in some cases (Table 2, Figure 77).

For instance, in hexane at room temperature, **114** has a maximum wavelength excitation at λ_{max}^{exc} = 525 nm for a detectable emission intensity (λ_{em} = 610 nm), while a maximum emission wavelength (λ_{max}^{em} = 574 nm) occurs at an excitation wavelength of 450 nm.

Although the red-shift of the excitation spectra compared to the absorption spectra presumably results from an optical artefact due to the relatively high concentrations used for recording, the emission spectra barely overlap with the absorption spectra and therefore represent the actual transition wavelength from S_1 to S_0. In solid state at room temperature, **112** shows a red fluorescence with an emission maximum at λ_{max}^{em} = 619 nm, while **114** exhibits an orange fluorescence with an emission maximum at λ_{max}^{em} = 587 nm close to the solution value. Here, the exact emission wavelength not only depends on the extent of excitonic interaction of neighbouring molecules but also is sensitive to the crystal morphology,[107] and is therefore hardly predictable.

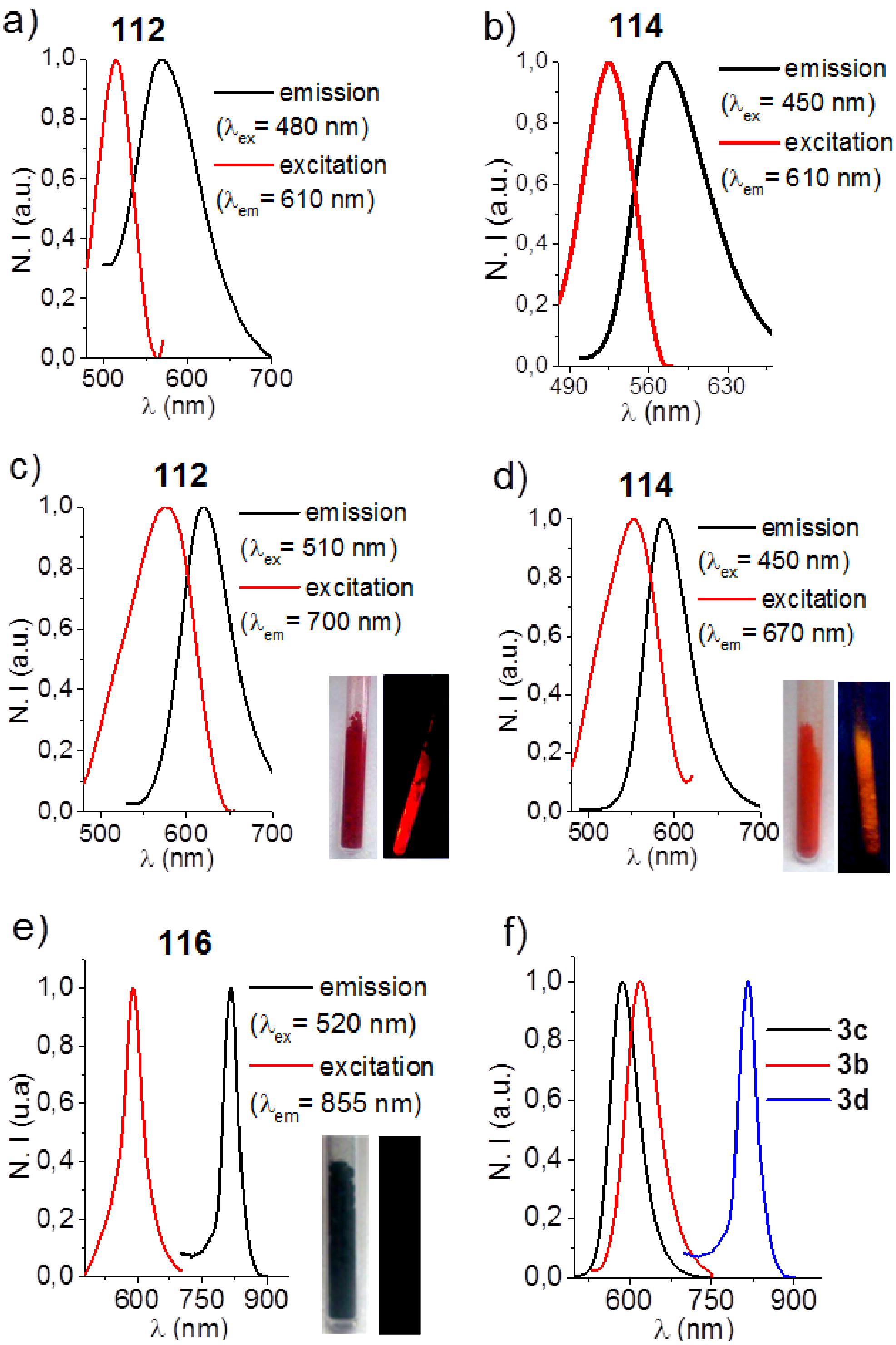

Figure 77. a), b) Excitation and emission spectra of **112** and **114** in hexane solution at room temperature; c), d), e) excitation and emission spectra of **112-116** in solid state at room temperature; f) emission spectra of **112-116** in solid state at room temperature grouped together for comparison. The inserts show photographic images of the fluorescence caused by a handheld UV-lamp with λ_{max} = 360 nm (dark in case of **116** due to emission in the near IR.

The most intriguing feature, however, is certainly the near-IR emission of **116** with an emission maximum at λ_{max}^{em} = 816 nm. Although, near-IR emission at room temperature is a rare phenomenon in main group chemistry in itself,[108] the emission response of **116** in the solid state is unlikely to be due to impurities as it is clearly related to the absorption maximum at about 600 nm (which was also predicted by TD-DFT calculations). The remarkably large Stokes-shift of $\Delta\lambda$ = 226 nm in **116** (about 4400 cm^{-1}) compared to **112** and **114** and other emissive disilenes[82,84] may partially result from the closer distance of the two Si=Si units within one molecule providing a larger excitonic splitting due to the r^{-3} dependence.[109] Unusually large Stokes shifts of more than 200 nm in the solid state may also be related to intermolecular coupling.[110] Such shifts can be observed in crystalline entities in dependence of the mutual orientation and strength of the individual, molecular transitions thus modifying the supramolecular emission. The apparent crystalline emission may be further influenced by the morphology of the crystals.[102] As a consequence, the Stokes-shift within a solid is not readily interpretable on a molecular basis and thus beyond the scope of this publication.[111]

Unfortunately, the quality of the emission data was insufficient for the determination of reliable lifetime data for these compounds. The low quantum yields both in solution and solid state of tetrasiladienes **112-116** are likely due to a rapid non-radiative relaxation of the excited states via the many vibrational modes that can be envisaged for these molecules. On the other hand, the fact that fluorescence can be readily observed, indicates that bulky substituents are appropriate for suppressing these movements and provide a strategy for further enhancement. Indeed, the photoemission of **112-116** is enhanced in the solid state, presumably due to the restricted motion of substituents.

3.2. Reactivity of Aryl Disilenes and *para*-Arylene Bridged Tetrasiladienes towards Phenyl Acetylene

After the successful synthesis of a variety of disilenes and tetrasiladienes, the use of these compounds as precursors of new ring systems was envisaged.

As reviewed in section 1.9, the [2+2] cycloadducts **89a** and **90** derived from the addition of phenyl acetylene to phenyl disilene **66** and tetrasiladiene *p*-**67** were isolated by Scheschkewitz group.[92] Based on this finding, the reaction of the different disilenes and tetrasiladienes introduced in the previous section towards acetylene should be investigated.

3.2.1. [2+2] Cycloadditions with Regular Regioselectivity

3.2.1.1. [2+2] Reaction with Species with One Si=Si Unit

Although 9-(2-naphthyl)carbazole substituted disilene **104** could not be isolated in crystalline form, it precipitates from solution in increased purity. Sufficiently clean samples for testing the reactivity of **104** towards phenyl acetylene could thus be obtained. This reaction was assumed to give insight not only to the structure of the final product but also the constitution of the substrate **104** itself.

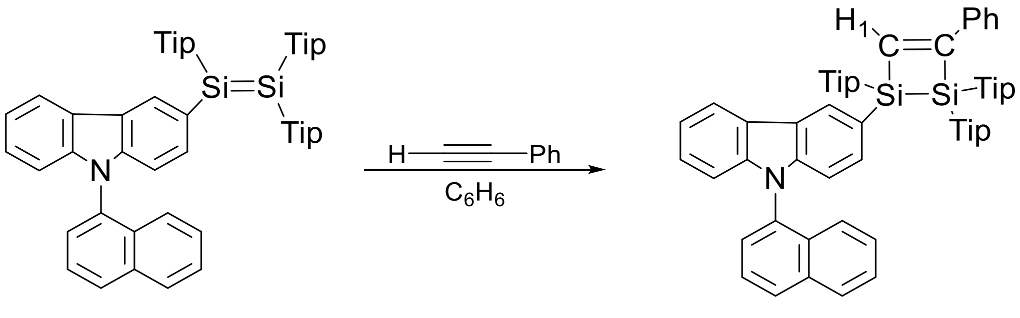

104 **120**

Scheme 47. Synthesis of disilacyclobutene **120**.

The reaction of one equivalent of phenyl acetylene with crude disilene **104** in benzene at ambient temperature is completed over the course of one hour (Scheme 47) as indicated by the color change from intense red orange to fade yellow.

In the ^{29}Si NMR, chemical shifts of equal intensity at δ = −11.16 and −11.58 ppm are observed (Figure 78), suggesting that the expected formal [2+2] cycloaddition product **120** is obtained in a regiospecific manner*.*

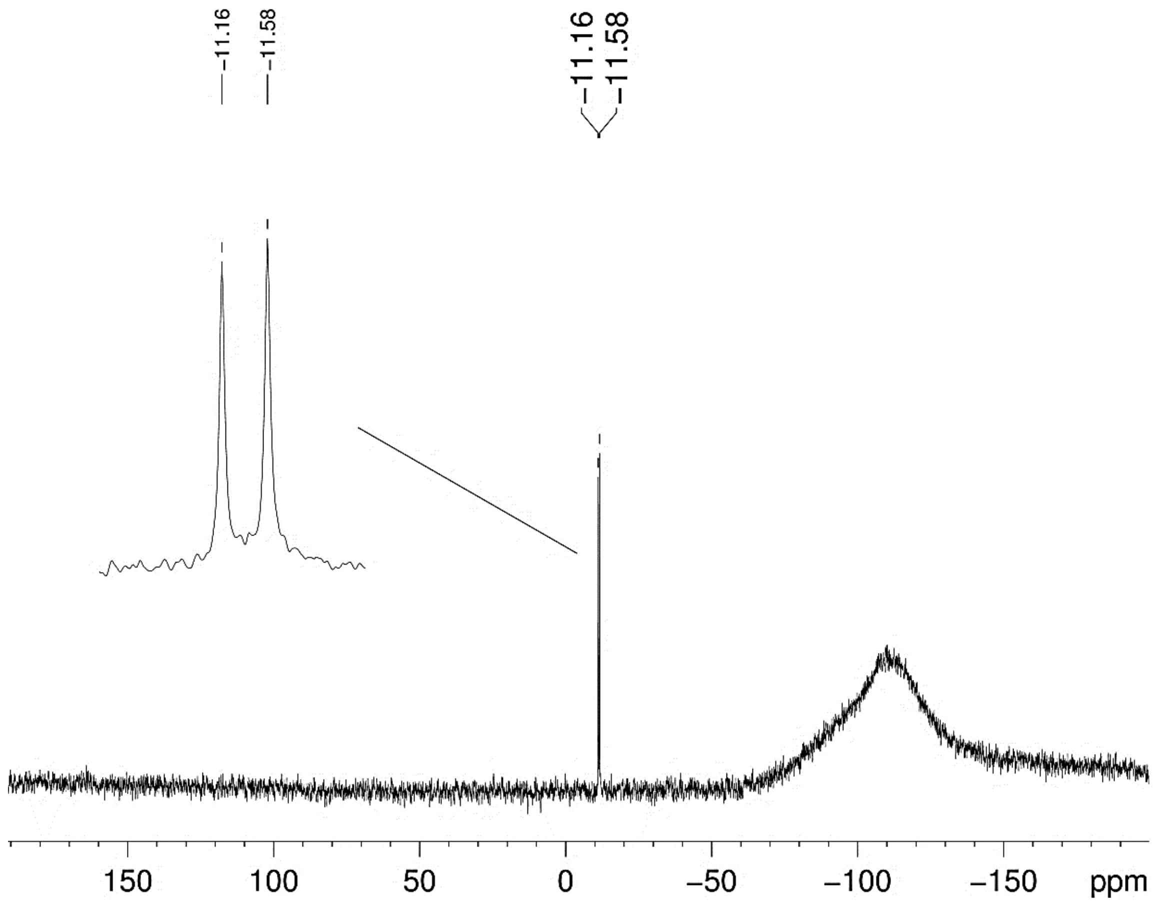

Figure 78. ^{29}Si NMR of the reaction mixture of disilene **104** with phenyl acetylene.

In the ^{1}H NMR spectrum, the resonance at δ = 8.33 ppm is attributed to the carbazole moiety while the vinylic proton shows a resonance at 7.94 ppm with satellite signals arising from coupling to the two endocyclic silicon atoms (^{2}J = 30 Hz and ^{3}J = 8 Hz). Additionally, distinct heptets in the isopropyl region and numerous doublets of comparable intensity in the alkyl region are visible suggesting selective conversion to a single product (Figure 79).

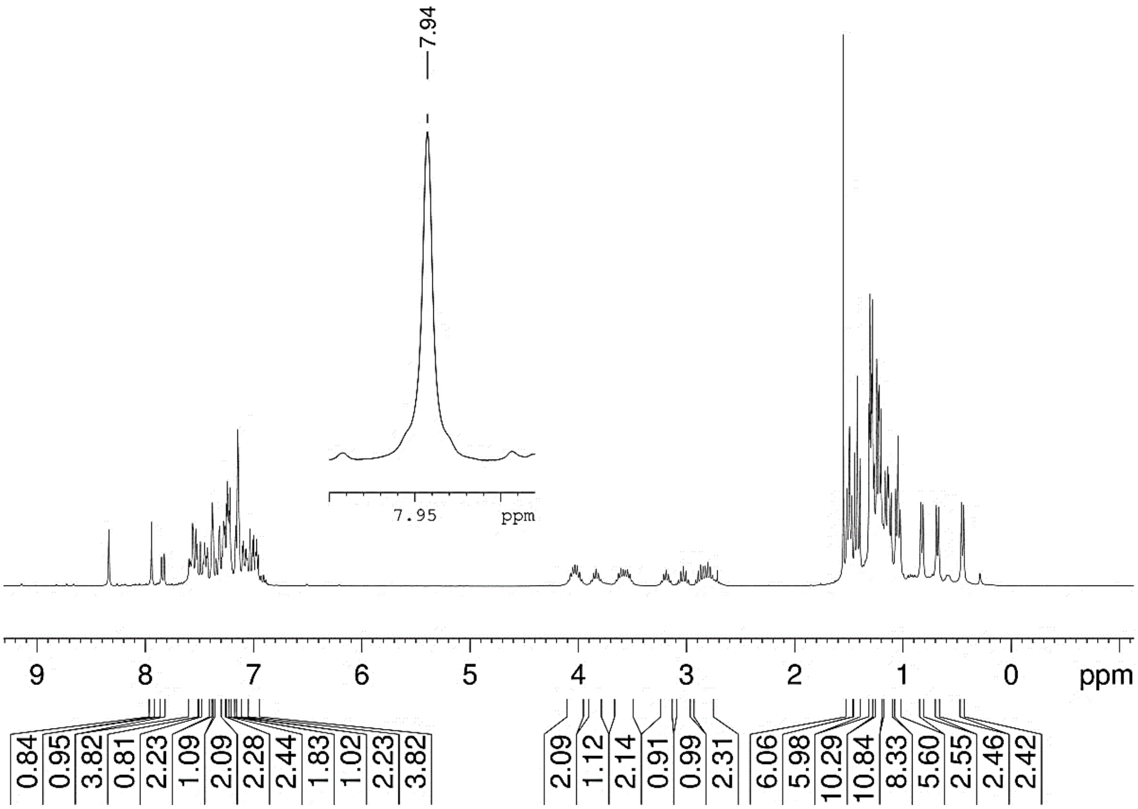

Figure 79. ^{1}H NMR of the reaction mixture of disilene **104** with phenyl acetylene.

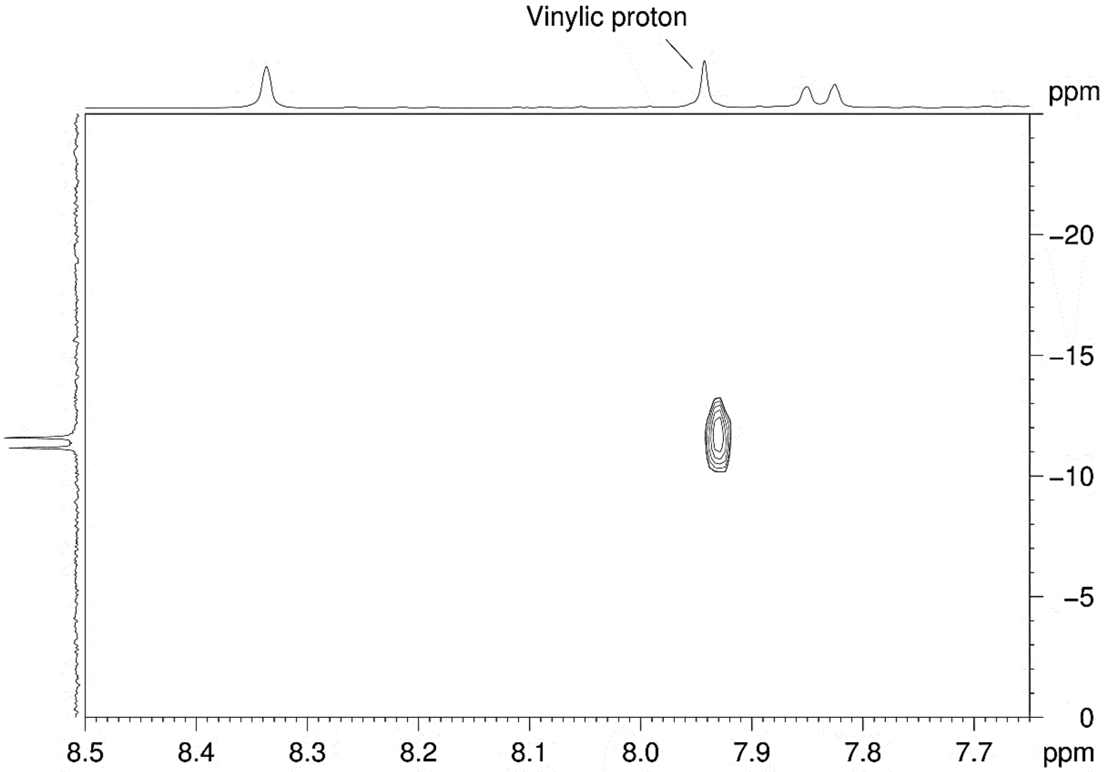

Figure 80. ^{1}H-^{29}Si NMR of the reaction mixture of disilene **104** with phenyl acetylene.

The ^{13}C NMR spectrum shows the endocyclic carbon atoms of the disilacyclobutene rings at δ = 172.91 and 156.91 ppm. In the 2D ^{1}H-^{29}Si NMR correlation, the two silicon atoms show one intense cross-peak to the endocyclic vinylic proton (Figure 80).

Colorless single crystals were obtained in excellent yield (94%) from a concentrated solution of acetone and benzene mixture (1 : 0.5).

The molecular structure was substantiated by single-crystal X-ray diffraction analysis (Figure 81).

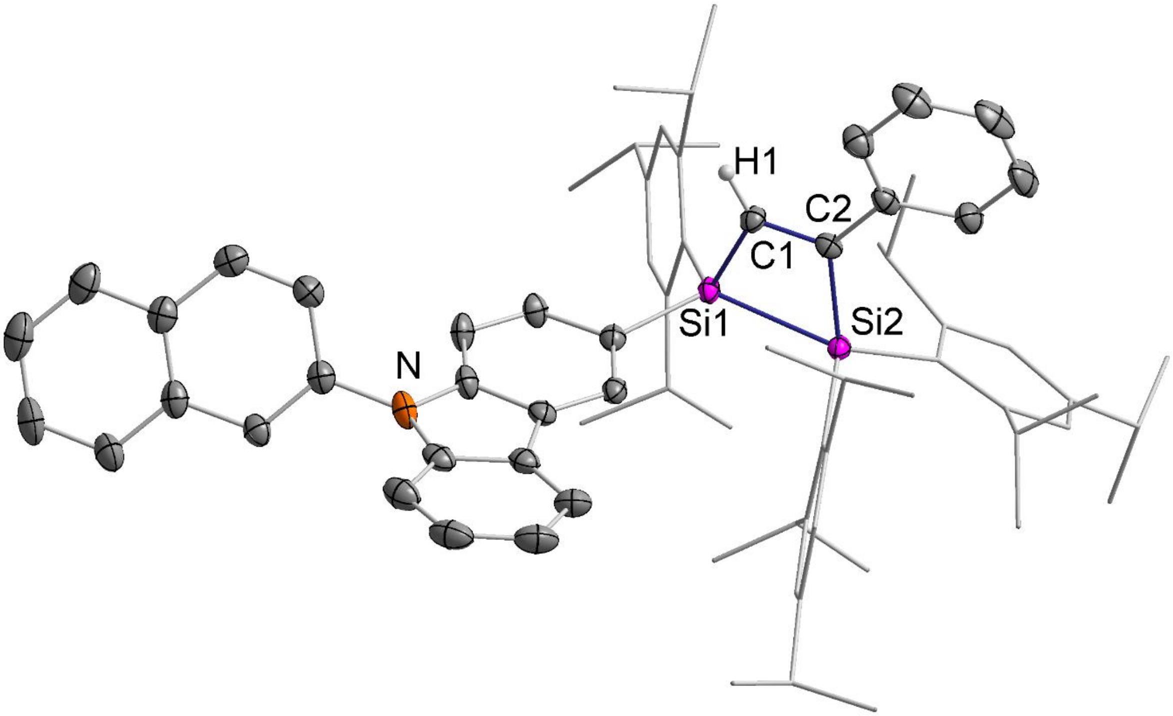

Figure 81. Molecular structure of **120** in the solid state (thermal ellipsoids at 50%, H atoms and disordered ^{i}Pr groups are omitted for clarity). Selected bond lengths [Å] and bond angles [°]: Si1-Si2 2.4197 (8), Si1-C1 1.876(2), Si1-C9 1.876(2), Si1-C32 1.914(2), Si2-C47 1.923(2), Si2-C2 1.910(2), Si2-C62 1.925(2), C(1)-Si(1)-Si(2) 73.02(7), C(2)-Si(2)-Si(1) 73.95(7), C(1)-C(2) 1.350(3), C(1)-C(2)-Si(2) 104.07(16), C(2)-C(1)-Si(1) 108.51(17).

The disilabutene **120** crystallizes in a triclinic space group (P-1). The endocyclic Si-Si single bond distance (2.4197(8) Å) is slightly longer than that of phenyl disilacyclobutene **89a** (2.4085(5) Å).[92] Due to the different covalent radii of silicon and carbon, the planar disilacyclobutene ring is also strongly distorted: the endocyclic angles to Si atoms are relatively acute (C(1)-Si(1)-Si(2) 73.02(7)° and C(2)-Si(2)-Si(1)

73.95(7)°), while the corresponding angles of the carbon atoms are both larger than 90° (C(1)-C(2)-Si(2) 104.07(16) and C(2)-C(1)-Si(1) 108.51(17)°.

The X-ray diffraction of the disilacyclobutene **120** serves also as prove of the constitution of the disilene **104** deduced from spectroscopic data.

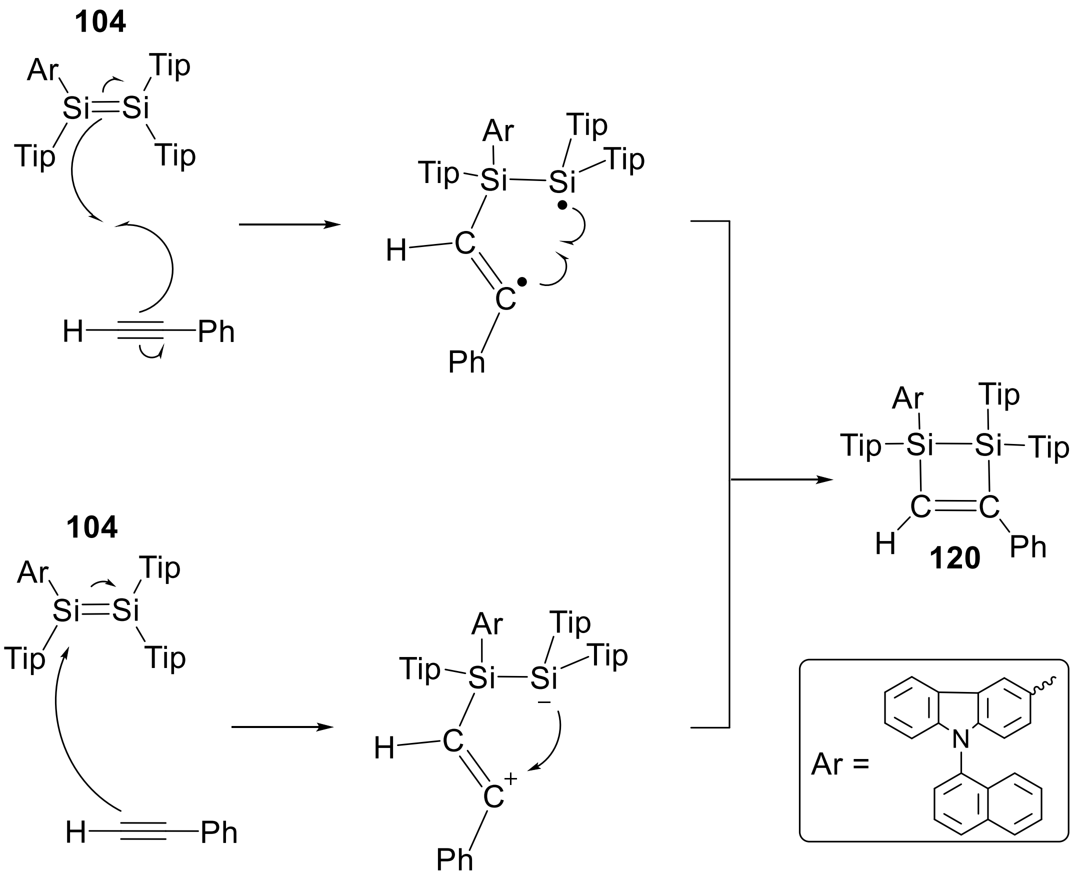

Scheme 48. Proposed mechanism for the addition of phenyl acetylene to disilene **104** to form **120** via the formation of of a biradical or zwitterionic intermediate.

Indeed, the formation of **120** provides further evidence for a stepwise mechanism for this type of reactions.

The simplest process that could lead to this result would involve addition of phenyl acetylene to disilene **104**, giving either a biradical or zwitterionic intermediate (Scheme 48). The initial attack presumably occurs to the sterically less hindered end of the Si=Si bond (i.e. the Ar-substituted silicon atom) and with the H-substituted end of phenylacetylene. Like in the case of **89a**,[92] the resulting species would then close, with the phenyl-substituted carbon atom is bonded to $SiTip_2$ moiety to give **120**. A concerted mechanism would presumably give rise to the other regio chemistry with the less hindered ends of the original substrates at opposing corners of the four-membered **120**.

3.2.1.2. [2+2] Reactions with Species with Two Si=Si Units

The addition of two equivalents of phenyl acetylene to the different *para*-tetrasiladienes derivatives **108**, **110**, **112** and **114** in benzene at room temperature (Scheme 49) results in a color change from intense red to bright yellow, indicating complete conversion to a new product. According to multinuclear NMR spectroscopy, all reactions proceed cleanly within less than two hours of stirring, under formation of the desired air-stable arylene-bridged bis(disilacyclobutene)s **121a-d**.

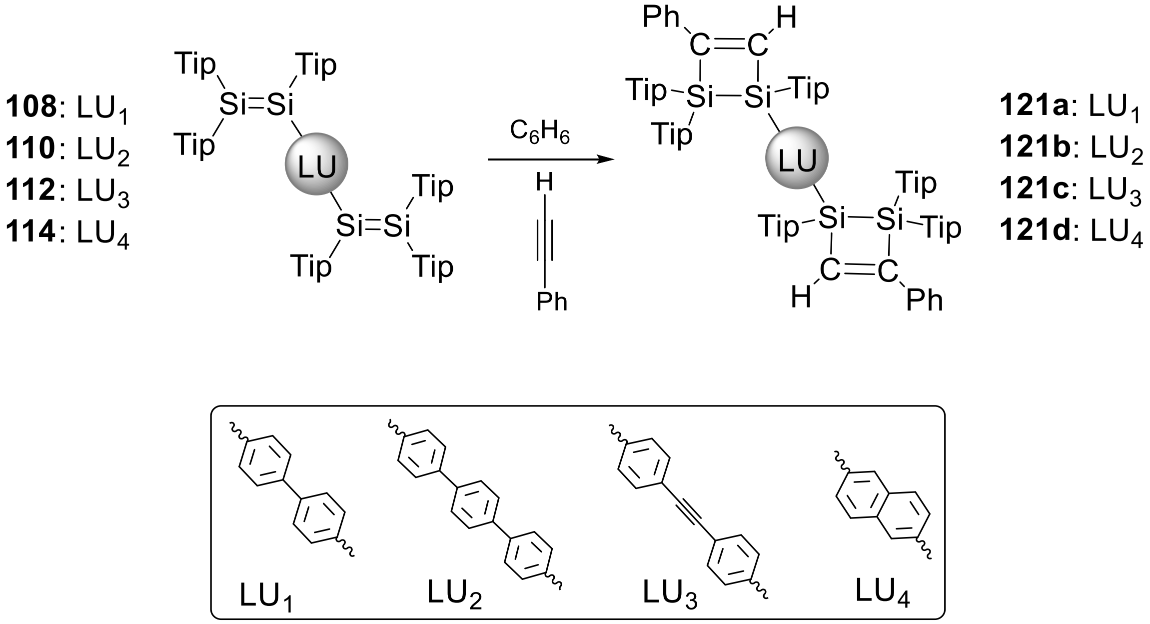

Scheme 49. Reactivity of different arylene bridged tetrasiladienes with two equivalents phenyl acetylene as well as example of the different linking units employed in this study.

Compounds **121a** and **121d** were successfully isolated as colorless crystals (mp. > 230°C) in high, coincidentally identical yields (**121a**: 86%; **121b**: 86%) after crystallization from a concentrated solution in a 1 : 1 mixture (hexane-isopropanol) and (thf-benzene) solution, respectively.

In contrast, crystallization of **121b** and **121c** from hexane, isopropanol, benzene and thf solvents remained unsuccessful. While the crude product of **121b** was obtained from a concentrated hexane solution as pure colorless solid in 84% yield, **121c** was obtained as slightly yellow solid with a small amount of impurities (< 10%) by removal of all volatiles in vacuum in 83% yield (mp. > 230°C).

All arylene-bridged bis(disilacyclobutene)s **121a-d** were completely characterized by multinuclear NMR (Table 3).

Table 3. NMR data of arylene bridged-bis(disilacyclobutene) **121a-d** as well as structural parameters of **121a** and **121d**. [a] saturated silicon atoms in disilacyclobutenes, [b] vinylic proton of the disilacyclobutenes and [c] endocyclic carbon atoms of the disilacyclobutene rings.

	121a	**121b**	**121c**	**121d**
δ ^{29}Si, ppm [a]	−11.28; −11.77	−11.25; −11.74	−11.30; −11.94	−10.79; −11.07
δ ^{1}H, ppm [b]	7.77	7.84	7.70	7.73
δ ^{13}C, ppm [c]	171.92; 155.95	173.22; 157.20	173.29; 156.81	173.22; 157.58
d(Si1-Si2), Å	2.3953(15)	-	-	2.4121(11)
C1-Si1-Si2, °	73.27(13)	-	-	72.75(10)
C2-Si2-Si1, °	74.14(13)	-	-	74.22(9)
C1-C2-Si2, °	103.6(3)	-	-	103.7(2)
C2-C1-Si1, °	108.1(3)	-	-	109.1(2)

Bis(disilacyclobutene)s **121a-d** show very similar ^{29}Si NMR spectra with two high-field signals between −11.94 and −10.79 ppm (see example **121a** in Figure 82 and Table 3) in the typical range for saturated silicon atoms in disilacyclobutenes rings,[92] suggesting the clean formation of [2+2] cycloadducts. Apparently, the ^{29}Si NMR shift is almost independent from the nature of the substituents and hence very characteristic for this type of cyclo adduct.

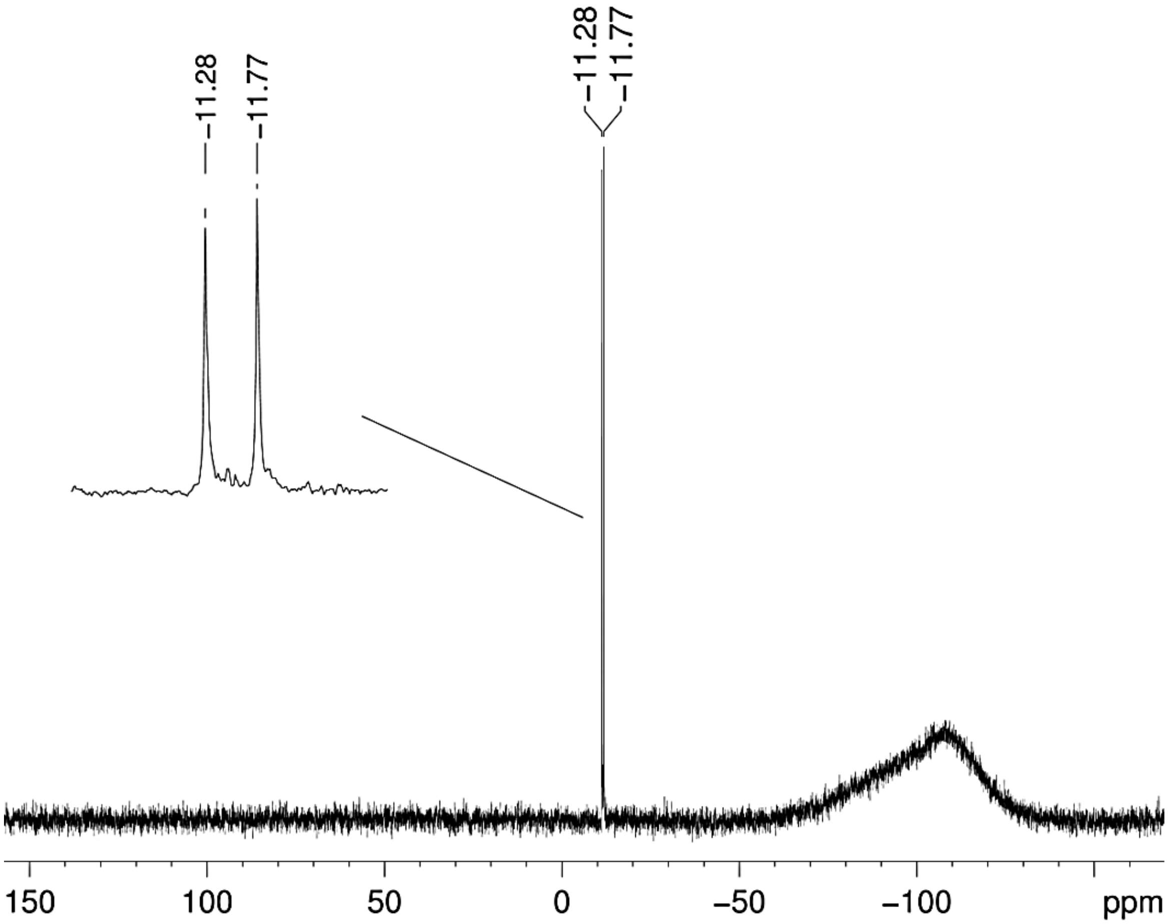

Figure 82. ^{29}Si NMR of biphenylene bridged bis(disilacyclobutene) **121a** exemplary for arylene bridged bis(disilacyclobutene) **121a-d**.

The ^{29}Si NMR spectra of **121c** show two major signals in the ratio 1 : 1 at $\delta = -11.94$ and −11.30 ppm in the usual typical range region for endoyclic saturated silicon species of disilacyclobutenes, alongside very minor signals of impurities (< 10%) of saturated silicon products ranging from −0.97 to −65.94 ppm (Figure 83). Competing reactions such as CH-additions or [2+2] cycloaddition with inversed regiochemistry would reasonably account for the side product **122** (Scheme 50) due to the different possibilities of permutation arising from the presence of two Si=Si units.

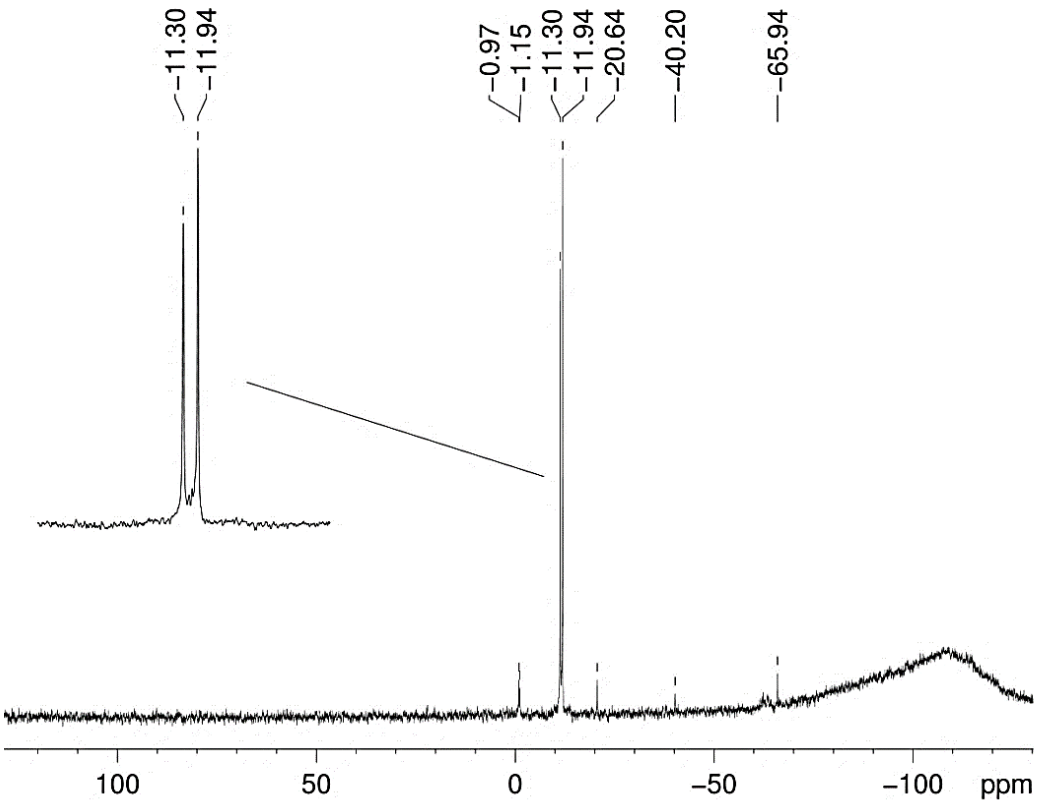

Figure 83. ^{29}Si NMR spectrum of the reaction of phenyl acetylene with bis(phenyl)acetylene-bridged tetrasiladiene **112**.

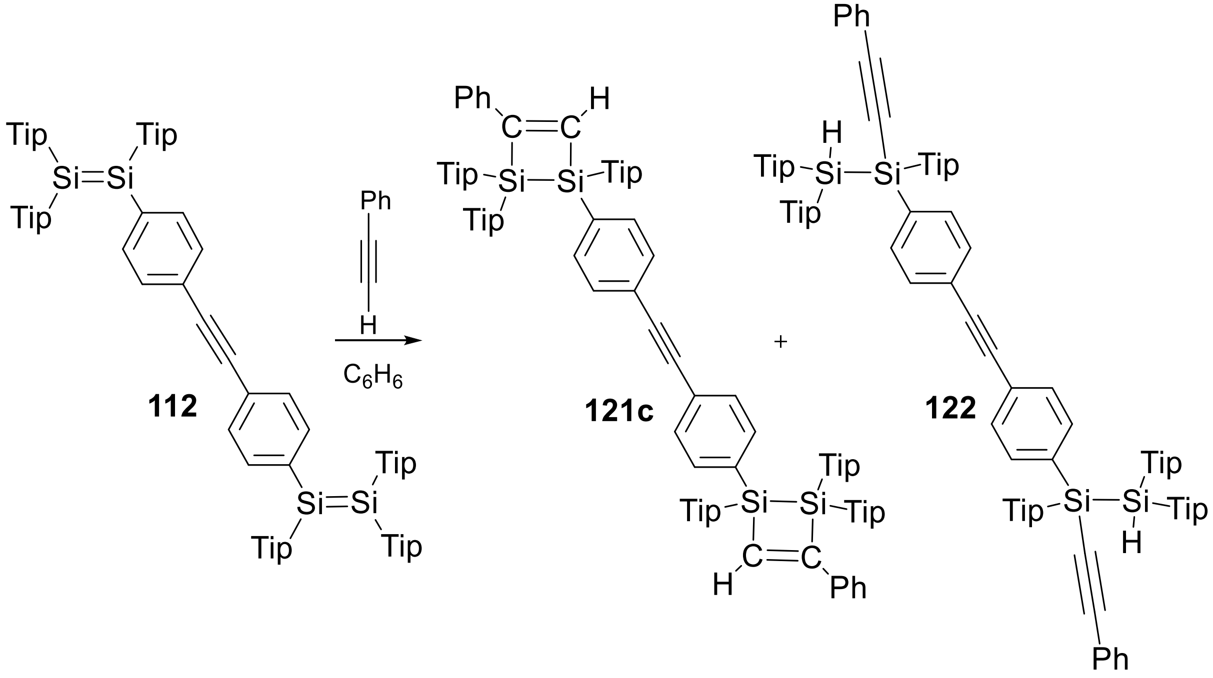

Scheme 50. Assumed reaction of tetrasiladiene **112** and phenyl acetylene, showing the expected [2+2] cycloadduct **121c** with the suspected side product **122** resulting from CH-addition.

In all cases, the examination of ^{1}H-NMR spectrum (see example **121a** in Figure 84 and Table 3) revealed the presence of the vinylic protons of the disilacyclobutene rings, which appear in the lowfield region of the spectrum as a singlet signal between 7.70 and 7.84 ppm with satellite signals arising from coupling to the two endocyclic silicon atoms (^2J = 29 Hz and ^3J = 8 Hz).

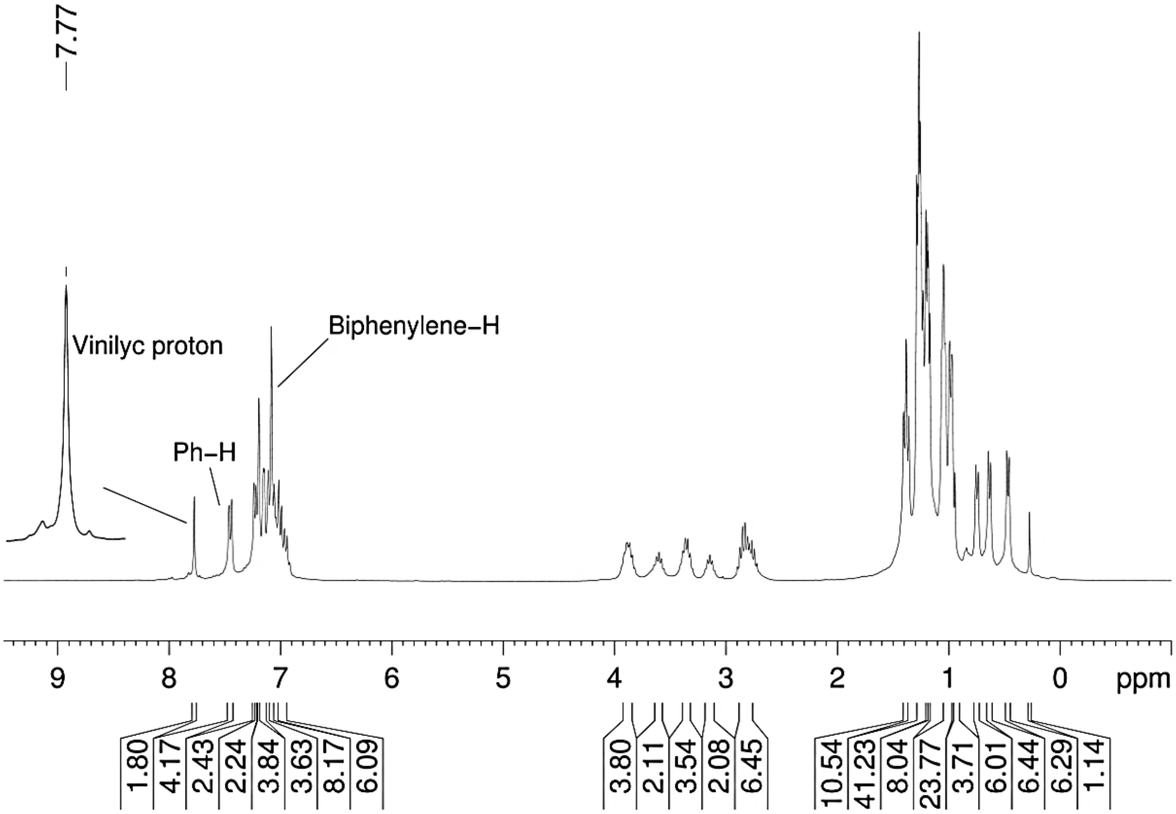

Figure 84. ^{1}H NMR of biphenylene bridged bis(disilacyclobutene) **121a** exemplary for arylene bridged bis(disilacyclobutene) **121a-d**. δ = 7.77 ppm is assigned to the vinylic protons of the disilacyclobutene ring appears.

The minor signal at δ = 5.51 ppm in the ^{1}H NMR of **121c** can be attributed to a silicon hydride species, which indicates the formation of the side products (< 10%) mentioned earlier and suggests that CH addition is indeed a competitive reaction pathway to some extend (Figure 85). As shown in Table 3, each of **121a-d** show the endocyclic carbon atoms of the disilacyclobutene rings between 155.95 and 173.29 ppm in the ^{13}C NMR spectrum. Furthermore, the central C-C triple bond connecting the two disilacyclobutene units of **121c** was observed at δ = 90.82 ppm (Figure 86).

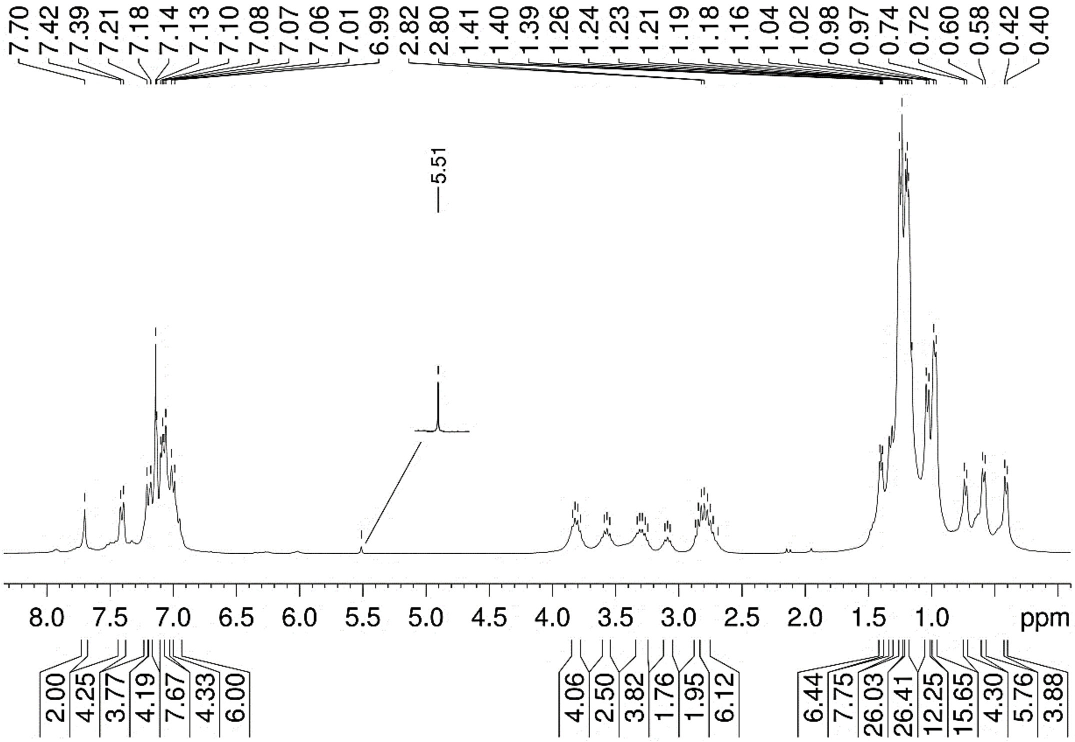

Figure 85. ^{1}H NMR spectrum of the reaction mixture of phenyl acetylene and bis(phenylene)acetylene-bridged tetrasiladiene **112**.

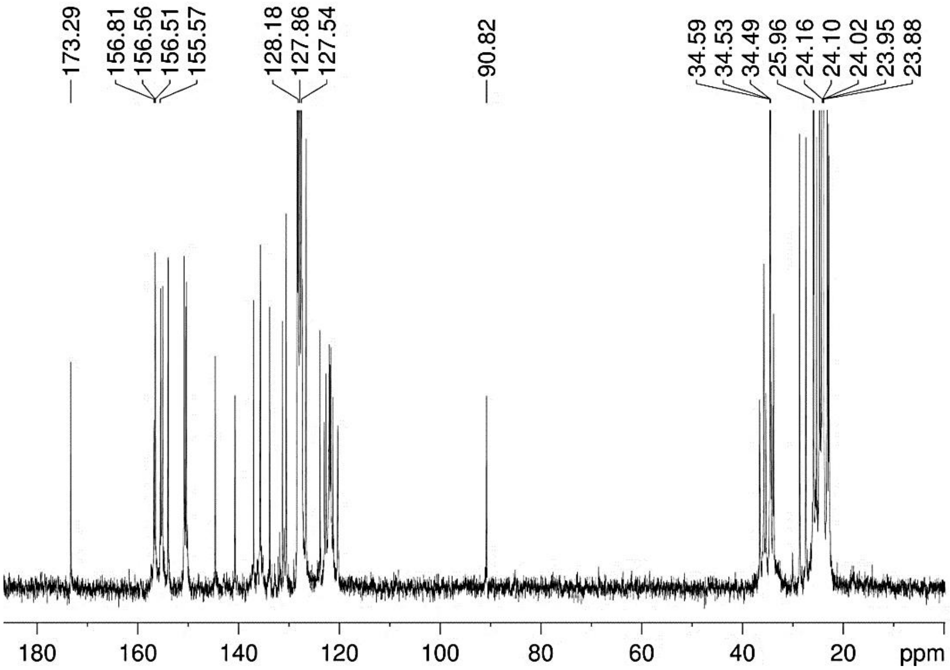

Figure 86. ^{13}C NMR of the reaction mixture of bis (phenyl) acetylene-bridged tetrasiladiene **121c** exemplary for arylene bridged bis(disilacyclobutene) **121a-d**. δ = 173.29 and 156.81 ppm the endocyclic carbon atoms of the disilacyclobutene rings and δ = 90.82 ppm for the central carbon carbon triple bond connecting the two disilacyclobutene units.

Coupling constants between the vinylic proton and the two endocyclic silicon atoms (SiTip and $SiTip_2$) of **121a-d** were derived from 2D ^{29}Si-^{1}H correlation spectra (see example **121a** in Figure 87). ^{2}J coupling constant for the correlation of the SiTip unit with the vinylic proton amounts to 29 Hz, while ^{3}J = 8 Hz is determined between $SiTip_2$ and the vinylic proton. The two coupling constants were verified in the ^{1}H NMR on the basis of the corresponding ^{29}Si satellite signals.

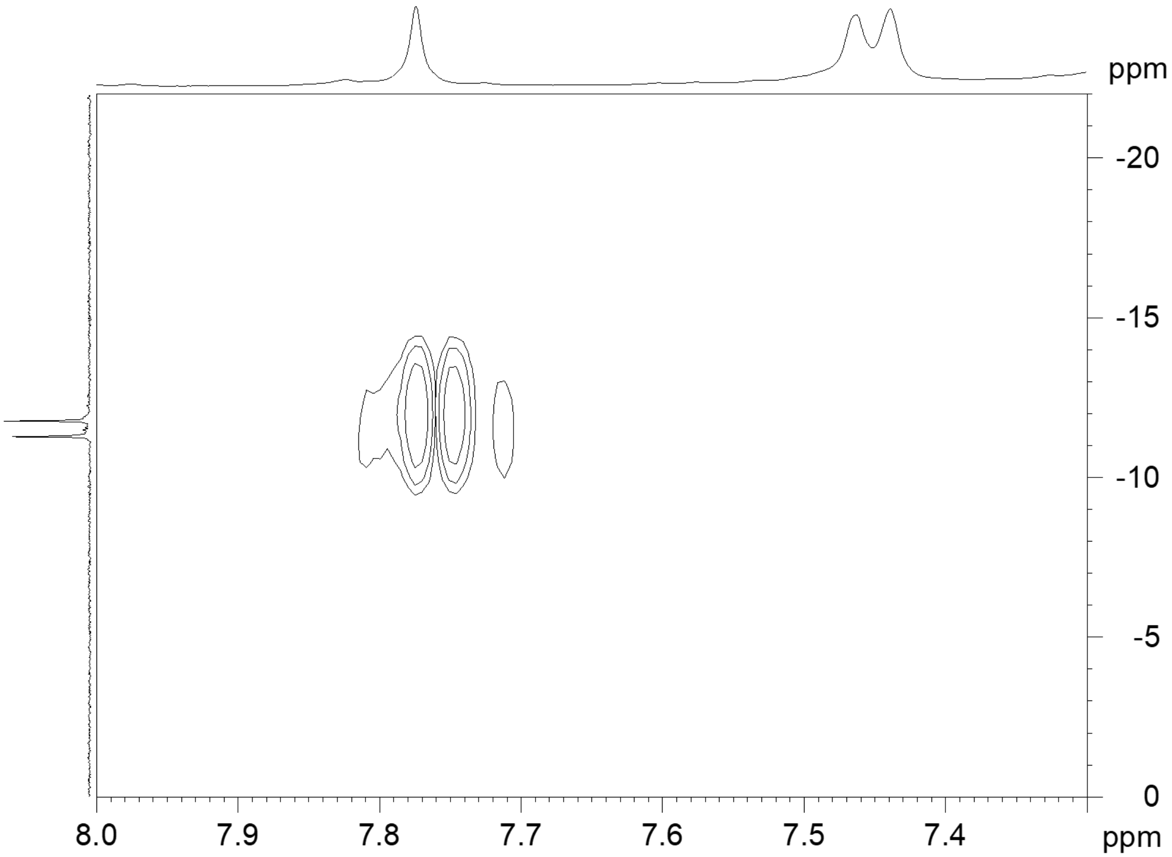

Figure 87. Section of a 2D NMR Spectrum of ^{29}Si-^{1}H correlation of **121a** used for the calculation of ^{2}J and ^{3}J coupling constant.

X-ray diffraction of **121a** and **121d** confirmed the NMR spectroscopic findings and revealed the structure of biphenylene and naphthalene- bridged bis(disilacyclobutene)s **121a** and **121d** (Figure 88 and 89), which also lends further support to the constitution of the other cycloadducts **121b-c** of which no single crystals could be obtained.

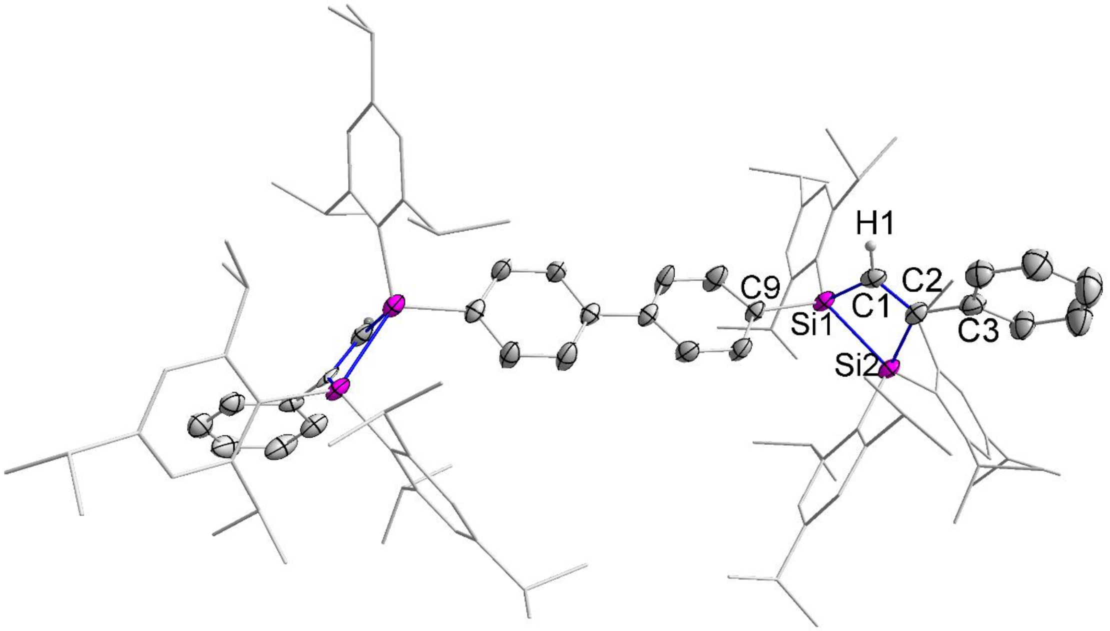

Figure 88. Molecular structure of **121a** in the solid state (thermal ellipsoids at 50%, H atoms and disordered ^{i}Pr groups are omitted for clarity). Selected bond lengths [Å] and bond angles [°]: Si1-Si2 2.3953 (15), Si1-C1 1.862(5), Si1-C9 1.882(4), Si1-C21 1.918 (4), Si2-C51 1.915(4), Si2-C2 1.899(4), Si2-C36 1.917 (4), C(1)-Si(1)-Si(2) 73.27(13), C(2)-Si(2)-Si(1) 74.14(13), C(1)-C(2) 1.352(5), C(1)-C(2)-Si(2) 103.6(3), C(2)-C(1)-Si(1) 108.1(3).

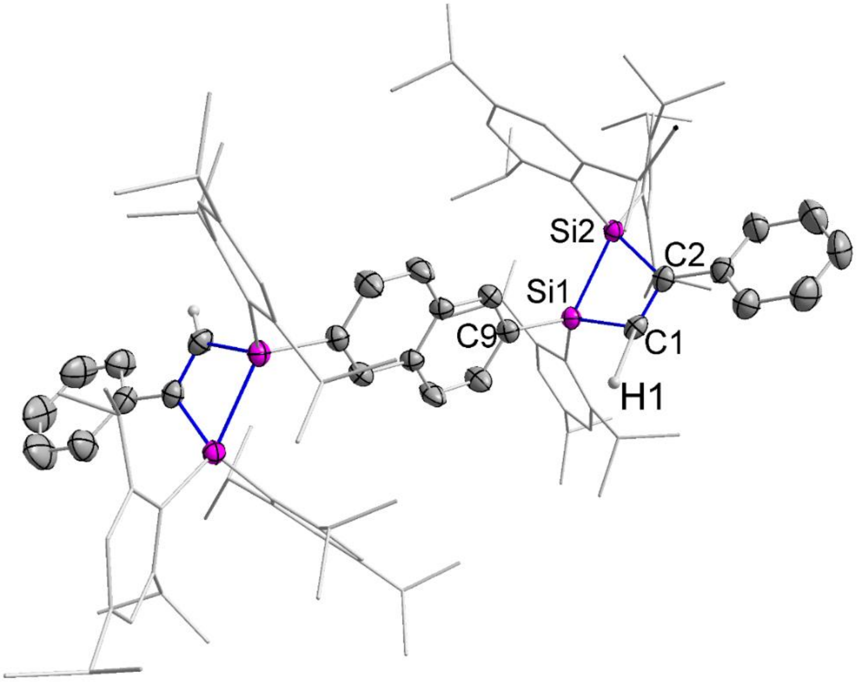

Figure 89. Molecular structure of **121d** in the solid state (thermal ellipsoids at 50%, H atoms and disordered ^{i}Pr groups are omitted for clarity). Selected bond lengths [Å] and bond angles [°]: Si1-Si2 2.4121 (11), Si1-C1 1.874(3), Si1-C9 1.878(3), Si1-C14 1.909(3), Si2-C29 1.902(3), Si2-C2 1.908(3), Si2-C44 1.917(3), C(1)-Si(1)-Si(2) 72.75(10), C(2)-Si(2)-Si(1) 74.22(9), C(1)-C(2) 1.341(4), C(1)-C(2)-Si(2) 103.7(2), C(2)-C(1)-Si(1) 109.1(2).

As shown in Figure 88 and 89, each bridged bis(disilacyclobutene) **121a** and **121d** crystallizes in the triclinic space group P-1 with only one half of the centrosymmetric molecule in the asymmetric unit. The Si2 atom is substituted by two Tip groups, whereas the Si1 is attached to the arylene linker and one Tip group. The two endocyclic Si-Si single bonds distances of **121d** (2.4121(11) Å) are comparable to what was found in phenylene-bridged bis(disilacyclobutene) **90** (2.4267(9) Å)[92] and slightly longer than in the biphenylene-bridged version **121a** (2.3953(15) Å). Due to the different covalent radii of silicon and carbon, the planar disilacyclobutene rings are strongly distorted: the endocyclic angles to Si atoms are relatively acute (C(1)-Si(1)-Si(2) 72.75(10)° and C(2)-Si(2)-Si(1) 74.22(9)°), while the corresponding angles of the carbon atoms with both are greater than 90° (C(1)-C(2)-Si(2) 103.7(2) and C(2)-C(1)-Si(1) 109.1(2)°.

In both cases, the C1, C2, Si1, and Si2 form an almost perfectly planar trapezoid (sum of internal angles about 359°) with the endocyclic angles to Si atoms are relatively acute [C1-Si1-Si2: 72.75(10)° to 73.27(13)° and C2-Si2-Si1 74.14(13)° to 74.22(9)° as well as the endocyclic angles to C atoms larger than 90° (C1-C2-Si2 103.6(3)° to 103.7(2)° and C2-C1-Si1 108.1(3)° to 109.1(2)°; Table 3).

3.2.2. [2+2] Cycloadditions with Reversed Regioselectivity

3.2.2.1. [2+2] Reaction with Species with One Si=Si Unit

When a mixture 1:1 of phenyl acetylene and duryl disilene **94** is dissolved in benzene at room temperature (Scheme 51) no color change is observed after 2 h and ^{29}Si NMR spectrum shows the presence of starting material. The reduced reactivity of **94** could be explained by the more severe steric congestion of the duryl group.

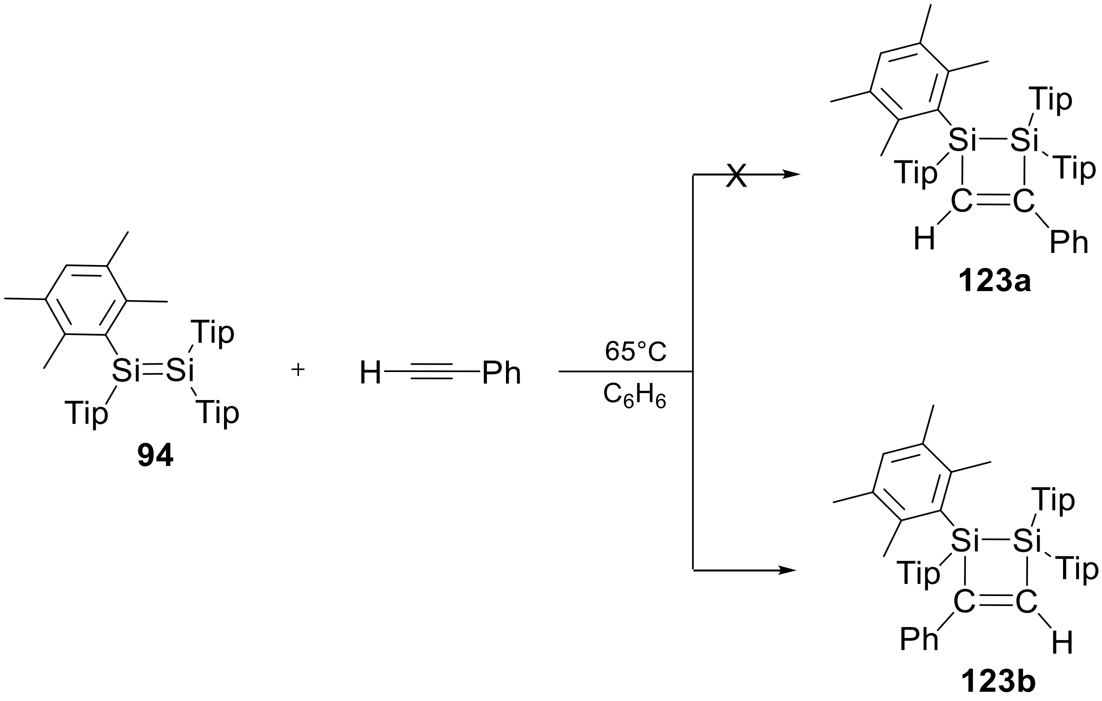

Scheme 51. Reaction of disilene **94** with phenyl acetylene in benzene at 65°C.

For this reason, the reaction mixture was heated up to 65 °C and left stirring overnight at this temperature. The solution turns colorless from bright yellow and the ^{29}Si NMR spectrum shows the disappearance of the two low field signals related to the Si-Si double bond. Three new signals at chemical shifts in the saturated region at δ = 2.89, 2.19 and −10.38 ppm in a ratio of 1.3 : 1: 2.5 (Figure 90) are distinctly different from those of the disilacyclobutene derivatives **120** and **121a-d** described in the previous section and therefore – initially in a tentative manner – attributed to the reversed regioisomer **123b**. The similarity of the signals at approx. 2 ppm indicated that an isomeric mixture could have formed during the reaction and thus the signal at δ = −10.38 ppm may correspond to a superposition of two coincidentally identical signals. As the product is unlikely to be a mixture of regioisomers given the close to invariant chemical shifts for **120** and **121a-d**, a plausible explanation for the occurrence of two very similar sets of signals would be conformational isomerism.

In the ^{1}H NMR spectrum (Figure 91), two diagnostic singlet signals in approximately ratio 1.2 : 1 at δ = 7.81 and 7.80 ppm for the two vinylic protons of the crude product with one set of resolved ^{29}Si satellite signals each.

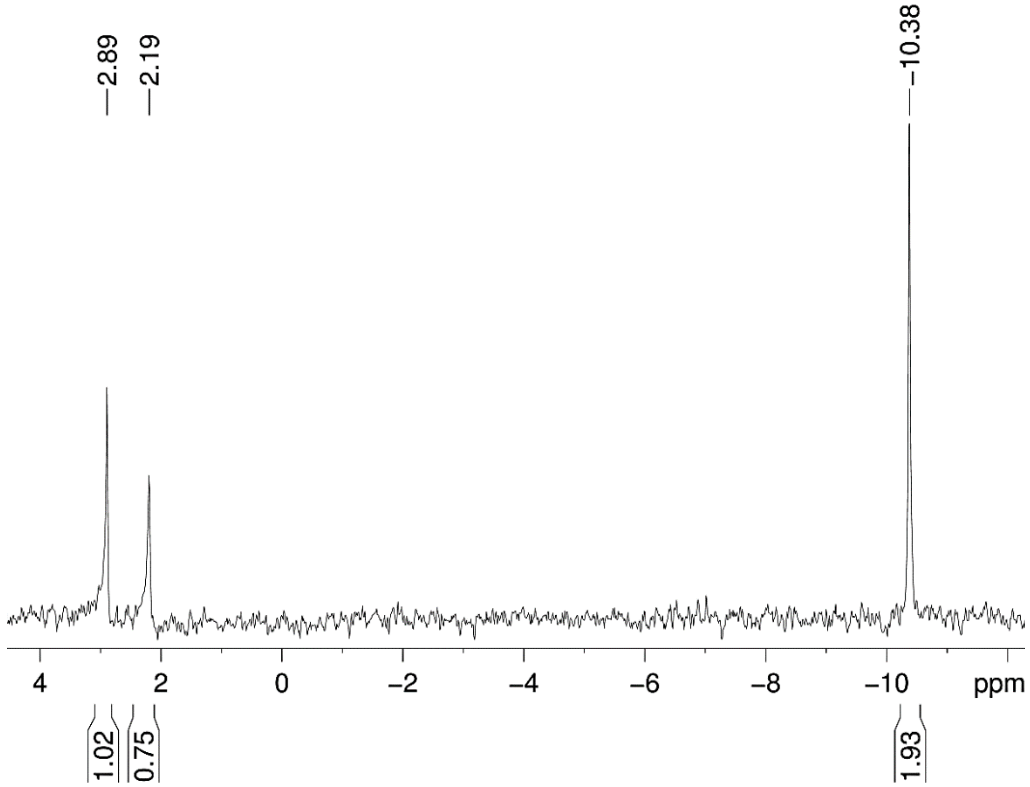

Figure 90. ^{29}Si NMR spectrum of the reaction mixture of phenyl acetylene and disilene **94**.

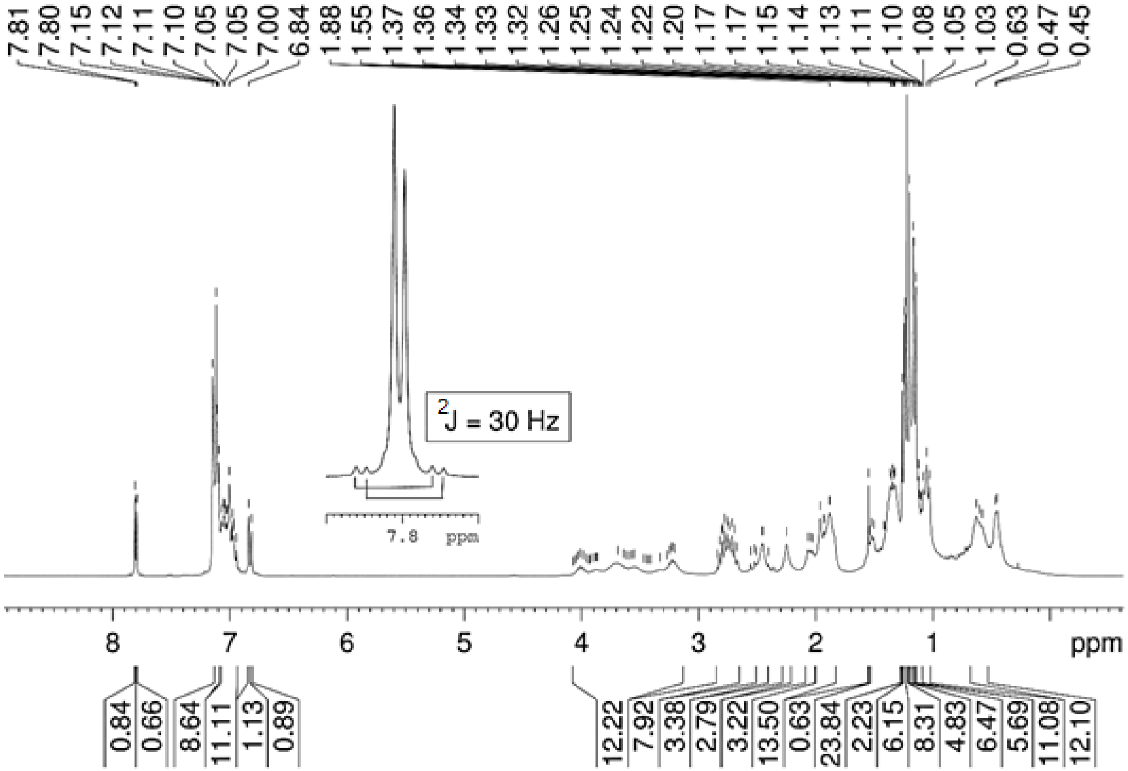

Figure 91. ^{1}H NMR spectrum of the reaction mixture of phenyl acetylene and disilene **94**.

The coupling constants between the vinylic proton and the two silicon centers (SiTip and SiTip$_2$) were calculated for each isomer from 2D ^{29}Si-^{1}H correlation spectrum (Figure 92) and verified in the ^{1}H NMR on the basis of the ^{29}Si satellite signals. Both isomers show nearly identical *J* values (^2J = 30 Hz and ^3J = 8 Hz). Notably, each two of the comparatively deshielded silicon resonances at δ = 2.89 and 2.19 ppm show cross-peaks to these signals with a coupling constant of ^2J = 30 Hz, in addition to further cross-peaks to two of the Tip substituents. Evidently, in both isomers the SiTip$_2$ moieties are directly bonded to the carbon atom carrying the vinylic proton, which clearly proves that conformational isomerism is responsible for the occurrence of two sets of signals rather than the presence of different regioisomers.

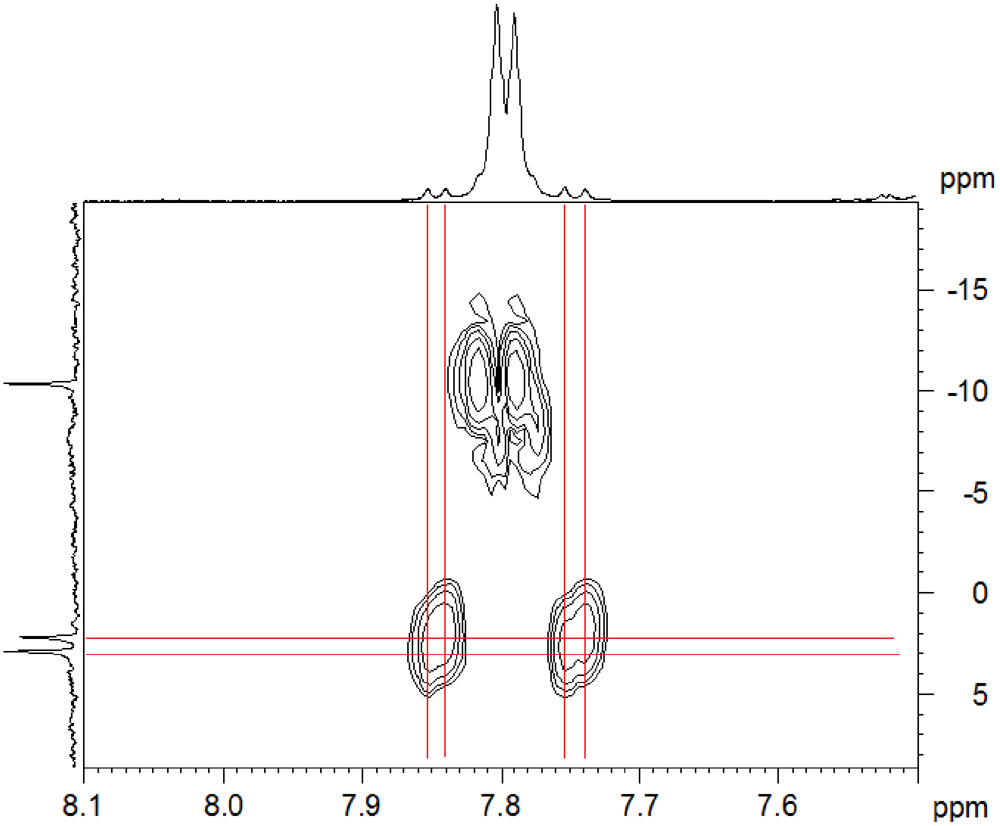

Figure 92. ^{1}H-^{29}Si NMR spectrum of the reaction mixture of phenyl acetylene and disilene **94**.

The final product was isolated as colorless crystals (mp. 182-188°C) from a concentrated hexane solution in 90% yield and it was therefore possible to confirm its constitution as disilacyclobutene **123b** with the opposite regiochemistry to that of the anticipated **123a** by X-ray diffraction on a single crystal (Figure 93). **123b** crystallizes in triclinic space group (P-1). Unlike the structure of the reported disilacyclobutene **89a**[91] and **120**, the phenyl-substituted carbon atom is bonded to the sterically less congested Si(Dur)Tip moiety. This may indicate a change of the mechanistic pathway from dipolar/diradical to concerted (Scheme 52). Currently, however, there is no further evidence available to back this assertion.

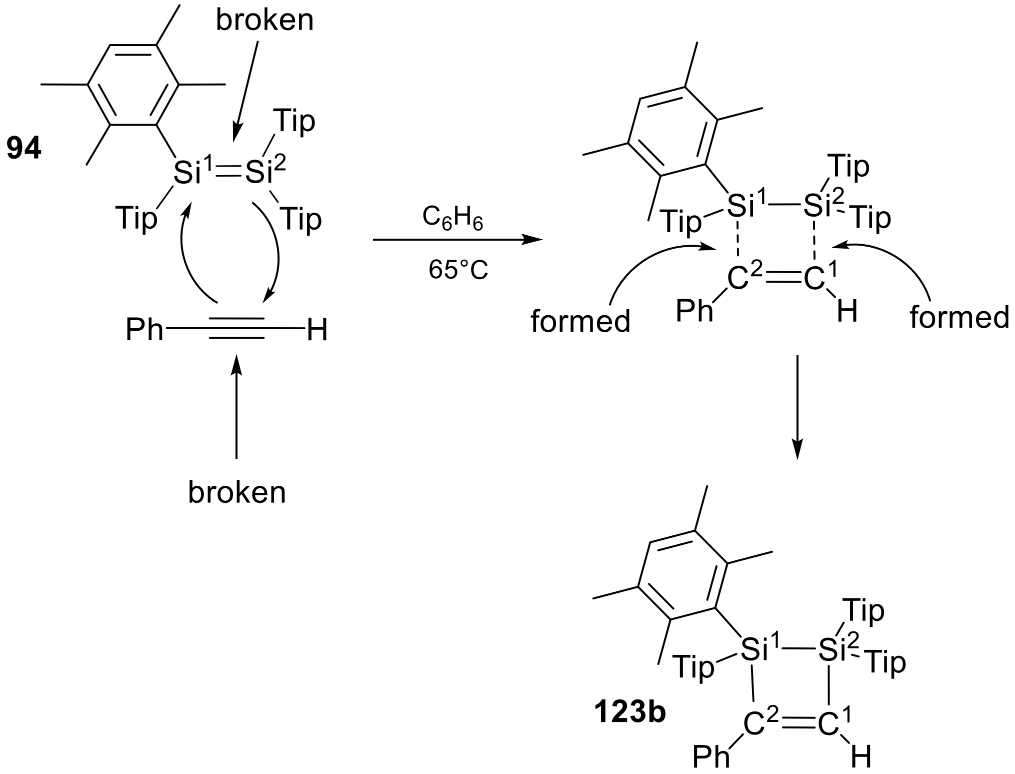

Scheme 52. Proposed concerted mechanism for the addition of phenyl acetylene to disilene **94** to form **123b**.

The endocyclic Si-Si single bond distance of **123b** (2.4535(19) Å) is remarkably longer than that of disilacyclobutene **89a** (2.4085(5) Å)[92] presumably due to the more pronounced steric bulk of the duryl moiety in **123b**. Due to the different covalent radii of silicon and carbon, the planar disilacyclobutene rings are as usual strongly distorted: the endocyclic angles to Si atoms are relatively acute (C(2)-Si(1)-Si(2) 73.45(14)° and C(1)-

Si(2)-Si(1) 72.49(14)°, whereas the corresponding angles of the carbon atoms with both are greater than 90° (C(1)-C(2)-Si(1) 103.4(3)° and C(2)-C(1)-Si(2) 110.0(17).°

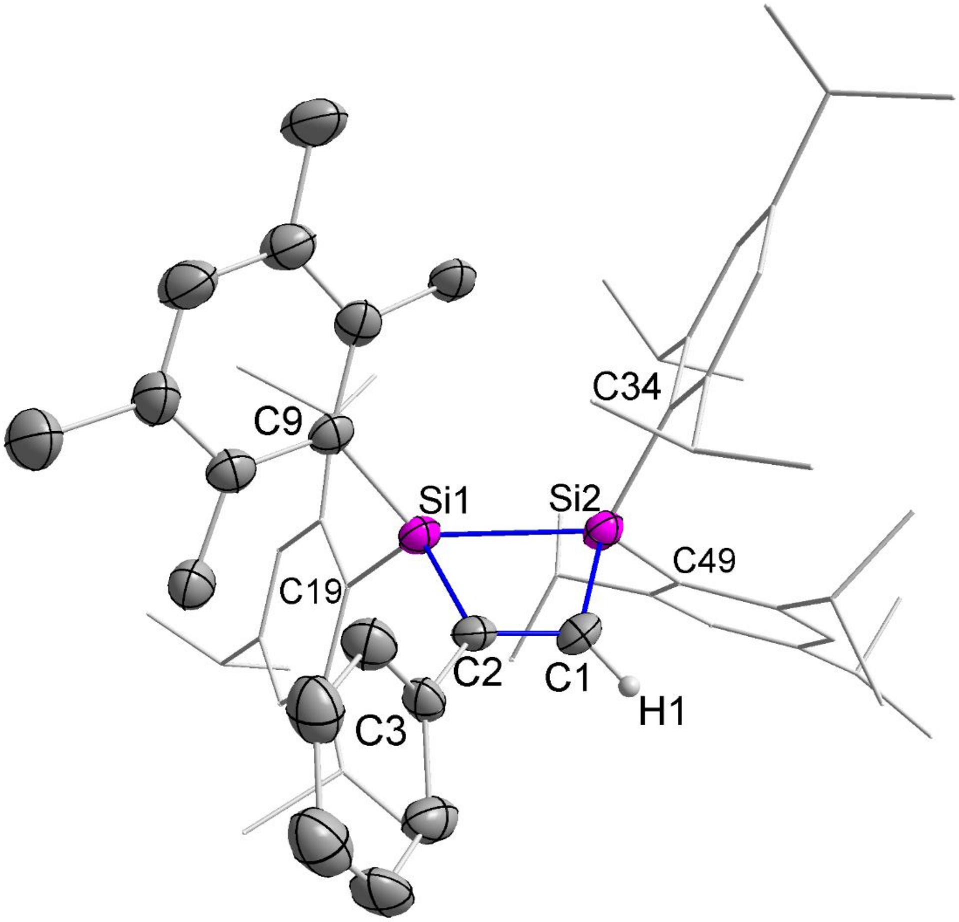

Figure 93. Molecular structure of **123b** in the solid state (thermal ellipsoids at 50%, H atoms and disordered ^{i}Pr groups are omitted for clarity). Selected bond lengths [Å] and bond angles [°]: Si1-Si2 2.4535(19), Si1-C2 1.921(4), Si1-C19 1.920(4), Si1-C9 1.924(2), Si2-C49 1.903(4), Si2-C1 1.862(5), Si2-C34 1.918(4), C(2)-Si(1)-Si(2) 73.45(14), C(1)-Si(2)-Si(1) 72.49(14), C(1)-C(2) 1.355(6), C(1)-C(2)-Si(1) 103.4(3), C(2)-C(1)-Si(2) 110.0(17).

Multinuclear NMR spectroscopy of the crystallized **123b** in C_6D_6 solution shows signals identical to those of the reaction mixture indicating that the assumed conformational isomers equilibrate rapidly after dissolving the crystalline samples, but slow on the NMR time scale. This seems to exclude the breaking of any bonds during this process and suggest the rotation of substituents to be responsible for the observations.

In the following section some further evidence for the presence of rotameric equilibria in the case of the [2+2] cycloaddition products with reversed regioselectivity will be gathered. In all cases, reduced reactivity due to more severe steric bulk necessitates heating of the reaction mixtures to complete conversion of the tetrasiladiene starting material.

3.2.2.2. [2+2] Reactions with Species with Two Si=Si Units

In the progress of the investigation into the reactivity of sterically more demanding Si=Si containing substrates towards phenyl acetylene, the reactivity of durylene and anthracene-bridged tetrasiladiene (**106** and **116**) with two equivalents of phenyl acetylene was tested in the expectation that they would behave similarly as the examples discussed in the previous sections and thus afford the bis(disilacyclobutene)s **121e,f** (Scheme 53). As will be shown in this section, however, the regioselectivity is reversed completely at the increased temperature necessary to complete conversion.

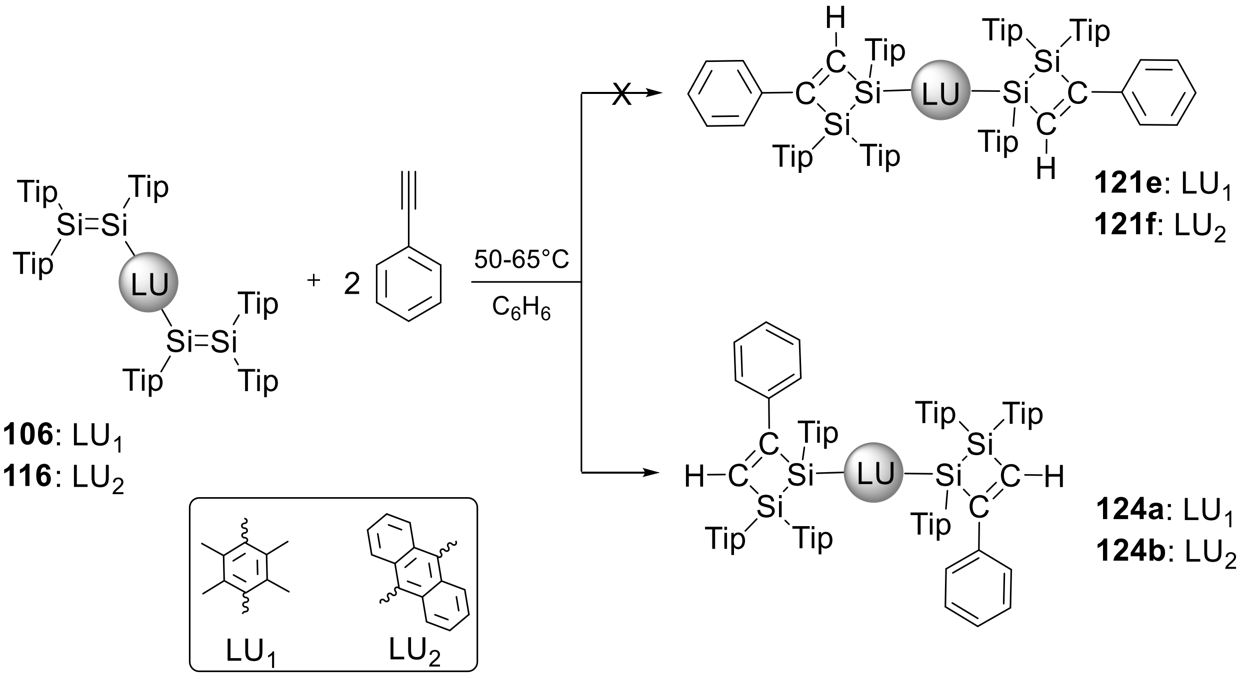

Scheme 53. Addition of two equivalents phenyl acetylene to each of arylene bridged tetrasiladienes **106** and **116**.

After stirring overnight at 65°C, the reaction mixture turns yellow in case of **106** as substrate whereas a yellow orange color was retained in case of **116**.

According to NMR analysis, most of the signals in the ^{1}H NMR spectrum for both reaction mixtures are overlapping and do not lend themselves to straightforward interpretation.

After stirring overnight at 65°C, the reaction mixture turns yellow in case of **106** as substrate whereas a yellow orange color was retained in case of **116**.

According to NMR analysis, most of the signals in the ^{1}H NMR spectrum for both reaction mixtures are overlapping and do not lend themselves to straightforward interpretation.

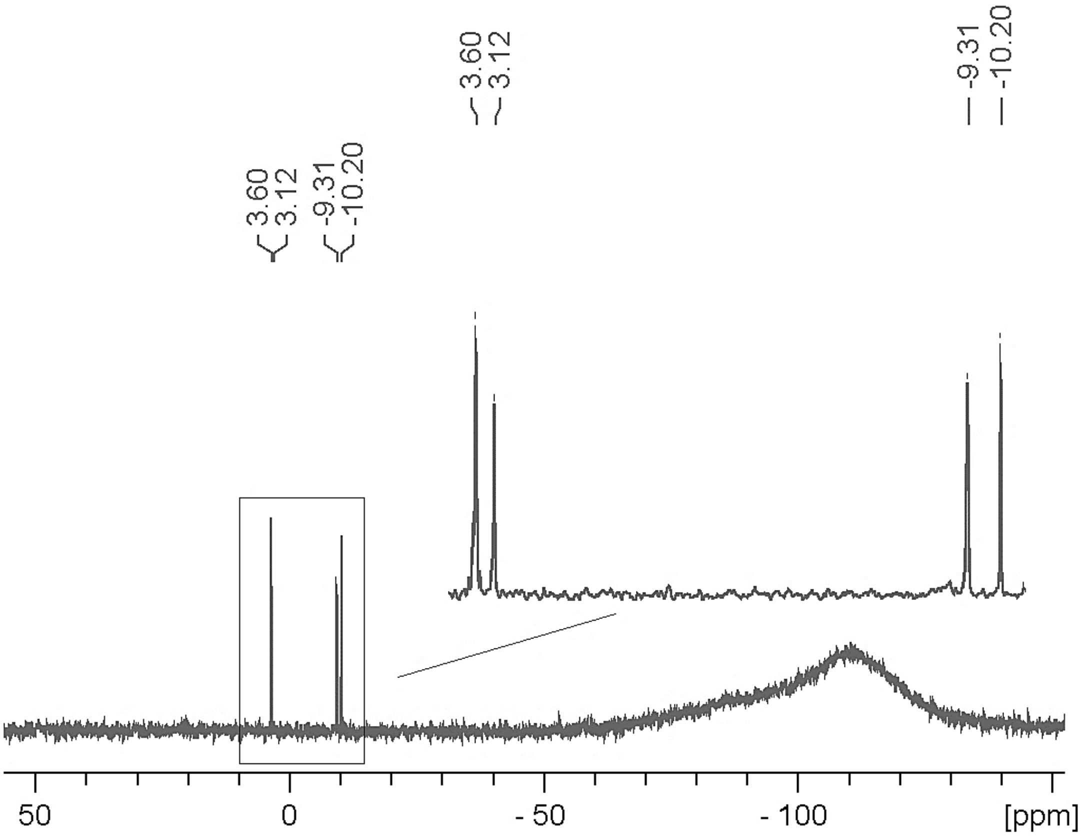

Figure 94. ^{29}Si NMR spectrum of the reaction mixture of two equivalents of phenylacetylene with durylene-bridged tetrasiladiene **106**.

The ^{29}Si NMR spectrum of the crude reaction mixture obtained from durylene-bridged **106** (LU$_1$) discloses the presence of at least two species with two sets of signals δ =

3.60, −10.21 ppm and δ = 3.12, −9.32 ppm (Figure 94). Similarly, two pairs of signals are observed in reaction from anthracene-bridged **116** (LU_2) at δ = 1.69, −7.89 ppm and δ = 1.83, −8.89 ppm. In the latter case, an additional signal at δ = −8.03 ppm of slightly smaller intensity is detected, which, however, is not present in purified samples and can therefore be attributed to an unknown sideproduct (Figure 95). As for the unbridged duryl-substituted mono(disilacyclobutene) **123b**, the similarity of the ^{29}Si NMR chemical shifts strongly suggests the formation of stereoisomers. Unlike in the case of **123b**, two Si=Si moieties were subject to the [2+2] cycloaddition presumably creating two stereogenic silicon centers. Therefore, in addition to the postulated possibility of a rotameric equilibrium, the formation of diastereomers has to be considered as an alternative explanation for the occurrence of two sets of signals.

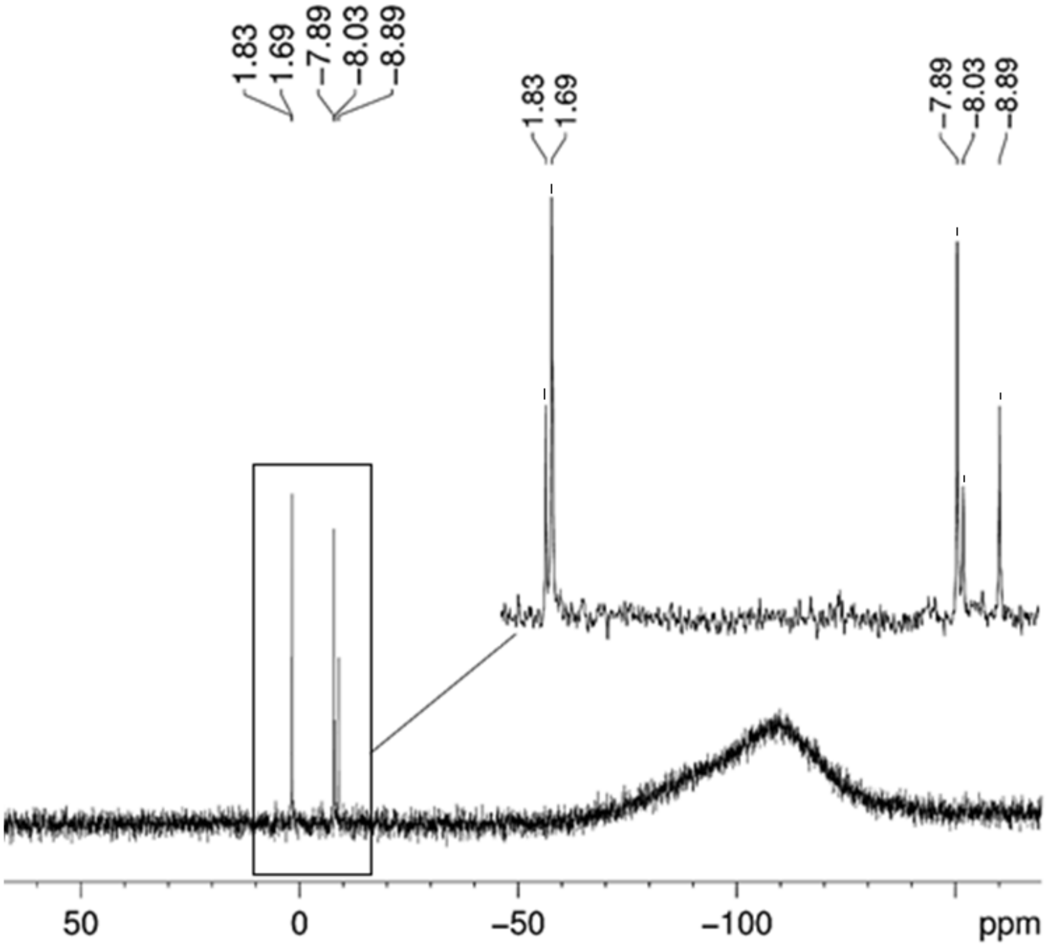

Figure 95. ^{29}Si NMR spectrum of the reaction mixture of two equivalents of phenyl acetylene with anthracenylene bridged tetrasiladiene **116**.

Both products were purified by crystallization: while the one derived from the reaction of durylene-bridged tetrasiladiene **106** was isolated as colorless crystals in 83% yield from a concentrated hexane solution, the product from anthracene-bridged **116** was obtained in 80% yield as yellow crystals from a minimum amount of benzene.

The ^{29}Si NMR spectra of the crystalline materials in C_6D_6, however, are virtually identical to those of the crude reaction mixtures in both cases with the exception that the single signal of the impurity at $\delta = -8.03$ ppm in case of (LU2) has almost completely disappeared after crystallization (Figure 96).

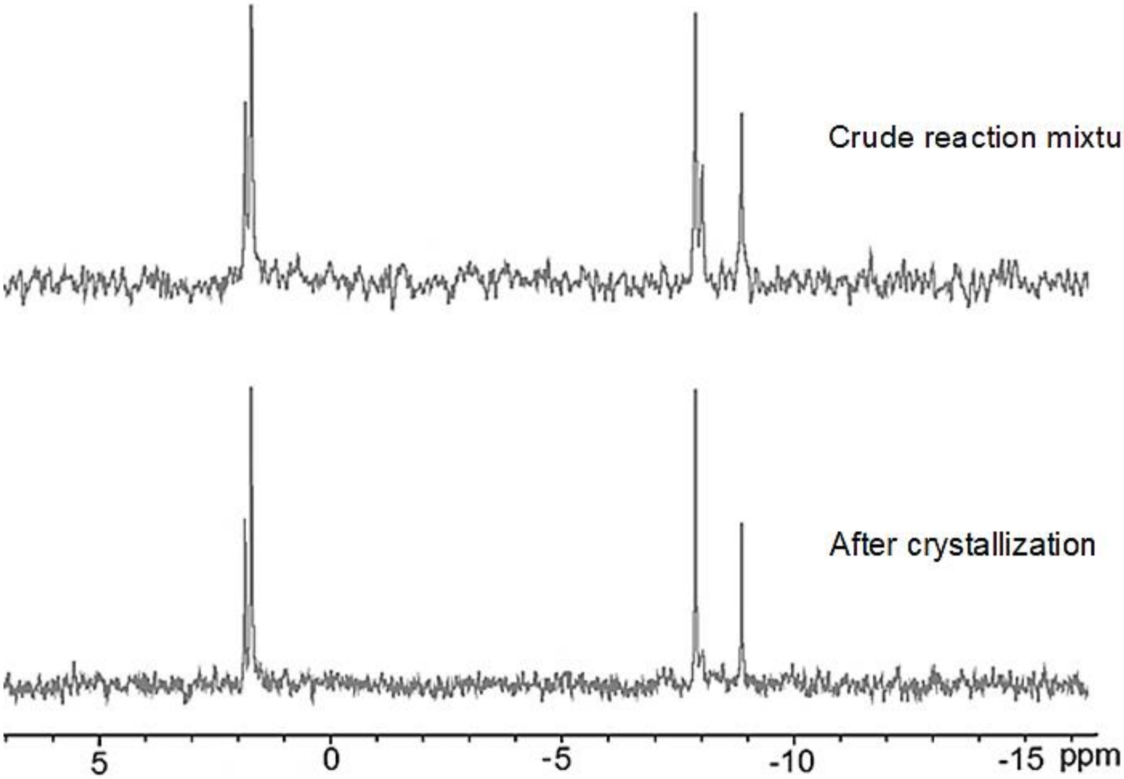

Figure 96. ^{29}Si NMR spectrum of the reaction mixture of two equivalents of phenyl acetylene with anthracenylene bridged tetrasiladiene **116** and after crystallization as yellow crystalline materials.

Nonetheless, X-ray diffraction verified the constitutions as the [2+2] cycloadducts **124a,b** (Figure 97 and 98). Like in case of disilacyclobutene **123b**, both bis(disilacyclobutene)s **124a,b** show a connectivity with the more sterically encumbered phenyl-substituted carbon atom attached to the less bulky substituted silicon atom (bonded to the linking unit and one Tip group).

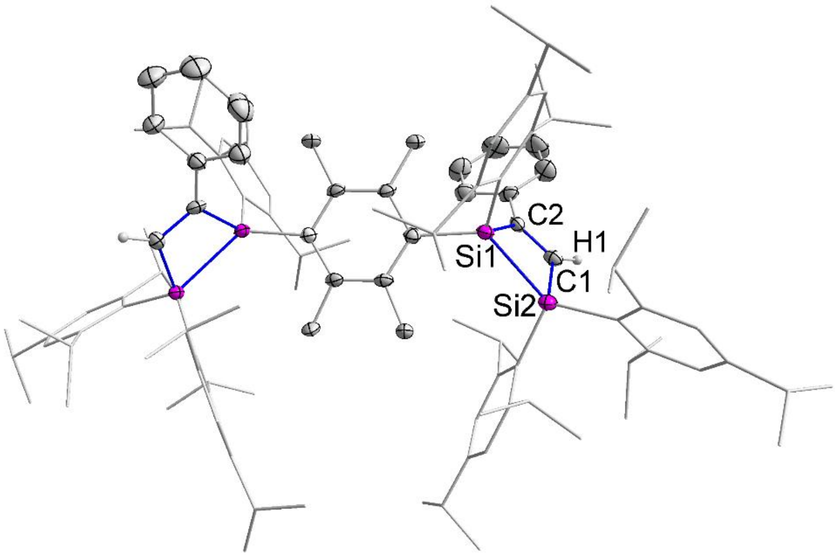

Figure 97. Molecular structure of **124a** in the solid state (thermal ellipsoids at 50%, H atoms and disordered ^{i}Pr groups are omitted for clarity). Quality of data insufficient for discussion of bonding parameters.

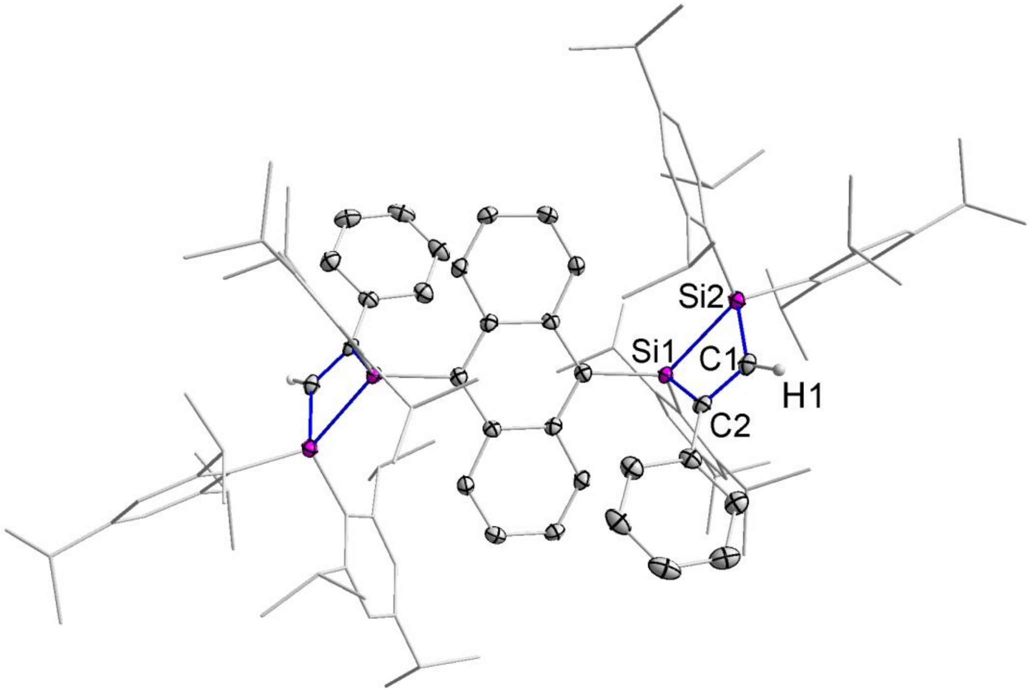

Figure 98. Molecular structure of **124b** in the solid state (thermal ellipsoids at 50%, H atoms and disordered ^{i}Pr groups are omitted for clarity). Selected bond lengths [Å] and bond angles [°]: Si1-Si2 2.4365(7), Si1-C 2 1.9113(19), Si1-C16 1.9250(17), Si1-C9 1.9185(17), Si2-C46 1.9183(18), Si2-C1 1.869(2), Si2-C31 1.9137(18), C(2)-Si(1)-Si(2) 73.50(6), C(1)-Si(2)-Si(1) 72.72(6), C(1)-C(2) 1.349(2), C(1)-C(2)-Si(1) 104.04(14), C(2)-C(1)-Si(2) 108.85(14).

In contrast to **124b**, the strong distortion of **124a** in the crystal packing and the resulting high R value for the calculated geometries prevent reliable interpretation of bonding parameters (Figure 97). The discussion is therefore restricted to the anthracene-bridged bis(disilacyclobutene) **124b** (Figure 98), which crystallizes in the triclinic space group P-1. The endocyclic Si-Si single bond distance (2.4365(7)) is comparable to the corresponding distance in naphtyl-bridged bis(disilacyclobutene) **121d** 2.4121(11) and slightly longer than in biphenyl-bridged bis(disilacyclobutene) **121a** (2.3953(15) Å). Furthermore, C1 and C2, Si1, and Si2 form an almost perfectly planar trapezoid (sum of internal angles 359.59) with the endocyclic angles to Si atoms are also relatively acute (C(2)-Si(1)-Si(2) 73.50(6) and C(1)-Si(2)-Si(1) 72.72(6)°), and the endocyclic angles to C atoms are larger than 90° (C(1)-C(2)-Si(1) 104.04(14) and C(2)-C(1)-Si(2) 110.0(17).°

Table 4. NMR data of arylene bridged-bis(disilacyclobutene) **123b** and **124a,b** in C_6D_6 as well as structural parameters of **123b** and **124b.** ^{a} saturated silicon atoms in disilacyclobutenes.

	123b	**124a**	**124b**
δ ^{29}Si, ppm ^{a}	2.89; 2.19; −10.38	3.60; 3.12; −9.32; −10.21	1.83; 1.69; −7.89; −8.89
d(Si1-Si2), Å	2.4535(19)	-	2.4365(7)
C2-Si1-Si2, °	73.45(14)	-	73.50(6)
C1-Si2-Si1, °	72.49(14)	-	72.72(6)
C1-C2-Si1, °	103.4(3)	-	104.04(14)
C2-C1-Si2, °	110.0(17)	-	108.85(14)

Remarkably, the two sets of signals in the ^{29}Si NMR spectrum of **124a,b** are very close to those of disilacyclobutene **123b** (Table 4), which confirms that the reverse regioisomers show characteristic chemical shifts as well, decidedly different from those of **120** and **121a-d** with regular stereo chemistry. This circumstance also leads to the assumption that an equilibrium between two conformers may be responsible for the increased number of signals rather than the presence of diastereomers.

In order to prove this hypothesis, **124a,b** were investigated by NMR at variable temperature in *d*$_8$-toluene.

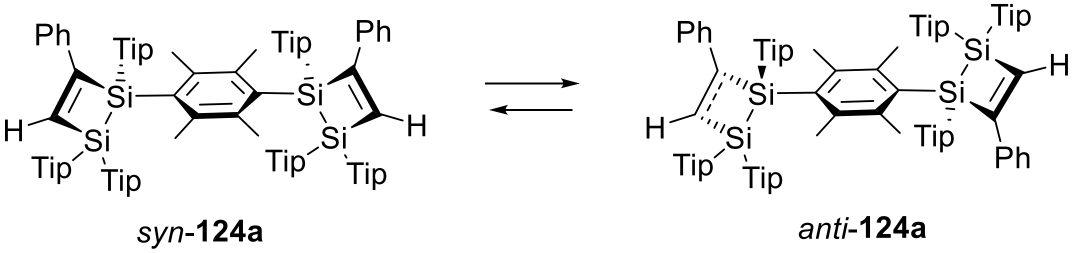

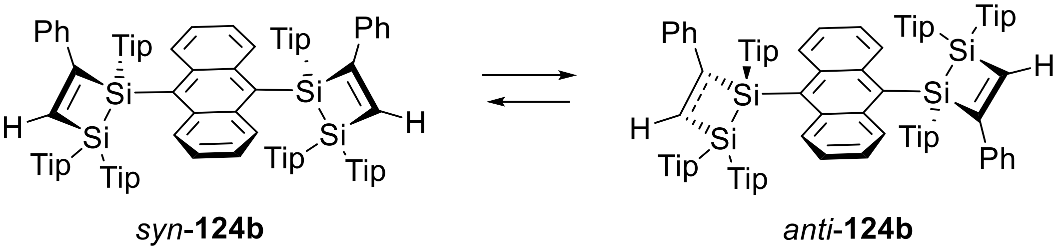

Scheme 54. Possible equilibrium between the postulated *syn*-, *anti*-conformations of resulting bridged bis(disilacyclobutenes) **124a,b**.

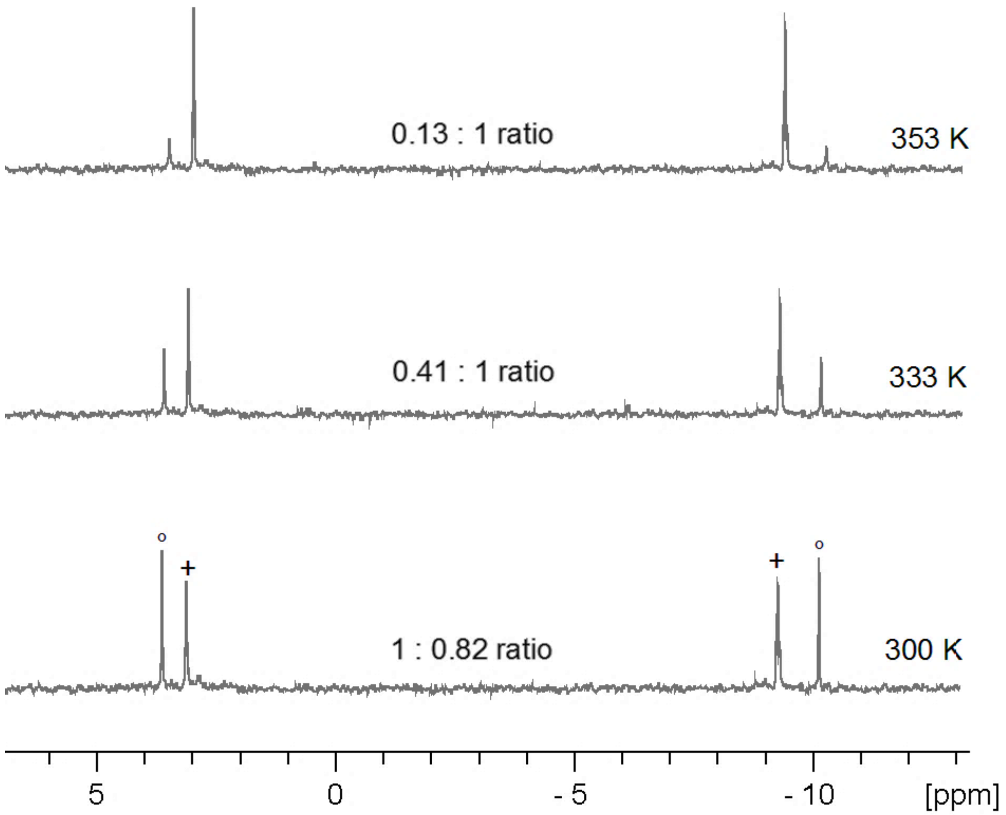

Figure 99. ^{29}Si VT-NMR of durene- bridged bis(disilacyclobutene) **124a** at different temperatures in d_8-toluene (333 and 353 K), and the resonances for the expected 2 rotamers, (+): signals can be assigned to *anti*-**124a**, (°): signals can be assigned to *syn*-**124a.**

As similarly observed in C_6D_6, the ^{29}Si NMR spectrum of compound **124a** in *d*$_8$-toluene at 300 K (Figure 99) exhibits two set of signals at δ = 3.49, −10.26 ppm and δ = 2.97, −9.40 ppm (ratio approximately 1 : 0.82). Even though it is impossible to reach coalescence by increasing the temperature, a significant and reversible change in the ratio of the two isomers is observed, indicating the expected temperature-dependance of the equilibrium. This finding provides strong support for the postulated equilibrium conformers *(anti*-**124a**, C_i symmetry) and (*syn*-**124a**, C_s symmetry) present in solution (Scheme 54).

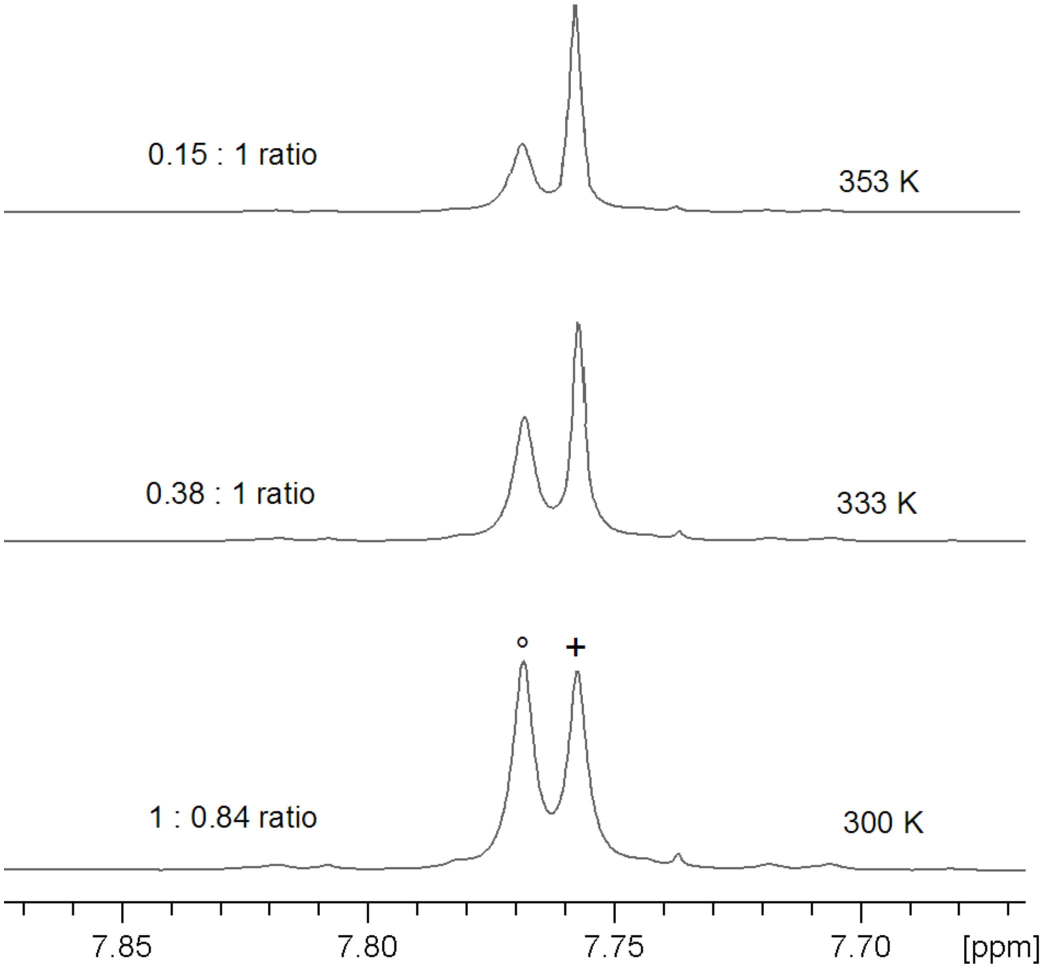

Figure 100. Low field Vinylic protons section of the ^{1}H VT-NMR spectrum from durene- bridged bis(disilacyclobutene) **124a** at different temperatures in *d*$_8$-toluene (300-353 K), and the resonances for the expected 2 rotamers, (+): signals can be assigned to *anti*-**124a**, (°): signals can be assigned to *syn*-**124a.**

The ^{1}H VT-NMR of **124a** (Figure 100) allows for an estimation of the thermodynamic parameters of the *syn-anti* isomerization by integration of the vinylic ^{1}H NMR signals at δ = 7.75 and 7.77 ppm (+ and °) at various temperatures. From the equilibrium constants thus determined, the thermodynamic parameters for *syn-anti* isomerization were estimated to $\Delta H \cong 29$ kJ.mol^{-1} and $\Delta S \cong 93$ J mol^{-1} (see Appendix). On the basis of the strong entropic contribution, it is assumed that *anti*-**124a** is increasingly favoured at higher temperatures as it should allow for significantly more degrees of freedom.

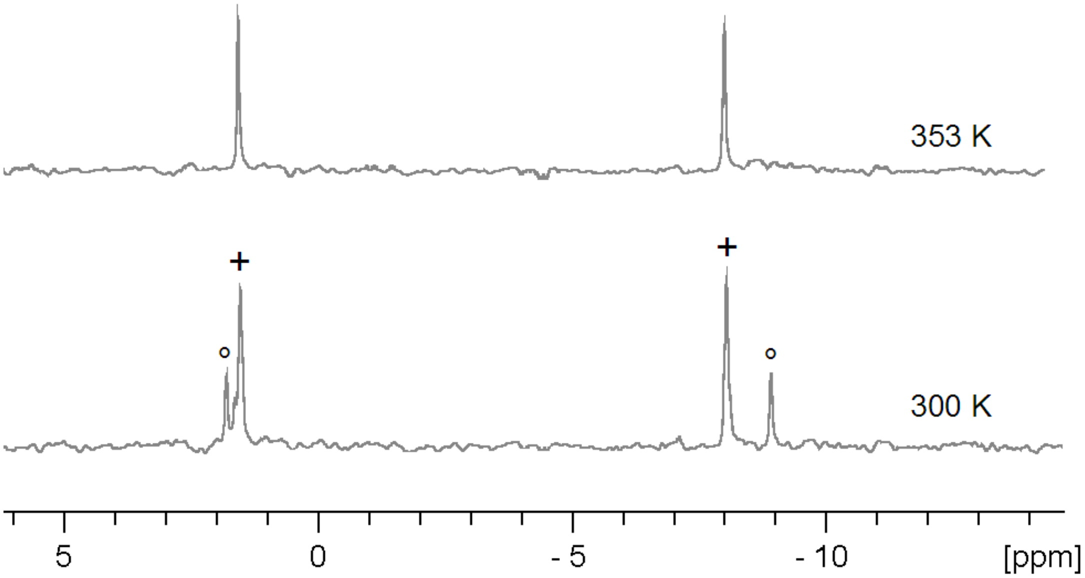

Figure 101. ^{29}Si VT-NMR of anthracene- bridged bis(disilacyclobutene) **124b** at higher temperature in d_8-toluene (353 K), and the resonances for the expected 2 rotamers, (+): signals can be assigned to *anti*-**124b**, (°): signals can be assigned to *syn*-**124b.**

The ^{29}Si NMR of **124b** in d_8-toluene at 300 K (Figure 101) shows one set of signals of higher intensity at δ = 1.67, −8.03 ppm and a lower intensity pair at δ = 1.81, −8.87 ppm in a ratio approximately 0.35 : 1. As in the case of **124a**, both *syn* (minor) and *anti*-**124b** (major) conformations are observed in solution due to the slow rotation about the Si-C bonds on the NMR time scale (Scheme 54). Increasing the temperature (353 K) did not lead to coalescence but to the completely disappearance of one set of signals in the ^{29}Si NMR due to an apparent complete shift of the equilibrium towards *anti*-**124b** (Figure 101), presumably more favored at higher temperature on the basis of more degrees of freedom with maximal distance between the two disilacyclobutene groups.

3.2.3. Evidence for Diradical Intermediacy: Addition of Phenyl Acetylene to Anthracenyl Substituted Disilene 100 between Ligand and Si=Si Unit

In order to further probe the influence of steric bulk of the oligoaromatic substituents, the reaction of 9-anthracenyl disilene **100** with one equivalent of phenyl acetylene in benzene was investigated. As in case of duryl disilene **94**, the reaction did not take place until heated to 50 °C and left stirring at this temperature overnight (Scheme 55). The color of the reaction mixture changes from purple to yellow orange and yellow crystals (mp. 200°- 205°C) were obtained from a concentrated (1:0.5) benzene/ethanol mixture in good yield (77%).

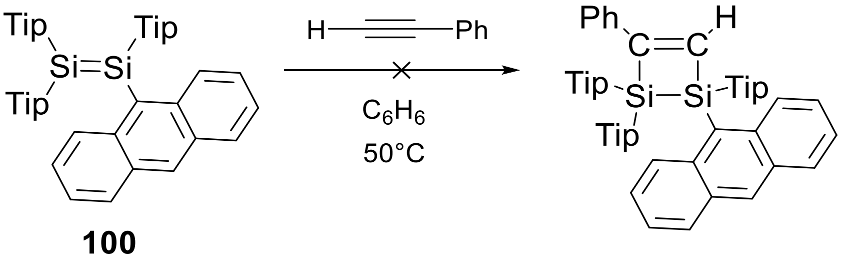

100

Scheme 55. Reaction of disilene **100** with phenyl acetylene in benzene at 50°C.

The ^{29}Si NMR spectrum of the crystals (Figure 102) shows the anticipated disappearance of the two lowfield signals of the Si-Si double bond. In this case, however, the two new highfield resonances in the saturated region at $\delta = -25.39$ and -36.40 ppm appear at significantly higher field than expected for a disiladicyclobutene[92] of either of the regiochemistry described in the previous sections.

The ^{1}H NMR spectrum (Figure 103) shows a singlet at $\delta = 6.00$ ppm in the region, typically observed for silicon hydrides, thus excluding a disilabicyclobutene structure. The presence of satellite peaks corresponding to a $^{1}J_{\text{Si-H}}$ coupling constant of 196 Hz confirms the formation of an Si-H bond.

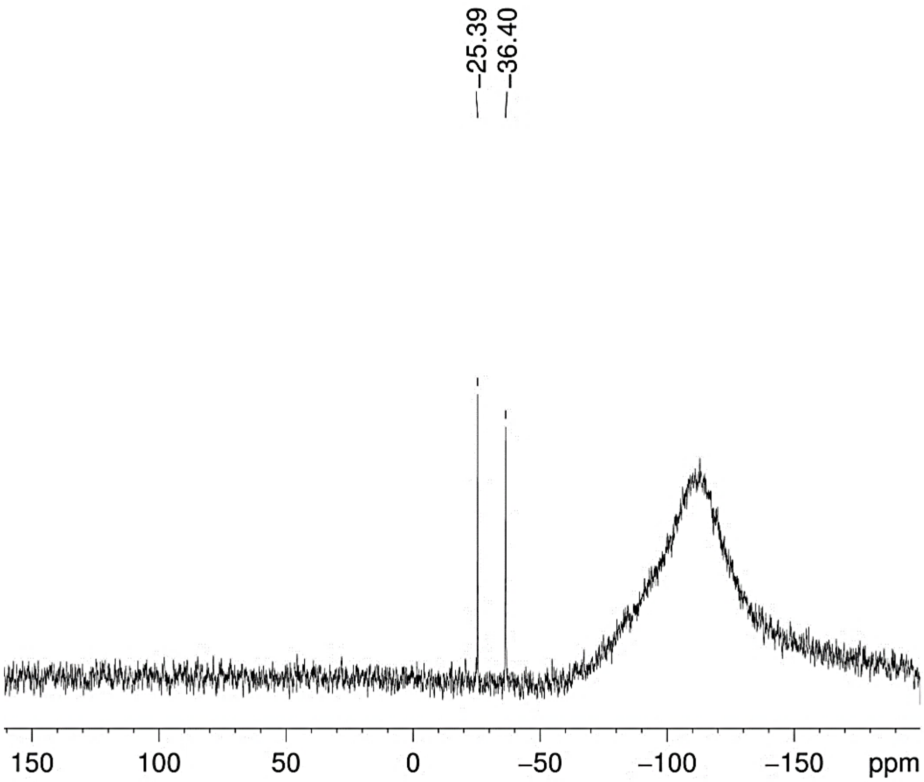

Figure 102. ^{29}Si NMR spectrum of the crystals derived from the reaction of disilene **100** with phenyl acetylene in benzene at 50°C.

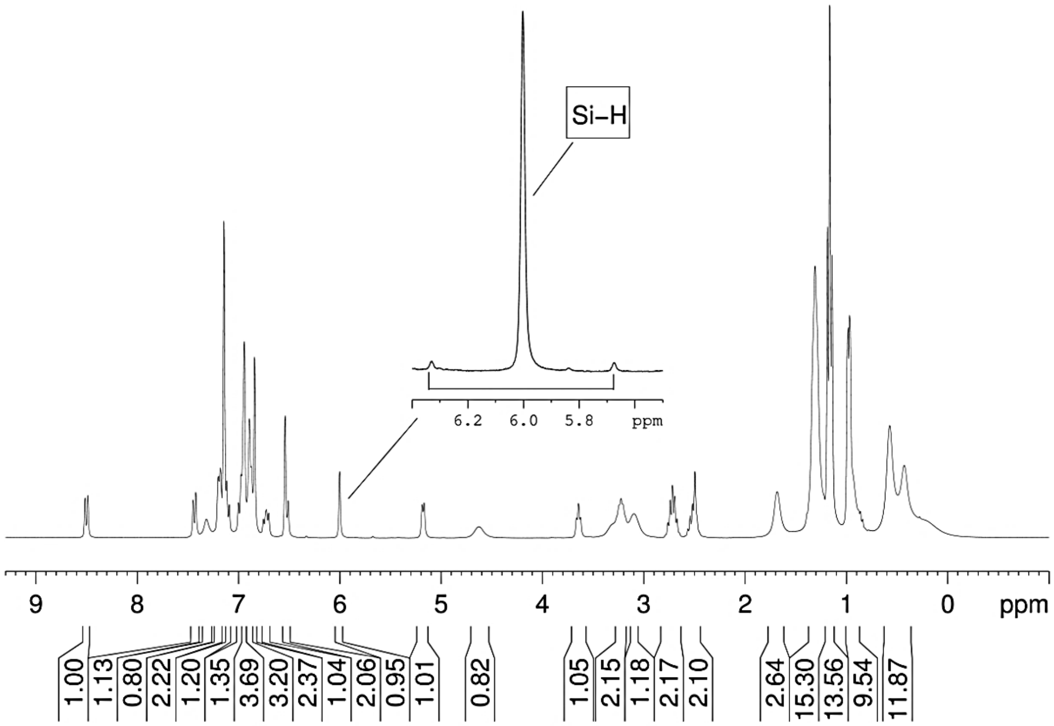

Figure 103. ^{1}H NMR spectrum of the crystals derived from the reaction of disilene **100.**

The Si-*H* corresponds to the signal at δ = −36.40 ppm in the ^{29}Si NMR by the occurrence of the cross-peaks to the satellite signals in the 2D ^{1}H-^{29}Si NMR correlation spectrum (Figure 104). Although the formation of a silicon hydride could readily be explained by the CH addition of phenylacetylene to the Si-Si double bond, the absence of signals in the alkyne region of the ^{13}C NMR spectrum definitely excludes this option. Instead two ^{13}C signals at δ = 128.28 and 128.18 ppm show crosspeaks to a doublet in the ^{1}H NMR at δ = 5.18 ppm (^{4}J = 5.9 Hz). As all these signals in accordance with a vinylic proton a considerably more complication reaction outcome than a simple C-H addition was anticipated.

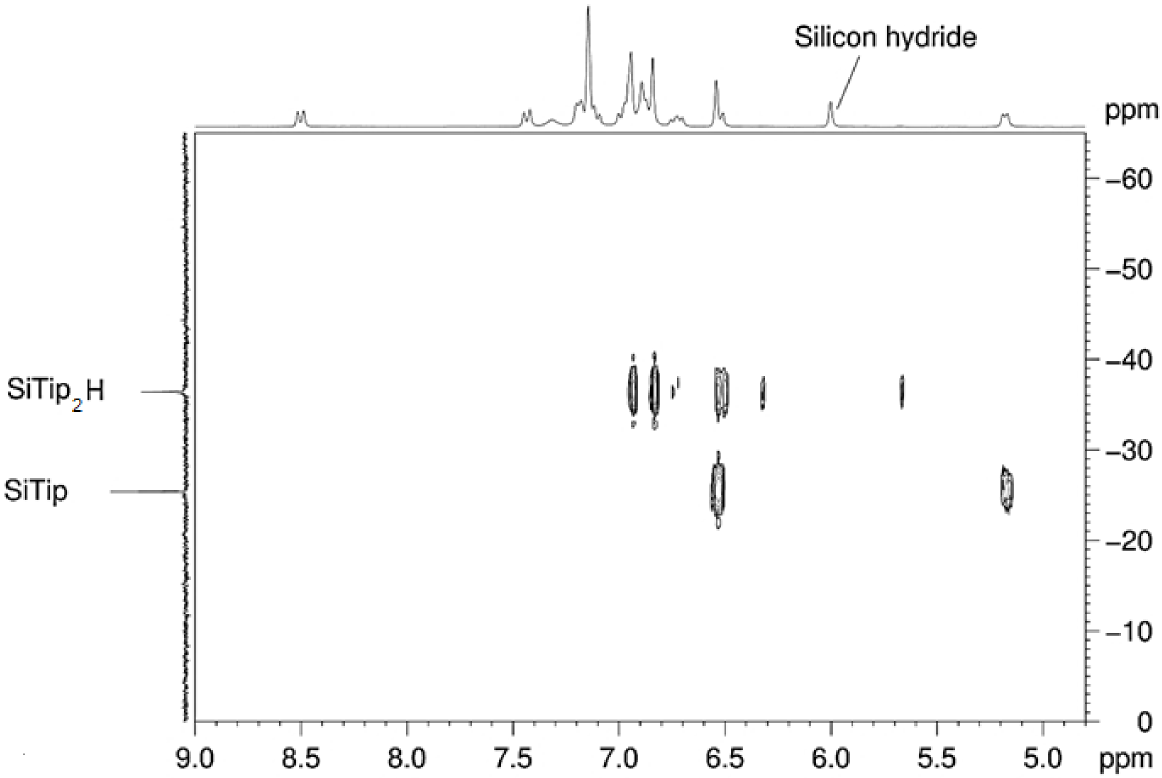

Figure 104. ^{1}H-^{29}Si NMR spectrum of the crystals derived from the reaction of disilene **100** with phenyl acetylene in benzene at 50°C.

High quality single crystals were readily obtained from a concentrated benzene solution at room temperature and the molecular structure of the product determined by an X-ray diffraction study on a single crystal (Figure 105). The cycloadduct **125** crystallizes in monoclinic space group ($P2_1/c$).

The incoming PhCC unit forms a six-membered ring annulated across one of the "bay-regions" of the former anthryl substituent and the adjacent silicon atom resulting in the tetracyclic structure **125**. The exocyclic Si-Si bond length (2.3786(6) Å) is much shorter than the endocyclic Si-Si single bond distance in disilacyclobutene **123b** (2.4535(19) Å), which is the result of significantly lower strain of exocyclic position.

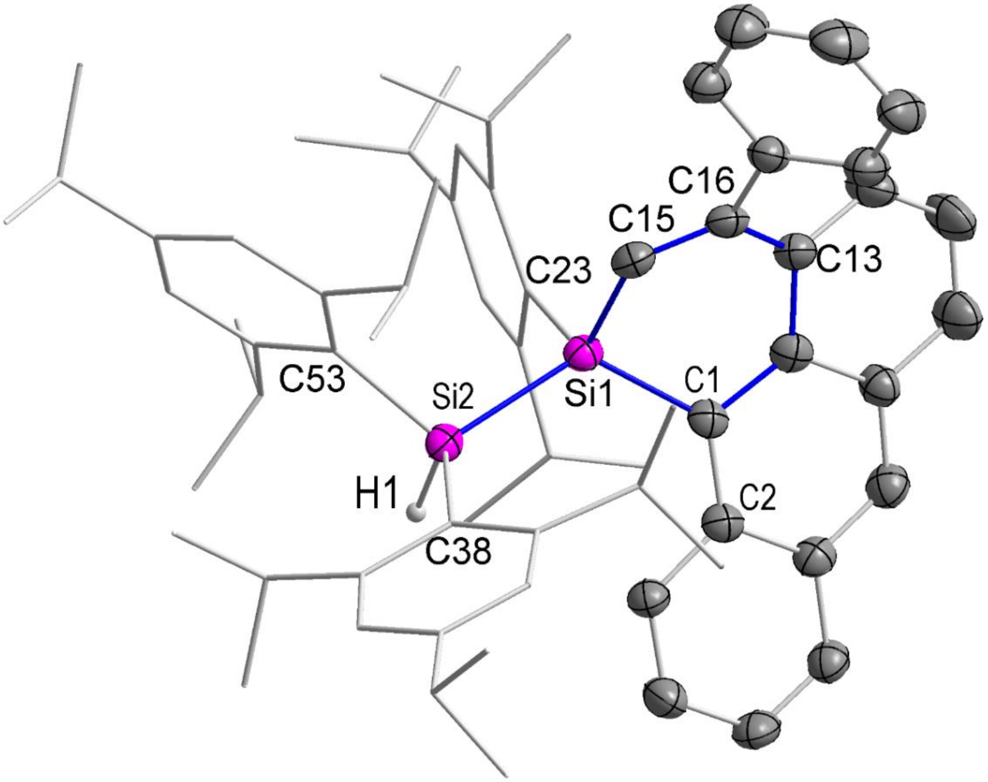

Figure 105. Molecular structure of **125** in the solid state (thermal ellipsoids at 50%, H atoms and disordered iPr groups are omitted for clarity). Selected bond lengths [Å] and bond angles [°]: Si1-Si2 2.3786(6), Si1-C1 1.9085(17), Si1-C23 1.9276(17), Si1-C15 1.8548(17), Si2-C53 1.9106(17), Si2-C38 1.9160(17), C13-C16 1.480(2), C(15)-Si(1)-Si(2) 110.34(6), C(15)-Si(1)-C(1) 97.67(7), C(15)- Si(1)-C(23) 112.72(7), C(1)- Si(1)-C(23) 110.67(7), C(1)- Si(1)-Si(1) 121.61(5), C(23)- Si(1)-Si(2) 104.07(5), C(53)-Si(2)-C(38) 108.50(7), C(53)- Si(2)-Si(1) 107.56(5), C(38)- Si(2)-Si(1) 124.31(5).

Mechanistically, the formation of tetracyclic **125** probably involves initial attack of phenyl acetylene to sterically slightly less encumbered end of the Si=Si bond of disilene **100** to give the intermediate **126** of the frequently proposed biradical-type (see section 1.11).

Biradical **126** could feasibly abstract one of the aryl hydrogens in 1-position of the anthracenyl group. Simple ring closure would then afford the isolated product **125** (Scheme 56).

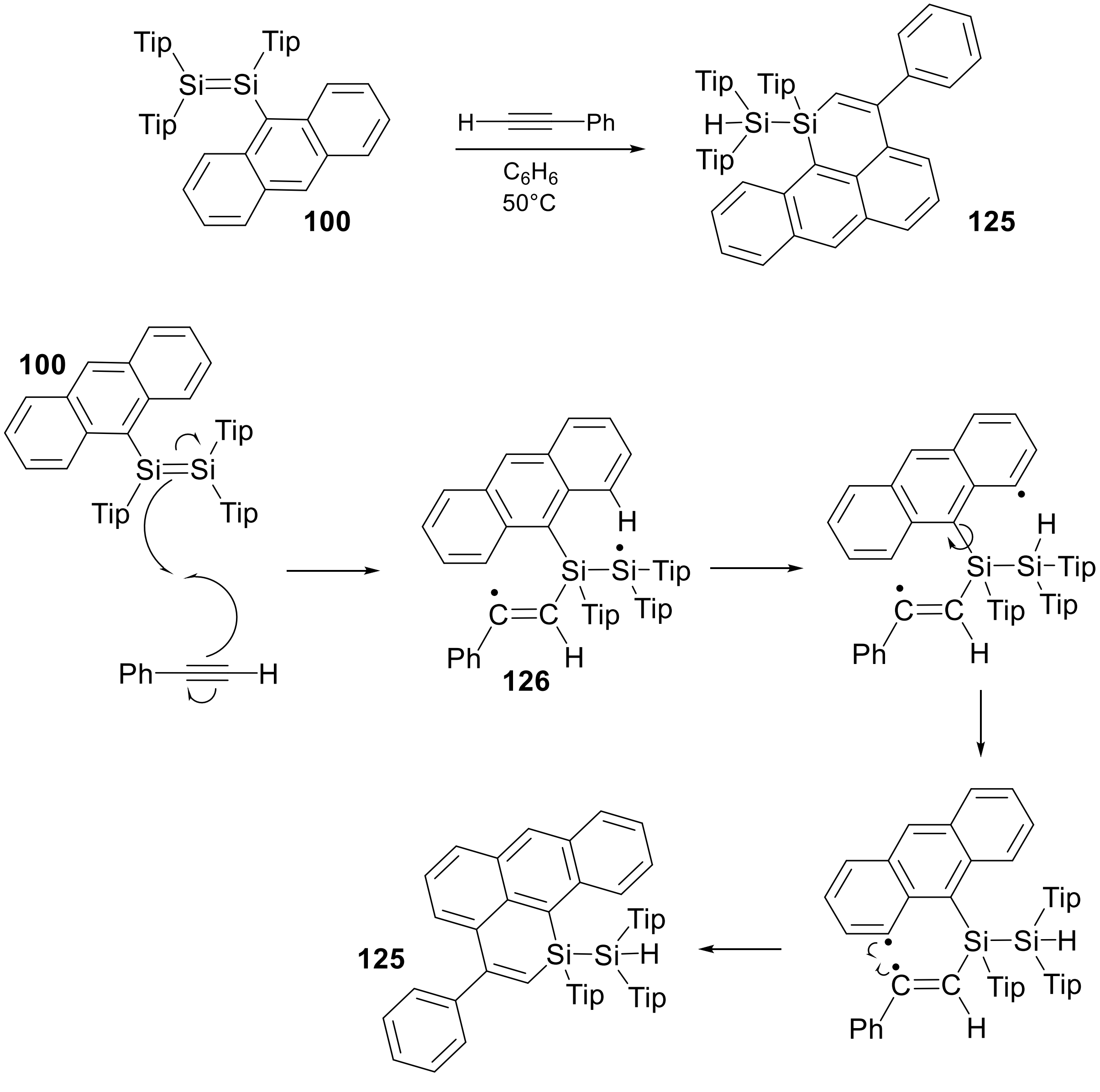

Scheme 56. Proposed mechanism of reaction between **100** and phenyl acetylene.

3.3. Synthesis of Bifunctional Monomers for Step-Growth Polymerization

As described in the introductory section 1.9, our group has reported the synthesis of air-stable ethynyl-terminated extended monomers from 1,4-bis(ethynyl)benzene and the *para*-phenylene bridged tetrasiladiene **67** based on the principle of regioselective cycloaddition of polar multiple bonds to Si=Si moieties.[92] As proof-of-principle, the step-growth polymerization of the bifunctional extended monomers and *para*-phenylene bridged tetrasiladiene in a 1:1 ratio led to σ–π conjugated organosilicon hybrid polymers. The synthesis of the extended monomer by RT reaction of the phenylene-bridged tetrasilabutadiene and 1,4-diethynylbenzene in 1:10 ratio was found to be less stereospecific than hoped for as it leads to the formation of two diastereomers in 4 : 1 ratio (*meso* vs. R,R and S,S). Among the two isomers only the *meso*-isomer (major isomer) was isolated in pure form and this stereochemically predefined co-monomer was further subjected to polymerization.[92] The facile rotation about the C-Si bond to the *para*-phenylene linker could be the reason for limited stereoselective nature of this reaction.

In order to understand the influence of the organic linking unit on the selectivity of the first step reaction, the use of tetrasiladienes **108**, **112** and **116** as precursors for the synthesis of air-stable ethynyl-terminated extended monomers from 1,4-bis(ethynyl)benzene was probed following similar protocols as had been established through the model reactions with phenyl acetylene described in the previous section.

A benzene solution of the tetrasiladiene of choice (**108, 112** and **116**) was added dropwise to a benzene solution of a large excess (10 equivalents) of 1,4-diethynyl benzene at room temperature (Scheme 57).

After three hours of stirring, the reaction mixture turned colorless in all cases and quantitative conversion to the anticipated new air-stable ethynyl-terminated extended monomers **127a**, **127b** and **127c** was confirmed by multinuclear NMR spectroscopy (Table 5).

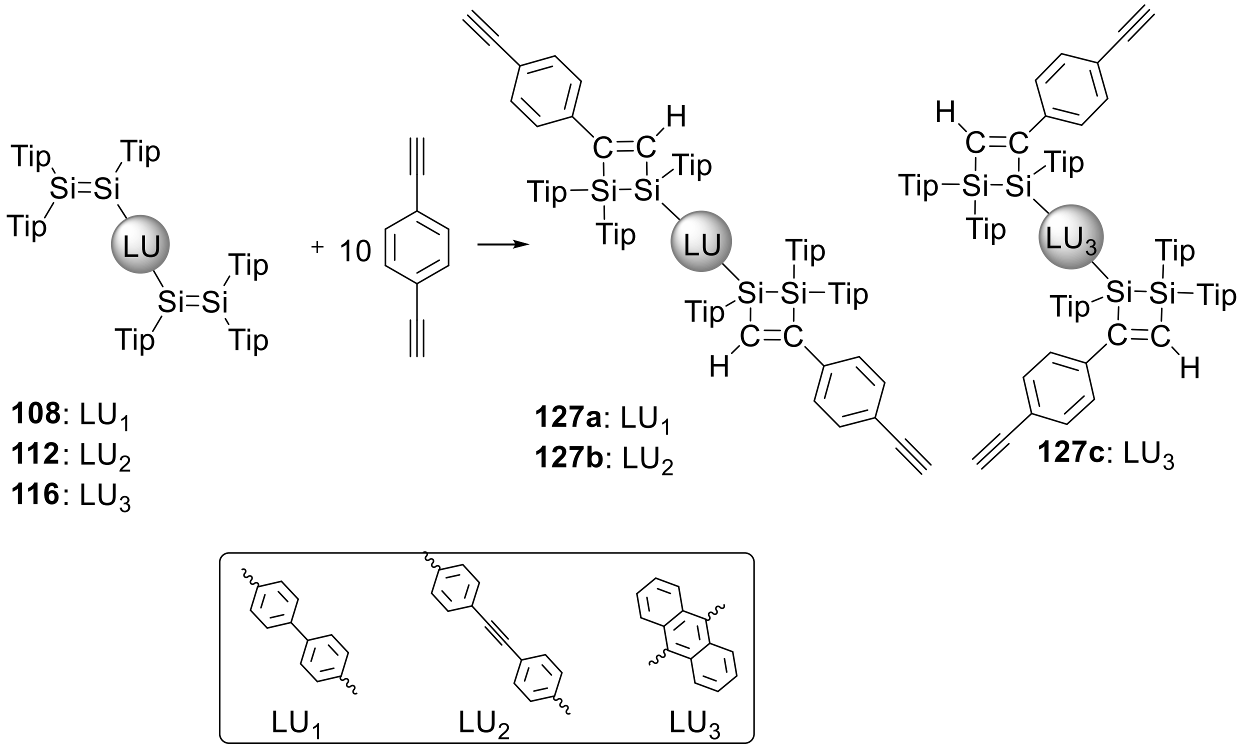

108: LU$_1$
112: LU$_2$
116: LU$_3$

127a: LU$_1$
127b: LU$_2$

127c: LU$_3$

Scheme 57. Reactivity of tetrasiladienes **108**, **112** and **116** towards excess of bis(ethynyl)benzene.

Table 5. NMR data of air-stable ethynyl-terminated extended monomers **127a-c**. [a] saturated silicon atoms in disilacyclobutenes, [b] vinylic proton of the disilacyclobutenes, [c] ethynyl-proton, [d] endocyclic carbon atoms of the disilacyclobutene rings, [e] C-C triple bond of ethynyl-terminus.

	127a	**127b**	**127c**
δ ^{29}Si, ppm [a]	−11.43; −11.74	−11.37; −11.85	1.36; −8.07
δ ^{1}Ha, ppm [b]	7.71	7.66	7.78
δ ^{1}Hb, ppm [c]	2.67	2.61	2.59
δ ^{13}C, ppm [d]	172.07; 157.94	172.22; 157.65	168.38; 163.40
δ ^{13}C, ppm [e]	83.89; 78.00	83.81; 78.04	83.85; 77.90

The extended monomers **127a,b** each show only two high-field resonances between −11.85 and −11.37 in the ^{29}Si NMR spectrum (see exemplary **127b** in Figure 106 and Table 5), which are very similar to the corresponding resonances of arylene bridged-bis(disilacyclobutene). The characteristic chemical shifts suggest that in case of **127a,b** the [2+2] cycloaddition had taken place with the same regioselectivity as in case of the prodcuts from the model reaction with phenyl acetylene **121a-d** (*cf.* previous section).

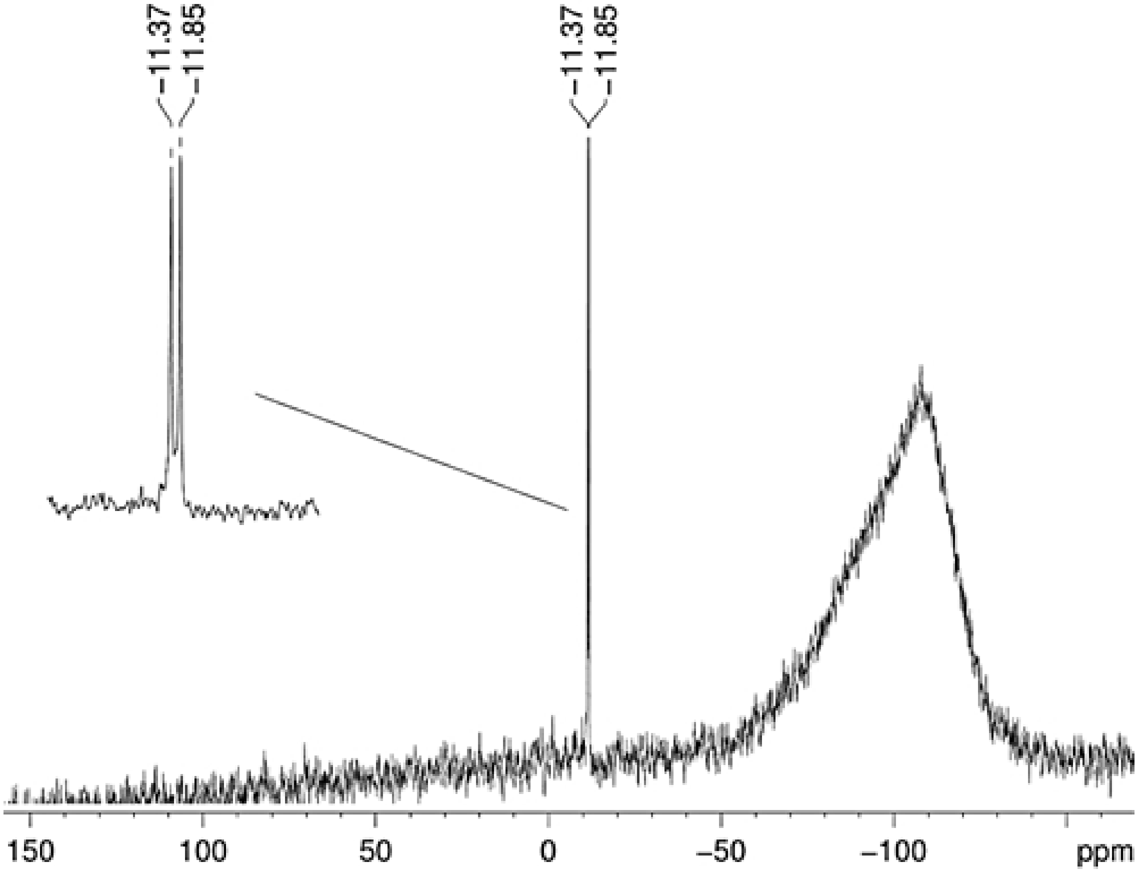

Figure 106. ^{29}Si NMR spectrum of the reaction mixture between 10 equivalents 1.4 diethynylbenzene and diphenylacetylene-bridged tetrasiladiene **112**.

In contrast, the two resonances of **127c** appear more deshielded at δ = 1.36 and −8.07 ppm (Figure 107 and Table 5) in comparison with **127a-b**. The ^{29}Si NMR data of **127c** compare well with observed in case of the addition of two equivalents of phenylacetylene to anthracene bridged tetrasiladienes **116**, again strongly suggesting that **127c** would also exhibit reversed regiochemistry. Notably**,** the reactions between **116** and excess 1,4-diethynyl benzene are in either case completely regio and diastereoselective.

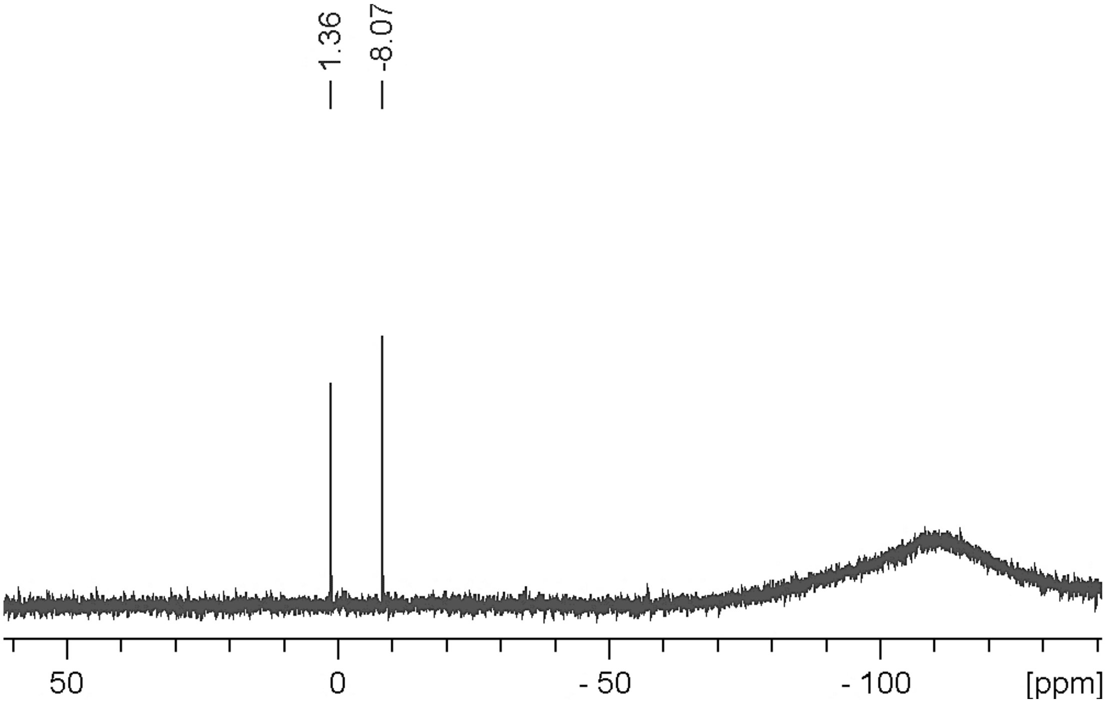

Figure 107. ^{29}Si NMR spectrum of the reaction mixture between 10 equivalents 1.4-diethynylbenzene and anthracene-bridged tetrasiladiene **116**.

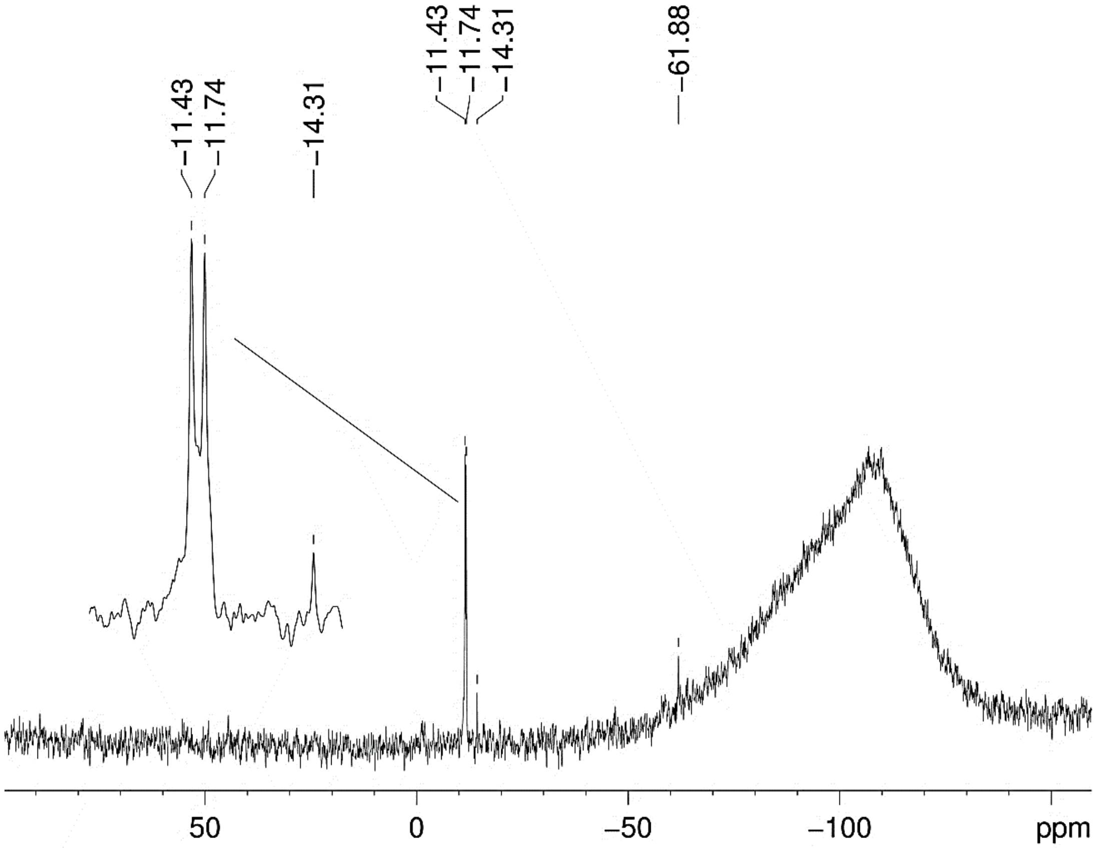

Figure 108. ^{29}Si NMR spectrum of the reaction mixture between 10 equivalents 1.4-diethynylbenzene and biphenylene-bridged tetrasiladiene **108**.

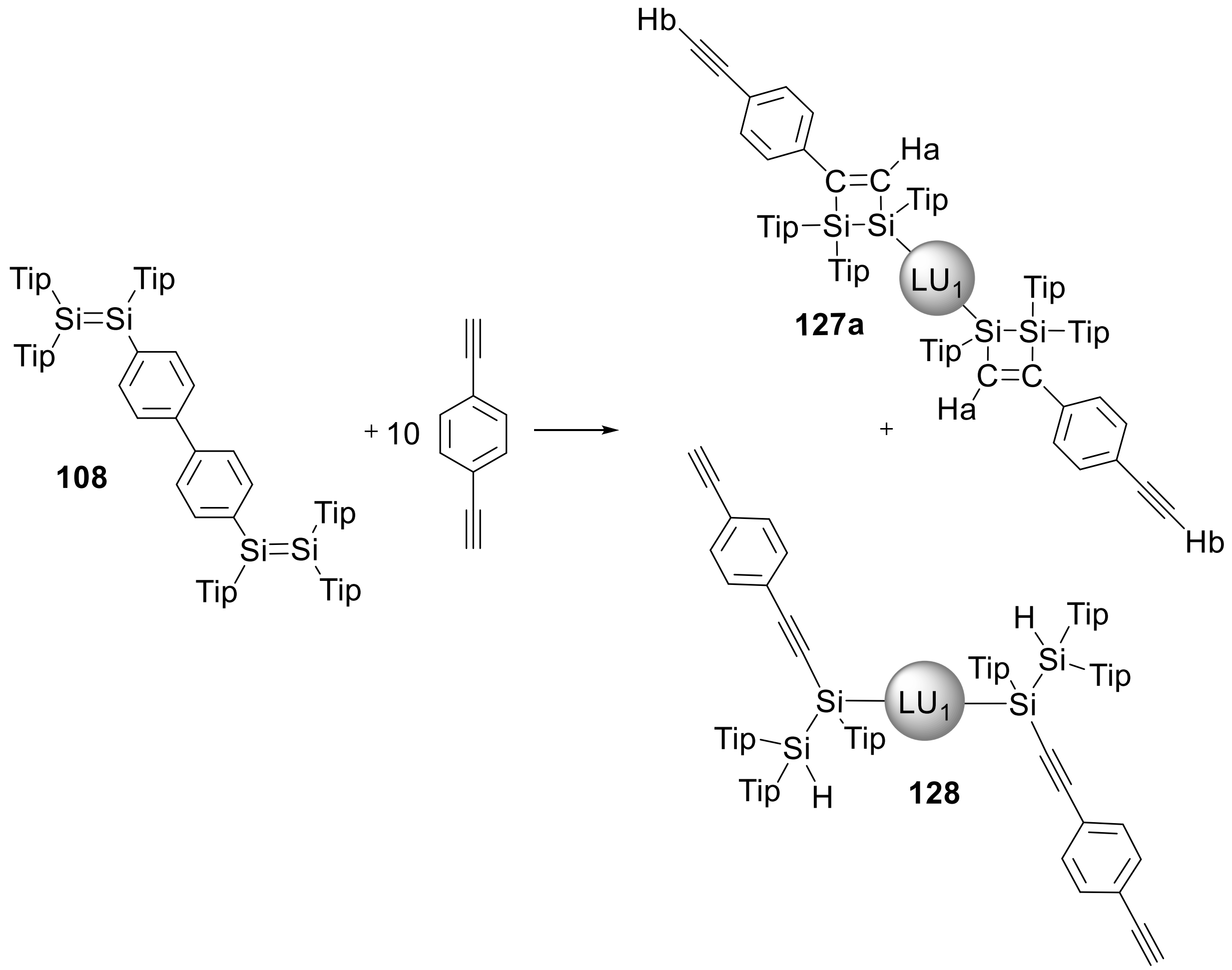

Scheme 58. Reaction between tetrasiladiene **108** and 10 equivalents of 1,4-diethynyl benzene in benzene at room temperature.

It should be mentioned that about 10% of impurities at $\delta = -14.31$ and -61.88 ppm were detected in case of using tetrasiladiene **108** as a substrate (Figure 108). This observation strongly suggests that tetrasiladiene **108** not only undergo facile [2+2] cycloaddition with the terminal alkyne to form the main product **127a** but also a C-H insertion to form the minor side product **128** (Scheme 58). The assignment is based on the comparison of chemical shifts with the CH addition product of phenyl acetylene to phenyl disilene **66a**, which can be obtained selectively in the presence of a base. [112]

The ^{1}H-NMR spectra of all the crude products **127a-c** show the vinylic protons (Ha) of the disilacyclobutene rings appear deshielded as a singlet between 7.66 and 7.78 ppm. Furthermore, the protons attached to ethynyl-terminated (Hb) are found between 2.59 and 2.67 ppm. Next to Hb signal, a singlet resonance, which can be assigned to residual 1,4-diethynylbenzene, is detected at δ = 2.70 ppm. Additionally, a distinct heptet in the isopropyl region and numerous doublets of comparable intensity in the alkyl region are visible (Table 5 and exemplary **127a** in Figure 109).

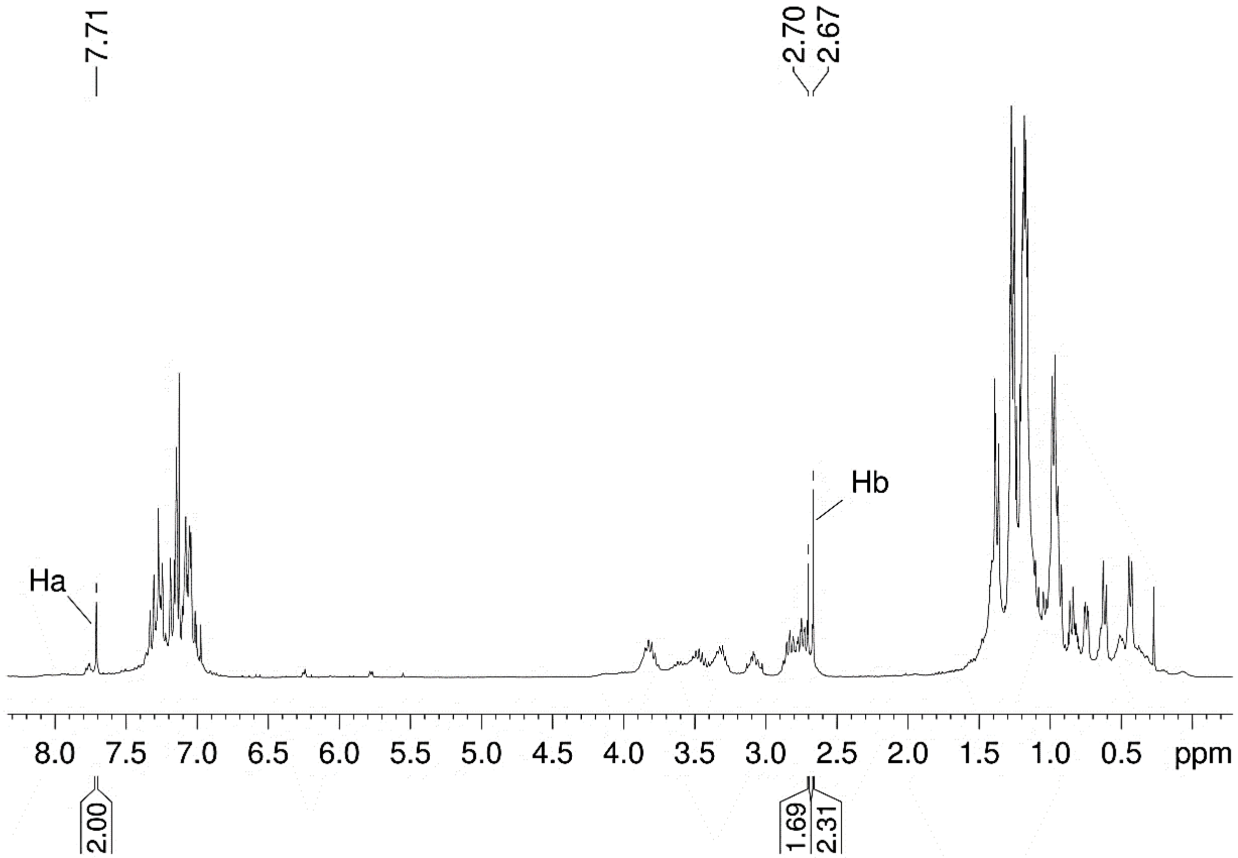

Figure 109. ^{1}H NMR spectrum of the reaction mixture between 10 equivalents 1,4-diethynylbenzene and biphenylene-bridged tetrasiladiene **108**.

In the ^{13}C NMR spectrum, the chemical shift of the endocyclic carbon atoms of the disilacyclobutene rings **127a** are very similar to those of **127b** at about 172 and 157 ppm, while the resonances of the endocyclic carbon atoms in case of **127c** show significantly differing shifts at δ = 168.38 and 163.40 ppm (Table 5). This observation strongly suggests that the regiochemistry in case of **127c** is switched in comparison to **127a-b**. In contrast, ^{13}C signals corresponding to the carbon-carbon triple bond of the ethynyl-terminus of the postulated products **127a-c** are detected in the range of 77.90 to 83.89 ppm. The signals at δ = 79.43 and 83.08 are assigned to the remaining excess of

1,4-diethynylbenzene. Additionally, the ^{13}C NMR spectrum of the postulated **127b** exhibits one more resonance at δ = 90.86 ppm attributed to the two equivalent C≡C carbon atoms between the biphenylene linker (exemplary **127b** in Figure 110**)**.

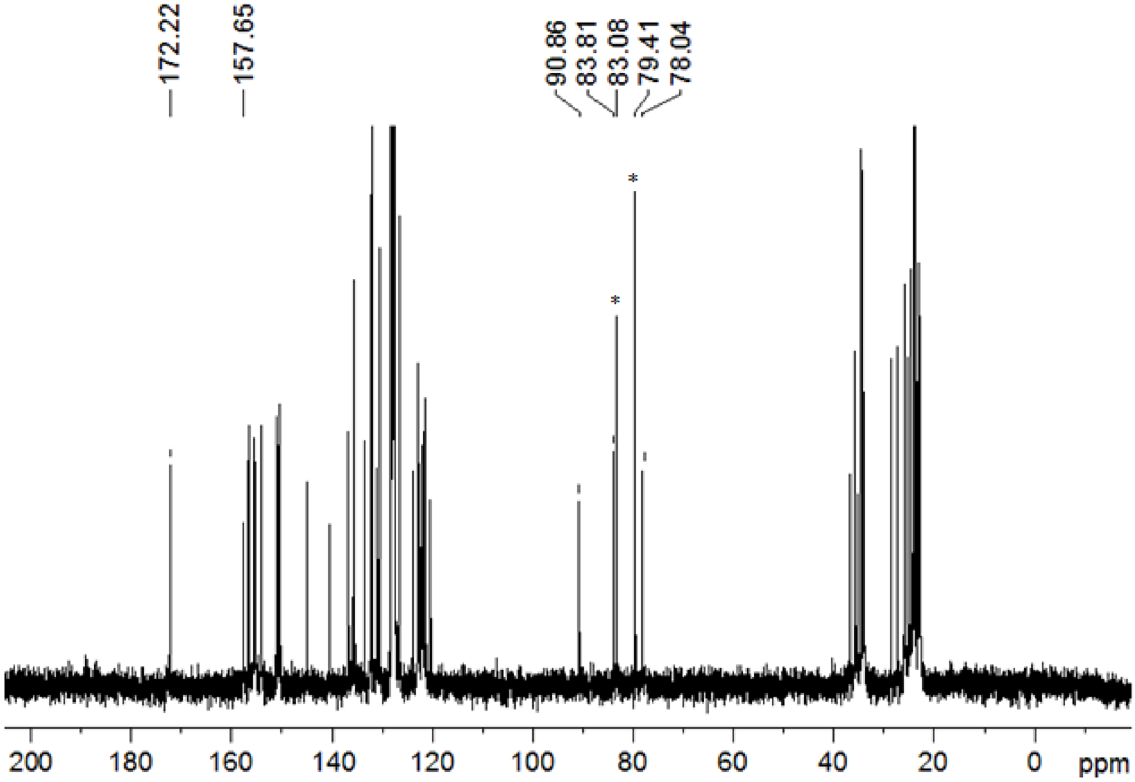

Figure 110. ^{13}C NMR spectrum of the reaction mixture between 10 equivalents 1.4 diethynylbenzene and diphenylacetylene-bridged tetrasiladiene **112**. ∗ = signals at δ = 79.43 and 83.08 for the remaining excess of 1,4-diethynylbenzene.

After removing excess of 1,4-diethynylbenzene by sublimation, all attempts so far to obtain single crystals suitable for X-ray diffraction were unsuccessful. The crude products **127a** and **127c** were obtained as colorless pure solid from concentrated hexane solution in 84% and 88% yield, respectively, while **127b** was obtained as colorless pure solid in 92% yield after removing hexane under vacuum.

Unfortunately, single crystals of the ethynyl-terminated extended monomers **127a-c** to finally confirm its constitution could not be obtained.

Analysis of products showed the selective formation of the anticipated co-monomers **127a-c** in high yield along with the expected change in region selectivity in case of

127c. Notably, the structure of organic linking units employed in the co-monomers were found to be essential for selective product formation. These findings lead to the conclusion that more sterically organic linking units employed in the co-monomers instead of phenyl group could restrain the free rotation about C-Si bond and therefore improve the diastereoselectivity of such kind of reactions.

4. Summary and Outlook

A series of aryl disilenes **92-104** and *para*-arylene bridged tetrasiladienes **106-119** were prepared from disilenide **27** and the corresponding aryl or arylene (di)halides (Scheme 59).

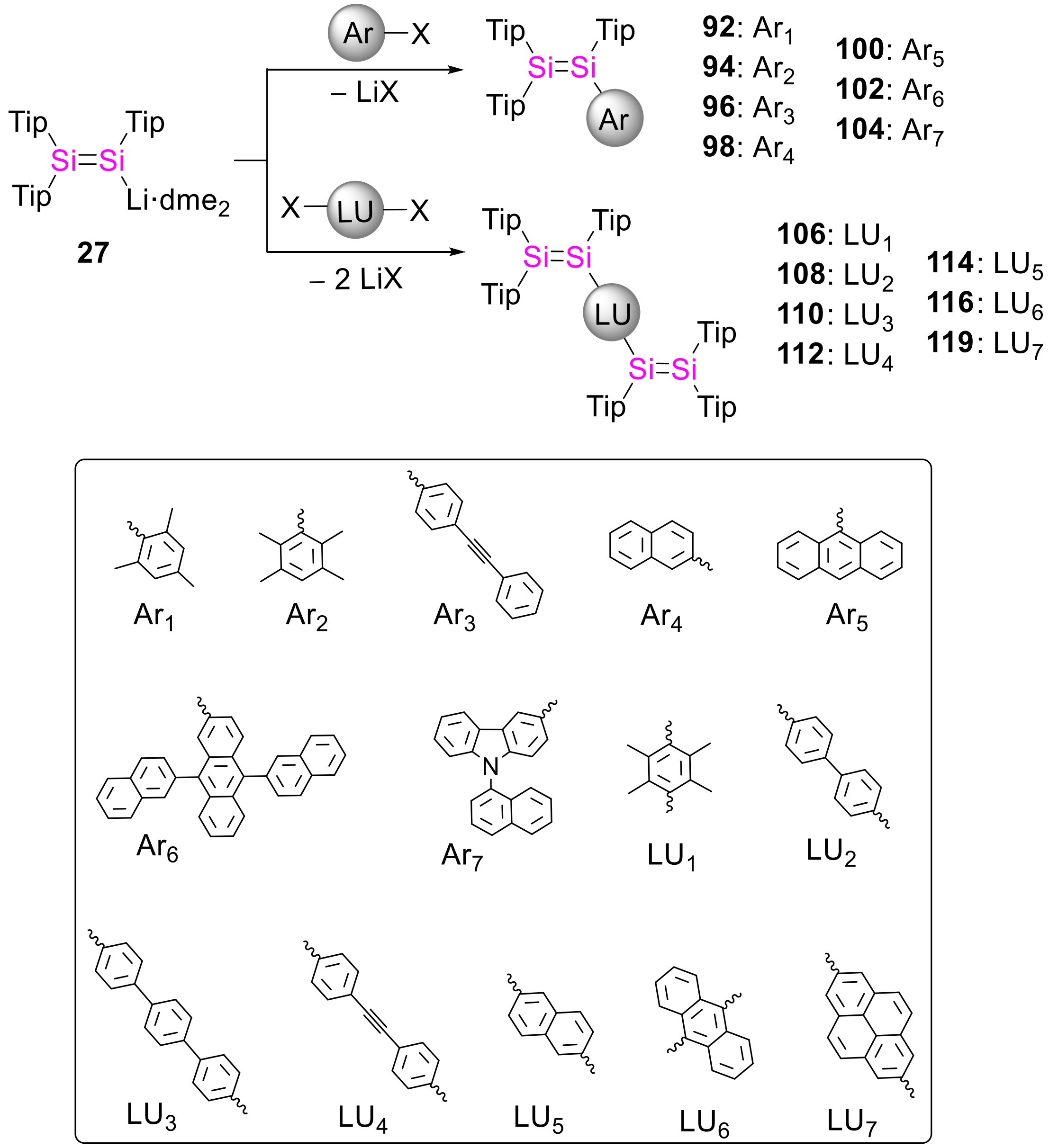

Scheme 59. Synthesis of aryl bridged disilenes **92-104** and tetrasiladienes **106-119** (Tip = 2,4,6-^{i}Pr$_3$C$_6$H$_2$; X = I or Br).

Single crystals were obtained in case of aryl disilenes **92, 94, 98** and **100** as well as in case of para-arylene bridged tetrasiladienes **106, 108, 112, 114** and **116**. Furthermore, the well-resolved CP-MAS ^{29}Si NMR in case of **106** and **116** as well as the coalescence at elevated temperature in **106** suggest the presence of different rotamers in solution.

Notably, even considerable steric demand of the linker does not adversely affect the yields of this reaction. It was found also that the electronic communication of bridged disilenyl moieties strongly depends on the overlap of π-orbitals and the conformational freedom of the conjugated scaffold, which can influence the HOMO-LUMO gap significantly. The twisted conformation of the biphenylene in case of **108** leads to a lower λ_{max} value compared to tetrasiladiene *p*-**67** although the π-conjugated system is potentially extended.

The photophysical data as well as DFT calculations provide strong evidence for the extended π -conjugation through the entire backbone of **92-98** and **108-114**. Although intermolecular charge transfer becomes increasingly more relevant when the dihedral distortion of the Si=Si moieties with respect to the organic π-system is increased, there does not seem to exist a clear-cut distinction to the more conventional π-π* transition typical for disilenes in the present case. It can be proposed, however, that a more perfect orthogonality (such as observed by the Iwamoto group)[81] may result in a more intense fluorescence.

Indeed, it was found that the compounds **112** and **114** exhibit fluorescence in solid state and in a hexane solution at room temperature. More importantly, with the anthryl-substituted **116** the first example of a room temperature near infrared-emissive Si=Si species has been obtained.

In the second part of this thesis, it was shown that the cycloaddition to the Si=Si bond of these compounds with phenyl acetylene provided access to various cycloadducts products. The NMR data and the crystal structure analysis of compounds **120** and **121a-d** revealed that substrates **104** and **108-114** undergo facile and selective [2+2] cycloaddition with the terminal alkyne (Scheme 60).

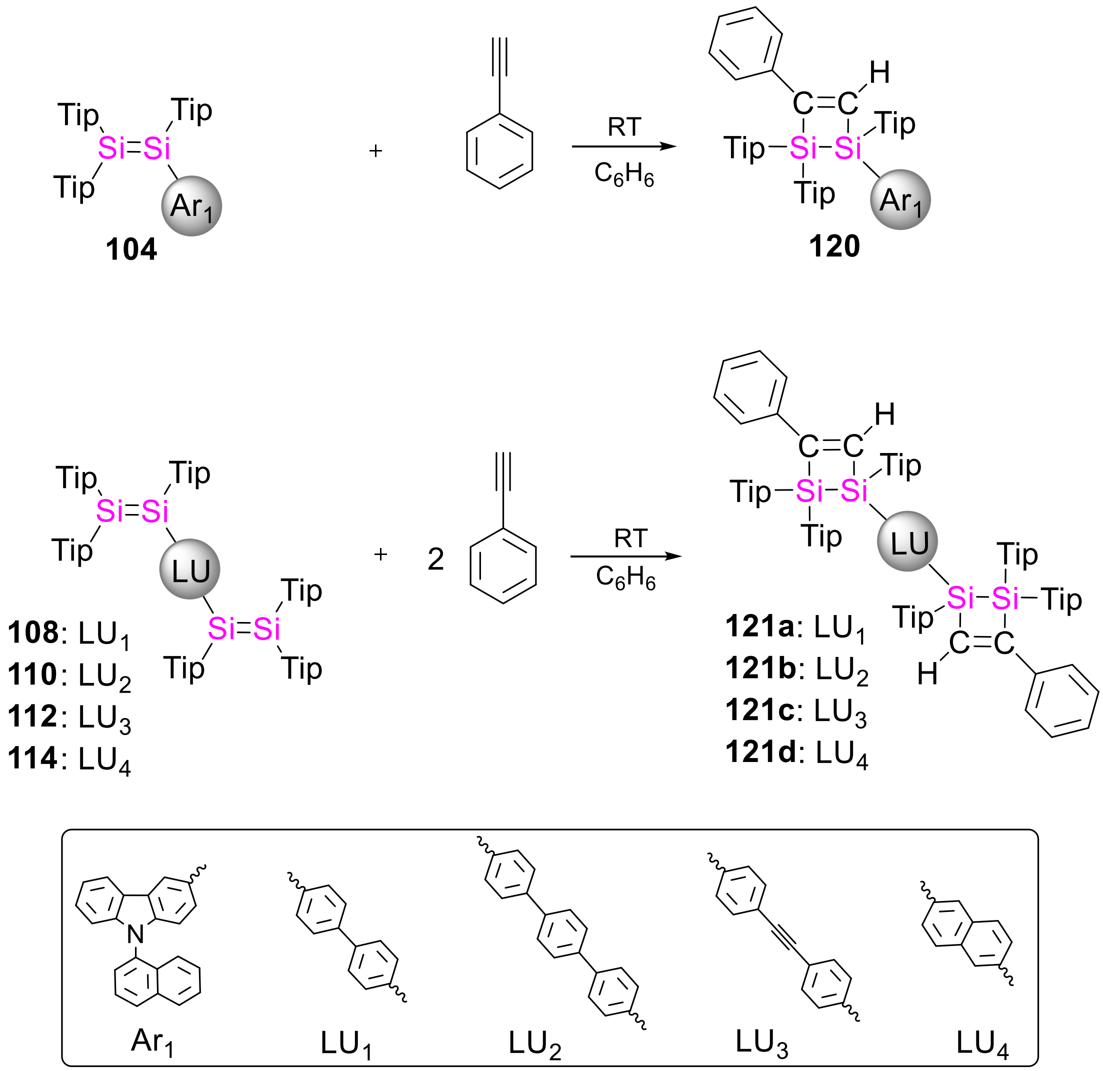

Scheme 60. Formation of various [2+2] cycloadducts **120** and **121a-d** with regular regioselectivity**.**

The addition of phenyl acetylene to substrates with more steric bulk such as disilene **94** or tetrasiladienes **106** and **116** can be achieved only at elevated temperature (Scheme 61). The NMR data of these reactions appeared to show the formation of a mixture of products, initially suggesting that substrates **94, 106** and **116** undergo an unselective [2+2] cycloaddition with the terminal alkyne. However, VT-NMR of **124a,b** showed that an equilibrium between the two rotational conformers *syn* and *anti* exists, where the isomerization from *syn*- to *trans*- conformation is more favorable at higher temperature.

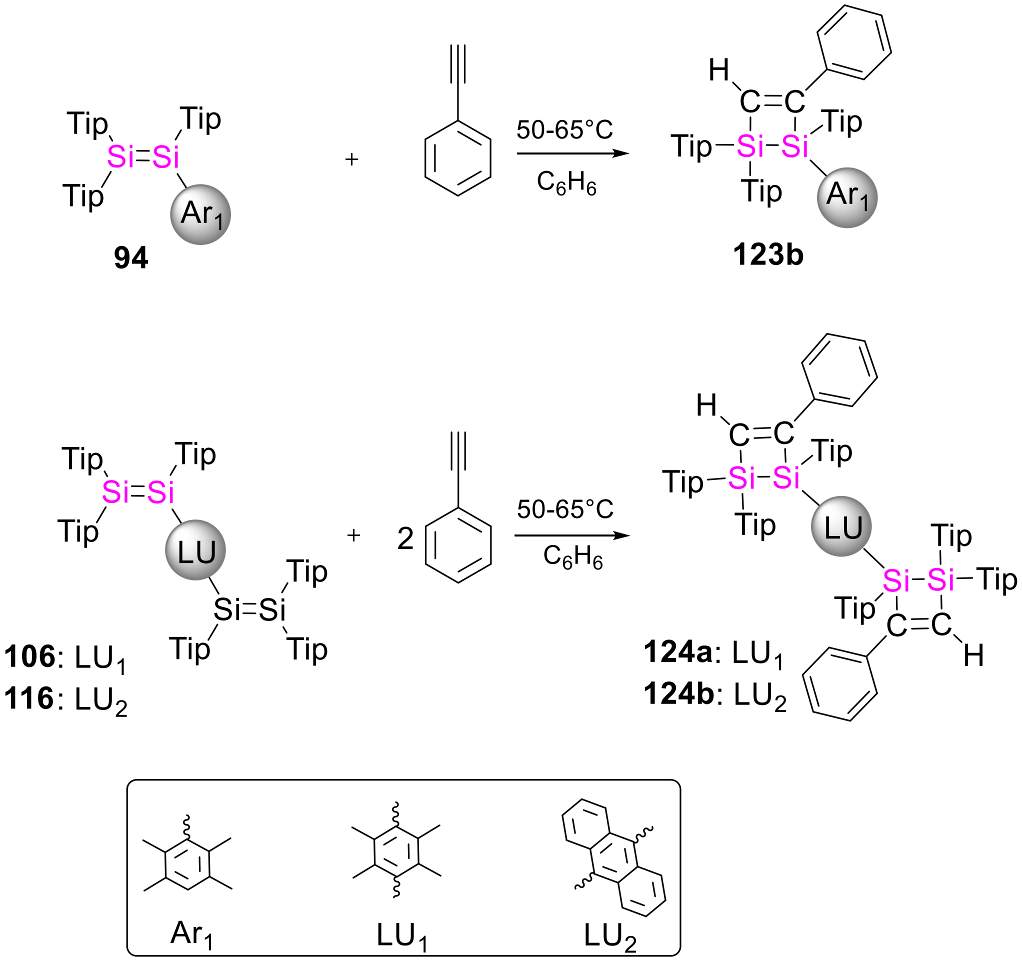

Scheme 61. Formation of various [2+2] cycloadducts **123b-124a,b** with reversed regioselectivity.

Furthermore, X-ray diffraction of the final products revealed the formation of [2+2] cycloadducts **123b-124a,b**. Unlike compounds **120** and **121a-d** derived from the selective [2+2] cycloaddition, the crystal structure analysis of **123b-124a,b** showed that the phenyl-substituted carbon atom is bonded to the sterically less congested Si(Ar)Tip moiety.

Although dipolar mechanisms are in general more favorable for the cycloaddition of unsymmetrically substituted disilenes and tetrasiladienes, the mechanism of the cycloaddition reactions in the present study seems to heavily depend on the substitution patter so that zwitterionic, biradical as well as concerted pathways appear to be active.

In the special case of the reaction of anthryl-substituted disilene **100** with phenyl acetylene, an unusual tetracyclic product **125** was obtained in good yield and completely characterized (Scheme 62). The formation of **125** provides strong evidence for diradical intermediates at least in this specific case.

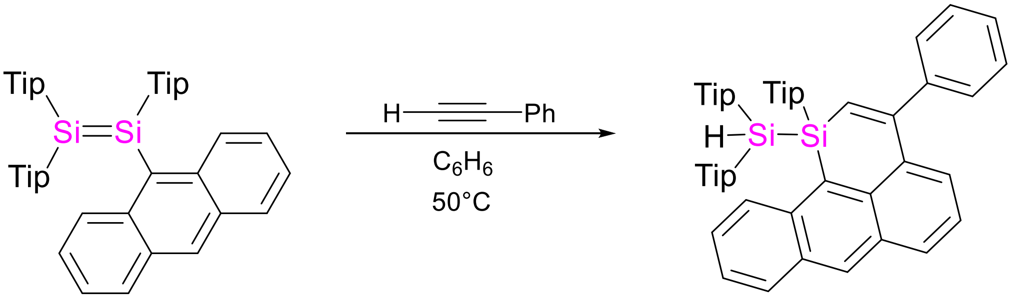

100 **125**

Scheme 62. Synthesis of tetracyclic product 125.

Finally, the reactions between a large excess of 1,4-diethynylbenzene and various tetrasiladisilenes **108**, **112** and **116** have been investigated (Scheme 57).

In contrast to M. Majumdar's work in our group[92], none of the reactions yielded any kind of isomers and hence allow for the selective formation of the postulated monomers **127a-c** in high yield. It is likely that the more sterically demanding organic linking units (compared to the *para*-phenylene unit) employed in the monomer could restrain the free rotation about C-Si bond, which results in the increased selectivity of the reactions. To date no molecular structures of the formed products **127a-c** could be obtained to confirm the proposed structures.

Although outside the scope of this thesis, the reactions of the bifunctional co-monomers **127a-c** described here with the corresponding tetrasiladienes **108**, **112** and **116** in 1:1 ratio promise to provide three types of organosilicon hybrid polymers $\mathbf{P_1}$, $\mathbf{P_2}$ and $\mathbf{P_3}$ (Scheme 63). Based on the diverse silicon motifs alternating with the different π-conjugated fragments (LU), an extended σ-π conjugation along the polymers backbone is expected and should be subject of future investigations.

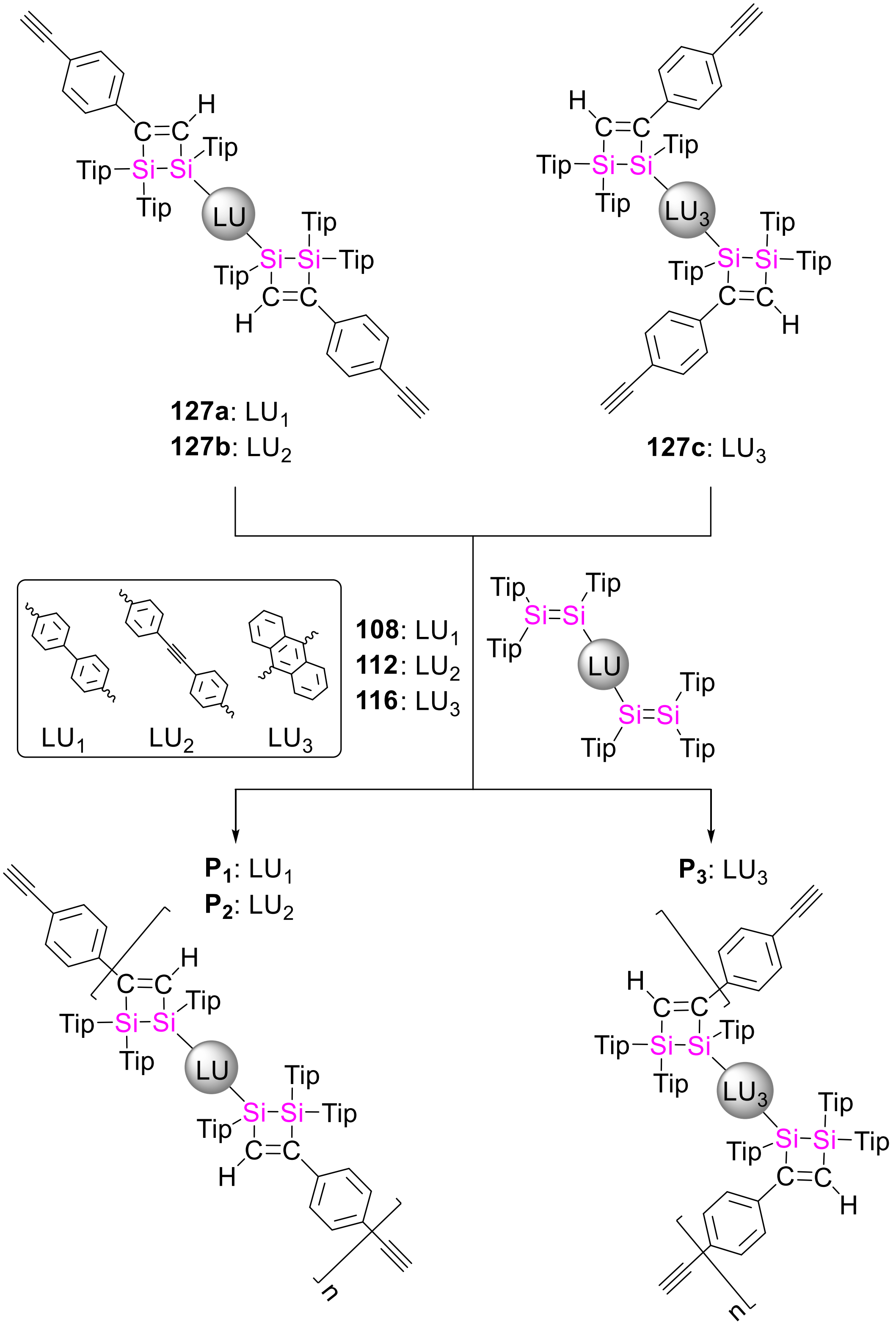

Scheme 63. Proposed reaction of extended bis (alkyne) co-monomers **127a-c** with their corresponding tetrasiladienes **108**, **112** and **116** giving polymers **$P_{1\text{-}3}$**.

5. Experimental Details

5.1. General Information

5.1.1. Experimental Conditions

Due to the high moisture and air sensitivity of the used compounds, all manipulations were carried out under a protective atmosphere of argon applying standard Schlenk techniques or in a dry glovebox. The protection gas employed was Argon 5.0 supplied by PraxAir and was used without further purification. All glassware was cleaned in a KOH solution, neutralized and cleaned again in an HCl bath and dried in an oven at 120 °C overnight. All reaction setups were evacuated to high vacuum and purged with argon four times. To generate a vacuum, a slide vane rotary vacuum pump RZ 6 from Vacuubrand was used.

5.1.2. Purification of Solvents

Benzene, diethylether (Et_2O), 1,2-dimethoxyethane (dme), pentane and toluene were refluxed over sodium/benzophenone. Hexane was dried by refluxing over sodium/benzophenone/tetra(ethyleneglycol)dimethylether (tetraglyme). Deuterated benzene and toluene were dried over potassium and distilled under argon. All solvents were distilled and stored under argon and degassed prior to use. The dry solvents were transferred with cannulas of PTFE or stainless steel under a protective atmosphere of argon into the reaction flasks.

5.1.3. Methods of Analyses and Measurement

NMR spectra were recorded on a Bruker Avance III 300 spectrometer (H = 300.13 MHZ, C = 75.46 MHz, Si = 59.6 MHz) and analyzed with the TopSpin suite of programs. All chemical shifts are reported in parts per million (ppm). The ^{1}H spectra chemical shifts were referenced to the peaks of the residual protons of the used deuterated solvents and the ^{13}C NMR shifts to the triplets of the deuterated solvent itself. ^{1}H-NMR: $CDCl_3$: δ = 7.26 ppm; benzene-d_6: δ = 7.16 ppm; toluene-d_8: δ = 2.08 ppm; thf-d_8: δ = 1.72 ppm; ^{13}C-NMR: $CDCl_3$: δ = 77.0 ppm; benzene-d_6: δ = 128.06 ppm; toluene-d_8: δ = 20.04 ppm; thf-d_8: δ = 25.31 ppm. Coupling constants are reported in Hertz (Hz) and are given in the usual notion that ^{n}j(X,Y) means a coupling of nucleus X over n bonds with nucleus Y. Coupling constants are determined by observing satellite signals next to main signal. The multiplicity and shape of the observed signals are given as s = singlet, d = doublet, t = triplet, hept. = septet, m = multiplet or convoluted signals, br = broad signal.

The UV-vis spectra were recorded on a Perkin-Elmer lambda 35 spectrometer, using quartz cell with a path length of 0.1 cm. The UV/VIS absorption spectra analyzed with Spekwin32 and the linear fits with Origin. The fluorescence spectra were recorded using a Jasco Spectrofluorometer FP-6500. The fluorescence quantum yields were measured by a Hamamatsu Quantaurus-QY Absolute PL Quantum Yield Spectrometer C11347 and the fluorescence spectra analyzed with origin. Melting points were determined under argon in closed NMR tubes and are uncorrected. CHN elemental analysis was carried out through a combustion analysis for the isolated pure products using Leco CHN-900 analyzer.

5.1.4. Computational Details

Computations have been performed by Lukas Klemmers from our group. Optimized structures as well as orbitals from natural bond orbital (NBO) [113,114] analysis were visualized with the ChemCraft[115] program. Data from TD-DFT calculations was processed and visualized with the GaussSum[116] and OriginPro 2016G[117] programmes.

5.2. Starting Materials

5.2.1. General Starting Materials

Deuterated solvents were purchased from Sigma-Aldrich and were dried if necessary as mentioned above. 2-bromomesitylene; 1-Iodo-2,3,5,6-tetramethylbenzene**;** 1,4-diodo-2,3,5,6-tetramethylbenzene**;** 2-bromonaphtalene; 9-bromoanthracene; 1-bromo-4 (phenylethynyl)benzene; 3-bromo-9-(2-naphthyl)carbazole; 2-bromo-9,10-di(2 naphthyl)anthracene; 4,4´-diiodobiphenyl; 4,4′-dibromo-p-terphenyl; 2,6-dibromonaphthalene; bis(4-bromophenyl)acetylene; 1.4-diehtynylbenzene; phenylacetylene, 9,10-dibromoanthracene; phenylacetylene were purchased from Sigma-Aldrich, TCI Deutschland or ALFA AESAR. Silicon tetrachloride was distilled from magnesium under a protecting atmosphere of argon. 2,7-dibromopyrene were generously supplied by the group of Todd Marder at the Julius-Maximilians-Universität (JMU) Würzburg. All other starting materials were prepared according to published procedures referenced in the corresponding protocols.

5.2.2. Preparation of Starting Materials

5.2.2.1. Preparation of 1-Bromo-2,4,6-triisopropylbenzene (*TipBr*)

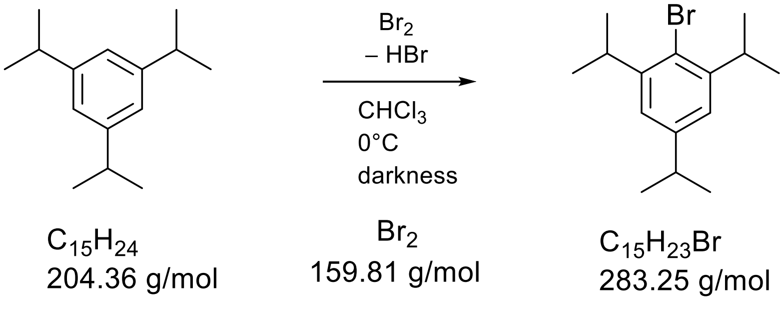

Based on existing publication,[118] a modified procedure is carried out. Br_2 (35 ml, 110.46 g, 0.69 mol) is added dropwise to a stirred and light protected solution of 2,4,6-

triisopropylbenzene Tip-H (143 g, 0.7 mol) in 700 ml of $CHCl_3$ at 0°C. The HBr gas generated is neutralized by passing through three sequentially connected wash bottles, the last two filled with isopropanol. After the Br_2 addition is finished, the reaction mixture is allowed to warm up slowly to room temperature in thawing ice-bath and stirring is continued overnight. Solid NaOH was added under stirring to the resulting brown suspension until all remaining HBr is neutralized and the reaction mixture is basic. The organic layer is separated off and washed three times with water until it is neutral. After drying over Na_2SO_4 the organic layer is concentrated on a rotary evaporator by removing the $CHCl_3$. The remaining residue is distilled in vacuum to give TipBr as a colorless liquid (81%, 159 g, 0.56 mol).

^{1}H NMR (300.13 MHz, $CDCl_3$, 300 K): $\delta =$ 6.98 (s, 2H, Tip-*H*); 6.97 (s, 1H, Tip-*H*); 3.51(hept., $^3J_{H\text{-}H}$ = 7 Hz, 2H, iPr-C*H*); 2.83 (hept., $^3J_{H\text{-}H}$ = 7 Hz, 2H, iPr-C*H*); 1.21, 1,24(each d, $^3J_{H\text{-}H}$ = 7 Hz, altogether 18H, iPr-CH_3) ppm.

5.2.2.2. Preparation of 2,4,6-Triisopropylphenyllithium (*TipLi*)

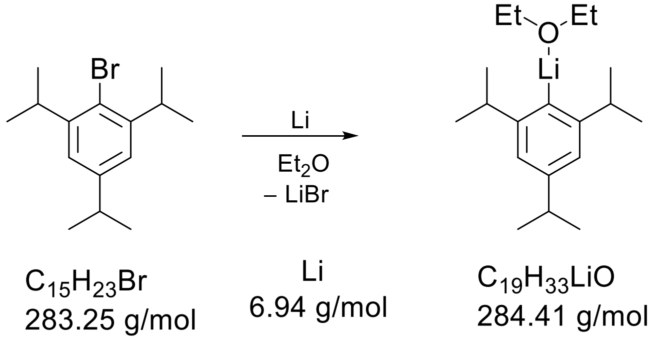

TipLi is prepared according to a modified literature procedure.[118] To a suspension of 2.2 equivalents of Li granules (7.63 g, 1.1 mol) in 1 L of dry Et_2O, TipBr (156 g, 0.55 mol) is added dropwise at room temperature. After the addition is finished, the mixture is slightly cooled with water bath and stirring is continued overnight. The conversion of TipLi is checked by ^{1}H-NMR spectroscopy on a hydrolyzed aliquot, which showed quantitative conversion of TipBr to TipLi. The remaining Li granules are filtered off under argon atmosphere and the diethylether is removed from the filtrate under reduced pressure to afford (72%, 114 g, 0.4 mol) TipLi. The crude product is used without further purification.

^{1}**H NMR** (300.13 MHz, CDCl$_3$, 300 K): $\delta =$ 7.09 (br., 2H, Tip-*H*); 3.19 (br., 2H, iPr-C*H*); 3.01 (br., 1H, iPr-C*H*); 2.83 (q, 4H, Et$_2$O-CH$_2$); 1.52, 1,36(br., altogether 18H, iPr-C*H*$_3$); 0.60 (t, 6H, Et$_2$O-CH$_2$) ppm.

5.2.2.3. Preparation of Dichlorobis(2,4,6-triisopropylphenyl)silane (Tip$_2$SiCl$_2$)

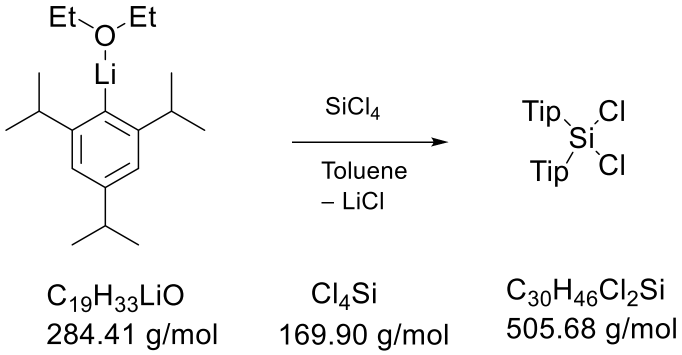

Tip$_2$SiCl$_2$ is prepared according to a modified literature procedure.[118] To the TipLi isolated by the previous procedure, 1 L of dry toluene is added and the mixture is cooled in an ice bath. Silicon tetrachloride (21 ml, 30.58 g, 0.18 mol) is added dropwise and after addition the reaction mixture is stirred overnight in the thawing cold bath. Stirring is continued for another day to complete the reaction. All insoluble components are removed by filtration. The filtrate is reduced completely under vacuum to remove the toluene. The remaining residue is dissolved in pentane (4 ml/g) and kept at −78 °C overnight. The crystallized product is further purified by two further crystallizations from pentane yielding 56 g (61%, 0.11 mol) of pure Tip$_2$SiCl$_2$.

^{1}H NMR (300.13 MHz, $CDCl_3$, 300 K): $\delta = 6.98$ (s, 4H, Tip-*H*); 3.66 (hept., $^3J_{H\text{-}H} = 6.8$ Hz, 4H, iPr-C*H*); 2.83 (hept., $^3J_{H\text{-}H} = 6.8$ Hz, 2H, iPr-C*H*); 1.20 (d, $^3J_{H\text{-}H} = 6.8$ Hz, 12H, iPr-C*H*$_3$), 1.18 (d, $^3J_{H\text{-}H} = 6.8$ Hz, 24H, iPr-C*H*$_3$) ppm.

5.2.2.4. Preparation of Lithium Powder

In a concial flask 100 ml heavy paraffin oil and 50.00 g lithium rods are heated to 210 °C under a constant argon flow over the surface of paraffin oil through rubber tubing. The molten lithium is thoroughly dispersed with a high speed dispersion tool (CAUTION! DANGER OF FIRE AND/OR EXPLOSION: Please use fresh, dry paraffin oil and oven-dried vessels for the procedure. Extreme caution must be taken that no trace amounts of water are present. Heat the floating lithium pieces to 210 °C with stirring as a safeguard to remove eventual traces of water prior to the use of the dispersion tool). The dispersion of lithium in paraffin oil is allowed to cool down to rt filtered through a reverse frit under argon. The lithium powder is washed with hexane twice and thoroughly dried in vacuum. It can be stored under a protective argon atmosphere for extended perios of time (> 1 year).

5.2.2.5. Preparation of 1,2,2-Tris(2,4,6-triisopropylphenyl)-Disilenyl-Lithium

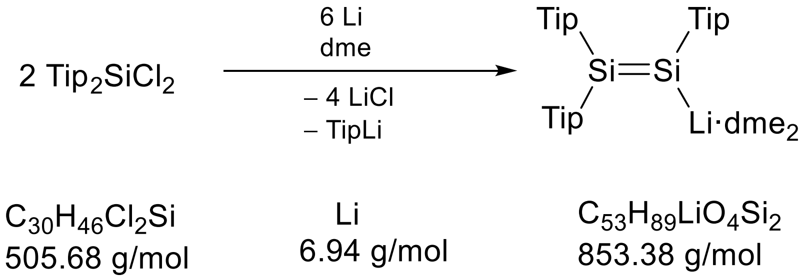

Disilenide is prepared according to a modified published procedure.[69] Dry dme (200 ml) is added under mixture of Tip_2SiCl_2 (40 g, 79 mmol) and lithium powder (2.4 g, 340 mmol). After stirring overnight, the reaction mixture turned deep red and the solvent is distilled of under reduced pressure. The residue is digested in 250 ml hexane and all precipitate is filtered off at 50°C. The dark red filtrate is kept at room temperature overnight. Pure disilenide crystallizes in (50%, 17 g, 20 mmol).

^{1}H NMR (300.13 MHz, C_6D_6, 300 K): $\delta =$ 7.13, 7.09,7.07 (each br., each 2H, Tip-*H*); 4.79 (m, 4H, iPr-C*H*); 4.28 (br., 2H, iPr-C*H*); 2.92 (s, 12H, dme-CH_3); 2.84 (s, 8H, dme-CH_2); 2.90-2.74 (br., 3H, iPr-C*H*); 1.43, 1.41, 1.33, 1.26, 1.21, 1.20, 1.14 (each d, altogether 54H, iPr-CH_3) ppm.

5.3. General Procedure for the Preparation of Aryl Disilenes and *para*-Arylene Bridged Tetrasiladienes

A 7 °C cold benzene solution of the required stoichiometric amount of disilenide **27** is added dropwise to a solution of the appropriate aryl halide or aryl dihalides in benzene using a dropping funnel pre-cooled with ice water in the cooling mantle. During the addition period of 2h care is to be taken that the temperature of both dropping funnel and receiving flask is kept at 7°C. The reaction mixture is brought to room temperature and stirred for additional 22 hours. All volatiles are removed in vacuum and the residue is digested in hexane. Insoluble material (LiX) is separated from the solution by filtration. Crystallization from a minimum amount of the indicated solvent affords the corresponding product.

5.3.1. Synthesis of 1-Mesityl-1,2,2-tris(2,4,6-triisopropylphenyl)Disilene 92

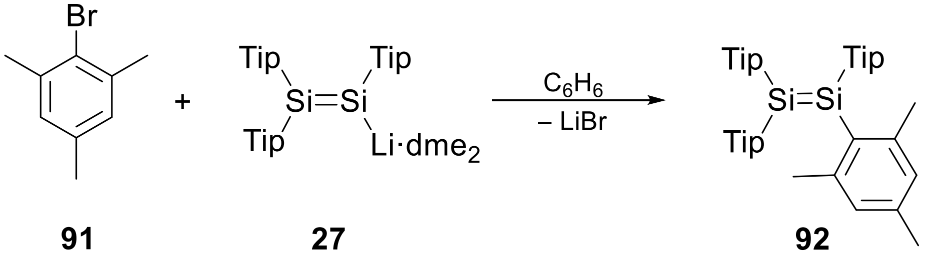

91 **27** **92**

$C_9H_{11}Br$
199.09 g.mol^{-1}

$C_{53}H_{89}LiO_4Si_2$
853.38 g.mol^{-1}

$C_{54}H_{80}Si_2$
784.57 g.mol^{-1}

Quantities: MesBr **91** (0.14 g, 0.72 mmol) in 20 ml of benzene, lithium disilenide **27** (0.62 g, 0.72 mmol) in 20 ml of benzene.

Isolation: Yellow orange pure solid product after removal of solvent, 0.52 g (93%, mp. 160°C, no dec.) and single crystals are grown from hexane.

Characterization:

^{1}**H NMR** (300 MHz, $[D_6]$benzene, TMS) δ 7.08 (s, 3H, Tip-*H*); 7.02 ,7.00, 6.98 (each s, each 1H, Tip-*H*); 6.67, 6.65 (s, 2H, Mes-*H*); 4.64 (hept., $^{3}J(H,H)$ = 6.7 Hz 1H, ^{i}Pr-C*H*), 4.53 (hept., $^{3}J(H,H)$ = 6.6 Hz, 2H, ^{i}Pr-C*H*); 3.81 (hept., $^{3}J(H,H)$ = 6.7 Hz, 3H, ^{i}Pr-C*H*); 2.72 (hept., $^{3}J(H,H)$ = 6.7 Hz, 3H, ^{i}Pr-C*H*); 2.66, 2.53, 2.02 (s, each 3H, Me-*H*); 1.46, 1.45, 1.44, 1.42, 1.40, 1.18, 1.17. 1.16, 1.15, 1.13, 0.72, 0.70, 0.66, 0.63, 0.58 (each d, $^{3}J(H,H)$ = 6.7 Hz, altogether 54H, iPr-CH_3) ppm.

^{13}**C NMR** (75.46 MHz, $[D_6]$benzene, TMS) δ 155.83, 155.44, 155.40, 155.11, 155.00, 154.43 (Tip-C_o); 150.75, 150.69, 150.49 (Tip-C_p);144.56, 143.85 (Mes-C_p); 138.57 (Mes-C_o); 137.79 (Mes-C_i); 134.79, 134.43, 132.16 (Tip-C_i); 128.62, 128.17 (Mes-C_m); 122.48, 122.40, 122.25, 121.41, 121.25, 121.21 (Tip-C_m); 39.00, 38.53, 38.20, 37.04, 36.76, 36.34, 34.55, 34.52, 34.46 (^{i}Pr-*C*H); 25.85, 25.76 (Me-C_o); 25.18, 25.14, 25.07, 24.76, 24.73, 24.60, 24.47, 24.34, 24.11, 24.05, 24.02, 23.99, 23.91 (^{i}Pr-CH_3); 21.13 (Me-C_p) ppm.

^{29}**Si NMR** (59.62 MHz, $[D_6]$benzene, TMS) δ 55.95 (*Si*PhTip); 55.58 (*Si*Tip_2) ppm.

UV-Vis(hexane) λ_{max} (ε) 430 nm (21200 $M^{-1}cm^{-1}$).

Exact mass (EI): found, 784.5800; calcd for $C_{54}H_{80}Si_2$, 784.5799.

5.3.2. Synthesis of 1-(2,3,5,6-Tetramethylphenyl)-1,2,2-tris(2,4,6-triisopropylphenyl)Disilene 94

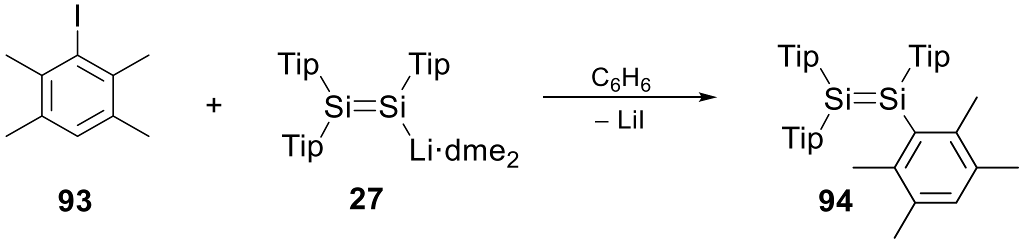

93 **27** **94**

$C_{10}H_{13}I$
260,12 g.mol^{-1}

$C_{53}H_{89}LiO_4Si_2$
853.38 g.mol^{-1}

$C_{55}H_{82}Si_2$
799.43 g.mol^{-1}

Quantities: 1-Iodo-2,3,5,6-tetramethylbenzene **93** (0.85 g, 3.27 mmol) in 30 ml of benzene, disilenide **27** (2.79 g, 3.27 mmol) in 35 ml of benzene.

Isolation: Yellow crystals at room temperature from hexane, 2.30 g (88%, mp. 145°C, dec.).

Characterization:

^{1}**H NMR** (300 MHz, [D$_6$]benzene, TMS): coupling constants in Tip-*H* doublet: ^{4}J = 1.65 Hz; $\delta =$ 7.09, 7.07, 7.04, 6.99 (each d, each 1H, Tip-*H*); 6.97 (s, 1H, Tip-*H*); 6.77 (s, 1H, $C_6Me_4\mathit{H_1}$); 4.60, 4.49, 3.80 (each hept., each 2H, iPr-C*H*); 2.76, 2.70, 2.68 (hept., each 1H, iPr-C*H*); 2.73, 2.54, 1.95, 1.90 (each s, each 3H, $C_6\mathit{Me_4}H_1$); 1.43 (d, 3H, iPr-C$\mathit{H_3}$); 1.37 (d, 3H, iPr-C$\mathit{H_3}$); 1.30 (s, 3H, iPr-C$\mathit{H_3}$); 1.27-1.24 (m, 14H, iPr-C$\mathit{H_3}$); 1.22 (d, 3H, iPr-C$\mathit{H_3}$); 1.20 (d, 3H, iPr-C$\mathit{H_3}$); 1.18 (s, 2H, iPr-C$\mathit{H_3}$); 1.08-0.99 (m, 14H, iPr-C$\mathit{H_3}$); 0.77, 0.63, 0.52 (each d, 9H, iPr-C$\mathit{H_3}$) ppm.

^{13}**C NMR** (75.46 MHz, [D$_6$]benzene, TMS) $\delta =$ 155.68, 155.52, 155.12, 154,68. 150.76 ,150.06 (Tip-*Co/p*), 139.96, 139.28, 134.12, 133.97, 133.46, 132.75 (Ar-C_i); 133.05 (Ar-*C*H); 127.80, 127.54 ($C_6Me_4H_1$-$\mathit{C}_{q.}$); 122.53, 122.39, 122.33, 121.43, 121.28, 121.15 (Tip-*C*H); 38.92, 38.57, 38.25, 36.97, 36.62, 36.47 (iPr-*C*H); 34.57, 34.51, 34.41

($C_6Me_4H_1$-CH_3); 25.19, 24.77, 24.39, 24.11, 23.99, 23.44, 22.80, 20.73, 20.32 (iPr-CH_3) ppm.

^{29}Si NMR (59.62 MHz, [D$_6$]benzene, TMS) δ = 57.88 ($^1J_{Si\text{-}Si}$ = 293.97 Hz, *Si*Tip); 52.95 ($^1J_{Si\text{-}Si}$ = 293.97 Hz, *Si*Tip$_2$) ppm.

UV-Vis (hexane) λ_{max} (ε) 430 nm (17300 M^{-1}cm^{-1}); λ_{max} (ε) 335 nm (15000 M^{-1}cm^{-1}).

Combustion Analysis: Calcd. for $C_{55}H_{82}Si_2$: C, 82.63; H, 10.34. Found: C, 82.52; H, 10.26.

5.3.3. Reaction of 1-Bromo-4 (phenylethynyl)benzene 95 with Disilenide 27

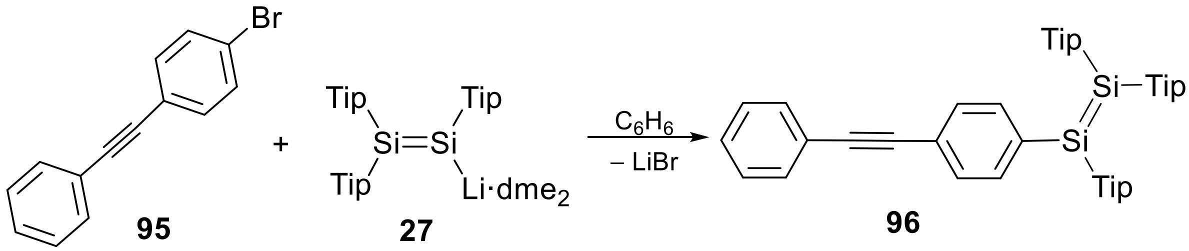

95 **27** **96**

$C_{14}H_9Br$
257,17 g.mol^{-1}

$C_{53}H_{89}LiO_4Si_2$
853.38 g.mol^{-1}

$C_{59}H_{78}S_{i2}$
843.44 g.mol^{-1}

Quantities: 1-bromo-4 (phenylethynyl)benzene **95** (0.45 g, 1.76 mmol) in 25 ml of benzene, disilenide **27** (1.51 g, 1.76 mmol) in 25 ml of benzene.

Isolation: Since crystallization attempts remained unsuccessful, the crude product is obtained as a pure red solid in 94% yield (mp. 155°C, dec.) after removal of hexane solvent under completely reduced pressure.

Characterization:

^{1}H NMR (300 MHz, [D$_6$]benzene, TMS) δ = 7.32 (m, 4H, Ph-*H*); 7.17 (s, 1H, Ph-*H*); 7.12, 7.09, 7.03 (each s, each 2H, Tip-*H*); 6.93 (m, 4H, Ph-*H*); 4.24, 4.19, 3.99 (each hept., each 2H, iPr-C*H*); 2.79, 2.74, 2.68 (each hept., each 1H, iPr-C*H*); 1.22, 1.183, 1.24, 1.05 (each d, altogether 54H, iPr-CH_3) ppm.

^{13}C NMR (75.46 MHz, [D$_6$]benzene, TMS) δ = 156.20, 155.53, 155.04, 151.71, 151.42, 150.73 (Tip-*C*o/p); 148.93 (Ar-*C*H); 139.79 (Ar-*C*i); 135.58, 133.11, 132.87, 132.64, 131.74, 130.89 (Tip-*C*i); 129.85, 128.32 (Ar-*C*H); 128.19 (C_6D_6); 127.87, 127.55 (Ar-*Cq*); 121.81, 121.37 (Ar-*C*H); 122.23, 121.97, 121.61 (Tip-*C*H); 90.79, 90.52 (Carbon-Carbon.triple bond); 38.27, 38.21, 37.34, 34.75, 34.63, 34.59, 34.39 (iPr-*C*H); 24.52, 24.29, 24.12, 24.00, 23.96, 23.80 (iPr-*C*H_3) ppm.

^{29}Si NMR (59.62 MHz, [D$_6$]benzene, TMS) $\delta = 69.70$ (*Si*Tip); 57.76 (*Si*Tip2) ppm.

UV-Vis (hexane) λ_{max} (ε) 472 nm (4880 $M^{-1}cm^{-1}$).

Combustion Analysis: Calcd. for $C_{59}H_{78}Si_2$: C, 84.02; H, 9.32. Found: C, 82.51; H, 9.03.

5.3.4. Synthesis of 1-(naphthalen-2-yl)-1,2,2-tris(2,4,6-triisopropylphenyl)Disilene 98

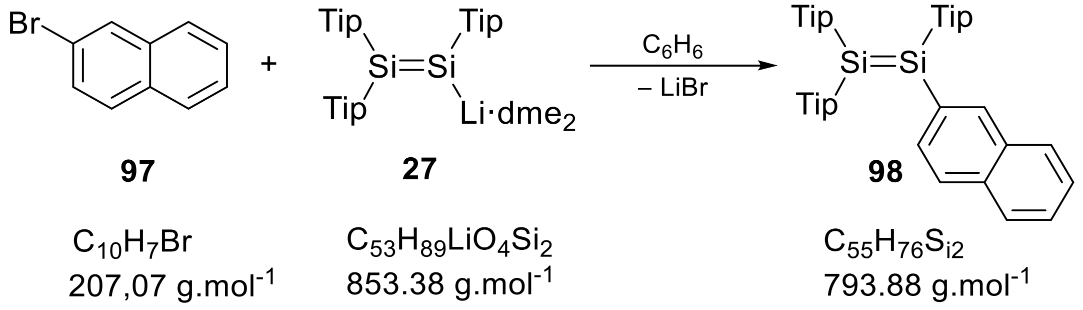

Quantities: 2-bromonaphtalene **97** (0.37 g, 1.79 mmol) in 25 mL of benzene, disilenide **27** (1.53 g, 1.79 mmol) in 25 ml of benzene.

Isolation: red orange crystals at room temperature from hexane, 1.21 g (85%, mp. 120°C, dec.).

Characterization:

^{1}H NMR (300 MHz, [D$_6$]benzene, TMS) $\delta = 7.90$ (s, 1H, $C_{10}H_7$); 7.43 (t, 2H, $C_{10}H_7$); 7.30 (d, 2H, $C_{10}H_7$), 7.15, 7.09, 7.06 (each s, each 2H, Tip-*H*); 7.07 (br., overlapping, 1H, $C_{10}H_7$); 7.04 (br., overlapping, 1H, $C_{10}H_7$); 4.34, 4.27, 4.06 (each hept., each 2H, iPr-C*H*); 2.70, 2.75, 2.70 (each hept., each 1H, iPr-C*H*); 1.23, 1.20, 1.17, 1.14, 1.26, 1.09, 1.07 (each d, altogether 54H, iPr-CH_3) ppm.

^{13}C NMR (75.46 MHz, [D$_6$]benzene, TMS) $\delta = 156.32$, 156.07, 155.68, 155.06, 151.68, 151.15, 150.63 (Tip-*Co/p*); 136.32 ($C_{10}H_7$-*C*H); 136.29 ($C_{10}H_7$-C_i); 133.79, 133.47, 133.13, 133.01, 130.16 (Tip-*C*i); 132.47, 129.69, 129.29 ($C_{10}H_7$-*C*H); 127.87, 127.55 ($C_{10}H_7$-*C*q.); 126.99, 126.14, 124.83 ($C_{10}H_7$-*C*H); 121.97, 121.62 (Tip-*C*H); 38.27, 38.14, 37.34, 34.76, 34.60, 34.51, 34.41 (iPr-*C*H); 25.59, 24.55, 24.14, 23.97, 23.82 (iPr-CH_3) ppm.

^{29}Si NMR (99.36 MHz, [D$_6$]benzene, TMS) $\delta = 71.05$ (*Si*Tip); 56.74 (*Si*Tip$_2$) ppm.

UV-Vis (hexane) λ_{max} (ε) 463 nm (6800 M^{-1}cm^{-1}).

Combustion Analysis: Calcd. for $C_{55}H_{76}Si_2$: C, 83.26; H, 9.66. Found: C, 83.51; H, 9.77.

5.3.5. Synthesis of 1-(anthracen-9-yl)-1,2,2-tris(2,4,6-triisopropylphenyl)Disilene 100

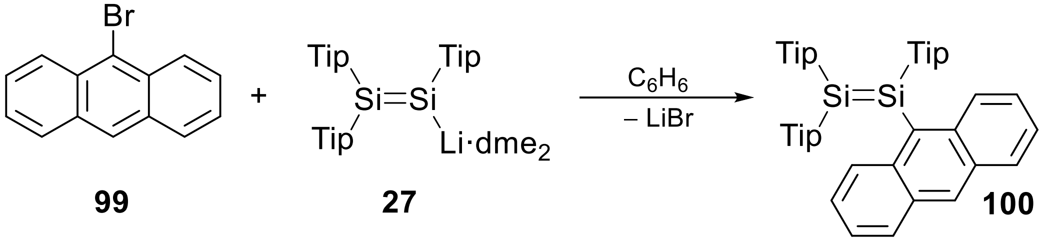

99 **27** **100**

$C_{14}H_9Br$
257,17 g.mol^{-1}

$C_{53}H_{89}LiO_4Si_2$
853.38 g.mol^{-1}

$C_{59}H_{78}Si_2$
843.44 g.mol^{-1}

Quantities: 9-bromoanthracene **99** (0.38 g, 1.49 mmol) in 20 mL of benzene, of disilenide **27** (1.273 g, 1.49 mmol) in 25 ml of benzene.

Isolation: Purple crystals at −26 °C from pentane, 2.30 g (87%, mp. 168°C, dec.).

Characterization:

^{1}H NMR (300 MHz, [D$_6$]benzene, TMS) $\delta = 9.75$ (d, 1H, C_{14}*H*$_9$); 9.09 (d, 1H, C_{14}*H*$_9$); 8.18 (s, 1H, C_{14}*H*$_9$); 7.69 (dd, 2H, C_{14}*H*$_9$); 7.27-7.18, 7.12-7.11, 7.10-7.03 (each m, each 2H, overlapping with $C_{14}H_9$, Tip-*H*); 7.01, 6.93, 6.84, 6.68 (each s, each 1H, C_{14}*H*$_9$); 5.03, 4.67, 4.31 (each hept., each 1H, iPr-C*H*); 4.03 (hept., 2H, iPr-C*H*); 3.81, 2.75, 2.65, 2.51 (each hept., each 1H, iPr-C*H*); 1.68, 1.53, 1.33, 1.30, 1.76, 1.10, 0.98, 0.84, 0.61, -0.06, -0.39 (each d, altogether 54H, iPr-C*H*$_3$) ppm.

^{13}C NMR (75.46 MHz, [D$_6$]benzene, TMS) δ = 156.02, 155.54, 155.29, 155.20, 155.17, 154.37, 151.01, 150.98 (Tip-$C_{o/p}$); 137.69, 137.14, 136.46 ($C_{14}H_9$-C_i); 133.32, 133.20, 132.31, 131.51 (Tip-C_i); 131.46, 130.02, 129.16, 129.01, 128.40, 128.37 ($C_{14}H_9$-*CH*); 127.87, 127.55 ($C_{14}H_9$-$C_{q.}$); 125.61, 125.40 ($C_{14}H_9$-*C*H); 122.64, 122.47, 122.28, 121.55, 121.47, 121.28, 121.05 (Tip-*C*H); 39.18, 38.65, 38.43, 37.80, 36.64, 36.45, 34.63, 34.53, 34.25 (iPr-*C*H); 25.65, 25.23, 24.84, 24.76, 24.65, 24.15, 24.04, 23.99, 23.84, 23.75, 23.62, 23.32 (iPr-CH_3); 34.49, 22.54, 14.11 (pentane) ppm.

^{29}Si NMR (59.62 MHz, [D$_6$]benzene, TMS) δ = 60.08 (*Si*Tip); 52.68 (*Si*Tip$_2$) ppm.

UV-Vis (hexane) λ_{1max} (ε_1) 412 nm (21500 M^{-1}cm^{-1}), λ_{2max} (ε_2) 550 nm (3800 M^{-1}cm^{-1}).

Combustion Analysis: Calcd. for $C_{59}H_{78}Si_2$: C, 84.02; H, 9.32. Found: C, 84.17; H, 9.46.

5.3.6. Reaction of 2-Bromo-9,10-di(2-naphthyl)Anthracene 101 with Disilenide 27

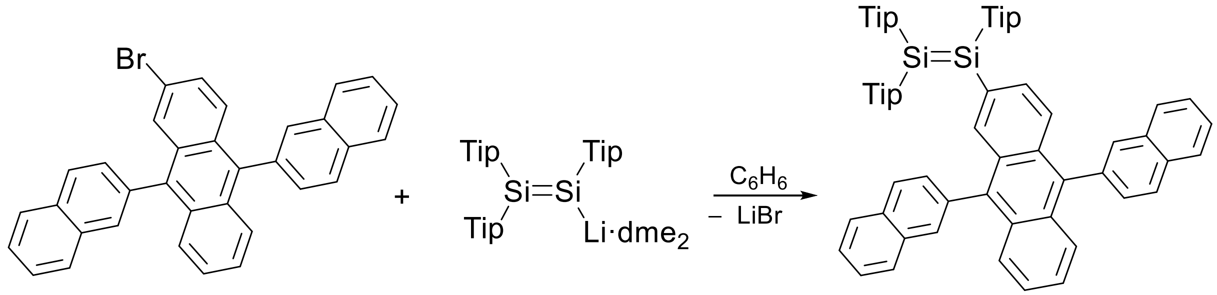

101

$C_{34}H_{21}Br$
509.38 g.mol^{-1}

27

$C_{53}H_{89}LiO_4Si_2$
853.38 g.mol^{-1}

102

$C_{79}H_{90}Si_2$
1095.76 g.mol^{-1}

Quantities: 2-bromo-9,10-di(2-naphthyl)anthracene **101** (0.48 g, 0.94 mmol) in 27 mL of benzene, disilenide **27** (0.81 g, 0.94 mmol) in 22 ml of benzene.

Isolation: Standing overnight at room temperature affords 0.89 g (mp. 180°C, no dec.) in 86% yield as burgundy red microcrystals from a concentrated hexane solution.

Characterization:

^{1}H NMR (300 MHz, [D$_6$]benzene, TMS) δ = 8.13 (br., 1H, Ar-*H*); 7.76 (m, 7H, Ar-*H*); 7.59 (m, 2H, Ar-*H*); 7.47 (m, 3H, Ar-*H*); 7.33 (m, 5H, Ar-*H*); 7.08 (m, 3H, Ar-*H*); 7.03, 6.99

(each s, each 2H, Tip-*H*); 6.92 (br., 2H, Tip-*H*); 4.18 (br., 3H, iPr-C*H*); 3.94 (br., 2H, iPr-C*H*), 3.54 (br., 1H, iPr-C*H*); 2.68 (hept., 3H, iPr-C*H*); 1.22, (br.); 1.18, 1.10, 0.88 (each d, altogether 54H, iPr-C*H*$_3$) ppm.

^{13}C NMR (75.46 MHz, [D_6]benzene, TMS) $\delta =$ 156.10, 155.74, 155.56, 154.85, 151.19, 150.48 (Tip-*C*o/p); 137.28, 137.17, 136.94, 136.48 (Ar-*C*i); 135.70 (Ar-*C*H); 133.93, 133.67, 133.33, 133.15, 132.92, 131.02. 130.91, 130.11 (Tip-*C*i); 131.65, 130.44, 130.37, 129.72, 129.38, 128.43, 128.35 (Ar-*C*H); 128.20 (C_6D_6) ; 127.88, 127.55 (Ar-*Cq*); 127.98, 127.77, 127.37, 126.36, 126.18, 126.06, 125.92, 125.92, 125.80, 125.42, 125.37 (Ar-*C*H); 121.87, 121.11 (Tip-*C*H); 38.56, 38.35, 37.36, 34.51, 34.36, 33.59; (iPr-*C*H); 25.56, 25.26, 24.45, 24.30, 24.03, 23.95, 23.79 (iPr-*C*H$_3$); 31.79, 22.88, 14.20 (Hexane) ppm.

^{29}Si NMR (59.62 MHz, [D_6]benzene, TMS) $\delta =$ 70.79 (*Si*Tip); 57.56 (*Si*Tip2) ppm.

UV-Vis (hexane) λ_{1max} (ε_1) 406 nm (38800 $M^{-1}cm^{-1}$); λ_{2max} (ε_2) 530 nm (23000 $M^{-1}cm^{-1}$).

Combustion Analysis: Calcd. for $C_{79}H_{90}Si_2$: C, 86.59; H, 8.28. Found: C, 83.74; H, 8.48.

5.3.7. Reaction of 3-Bromo-9-(2-naphthyl)Carbazole 103 with Disilenide 27

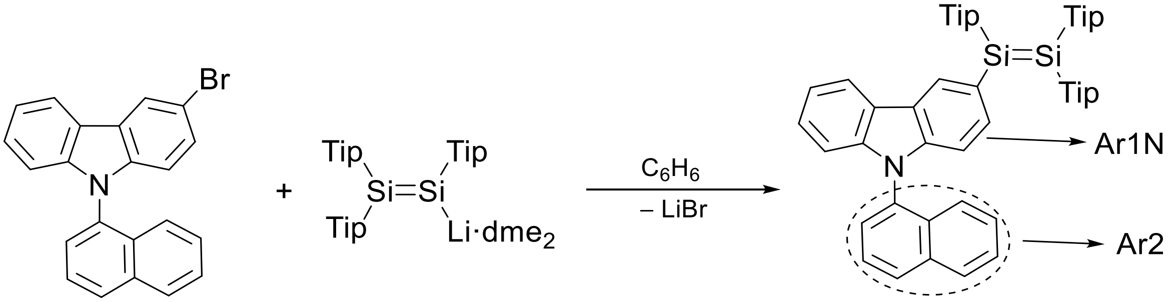

103
$C_{22}H_{14}BrN$
372.27 g.mol^{-1}

27
$C_{53}H_{89}LiO_4Si_2$
853.38 g.mol^{-1}

104
$C_{67}H_{83}NS_{i2}$
958.58 g.mol^{-1}

Quantities: 3-bromo-9-(2-naphthyl)carbazole **103** (0.38 g, 1.49 mmol) in 20 mL of benzene, disilenide **27** (0.70 g, 0.82 mmol) in 20 ml of benzene.

Isolation: An orange pure solid (mp. 163°C) in 90% yield was obtained as precipitate from a concentrated hexane solution.

Characterization:

^{1}H NMR (300 MHz, [D$_6$]benzene, TMS) $\delta = 8.35$ (s, 1H, Ar-*H*); 7.62 (dd, 2H, Ar-*H*); 7.51 (m, 3H, Ar-*H*); 7.43 (s, 2H, Ar-*H*), 7.23 (br, 2H, Ar-*H*); 7.20 (s, overlapping between Ar-H and Tip-H, 5H, Ar-*H and* Tip-*H*); 7.14 (s, overlapping with C_6D_6, 6H, Tip-*H*); 7.09 (s, 2H, Tip-*H*); 7.01 (d, 1H, Ar-*H*); 4.50, 4.40, 4.13 (each hept., 2H, iPr-C*H*); 2.82 2.76, 2.72 (each hept., 1H, iPr-*CH)*; 1.31 (d, 6H, *i*Pr-CH_3); 1.26 (d, 8H, *i*Pr-CH_3); 1.23 (s, 8H, *i*Pr-CH_3); 1.20 (s, 6H, *i*Pr-CH_3); 1.17-1.12 (m, 26H, *i*Pr-C*H)* ppm.

^{13}C NMR (75.46 MHz, [D$_6$]benzene, TMS) $\delta = 156.29$, 155.72, 154.99, 151.55, 151.01, 150.39 (Tip-*C*o/p), 141.76, 141.38 (Ar-*C*i), 135.12, 134.23, 133.74, 133.63, 132.55, 130.99, 129.26 (Tip-*Ci*); 133.95, 128.45, 128.03, 126.68, 126.32, 126.13, 125.37, 125.20, 121.87, 121.71 (Ar-*C*H); 128.2 (C_6D_6), 127.88, 127.55 (Ar-*Cq*); 121.93, 121.88, 121.57, 120.74, 120.58, 120.47 (Tip-*C*H), 109.99, 109.72 (Ar-*C*H); 38.31, 38.11, 37.47, 34.81, 34.55, 34.44, 31.80 (iPr-*C*H); 25.80, 24.62, 24.33, 24.03, 23.95, 23.87, 22.89 (iPr-*C*H_3), 14.17 (Hexane) ppm.

^{29}Si NMR (59.62 MHz, [D$_6$]benzene, TMS) $\delta = 74.39$ (*Si*Tip), 52.28; (*Si*Tip2) ppm.

UV-Vis (hexane) λ_{max} (ε) 447 nm (17300 $M^{-1}cm^{-1}$).

Combustion Analysis: Calcd. for $C_{67}H_{83}NSi_2$: C, 83.95; H, 8.73. Found: C, 83.09; H, 7.96.

5.3.8. Synthesis of 1,4-Bis{1,2,2-[tris(2,4,6-triisopropylphenyl)]}DisilenylDurene 106

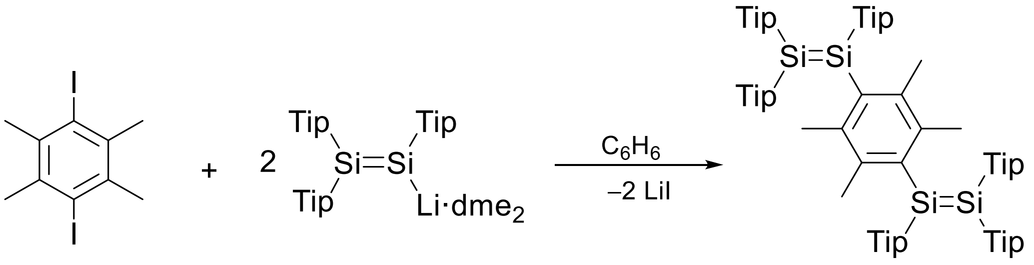

105 $C_{10}H_{12}I_2$ 386.01 g/mol

27 $C_{53}H_{89}LiO_4Si_2$ 853.38 g/mol

106 $C_{100}H_{150}Si_4$ 1464.64 g/mol

Quantities: diiododurene (0.237 g, 0.708 mmol) **105** in 20 mL of benzene, disilenide **27** (1,21g, 1.41 mmol) in 25 ml of benzene.

Isolation: Crystallization at room temperature overnight from hexane yields 0.67 g (65 %) as orange microcrystals (mp. 174°C, no dec.). A single crystal surrounded by microcrystals is detected by X-ray diffraction.

Characterization:

^{29}Si NMR at 300 K (59.62 MHz, [D$_6$]benzene, TMS) δ = 58.73; 58.01; 57.87; 57.52; 56.30; 55.60; 53.21; 52.10 ppm.

^{29}Si NMR at 353 K (59.62 MHz, [*d*$_8$]toluene, TMS) δ = 57.84 and 52.92 ppm.

CP-MAS ^{29}Si NMR (79.49 MHz) δ = 55.42 ppm.

UV-Vis (hexane) λ_{max} (ε) 450 nm (19700 M^{-1}cm^{-1}).

Combustion Analysis: Calcd. for $C_{100}H_{150}Si_4$: C, 82.01; H, 10.32. Found: C, 80.71; H, 9.35.

5.3.9. Synthesis of 4,4´-Bis{1,2,2-[tris(2,4,6-triisopropylphenyl)]}Disilenylbiphenyl 108

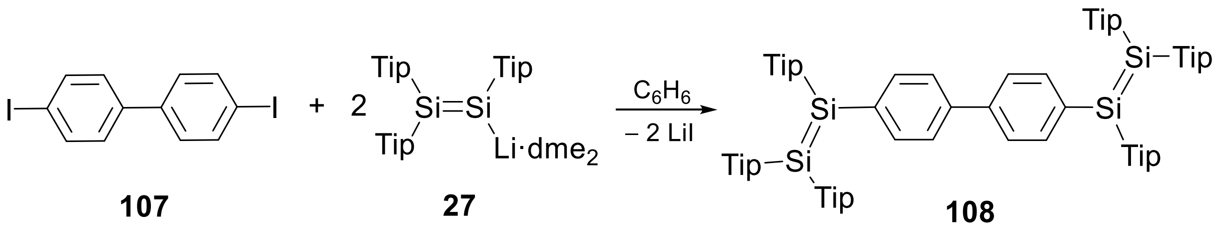

$C_{12}H_8I_2$
406.00 g.mol^{-1}

$C_{53}H_{89}LiO_4Si_2$
853.38 g.mol^{-1}

$C_{102}H_{146}Si_4$
1095.76 g.mol^{-1}

Quantities: 4,4´-diiodobiphenyl (0.237 g, 0.585 mmol) **107** in 20 ml of benzene, disilenide **27** (1g, 1.17 mmol) in 20 ml of benzene.

Isolation: Red crystals at room temperature from hexane, 0.75 g (88%, mp. 178°C, dec.).

Characterization:

^{1}H NMR (300 MHz, [D$_6$]benzene, TMS) $\delta =$ 7.35 (d, 4H, -(C_6H_4)$_2$-); 7.13, 7.10, 7.03 (each s, each 4H, Tip-*H*); 6.99 (d, 4H, -(C_6H_4)$_2$-); 4.29, 4.20, 4.0, 2.76 (each hept., each 4H, iPr-C*H*); 2.69 (hept., 2H, iPr-C*H*); 1.24, 1.22, 1.18, 1.14, 1.12, 1.04 (each d, altogether 108H, iPr-C*H*$_3$) ppm.

^{13}C NMR (75.46 MHz, [D$_6$]benzene, TMS) $\delta =$ 156.19, 155.59, 155.09, 154.97, 151.55, 151.15, 150.54, 148.92 (Tip-$C_{o/p}$); 140.75, 137.41 ((C_6H_4)$_2$-C_i); 136.37 ((C_6H_4)$_2$-*C*H); 133.34, 133.19, 130.24 (Tip-C_i); 127.86, 127.54 ((C_6H_4)$_2$-$C_{q.}$); 126.12 ((C_6H_4)$_2$-*C*H); 122.22, 121.92, 121.53 (Tip-*C*H); 38.25, 38.06, 37.43, 34.75, 34.58, 34.40 (iPr-*C*H); 25.95, 24.51, 24.28, 24.15, 24.29, 23.99, 23.80 (iPr-*C*H$_3$) ppm.

^{29}Si NMR (59.62 MHz, [D$_6$]benzene, TMS) $\delta =$ 71.04 (*Si*Tip); 56.00 (*Si*Tip$_2$) ppm.

UV-Vis (hexane) λ_{1max} (ε_1) 277 nm (35000 $M^{-1}cm^{-1}$); λ_{2max} (ε_2) 463 nm (21000 $M^{-1}cm^{-1}$).

Combustion Analysis: Calcd. for $C_{102}H_{146}Si_4$: C, 82.44; H, 9.83. Found: C, 82.60; H, 9.97.

5.3.10. Reaction of Disilenide 27 with 4,4′-Dibromo-*p*-terphenyl 109

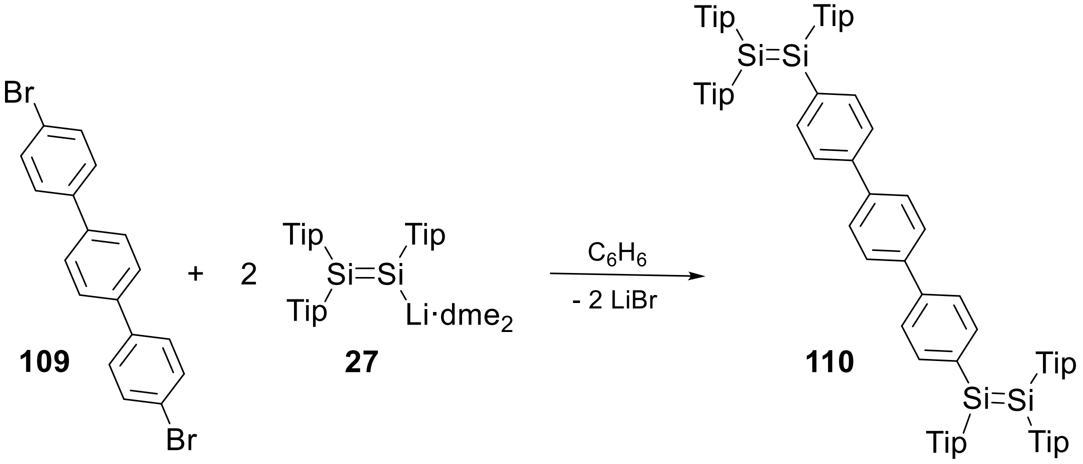

109 **27** **110**

$C_{18}H_{12}Br_2$ 388.10 g.mol^{-1}

$C_{53}H_{89}LiO_4Si_2$ 853.38 g.mol^{-1}

$C_{108}H_{150}Si_4$ 1560.73 g.mol^{-1}

Quantities: 4,4′-dibromo-p-terphenyl **109** (0.316 g, 0.81 mmol) in 30 ml of benzene, disilenide **27** (1.39 g, 1.62 mmol) in 30 ml of benzene.

Isolation: Crystallization at room temperature from hexane overnight yields 0.95 g (75%) of **110** as red orange microcrystals (mp. 177°C, dec.).

Characterization:

^{1}H NMR (300 MHz, [D$_6$]benzene, TMS) $\delta = 7.46$ (d, 4H, Ar-*H*); 7.30, 7.16, 7.06 (each s, each 4H, Tip-*H*); 7.17 (br., 2H, Ar-H); 7.14 (s, 17H, overlapping between Ar-*H* and C_6D_6); 4.30, 4.27, 4.05, 2.77 (each hept., each 4H, iPr-C*H*); 3.14 (dme, 3H); 2.68 (hept., 2H, iPr-C*H*); 1.24, 1.22, 1.18, 1.14 (br.), 1.12, 1.04 (each d, altogether 108H, iPr-C*H*3) ppm.

^{13}C NMR (75.46 MHz, [D$_6$]benzene, TMS) $\delta = 156.21$, 155.64, 155.01, 151.65, 151.25, 150.62 (Tip-*C*o/p); 140.60, 139.76 (Ar-*C*i); 137.57, 136.56 (Ar-*C*H), 133.28, 133.19, 130.32 (Tip-*C*i); 128,79 (Ar-*C*H); 128.19 (C_6D_6), 127.78, 127.55, 126.14 (Ar-*Cq.*); 121.97, 121.58 (Tip-*C*H); 71.16, 58.75 (dme); 38.32, 38.06, 37.43, 34.75, 34.58, 34.41 (iPr-*C*H); 25.61, 24.51, 24.28, 24.15, 24.29, 23.99, 23.82 (iPr-*C*H3) ppm.

^{29}Si NMR (59.62 MHz, [D$_6$]benzene, TMS) $\delta = 70.90$ (*Si*Tip); 56.11 (*Si*Tip2) ppm.

UV-Vis (hexane) λ_{1max} (ε_1) 296 nm (44600 M^{-1}cm^{-1}); $\lambda_2$max (ε_2) 463 nm (8300 M^{-1}cm^{-1}).

Combustion Analysis: Calcd. for $C_{108}H_{150}Si_4$: C, 83.11; H, 9.69. Found: C, 82.31; H, 9.11.

5.3.11. Synthesis of 1,2-Bis(4-(1,2,2-tris(2,4,6-isopropylphenyl)Disilenyl)phenyl)ethyne 112

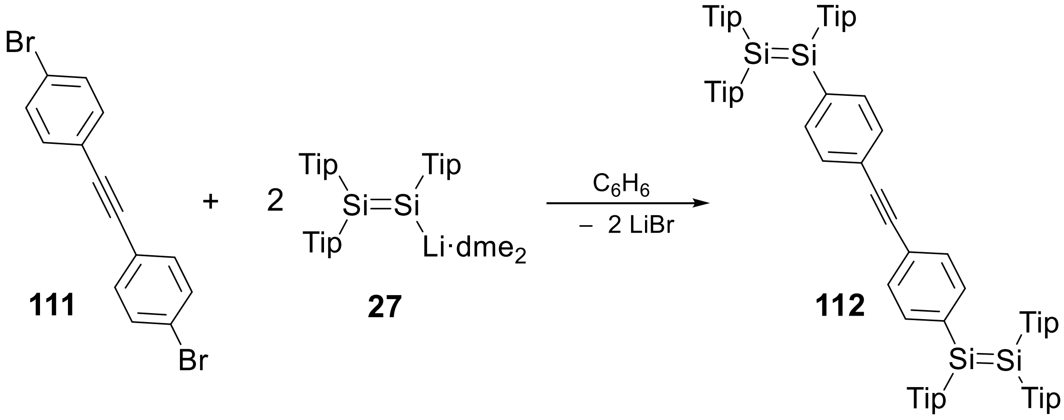

111 $C_{14}H_8Br_2$ 336.03 g.mol^{-1}

27 $C_{53}H_{89}LiO_4Si_2$ 853.38 g.mol^{-1}

112 $C_{104}H_{146}Si_4$ 1508.65g.mol^{-1}

Quantities: bis(4-bromophenyl)acetylene **111** (0.296 g, 0.88 mmol) in 20 ml of benzene, disilenide **27** (1.60 g, 1.87 mmol) in 23 ml of benzene.

Isolation: Red crystals at room temperature from benzene, 1.25 g (94%, mp. 184°C, dec.).

Characterization:

^{1}H NMR (300 MHz, [D$_6$]benzene, TMS) $\delta = 7.25$ (d, 4H, -C_6H_4-); 7.11; 7.08; 7.032 (each s, each 4H, Tip-*H*); 7.02 (d, 4H, -C_6H_4-); 4.24, 4.17, 3.98, 2.76 (each hept., each 4H, iPr-C*H*); 2.69 (hept., 2H, iPr-C*H*); 1.20, 1.19, 1.16, 1.15, 1.13, 1.10 1.06; 1.04 (each d, altogether 108H, iPr-C*H*$_3$) ppm.

^{13}C NMR (75.46 MHz, [D$_6$]benzene, TMS) $\delta = 156.20$, 155.54, 155.05, 151.69, 151.38, 150.72 (Tip-*C*o/p); 139.55 (C_6H_4-*C*i); 135.75 (C_6H_4-*C*H); 132.92, 132.69, 129.88, 121.50 (Tip-*C*i); 130.88 (C_6H_4-*C*H); 127.87, 127.55 (C_6H_4-*C*q.); 121.97, 121.60 (Tip-*C*H); 91.43

(Carbon-Carbon.triple bond); 38.26, 38.21, 37.34, 34.74, 34.59, 34.39 (iPr-*C*H); 25.51, 24.51, 24.11, 23.99, 23.93, 23.87 (iPr-*C*H_3) ppm.

^{29}Si NMR (59.62 MHz, [D_6]benzene, TMS) $\delta = 69.91$ (*Si*Tip); 57.52 (*Si*Tip_2) ppm.

UV-Vis (hexane) λ_{max} (ε) 309 nm (47690 $M^{-1}cm^{-1}$); λ_{max} (ε) 488 nm (46000 $M^{-1}cm^{-1}$).

Combustion Analysis: Calcd. for $C_{104}H_{146}Si_4$: C, 82.72; H, 9.67. Found: C, 77.55; H, 9.12.

Combustion analysis and mass spectrometry did not yield satisfactory results presumably due to the oxygen sensitivity of **112.**

5.3.12. Synthesis of 2,6-Bis{1,2,2-[tris(2,4,6-triisopropylphenyl)]}Dsilenylnaphthalene 114

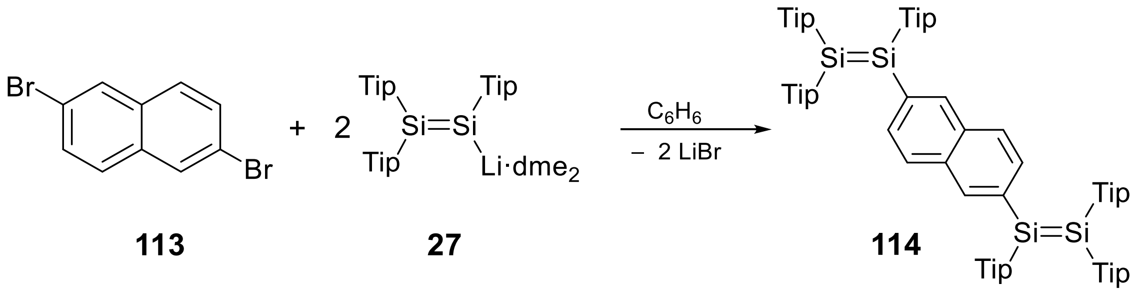

113 **27** **114**

$C_{10}H_6Br_2$
285.97 g.mol^{-1}

$C_{53}H_{89}LiO_4Si_2$
853.38 g.mol^{-1}

$C_{100}H_{144}Si_4$
1458.59g.mol^{-1}

Quantities: 2,6-dibromonaphthalene **113** (0.22 g, 0.73 mmol) in 25 ml of benzene, disilenide **27** (1.32 g, 1.54 mmol) in 22 ml of benzene.

Isolation: Red crystals at room temperature from benzene, 0.79 g (74%, mp. 150°C, dec.).

Characterization:

^{1}H NMR (300 MHz, [D_6]benzene, TMS) $\delta = 7.67$ (s, 2H, -C_{10}*H_6*-); 7.27(d, 2H, -C_{10}*H_6*-); 7.12, 7.06, 7.04 (each s, each 4H, Tip-*H*); 6.75 (d, 2H, -C_{10}*H_6*-); 4.28, 4.24, 4.05, 2.77 (each hept., each 4H, iPr-C*H*); 2.68 (hept., 2H, iPr-C*H*); 1.24, 1.22, 1.18, 1.14 (br.), 1.12, 1.06 (each d, altogether 108H, iPr-C*H_3*) ppm.

^{13}C NMR (75.46 MHz, [D_6]benzene, TMS) $\delta = 156.25$, 155.594, 155.06, 151.67, 151.02, 150.61 (Tip-*$C_{o/p}$*); 136.65 ($C_{10}H_6$-*C_i*); 136.06 ($C_{10}H_6$-*CH*); 133.18, 133.15, 130.22 (Tip-

C$_i$); 132.43, 128.42 ($C_{10}H_6$-*C*H); 127.87, 127.55 ($C_{10}H_6$-*C*$_{q.}$); 127.12 ($C_{10}H_6$-*C*H); 122.3, 121.91, 121.52 (Tip-*C*H); 38.32, 38.06, 37.43, 34.75, 34.58, 34.41 (iPr-*C*H); 25.61, 24.51, 24.28, 24.15, 24.29, 23.99, 23.82 (iPr-*C*H_3) ppm.

^{29}Si NMR (59.62 MHz, [D$_6$]benzene, TMS) $\delta = 71.46$ (*Si*Tip); 56.67 (*Si*Tip$_2$) ppm.

UV-Vis (hexane) λ_{max} (ε) 484 nm (12200 $M^{-1}cm^{-1}$).

Combustion Analysis: Calcd. for $C_{100}H_{144}Si_4$: C, 82.35; H, 9.95. Found: C, 75.49; H, 9.07.

Combustion analysis and mass spectrometry did not yield satisfactory results presumably due to the oxygen sensitivity of **114.**

5.3.13. Synthesis of 9,10-Bis{1,2,2-[tris(2,4,6-triisopropylphenyl)]}Disilenylanthracene 116

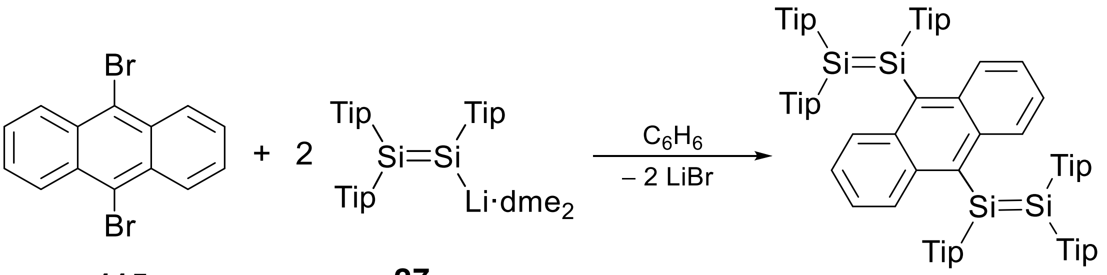

115 **27** **116**

$C_{14}H_9Br_2$
336.03 g.mol^{-1}

$C_{53}H_{89}LiO_4Si_2$
853.38 g.mol^{-1}

$C_{104}H_{146}Si_4$
1508.65 g.mol^{-1}

Quantities: 9,10-dibromoanthracene **115** (0.98 g, 2.92 mmol) in 80 ml of benzene, disilenide **27** (5g, 5.86 mmol) in 80 ml of benzene.

Isolation: dark blue-green microcrystals at −10 °C from thf, 3.89 g (88%, mp. 189°C, dec.) and single crystals are grown from benzene.

Characterization:

^{29}Si NMR (59.62 MHz, [D$_6$]benzene, TMS) δ 62.72; 60.65; 60.08; 59.71; 53.94; 52.69; 52.24 ppm.

CP-MAS ^{29}Si NMR (79.49 MHz) δ 65.14; 54.01; −2.25; −6.30 ppm.

UV-Vis (hexane) λ_{1max} (ε_1) 422 nm (36600 $M^{-1}cm^{-1}$); λ_{2max} (ε_2) 597 nm (7500 $M^{-1}cm^{-1}$).

Combustion Analysis: Calcd. for $C_{104}H_{146}Si_4$: C, 82.80; H, 9.75. Found: C, 79.27; H, 8.04.

Combustion analysis did not yield satisfactory results presumably due to the oxygen sensitivity of **116.**

5.3.14. Reaction of Disilenide 27 with exces 2,7-Dibromopyrene 115

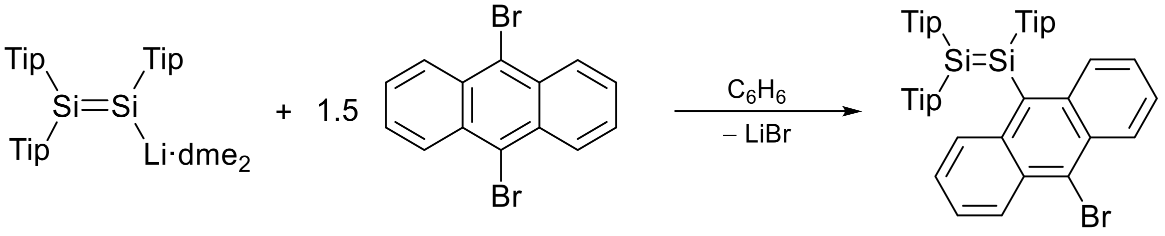

27
$C_{53}H_{89}LiO_4Si_2$
853.38 g.mol^{-1}

115
$C_{14}H_9Br_2$
336.03 g.mol^{-1}

117
$C_{59}H_{77}Si_2Br$
922.34 g.mol^{-1}

Quantities: 9,10-dibromoanthracene **115** (0.3 g, 0.89 mmol) in 20 ml of benzene, disilenide **27** (0.51g, 0.59 mmol) in 15 ml of benzene.

Isolation: Crystallization at room temperature affords only excess of starting material as yellow crystals. Starting material is removed via filtration and the remaining solution is characterized spectroscopically. Attempts to crystallize the main product failed, however.

Characterization:

^{1}H NMR (300 MHz, [D_6]benzene, TMS) δ 9.84 (d, 1H, anthracene-*H*); 9.14 (d, 1H, anthracene-*H*); 8.58 (dd, 2H, anthracene-*H*); 8.47 (dd, 1H, anthracene-*H*); 7.27-7.18, 7.12-7.11, 7.10-7.03 (each m, each 2H, overlapping with $C_{14}H_8$, Tip-*H*); 7.01, 6.93, 6.84, 6.68 (each s, each 1H, anthracene-*H*); 5.03, 4.67, 4.31 (each hept., each 1H, iPr-C*H*); 4.03 (hept., 2H, iPr-C*H*); 3.81, 2.75, 2.65, 2.51 (each hept., each 1H, iPr-C*H*); 1.68, 1.53, 1.33, 1.30, 1.76, 1.10, 0.98, 0.84, 0.61, -0.06, -0.39 (each d, altogether 54H, iPr-C*H*$_3$) ppm.

^{13}C NMR (75.46 MHz, [D$_6$]benzene, TMS) δ 155.99, 155.44, 155.29, 155.18, 154.35, 151.01, 150.98 (Tip-*C*$_{o/p}$); 137.69, 137.14, 136.46 (C$_{14}$H$_8$-*C*$_i$); 133.32, 133.20, 132.31, 131.12 (Tip-*C*$_i$); 131.46, 130.02, 129.16, 129.01, 128.42 (C$_{14}$H$_8$-*CH*); 127.87, 127.55 (C$_{14}$H$_8$-*C*$_{q.}$); 125.61, 125.54 (C$_{14}$H$_8$-*C*H); 122.64, 122.47, 122.28, 121.55, 121.47, 121.28, 121.05 (Tip-*C*H); 39.18, 38.65, 38.43, 37.80, 36.64, 36.45, 34.63, 34.53, 34.25 (iPr-*C*H); 25.65, 25.23, 24.84, 24.76, 24.65, 24.15, 24.04, 23.99, 23.84, 23.75, 23.62, 23.32 (iPr-*CH*$_3$); 34.49, 22.54, 14.11 (pentane) ppm.

^{29}Si NMR (59.62 MHz, [D$_6$]benzene, TMS) δ 60.08 (*Si*Tip); 52.68 (*Si*Tip$_2$) ppm.

5.3.15. Reaction of Disilenide 27 with 2,7-Dibromopyrene 118

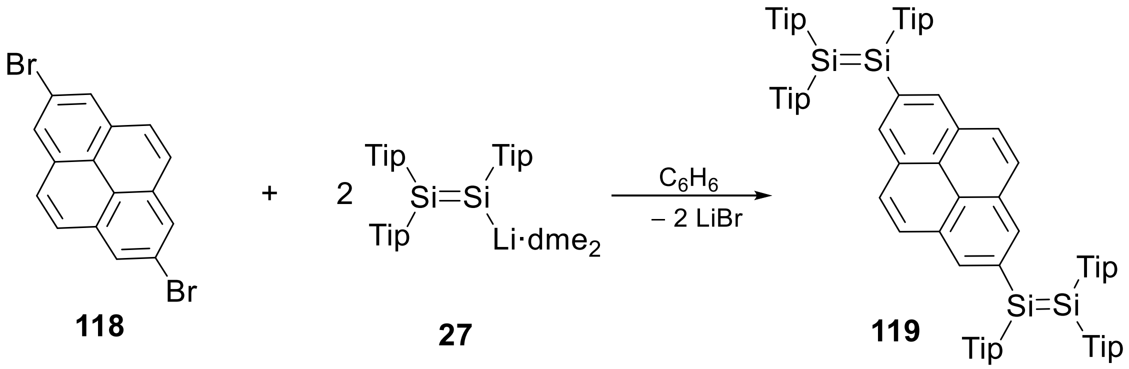

$C_{16}H_8Br_2$
360.05 g.mol^{-1}

$C_{53}H_{89}LiO_4Si_2$
853.38 g.mol^{-1}

$C_{106}H_{146}Si_4$
1532.67g.mol^{-1}

Quantities: 2,7-dibromopyrene **118** (0.221 g, 0.613 mmol) in 20 ml of benzene, disilenide **27** (1.066 g, 1.249 mmol) in 25 ml of benzene.

Isolation: Crystallization at room temperature from hexane overnight yields 0.89 g (95 %) of **119** as red-orange microcrystals (mp. 189°C, dec.).

Characterization:

^{1}H NMR (300 MHz, [D$_6$]benzene, TMS) $\delta = 8.00$ (s, 4H, Ar-*H*); 7.19 (s, 4H, Tip-*H*); 7.17 (s, 4H, Ar-*H*); 7.12, 7.087 (each s, each 4H, Tip-*H*); 4.36, 4.28, 4.10, 2.81 (each hept., each 4H, iPr-C*H*); 2.69 (hept., 2H, iPr-C*H*); 1.28, 1.23, 1.20, 1.14, 1.12, 1.10 (each d, altogether 108H, iPr-C*H*$_3$) ppm.

^{13}C NMR (75.46 MHz, [D$_6$]benzene, TMS) $\delta = 156.49$, 155.81, 155.10, 151.77, 151.23, 150.63 (Tip-*C*o/p); 136.51 (Ar-*C*i); 133.11, 133.03, 130.11, 124.09 (Tip-*C*i); 130.84 (Ar-*CH*); 128.19 (C$_6$D$_6$); 127.87, 127.55 (Ar-*Cq*); 122.09, 122.01, 121.74 (Tip-*C*H); 38.28, 38.16, 37.26, 34.80, 34.65, 34.40, 34.17 (iPr-*C*H); 25.65, 24.60, 24.49, 24.15, 24.09, 23.98, 23.80 (iPr-*CH$_3$*); 31.79, 22.87, 14.17 (Hexane) ppm.

^{29}Si NMR (59.62 MHz, [D$_6$]benzene, TMS) $\delta = 71.13$ (*Si*Tip); 56.93 (*Si*Tip2) ppm.

UV-Vis (hexane) λ_{max} (ε) 470 nm (9700 M^{-1}cm^{-1}).

Combustion Analysis: Calcd. for $C_{106}H_{146}Si_4$: C, 83.07; H, 9.60. Found: C, 81.49; H, 9.52.

5.4. Reactivity of Aryl Functionalized Disilenes or Tetrasiladienes towards PhenylAcetylene

5.4.1. Reaction of Carbazole Substituted Disilene 103 with PhenylAcetylene

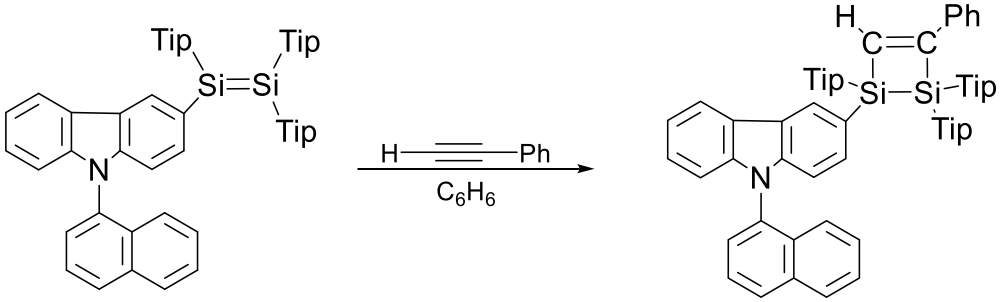

104

$C_{67}H_{83}NS_{i2}$

958.58 g.mol^{-1}

120

$C_{75}H_{89}NSi_2$

1060.71 g/mol

0.067 g (0.66 mmol) of neat phenyl acetylene is added via syringe to a solution of 0.63 g (0.66 mmol) of carbazole bridged disilene **104** in 16 mL of benzene at room temperature. The reaction mixture instantaneously turns bright yellow and is stirred for additional one hour. The solvent is removed completely under vacuum. Colorless single crystals were obtained in excellent yield (94%) from concentrated solution of acetone and benzene.

^{1}H NMR (300 MHz, [D$_6$]benzene, TMS) δ = 8.33 (s, 1H, Ar-*H*); 7.94 (s, 1H, SiPhC=C*H*Si); 7.83 (d, 1H, Ar-*H*); 7.54 (m, 4H, Ar-*H*); 7.49 (s, 1H, Ar-*H*); 7.43 (m, 2H, Ar-*H*); 7.38 (s, 1H, Ar-*H*); 7.32 (m, 2H, Ar-*H*); 7.28, 7.24 (each m, each 2H, Tip-*H*); 7.22 (br., 2H, Tip-*H*); 7.16 (s, 1H, *p*-Ph-*H*); 7.08 (dd, 2H, Ar-*H*); 7.00 (m, 4H, Ph-*H*); 4.03 (hept., 2H, *i*Pr-C*H*); 3.83 (hept., 1H, *i*Pr-C*H*); 3.58 (hept., 2H, *i*Pr-C*H*); 3.18 (hept., 1H, *i*Pr-C*H*); 3.03 (hept., 1H, iPr-C*H*); 2.84 (hept., 2H, *i*Pr-C*H*); 1.55 (Acetone); 1.49(t, 6H, *i*Pr-CH_3); 1.42 (t, 6H, *i*Pr-CH_3); 1.29 (m, 10H, *i*Pr-CH_3); 1.21 (m, 11H, *i*Pr-CH_3); 1.13 (m, 8H, *i*Pr-CH_3); 1.04 (t, 6H, *i*Pr-CH_3); 0.83 (d, 2H, *i*Pr-CH_3); 0.68 (d, 2H, *i*Pr-CH_3); 0.45(d, 2H, *i*Pr-CH_3) ppm.

^{13}C NMR (75.46 MHz, [D$_6$]benzene, TMS) δ = 203.59 (CO, acetone); 172.90 (SiPh*C*=CHSi); 157.99; 156.91, 156.47, 155.62, 154,72, 154.58, 150.80, 150.43, 150.23 (Tip-*C*o/p); 144.79, 141.88, 141.39; 138.25 (Ar-*Ci*); 135.20 (Ar-*CH*); 134.23, 133.96, 132.65, 132.54, 130.11; 129.59, 128.43 (Ar-*Ci*); 132.22 (Ar-*CH*); 128.20 (C_6D_6) ; 127.88, 127.56 (Ar-*Cq*); 127.38, 126.77, 126.56, 126.29, 125.97, 125.40, 125.29, 124.17, 121.48, 121.22, 122.68, 122.35, 122.23, 121.51, 120.08, 120.33, 120.17 (Tip-*CH*); 109.95, 109.08 (dendrimer backbone); 36.59-33.88 (*i*Pr-*C*H); 29.94- 22.62 (*i*Pr-*C*H$_3$) ppm.

^{29}Si NMR (59.62 MHz, [D$_6$]benzene, TMS) δ = −11.56, −11.58 ppm.

Combustion Analysis: Calcd. for $C_{75}H_{89}NSi_2$: C, 84.93; H, 8.46. Found: C, 83.42; H, 8.74.

5.4.2. Synthesis of 4,4´-Bis(2-phenyl-1,2,2-tris(2,4,6-isopropylphenyl)Disilacyclobut-3enyl)biphenyl 121a

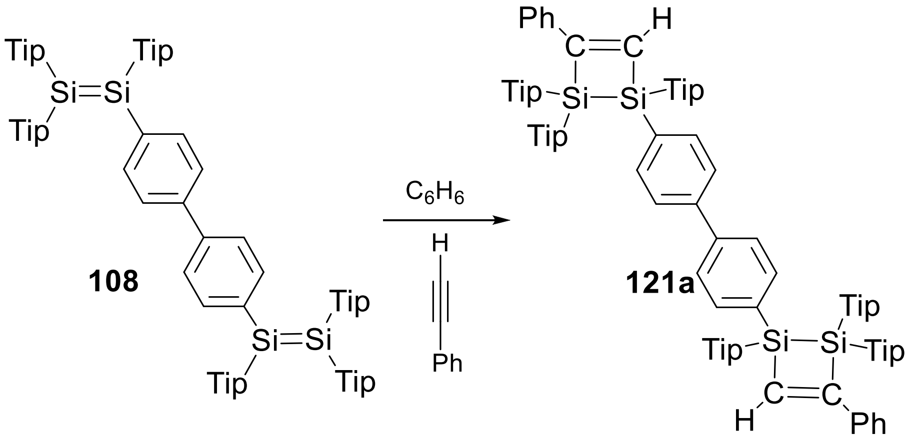

$C_{102}H_{146}Si_4$
1095.76 g/mol

$C_{118}H_{158}Si_4$
1688.9 g/mol

0.067 g (0.66 mmol) of neat phenyl acetylene is added via syringe to a solution of 0.36 g (0.33 mmol) biphenyl bridged tetrasiladiene **108** in 10 mL of benzene at room temperature. The reaction mixture instanteneously turns bright yellow and is stirred for additional three hours. The solvent is removed completely under vacuum. Crystallization at room temperature from hexane and isopropanol overnight yields 0.48 g (86%) as colorless crystals (mp. > 220°C).

^{1}H NMR (300 MHz, $[D_6]$benzene, TMS) δ = 7.77 (s, 2H, SiPhC=C*H*Si); 7.45 (d, 4H, *o*-Ph-*H*); 7.23, 7.19, 7.11 (br., each 4H, Tip-*H*); 7.08 (s, 8H, Ar-*H*); 6.97 (dd, 6H, Ph-*H*); 3.83 (hept., 4H, *i*Pr-C*H*); 3.60 (hept., 2H, *i*Pr-C*H*); 3.35 (hept., 4H, *i*Pr-C*H*); 3.84 (hept., 2H, *i*Pr-C*H*); 2.829 (hept., 6H, iPr-C*H*), 1.38 (m, 12H, *i*Pr-CH_3); 1.28-1.20 (m, 41H, *i*Pr-C*H3*); 1.17 (d, 8H, *i*Pr-CH_3); 1.04-0.99 (m, 24H, *i*Pr-CH_3); 0.94 (s, 4H, *i*Pr-CH_3); 0.74, 0.63, 0.46 (each d, 18H, *i*Pr-CH_3); 0.27 (s, 1H, *i*Pr-CH_3) ppm.

^{13}C NMR (75.46 MHz, $[D_6]$benzene, TMS) δ = 171.91 (SiPh*C*=CHSi); 155.94 (SiPh*C*=CHSi); 155.31 155.21, 154.22, 153,96, 152.88, 152.83, 149.56, 149.19, 148.94 (Tip-*Co/p*); 143.51, 139.99, 137.52, 135.97 (Ar-*Ci*); 135.07 (Ar-*CH*); 132.83, 130.62 (Ar-

Ci); 127.11 (Ar-*C*H); 126.94, 126.62, 126.30 (Ar-*Cq*); 126.08, 125.43, 124.68, 121.64, 121.38, 120.79, 120.59, 120.33, 119.12 (Ar-*CH*); 62.47 (2-Propanol-*CH*.); 35.32-32.56 (*i*Pr-*C*H); 27.36- 21.56 (*i*Pr-*C*H_3) ppm.

^{29}Si NMR (59.62 MHz, [D_6]benzene, TMS) δ = −11.27, −11.76 ppm.

Combustion Analysis: Calcd. for $C_{118}H_{158}Si_4$: C, 83.92; H, 9.43. Found: C, 81.69; H, 9.83.

5.4.3. Reaction of Crude Terphenyl Bridged Tetrasiladiene 110 with PhenylAcetylene

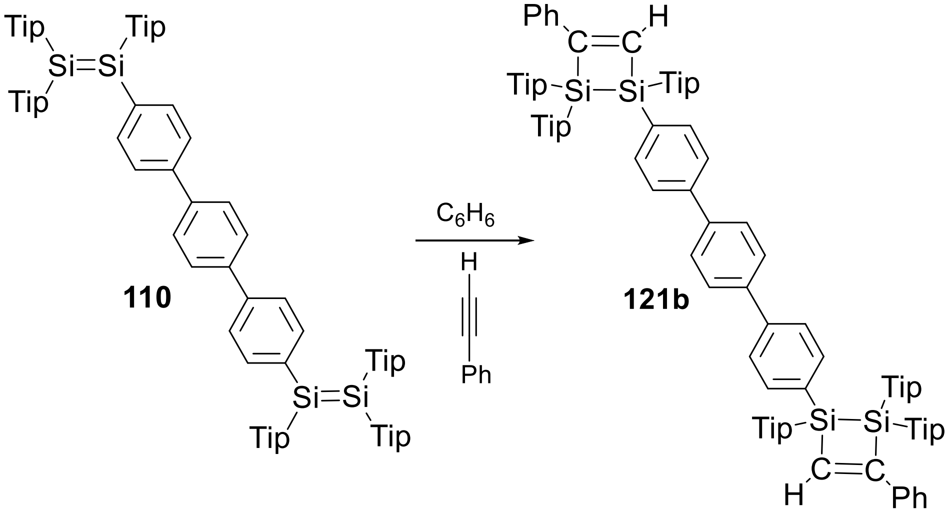

$C_{108}H_{150}Si_4$
1560.73 g/mol

$C_{124}H_{162}Si_4$
1765 g/mol

To a solution of 0.51 g (0.33 mmol) terphenyl bridged tetrasiladiene **110** in 15 mL of benzene, 0.067 g (0.66 mmol) of neat phenyl acetylene is added via syringe at room temperature. The reaction mixture instanteneously turns bright yellow and is stirred for additional three hours. The solvent is removed completely under vacuum and the crude product is obtained as pure colorless solid (mp. > 230°C). Crystallization from different solvent was failed.

^{1}**H NMR** (300 MHz, [D$_6$]benzene, TMS) δ = 7.85 (s, 2H, SiPhC=C*H*Si); 7.48 (d, 4H, *o*-Ph-*H*); 7.35, 7.33, 7.27, 7.10,7.03 (each s, 12H, Tip-*H*); 7.21 (m, 12H, Ar-*H*); 7.07, 7.00, 6.97, 6.95, 6.93 (m, 6H, Ph-*H*); 3.94 (hept., 4H, *i*Pr-C*H*); 3.66 (hept., 2H, *i*Pr-C*H*); 3.42 (hept., 4H, *i*Pr-C*H*); 3.17 (hept., 2H, *i*Pr-C*H*); 2.82 (hept., 6H, iPr-C*H*); 1.44 (m, 12H, *i*Pr-CH_3); 1.30-1.22 (m, 40H, *i*Pr-CH_3); 1.20 (d, 10H, *i*Pr-CH_3); 1.14 (d, 8H, *i*Pr-CH_3); 1.07 (m, 10H, *i*Pr-CH_3); 1.02 (d, 10H, *i*Pr-CH_3); 0.86, 0.66, 0.48 (each d, 18H, *i*Pr-CH_3) ppm.

^{13}**C NMR** (75.46 MHz, [D$_6$]benzene, TMS) δ = 173.21 (SiPh*C*=CHSi); 157.20 (SiPh*C*=CHSi); 156.63 156.55, 155.51, 155,25, 154.19, 154.16, 150.87, 150.55, 150.32 (Tip-*C*o/p); 144.75, 141.05, 139.89, 138.94, 137.31, 136.47 (Ar-*Ci*); 136.47 (Ar-*CH*); 134.04, 131.97 (Ar-*Ci*); 131.18 (Ar-*CH*); 128.20(C_6D_6) ; 127.87, 127.55 (Ar-*Cq*); 126.71, 125.98, 122.96, 122.66, 122.13, 121.92, 121.66, 120.39, 119.12 (Tip-*CH*); 36.64-33.86 (*i*Pr-*C*H); 28.69- 22.82 (*i*Pr-*C*H$_3$) ppm.

^{29}**Si NMR** (59.62 MHz, [D$_6$]benzene, TMS) δ = −11.25, −11.74 ppm.

Combustion Analysis: Calcd. for $C_{124}H_{162}Si_4$: C, 84.38; H, 9.25. Found: C, 83.18; H, 9.32.

5.4.4. Reaction of crude Bis(phenyl)Acetylene Bridged Tetrasiladiene 112 with PhenylAcetylene

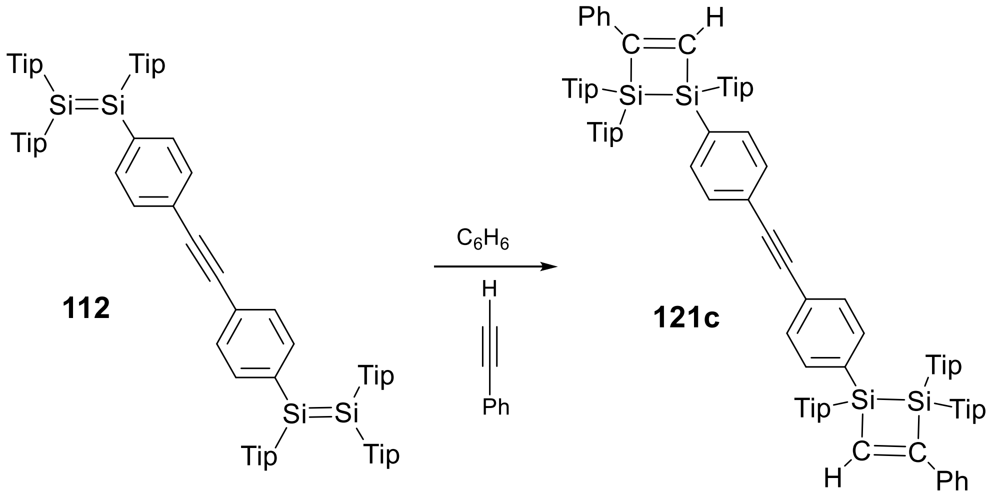

112

121c

$C_{104}H_{146}Si_4$
1508.65g/mol

$C_{120}H_{158}Si_4$
1712.92 g/mol

0.067 g (0.66 mmol) of neat phenyl acetylene is added via syringe to a solution of 0.49 g (0.33 mmol) bis(phenyl)acetylene bridged tetrasialdiene **112** in 25 mL of benzene. The reaction mixture instantaneously turns bright yellow and is stirred for additional two hours. The solvent is removed completely under vacuum and the crude product is obtained as colorless solid in 83% yield (mp. > 230°C). Crystallization from different solvent was failed.

^{1}H NMR (300 MHz, [D$_6$]benzene, TMS) δ = 7.69 (s, 2H, SiPhC=C*H*Si); 7.40 (d, 4H, *o*-Ph-*H)*; 7.20, 7.17, 7.01, (each s, each 4H, Tip-*H*); 7.08 (m, 8H, Ar-*H*); 6.94 (m, 6H, Ph-*H*); 3.82 (hept., 4H, *i*Pr-C*H*); 3.56 (hept., 2H, *i*Pr-C*H*); 3.28 (hept., 4H, *i*Pr-C*H*); 3.08 (hept., 2H, *i*Pr-C*H*); 2.79 (hept., 6H, iPr-C*H*); 1.39(d, 6H, *i*Pr-C*H$_3$*); 1.32 (d, 8H, *i*Pr-C*H$_3$)*; 1.23 (d, 26H, *i*Pr-C*H$_3$*); 1.19 (m, 26H, *i*Pr-C*H$_3$*); 1.03 (d, 12H, *i*Pr-C*H$_3$)*; 0.96 (d, 16H, *i*Pr-C*H$_3$*); 0.73 (d, 4H, *i*Pr-C*H$_3$*); 0.58(d, 6H, *i*Pr-C*H$_3$)*; 0.41 (d, 4H, *i*Pr-C*H$_3$*) ppm.
^{13}C NMR (75.46 MHz, [D$_6$]benzene, TMS) δ = 173.29 (SiPh*C*=CHSi); 156.80 (SiPh*C*=CHSi); 156.55, 156.51, 155.56, 155.43, 155.07, 154.82, 154.00, 153.95, 150.83, 150.76, 150.54, 150.39, 150.18 (Tip-*C*o/p); 144.62, 140.71, 137.02 (Ar-*Ci*); 135.69 (Ar-*CH*); 133.84, 132.77, 131.30 (Ar-*Ci*); 130.96, 130.57 (Ar-*CH*); 128.17(C_6D_6) ;

127.85, 127.53 (Ar-*Cq*); 126.62, 121.85, 122.96, 122.62, 122.06, 121.85, 121.65, 121.22, 120.35 (Tip-*CH*); 90.82 (Ar-C≡C-Ar); 36.57-33.79 (*i*Pr-*C*H); 28.64- 22.82 (*i*Pr-*C*H$_3$) ppm.

^{29}Si NMR (59.62 MHz, [D$_6$]benzene, TMS) δ = −11.30, −11.94 ppm.

5.4.5. Synthesis of 4,4´-Bis(2-phenyl-1,2,2-tris(2,4,6-isopropylphenyl)Disilacyclobut-3enyl)naphthalene 121d

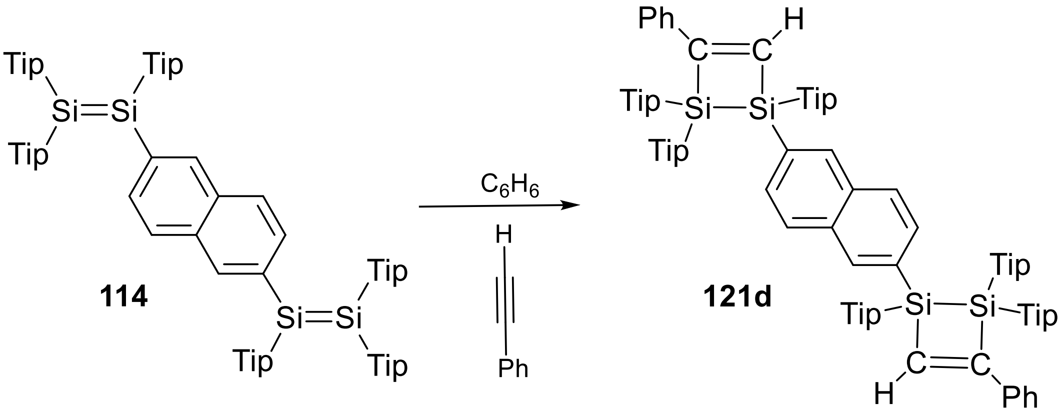

114

121d

$C_{100}H_{144}Si_4$
1458.59g.mol^{-1}

$C_{116}H_{156}Si_4$
1662.86 g/mol

0.067 g (0.66 mmol) of neat phenyl acetylene is added via syringe to a solution of 0.48 g (0.33 mmol) naphthalene bridged tetrasiladiene **114** in 18 mL of benzene. The reaction mixture instantaneously turns bright yellow and is stirred for additional one hour. The solvent is removed completely under vacuum. Crystallization at room temperature from thf overnight yields 0.47 g (86%) of **121d** as colorless crystals (mp. > 230°C).

^{1}H NMR (300 MHz, [D$_6$]benzene, TMS) δ = 7.73 (s, 2H, SiPhC=C*H*Si); 7.62 (s, 1H, Ar-*H*); 7.38 (m, 5H, Ar-*H*); 7.24 (br., 2H, *o*-Ph-*H*); 7.18 (br., 2H, *o*-Ph-*H*); 7.11, 7.07, 7.01, (each s, each 4H, Tip-*H*); 6.90 (m, 6H, Ph-*H*); 3.89 (hept., 4H, *i*Pr-C*H*); 3.67 (hept., 2H, *i*Pr-C*H*); 3.37 (hept., 4H, *i*Pr-C*H*); 3.08 (hept., 2H, *i*Pr-C*H*); 2.79 (hept., 6H, iPr-C*H*); 1.41(m, 12H, *i*Pr-C*H*$_3$); 1.33-1.21 (m, 28H, *i*Pr-C*H*$_3$); 1.20 (s, 6H, *i*Pr-C*H*$_3$); 1.18 (d, 10H, *i*Pr-C*H*$_3$); 1.17 (s, 12H, *i*Pr-C*H*$_3$); 1.04 (d, 12H, *i*Pr-C*H*$_3$); 0.99 (m, 8H, *i*Pr-C*H*$_3$); 0.85 (d, 6H, *i*Pr-C*H*$_3$); 0.65(d, 4H, *i*Pr-C*H*$_3$); 0.60 (d, 4H, *i*Pr-C*H*$_3$) ; 0.42 (d, 4H, *i*Pr-C*H3*) ppm.

^{13}C NMR (75.46 MHz, $[D_6]$benzene, TMS) δ = 173.22 (SiPh*C*=CHSi); 157.58 (SiPh*C*=CHSi); 156.58, 155.61, 155.15, 154,12, 154.01, 150.80, 150.51, 150.20 (Tip-*C*o/p); 144.92, 137.74, 137.55 (Ar-*Ci*); 137.04 (Ar-*CH*); 134.01, 133.05, 131.52 (Ar-*Ci*); 131.44 (Ar-*CH*); 128.20 (C_6D_6) ; 127.87, 127.55 (Ar-*Cq*); 127.12, 126.71, 121.03, 122.61, 121.95, 121.63, 121.95, 121.63, 121.27, 120.42 (Tip-*CH*); 36.65-33.85 (*i*Pr-*C*H); 28.63- 22.89 (*i*Pr-*C*H_3) ppm.

^{29}Si NMR (59.62 MHz, $[D_6]$benzene, TMS) δ = −10.79, −11.07 ppm.

Combustion Analysis: Calcd. for $C_{116}H_{156}Si_4$: C, 82.35; H, 9.95. Found: C, 82.11; H, 9.36.

5.4.6. Synthesis of 3-Phenyl-1-(2,3,5,6-tetramethylphenyl)-1,2,2-tris(2,4,6-triisopropylphenyl)-1,2-dihydro-1,2-Disilete 123b

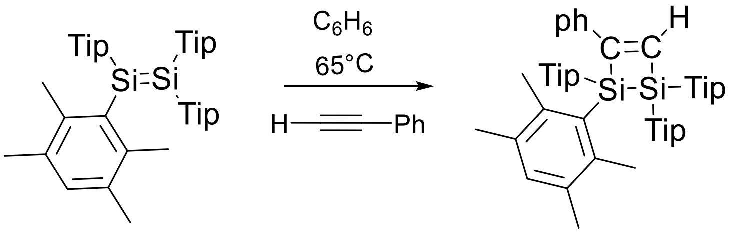

94

$C_{55}H_{82}Si_2$
799.43 g.mol^{-1}

123b

$C_{63}H_{88}Si_2$
901.57 g.mol^{-1}

0.067 g (0.66 mmol) of neat phenyl acetylene is added via syringe to a solution of 0.52 g (0.66 mmol) durene disilene **94** in 20 mL of benzene at 65°C. Stirring overnight at 65 °C resulted in a colorless reaction mixture that was thoroughly dried in vacuo. The residue is redissolved with a minimum amount of benzene and standing overnight at room temperature affords 0.53 mg of **123b** in 90% (mp. 182-188°C) as colorless crystals. The ^{29}Si NMR of the crystals in C_6D_6 revealed three signals at δ = 2.89, 2.21, -10.37 ppm.

Exact integration difficult due to partially overlapping resonances of two isomers

^{1}H NMR (300 MHz, [D$_6$]benzene, TMS) δ = 7.81 (s, 0.84H, SiPhC=C*H*Si); 7.68 (s, 0.66H, SiPhC=C*H*Si); 7.11-7.09 (m, 8.68H, *o*-Ph-*H*); 7.07-6.94 (m, 11.16H, Tip-*H*); 6.83 (s, 1.13H, durene-*H*); 6.81 (s, 0.89H, durene-*H*); 4.00-3.22 (m, 12H, *i*Pr-C*H*); 2.75 (hept., 8H, *i*Pr-C*H*); 2.45, 2.24, 1.96, 1.88 (br., 21H, Ph-*C*H_3); 1.55 (Acetone); 1.52-1.34 (br, 23.8H, *i*Pr-CH_3); 1.26 (s, 2H, *i*Pr-CH_3); 1.24 (d, 6H, *i*Pr-C*H3*); 1.22 (s, 8H, *i*Pr-C*H3*); 1.20 (s, 4H, *i*Pr-CH_3); 1.16 (d, 6H, *i*Pr-CH_3); 1.14 (d, 6H, *i*Pr-CH_3) ; 1.05 (m, 11H, *i*Pr-CH_3); 0.63 (br, 12H, *i*Pr-CH_3); 0.45 (br, 8H, *i*Pr-CH_3) ppm.

^{13}C NMR (75.46 MHz, [D$_6$]benzene, TMS) δ = 172.99 (SiPh*C*=CHSi); 162.41 (SiPhC=*C*HSi); 154.72-149.67 (Tip-*Co/p*); 147.60, 140.63, 140.37, 137.29, 135.75, 135.6 (Ar-*Ci*); 133.11, 132.54 (Ar-*CH*); 127.87, 127.55 (Durene-*Cq*); 126.35, 126.31, 122.67, 122.30, 121.93, 121.51 (Ar-*C*H); 36.71-32.59 (*i*Pr-*C*H); 27.36-20.37 (*i*Pr-*C*H$_3$) ppm.

^{29}Si NMR (59.62 MHz, [D$_6$]benzene, TMS) δ = 2.89, 2.21, −10.37 ppm.

Combustion Analysis: Calcd. for $C_{63}H_{88}Si_2$: C, 83.93; H, 9.84. Found: C, 80.91; H, 9.12.

5.4.7. Synthesis of 2,2'-(2,3,5,6-tetramethyl-1,4-phenylene)bis(4-phenyl-1,1,2-tris(2,4,6-triisopropylphenyl)-1,2-dihydro-1,2-Disilete) 124a

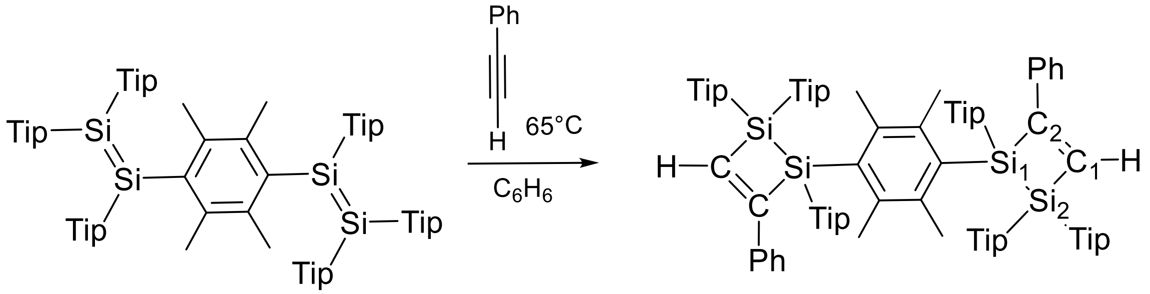

106

124a

$C_{100}H_{150}Si_4$
1464.64 g/mol

$C_{116}H_{162}Si_4$
1668,91 g/mol

0.067 g (0.66 mmol) of neat phenyl acetylene is added via syringe to a solution of 0.48 g (0.33 mmol) durene bridged tetrasiladiene **106** in 20 mL of benzene at 65°C. After stirring over night at 65°C, the reaction mixture turns yellow. The solvent is removed completely under vacuum to afford yellow solid. The yellow residue is dissolved with a minimum amount of hexane. Standing overnight affords 83% of **124a** as colorless crystals (mp. > 230°C).

Most of the signals in the ^{1}H NMR spectrum are overlapping and not suitable for analysis.

^{29}Si NMR (59.62 MHz, [D$_6$]benzene, TMS) δ = 3.60, 3.12, −9.32 and −10.21 ppm,

Elemental Analysis: Calcd. for $C_{116}H_{162}Si_4$: C, 83.48; H, 9.78. Found: C, 82.53; H, 9.04.

5.4.8. Synthesis of 9,10-Bis(2-phenyl-1,2,2-tris(2,4,6-isopropylphenyl)Disilacyclobut-3enyl)anthracene 124b

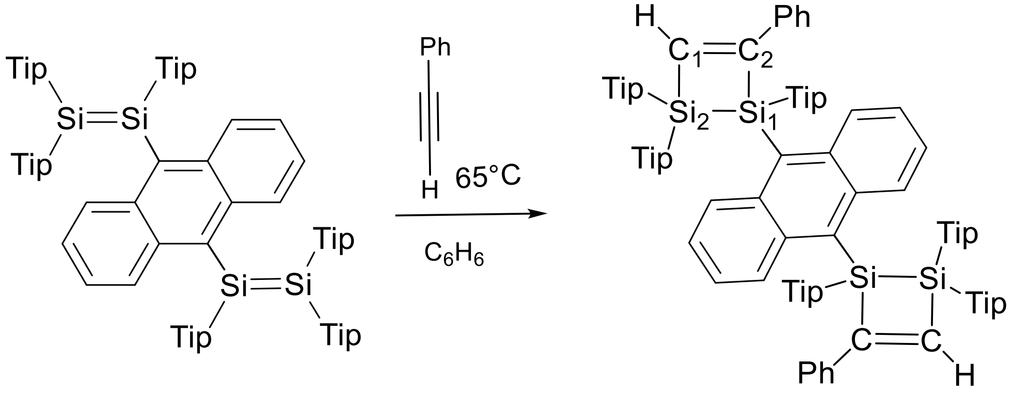

116

$C_{104}H_{146}Si_4$
1508.65 g.mol

124b

$C_{120}H_{158}Si_4$
1712.92 g/mol

0.067 g (0.66 mmol) of neat phenyl acetylene is added via syringe to a solution of 0.5 g (0.33 mmol) anthracene bridged tetrasiladiene **116** in 15 mL of benzene at 65°C. After stirring overnight at 65°C, the reaction mixture turned yellow. The solvent is removed under reduced pressure to afford a bright yellow. The yellow residue is dissolved with a minimum amount of benzene (1ml) and standing overnight at room temperature affords 0.45g of 124b in 80% as yellow crystals (mp. > 230°C).

Most of the signals in the ^{1}H NMR spectrum are overlapping and not suitable for analysis.

^{29}Si NMR (59.62 MHz, [D$_6$]benzene, TMS) δ = 1.75; 1.47; −8.09; −8.97 ppm.
Combustion Analysis: C, 84.14; H, 9.30. Found: C, 83.9; H, 9.89.

5.4.9. Reaction of Anthracene Substituted Disilene 100 with PhenylAcetylene

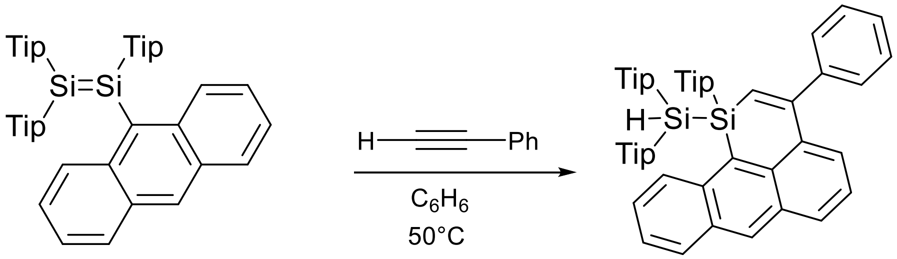

100
$C_{59}H_{78}S_{i2}$
843.44 g/mol

125
$C_{67}H_{86}Si_2$
947.60 g/mol

0.067 g (0.66 mmol) of neat phenyl acetylene is added via syringe to a solution of 0.55 g (0.66 mmol) anthracene bridged disilene **100** in 10 mL of benzene. After stirring overnight at 50 °C the reaction mixture turns yellow. The solvent is removed completely under vacuum. Crystallization at room temperature from ethanol overnight yields 0.40 g (77%) of **125** as yellow crystals (mp. 200°- 205°C).

^{1}H NMR (300 MHz, [D$_6$]benzene, TMS) δ = 8.50, 7.43 (each d, each 1H, Ar-*H*); 7.31 (br., 1H, Ar-*H*); 7.19-7.17 (m, 2H, Ar-*H*); 7.10, 6.99 (each d, each 1H, Ar-*H*); 6.94 (br., 4H, Tip-*H*); 6.89 (br., 3H, Ar-*H*); 6.87-6.84 (m, 2H, Tip-*H*); 6.72 (t, 1H, Ar-*H*); 6.54, 6.51 (each s, each 1H, Ar-*H*); 6.00 (s, 1H, Si-*H*); 5.18 (d, 1H, ^{4}J = 5.9 HZ, vinylic-*H*), 4.62, 3.64, 3.09 (each br.hept., each 1H, *i*Pr-C*H*); 3.23 (br. hept., 2H, *i*Pr-C*H*); 2.71, 2.51 (each hept., each 2H, *i*Pr-C*H*); 1.68 (br., 3H, *i*Pr-CH_3); 1.31 (s, 15H, *i*Pr-CH_3); 1.16 (t, 14H, *i*Pr-CH_3); 0.97 (d, 10H, *i*Pr-CH_3); 0.49 (d, 12H, *i*Pr-CH_3) ppm.
^{13}C NMR (75.46 MHz, [D$_6$]benzene, TMS) δ = 160.05, 155.77, 155.68, 155.40, 149.91 (Tip-*C*o/p); 147.12, 141.54, 137.20 (Ar-*Ci*); 133.71 (Ar-*CH*); 133.46, 133.42, 132.59,

129.69 (Tip-*C*i); 130.08, 129.18 (Ar-*CH*); 128.28, 128.18 (vinylic-*C*) ; 127.88, 127.56 (Ar-*Cq*); 127.70, 127.10, 126.93, 126.72, 125.91, 125.82, 121.87 (Tip-*CH*); 47.37, 34.47, 34.28, 34.22, 32.65, 32.02 (*i*Pr-*C*H); 25.87, 25.50, 24.46, 23.94, 23.88, 23.85, 23.68, 23.61, 23.29 (*i*Pr-*C*H$_3$) ppm.

^{29}Si NMR (59.62 MHz, [D$_6$]benzene, TMS) $\delta = -25.38, -36.39$ ppm.

Combustion Analysis: Calcd. for $C_{67}H_{86}Si_2$: C, 84.92; H, 9.15. Found: C, 84.01; H, 9.18.

5.5. Synthesis of Bifunctional Monomers

5.5.1. Reactivity of Tetrasiladiene 108 towards Bis(ethynyl)benzene

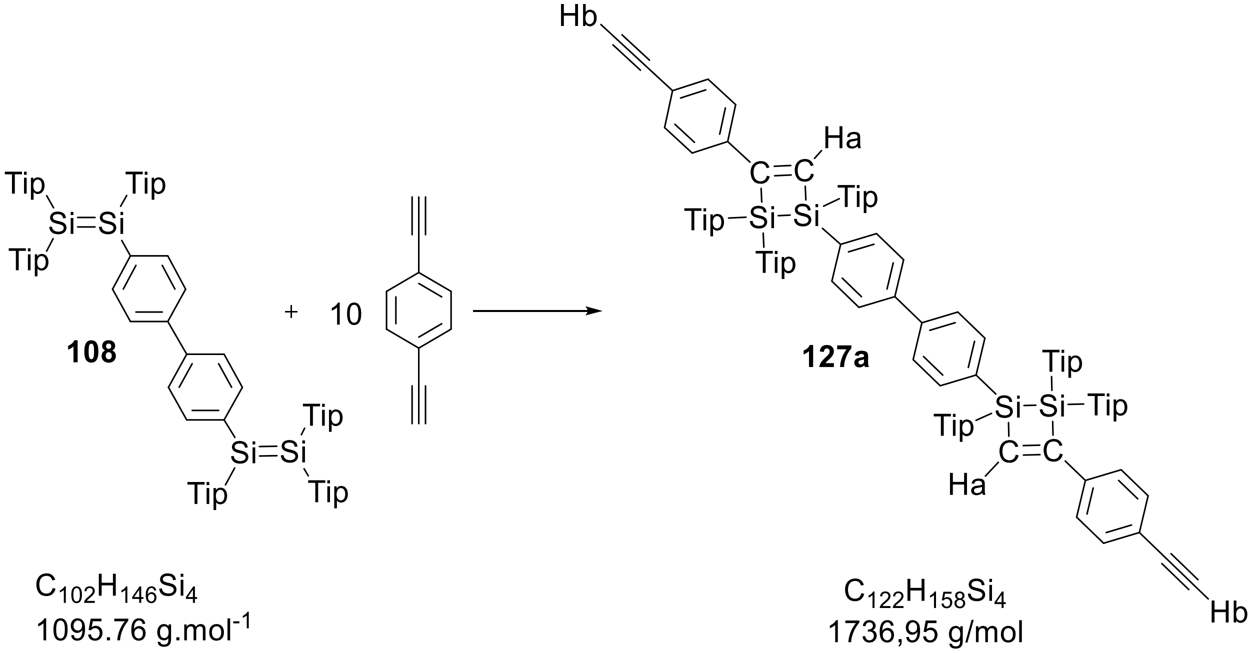

108

127a

$C_{102}H_{146}Si_4$
1095.76 g.mol^{-1}

$C_{122}H_{158}Si_4$
1736,95 g/mol

A 15 mL benzene solution of 0.65g (0.44 mmol) 4,4´-bis{1,2,2-[tris(2,4,6 triisopropylphenyl)]}disilenylbiphenyl 1**08** is added dropwise to a 15 mL benzene solution of 1,4-diethynyl benzene (0.56 g, 4.43 mmol) at room temperature. The solution is stirred at room temperature for 3 hours. The solvent is removed under vacuum. The excess 1.4-diethynylbenzene is removed by sublimation. The crude product is obtained as pure colorless solid in 84% yield (mp. > 230°C). Crystallization from different solvent is failed.

^{1}H NMR (300 MHz, [D$_6$]benzene, TMS) $\delta =$ 7.71 (s, 2H, (HC≡C-C$_4$H$_4$-)SiC=C*H*Si); 7.41 (d, 4H, *o*-Ph-*H*); 7.33 (s, 4H, HC≡C-C$_4$*H*$_4$-); 7.30 (s, 4H, HC≡C-C$_4$*H*$_4$-); 7.21, 7.18, 7.12 (br., each 4H, Tip-*H*); 7.09 (s, 8H, Ar-*H*); 6.90 (dd, 6H, Ph-*H*); 3.73 (hept., 4H, *i*Pr-C*H*); 3.65 (hept., 2H, *i*Pr-C*H*); 3.45 (hept., 4H, *i*Pr-C*H*); 3.86 (hept., 2H, *i*Pr-C*H*); 2.89 (hept., 6H, iPr-C*H*); 2.66 (s, 2H, *H*C≡C-C$_4$H$_4$-); 1.48 (m, 12H, *i*Pr-C*H$_3$*); 1.27-1.21 (m, 41H, *i*Pr-C*H3*); 1.19 (d, 8H, *i*Pr-C*H$_3$*); 1.05-0.97 (m, 24H, *i*Pr-C*H$_3$*); 0.95 (s, 4H, *i*Pr-C*H$_3$*); 0.75, 0.61, 0.44 (each d, 18H, *i*Pr-C*H$_3$*); 0.28 (s, 1H, *i*Pr-C*H$_3$*) ppm.

^{13}C NMR (75.46 MHz, [D$_6$]benzene, TMS) $\delta =$ 172.06 ((HC≡C-C$_4$H$_4$-)Si*C*=CHSi); 157.95 ((HC≡C-C$_4$H$_4$-)SiC=*C*HSi); 155.33 155.22, 154.20, 153,86, 152.78, 152.63, 149.46, 149.15, 148.93 (Tip-*Co/p*); 143.52, 139.91, 137.53, 135.98 (Ar-*Ci*); 135.03 (Ar-*CH*); 132.33, 130.61 (Ar-*Ci*); 127.12 (Ar-*C*H); 126.92, 126.61, 126.40 (Ar-*Cq*); 126.07, 125.33, 124.64, 121.61, 121.33, 120.72, 120.51, 120.31, 119.12 (Ar-*CH*); 83.81 (HC≡*C*-C$_4$H$_4$-); 78.02 (H*C*≡C-C$_4$H$_4$-); 35.31-32.52 (*i*Pr-*C*H); 27.32- 21.53 (*i*Pr-*C*H$_3$) ppm

^{29}Si NMR (59.62 MHz, [D$_6$]benzene, TMS) $\delta =$ −11.42, −11.74 ppm.

5.5.2. Reactivity of Tetrasiladiene 112 towards Bis(ethynyl)benzene

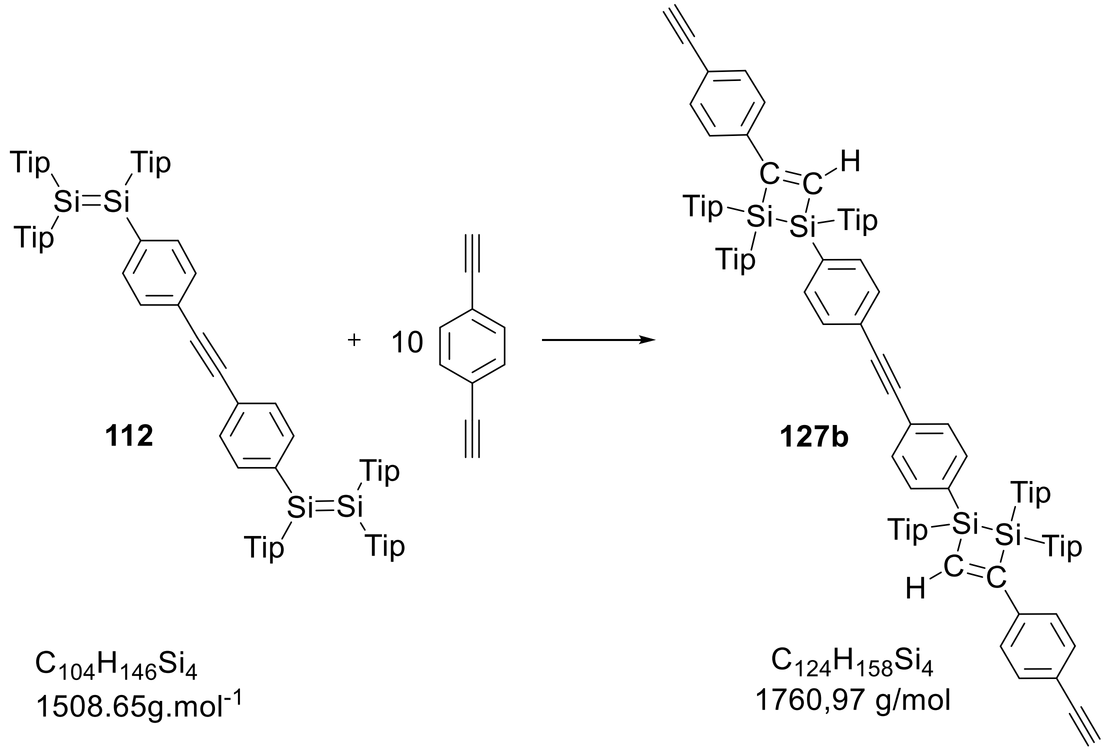

112

$C_{104}H_{146}Si_4$
1508.65g.mol^{-1}

127b

$C_{124}H_{158}Si_4$
1760,97 g/mol

A 15 mL benzene solution of 0.4g (0.26 mmol) 1,2-bis(4-(1,2,2-tris(2,4,6-isopropylphenyl)disilenyl)phenyl)ethyne **112** is added dropwise to a 15mL benzene solution of 1,4-diethynyl benzene (0.33 g, 2.65 mmol). The solution is stirred at room temperature for 3 hours. The solvent is removed under vacuum. The excess 1.4-diethynylbenzene is removed by sublimation. The crude product is obtained as pure colorless solid in 92% yield (mp. > 230°C). Crystallization from different solvent is failed.

^{1}H NMR (300 MHz, [D$_6$]benzene, TMS) $\delta =$ 7.66 (s, 2H, (HC≡C-C$_4$H$_4$-)SiC=C*H*Si); 7.28 (d, 8H, HC≡C-C4*H*4-); 7.21, 7.16, 7.02, (each s, each 4H, Tip-*H*); 7.07 (m, 8H, Ar-*H*); 6.84 (m, 6H, Ph-*H*); 3.81 (hept., 4H, *i*Pr-C*H*); 3.55 (hept., 2H, *i*Pr-C*H*); 3.27 (hept., 4H, *i*Pr-C*H*); 3.09 (hept., 2H, *i*Pr-C*H*); 2.78 (hept., 6H, iPr-C*H*); 2.67 (s, 2H, *H*C≡C-C$_4$H$_4$-); 1.38 (d, 6H, *i*Pr-C*H*$_3$); 1.33(d, 8H, *i*Pr-C*H*$_3$); 1.24 (d, 26H, *i*Pr-C*H*$_3$); 1.18 (m, 26H, *i*Pr-C*H*$_3$); 1.05 (d, 12H, *i*Pr-C*H*$_3$); 0.94 (d, 16H, *i*Pr-C*H*$_3$); 0.72 (d, 4H, *i*Pr-C*H*$_3$); 0.57 (d, 6H, *i*Pr-C*H*$_3$); 0.40 (d, 4H, *i*Pr-C*H*$_3$) ppm.

^{13}C NMR (75.46 MHz, [D$_6$]benzene, TMS) δ = 172.22 ((HC≡C-C$_4$H$_4$-)Si*C*=CHSi); 157.64 ((HC≡C-C$_4$H$_4$-)SiC=*C*HSi); 156.54, 156.50, 155.55, 155.42, 155.05, 154.80, 154.00, 153.94, 150.83, 150.75, 150.53, 150.36, 150.17 (Tip-*C*o/p); 144.60, 140.72, 137.01 (Ar-*Ci*); 135.65 (Ar-*CH*); 133.81, 132.74, 131.29 (Ar-*Ci*); 130.94, 130.54 (Ar-*CH*); 128.17(C$_6$D$_6$) ; 127.83, 127.51 (Ar-*Cq*); 126.61, 121.83, 122.94, 122.62, 122.04, 121.81, 121.61, 121.20, 120.31 (Tip-*CH*); 90.00 (Ar-C≡C-Ar); 83.81 (HC≡*C*-C$_4$H$_4$-); 78.04 (H*C*≡C-C$_4$H$_4$-); 36.51-33.73 (*i*Pr-*C*H); 28.63- 22.80 (*i*Pr-*C*H$_3$) ppm.

^{29}Si NMR (59.62 MHz, [D$_6$]benzene, TMS) δ = −11.36, −11.85 ppm.

5.5.3. Reactivity of Tetrasiladiene 116 towards Bis(ethynyl)benzene

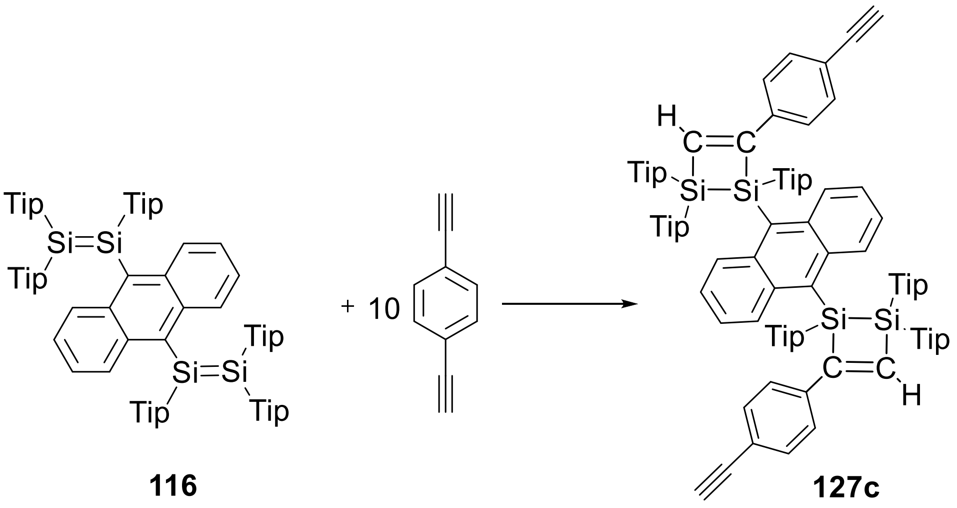

116

$C_{104}H_{146}Si_4$
1508.65 g.mol^{-1}

127c

$C_{124}H_{158}Si_4$
1760,97 g/mol

A 15 mL benzene solution of 0.5g (0.33 mmol) 9,10-bis{1,2,2-[tris(2,4,6-triisopropylphenyl)]}disilenylanthracene **116** is added dropwise to a 15mL benzene solution of 1,4-diethynyl benzene (0.41 g, 3.3 mmol) at room temperature. The solution is stirred at room temperature for 3 hours. The solvent was removed under vacuum. The excess 1.4-diethynylbenzene is removed by sublimation. The crude product is obtained as pure colorless solid in 88% yield (mp. > 230°C). Crystallization from different solvent is failed.

^{1}H NMR (300 MHz, [D$_6$]benzene, TMS) δ = 9.48, 7.83 (each d, each 2H, Ar-*H*); 7.78 (s, 2H, HC≡C-C$_4$H$_4$-)SiC=C*H*Si); 7.18, 6.99 (each d, each 2H, Ar-*H*); 6.92 (br., 4H, Tip-*H*); 6.85-6.82 (m, 2H, Tip-*H*); 3.91, 3.62, 3.04 (each br.hept., each 1H, *i*Pr-C*H*); 3.21 (br.hept., 2H, *i*Pr-C*H*); 2.61, 2.41 (each hept., each 2H, *i*Pr-C*H*); 2.59 (s, 2H, *H*C≡C-C$_4$H$_4$-); 1.65 (br., 3H, *i*Pr-C*H$_3$*); 1.41 (s, 15H, *i*Pr-C*H$_3$*); 1.13 (t, 14H, *i*Pr-C*H$_3$*); 0.94 (d, 10H, *i*Pr-C*H$_3$*); -0.45 (d, 12H, *i*Pr-C*H$_3$*) ppm.

^{13}C NMR (75.46 MHz, [D$_6$]benzene, TMS) δ = 168.38 ((HC≡C-C$_4$H$_4$-)Si*C*=CHSi); 163.40 ((HC≡C-C$_4$H$_4$-)SiC=*C*HSi); 155.76, 155.67, 155.41, 149.71 (Tip-*C*o/p); 145.12, 141.52, 137.25 (Ar-*Ci*); 133.70 (Ar-*CH*); 133.44, 133.41, 132.55, 129.61 (Tip-*C*i); 130.05, 129.15, 128.85 (Ar-*CH*); 128.24 (C$_6$D$_6$) ; 127.85, 127.54 (Ar-*Cq*);127.71, 127.12, 126.92, 126.70, 125.90, 125.81, 121.83 (Tip-*CH*); 83.85 (HC≡*C*-C$_4$H$_4$-); 77.90 (H*C*≡C-C$_4$H$_4$-); 47.31, 34.46, 34.27, 34.20, 32.64, 32.01 (*i*Pr-*C*H); 25.83, 25.51, 24.43, 23.92, 23.83, 23.82, 23.61, 23.60, 23.21 (*i*Pr-*C*H$_3$) ppm.

^{29}Si NMR (59.62 MHz, [D$_6$]benzene, TMS) δ = 1.36, −8.07 ppm.

6. References

---

[1] M. Schulenburg, *Bundesministerium für Bildung und Forschung (BMBF) Referat Publikationen*; Internetredaktion, 11055 Berlin **2004**, Vom Sand zum Superchip.

[2] W. Emmett, Geolocigal Survey (US), *Geological Survey Professional Paper* **1975,** 870-A, A54.

[3] M. Norton, C. Carter, Ceramic materials: Science and engineering, *Springer* **2007**.

[4] Lavoisier, A., *Traite Elementaire de Chemie,* Paris*: Masson*, **1789**, vol. *1*, pp. 174, 194−195.

[5] Davy, H.*, Phil. Trans. Roy. Soc*. (London), **1808**, vol. *98*. pp. 333−370; Davy, H., *Ann. Physik*, **1809**, vol. *32*., pp. 365−396; Davy, H., *Phil. Trans. Roy. Soc.* (London), **1810**, vol. *10*, pp. 16−74.

[6] Berzelius, J.J., *Ann. Phys. Chem.*, **1824**, vol. *1*, pp. 204−230; Soderbaum, H.G., *Jac. Berzelius Lettres,* vol. *1*, pt. 2. Correspondance entre Berzelius et Sir Humphry Davy,1806−1825, Uppsala, **1912**, pp. 67−73; Woehler, F., *Ber. Deut. Chem. Ges.*, **1875**, vol. *8*, pp. 838− 852.

[7] Thomson, T., *A System of Chemistry of Inorganic Bodies*, London−Edinburg, **1831**, 7th Ed., p. 222.

[8] Woehler, F., *Journ. Pharm*., **1858**, vol. *34*, pp. 135−137.

[9] M. Schulze, G. Wagner, H. Moretto, Silicones*, Ullmann´s Encyclopedia of Industrial Chemistry*, Weinheim, **2000**.

[10] Rochow, E.G., *An Introduction to the Chemistry of the Silicones*, Second Ed., New York: John Wiley & Sons, Inc., **1951**.

[11] Stuart Bondurant, Virginia Ernster, and Roger Herdman, Editors; *Committee on the Safety of Silicone Breast Implants*, Institute of Medicine, ISBN: 0-309-51931-4, 560 pages, 6 x 9, (**1999**).

[12] W. Pikard, *Patent US836531*: Means For Receiving Intelligence Communicated By Electric Waves, **1905**.

[13] Martin A. Green, ARC Photovoltaics Centre of Excellence, University of New South Wales (UNSW), *John Wiley & Sons, Ltd*. **2009**; *17*:183–189.

[14] P. Siffert, E. Krimmel, *Science and Business Media*, Silicon, Springer, **2004**.

---

[15] Lidia Lukasiak and Andrzej Jakubowski, *history of semiconductors, Journal of telecommunications and information technology,* **2010.**

[16] F. S. Kipping, L. L. LIoyd, *J. Chem. Soc. Trans*. **1901**, *79*, 449-459.

[17] F. S. Kipping, J. E. Sands, *J. Chem. Soc. Trans*. **1921**, *119*, 647-653.

[18] H. Köhler, A. Michaelis, *Ber. Dtsch, Chem. Ges*. **1877**, *10*, 807-814.

[19] J. J. Daly, J. Maier, *Nature* **1964**, *203*, 1167-1168.

[20] K. S. Pitzer, *J. Am. Chem. Soc.* **1948**, *70*, 2140-2145.

[21] R. S. Mulliken, *J. Cem. Phys. **1950***, *72*, 4493-4503.

[22] P. Jutzi, *Angew. Chem. Int. Ed. Engl.* **1975**,*14*, 232-245.

[23] M. Series, D. E. Goldberg, P. B. Hitchcock, M. F. Lappert, K. Markthomas, A. J. Thorne, A. Haaland, B. E. R. Schilling, *Dalt. Trans.* **1986**, 2387-2394.

[24] A. G. Brook, S. C. Nyburg, F. Abdesaken, B. Gutekunst, R. Krishna, M. R. Kallury, Y. C. Poon, Y. M. Chang, W. N. Winnie, J*. Am. Chem. Soc., Chem. Commun.* **1981**, *104*, 191-192.

[25] R. West, J. M. Fink, J. Michl, *Science.* **1981,** *214*, 1343-1344.

[26] M. Yoshifuji, I. Shima, N. Inamoto, K. Hirotsu, T. Higuchi, *J. Am. Chem. Soc.* **1981**, *103*, 4587-4589.

[27] D. N. Roark, G. J. D. Peddle, *J. Am. Chem. Soc.* **1973**, *94*, 5837-5841.

[28] M. A. Pearsall, R. West, *J. Am. Chem. Soc.* **1988**, *110*, 7228-7229.

[29] R. Janoschek, *Chemie in unserer Zeit* **1988**, *22*, 128.

[30] L. Pauling, *J. Am. Chem. Soc.* **1931**, *53*, 1367.

[31] (a) E. A. Carter, W. Goddard, *J. Phys. Chem.* **1986**, *90*, 998-1001; (b) G. Trinquier, J. P. Malrieu, *J. Am. Chem. Soc.* **1987**, *109*, 5303-5315; (c) J. P. Malrieu; G. Trinquier, *J. Am. Chem. Soc.* **1990**, *94*, 6184-6196.

[32] (a) Vladimir Ya. Lee and Akira Sekiguchi, *Organometallic Compounds of Low-Coordinate Si, Ge, Sn and Pb: From Phantom Species to Stable Compounds*, **2010** John Wiley and Sons; (b) P. P. Power, *Chem. Rev. (Washington, D. C.)* **1999**, *99*, 3463-3503.

[33] M. Karni, Y. Apeloig, J. Am. *Chem. Soc.* **1999**, *112*, 8589-8590.

---

[34] Kira, M.; Maruyama, T.; Kabuto, C.; Ebata, K.; Sakurai, H. *Angew. Chem.* **1994**, *106*, 1575; *Angew. Chem., Int. Ed. Engl.* **1994**, *33*, 1489.

[35] A. Sekiguchi, S. Inoue, M. Ichinohe, Y. Arai, *J. Am. Chem. Soc.* **2004**, *126*, 9626.

[36] R. Tanaka, T. Iwamoto, M. Kira, *Angew. Chem.* **2006**, *118*, 6519; *Angew. Chem. Int. Ed.* **2006**, *45*, 6371.

[37] M. J. Fink, M. J. Michalczyk, K. J. Haller, R. West, J. Michl, *organometallics,* **1984**, 793-800.

[38] M. Wind, D. R. Powell, R. West, *organometallics,* **1996**, *15*, 5773-5773.

[39] B. D. Shehered, C. F. Campana, R. West, *Heteroat. Chem.* 1**990**, *1*, 1-7.

[40] M. Kira, T. Iwamoto*, Adv. Organomet.Chem*. **2006**, *54*, 73- 148.

[41] D. Scheschkewitz, *Chem. Lett*. **2011,** *40***,** 2-11.

[42] M. Weidembruch, S. Wilms, W. Saak, G. Henkl, *Angew. Chem. Int. Ed*. **1997**, *36*, 3090.

[43] A. Fukazawa, Y. Li, S. Yamaguchi, H. Tsuji, K. Tamao, *J. Am. Chem. Soc.* **2007***, 129,* 14164-14165.

[44] a) Tamao, *Dalton Trans.* **2010**, *39*, 9203–9208; c) M. Kobayashi, T. Matsuo, T. Fukunaga, D. Hashizume, H. Fueno, K. Tanaka, K. Tamao; b) K. Tamao, M. Kobayashi, T. Matsuo, H. Tsuji, *Chem. Commun.,* **2012**, *48*, 1030–1032.

[45] R. Okazaki, R. West, *Adv. Organomet. Chem.* **1996**, *39*, 231-273.

[46] S. Masamune, Y. Hanzawa, S. Murakami, T. Bally, J. F. Blount, J. Am*. Chem.* Soc. **1982**, *104*, 1150-1153.

[47] M. Kira, T. Maruryama, C. Kabuto, K. Ebata, H. Sakurai, *Angew. Chem.* **1994**, *106*, 1575-1577.

[48] A. Schaefer, M. Weidenbruch, K. Peters, H. G. Von Schnering, *Angew. Chem.* **1984**, *96*, 311-312; *Angew. Chem. Int. Ed. Engl*. **1984**, *23*, 302-303.

[49] H. Watanabe, K. Takeuchi, N. Fukawa, M. Kato, Y. Nagai, *Chem. Lett.* **1987**, 1341-1344.

[50] S. Masamune, Y. Eriyama, T. Kawase, *Angew. Chem.* **1987**, *99*, 601-602; *Angew. Chem. Int. Ed. Engl*. **1987**, *26*, 584-585.

[51] T.Iwamoto, J. Okita, C. Kabuto, M. Kira, *J. Am. Chem. Soc.* **2002**, *124*, 11604-11605.

---

[52] A. Sekiguchi, M. Ichinohe, S. Yamaguchi, *J. Am. Chem. Soc.* **1999,** *121*, 10231-10232.

[53] M. Ichinohe, Y. Arai, A. Sekiguchi, N. Takagi, S. Nagase, *Organometallics* **2001**, *20*, 4141-4143.

[54] a) T. Iwamoto, S. Ishida in *Functional Molecular Silicon Compounds II Low Oxidation states* (Ed. D. Scheschkewitz), Springer, **2015**, p. 128; b) C. Präsang, D. Scheschkewitz, *Chem. Soc. Rev.* **2015**, *in press*, DOI: 10.1039/c5cs00720h.

[55] J. Park, S. A. Batcheller, S. Masamune, *J. Organomet. Chem.* **1989**, *367*, 39-45.

[56] M. Weindenbruch, S. Willms, W. Saak, G. Henkel, *Angew. Chem.* **1997**, *109*, 2612-2613; *Angew. Chem., Int. Ed. Engl.* **1997**, *36*, 2503-2504.

[57] D. Scheschkewitz, *Angew. Chem.* **2004**, *116*, 3025-3028; *Angew. Chem., Int. Ed.* **2004**, *43*, 2965-2967.

[58] M. Ichinohe, K. Sanuki, S. Inoue, A. Sekiguchi, *Organometallics* **2004**, *23*, 3088-3090.

[59] M. Ichinohe, K. Sanuki, S. Inoue, A. Sekiguchi, *Silicon Chem.* **2005**, *3*, 111-116.

[60] S. Inoue, M. Ichinohe, A. Sekiguchi*, Chem. Lett.* **2005**, *34*, 1564-1565.

[61] R. Kinjo, M. Ichinohe, A. Sekiguchi, N. Takagi, M. Sumimoto, S. Nagase, *J. Am. Chem. Soc.* **2007**, *129*, 7766-7767.

[62] T. Yamaguchi, M. Ichinohe, A. Sekiguchi*, New j. Chem.* **2010**, *34*, 1544-1546.

[63] T. Iwamoto, M. Kobayshi, K. Uchiyama, S. Sasaki, S. Nagendram, H. Isobe, M. Kira, *J. Am. Chem. Soc.* **2009**, *131*, 3156-3157.

[64] M. J. Cowely, K. Abersfelder, A. J. P. White, M. Majumdar, *D. Scheschkewitz, Chem. Commun.* **2012**, *48*, 6595-6597.

[65] K. Abersfelder, D. Guclu, D. Scheschkewitz, *Angew. Chem.* **2006**, *118*, 1673-1675; *Angew. Chem. Int. Ed.* **2006**, *45*, 1643-1645.

[66] H. Yasuda, V. Y. Lee and A. Sekiguchi, *J. Am. Soc.* **2009**, *131*, 6352-6353.

[67] S. Inoue, M. Ichinohe, A. Sekiguchi*, Chem. Lett.* **2008**, *37*, 1044-1045.

[68] M. Hartman, A. Haji-Abdi, K. Abersfelder, P. R. Haycock, A. J. P. White, *D. Scheschkewitz, Dalton Trans.* **2010**, 9288-9295.

[69] K. Abersfelder, *D. Scheschkewitz, J. Am. Chem. Soc.* **2008**, *130*, 4114-4121.

---

[70] K. Abersfelder, T. -I. Nguyen, D. Scheschkewitz*, Z. Aorg. Allg. Chem.* **2009**, *635*, 2093-2098.

[71] K. Abersfelder, A. J. P. White*,* H. S. Rzepa, D. Scheschkewitz, *Science* **2010**, *327*, 564-566.

[72] T. -I. Nguyen, D. Scheschkewitz*, J. Am. Chem. Soc.* **2005**, *127*, 10174-10175.

[73] N. Takagi, S. Nagase, *Eur. J. Inorg. Chem.* **2002**, 2775-2778.

[74] T. Sasamori, K. Hironaka, Y. Sugiyama, N. Takagi, S. Nagase, Y. Hosoi, Y. Furukawa, N. Tokitoh, *J. Am. Chem. Soc.* **2008**, *130*, 13856-13857.

[75] K. Suzuki, T. Mastuo, D. Hashizume, K. Tamao, *J. Am. Chem. Soc.* **2011**, *133*, 19710-19713.

[76] N. Wiberg, S. K. Vasisht, G. Fischer, P. Mayer, *Z. Aorg. Allg. Chem.* **2004**, *630*, 1823-1828.

[77] T. Sasamori, K. Hironaka, Y. Sugiyama, N. Takagi, S. Nagase, N. Tokitoh, *Pure Appl. Chem.* **2010**, *82*, 603-612.

[78] Uchiyama, K.; Nagendran, S.; Ishida, S.; Iwamoto, T.; Kira, M. *J. Am. Chem. Soc.* **2007**, *129*, 10638.

[79] a) S. Parke, M. Boone, E. Rivard, *Chem. Commun.,* **2016**, *52*, 9485, b) M.P. Duffy, W. Delaunay, P.-A. Bouit and M. Hissler, *Chem. Soc. Rev.,* **2016**, *45*, 5296-5310; c) A. C. Grimsdale, K. Müllen, *Macromol. Rapid Commun.,* **2007**, *28*, 1676−1702; d) M. Hissler, P. W. Dyer, R. Reau, *Top. Curr. Chem*., **2005**, *250*, 127−163 e) M. Hissler, P. W. Dyer, R. Reau, *Coord. Chem. Rev.,* **2003**, *244*, 1−44.

[80] a) I. Bejan and D. Scheschkewitz, *Angew. Chem.,* **2007***, 119,* 5885-5888*; Angew. Chem. Int Ed.,* **2007**, *46*, 5783-5786; b) J. Jeck, I. Bejan, A. J. P. White, F. Breher and D. Scheschkewitz, *J. Am. Chem. Soc.* **2010**, *132*, 17306-17315.

[81] T. Iwamoto, M. Kobayashi, K. Uchiyama, S. Sasaki, S. Nagendran, H. Isobe, and M. Kira *J. AM. CHEM. SOC.* **2009**, *131*, 3156–3157.

[82] a) T. Matsuo, M. Kobayashi, K. Tamao, *Dalton Trans.* **2010**, *39*, 9203–9208; b) M. Kobayashi, T. Matsuo, T. Fukunaga, D. Hashizume, H. Fueno, K. Tanaka, K. Tamao, *J. Am. Chem. Soc.* **2010**, *132*, 15162; c) M. Kobayashi, N. Hayakawa, K. Nakabayashi, T. Matsuo, D. Hashizume, H. Fueno, K. Tanaka, K. Tamao, *Chem. Lett.* **2014**, *43*, 432-

---

434; d) M. Kobayashi, D. Hashizume, T. Fukunaga, T. Mastuo, and K. Tamao, *The 90th Annual Meeting of Chemical Society of Japan,* March **2010**, Higashi-Osaka (Abstract No. 2C2-19).

[83] Li, L.; Matsuo, T.; Hashizume, D.; Fueno, H.; Tanaka, K.; Tamao, K. *J. Am. Chem. Soc.,* **2015**, *137*, 15026.).

[84] M. Kobayachi, T. Matsuo, K. Tamoa, *J. Am. Chem. Soc.* **2016**, *138*, 758-761.

[85] D. J. De Young, M. J. Fink, R. West, J. Michl, *Main Group Met. Chem.* **1987**, *10*, 19-43.

[86] A: Sekiguchi, I. Maruki, H. Sakurai, *J. Am. Chem. Soc.* **1993**, *115*, 11460-11466.

[87] S. Boomgaarden, W. Saak, M. Weindenbruch, H. Marsman, *Z. Anorg. Allg. Chem.* **2001**, *627*, 349-352.

[88] M. Kira, T. Ishima, T. Iwamoto, M Ichinohe, *J. Am. Chem. Soc.* **2001**, *123*, 1676-1682.

[89] Y. Nakadaira, R. Sato, H. Sakurai, *Chem. Lett.* **1985**, 643.

[90] D. J. DeYoung, R. West, *Chem. Lett.* **1986**, 883.

[91] A. Meltzer, M. Majumdar, A. J. P. White, V. Huch, D. Scheschkewitz, *Organometallics* **2013**, *32*, 6844 –6850.

[92] M. Majumdar, I. Bejan, V. Huch, A. J. P. White, G. R. Whittell, A. Schäfer, I. Manners and D. Scheschkewitz, *Chem. Eur. J.*, **2014**, *20*, 9225.

[93] a) C. Präsang and D. Scheschkewitz, *Chem. Soc. Rev.,* **2016**, *45,* 900-921; b) A. M. Priegert, B. W. Rawe, S. C. Serin and D. P. Gates, *Chem. Soc. Rev.*, **2016**, *45*, 922-953; c) D. Protasiewicz, *Pure Appl. Chem.* **2013**, *85*, 801−815; d) D. Scheschkewitz, *Chem. Lett*. **2011**, *40*, 2-11; e) T. Matsuo, M. Kobayashi and K. Tamao, *Dalton Trans.,* **2010**, *39*, 9203−9208; f) D. Scheschkewitz, *Chem. Eur. J.,* **2009**, *15*, 2476-2485.

[94] a) V. A. Wright and D. P. Gates, *Angew. Chem.* **2002***, 114*, 2495; *Angew. Chem. Int. Ed.,* **2002**, *41*, 2389-2392; b) R. C Smith and J. D. Protasiewicz, *J. Am. Chem. Soc.,* **2004**, *12*6, 2268-2269; c) V.A. Wright, B. O. Patrick, C. Schneider and D. P. Gates, *J. Am. Chem. Soc.,* **2006**, *128*, 8836-8844.

---

[95] a) D. M. Salazar, E. Mijangos, S. P. Len, M. Gao and A. Orthaber, *Chem. Commun.,* **2017**, *53*, 1120-1123; b) A. Arkhypchuk, A. Orthaber and S. Ott, *Eur. J. Inorg. Chem*. **2014**, 1760-1766*;* c) A. Arkhypchuk, M-P. Santoni and S. Ott, *Angew. Chem. Int Ed.,* **2012**, *51*, 7776-7780, d) B. Li, T. Matsuo, T. Fukunaga, D. Hashizume, H. Fueno, K. Tanaka and K. Tamao, *J. Am. Chem. Soc.,* **2009**, *131*, 13222-12223.

[96] a) M. Kira, *Organometallics,* **2011**, *30*, 4459-4465; b) H. Tomioka, K. Kimoto, H. Murata and Y. Izawa, J. CHEM. SOC. PERKIN TRANS, *1,* **1991**.

[97] D. Auer, C. Strohmann; A. V. Arbuznikov and M. Kaupp, Organometallics, **2003**, *22*, 2442-2449.

[98] I. J. Bruno, J. C. Cole, M. Kessler, J. Luo, W. D. S. Motherwell, L. H. Purkis, B. R. Smith, R. Taylor, R. I. Cooper, S. E. Harris, A.G. Orpen, *J. Chem. Inf. Comput. Sci*., **2004**, *44*, 2133-2144.

[99] N. M. Obeid, L. Klemmer, D. Maus, M. Zimmer, I. Bejan, V. Huch, A. J. P. White, G. Jung, D. Scheschkewitz, *Dalton Trans.* **2017.**

[100] M. R. Wortmann, K. Elich, S. Lebus and W. Liptay, *J. Chem. Phys.,* **1991**, *95*, *6371*-6381.

[101] M P. Chen and T. J. Meyer, *Chem. Rev.,* **1998**, *98*, 1439−1477.

[102] R. Wortmann, S. Lebus, K. Elich, S. Assar, N. Detzer and W. Liptay, *Chemical Physics Letters.,* **1992**, *198*,220-228.

[103] F. C. Grozema, M. Swart, R. W. J. Zijlistra, J. J. Piet, D. A. Siebbeles and P. Van Duijnen, *J. Am. Chem. Soc.,* **2005**, *127*, 11019-11028.

[104] F Y. Sato, Y. Ueki, M. Ishikawa and M. Kumada, *J. Chem. Soc., Faraday Trans.,* 1984, **80**, 341.

[105] a) A. D. Becke, *J. Chem. Phys.* **1993**, *98*, 5648-52, b) R. Ditchfield, W. J. Hehre and J. A. Pople, *J. Chem. Phys.,* **1971**, *54*, 724–728, c) W. J. Hehre, R. Ditchfield and J. A. Pople, *J. Chem. Phys.,* **1972**, *56*, 22572261, d) M. M. Francl, W. J. Pietro, W. J. Hehre, J. S. Binkley, M. S. Gordon, D. J. DeFrees and J. A. Pople, *J. Chem. Phys.,* **1982**, *77*, 3654–3665, e) V. A. Rassolov, *J. Comput. Chem.,* **2001**, *22*, 976–984.

---

[106] M. J. Frisch, G. W. Trucks, H. B. Schlegel, G. E. Scuseria, M. A. Robb, J. R. Cheeseman, G. Scalmani, V. Barone, B. Menucci, G. A. Petersson, *et al.*, *Gaussian 09 Revision B*.

[107] C. Spies, A.-M. Huynh, V. Huch and G. Jung, *J. Phys. Chem. C*, **2013**, *117*, 18163−18169.

[108] C. Stoumpos, D. Malliakas and G. Kanatzidis*, Inorg. Chem.,* **2013**, *52*, 9010-9038.

[109] M. Kasha, H. R. Rawls and M. A. El-Bayoumi, *Eighth European Congress on Molecular Spectroscopy*, Copenhagen **1965**, 371-392.

[110] R. M. Hochstrasser, Rev. Mod. Phys., **1962**, *34*, 531-549.

[111] It was nonetheless attempted to optimize (and thus relax) the vertically excited state of the model system **116Dip**. A preliminary assessment of this computationally demanding calculations after one week (and thus the first few cycles) suggested an instability of the wave function and the attempt was therefore abandoned.

[112] A. Kell, *Master thesis*, Saarland University **2016.**

[113] J. P. Foster and F. J. Weinhold, *J. Am. Chem. Soc.,* 1980, **102**, 7211-7218.

[114] A. E. Reed, L. A. Curtiss and F. Weinhold, *Chem. Rev.,* 1988, **88**, 899-926.

[115] http://www.chemcraftprog.com

[116] N. M. O'Boyle, A. L. Tenderholt and K. M. Langner, *J. Comp. Chem.* 2008, **29**, 839–845.

[117] http://www. OriginLab.com.

[118] (a) G. M. Whitesides, M. Eisenhut, W. M. Bunting, J. Am. Chem. Soc. 1974, 96, 5398−5407; (b) A. R. Miller, D. Y. Curtin, J. Am. Chem. Soc. 1976, 98, 1860−1865.

7. Appendix

7.1. List of Compounds

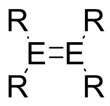

1,2

(**1**: E=Sn, **2**: E=Ge)

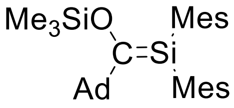

3

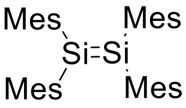

4

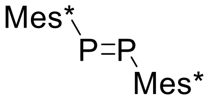

5

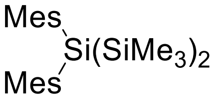

6

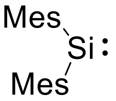

7

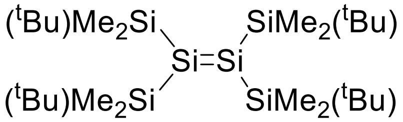

8

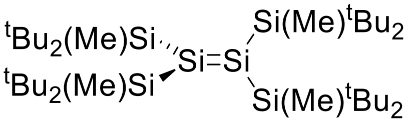

9

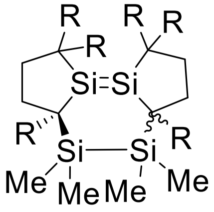

cis/trans-**10**

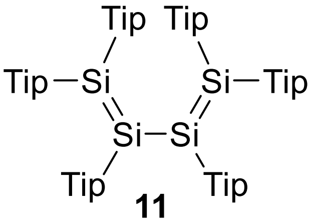

11

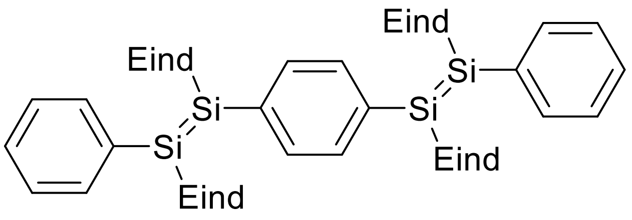

12

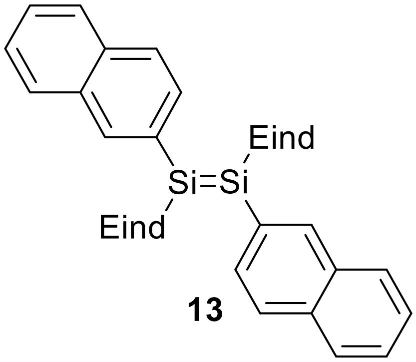

13

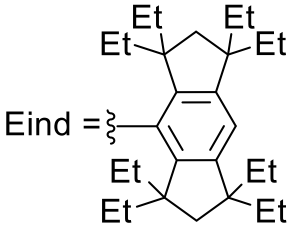

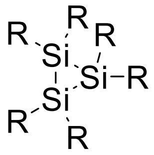

14

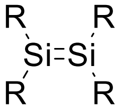

15 : R = 2,6-dimethylphenyl

16 : R = $^{t}BuMe_2Si$

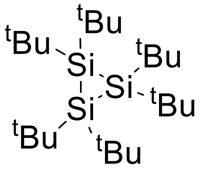

17

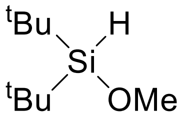

18

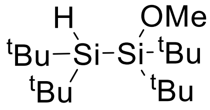

19

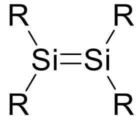

20 : R = Tip

21 : R = $(Me_3Si)_2CH$

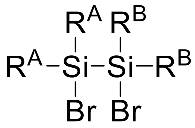

22a,b

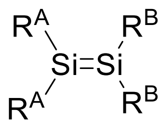

R^A = $^{t}BuMe_2Si$

23a : R^B = $^{i}PrMe_2Si$

23b R^B = $^{i}Pr_3Si$

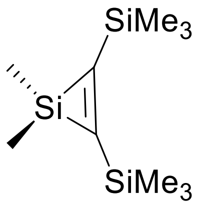

24a,b

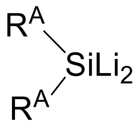

25a,b

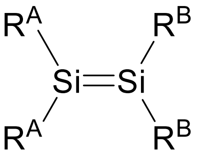

26a,d

26a : R^A = $^{i}Pr_3Si$, R^B = Mes

26b : R^A = $^{t}Bu_3Si$, R^B = Mes

26c : R^A = $^{i}Pr_3Si$, R^B = Tip

26d : R^A = $^{t}Bu_3Si$, R^B = Tip

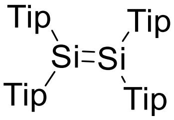

20

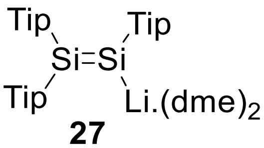

27

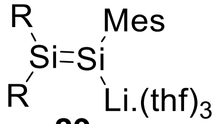

29

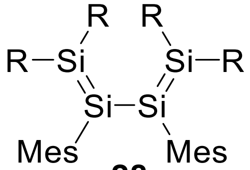

28

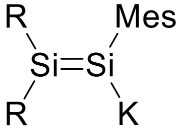

30

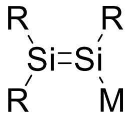

31a-c

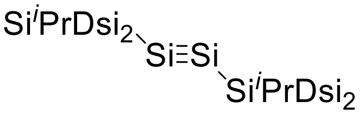

32

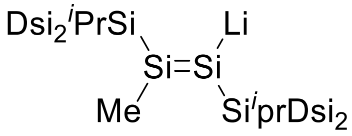

33

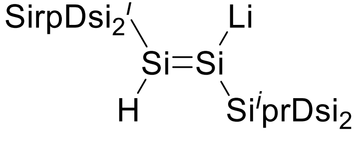

34

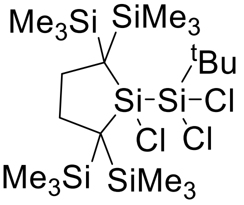

35

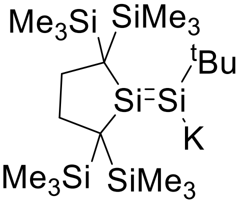

36

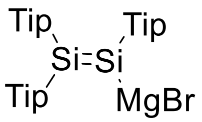

37

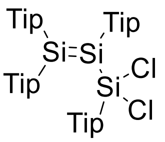

38

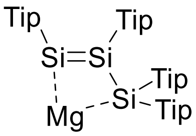

39

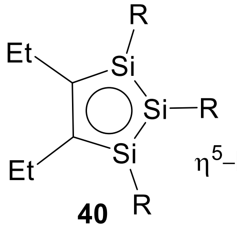

40

η^5–Li^+(thf)

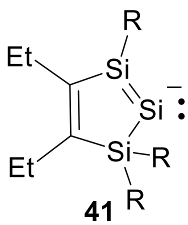

41

Li^+(12-crown-4)$_2$

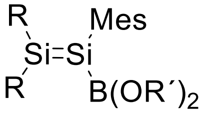

42a,b

B(OR´)$_2$ =

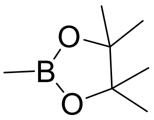

42a

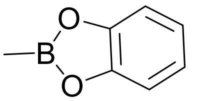

42b

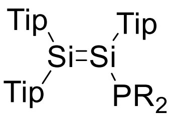

43a-d

a: R = Ph
b: R = ipr
c: R = Cy
d: R = tBu

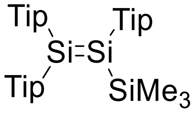

44

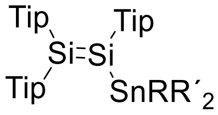

45a-d

a: R = R´= Me
b: R = R´ = Ph;
c: R = R´ = nBu
d: R = Cl, R´ = tBu)

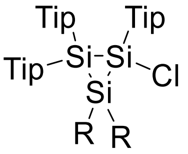

46a-c

a: R = Me
b: R = Ph
c: R = Cl

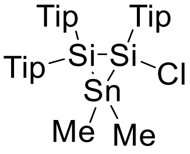

47

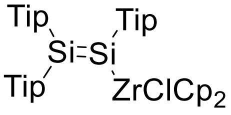

48

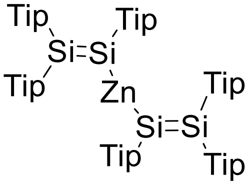

49

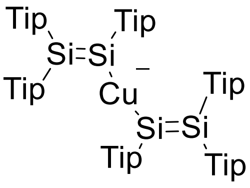

50

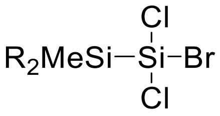

51

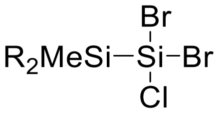

52

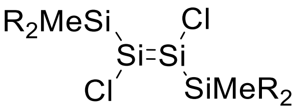

53

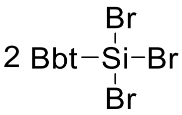

54

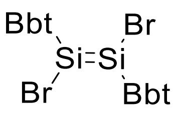

55

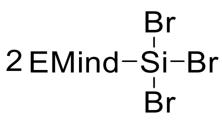

56

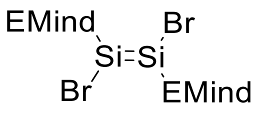

57

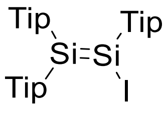

58

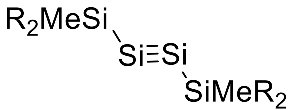

59

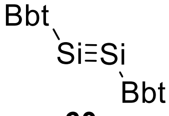

60

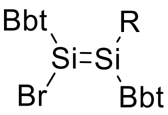

61a-d

a: R = Me
b: R = Et
c: R = nBu
d: R = Ph

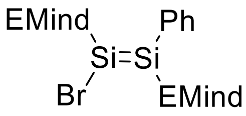

62

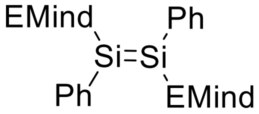

63

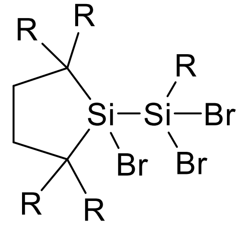

64

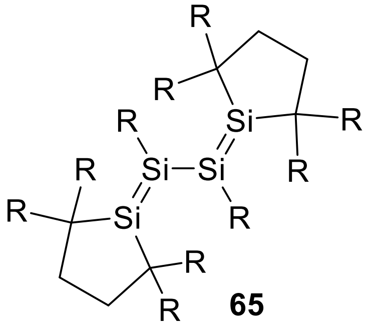

65

R = SiMe3

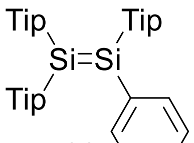

66

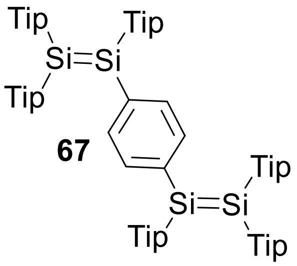

67

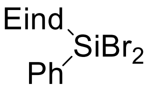

68

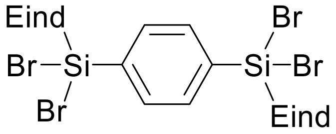

69

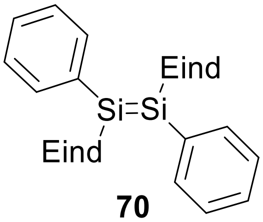

70

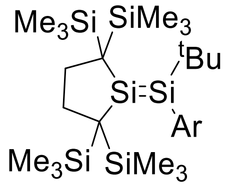

71a-c

Ar =

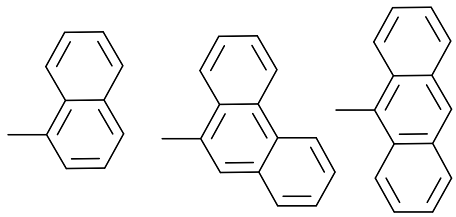

a **b** **c**

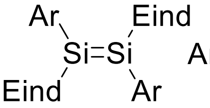

72

Ar =

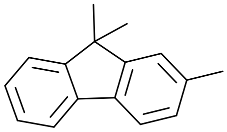

73

EindM(OHex) =

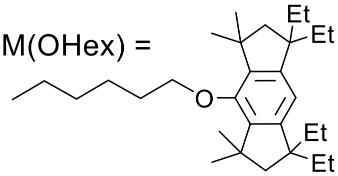

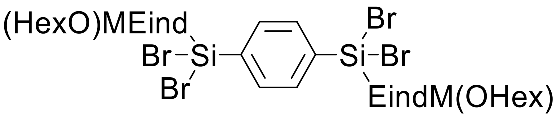

74

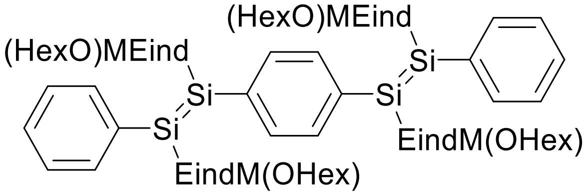

75: n=1
76: n=2
77: n=3
78: n=4

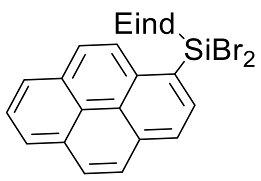

79

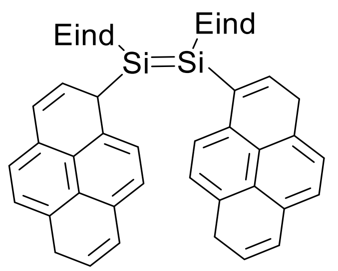

80

Eind =

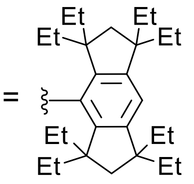

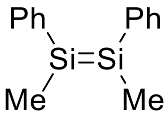

cis **81**

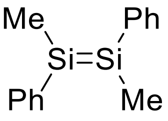

trans **81**

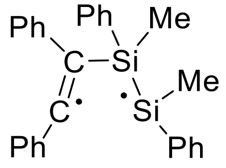

82

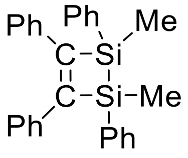

83

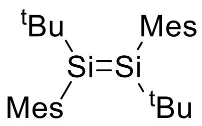

84

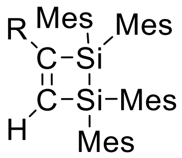

85a, R = Ph
85b, R = OEt
85c, R = CO_2Me
85d, R = $SiMe_3$

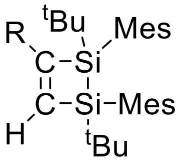

86a, R = Ph
86b, R = OEt

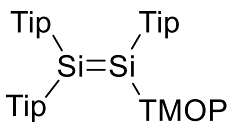

87

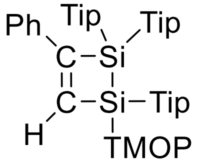

88

TMOP = 2,4,6-$(MeO)_3C_6H_2$

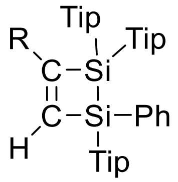

89a, R = Ph
89b, R = ^tBu

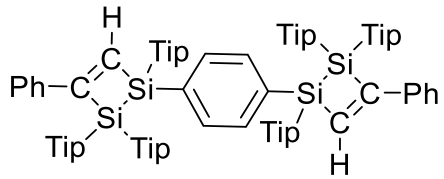

90

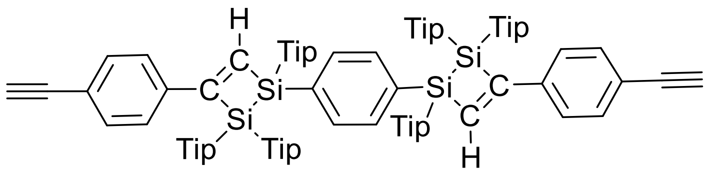

M1 (34%)
M2 (8%)

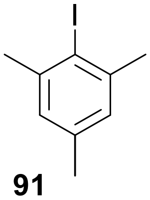

91

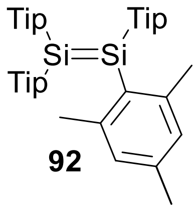

92

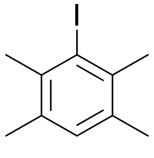

93

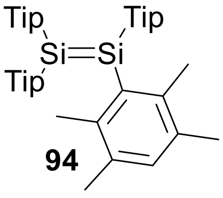

94

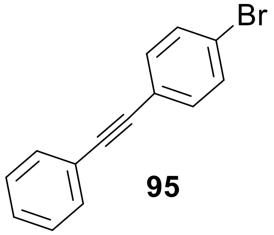

95

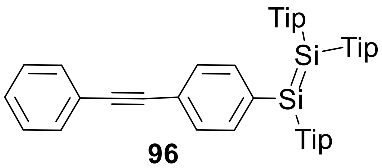

96

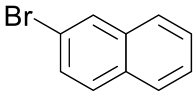

97

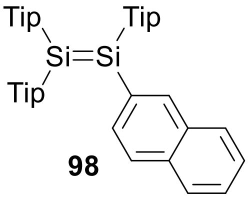

98

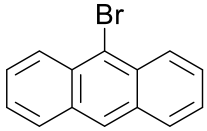

99

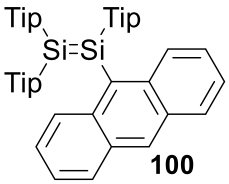

100

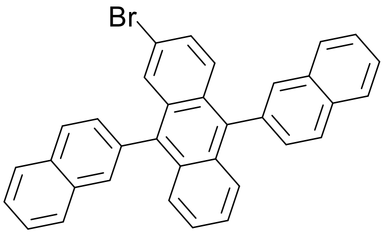

101

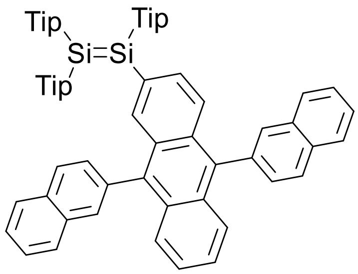

102

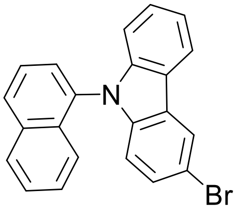

103

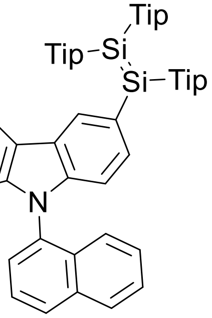

104

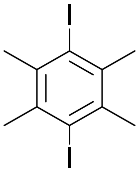

105

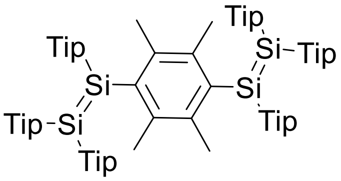

106

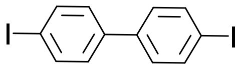

107

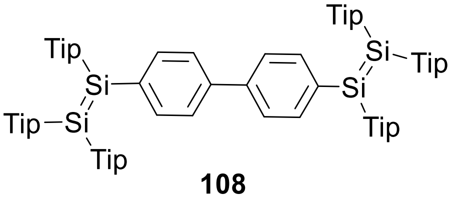

108

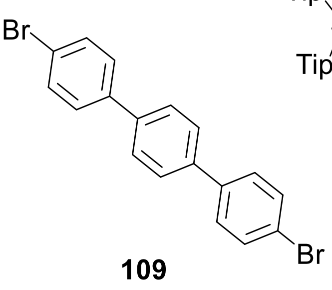

109

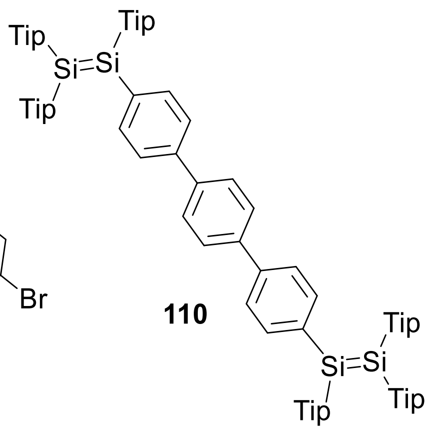

110

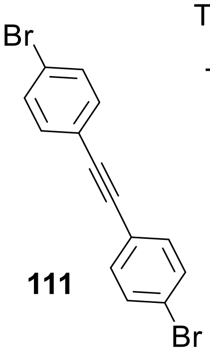

111

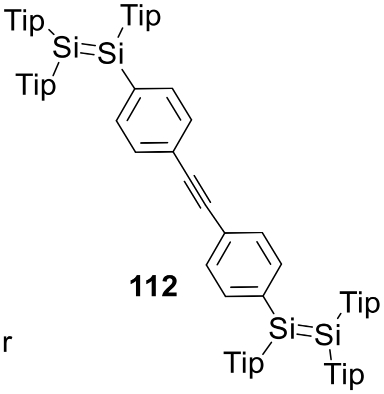

112

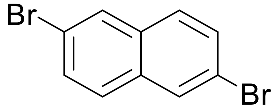

113

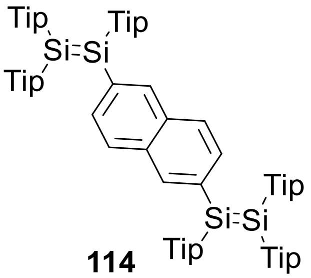

114

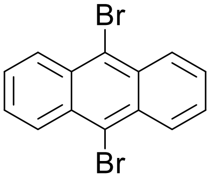

115

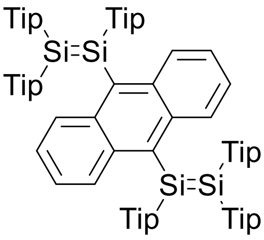

116

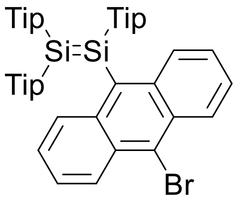

117

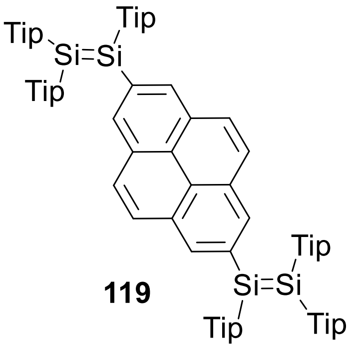

119

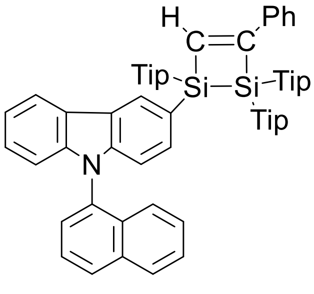

120

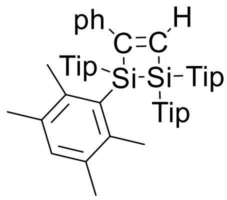

123b

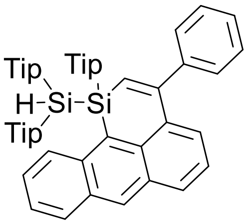

125

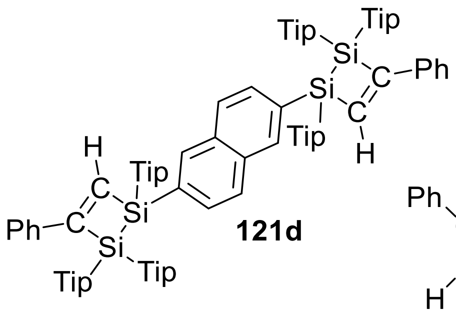

121d

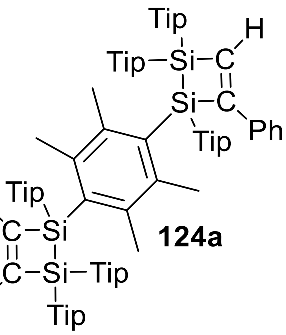

124a

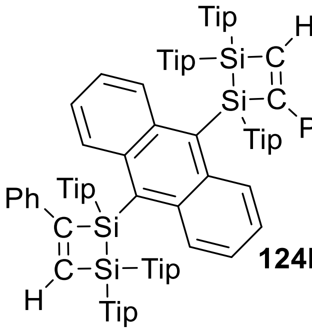

124b

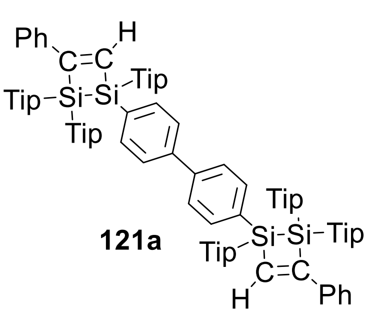

121a

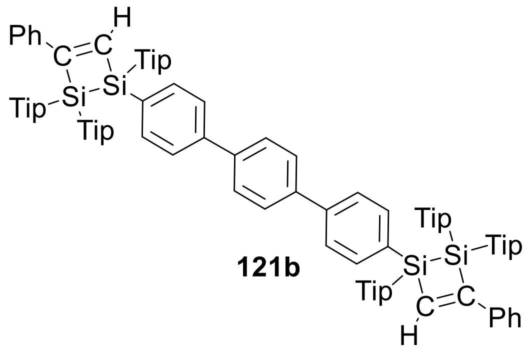

121b

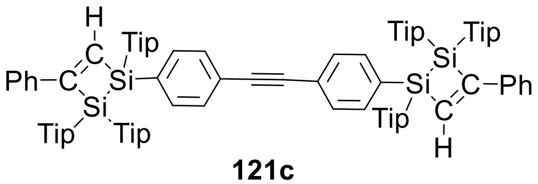

121c

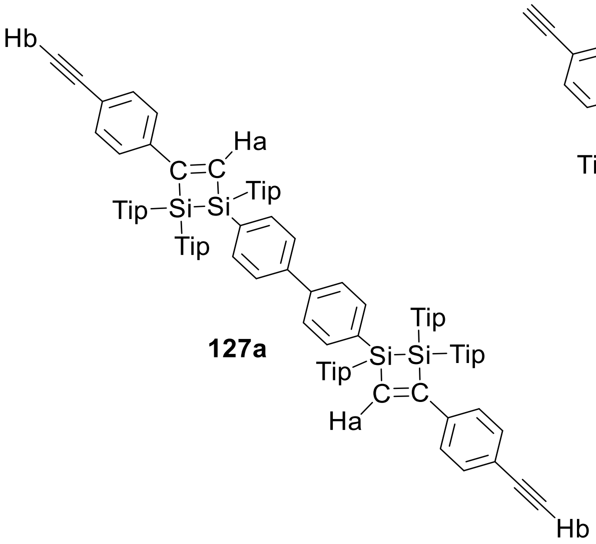

127a

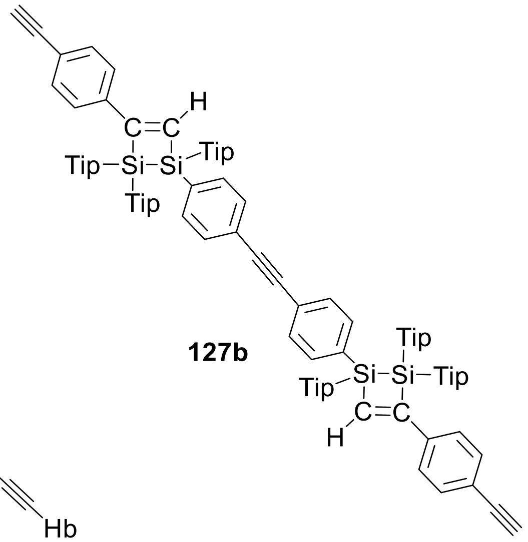

127b

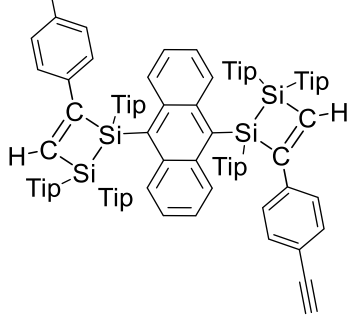

127c

7.2. X-ray Structure Determination

7.2.1. Crystal Data and Structure Refinement for 92

$C_{54}H_{80}Si_2$, M = 785.36, triclinic, P-1 (no. 2), a = 14.5604(3), b = 18.2609(4), c = 19.9406(4) Å, α = 98.3330(17), β = 102.4825(18), γ = 91.8560(17)°, V = 5110.79(19) Å^3, Z = 4 (2 independent molecules), D_c = 1.021 g cm^{-3}, μ(Mo-Kα) = 0.101 mm^{-1}, T = 173 K, yellow blocks, Oxford Diffraction Xcalibur 3 diffractometer; 33378 independent measured reflections (R_{int} = 0.0179), F^2 refinement,[X1] R_1(obs) = 0.0658, wR_2(all) = 0.1874, 23950 independent observed absorption-corrected reflections [$|F_o| > 4\sigma(|F_o|)$, $2\theta_{max}$ = 66°], 1028 parameters. CCDC 976704.

Reciprocal space analysis of the data set for the structure of **92** clearly showed the crystal to be twinned. Despite numerous attempts, modelling this twinning at the data processing stage gave unsatisfactory results, and so the data was processed without any twin modelling. However, signs of the unresolved twinning are evident in the final ΔF map, with one residual electron density peak (Q1) significantly larger than the rest at 2.24 eÅ^{-3} (the next four are 1.20, 0.84, 0.80 and 0.73 eÅ^{-3}). This peak sits in relatively empty space, its closest approach being *ca*. 1.84 Å to the methine hydrogen of the C37-based isopropyl group. This site is *ca*. 2.69 Å away from Si2B, and the Si2B···Q1 vector is almost orthogonal to the Si1B–Si2B bond, the Si1B–Si2B···Q1 angle being *ca*. 88.7°. Since there seems no sensible chemical explanation for this peak, it is most likely that it is an artefact of the unresolved twinning.

The structure was found to contain two crystallographically independent molecules, **92-A** and **92-B**. The C34-based isopropyl unit in molecule **92-A** was found to be disordered. Two orientations were identified of *ca*. 81 and 19% occupancy, their geometries were optimised, the thermal parameters of adjacent atoms were restrained to be similar, and only the non-hydrogen atoms of the major occupancy orientation were refined anisotropically (those of the minor occupancy orientation were refined isotropically).

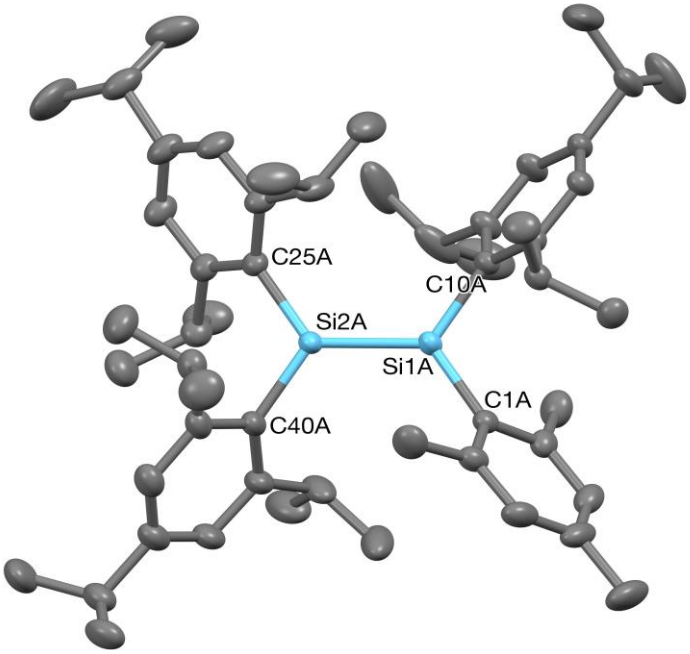

Figure 111. The crystal structure of one (**92-A**) of the two independent molecules present in the crystal of **92** (50% probability ellipsoids).

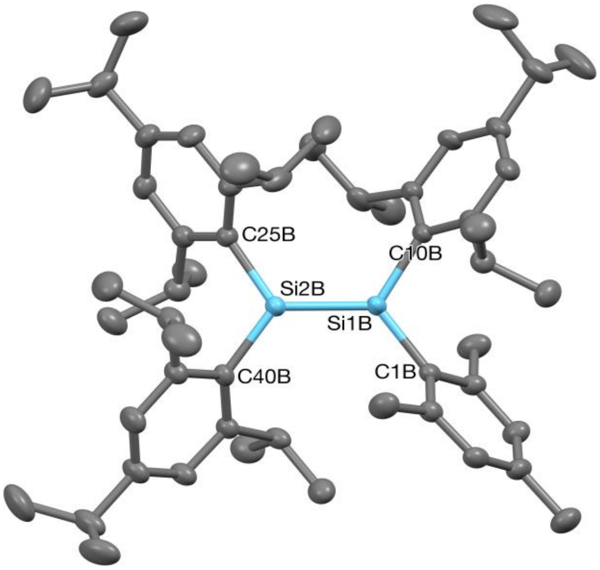

Figure 112. The crystal structure of one (**92-B**) of the two independent molecules present in the crystal of **92** (50% probability ellipsoids).

7.2.2. Crystal Data and Structure Refinement for 94

Identification code	sh3611	
Empirical formula	$C_{55} H_{82} Si_2$ x 0.5 $C_6 H_{14}$	
Formula weight	842.47	
Temperature	163(2) K	
Wavelength	0.71073 Å	
Crystal system	Triclinic	
Space group	P-1	
Unit cell dimensions	a = 12.8482(9) Å	α= 109.835(4)°.
	b = 13.2841(12) Å	β= 101.906(4)°.
	c = 17.9857(14) Å	γ = 97.497(4)°.
Volume	2757.7(4) Å^3	
Z	2	
Density (calculated)	1.015 Mg/m^3	
Absorption coefficient	0.097 mm^{-1}	
F(000)	930	
Crystal size	0.489 x 0.308 x 0.128 mm^3	
Theta range for data collection	1.250 to 28.122°.	
Index ranges	-16<=h<=16, -17<=k<=17, -23<=l<=23	
Reflections collected	50119	
Independent reflections	13225 [R(int) = 0.0382]	
Completeness to theta = 25.242°	99.9 %	
Absorption correction	Semi-empirical from equivalents	
Max. and min. transmission	0.7456 and 0.7087	
Refinement method	Full-matrix least-squares on F^2	
Data / restraints / parameters	13225 / 163 / 594	
Goodness-of-fit on F^2	1.038	
Final R indices [I>2sigma(I)]	R1 = 0.0553, wR2 = 0.1364	
R indices (all data)	R1 = 0.0888, wR2 = 0.1545	
Extinction coefficient	n/a	
Largest diff. peak and hole	0.427 and -0.340 e.Å^{-3}	

7.2.3. Crystal Data and Structure Refinement for for 98

Identification code	sh3783	
Empirical formula	$C_{55} H_{76} Si_2$	
Formula weight	793.33	
Temperature	152(2) K	
Wavelength	0.71073 Å	
Crystal system	Triclinic	
Space group	P-1	
Unit cell dimensions	a = 11.7724(7) Å	α= 88.036(3)°.
	b = 13.4029(8) Å	β= 89.589(3)°.
	c = 16.1636(10) Å	γ = 76.942(3)°.
Volume	2483.0(3) $Å^3$	
Z	2	
Density (calculated)	1.061 Mg/m^3	
Absorption coefficient	0.105 mm^{-1}	
F(000)	868	
Crystal size	0.253 x 0.203 x 0.203 mm^3	
Theta range for data collection	1.261 to 27.582°.	
Index ranges	-15<=h<=15, -17<=k<=17, -21<=l<=19	
Reflections collected	42683	
Independent reflections	11462 [R(int) = 0.0217]	
Completeness to theta = 25.242°	100.0 %	
Absorption correction	Semi-empirical from equivalents	
Max. and min. transmission	0.7456 and 0.7006	
Refinement method	Full-matrix least-squares on F^2	
Data / restraints / parameters	11462 / 204 / 572	
Goodness-of-fit on F^2	1.030	
Final R indices [I>2sigma(I)]	R1 = 0.0534, wR2 = 0.1392	
R indices (all data)	R1 = 0.0670, wR2 = 0.1506	
Extinction coefficient	n/a	
Largest diff. peak and hole	1.086 and -0.287 e.$Å^{-3}$	

7.2.4. Crystal Data and Structure Refinement for 100

Identification code	sh3782	
Empirical formula	$C_{59} H_{78} Si_2$ x 0.5($C_5 H_{12}$) x 0.25($C_6 H_6$)	
Formula weight	898.99 g/mol	
Temperature	122(2) K	
Wavelength	0.71073 Å	
Crystal system	Triclinic	
Space group	P-1	
Unit cell dimensions	a = 14.5999(9) Å	α= 95.878(3)°.
	b = 19.1502(11) Å	β= 101.103(3)°.
	c = 20.8629(13) Å	γ = 96.251(3)°.
Volume	5644.2(6) Å^3	
Z	4	
Density (calculated)	1.058 Mg/m^3	
Absorption coefficient	0.099 mm^{-1}	
F(000)	1966	
Crystal size	0.539 x 0.220 x 0.092 mm^3	
Theta range for data collection	1.003 to 26.555°.	
Index ranges	-18<=h<=18, -23<=k<=23, -24<=l<=26	
Reflections collected	66625	
Independent reflections	21894 [R(int) = 0.1047]	
Completeness to theta = 25.242°	95.3 %	
Absorption correction	Semi-empirical from equivalents	
Max. and min. transmission	0.7454 and 0.6219	
Refinement method	Full-matrix least-squares on F^2	
Data / restraints / parameters	21894 / 976 / 1183	
Goodness-of-fit on F^2	1.606	
Final R indices [I>2sigma(I)]	R1 = 0.2122, wR2 = 0.2552	
R indices (all data)	R1 = 0.2892, wR2 = 0.2733	
Extinction coefficient	n/a	
Largest diff. peak and hole	1.129 and -0.770 e.Å^{-3}	

7.2.5. Crystal Data and Structure Refinement for 106

Identification code	sh3666	
Empirical formula	C100 H150 Si4	
Formula weight	1464.55	
Temperature	152(2) K	
Wavelength	0.71073 Å	
Crystal system	Triclinic	
Space group	P-1	
Unit cell dimensions	a = 10.502(2) Å	α= 78.167(11)°.
	b = 13.184(3) Å	β= 79.475(12)°.
	c = 18.070(4) Å	γ = 71.433(13)°.
Volume	2302.7(8) Å^3	
Z	1	
Density (calculated)	1.056 Mg/m^3	
Absorption coefficient	0.108 mm^{-1}	
F(000)	806	
Crystal size	0.244 x 0.119 x 0.028 mm^3	
Theta range for data collection	1.161 to 26.588°.	
Index ranges	-11<=h<=12, -15<=k<=16, -21<=l<=22	
Reflections collected	23782	
Independent reflections	8485 [R(int) = 0.2274]	
Completeness to theta = 25.242°	89.8 %	
Absorption correction	Semi-empirical from equivalents	
Max. and min. transmission	0.7454 and 0.6813	
Refinement method	Full-matrix least-squares on F^2	
Data / restraints / parameters	8485 / 0 / 489	
Goodness-of-fit on F^2	1.141	
Final R indices [I>2sigma(I)]	R1 = 0.1500, wR2 = 0.2858	
R indices (all data)	R1 = 0.3973, wR2 = 0.3607	
Extinction coefficient	n/a	
Largest diff. peak and hole	1.449 and -0.401 e.Å^{-3}	

7.2.6. Crystal Data and Structure Refinement for 108

Identification code	sh3659	
Empirical formula	$C_{102} H_{146} Si_4$	
Formula weight	1484.54	
Temperature	122(2) K	
Wavelength	0.71073 Å	
Crystal system	Monoclinic	
Space group	C2/c	
Unit cell dimensions	a = 37.053(5) Å	α= 90°.
	b = 18.096(2) Å	β= 111.333(7)°.
	c = 15.4097(18) Å	γ = 90°.
Volume	9625(2) Å^3	
Z	4	
Density (calculated)	1.025 Mg/m^3	
Absorption coefficient	0.104 mm^{-1}	
F(000)	3256	
Crystal size	0.671 x 0.231 x 0.066 mm^3	
Theta range for data collection	1.180 to 27.150°.	
Index ranges	-46<=h<=47, -23<=k<=23, -19<=l<=14	
Reflections collected	73251	
Independent reflections	10663 [R(int) = 0.0848]	
Completeness to theta = 25.242°	100.0 %	
Absorption correction	Semi-empirical from equivalents	
Max. and min. transmission	0.7455 and 0.6793	
Refinement method	Full-matrix least-squares on F^2	
Data / restraints / parameters	10663 / 0 / 770	
Goodness-of-fit on F^2	1.016	
Final R indices [I>2sigma(I)]	R1 = 0.0521, wR2 = 0.1053	
R indices (all data)	R1 = 0.1098, wR2 = 0.1278	
Extinction coefficient	n/a	
Largest diff. peak and hole	0.375 and -0.358 e.Å^{-3}	

7.2.7. Crystal Data and Structure Refinement for 112

Identification code	sh3697	
Empirical formula	$C_{104} H_{146} Si_4$ x 4($C_6 H_6$)	
Formula weight	1820.99	
Temperature	123(2) K	
Wavelength	0.71073 Å	
Crystal system	Triclinic	
Space group	P-1	
Unit cell dimensions	a = 11.0556(12) Å	α= 76.026(4)°.
	b = 13.8116(15) Å	β= 80.911(4)°.
	c = 20.163(2) Å	γ = 72.584(3)°.
Volume	2838.5(5) Å^3	
Z	1	
Density (calculated)	1.065 Mg/m^3	
Absorption coefficient	0.099 mm^{-1}	
F(000)	994	
Crystal size	0.428 x 0.369 x 0.080 mm^3	
Theta range for data collection	1.045 to 26.462°.	
Index ranges	-13<=h<=13, -15<=k<=17, -25<=l<=24	
Reflections collected	39573	
Independent reflections	11469 [R(int) = 0.0344]	
Completeness to theta = 25.242°	98.9 %	
Absorption correction	Semi-empirical from equivalents	
Max. and min. transmission	0.7454 and 0.6675	
Refinement method	Full-matrix least-squares on F^2	
Data / restraints / parameters	11469 / 709 / 961	
Goodness-of-fit on F^2	1.033	
Final R indices [I>2sigma(I)]	R1 = 0.0524, wR2 = 0.1197	
R indices (all data)	R1 = 0.0850, wR2 = 0.1391	
Extinction coefficient	n/a	
Largest diff. peak and hole	0.382 and -0.357 e.Å^{-3}	

7.2.8. Crystal Data and Structure Refinement for 114

Identification code	sh3658	
Empirical formula	$C_{100} H_{144} Si_4 \times 0.5(C_{18} H_{18}) \times 2(C_6 H_6)$	
Formula weight	1692.83	
Temperature	122(2) K	
Wavelength	0.71073 Å	
Crystal system	Triclinic	
Space group	P-1	
Unit cell dimensions	a = 10.4614(5) Å	α= 114.7130(10)°.
	b = 16.0181(7) Å	β= 98.7550(10)°.
	c = 18.0405(9) Å	γ = 93.023(2)°.
Volume	2691.3(2) $Å^3$	
Z	1	
Density (calculated)	1.044 Mg/m^3	
Absorption coefficient	0.100 mm^{-1}	
F(000)	926	
Crystal size	0.650 x 0.522 x 0.306 mm^3	
Theta range for data collection	1.266 to 29.661°.	
Index ranges	-14<=h<=14, -22<=k<=22, -25<=l<=25	
Reflections collected	56249	
Independent reflections	15141 [R(int) = 0.0288]	
Completeness to theta = 25.242°	100.0 %	
Absorption correction	Semi-empirical from equivalents	
Max. and min. transmission	0.7459 and 0.7068	
Refinement method	Full-matrix least-squares on F^2	
Data / restraints / parameters	15141 / 638 / 691	
Goodness-of-fit on F^2	1.254	
Final R indices [I>2sigma(I)]	R1 = 0.0623, wR2 = 0.1567	
R indices (all data)	R1 = 0.0844, wR2 = 0.1684	
Extinction coefficient	n/a	
Largest diff. peak and hole	1.384 and -0.359 e.$Å^{-3}$	

7.2.9. Crystal Data and Structure Refinement for 116

Identification code	sh3747	
Empirical formula	$C_{104} H_{146} Si_4,C_{12} H_{12},3(C_1 H_4),2()n,2(H_1)$	
Formula weight	1703.83	
Temperature	192(2) K	
Wavelength	0.71073 Å	
Crystal system	Triclinic	
Space group	P-1	
Unit cell dimensions	a = 10.9487(6) Å	α= 83.163(3)°.
	b = 12.7883(8) Å	β= 77.072(3)°.
	c = 21.4719(14) Å	γ = 65.079(3)°.
Volume	2656.3(3) Å^3	
Z	1	
Density (calculated)	1.065 Mg/m^3	
Absorption coefficient	0.102 mm^{-1}	
F(000)	931	
Crystal size	0.525 x 0.115 x 0.102 mm^3	
Theta range for data collection	0.973 to 27.174°.	
Index ranges	-14<=h<=14, -16<=k<=16, -27<=l<=27	
Reflections collected	38197	
Independent reflections	11426 [R(int) = 0.0529]	
Completeness to theta = 25.242°	98.1 %	
Absorption correction	Semi-empirical from equivalents	
Max. and min. transmission	0.7455 and 0.6215	
Refinement method	Full-matrix least-squares on F^2	
Data / restraints / parameters	11426 / 216 / 628	
Goodness-of-fit on F^2	1.027	
Final R indices [I>2sigma(I)]	R1 = 0.0595, wR2 = 0.1467	
R indices (all data)	R1 = 0.1008, wR2 = 0.1665	
Extinction coefficient	n/a	
Largest diff. peak and hole	0.614 and -0.510 e.Å^{-3}	

7.2.10. Crystal Data and Structure Refinement for 120

Identification code	sh3784	
Empirical formula	$C_{75} H_{83} N S_{i2} x C_6 H_6$	
Formula weight	1132.71	
Temperature	152(2) K	
Wavelength	0.71073 Å	
Crystal system	Triclinic	
Space group	P-1	
Unit cell dimensions	a = 14.0239(7) Å	α= 76.720(2)°.
	b = 14.8033(7) Å	β= 75.529(2)°.
	c = 17.6085(8) Å	γ = 79.975(2)°.
Volume	3418.4(3) $Å^3$	
Z	2	
Density (calculated)	1.100 Mg/m^3	
Absorption coefficient	0.095 mm^{-1}	
F(000)	1220	
Crystal size	0.523 x 0.251 x 0.140 mm^3	
Theta range for data collection	1.218 to 26.506°.	
Index ranges	-17<=h<=17, -18<=k<=17, -22<=l<=22	
Reflections collected	45817	
Independent reflections	13857 [R(int) = 0.0408]	
Completeness to theta = 25.242°	99.0 %	
Absorption correction	Semi-empirical from equivalents	
Max. and min. transmission	0.7454 and 0.6948	
Refinement method	Full-matrix least-squares on F^2	
Data / restraints / parameters	13857 / 205 / 850	
Goodness-of-fit on F^2	1.051	
Final R indices [I>2sigma(I)]	R1 = 0.0583, wR2 = 0.1482	
R indices (all data)	R1 = 0.0891, wR2 = 0.1646	
Extinction coefficient	n/a	
Largest diff. peak and hole	0.742 and -0.309 e.$Å^{-3}$	

7.2.11. Crystal Data and Structure Refinement for 121a

Identification code	sh3652	
Empirical formula	$C_{118} H_{158} Si_4 \times 4(C_6 H_6)$	
Formula weight	2001.23	
Temperature	132(2) K	
Wavelength	0.71073 Å	
Crystal system	Triclinic	
Space group	P-1	
Unit cell dimensions	a = 19.3602(19) Å	α= 70.157(4)°.
	b = 19.552(2) Å	β= 65.849(4)°.
	c = 20.072(2) Å	γ = 84.962(5)°.
Volume	6509.6(12) $Å^3$	
Z	2	
Density (calculated)	1.021 Mg/m^3	
Absorption coefficient	0.092 mm^{-1}	
F(000)	2180	
Crystal size	0.584 x 0.337 x 0.076 mm^3	
Theta range for data collection	1.109 to 27.357°.	
Index ranges	-24<=h<=23, -25<=k<=25, -25<=l<=25	
Reflections collected	94516	
Independent reflections	28182 [R(int) = 0.1010]	
Completeness to theta = 25.242°	97.7 %	
Absorption correction	Semi-empirical from equivalents	
Max. and min. transmission	0.7455 and 0.6280	
Refinement method	Full-matrix least-squares on F^2	
Data / restraints / parameters	28182 / 349 / 1431	
Goodness-of-fit on F^2	1.410	
Final R indices [I>2sigma(I)]	R1 = 0.1011, wR2 = 0.2391	
R indices (all data)	R1 = 0.2080, wR2 = 0.2650	
Extinction coefficient	n/a	
Largest diff. peak and hole	1.465 and -0.538 $e.Å^{-3}$	

7.2.12. Crystal Data and Structure Refinement for 121d

Identification code	sh3679	
Empirical formula	$C_{116} H_{156} Si_4$ x 6($C_6 H_6$) x 0.5($C_4 H_8 O$)	
Formula weight	2167.46	
Temperature	152(2) K	
Wavelength	0.71073 Å	
Crystal system	Triclinic	
Space group	P-1	
Unit cell dimensions	a = 16.9099(7) Å	α= 89.172(2)°.
	b = 18.3728(8) Å	β= 72.613(2)°.
	c = 23.0313(8) Å	γ = 78.895(2)°.
Volume	6693.5(5) $Å^3$	
Z	2	
Density (calculated)	1.075 Mg/m^3	
Absorption coefficient	0.094 mm^{-1}	
F(000)	2360	
Crystal size	0.822 x 0.706 x 0.168 mm^3	
Theta range for data collection	0.927 to 27.593°.	
Index ranges	-21<=h<=22, -23<=k<=23, -29<=l<=29	
Reflections collected	110354	
Independent reflections	30708 [R(int) = 0.0364]	
Completeness to theta = 25.242°	99.7 %	
Absorption correction	Semi-empirical from equivalents	
Max. and min. transmission	0.7456 and 0.7115	
Refinement method	Full-matrix least-squares on F^2	
Data / restraints / parameters	30708 / 637 / 1590	
Goodness-of-fit on F^2	2.395	
Final R indices [I>2sigma(I)]	R1 = 0.0864, wR2 = 0.2458	
R indices (all data)	R1 = 0.1253, wR2 = 0.2591	
Extinction coefficient	n/a	
Largest diff. peak and hole	1.412 and -0.765 e.$Å^{-3}$	

7.2.13. Crystal Data and Structure Refinement for 123b

Identification code	sh3616	
Empirical formula	$C_{63}H_{88}Si_2 \times C_6H_{14}$	
Formula weight	987.68	
Temperature	163(2) K	
Wavelength	0.71073 Å	
Crystal system	Triclinic	
Space group	P-1	
Unit cell dimensions	a = 12.592(6) Å	α= 91.535(11)°.
	b = 13.694(8) Å	β= 101.63(2)°.
	c = 19.072(11) Å	γ = 101.374(15)°.
Volume	3150(3) $Å^3$	
Z	2	
Density (calculated)	1.041 Mg/m^3	
Absorption coefficient	0.094 mm^{-1}	
F(000)	1088	
Crystal size	0.277 x 0.185 x 0.048 mm^3	
Theta range for data collection	1.093 to 26.498°.	
Index ranges	-15<=h<=15, -17<=k<=17, -23<=l<=23	
Reflections collected	39913	
Independent reflections	12302 [R(int) = 0.1138]	
Completeness to theta = 25.242°	96.0 %	
Absorption correction	Semi-empirical from equivalents	
Max. and min. transmission	0.7454 and 0.6659	
Refinement method	Full-matrix least-squares on F^2	
Data / restraints / parameters	12302 / 183 / 733	
Goodness-of-fit on F^2	1.120	
Final R indices [I>2sigma(I)]	R1 = 0.0886, wR2 = 0.1774	
R indices (all data)	R1 = 0.2080, wR2 = 0.2184	
Extinction coefficient	0.0101(10)	
Largest diff. peak and hole	0.439 and -0.363 e.$Å^{-3}$	

7.2.14. Crystal Data and Structure Refinement for 124b

Identification code	sh3653	
Empirical formula	$C_{132} H_{170} Si_4$	
Formula weight	1869.03	
Temperature	132(2) K	
Wavelength	0.71073 Å	
Crystal system	Triclinic	
Space group	P-1	
Unit cell dimensions	a = 12.9721(13) Å	α= 108.415(6)°.
	b = 15.0516(15) Å	β= 93.488(6)°.
	c = 15.2149(15) Å	γ = 92.687(6)°.
Volume	2806.5(5) $Å^3$	
Z	1	
Density (calculated)	1.106 Mg/m^3	
Absorption coefficient	0.102 mm^{-1}	
F(000)	1018	
Crystal size	0.315 x 0.161 x 0.040 mm^3	
Theta range for data collection	1.415 to 27.237°.	
Index ranges	-16<=h<=16, -19<=k<=17, -19<=l<=19	
Reflections collected	42459	
Independent reflections	12372 [R(int) = 0.0562]	
Completeness to theta = 25.242°	99.2 %	
Absorption correction	Semi-empirical from equivalents	
Max. and min. transmission	0.7455 and 0.6844	
Refinement method	Full-matrix least-squares on F^2	
Data / restraints / parameters	12372 / 0 / 953	
Goodness-of-fit on F^2	1.008	
Final R indices [I>2sigma(I)]	R1 = 0.0475, wR2 = 0.0963	
R indices (all data)	R1 = 0.0864, wR2 = 0.1115	
Extinction coefficient	n/a	
Largest diff. peak and hole	0.325 and -0.328 e.$Å^{-3}$	

7.2.15. Crystal Data and Structure Refinement for 125

Identification code	sh3764	
Empirical formula	$C_{67} H_{84} Si_2$ x 0.5($C_6 H_6$)	
Formula weight	984.57	
Temperature	142(2) K	
Wavelength	0.71073 Å	
Crystal system	Monoclinic	
Space group	$P2_1/c$	
Unit cell dimensions	a = 11.0117(7) Å	α= 90°.
	b = 20.9190(12) Å	β= 96.136(2)°.
	c = 26.6418(14) Å	γ = 90°.
Volume	6101.9(6) $Å^3$	
Z	4	
Density (calculated)	1.072 Mg/m^3	
Absorption coefficient	0.097 mm^{-1}	
F(000)	2140	
Crystal size	0.465 x 0.159 x 0.146 mm^3	
Theta range for data collection	1.240 to 26.422°.	
Index ranges	-13<=h<=13, -26<=k<=24, -33<=l<=32	
Reflections collected	91650	
Independent reflections	12533 [R(int) = 0.0393]	
Completeness to theta = 25.242°	100.0 %	
Absorption correction	Semi-empirical from equivalents	
Max. and min. transmission	0.7454 and 0.7077	
Refinement method	Full-matrix least-squares on F^2	
Data / restraints / parameters	12533 / 14 / 656	
Goodness-of-fit on F^2	1.051	
Final R indices [I>2sigma(I)]	R1 = 0.0495, wR2 = 0.1244	
R indices (all data)	R1 = 0.0658, wR2 = 0.1318	
Extinction coefficient	n/a	
Largest diff. peak and hole	0.751 and -0.522 e.$Å^{-3}$	

7.3. Absorption Spectra

7.3.1. UV/vis Spectra and Determination of ε for 94

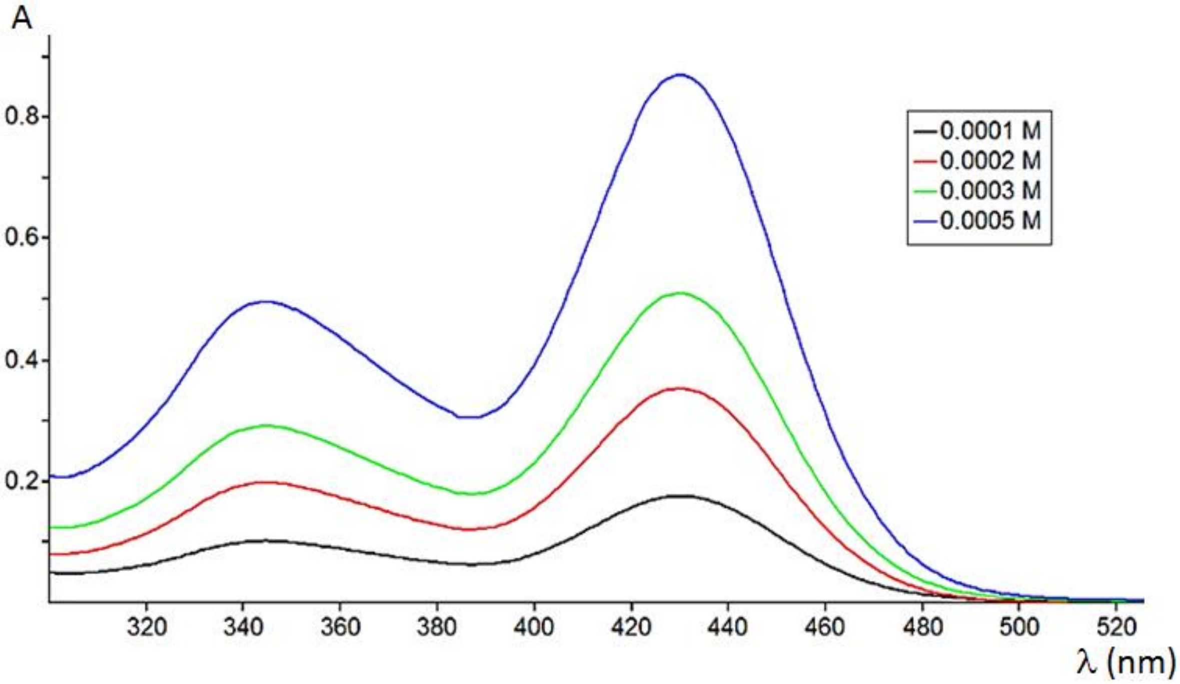

Figure 113. UV/vis (d = 1 mm) in hexane spectra of **94.**

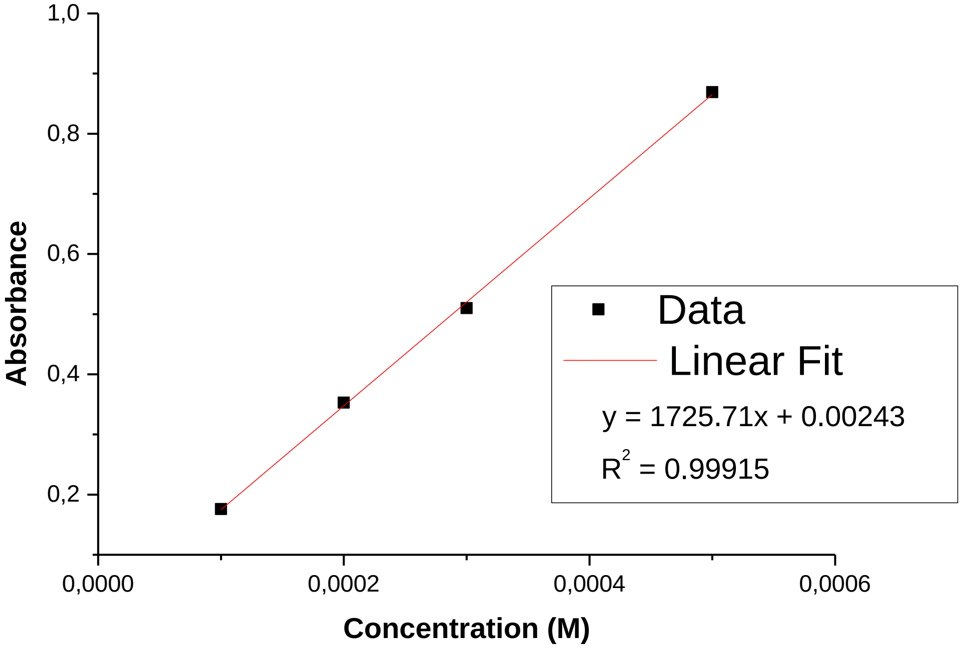

Figure 114. Linear fit for UV/vis data of **94** for (λ = 430 nm).

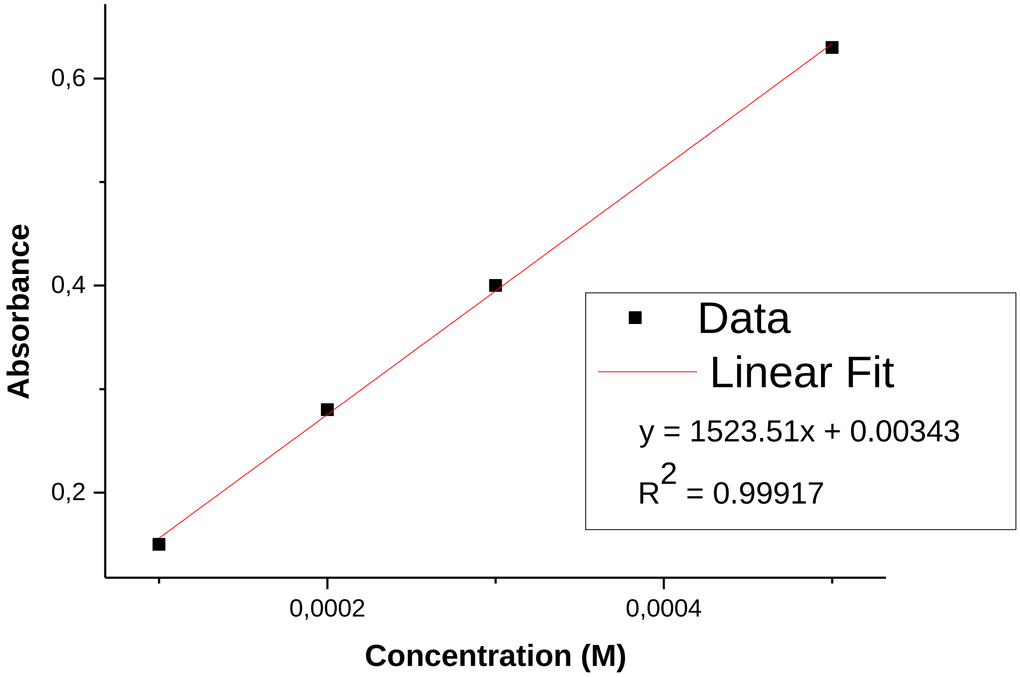

Figure 115. Linear fit for UV/vis data of **94** for (λ = 335 nm).

7.3.2. UV/vis Spectra and Determination of ε for 96

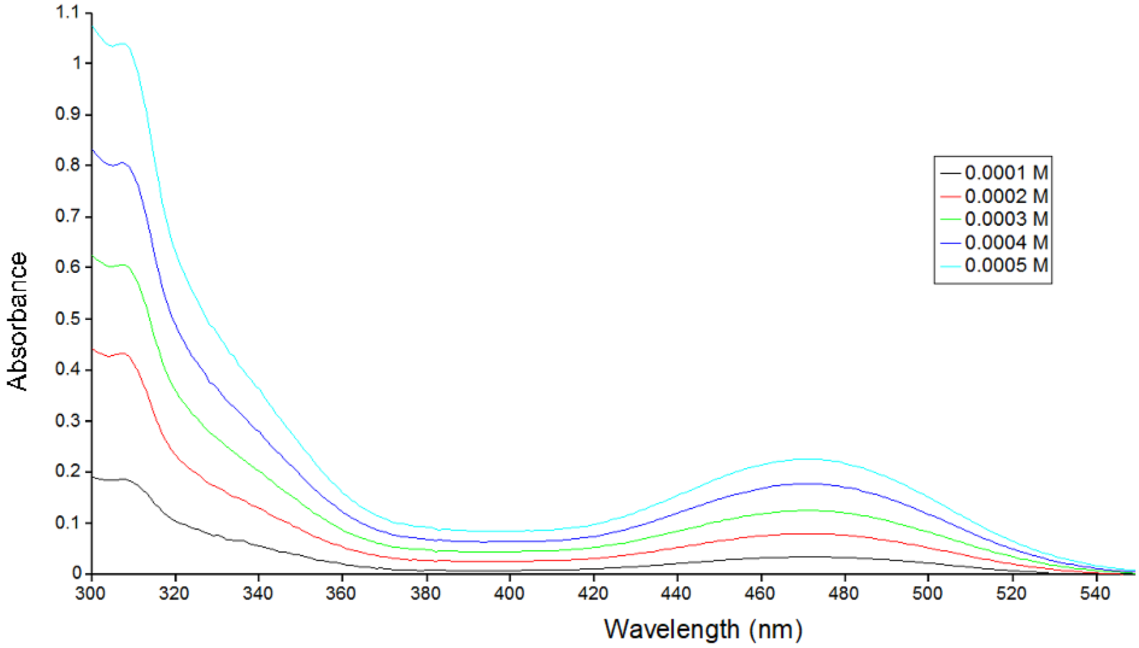

Figure 116. UV/vis (d = 1 mm) in hexane spectra of **96**.

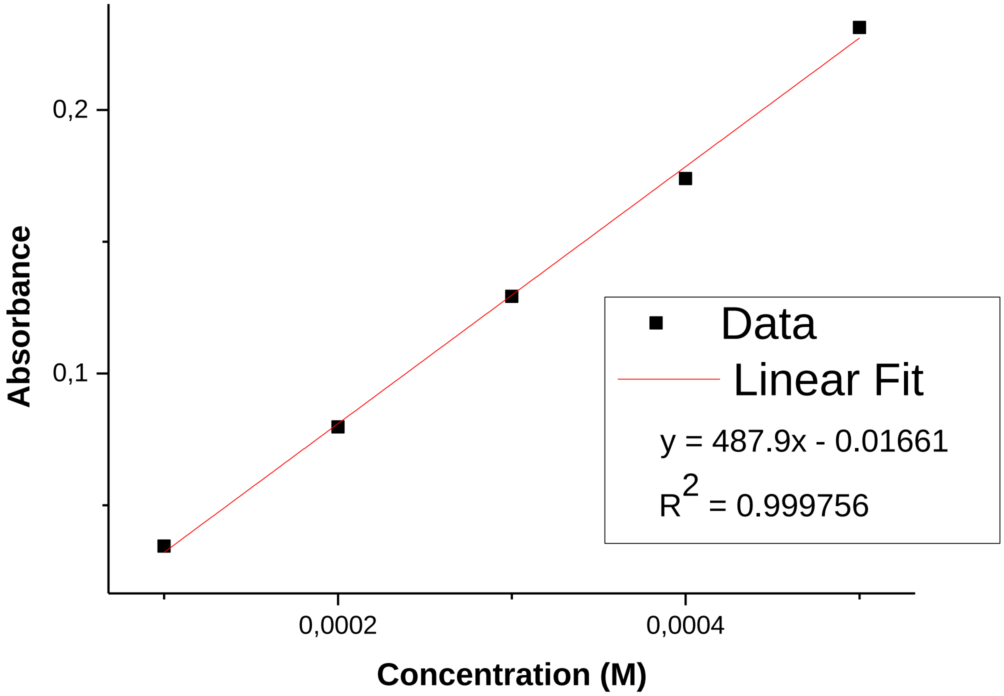

Figure 117. Linear fit for UV/vis data of **96** for (λ = 472 nm).

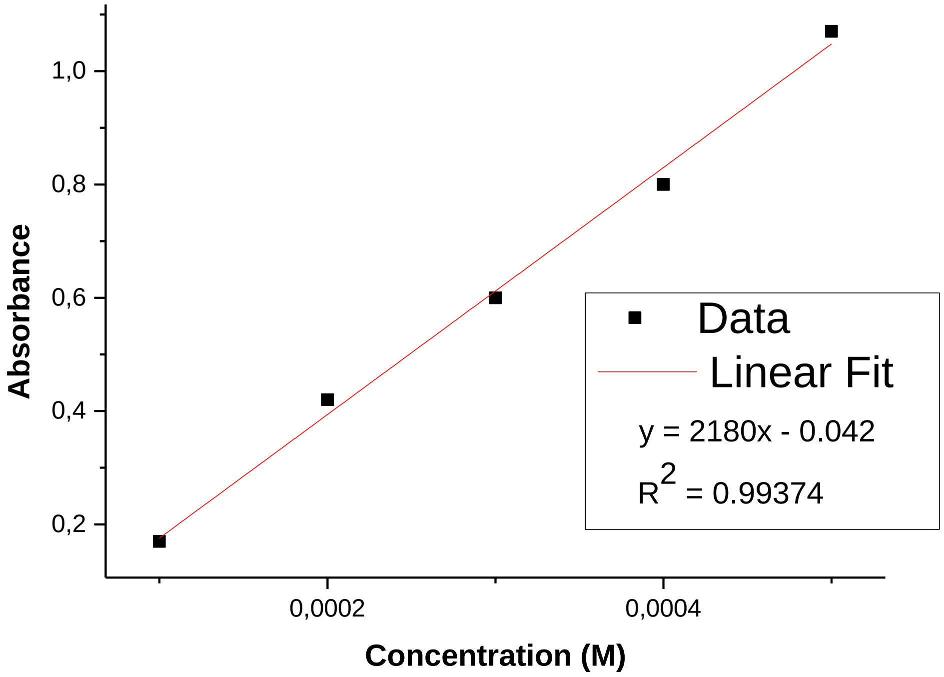

Figure 118. Linear fit for UV/vis data of **96** for (λ = 309 nm).

7.3.3. UV/vis Spectra and Determination of ε for 98

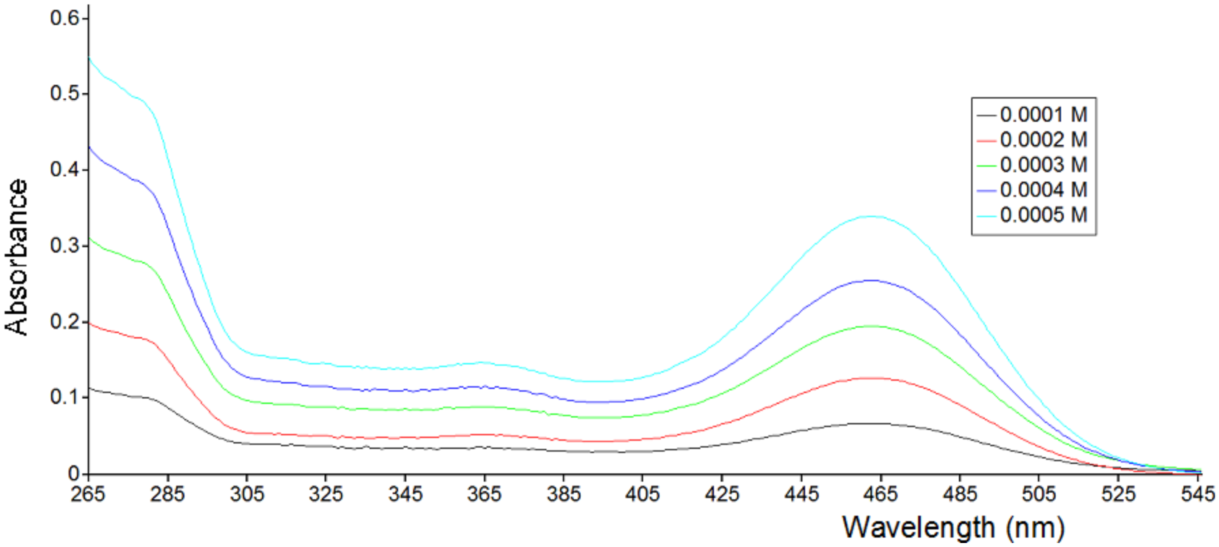

Figure 119. UV/vis (d = 1 mm) in hexane spectra of **98.**

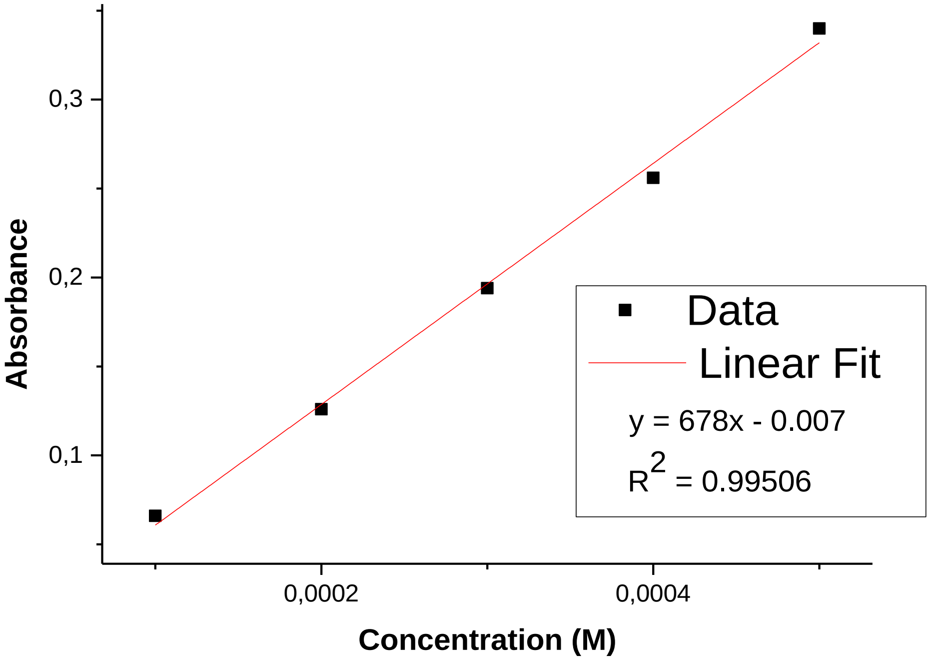

Figure 120. Linear fit for UV/vis data of **98.**

7.3.4. UV/vis Spectra and Determination of ε for 100

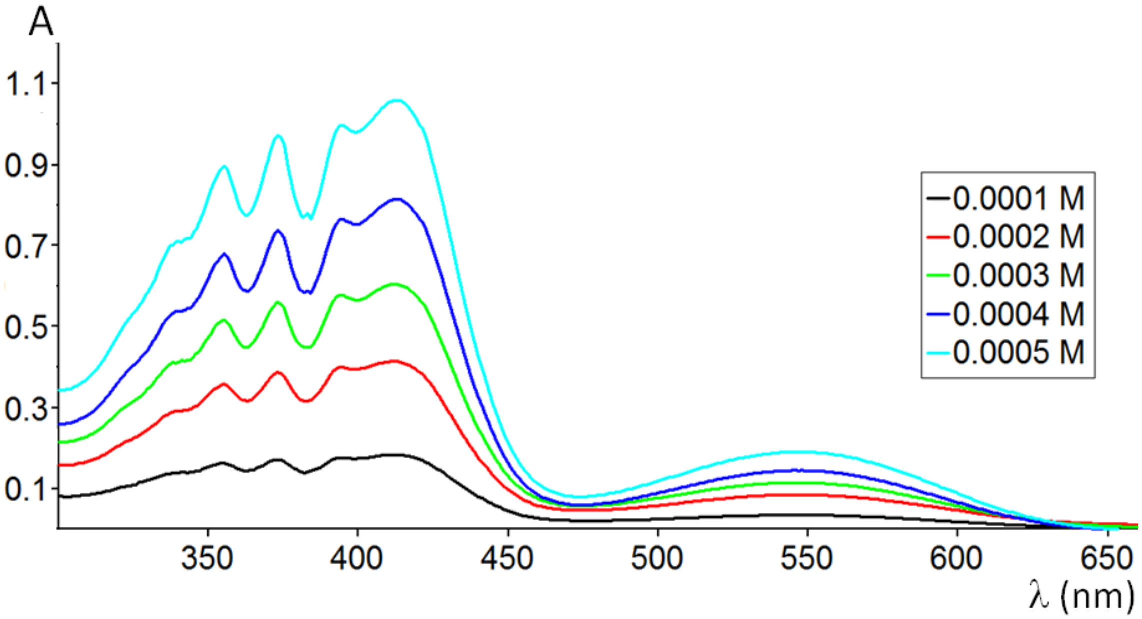

Figure 121. UV/vis (d = 1 mm) of 100 recorded in hexane.

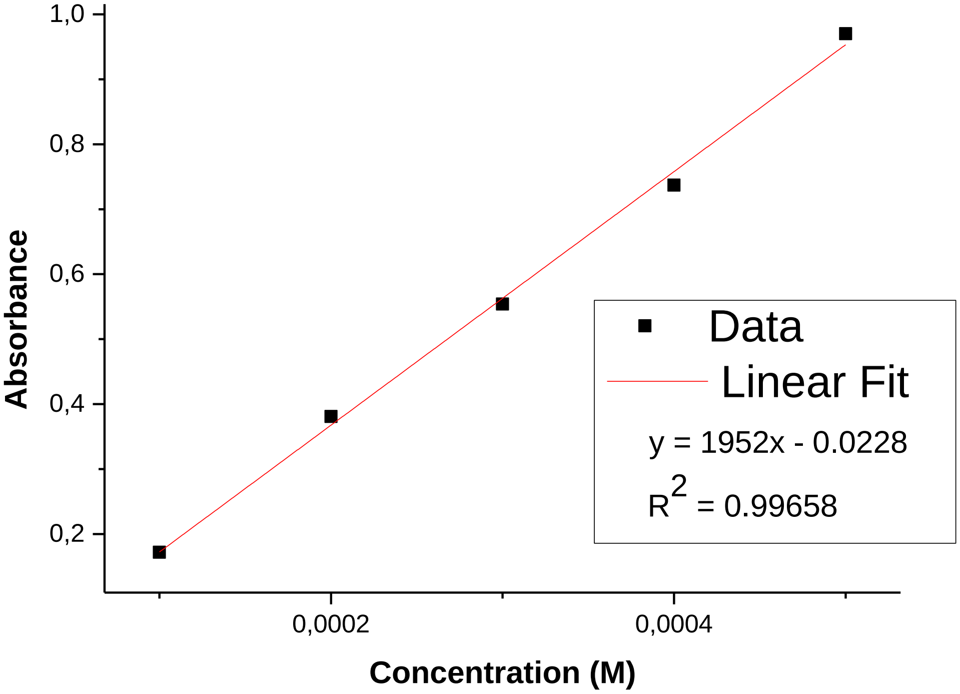

Figure 122. Linear fit for UV/vis data of **100** (λ = 373 nm).

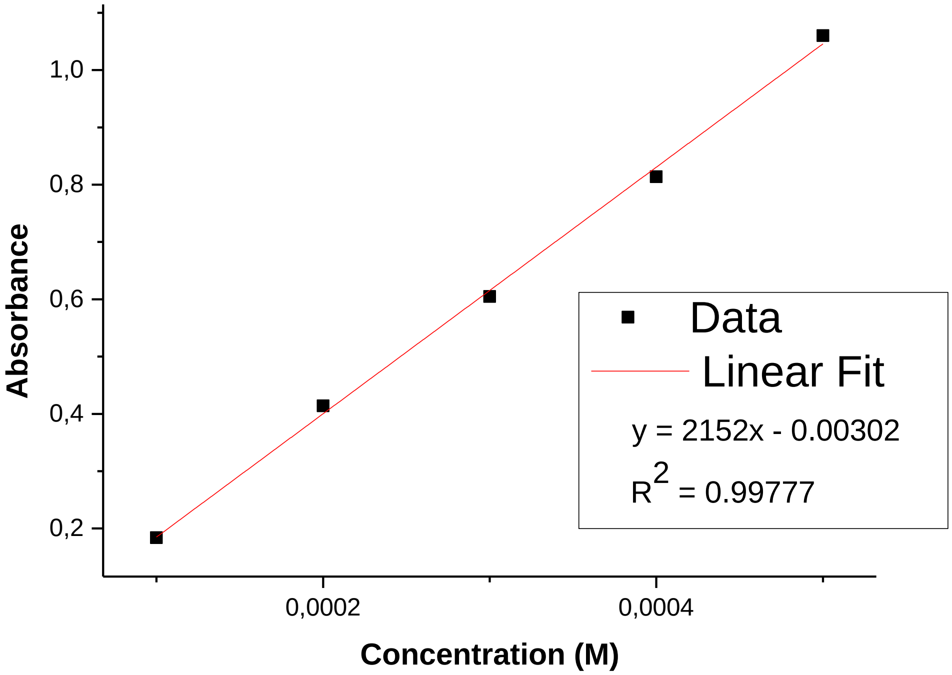

Figure 123. Linear fit for UV/vis data of **100** (λ = 412 nm).

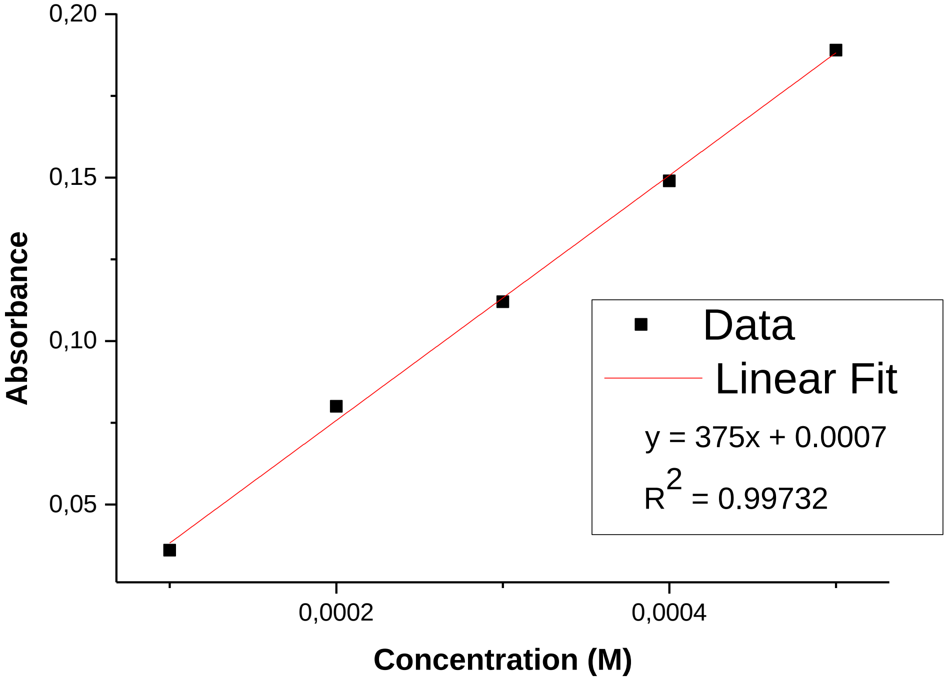

Figure 124. Linear fit for UV/vis data of **100** (λ = 550 nm).

7.3.5. UV/vis Spectra and Determination of ε for 102

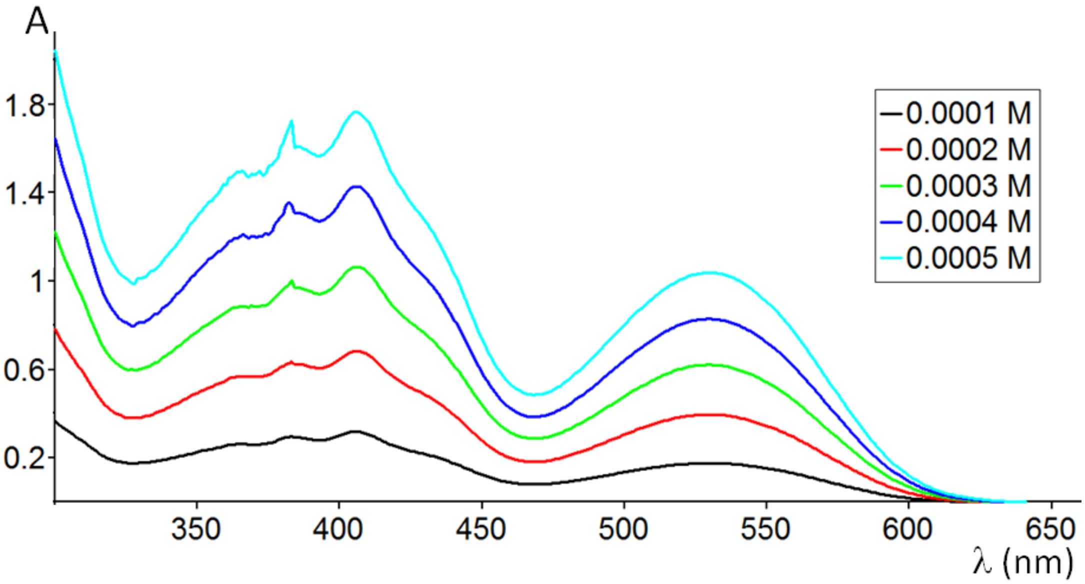

Figure 125. UV/vis (d = 1 mm) of **102** recorded in hexane.

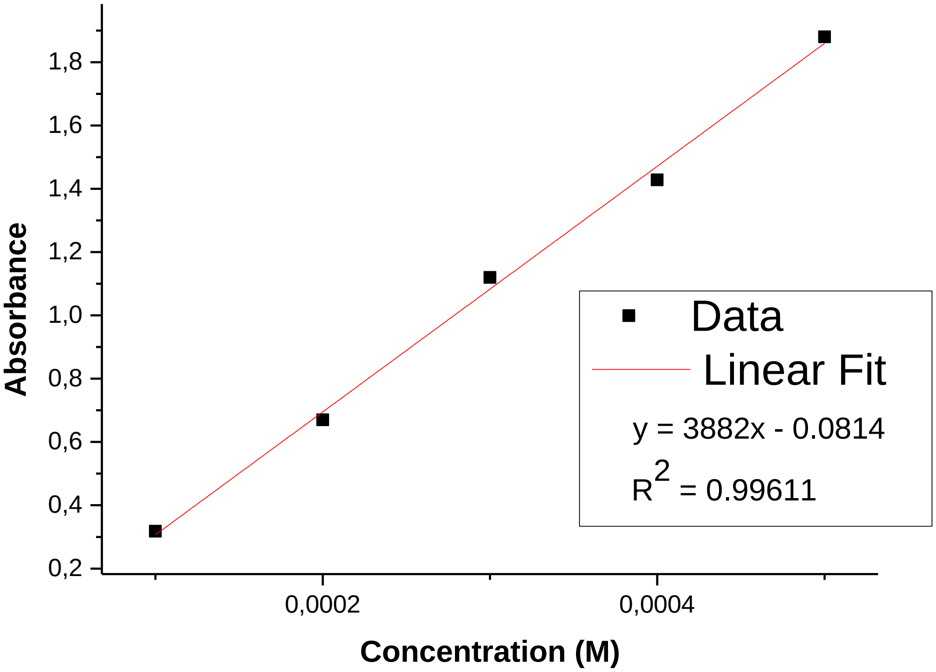

Figure 126. Linear fit for UV/vis data of **102** (λ = 406 nm).

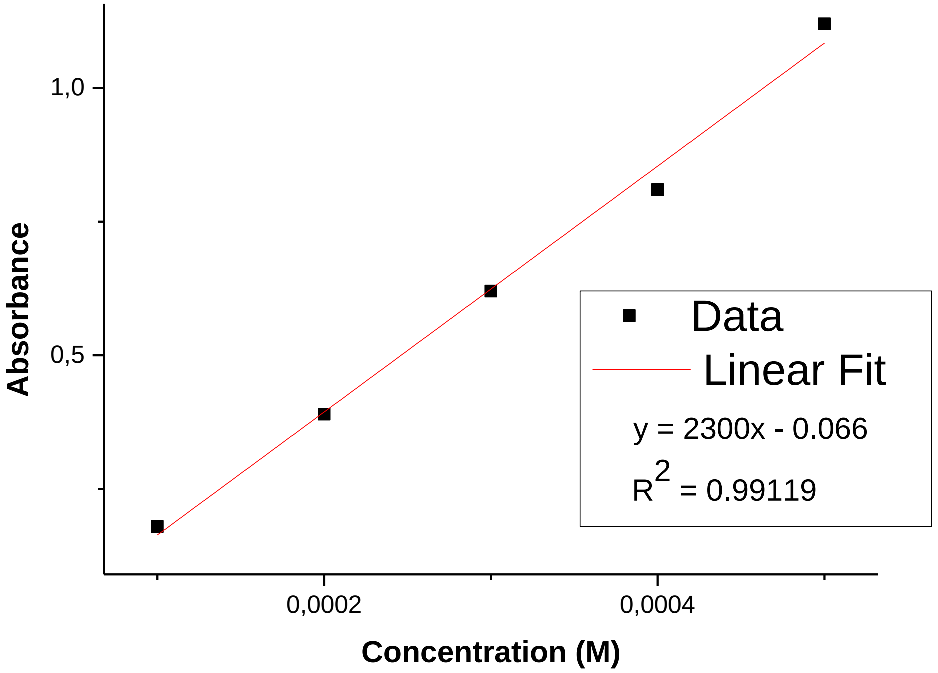

Figure 127. Linear fit for UV/vis data of **102** (λ = 530 nm).

7.3.6. UV/vis Spectra and Determination of ε for 104

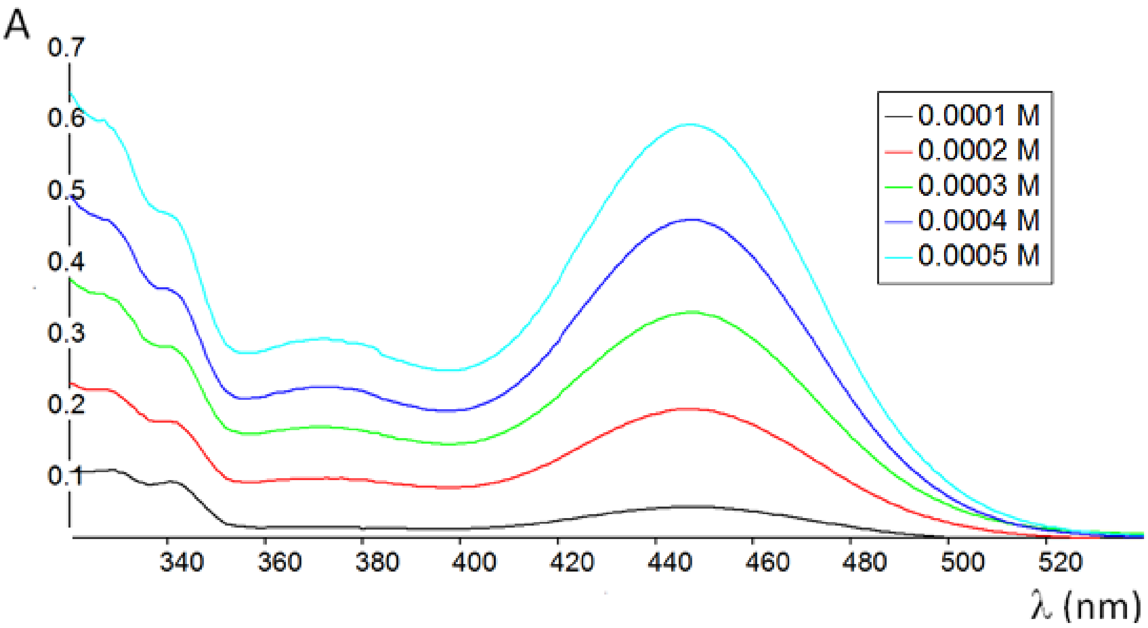

Figure 128. UV/vis (d = 1 mm) of **104** recorded in hexane.

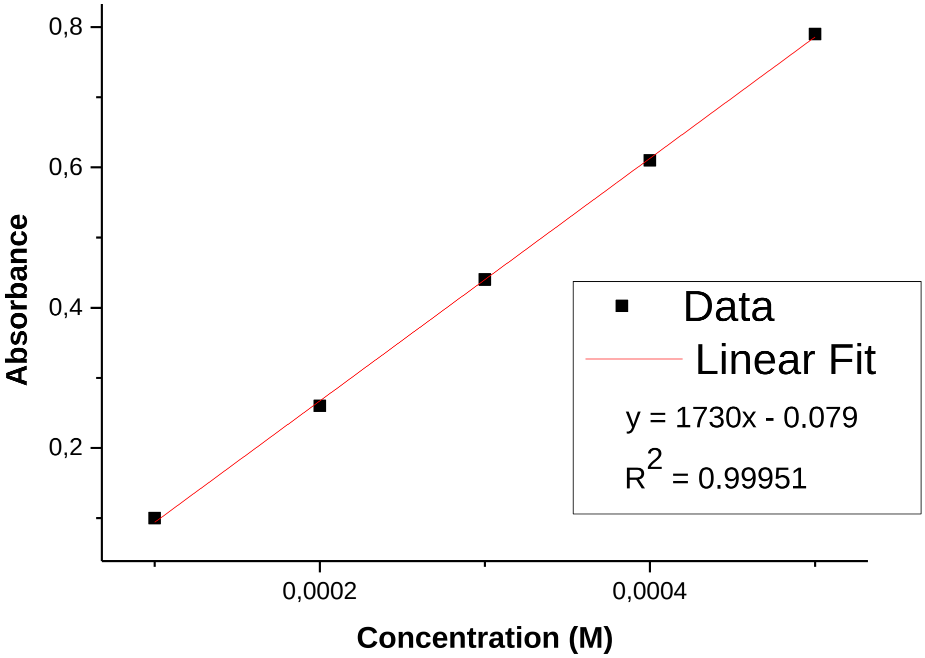

Figure 129. Linear fit for UV/vis data of **104.**

7.3.7. UV/vis Spectra and Determination of ε for 106

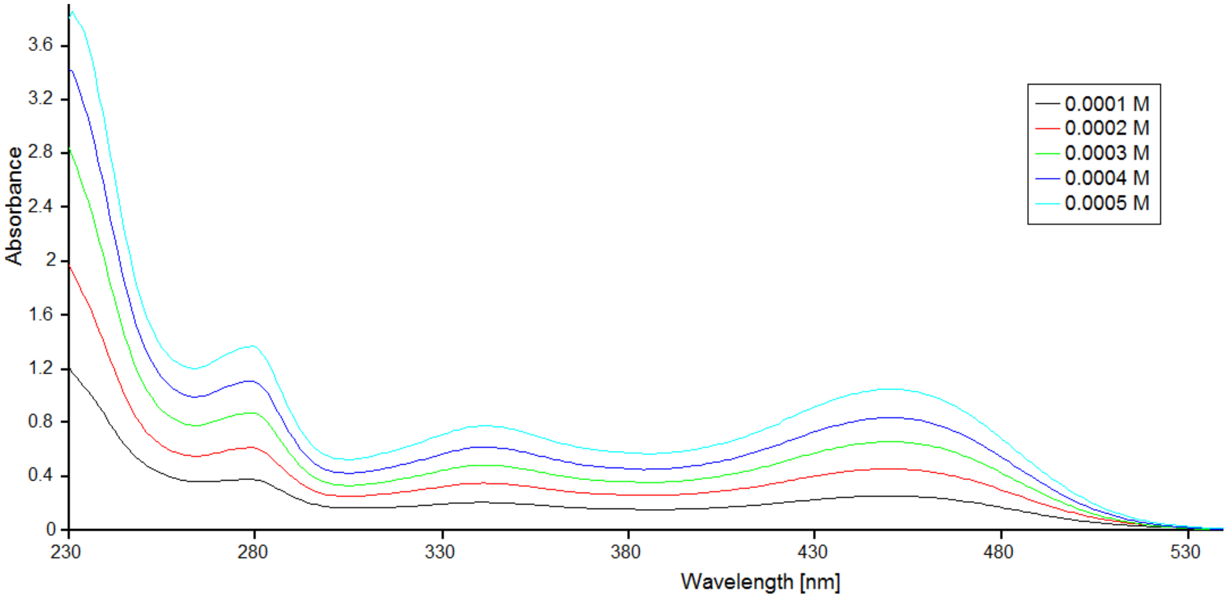

Figure 130. UV/vis (d = 1 mm) of 106 recorded in hexane.

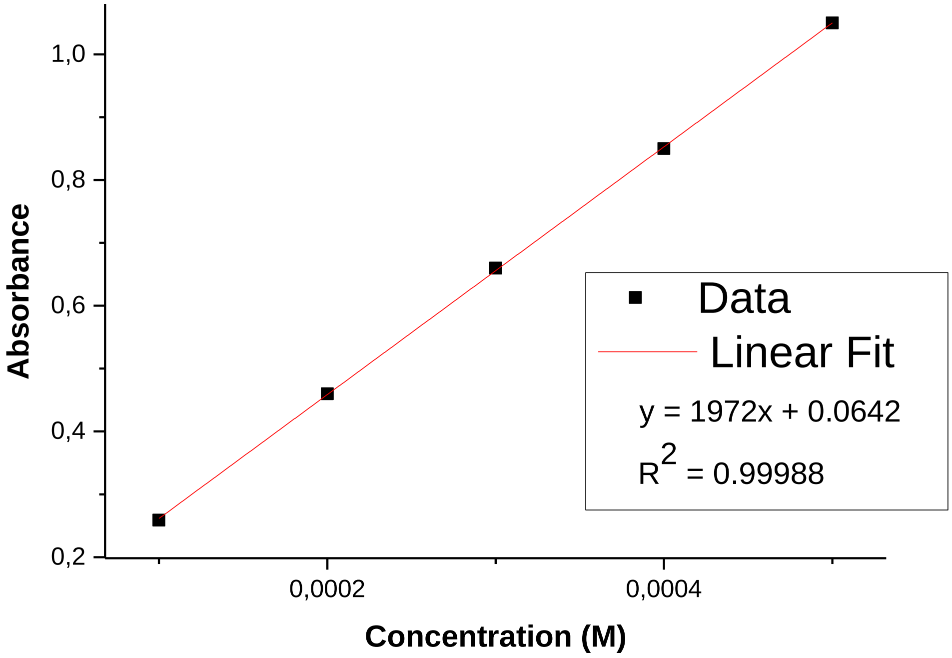

Figure 131. Linear fit for UV/vis data of **106** (λ = 450 nm).

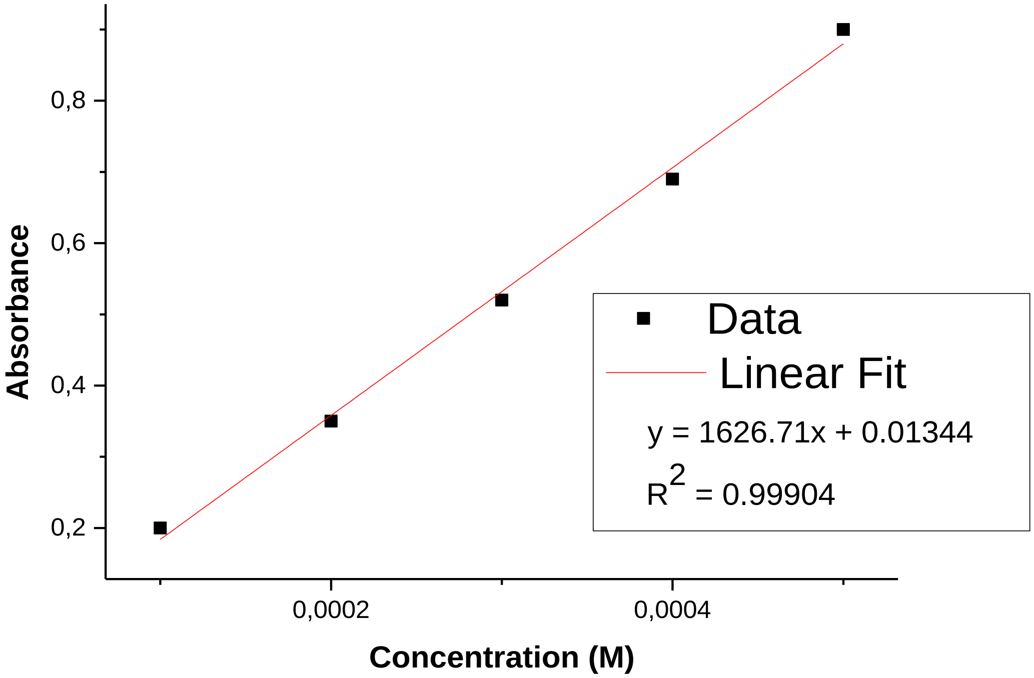

Figure 132. Linear fit for UV/vis data of **106** (λ = 335 nm).

7.3.8. UV/vis Spectra and Determination of ε for 108

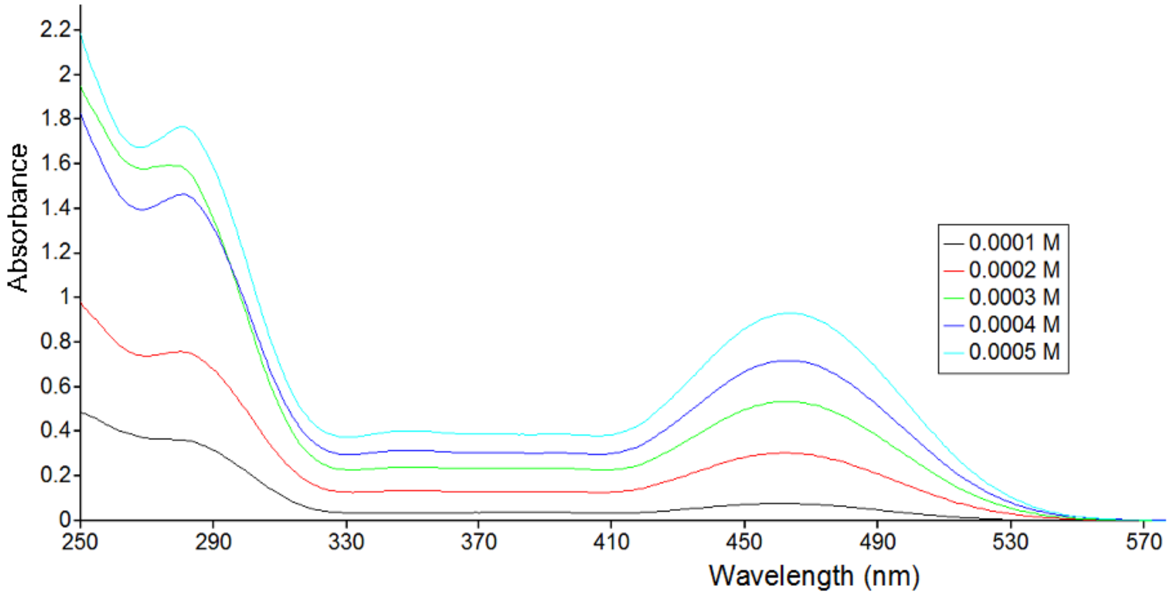

Figure 133. UV/vis (d = 1 mm) in hexane spectra of **108.**

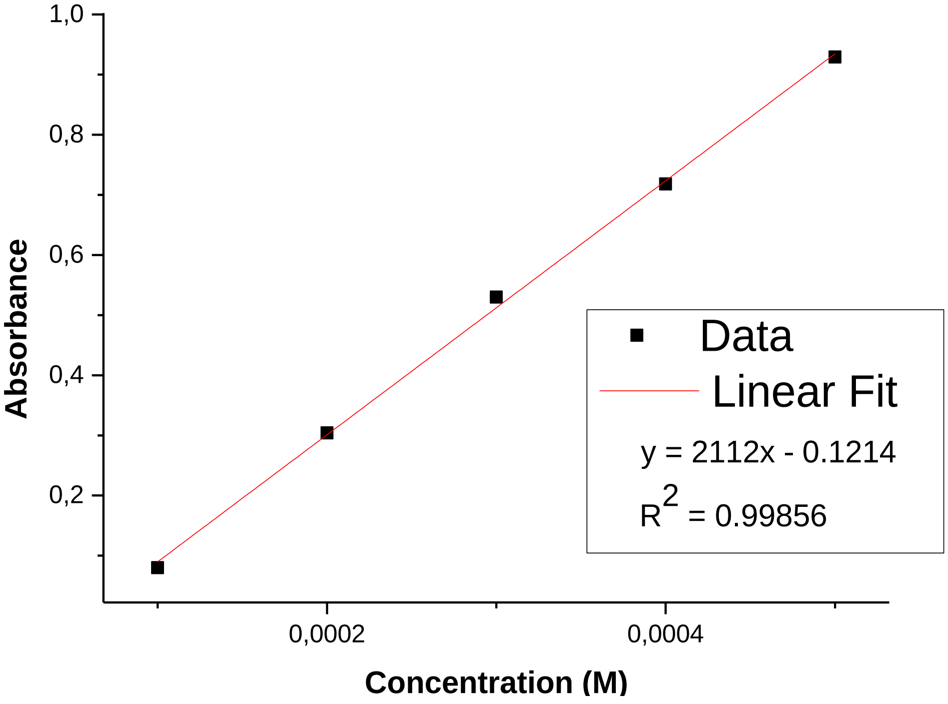

Figure 134. Linear fit for UV/vis data of **108** for (λ = 463 nm).

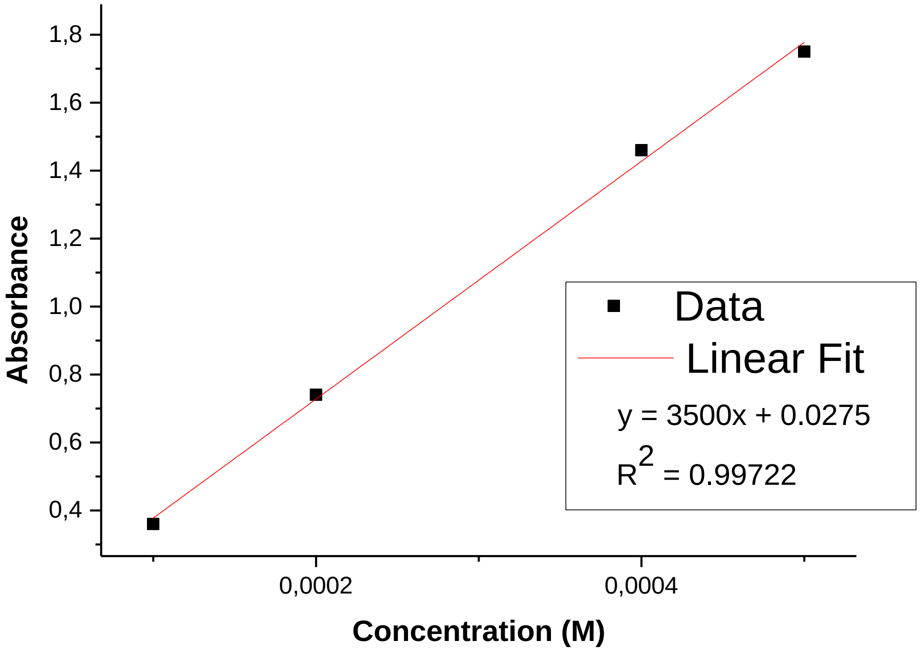

Figure 135. Linear fit for UV/vis data of **108** for (λ = 227 nm).

7.3.9. UV/vis Spectra and Determination of ε for 110

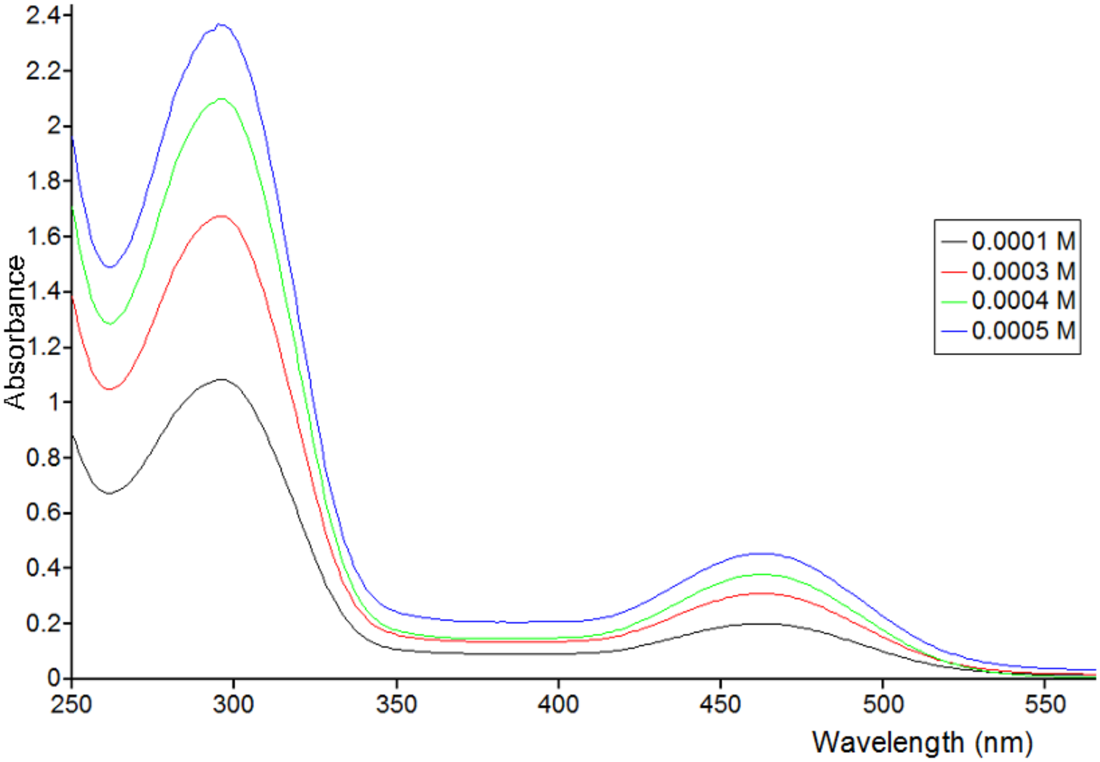

Figure 136. UV/vis (d = 1 mm) in hexane spectra of **110.**

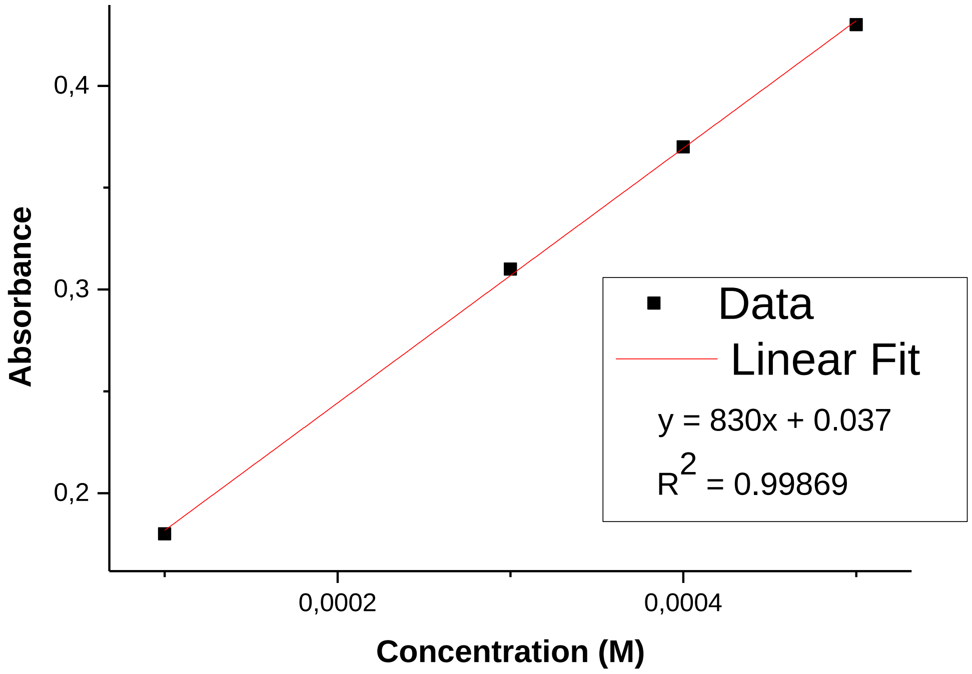

Figure 137. Linear fit for UV/ Vis data of **110** for (λ = 463 nm).

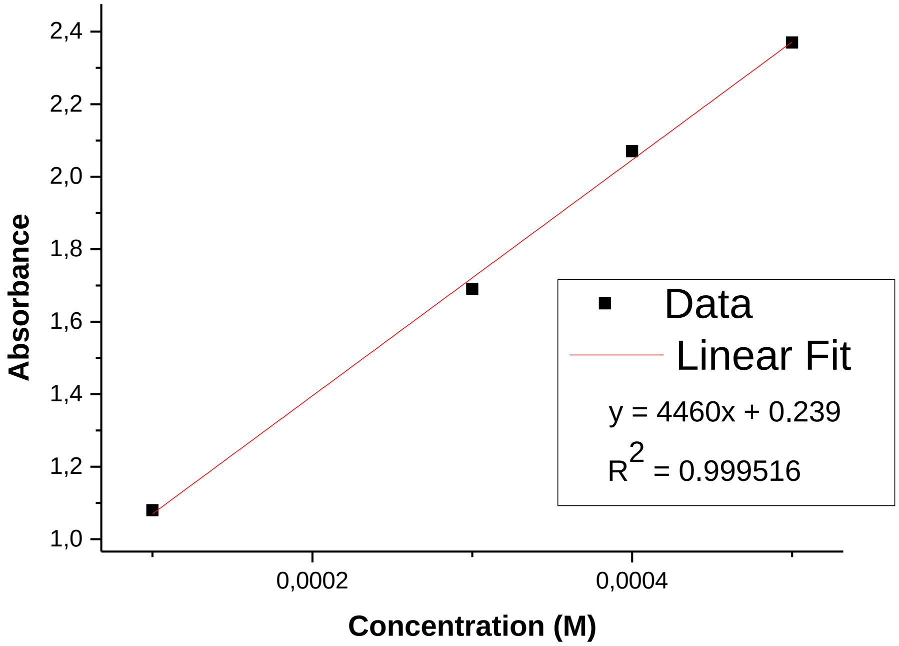

Figure 138. Linear fit for UV/vis data of **110** for (λ = 296 nm).

7.3.10. UV/vis Spectra and Determination of ε for 112

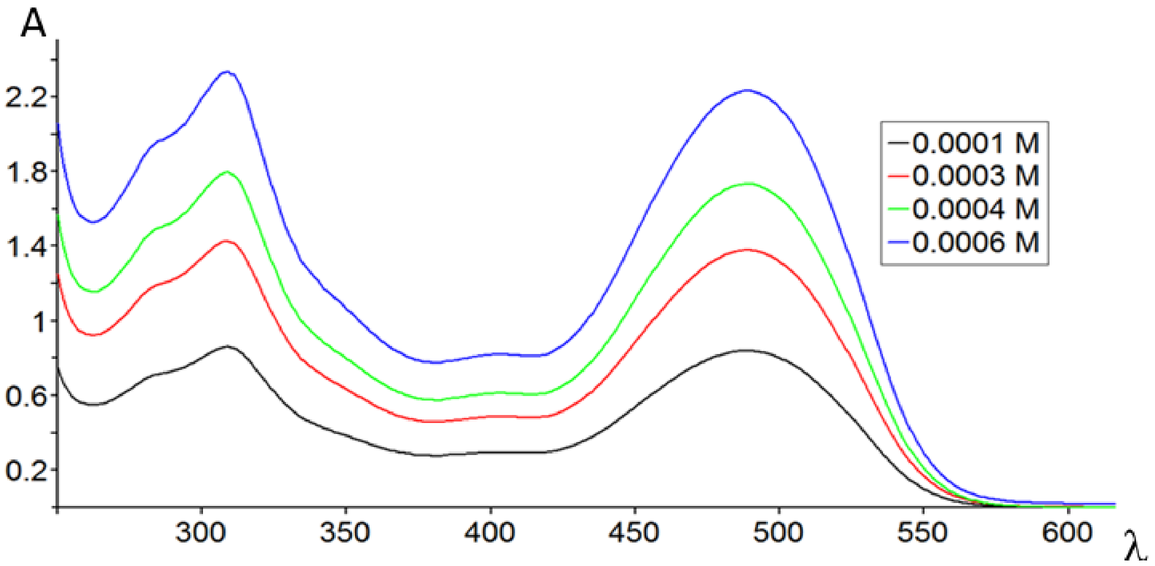

Figure 139. UV/vis (d = 1 mm) in hexane spectra of **112.**

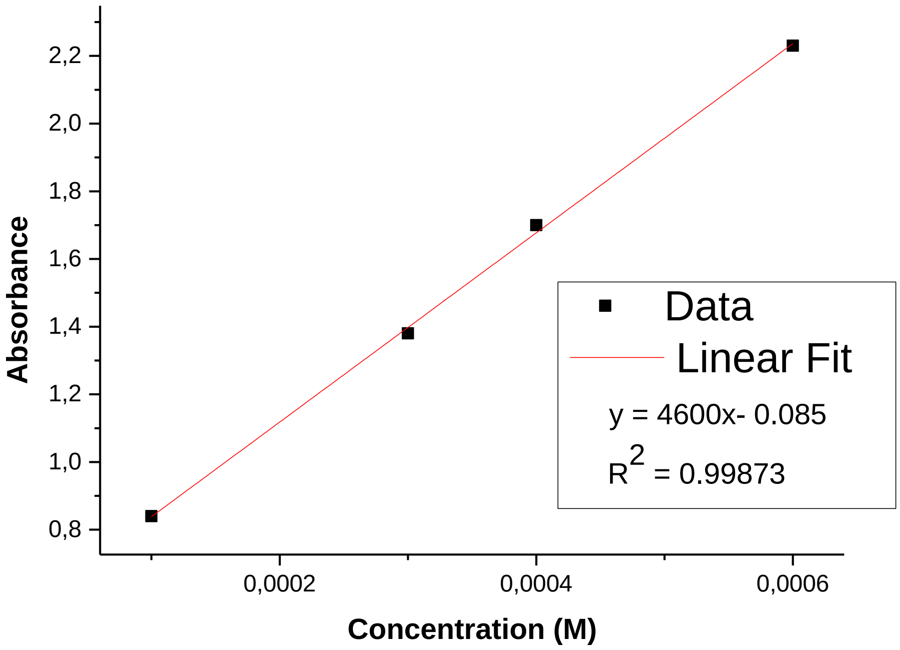

Figure 140. Linear fit for UV/vis data of **112** for (λ = 488 nm).

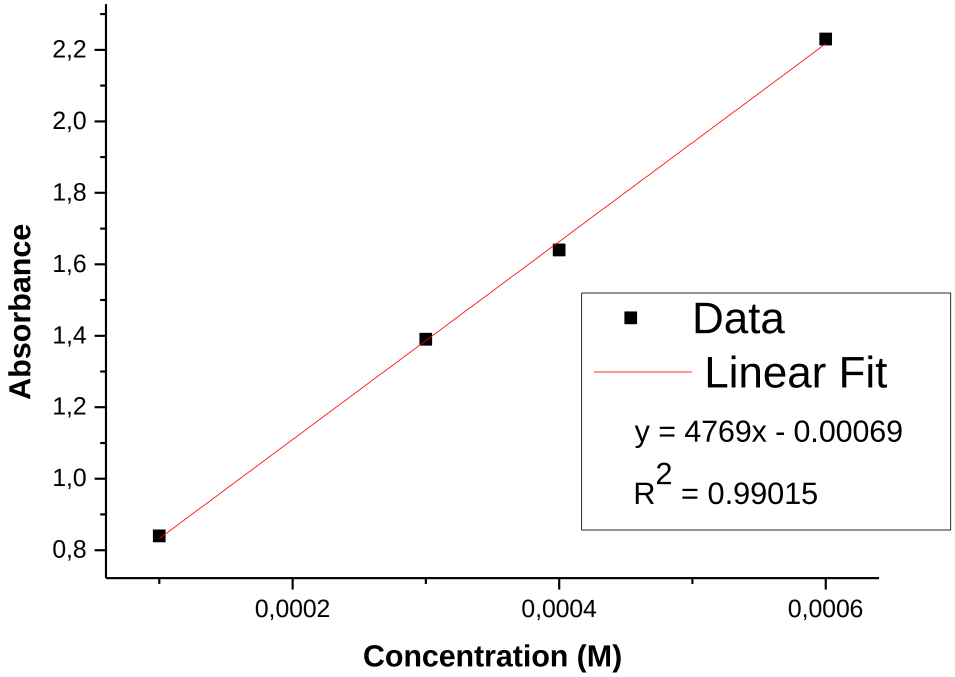

Figure 141. Linear fit for UV/vis data of **112** for (λ = 309 nm).

7.3.11. UV/vis Spectra and Determination of ε for 114

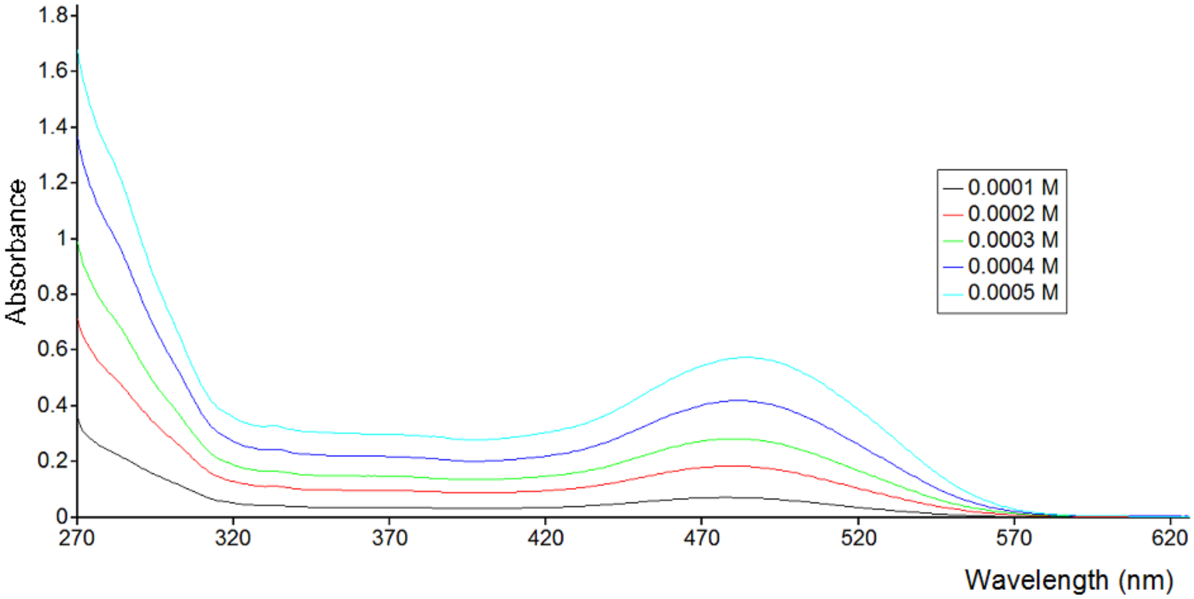

Figure 142. UV/vis (d = 1 mm) in hexane spectra of **114.**

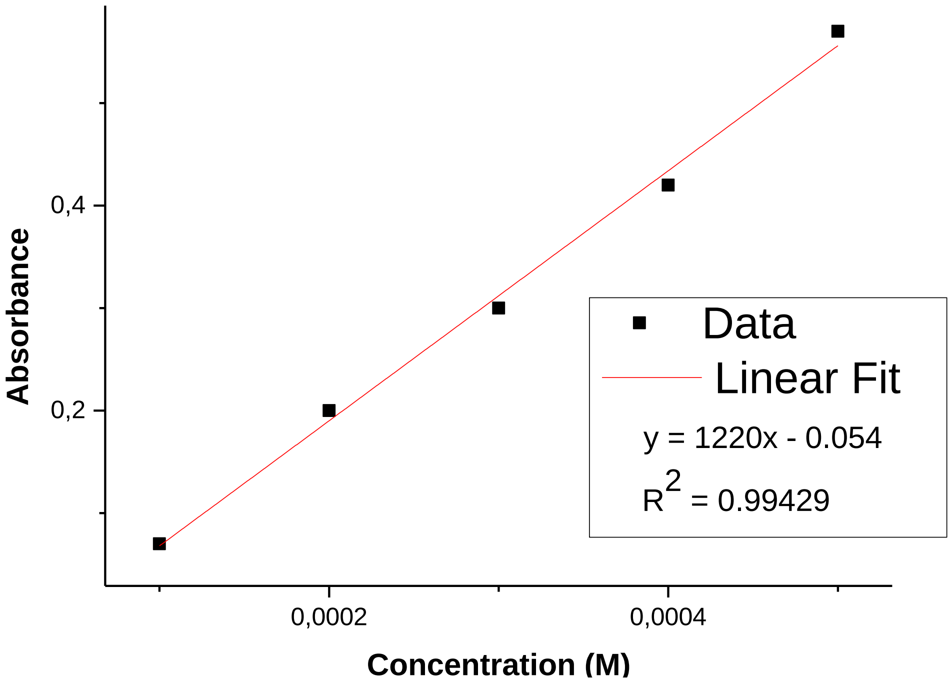

Figure 143. Linear fit for UV/vis data of **114.**

7.3.12. UV/vis Spectra and Determination of ε for 116

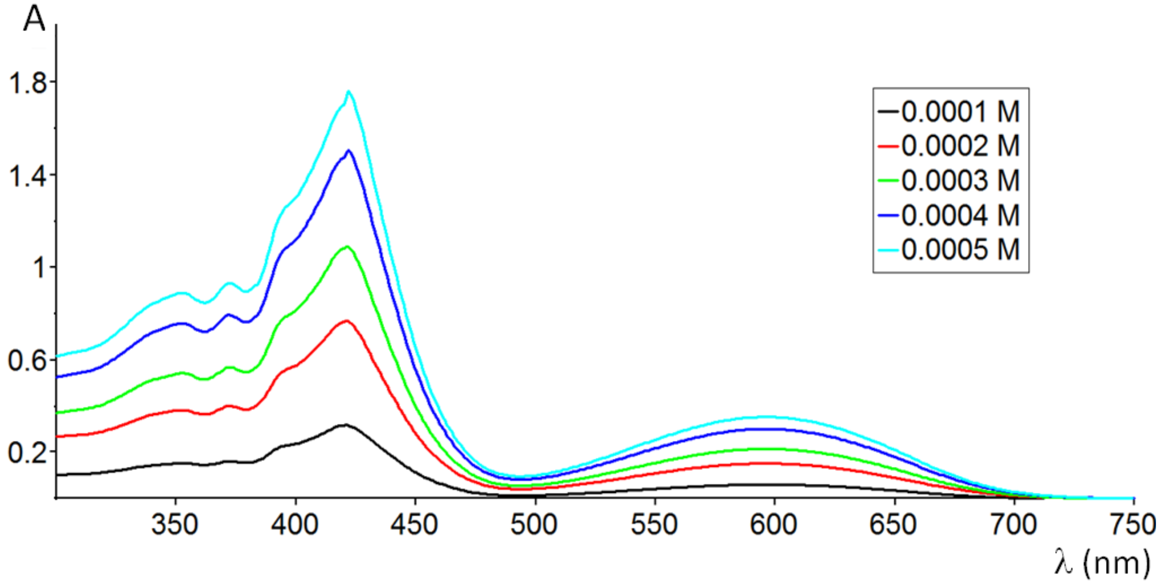

Figure 144. UV/vis (d = 1 mm) of **116** recorded in hexane.

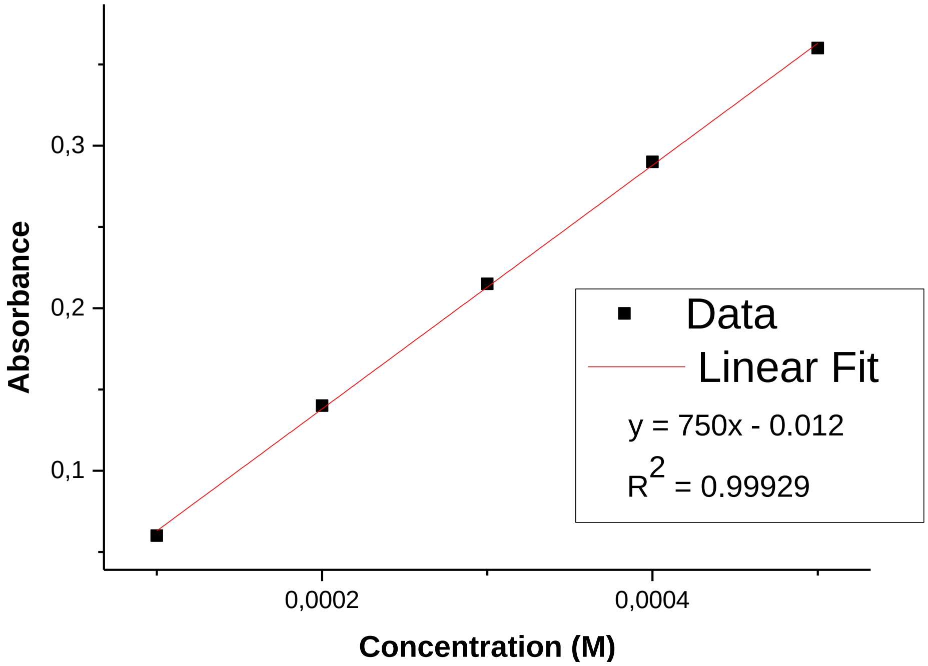

Figure 145. Linear fit for UV/vis data of **116** (λ = 597 nm).

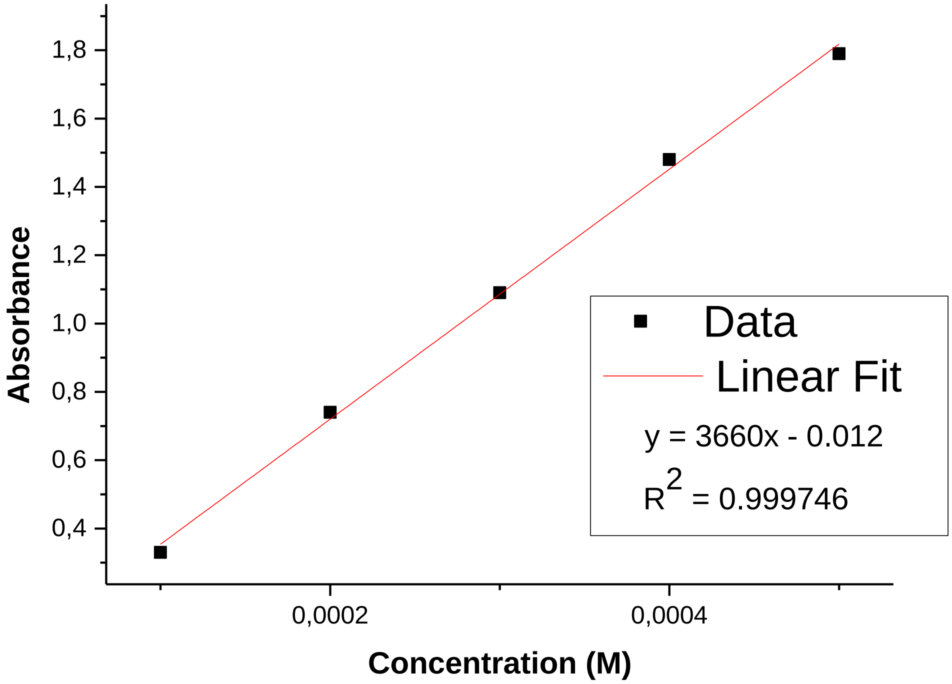

Figure 146. Linear fit for UV/vis data of **116** (λ = 422 nm).

7.3.13. UV/vis Spectra and Determination of ε for 118

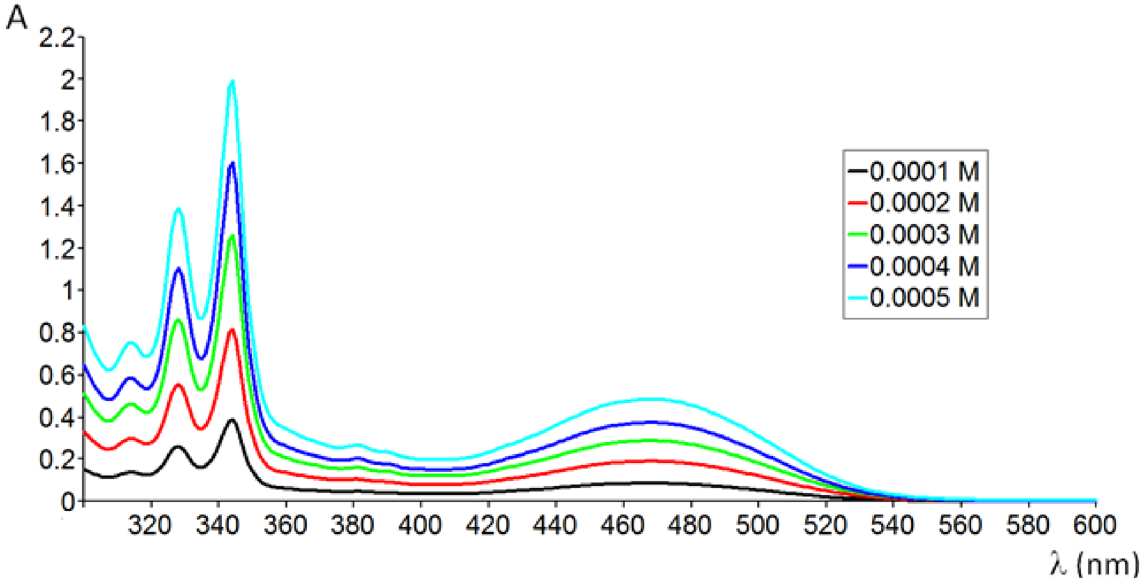

Figure 147. UV/vis (d = 1 mm) in hexane spectra of **119*.***

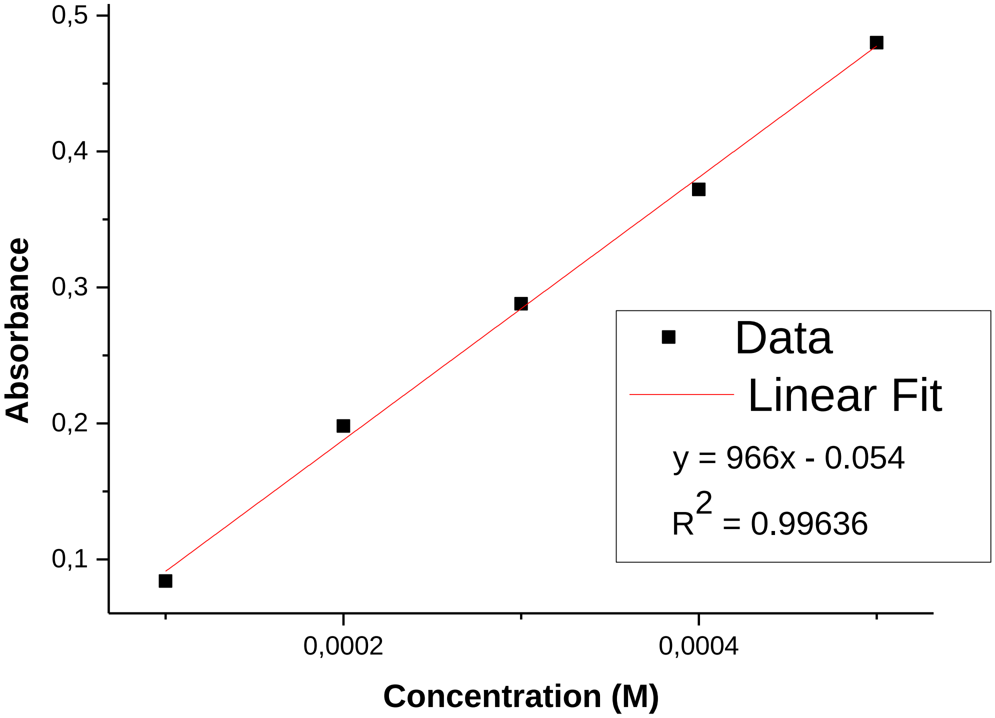

Figure 148. Linear fit for UV/vis data of **119** (λ = 470 nm).

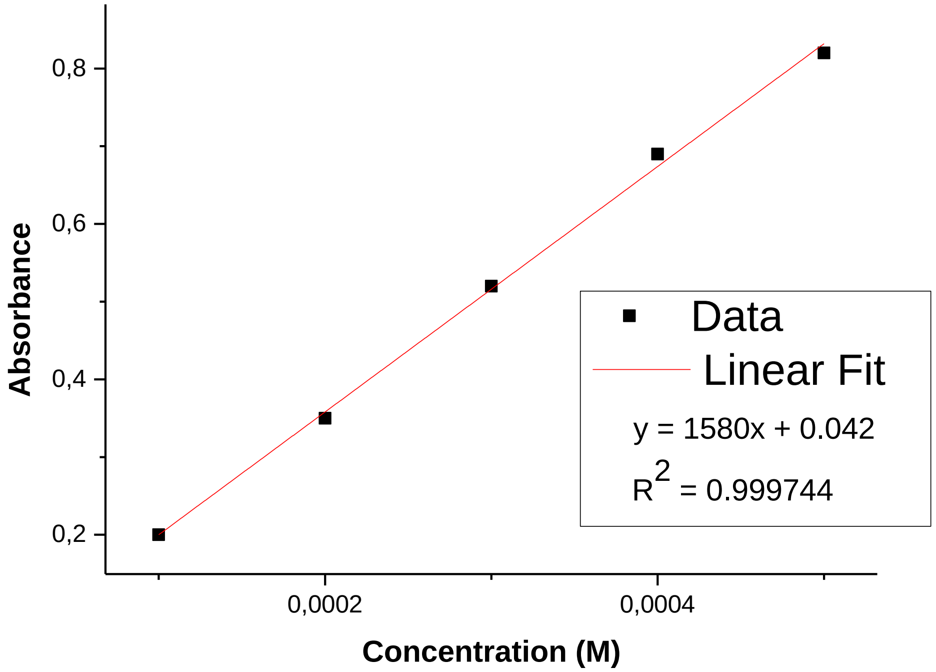

Figure 149. Linear fit for UV/vis data of **119** (λ = 315 nm).

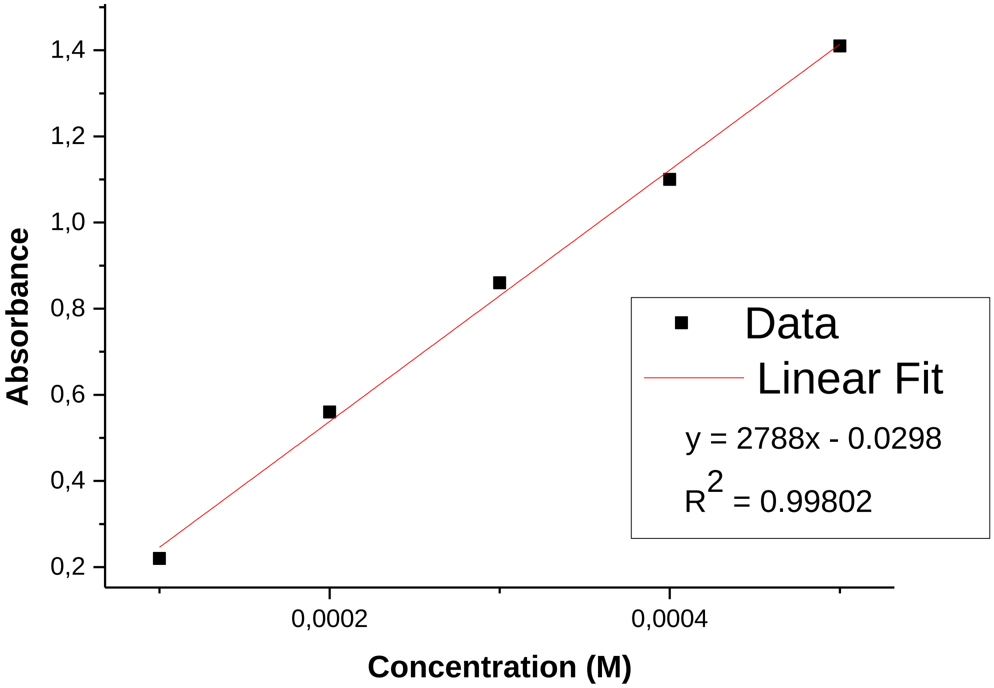

Figure 150. Linear fit for UV/vis data of **119** (λ = 328 nm).

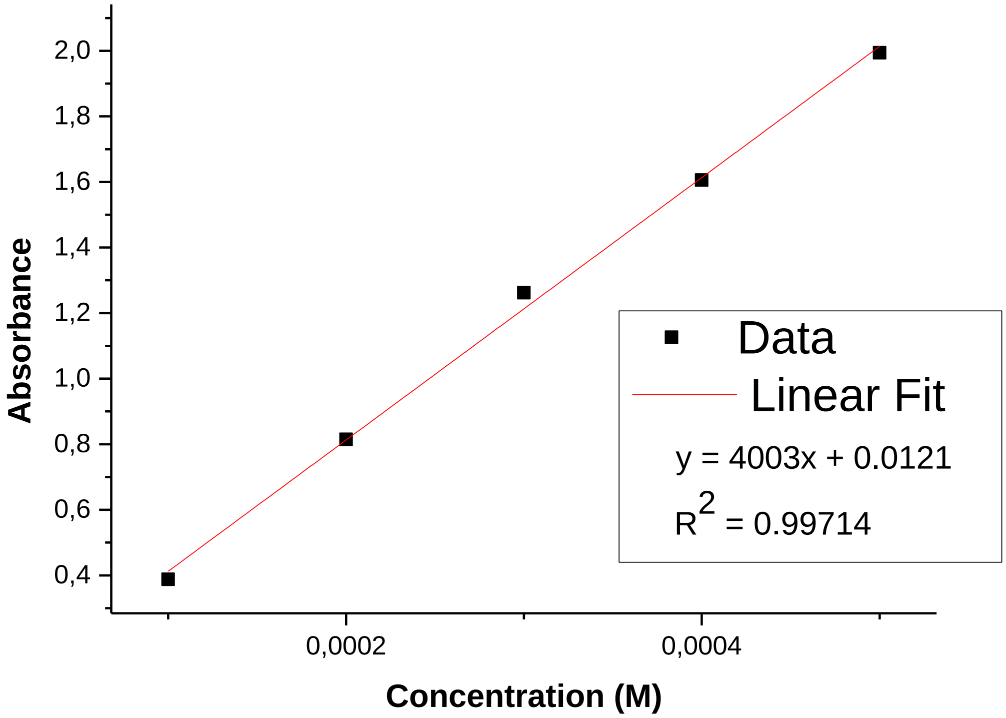

Figure 151. Linear fit for UV/vis data of **119** (λ = 344 nm).

7.4. DFT Calculations

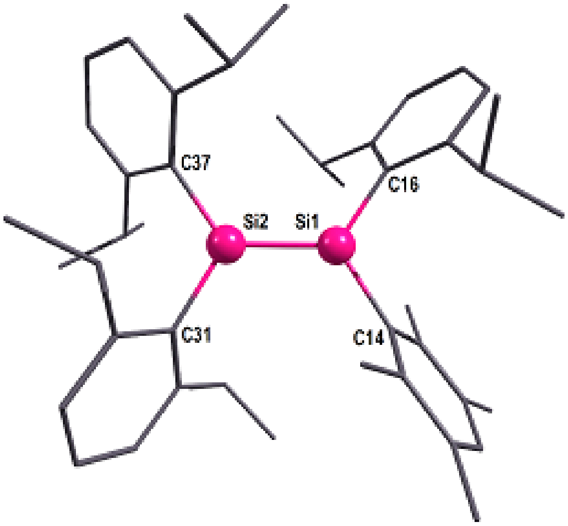

Bond lengths (Pm):	
Si1-Si2	216.75(5)
Si1-C14	190.70(8)
Si1-C16	190.99(1)
Si2-C31	191.67(4)
Si2-C37	191.55(6)

Bond Angles (°):	
Si2-Si1-C14	121.46(4)
Si2-Si1-C16	124.67(5)
Si1-Si2-C31	120.89(3)
Si1-Si2-C37	123.77(0)
Σ°(Si1)	359.95(5)
Σ°(Si2)	360.0(0)
θ(Si1)	1.97(1)
θ(Si2)	0.25(9)
τ	2.37(8)

Deviation from planarity (°):	
(Si1-Si2)-Duryl	59.26(6)

Figure 152. Optimized structure of **94Dip** including selected bond distances and bond angles.

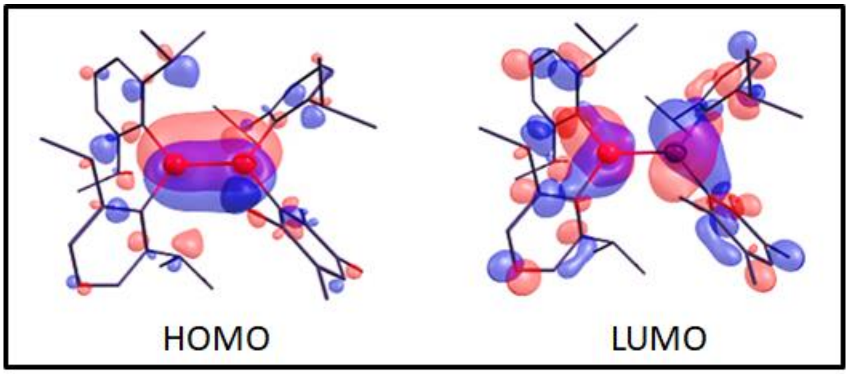

Figure 153. Selected Frontier orbitals of **94Dip**.

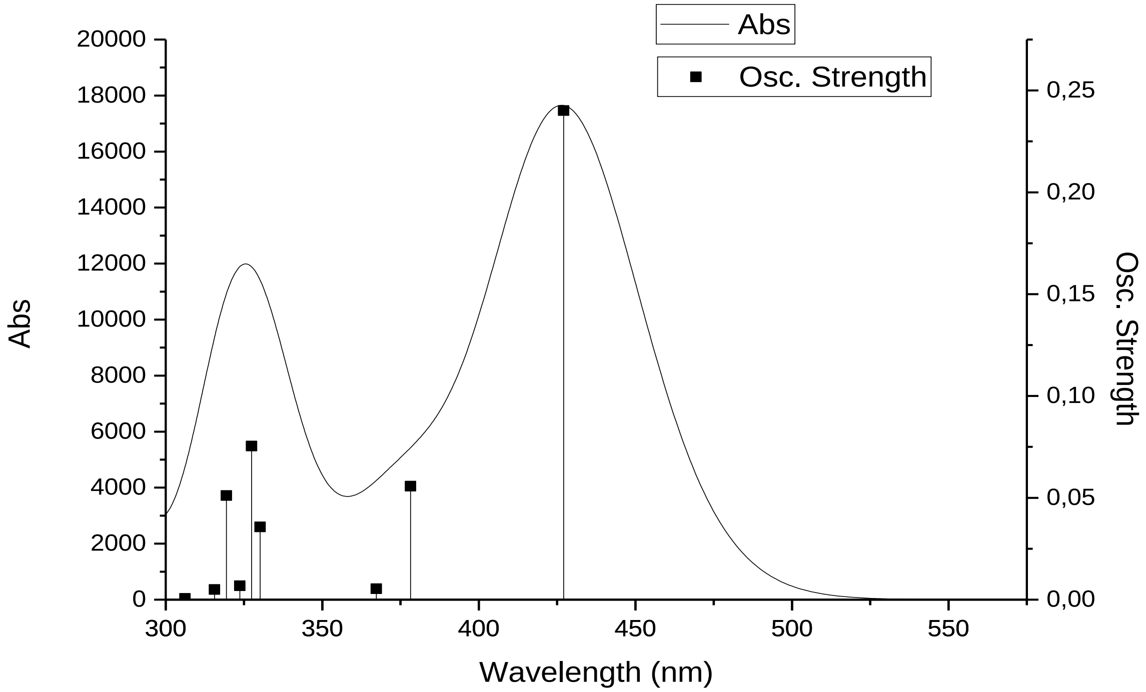

Figure 154. Calculated transitions (vertical bars) and simulated UV/vis absorption spectrum of **94Dip**.

Table 6. Selected electronic transitions and optical parameters of the theoretical calculations of **94Dip**.

Transition No.	$\lambda_{\text{calc. max}}$ (nm)	Transition energy (eV)	Transitions	*f c*	Contribution (%)
1	4 2 7.0 8	2.90	H→L	0.2401	90
2	378.02	3.27	H→L+1	0.0557	99
5	327.42	3.78	H→L+4	0.0754	91

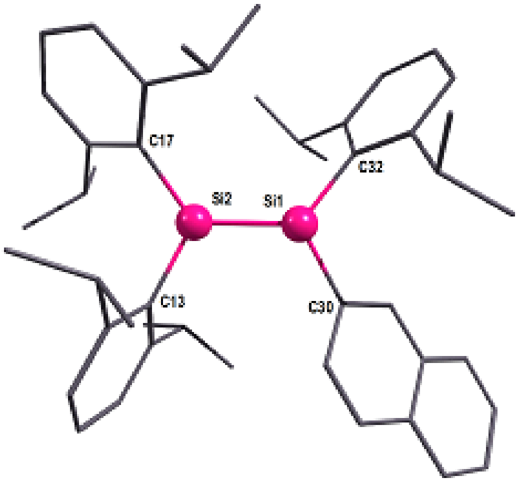

Bond lengths (Pm):	
Si1-Si2	217.87(5)
Si1-C30	187.9(4)
Si1-C32	190.0(6)
Si2-C13	191.4(8)
Si2-C17	191.7(3)

Bond Angles (°):	
Si2-Si1-C30	119.61(3)
Si2-Si1-C32	126.73(9)
Si1-Si2-C13	116.79(4)
Si1-Si2-C17	125.56(6)
Σ°(Si1)	358.59(5)
Σ°(Si2)	357.91(9)
θ(Si1)	10,956
θ(Si2)	13,767
τ	3,013

Deviation from planarity (°):	
(Si1-Si2)-Naphthyl	42.46(0)

Figure 155. Optimized structure of **98Dip** including selected bond distances and bond angles.

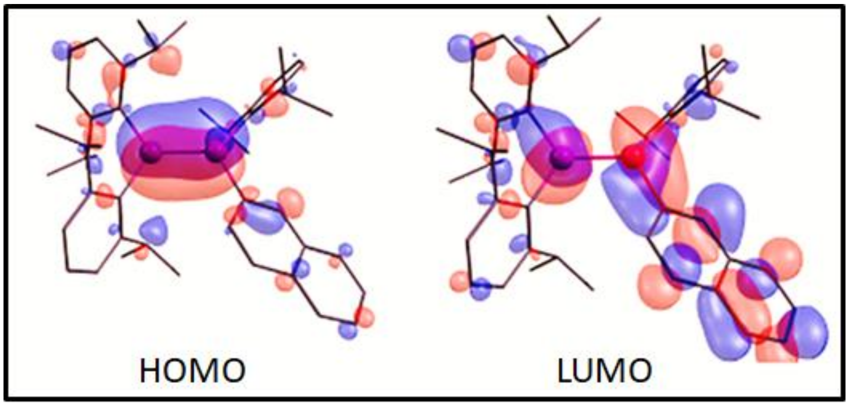

Figure 156. Selected Frontier orbitals of **98Dip.**

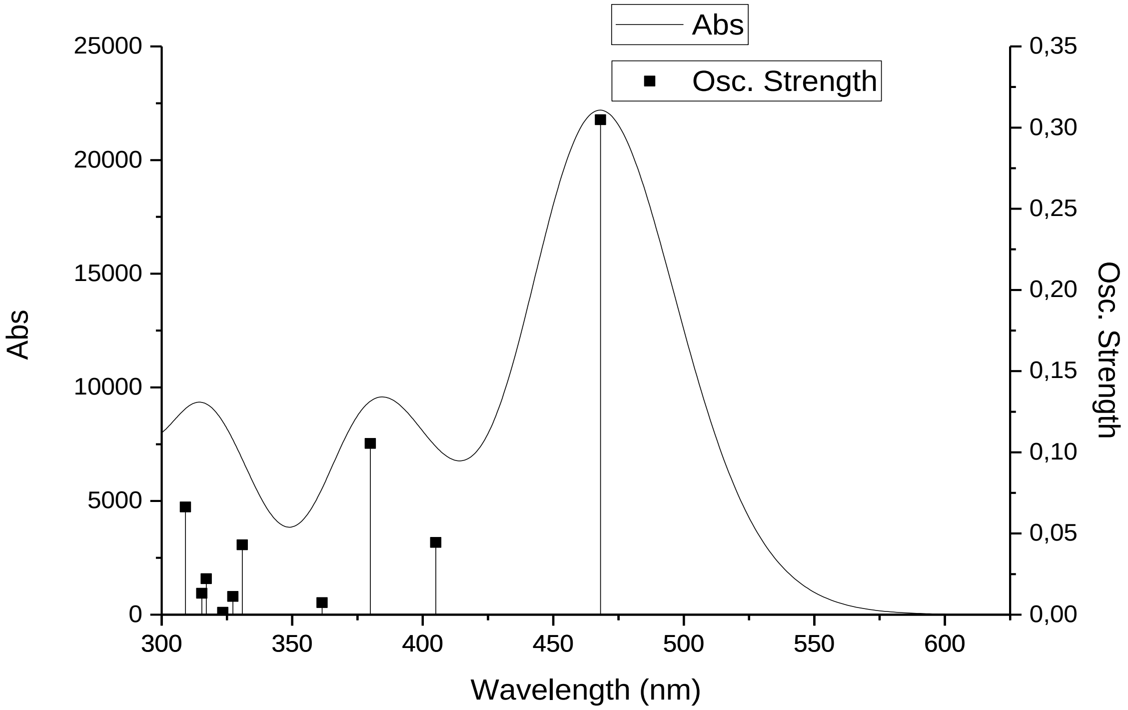

Figure 157. Calculated transitions (vertical bars) and simulated UV/vis absorption spectrum of **98Dip.**

Table 7. Selected electronic transitions and optical parameters of the theoretical calculations of **98Dip**.

Transition No.	**$\lambda_{\text{calc. max}}$ (nm)**	**Transition energy (eV)**	**Transitions**	***f c***	**Contribution (%)**
1	468.11	2.64	H→L	0.3048	93
2	404.97	3.06	H→L+1	0.0445	87
3	379.95	3.27	H→L+2	0.1054	87

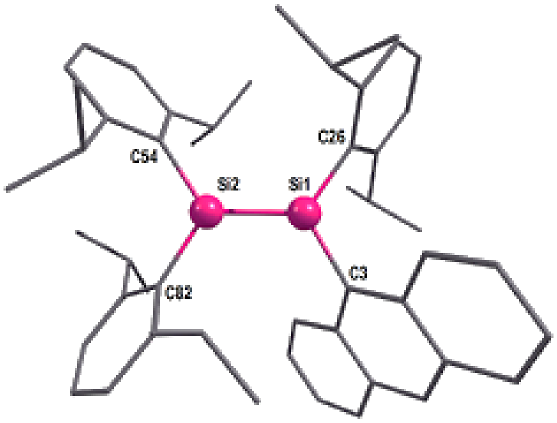

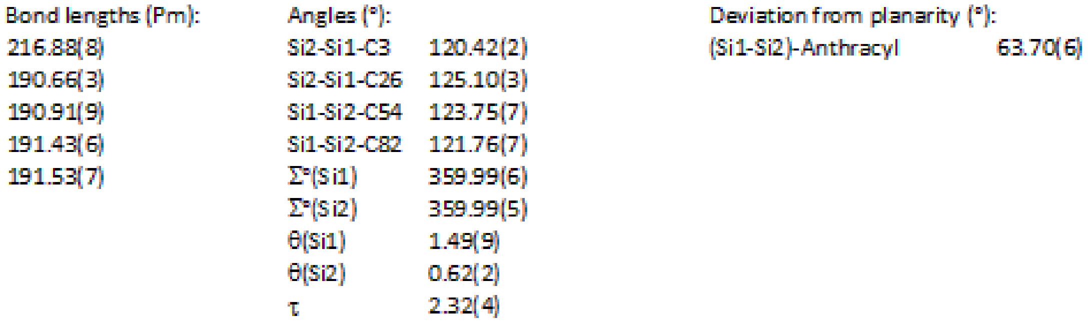

Bond lengths (Pm):	Angles (°):		Deviation from planarity (°):	
216.88(8)	Si2-Si1-C3	120.42(2)	(Si1-Si2)-Anthracyl	63.70(6)
190.66(3)	Si2-Si1-C26	125.10(3)		
190.91(9)	Si1-Si2-C54	123.75(7)		
191.43(6)	Si1-Si2-C82	121.76(7)		
191.53(7)	Σ°(Si1)	359.99(6)		
	Σ°(Si2)	359.99(5)		
	θ(Si1)	1.49(9)		
	θ(Si2)	0.62(2)		
	τ	2.32(4)		

Figure 158. Optimized structure of **100Dip** including selected bond distances and bond angles.

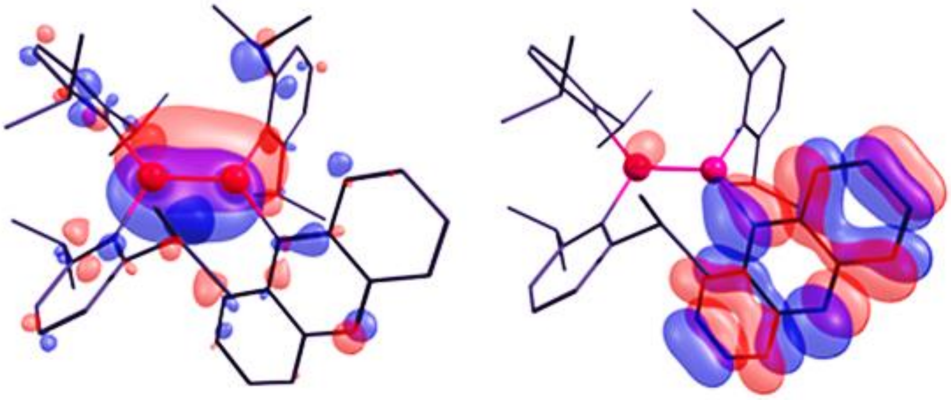

Figure 159. Selected Frontier orbitals of **100Dip.**

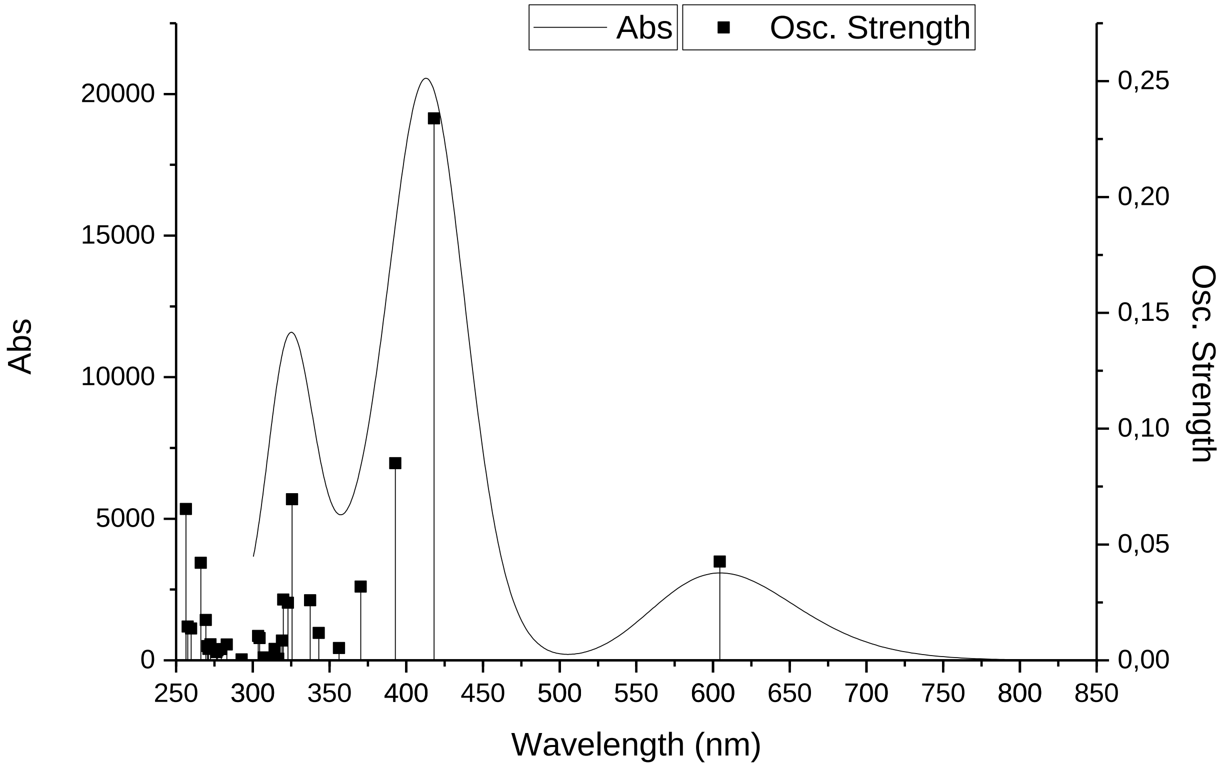

Figure 160. Calculated transitions (vertical bars) and simulated UV/vis absorption spectrum of **100Dip.**

Table 8. Selected electronic transitions and optical parameters of the theoretical calculations of **100Dip**.

Transition No.	$\lambda_{\text{calc. max}}$ **(nm)**	**Transition energy (eV)**	**Transitions**	***f c***	**Contribution (%)**
1	604.41	2.05	H→L	0.0426	98
2	418.10	2.96	H→L+1	0.2339	81
8	325.56	3.80	H→L+5 H→L+6	0.1054	70 10

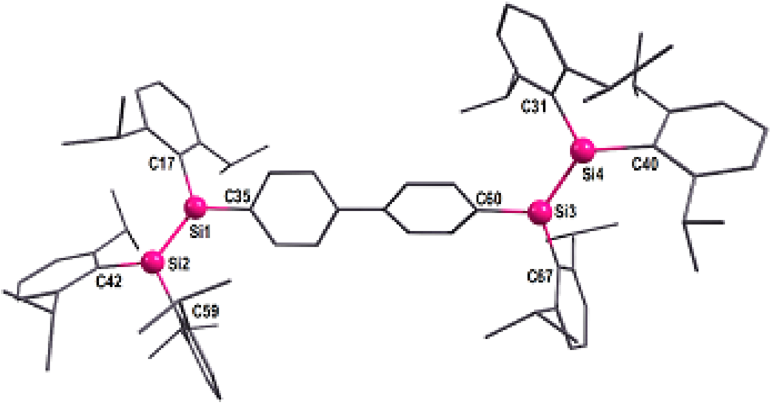

Bond lengths (pm):	
Si1-Si2	217.8(3)
Si1-C42	191.7(0)
Si1-C59	191.5(5)
Si2-C17	189.9(9)
Si2-C35	187.8(3)
Si3-Si4	217.3(2)
Si3-C60	187.8(4)
Si3-C67	189.9(1)
Si4-C31	191.4(4)
Si4-C40	191.6(4)

Bond angles (°):	
Si1-Si2-C17	126.86(9)
Si1-Si2-C35	119.60(0)
Si2-Si1-C42	125.83(0)
Si2-Si1-C59	116.16(5)
Si3-Si4-C31	117.24(8)
Si3-Si4-C40	125.55(3)
Si4-Si3-C60	119.54(4)
Si4-Si3-C67	127.28(2)
Σ°(Si1)	357,915
Σ°(Si2)	358,685
Σ°(Si3)	359,516
Σ°(Si4)	358,835
θ(Si1)	13,819
θ(Si2)	10,594
θ(Si3)	6,442
θ(Si4)	10,328
τ(Si1-Si2)	3,353
τ(Si3-Si4)	4,067

Deviation from planarity (°):	
(Si1-Si2)-Biphenyl	40.79(0)
Biphenyl-(Si3-Si4)	41.69(0)
(Si1-Si2)-(Si3-Si4)	34.10(2)

Figure 161. Optimized structure of **108Dip** including selected bond distances and bond angles.

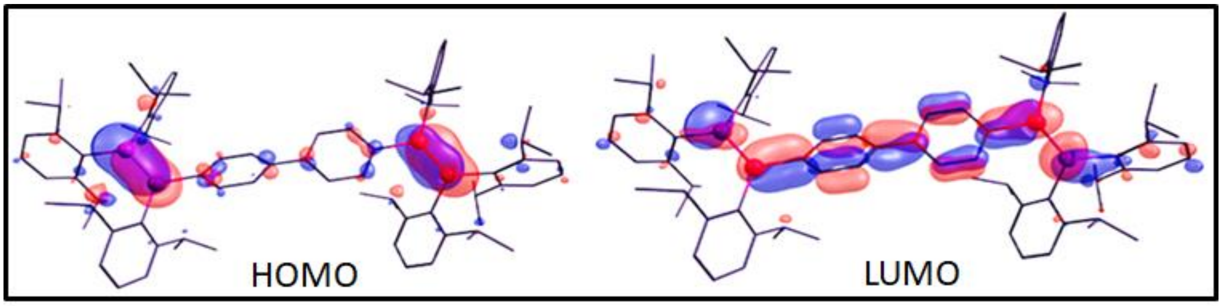

Figure 162. Selected Frontier orbitals of **108Dip**.

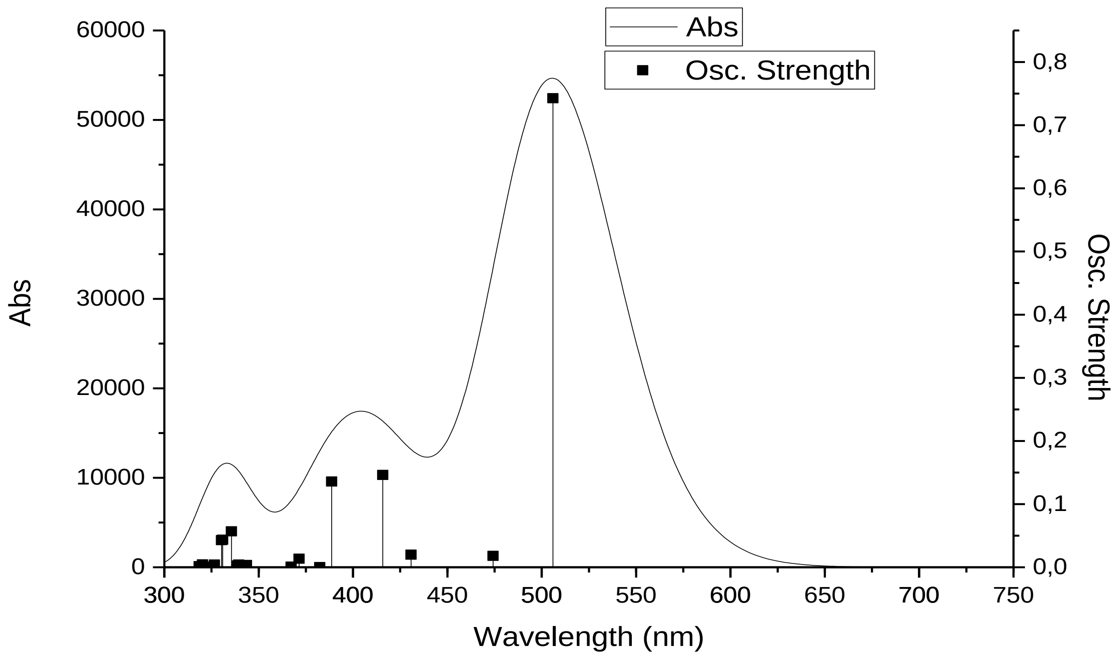

Figure 163. Calculated transitions (vertical bars) and simulated UV/vis absorption spectrum of **108Dip.**

Table 9. Selected electronic transitions and optical parameters of the theoretical calculations of **108Dip**.

Transition No.	$\lambda_{\text{calc. max}}$ (nm)	Transition energy (eV)	Transitions	*f c*	Contribution (%)
1	505.93	2.45	H→L	0.7427	97
4	415.77	2.98	H-1→L+1 H→L+2	0.1462	75 14
5	388.71	3.18	H-1→L+1 H-1→L+3 H→L+2	0.1357	20 13 60

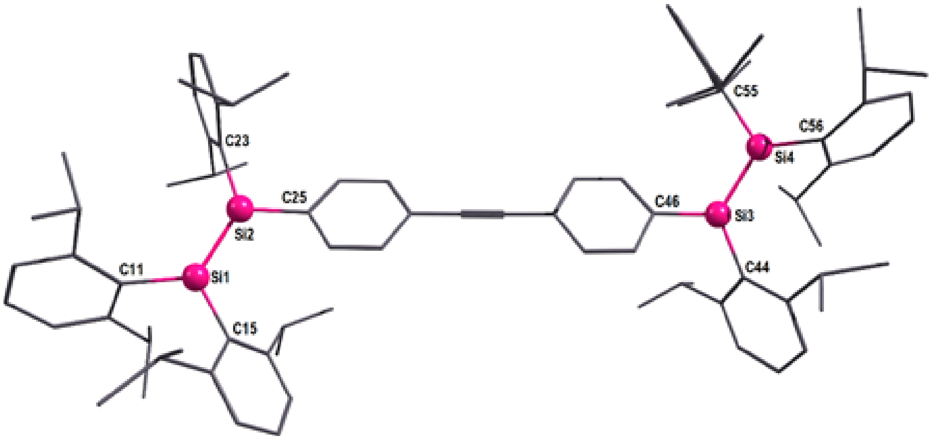

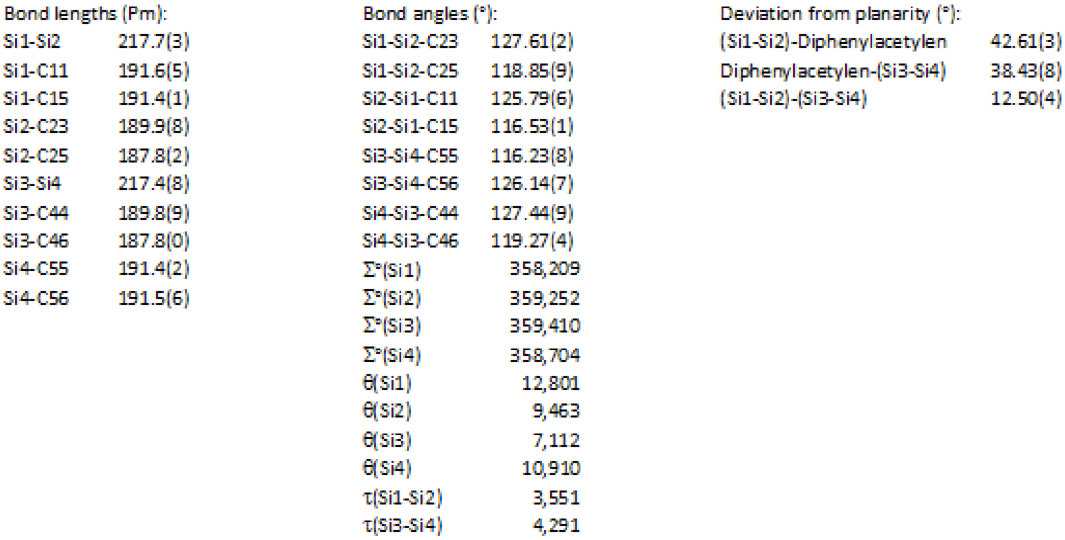

Bond lengths (Pm):	
Si1-Si2	217.7(3)
Si1-C11	191.6(5)
Si1-C15	191.4(1)
Si2-C23	189.9(8)
Si2-C25	187.8(2)
Si3-Si4	217.4(8)
Si3-C44	189.8(9)
Si3-C46	187.8(0)
Si4-C55	191.4(2)
Si4-C56	191.5(6)

Bond angles (°):	
Si1-Si2-C23	127.61(2)
Si1-Si2-C25	118.85(9)
Si2-Si1-C11	125.79(6)
Si2-Si1-C15	116.53(1)
Si3-Si4-C55	116.23(8)
Si3-Si4-C56	126.14(7)
Si4-Si3-C44	127.44(9)
Si4-Si3-C46	119.27(4)
Σ°(Si1)	358,209
Σ°(Si2)	359,252
Σ°(Si3)	359,410
Σ°(Si4)	358,704
θ(Si1)	12,801
θ(Si2)	9,463
θ(Si3)	7,112
θ(Si4)	10,910
τ(Si1-Si2)	3,551
τ(Si3-Si4)	4,291

Deviation from planarity (°):	
(Si1-Si2)-Diphenylacetylen	42.61(3)
Diphenylacetylen-(Si3-Si4)	38.43(8)
(Si1-Si2)-(Si3-Si4)	12.50(4)

Figure 164. Optimized structure of **112Dip** including selected bond distances and bond angles.

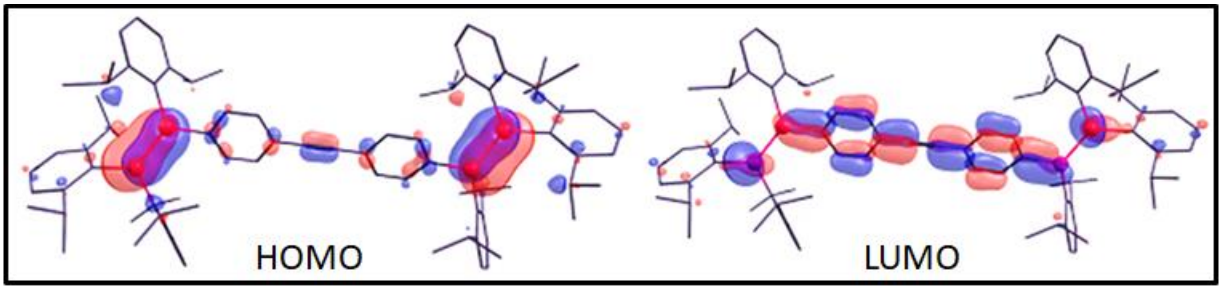

Figure 165. Selected Frontier orbitals of **112Dip.**

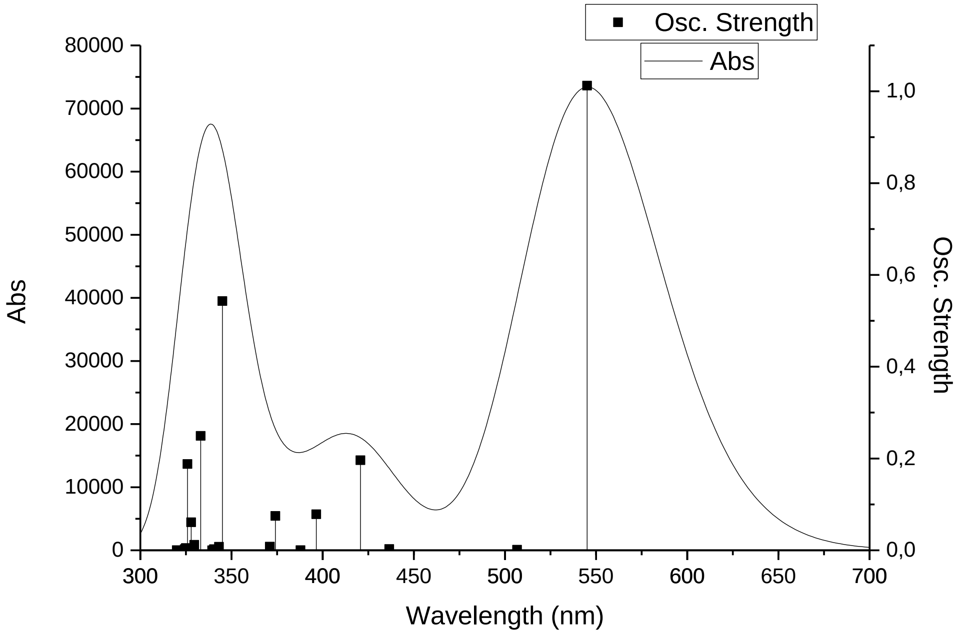

Figure 166. Calculated transitions (vertical bars) and simulated UV/vis absorption spectrum of **112Dip.**

Table 10. Selected electronic transitions and optical parameters of the theoretical calculations of **112Dip.**

Transition No.	**$\lambda_{\text{calc. max}}$ (nm)**	**Transition energy (eV)**	**Transitions**	***f c***	**Contribution (%)**
1	545.03	2.27	H→L	1.0124	98
4	420.77	2.94	H-1→L+1 H→L+2	0.1962	75 13
9	345.00	3.59	H-2→L H-1→L+5 H→L+8	0.5431	45 18 13

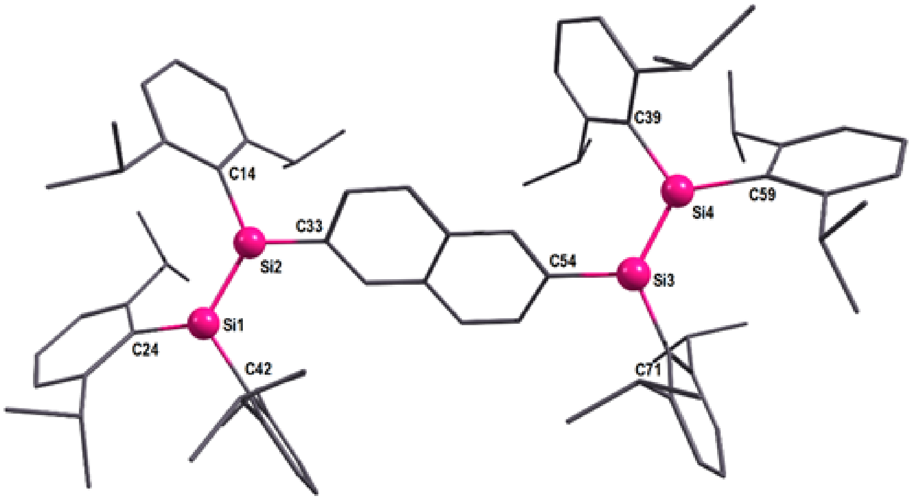

Bond lengths (Pm):	
Si1-Si2	217.9(4)
Si1-C24	191.7(1)
Si1-C42	191.5(7)
Si2-C14	190.0(7)
Si2-C33	187.9(8)
Si3-Si4	217.4(5)
Si3-C54	187.8(9)
Si3-C71	190.0(2)
Si4-C39	191.5(5)
Si4-C59	191.6(3)

Bond angles (°):	
Si1-Si2-C14	127.46(0)
Si1-Si2-C33	118.90(8)
Si2-Si1-C24	125.49(0)
Si2-Si1-C42	116.53(1)
Si3-Si4-C39	116.30(8)
Si3-Si4-C59	125.92(9)
Si4-Si3-C54	119.55(2)
Si4-Si3-C71	127.38(9)
Σ°(Si1)	357,566
Σ°(Si2)	358,413
Σ°(Si3)	359,294
Σ°(Si4)	358,485
θ(Si1)	14,899
θ(Si2)	11,615
θ(Si3)	7,756
θ(Si4)	11,804
τ(Si1-Si2)	3,295
τ(Si3-Si4)	4,249

Deviation from planarity (°):	
(Si1-Si2)-Naphthyl	46.82(4)
Naphthyl-(Si3-Si4)	39.81(1)
(Si1-Si2)-(Si3-Si4)	7.50(7)

Figure 167. Optimized structure of **114Dip** including selected bond distances and bond angles.

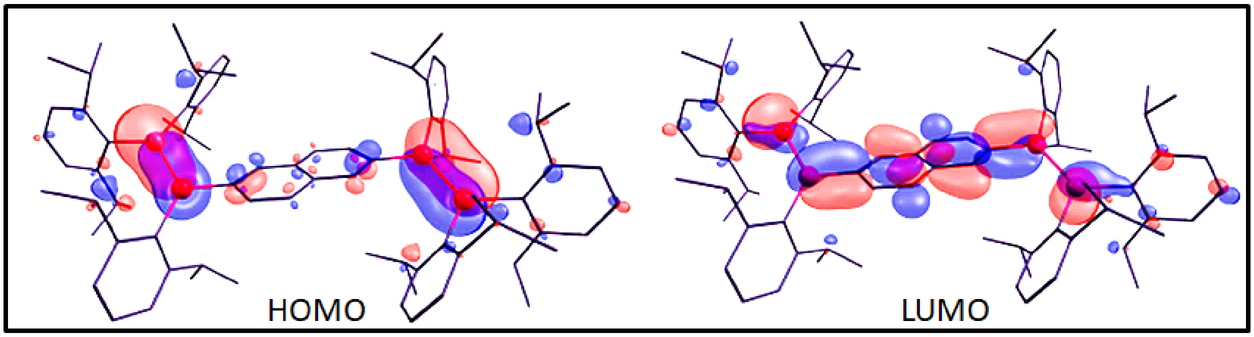

Figure 168. Selected Frontier orbitals of **114Dip**.

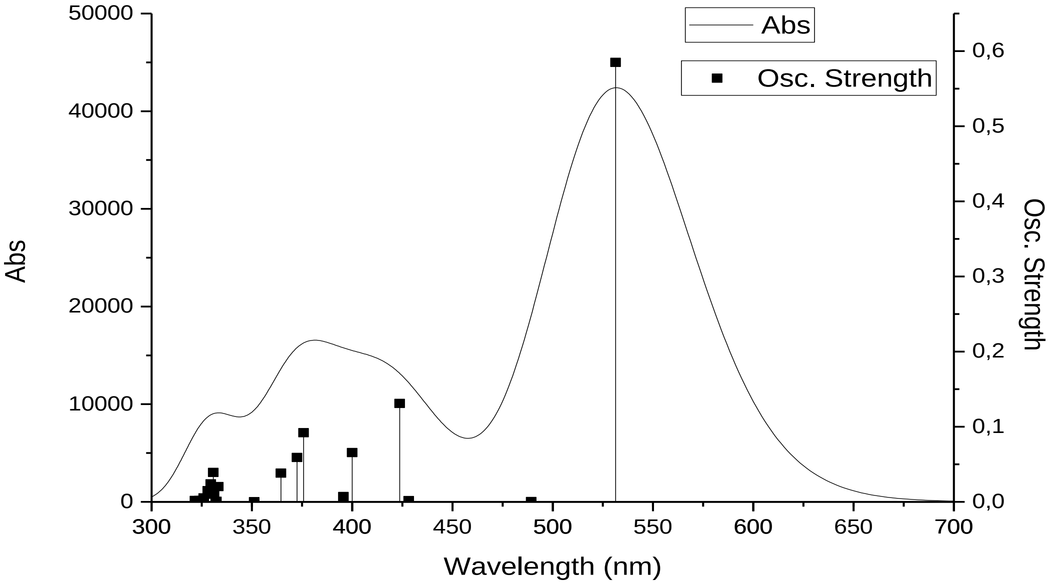

Figure 169. Calculated transitions (vertical bars) and simulated UV/vis absorption spectrum of **114Dip.**

Table 11. Selected electronic transitions and optical parameters of the theoretical calculations of **114Dip**.

Transition No.	$\lambda_{\text{calc. max}}$ **(nm)**	**Transition energy (eV)**	**Transitions**	$f\,c$	**Contribution (%)**
1	531.34	2.33	H→L	0.585	98
4	423.67	2.92	H→L+2	0.131	82

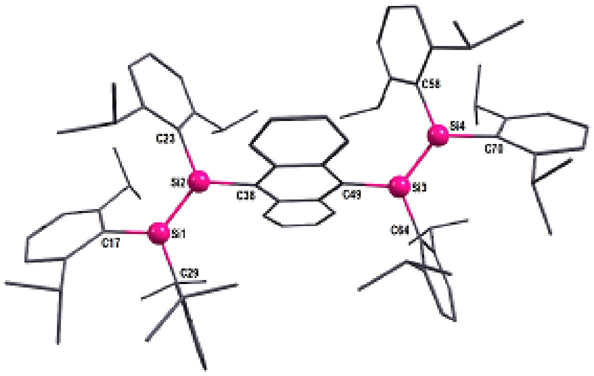

Bond lengths (Pm):	
Si1-Si2	218.2(6)
Si1-C17	192.6(4)
Si1-C29	191.2(6)
Si2-C23	191.5(2)
Si2-C38	193.2(0)
Si3-Si4	218.2(7)
Si3-C49	193.2(0)
Si3-C64	191.5(2)
Si4-C58	191.2(6)
Si4-C70	192.6(4)

Bond angles (°):	
Si1-Si2-C38	124.17(7)
Si1-Si2-C23	120.68(5)
Si2-Si1-C17	125.79(2)
Si2-Si1-C29	120.95(8)
Si3-Si4-C58	120.95(4)
Si3-Si4-C70	125.79(3)
Si4-Si3-C49	124.17(6)
Si4-Si3-C64	120.68(4)
Σ°(Si1)	359,909
Σ°(Si2)	359,993
Σ°(Si3)	359,993
Σ°(Si4)	359,908
θ(Si1)	2,819
θ(Si2)	0.800
θ(Si3)	0.788
θ(Si4)	2,830
τ(Si1-Si2)	4,970
τ(Si3-Si4)	4,971

Deviation from planarity (°):	
(Si1-Si2)-Anthracyl	65.23(6)
Anthracyl-(Si3-Si4)	65.24(1)
(Si1-Si2)-(Si3-Si4)	0.0(6)

Figure A60: Optimized structure of **116Dip** including selected bond distances and bond angles.

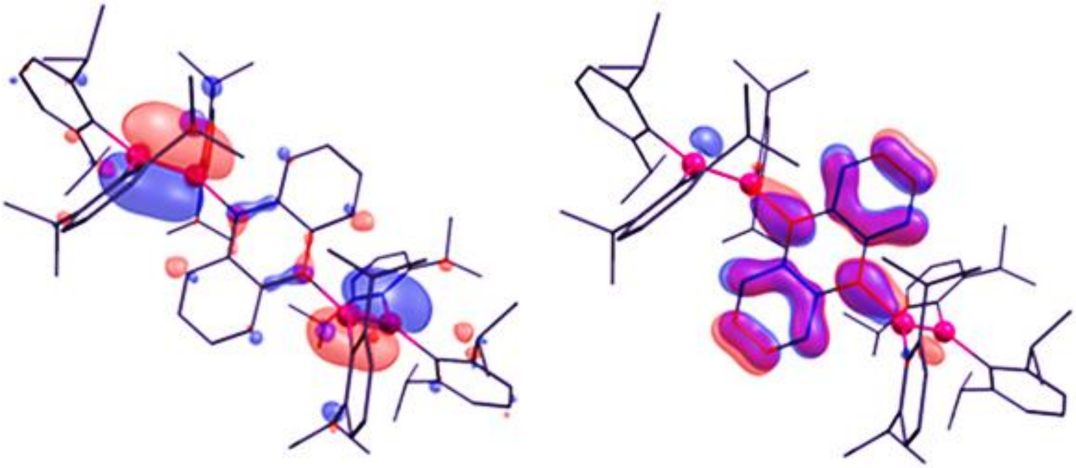

Figure 170. Selected Frontier orbitals of **116Dip.**

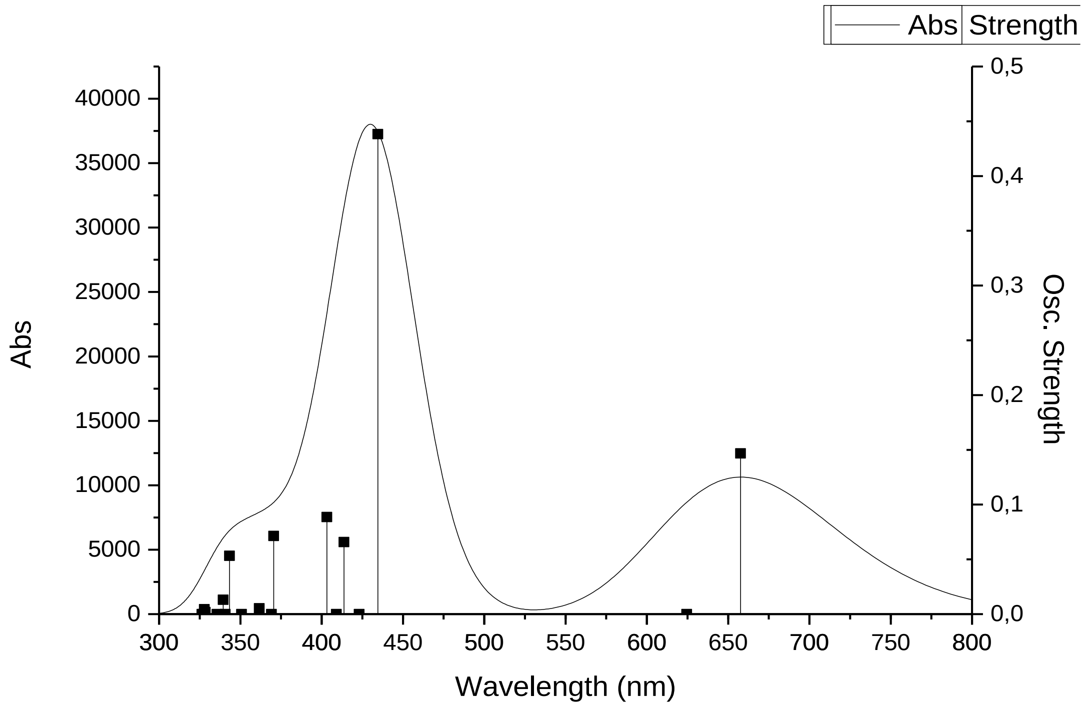

Figure 171. Calculated transitions (vertical bars) and simulated UV/vis absorption spectrum of **116Dip.**

Table 12. Selected electronic transitions and optical parameters of the theoretical calculations of **116Dip**.

Transition No.	**$\lambda_{\text{calc. max}}$ (nm)**	**Transition energy (eV)**	**Transitions**	***f c***	**Contribution (%)**
1	657.60	1.88	H→L	0.1468	99
2	624.57	1.98	H-1→L	0	99
3	423.67	2.85	H-2→L	0.4382	30
			H→L+1		60

7.5. Equilibrium between *Anti*-124a and *Syn*-124a

The equilibrium constants (K_{eq}) between *anti*-**124a** and *syn*-**124a** at various temperatures were determined by using integral ratio of vinylic proton signals in the ^{1}H NMR spectrum. The K_{eq} Values at various temperatures are summarized in Table 13. A plot of Ln K_{eq} at various temperatures is shown in Figure 171.

Method of calculation:

$\ln K_{eq} = -\Delta H/RT + \Delta S/R$

$\Delta H = -R \times \text{slope} = 28.83 \text{ kJ.mol}^{-1}$

$\Delta S = R \times \text{intercept} = 93.42 \text{ J.mol}^{-1}$

Table 13. Equilibrium Constant (K_{eq}) between *anti- and syn-* **124a** in *d$_8$*-toluene at various temperatures.

1/T (K^{-1})	ln k_{eq}	K_{eq}
0.0033	0.173	1.19
0.003	0.966	2.63
0.0028	1.89	6.66

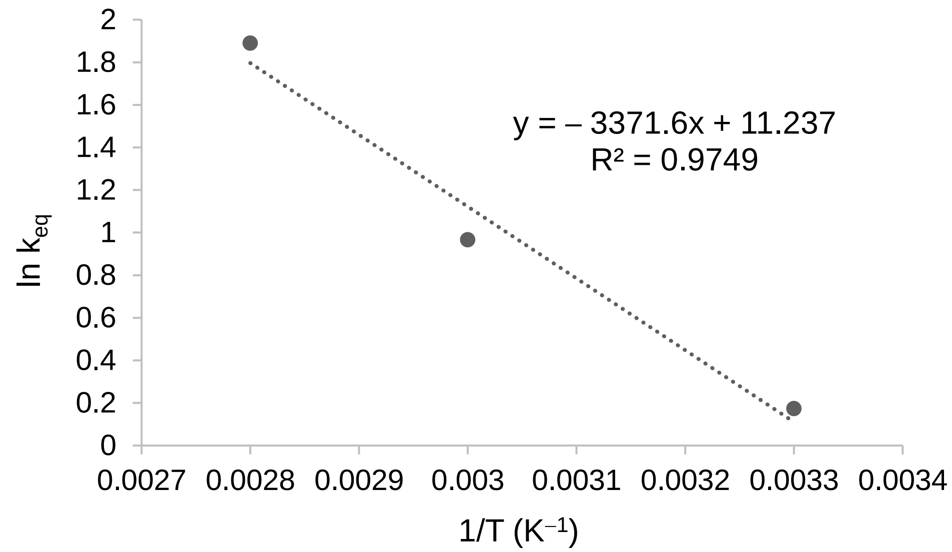

Figure 172. A plot of ln (K_{eq}) and 1/T.